frontiers | Research Topics

Myeloid cells in health and liver disease

Edited by
Evangelos Triantafyllou, Jack Leslie
and Carsten Deppermann

Published in
Frontiers in Immunology

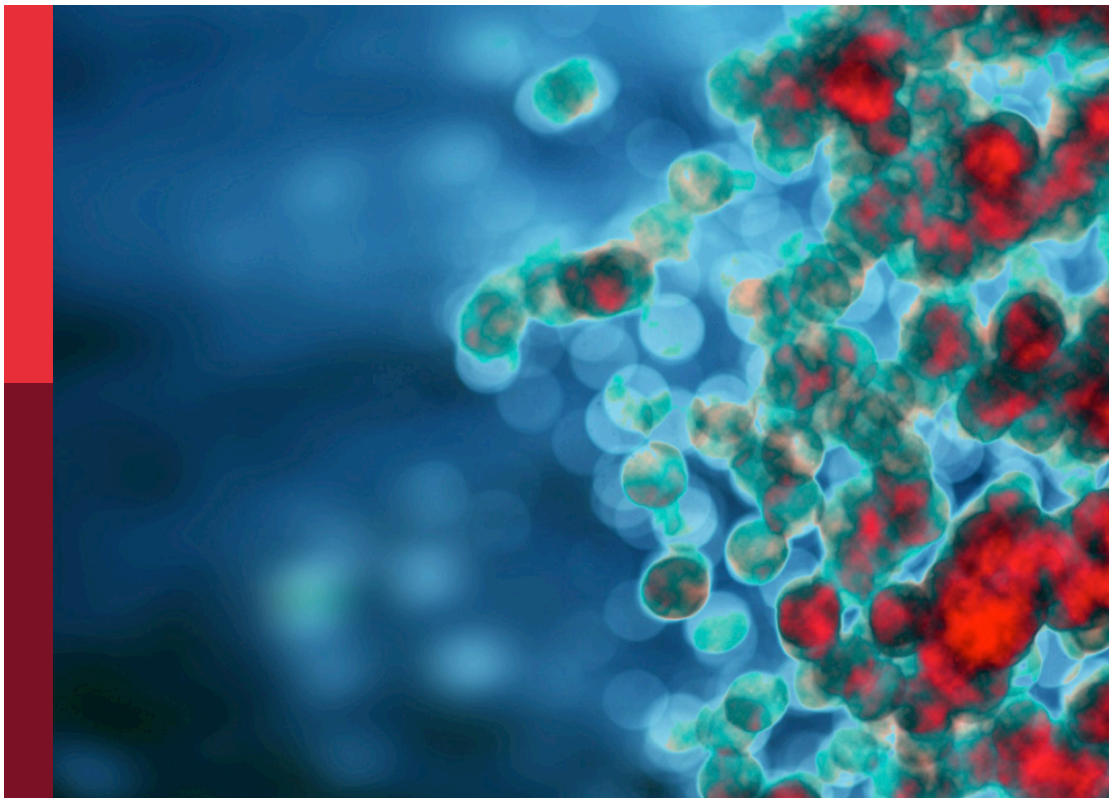

ISSN 1664-8714
ISBN 978-2-8325-5046-5
DOI 10.3389/978-2-8325-5046-5

About Frontiers

Frontiers is more than just an open access publisher of scholarly articles: it is a pioneering approach to the world of academia, radically improving the way scholarly research is managed. The grand vision of Frontiers is a world where all people have an equal opportunity to seek, share and generate knowledge. Frontiers provides immediate and permanent online open access to all its publications, but this alone is not enough to realize our grand goals.

Frontiers journal series

The Frontiers journal series is a multi-tier and interdisciplinary set of open-access, online journals, promising a paradigm shift from the current review, selection and dissemination processes in academic publishing. All Frontiers journals are driven by researchers for researchers; therefore, they constitute a service to the scholarly community. At the same time, the *Frontiers journal series* operates on a revolutionary invention, the tiered publishing system, initially addressing specific communities of scholars, and gradually climbing up to broader public understanding, thus serving the interests of the lay society, too.

Dedication to quality

Each Frontiers article is a landmark of the highest quality, thanks to genuinely collaborative interactions between authors and review editors, who include some of the world's best academicians. Research must be certified by peers before entering a stream of knowledge that may eventually reach the public - and shape society; therefore, Frontiers only applies the most rigorous and unbiased reviews. Frontiers revolutionizes research publishing by freely delivering the most outstanding research, evaluated with no bias from both the academic and social point of view. By applying the most advanced information technologies, Frontiers is catapulting scholarly publishing into a new generation.

What are Frontiers Research Topics?

Frontiers Research Topics are very popular trademarks of the *Frontiers journals series*: they are collections of at least ten articles, all centered on a particular subject. With their unique mix of varied contributions from Original Research to Review Articles, Frontiers Research Topics unify the most influential researchers, the latest key findings and historical advances in a hot research area.

Find out more on how to host your own Frontiers Research Topic or contribute to one as an author by contacting the Frontiers editorial office: frontiersin.org/about/contact

Myeloid cells in health and liver disease

Topic editors

Evangelos Triantafyllou – Imperial College London, United Kingdom
Jack Leslie – Newcastle University, United Kingdom
Carsten Deppermann – University Medical Centre, Johannes Gutenberg University Mainz, Germany

Citation

Triantafyllou, E., Leslie, J., Deppermann, C., eds. (2024). *Myeloid cells in health and liver disease*. Lausanne: Frontiers Media SA. doi: 10.3389/978-2-8325-5046-5

Topic editor Jack Leslie is a shareholder at FibroFind Ltd. All other Topic Editors declare no competing interests with regard to the Research Topic subject.

Table of contents

frontiers | Frontiers in Immunology

TYPE Original Research
PUBLISHED 08 September 2022
DOI 10.3389/fimmu.2022.968366

OPEN ACCESS

EDITED BY
Allan R. Brasier,
University of Wisconsin-Madison,
United States

REVIEWED BY
Juqiang Han,
People's Liberation Army General
Hospital, China
Young S. Hahn,
University of Virginia, United States

*CORRESPONDENCE
Ana C. Maretti-Mira
marettim@usc.edu

SPECIALTY SECTION
This article was submitted to
Molecular Innate Immunity,
a section of the journal
Frontiers in Immunology

RECEIVED 13 June 2022
ACCEPTED 12 August 2022
PUBLISHED 08 September 2022

CITATION
Maretti-Mira AC, Salomon MP,
Hsu AM, Kanel GC and
Golden-Mason L (2022) Hepatic
damage caused by long-term high
cholesterol intake induces a
dysfunctional restorative macrophage
population in experimental NASH.
Front. Immunol. 13:968366.
doi: 10.3389/fimmu.2022.968366

Hepatic damage caused by long-term high cholesterol intake induces a dysfunctional restorative macrophage population in experimental NASH

Ana C. Maretti-Mira[1,2]*, Matthew P. Salomon[1],
Angela M. Hsu[1,2], Gary C. Kanel[1,3] and Lucy Golden-Mason[1,2]

[1]USC Research Center for Liver Disease, Keck School of Medicine, University of Southern California, Los Angeles, CA, United States, [2]Division of Gastrointestinal and Liver Disease, Department of Medicine, Keck School of Medicine, University of Southern California, Los Angeles, CA, United States, [3]Department of Pathology, Keck School of Medicine, University of Southern California, Los Angeles, CA, United States

Excessive dietary cholesterol is preferentially stored in the liver, favoring the development of nonalcoholic steatohepatitis (NASH), characterized by progressive hepatic inflammation and fibrosis. Emerging evidence indicates a critical contribution of hepatic macrophages to NASH severity. However, the impact of cholesterol on these cells in the setting of NASH remains elusive. Here, we demonstrate that the dietary cholesterol content directly affects hepatic macrophage global gene expression. Our findings suggest that the modifications triggered by prolonged high cholesterol intake induce long-lasting hepatic damage and support the expansion of a dysfunctional pro-fibrotic restorative macrophage population even after cholesterol reduction. The present work expands the understanding of the modulatory effects of cholesterol on innate immune cell transcriptome and may help identify novel therapeutic targets for NASH intervention.

KEYWORDS

nonalcoholic fatty liver disease (NAFLD), Kupffer cells, tissue macrophages, RNAseq, innate immunity, cholesterol

Introduction

The liver is a crucial metabolic organ for lipid biosynthesis, processing, and elimination. Abnormal hepatic lipid accumulation is a hallmark of steatosis, a conditional part of the nonalcoholic fatty liver disease (NAFLD) spectrum. These lipids typically derive from diet, *de novo* lipogenesis, or adipose tissue lipolysis (1). Hepatic steatosis is frequently benign but can progress to nonalcoholic steatohepatitis (NASH), characterized by hepatic cellular injury and necroinflammation (2). NASH may progress to cirrhosis, end-stage liver failure, and hepatocellular carcinoma, representing the most common reason for terminal hepatic failure in western societies (3).

A significant change in lipid metabolism is also evident in NAFLD. A marked growth in free cholesterol (FC) levels occurs during the progression of steatosis to NASH, and total plasma cholesterol correlates to the presence of hepatic inflammation (4, 5). Increased cholesterol synthesis combined with a decrease in cholesterol elimination or the excessive intake of dietary cholesterol results in FC accumulation in the liver (6, 7). FC accumulation impacts several hepatic cells. FC accumulation in hepatocytes often triggers mitochondrial oxidative stress, sensitizes hepatocytes to pro-inflammatory cytokines, and later leads to cell death (8, 9). Hepatic stellate cells loaded with FC become sensitive to transforming growth factor (TGF) β-induced activation, which accelerates liver fibrosis (10), while FC exposure and accumulation in liver resident macrophages, termed Kupffer cells (KCs), contribute to liver inflammation (11).

KCs are part of a large family of innate immune effector cells known as macrophages. Hepatic macrophages fall into two categories: resident macrophages, the KCs, and infiltrating macrophages (IMs), derived from circulating monocytes that arrive at the liver during inflammation. Hepatic macrophages represent the first line of defense against products coming from the gastrointestinal tract and can play both pro- and anti-inflammatory roles in chronic liver diseases and directly contribute to fibrosis progression and resolution (12). Expansion of hepatic macrophages is a marker for NAFLD severity, and, in general, their participation is described as pro-inflammatory (13–15). Hepatic macrophage depletion prevents steatosis development and decreases hepatic levels of fibrosis (16). However, macrophage depletion during the NASH recovery phase accentuates liver fibrosis, suggesting a broader involvement of macrophages in liver homeostasis during NAFLD (14).

Although several studies support the participation of hepatic macrophages in NAFLD progression, the impact of dietary cholesterol on hepatic macrophage transcriptome and function in the setting of NASH remains elusive. Animal models of NASH based on long-term high-fat and high-fructose diets display the highest similarity to human NAFLD, not only phenotypically but also at the transcriptomic level (17). Therefore, we have selected an established prolonged fructose, palmitate, cholesterol, and trans-fat (FPC) diet to develop murine NASH and fed mice with different contents of cholesterol in two stages of our dietary intervention, starting with medium (0.2%) or high (1.25%) cholesterol content, and later reducing cholesterol to low levels (0.05%) (18). Our findings suggest that a decrease in cholesterol intake silences the inflammatory signal detected in macrophages from mice initially fed with medium cholesterol FPC diet. However, the effect of a long-term diet fueled by high cholesterol content is more harmful to the liver homeostasis since the hepatic macrophages do not completely deactivate after cholesterol reduction and further display a dysfunctional restorative macrophage phenotype.

Materials and methods

Murine model of diet-induced NASH

To evaluate the contribution of dietary cholesterol to NASH progression, we selected the well-established Fructose, Palmitate, Cholesterol, and Trans-Fat (FPC) diet (Envigo) to induce NASH as this model recapitulates human disease (17, 18). Seven-week-old male wild type C57BL/6J mice (Jackson Laboratory) were allowed to acclimate to housing in our facility for two weeks before the dietary intervention, which was subdivided into two phases: 1) Progression: mice received the FPC diet for 20 weeks and were divided into three groups according to the dietary cholesterol content - low (FPC + 0.05% cholesterol), medium (FPC + 0.2% cholesterol) and high (FPC + 1.25% cholesterol). 2) Regression: Cholesterol was reduced to 0.05% in all the FPC diet subgroups for additional ten weeks. The animal study was reviewed and approved by the University of Southern California Institutional Animal Care and Use Committee.

Liver non-parenchymal cell isolation

Hepatic non-parenchymal cells (NPCs) were isolated using liver perfusion. Livers were perfused with calcium/magnesium-free HBSS containing 3mg/mL of Liberase™ (Roche), excised, and then mechanically dissociated in calcium/magnesium-free HBSS containing 0.5% BSA and 2mM EDTA. The cell suspension was centrifuged at 20 x g for 2 minutes to remove hepatocytes and then transferred to a new tube and centrifuged at 365 x g for 8 minutes. Red blood cells were removed by lysis (RBC lysis buffer - BD Pharmlyse), and NPCs were isolated by density gradient centrifugation with 20% OptiPrep™ (StemCell Technologies). The NPC layer was collected and stained for cell sorting.

Hepatic macrophage sorting

To identify hepatic macrophages, we selected several markers that could identify hepatic macrophages with different phenotypes (19–21). We stained NPCs with anti-mouse CD45 (BD Horizon; 30-F11), MertK (eBio; DS5MMER), CD64 (BioLegend; X54-5/7.1), F4/80 (eBio; BM8), and CD11b (eBio; M1/70) antibodies. Cell incubation took place on ice in the dark for 25 minutes. Sorting was performed on a BD FACSAria™ Fusion Flow Cytometer, with 100µm nozzle, into 90% FBS media at 4˚C. After sorting, we checked population purity and centrifuged cells at 400 x g for 5min at 4°C. Cells were resuspended in RLT buffer (Qiagen) containing 2-mercaptoethanol, passed through QIAshredder (Qiagen), and stored at -80°C for subsequent processing.

Macrophage bulk mRNAseq

Macrophage RNA was isolated using the RNeasy kit (Qiagen) following the manufacturer's protocol. RNA quality and concentration were assessed by the 2100 Expert Bioanalyzer System (Agilent), using the RNA 6000 Pico Kit (Agilent). Transcriptome RNA sequencing was performed at the Norris Cancer Molecular Genomics Core. Library quality control was perform using Agilent BioAnalyzer 2100 and libraries were simultaneously prepared using Kapa mRNA Hyper kit (cat#08098123702, Roche Diagnostics) following the manufacturer's protocol. RNAseq libraries were sequenced on the Illumina Nextseq500 platform at a read length of 2x75 at 25 million reads per sample.

Raw sequencing reads were checked for overall quality and adapter contamination using FastQC (https://www.bioinformatics.babraham.ac.uk/projects/fastqc/) and trimmed using Trim Galore (https://www.bioinformatics.babraham.ac.uk/projects/trim_galore/) prior to downstream analysis. Reads were then used to quantifying transcript abundances with Salmon (22) using the GENCODE version M25 mouse reference. The resulting transcript abundances were summarized to gene level counts using functions in the Bioconductor package tximport (23). Significantly differentially expressed genes were identified using the Bioconductor package DESeq2 (24) with a significance threshold of FDR < 0.1. Volcano plots were generated using the Enhanced Volcano Bioconductor package (https://github.com/kevinblighe/EnhancedVolcano). Ingenuity Pathway Analysis (IPA) software (v01-20-04, Qiagen) was used to determine the hepatic biological processes altered by cholesterol intake level (25). Gene Set Enrichment analysis (GSEA) software v4.1.0 was used to identify relevant pathways and biological processes (26). The Gene Ontology Resource platform was used to identify the biological processes triggered by the commonly expressed genes during the progression phase of the dietary intervention (27).

Hepatic inflammation and fibrosis histological assessment

Liver fragments from each lobe were kept in 10% buffered neutral formalin overnight and dehydrated in 70% ethanol at 4°C. Fragments were then embedded in paraffin and cut into sections of 5µm thickness, deparaffinized, and hydrated. The serial sections were then stained for H&E and Sirius Red as per standard protocols at the USC Research Center for Liver Diseases (RCLD) Liver Histology Core.

Liver biopsies from 4 lobules from each mouse used in this study was evaluated and graded histologically as follows: Steatosis grades: "0" =none, "<1" = less than 5% of hepatocytes, "1" = 5-25%, "2" = 26-50%, "3" = 51-75%, "4" = >75%; Lobular inflammation grades (20x field): "0" = none, "1" = < 2 per field, "2" = 2-4 per field, "3" = > 4 per field; Fibrosis grades: "0" = None, "1" = Perisinusoidal or periportal, "2" = Perisinusoidal and portal/periportal, "3" = Bridging fibrosis, "4" = Cirrhosis. The scoring was performed by a pathologist (G.K) in coded fashion without knowledge of the treatment.

Statistical analyses

All statistical analyses, graphs, and heatmaps were generated using GraphPad Prism version 9 for macOS (GraphPad Software, www.graphpad.com). We used the non-parametrical Kruskal-Wallis test to evaluate hepatic inflammation and fibrosis scores.

Results

High dietary cholesterol intake exacerbates hepatic inflammation and fibrosis

To evaluate the contribution of dietary cholesterol to the progression of nonalcoholic steatohepatitis (NASH) induced by high-fat and high-fructose diet, we used the FPC diet as an established model mimicking human NASH (18). We combined the FPC diet with different cholesterol concentrations into two distinct phases. In the first phase (progression), mice were fed the FPC diet for 20 weeks with high (1.25%), medium (0.2%), or low (0.05%) cholesterol. In the second phase (regression), we reduced the cholesterol content of all FPC diets to 0.05% and fed all the groups for a further ten weeks. We euthanized six mice from each group at the end of the progression phase and four at the end of the regression phase, harvesting their livers to evaluate steatosis, inflammation, and fibrosis. We also isolated hepatic macrophages for transcriptomic analysis (Figure 1A).

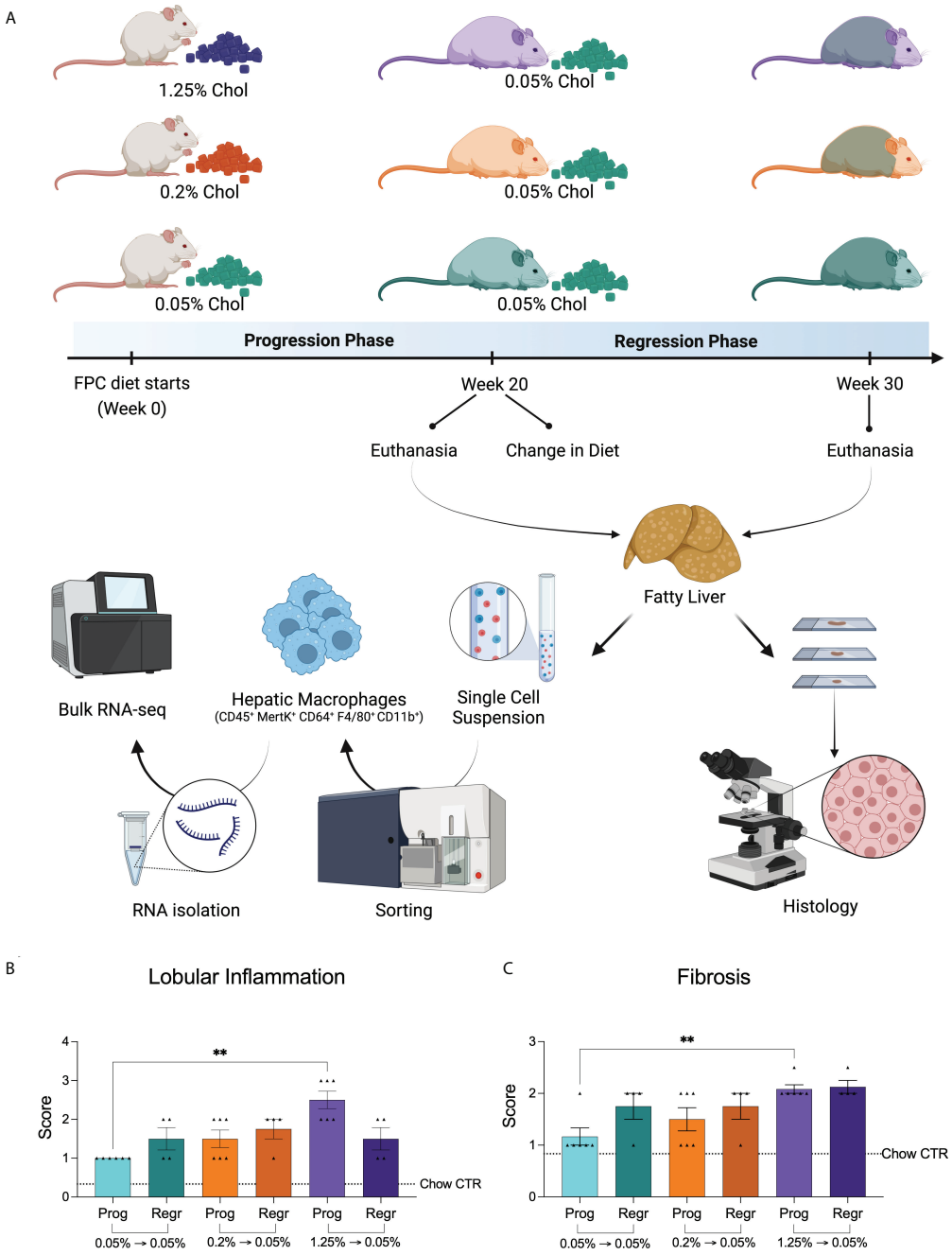

FIGURE 1
Experimental design and dietary cholesterol impact on murine NASH model. **(A)** For our NASH model, we selected the Fructose, Palmitate, Cholesterol, and Trans-Fat (FPC) diet. We evaluated the mice in two distinct phases. During the first 20 weeks (progression phase), we fed male C57BL/6J mice with the FPC diet containing different concentrations of cholesterol: 1.25% (high, purple), 0.2% (medium, orange), and 0.05% (low, green). At week 20, we reduced the dietary cholesterol intake for the 1.25% and 0.2% groups, keeping all mice on the FPC diet with 0.05% cholesterol for additional ten weeks (regression phase). At the end of each phase, we harvested mice livers, sorted hepatic macrophages, and processed them for RNA-seq analysis. NASH was assessed on the liver specimens based on histologic findings (Created with BioRender.com). **(B)** Lobular inflammation and Fibrosis **(C)** were exacerbated in mice fed with high cholesterol FPC diet during the progression phase (n = 6 for progression and n = 4 for regression phases). Statistical test used: Kruskal-Wallis, **P value < 0.01. Prog, Progression phase; Regr, Regression phase; CTR, control.

As expected, all FPC diet groups showed advanced steatosis (grade 4, Supplementary Figure 1A) without differences related to cholesterol intake. We observed a significant increase in lobular inflammation and fibrosis in the livers of mice fed with high cholesterol during the progression phase (Figures 1B, C; Supplementary Figures 1B, C). While inflammation slightly improved after cholesterol reduction (not significantly), fibrosis remained unchanged. In fact, the fibrosis scores of all groups became very similar by the end of the regression phase (Figure 1C).

Our findings suggest that high cholesterol intake combined with a high-fat and high-fructose diet aggravates hepatic inflammation and accelerates fibrosis.

Cholesterol intake affects hepatic macrophages transcriptome

Considering the significance of hepatic macrophages for NASH development, we evaluated the impact of dietary cholesterol on total hepatic macrophage transcriptome in a high-fat and high-fructose diet background. For this purpose, we sorted hepatic macrophages from the non-parenchymal cells obtained from mice livers, acquiring an average of 400,000 hepatic macrophages from each mouse. Cells were immediately preserved in RLT lysis buffer (Qiagen™) and later processed for RNAseq. Our findings revealed that cholesterol addition to the FPC diet significantly changed hepatic macrophage global gene expression (Figures 2A, B). We compared the medium and high cholesterol groups to the low cholesterol group in the different dietary phases to identify genes regulated by cholesterol. In macrophages from mice fed with medium cholesterol, we identified 1,774 differentially expressed (DE) genes (1,019 up and 755 down) during the progression phase and 229 genes (90 up and 139 down) during the regression phase. The most remarkable changes were observed in macrophages from the high cholesterol group, with 2,880 DE genes (1,373 up and 1,507 down) during the progression phase and 3,902 DE genes after cholesterol reduction (1,918 up and 1,984 down). Principal component analysis (PCA) indicated that macrophages' transcriptomes from mice fed with high and medium cholesterol are similar during the progression phase, fully separating from the low cholesterol group. However, during the regression phase, macrophages from the medium cholesterol group normalized their gene expression, becoming similar to macrophages from the low cholesterol group (Figure 2C). These results suggested that the transcriptomic modifications triggered by a high cholesterol diet are more robust and not as easily reversed as those resulting from medium cholesterol intake.

Identification of genes modulated by dietary cholesterol in hepatic macrophages

We analyzed the relationship among the DE genes from the high and medium cholesterol groups in both dietary phases and identified 32 genes commonly expressed, which were also strongly connected as a network (Figure 3A; Supplementary Figure 2; Supplementary Table 1). The biological processes enriched by those genes were related to differentiation and transformation of connective tissue cells, cell cycle, viability and activation, cell movement, and vasculogenesis. These processes were stimulated by cholesterol intake and inhibited by cholesterol reduction. Other processes also enriched by these genes were cell death, liver damage, and weight loss, downregulated by cholesterol ingestion and upregulated by cholesterol intake reduction (Figure 3B).

We highlighted genes with immune relevance in Figure 3C. Cholesterol intake upregulates the expression of *Ccl3, Cclr2, Dusp1, Osm*, and *Cd163*. Cholesterol reduction normalized the expression of *Ccl3, Cclr2, Dusp1*, and *Osm* in both medium and high cholesterol groups, while *Cd163* expression only decreased in the medium cholesterol macrophages. Conversely, *Cxcr5* expression was downregulated by cholesterol intake, recovering its levels after cholesterol reduction in the medium but not in the high cholesterol group.

We found 424 genes uniquely modified by cholesterol intake, regardless of its concentration, which included *Cnr2, Col4a3, Csf1, Cxcr2, Cxcr6, Gzma, Hbegf, Il16, Il1f9, Il33, Lamc1, Ncf1, Osmr, Prf1, Tnf*, and *Vegfa* (Figure 4A and Supplementary Table 1). Cholesterol reduction exclusively affected the expression of 55 genes, including *Ccl17, Cxcl12, Cd63, Clec7a, Tspan3, Erg1, Klf6, Ltc4s*, and *Mbl2* (Figure 4B and Supplementary Table 1). We applied the Gene Ontology enrichment test to these two sets of genes and observed that only genes from the progression phase could enrich relevant biological processes, such as wound healing, cytotoxic cell differentiation, neutrophil chemotaxis, and immune response (Figure 4C).

Dietary cholesterol induces macrophage genes related to extracellular matrix organization, inflammation and affects macrophage polarization

We identified the top 25 upregulated DE genes from the high and medium cholesterol groups during both the progression and regression phases, clustered the gene expression values of all six groups, and observed that the samples clustered into two main branches (Figure 5A and Supplementary Table 2). The first branch grouped all samples from the low cholesterol groups and

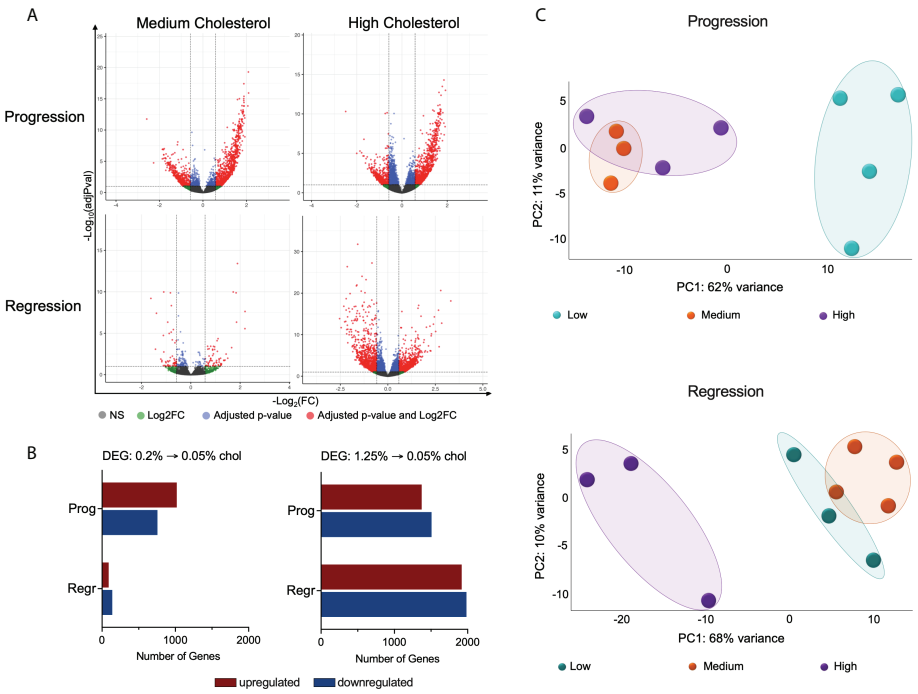

FIGURE 2
High cholesterol intake changes the global gene expression of hepatic macrophages. **(A)** Volcano plots show the hepatic macrophages' differentially expressed genes (DEGs) in the different dietary groups, emphasizing the cholesterol effect. DEG lists were acquired by normalizing the transcriptome from the high and medium cholesterol groups using the age-matched low cholesterol group. **(B)** Comparing the medium to the low cholesterol group, we found 1,774 genes modified during the progression phase (1,019 up and 755 down) and 229 genes in the regression phase (90 up and 139 down). The comparison between the high to the low cholesterol group revealed 2,880 genes differentially expressed during the progression phase (1,373 up and 1,507 down), and 3,902 DE genes in the regression phase (1,918 up and 1,984 down). **(C)** PCA plots clearly show that during the progression phase, the medium cholesterol (n = 3) and the high cholesterol (n = 3) groups differed from the low cholesterol group (n = 4) and that after cholesterol reduction (regression phase), the medium cholesterol group (n = 4) became comparable to the low cholesterol group (n = 3), while the high cholesterol group (n = 3) maintain the original difference. NS, non-significant; Log2FC, log2-foldchange based on low cholesterol age-matched group; Prog, Progression phase; Regr, Regression phase.

the samples of the medium cholesterol group during the regression phase. The other branch comprised samples from the medium cholesterol group during the progression phase and all the samples from the high cholesterol group. The samples of the high and medium cholesterol groups from the progression phase clustered together. The top upregulated genes related to cell migration (*Kdr, Il1r1, Flt4, Adamts1, Sele, Aqp1, Sema6a, Hspb1, Sema3f*), angiogenesis (*Kdr, Flt4, Hspb1, Col4a1, Col4a2, Sema6a*) and extracellular matrix organization (*Lama4, Col4a1, Col4a2, Pxdn, Adamts1, Adamts4, Adamts7, Hmcn1*) (Figure 5A).

Considering the participation of macrophages in tissue immune homeostasis, we specifically looked at genes for cytokines that shifted their expression pattern after cholesterol reduction. Dietary cholesterol upregulated the expression of *Ccl2, Ccl3, Ccl4, Ccl17, Csf1, Cxcl2, Hbegf, Il10, Il1a, Il33, Tnf, Trail*, and *Vegfa*, which normalized after cholesterol reduction (Figure 5B). Additionally, we searched for the cytokines that were not "turned off" by cholesterol reduction and found that *Bmp2, Bmp6, Fgf1, Il27, Il6st*, and *Tgfa* remained upregulated in the high cholesterol group but normalized their expression in the medium cholesterol group (Figure 5C).

We examined the pathways modified by dietary cholesterol and detected the upregulation of TNF-α, TGF-β, and IL-6 signaling during the progression phase and the downregulation of cholesterol and fatty acid metabolisms, FC-γ receptor activation, and PD-1 signaling pathways. Cholesterol reduction normalized most of these pathways (Figure 5D). Notably, the high cholesterol group showed a non-reversible upregulation of collagen formation and extracellular matrix organization processes. Cholesterol intake enhanced the expression of several genes encoding fibrillar collagen, fibrillin, and basement membrane components during the progression phase of medium and high cholesterol groups (Figure 5E). While most of these genes normalized their expression after cholesterol reduction in the medium cholesterol group, several genes were still highly expressed in the high cholesterol group. Matrix and disintegrin metalloproteinases genes (MMPs and ADAMs, respectively) followed a similar expression pattern, except for *Mmp12*,

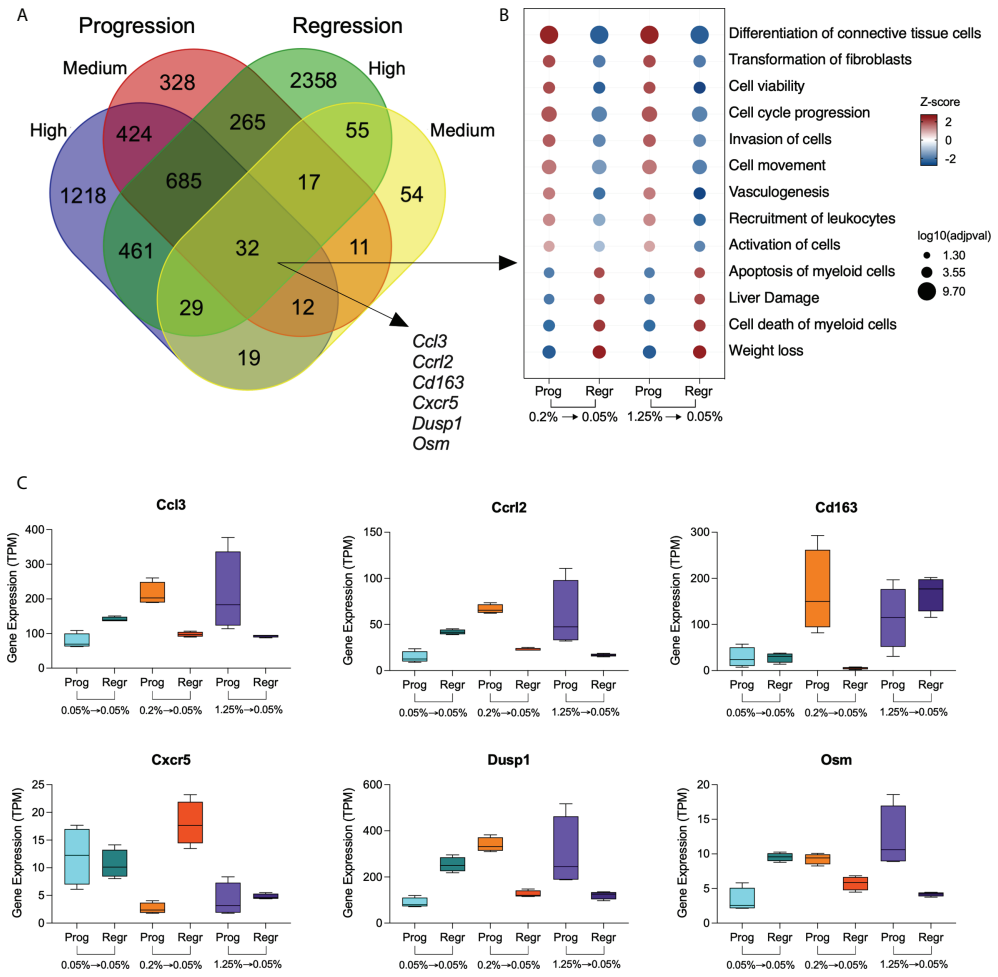

FIGURE 3
Genes modulated by dietary cholesterol in hepatic macrophages. **(A)** Venn diagram shows the overlapping differentially expressed genes among the comparison groups. The high and medium cholesterol groups were compared to the low cholesterol group during progression (Prog) and regression (Regr) phases. Thirty-two genes were commonly expressed by the four comparison groups. **(B)** Bubble plot shows the biological processes derived from the 32 genes commonly expressed genes by the four groups. Analysis performed using Ingenuity Pathway Analysis (IPA). **(C)** Expression of six genes with immunological significance were highlighted are shown in all six dietary groups included in this study. Prog, Progression phase; Regr, Regression phase.

Mmp13, and *Mmp19*, which were downregulated during the regression phase in both groups. *Timp3* was the only metalloproteinase inhibitor significantly expressed, displaying high levels in the medium and high cholesterol groups during the progression stage and the high cholesterol group in the regression phase.

Noticing the upregulation of pro-inflammatory pathways, we decided to evaluate the expression of macrophage polarization markers in both dietary intervention phases (Figure 6A). We found that hepatic macrophages from both cholesterol groups expressed mixed M1 and M2 polarization markers during the progression phase. After cholesterol reduction, these markers lowered their expression. Surprisingly, macrophages from the high cholesterol group displayed a more significant enrichment of genes that characterize restorative macrophages after cholesterol reduction (Figure 6B). These findings suggest that high cholesterol intake may promote more substantial hepatic damage with a further expansion of the restorative macrophage population after cholesterol reduction.

Additionally, we analyzed the FACS sorting data for the presence of Kupffer cells (KCs: F4/80^{hi} CD11b^{low}) and infiltrating macrophages (IMs: F4/80^{low} CD11b^{hi}) to verify if the results we observed would relate to the infiltrating macrophage influx rates. We did not find any significant change in the IMs/KCs ratios among the different groups during the dietary intervention (Supplementary Figure 3), which suggests that the phenotypic changes detected in our dataset are not linked to the reduction of recruited macrophages.

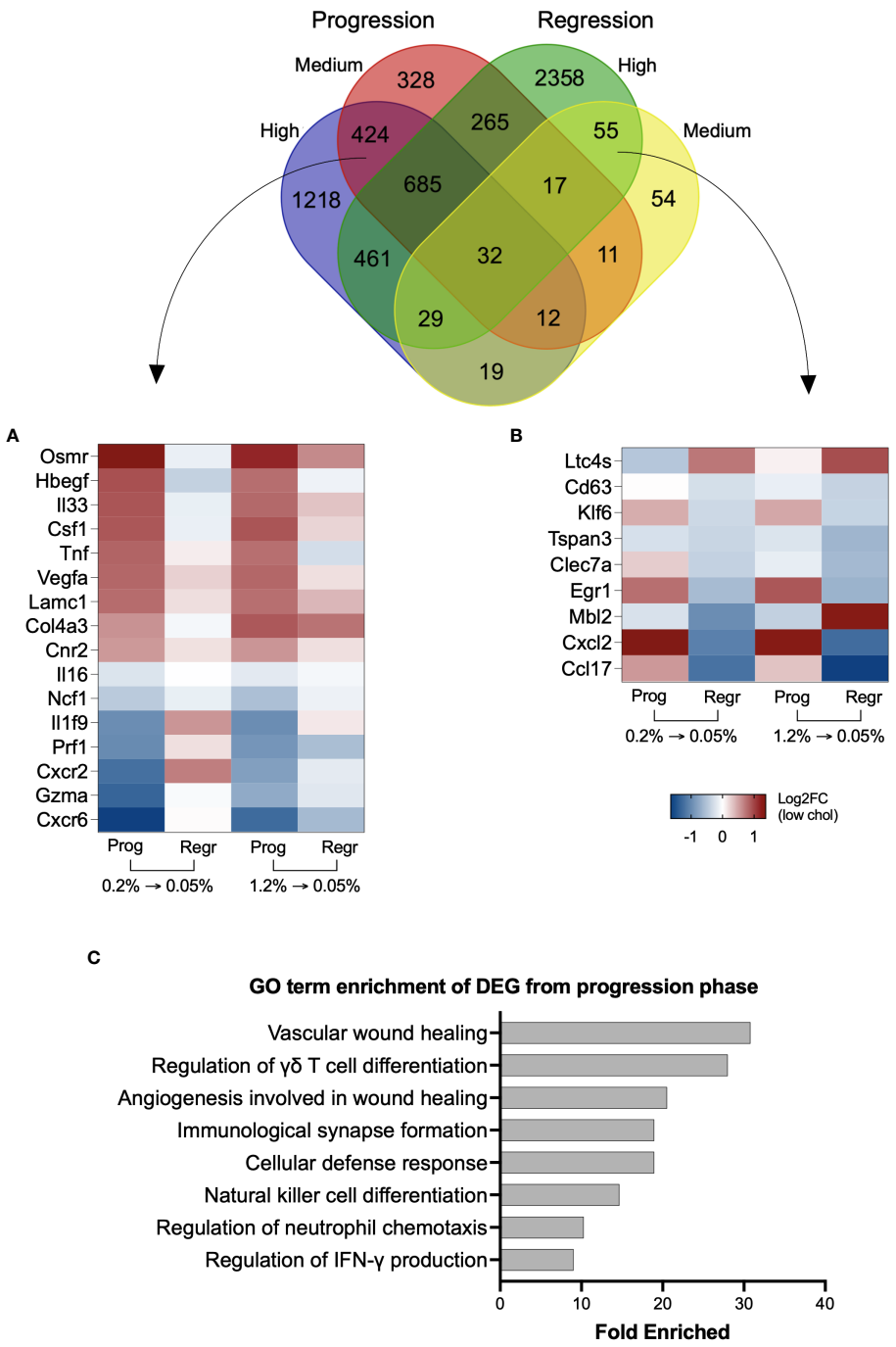

FIGURE 4
Genes uniquely modified by inclusion or reduction of dietary cholesterol can contribute to NASH. Venn diagram with the overlapping differentially expressed genes from the four groups. High and medium cholesterol groups commonly expressed 424 genes during the progression phase, while only 55 genes uniquely were commonly found during the regression phase. **(A)** Heatmap with 16 genes from the 424 genes upregulated by cholesterol introduction. The selected genes are previously correlated to NAFLD severity. Overall, these genes followed a similar expression pattern during the progression phase of medium and high cholesterol groups, with reversal of expression pattern on cholesterol reduction. **(B)** Heatmap showing 9 of the 55 genes commonly expressed in medium and high cholesterol groups after cholesterol reduction. The genes of interest are involved in NASH inflammation. **(C)** Gene Ontology (GO) terms enrichment using the differentially expressed genes (DEG) induced by cholesterol during the progression phase. Most of the biological functions were related to immune response. No significant results were found using the 55 genes commonly modified during the regression phase. Log2FC, log2-foldchange based on low cholesterol age-matched group. Prog, Progression phase; Regr, Regression phase.

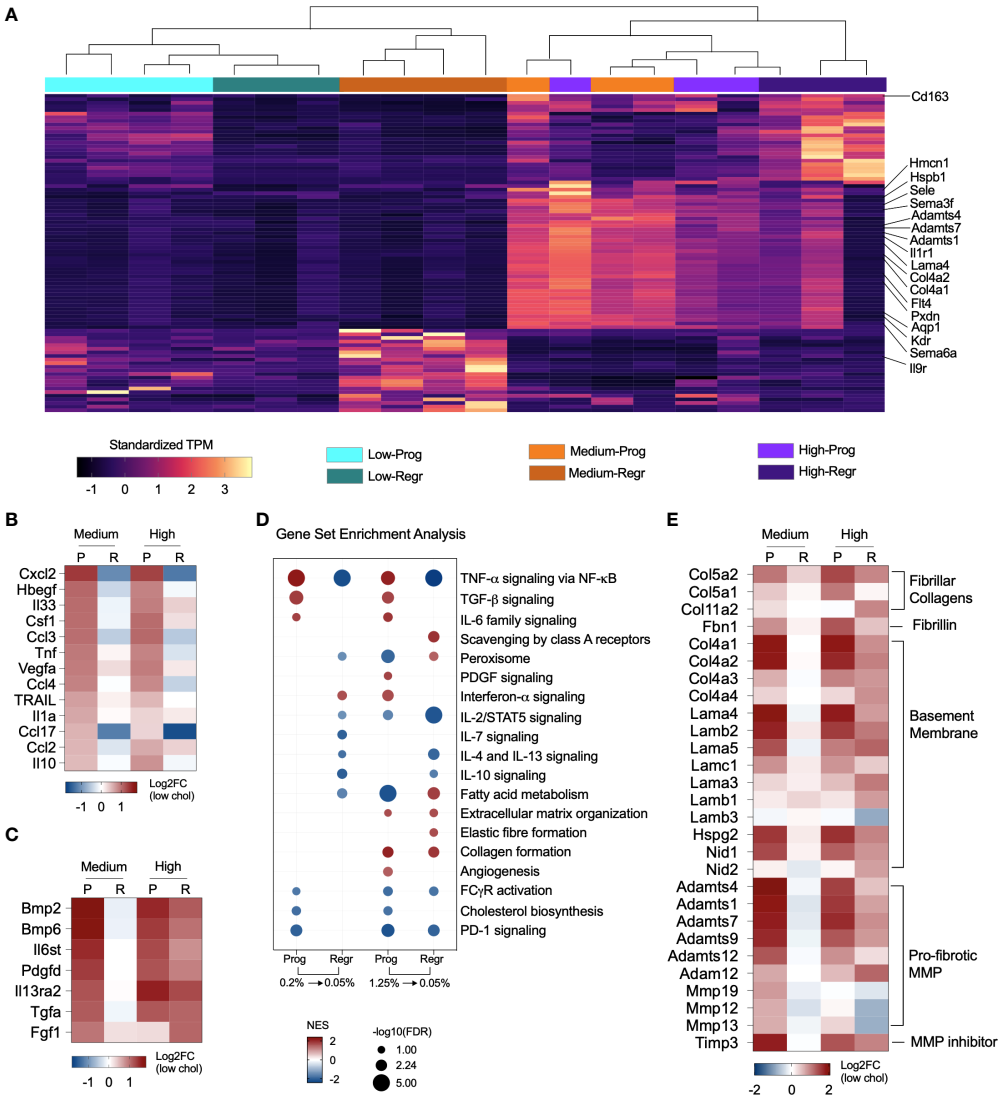

FIGURE 5
Cholesterol triggers expression of pro-fibrotic and pro-inflammatory genes. **(A)** Heatmap shows the standardized gene expression values of the 25 top upregulated genes found in each group. The highlighted genes commonly upregulated in the medium and high cholesterol groups during progression phase (Prog) and in the high cholesterol groups during regression phase (Regr) are mainly related to extracellular matrix organization, angiogenesis, and cell migration. **(B)** Expression of several cytokines relevant to NASH are affected by dietary cholesterol. In general, these cytokines were upregulated due to increased cholesterol dietary content and show an attenuated expression pattern after cholesterol reduction. **(C)** Cytokines upregulated during progression phase in both cholesterol groups and that maintained high expression in the high cholesterol groups after cholesterol reduction. Genes normalized in the medium cholesterol group during regression phase. **(D)** Gene Set Enrichment Analysis results, based on Hallmark and Reactome databases, highlighted the upregulation of TNF-α, TGF-β, and IL-6 signaling pathways during the progression phase of both cholesterol groups with subsequent downregulation/normalization after cholesterol reduction. The pathways for IL-10, IL-4/IL-13 signaling were downregulated by cholesterol reduction in both groups. Lipid metabolism, FC-γ receptor activation and PD-1 signaling are inhibited in both groups in the progression phase. The high cholesterol group showed continuous upregulation of collagen formation in both progression and regression phases. **(E)** Heatmap showing the fold changes in the expression of fibrillar collagens, fibrillin, type IV collagen and laminin, other basement membrane components, and pro-fibrotic proteases. Gene expression was upregulated in medium and high cholesterol groups during progression phase and stayed elevated in the high cholesterol after cholesterol reduction. P or Prog, Progression phase; R or Regr, Regression phase; Log2FC, log2-foldchange based on low cholesterol age-matched group.

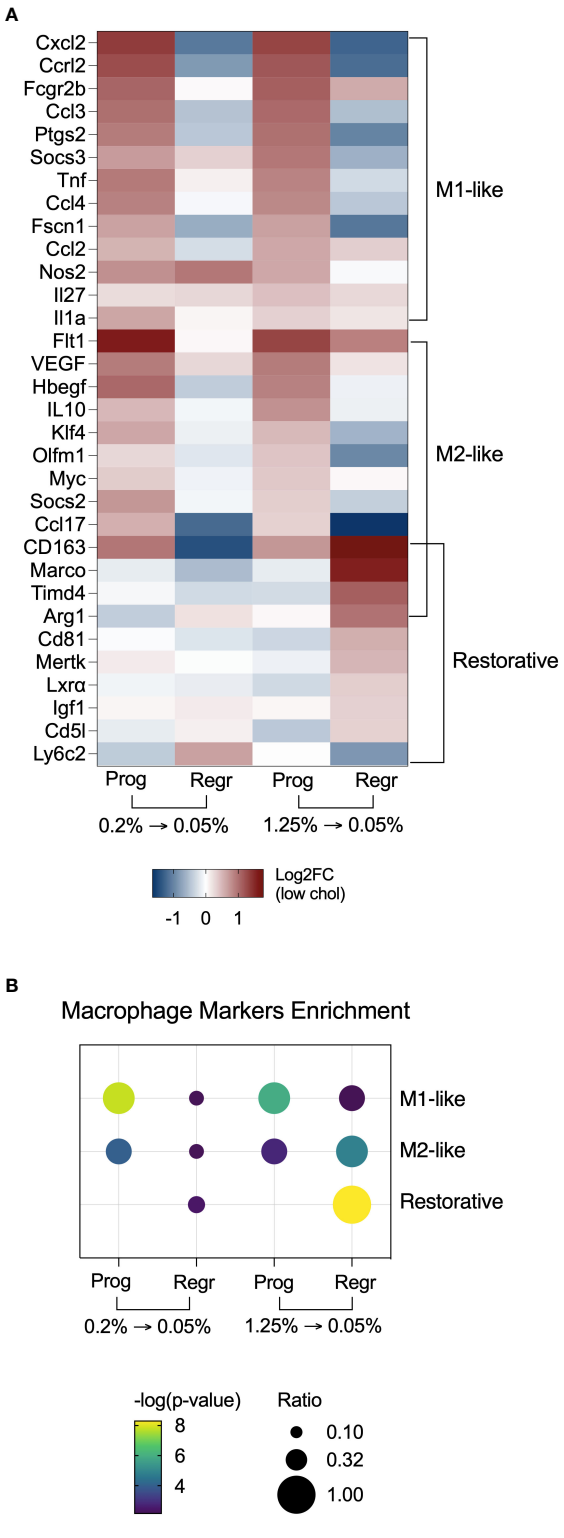

FIGURE 6
Hepatic macrophages from mice fed with high cholesterol FPC diet shift polarization towards a restorative phenotype after cholesterol reduction. **(A)** Heatmap with macrophage polarization markers shows enrichment of M1 and M2-like polarization markers during the progression of the FPC diet, and enrichment of restorative macrophages markers during the regression phase in the high cholesterol group. **(B)** Fisher's exact test confirmed the enrichment of polarization markers in hepatic macrophages during the different phases of the dietary intervention. Prog, Progression phase; Regr, Regression phase; Log2FC, log2-foldchange based on low cholesterol age-matched group.

High cholesterol intake triggers NASH-associated pathways in hepatic macrophages

We evaluated the most significant hepatotoxic pathways triggered in hepatic macrophages and identified upregulation of steatohepatitis, liver inflammation, and carcinoma in the high cholesterol group during the progression phase. Cholesterol reduction inhibited those processes (Figure 7A). Figure 7B shows the genes related to steatohepatitis significantly modified in macrophages of the high cholesterol group. We observed a shift in the expression pattern of anti-NASH genes, with upregulation of *Acox1*, *Nr1h3* (Lxr-a), *Gnmt*, and *Mat1* expressions after cholesterol reduction. Genes controlling liver inflammation were also affected by cholesterol intake and following reduction (Figure 7C). The pro-inflammatory genes *Jun*, *Ccl3L3*, *Tnf*, and *Ccl2*, initially upregulated during the progression phase, were inhibited in the regression phase. The most notable change is related to the anti-inflammatory genes *Pten*, *Atg5*, *Il6r*, *Pafah1b1*, and *Ptpn11*, which presented a low gene expression due to cholesterol intake, with further normalization after cholesterol reduction.

Discussion

Increasing evidence support the substantial contribution of innate and adaptive immunity in NASH progression. Among the innate immune cells, the hepatic macrophages play a pivotal

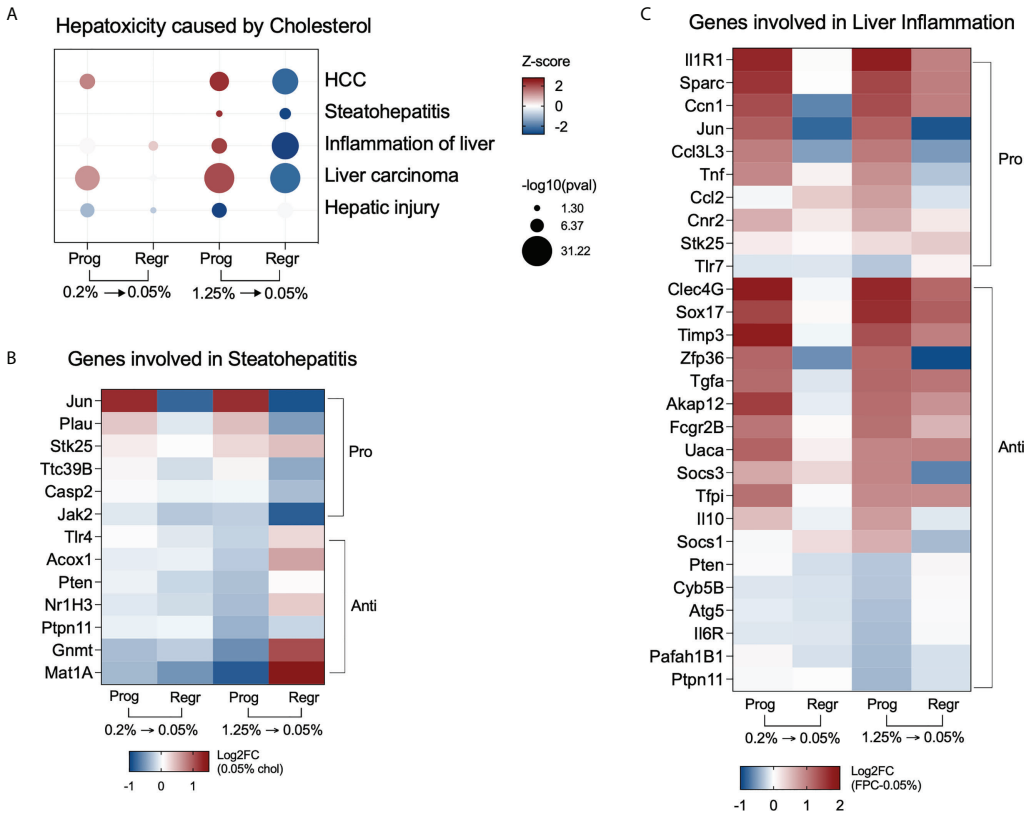

FIGURE 7
High cholesterol intake induces NASH-associated pathways in hepatic macrophages. **(A)** Hepatic macrophages from mice fed with high cholesterol displayed upregulation of steatohepatitis and liver inflammation processes during the progression phase and show inhibition of the same processes after cholesterol reduction. **(B)** Heatmap of the most variable genes involved in steatohepatitis in the high cholesterol group. During the progression phase, there is a strong downregulation of genes that can prevent NASH, such as Methionine adenosyltransferase (*Mat1*) and glycine N-methyltransferase (*Gnmt*), which were upregulated after cholesterol reduction. **(C)** Heatmap displaying the most variable genes related to liver inflammation in the high cholesterol group. Several pro-inflammatory genes triggered by high and medium cholesterol intake were normalized after cholesterol reduction, particularly *Jun, Ccl3l3, Tnf, Ccl2, and Cnr2*. The downregulation of the anti-inflammatory genes *Pten, Ptpn11, Cyb5b, Atg5, Il6r*, and *Pafah1b1* only in the high cholesterol group suggests their importance for NASH pathogenesis. Prog, Progression phase; Regr, Regression phase; Log2FC, log2-foldchange based on low cholesterol age-matched group.

role: they can cross-communicate with neutrophils, natural killer cells, innate lymphoid cells, and lymphocytes, coordinating cell recruitment, activation, and subsequent fate of hepatic inflammation (29–32).

By analyzing the impact of the dietary cholesterol reduction on NASH progression and on hepatic macrophage transcriptome, this work expands the understanding of the modulatory effects of cholesterol on the innate immune system, identifying potential new therapeutic targets for NASH intervention. High cholesterol intake combined with a high-fat diet contributes to hepatic lipid accumulation, liver oxidative stress, and consequent steatohepatitis development (6, 33). In our study, all animals on the FPC diet displayed high steatosis scores, regardless of cholesterol intake, indicating that cholesterol *per se* did not directly influence hepatic lipid accumulation. Instead, the cholesterol effect was related to tissue inflammation and scarring. Mice on high cholesterol diet displayed more lobular inflammation and fibrosis than mice fed with low cholesterol, corroborating our previous study (34). In the cholesterol reduction phase, we observed a slight decrease in lobular inflammation in the high cholesterol group, but fibrosis scores remained unchanged. The fact that we do not observe a reversion of fibrosis after reducing cholesterol may be due to the long-term high-fat and high-fructose diet that also culminates in fibrosis, even without cholesterol. The high cholesterol levels likely accelerate fibrosis progression. Alternatively, fibrosis may be irreversible at this stage.

Hepatic accumulation of free cholesterol during steatosis disturbs Kupffer cells and triggers a sterile inflammatory response (11, 35). Our findings demonstrate that prolonged medium or high cholesterol intake modifies total hepatic macrophage global gene expression. When we reduced cholesterol content in the FPC diet, the gene expression of macrophages from the medium and low cholesterol groups became very similar. However, cholesterol reduction did not normalize the gene expression in macrophages from mice fed high cholesterol diet, suggesting that the liver injury mediated by high cholesterol intake persists for longer. We also found that genes commonly affected by cholesterol intake and withdrawal, regardless of the initial cholesterol input, positively enriched biological processes linked to fibrosis during the progression stage and enhanced processes related to tissue repair during the regression phase. Of note, cholesterol upregulated the expression of some immunological genes in hepatic macrophages, which decreased after cholesterol reduction. Genes of interest include *Ccrl2*, an atypical chemokine receptor rapidly upregulated during inflammation (36); *Osm*, a cytokine that contributes to hepatic insulin resistance, fibrosis, development of NASH, and hepatocellular carcinoma (37–39); and *Ccl3*, a chemokine that favors the progression of steatohepatitis *via* macrophage recruitment (40).

Several pro-inflammatory and pro-fibrotic genes were exclusively induced in macrophages by medium and high cholesterol intake: *Osmr*, the receptor for Oncostatin M, is involved in macrophage recruitment and infiltration (41); *Il33*, a pro-inflammatory and pro-fibrotic cytokine that can activate hepatic stellate cells and macrophages (42, 43); *Tnf*, known to contribute to liver inflammation and strongly correlated to NASH severity (44); *Cnr2*, which participates in obesity-induced hepatic inflammation, macrophage infiltration, and TNF and CCL2 expression (45); and *Csf1*, highly expressed in NASH (46). Cholesterol reduction significantly inhibited the genes *Cxcl2* and *Ccl17*, known for neutrophil, macrophage, and Treg cell recruitment (47, 48). These findings support the significant impact of dietary cholesterol on macrophage-mediated hepatic inflammation in NASH.

We identified the most dramatic pathway changes in hepatic macrophage from mice fed with high cholesterol, with the upregulation of TNF-α, TGF-β, IFN-α, IL-6, and PDGF signaling pathways, all previously correlated to NASH progression. TNF-α signaling cross-regulates type I IFN signaling by eliciting interferon-stimulated gene expression and increasing inflammation, and IFN-α signaling would, in turn, favor steatosis (49, 50). IL-6 signaling also can contribute to NASH progression by increasing reactive oxygen species production and hepatocyte apoptosis (51). TGF-β and PDGF signaling pathways are well known to drive fibrosis progression, mainly by inducing hepatic stellate cell activation (52). In addition, these cells also upregulated steatohepatitis, inflammation, and cancer pathways during the progression phase, with their further silencing after cholesterol reduction.

Studies have shown that hypercholesterolemia impairs macrophage cholesterol efflux, driving their polarization into a pro-inflammatory phenotype (53). Our dataset showed a shift in macrophage polarization markers from the progression to the regression phase. Both medium and high cholesterol groups displayed M1 and M2-like markers enrichment during the progression phase. Intriguingly, macrophages from the high cholesterol group strongly expressed restorative macrophage markers after cholesterol reduction. Pro-restorative macrophages promote inflammation resolution and tissue repair, showing a distinct phenotype from the M1/M2 cells. Low expression of *Ly6C* and high expression of *Igf1, Cd81, Cd5l, Mertk*, and *Lxr* (54–56) characterize the pro-restorative phenotype. We also observed that the cholesterol intake or withdrawal does not influence the influx rates of infiltrating macrophages (IMs), suggesting that the polarization changes detected do not depend on the tissue ratios of KCs and IMs. Moreover, the increase of resident macrophages markers during the regression phase, such as *Cd163, Marco*, and *Timd4*, indicates that the restorative macrophage population expansion contributes to the repopulation of the resident macrophage pool during the late

resolution stage of liver repair, as already implied by other authors (54). Upregulation of *Lxr* and *Mertk* gene expression also supports inflammation suppression since the *Lxr-Mertk* axis in macrophages promotes cholesterol efflux and efferocytosis (53). Our findings suggest that reducing high cholesterol intake is enough to establish a restorative macrophage subset in the liver, even on the background of high-fat and high-fructose diets.

Other remarkable events triggered by cholesterol intake in the hepatic macrophages were collagen formation and extracellular matrix organization, with the upregulation of genes codifying several types of collagens, including those part of the basement membrane, fibrillar collagen, and pro-fibrotic proteases. The increase of type IV collagen and laminin deposition on the perisinusoidal areas is a hallmark of fibrotic livers from alcoholic fatty liver, hepatitis, and cirrhosis patients (57). Since hepatic sinusoids typically lack a basement membrane, the increase of type IV collagen and laminin in the sinusoids would favor the formation of a new basement membrane. Basement membrane formation in the sinusoids is associated with liver sinusoidal endothelial cells (LSEC) defenestration, which precedes the activation of hepatic stellate cells and fibrosis (58). These events, however, were not normalized in macrophages from the high cholesterol groups during the regression phase. Therefore, the presence of macrophages expressing high levels of type IV collagen and laminin could continuously drive hepatic sinusoid capillarization and favor fibrosis progression even after the reduction of cholesterol.

Additional pro-fibrogenic factors continuously expressed by macrophages from the high cholesterol group were the *Il6st* (gp130), which regulates collagen and laminin expression; *Fgf1*, *Tgfa*, and *Pdgfd*, which activates hepatic stellate cells; and *Il13ra2*, which participates of TGF-β transcription (59–64). In addition, the expression of genes that favor steatosis, such as *Bmp2* and *Bmp6*, remained high after cholesterol reduction in this group (65, 66). Furthermore, hepatic macrophages from mice fed with high cholesterol diet did not restore the expression of the anti-fibrotic proteases *Mmp9*, *Mmp12*, and *Mmp13*, suggesting an aberrant tissue repair mechanism favoring fibrosis progression.

A limitation of our study is the use of RNAseq as the only method to evaluate the hepatic macrophages. We were able to use only this technique due to the small number of macrophages recovered from each mouse and the need to include the significant variations carried by the biological replicates. RNAseq is a valuable tool for quantifying the gene expression of the whole transcriptome. However, further studies should be performed to evaluate the functional capacity of hepatic macrophages in the different stages of NASH induced by cholesterol and validate all pathways described in our results.

In conclusion, our data shed light on the immunological mechanisms behind the contribution of dietary cholesterol to NASH progression. Here we demonstrated that cholesterol intake levels directly contribute to hepatic injury and that prolonged high cholesterol intake damages are long-lasting and persistent, further promoting the expansion of a dysfunctional pro-fibrotic hepatic restorative macrophage phenotype which continues even after cholesterol reduction.

Data availability statement

The datasets presented in this study can be found in online repositories. The names of the repository/repositories and accession number(s) can be found below: https://www.ncbi.nlm.nih.gov/geo/query/acc.cgi?acc=GSE205776.

Ethics statement

The animal study was reviewed and approved by University of Southern California Institutional Animal Care and Use Committee.

Author contributions

AM-M and LG-M contributed to the conception and design of the study, analyzed the data, and wrote the manuscript. AM-M and AH executed the experiments. MS performed the bioinformatic analysis. GK performed the pathological evaluations. All authors contributed to manuscript revision, read, and approved the submitted version.

Funding

This work was primarily supported by the National Institutes of Health grant numbers DK117004 & DK106491 (LG-M) and the USC Research Center for Liver Disease (P30DK048522).

Acknowledgments

This manuscript is dedicated to the memory of Hugo R. Rosen, MD, who inspired a love for immunology and virology, and who inspired teamwork and respect for all. Dr. Rosen initiated and contributed significantly to this study. We would also like to thank Dr. Omar Lakhdari for performing the initial experiments.

Conflict of interest

The authors declare that the research was conducted in the absence of any commercial or financial relationships that could be construed as a potential conflict of interest.

Publisher's note

All claims expressed in this article are solely those of the authors and do not necessarily represent those of their affiliated organizations, or those of the publisher, the editors and the reviewers. Any product that may be evaluated in this article, or claim that may be made by its manufacturer, is not guaranteed or endorsed by the publisher.

Supplementary material

The Supplementary Material for this article can be found online at: https://www.frontiersin.org/articles/10.3389/fimmu.2022.968366/full#supplementary-material

References

1. Neuschwander-Tetri BA. Hepatic lipotoxicity and the pathogenesis of nonalcoholic steatohepatitis: The central role of nontriglyceride fatty acid metabolites. *Hepatology* (2010) 52(2):774–88. doi: 10.1002/hep.23719

2. Wree A, Broderick L, Canbay A, Hoffman HM, Feldstein AE. From NAFLD to NASH to cirrhosis-new insights into disease mechanisms. *Nat Rev Gastroenterol Hepatol* (2013) 10(11):627–36. doi: 10.1038/nrgastro.2013.149

3. Younossi ZM, Koenig AB, Abdelatif D, Fazel Y, Henry L, Wymer M. Global epidemiology of nonalcoholic fatty liver disease-meta-analytic assessment of prevalence, incidence, and outcomes. *Hepatology* (2016) 64(1):73–84. doi: 10.1002/hep.28431

4. Puri P, Baillie RA, Wiest MM, Mirshahi F, Choudhury J, Cheung O, et al. A lipidomic analysis of nonalcoholic fatty liver disease. *Hepatology* (2007) 46 (4):1081–90. doi: 10.1002/hep.21763

5. Wouters K, van Gorp PJ, Bieghs V, Gijbels MJ, Duimel H, Lütjohann D, et al. Dietary cholesterol, rather than liver steatosis, leads to hepatic inflammation in hyperlipidemic mouse models of nonalcoholic steatohepatitis. *Hepatology.* (2008) 48(2):474–86. doi: 10.1002/hep.22363

6. Bellanti F, Villani R, Facciorusso A, Vendemiale G, Serviddio G. Lipid oxidation products in the pathogenesis of non-alcoholic steatohepatitis. *Free Radic Biol Med* (2017) 111:173–85. doi: 10.1016/j.freeradbiomed.2017.01.023

7. Püschel GP, Henkel J. Dietary cholesterol does not break your heart but kills your liver. *Porto BioMed J* (2018) 3(1):e12. doi: 10.1016/j.pbj.0000000000000012

8. Marí M, Caballero F, Colell A, Morales A, Caballeria J, Fernandez A, et al. Mitochondrial free cholesterol loading sensitizes to TNF- and fas-mediated steatohepatitis. *Cell Metab* (2006) 4(3):185–98. doi: 10.1016/j.cmet.2006.07.006

9. Ioannou GN, Haigh WG, Thorning D, Savard C. Hepatic cholesterol crystals and crown-like structures distinguish NASH from simple steatosis. *J Lipid Res* (2013) 54(5):1326–34. doi: 10.1194/jlr.M034876

10. Tomita K, Teratani T, Suzuki T, Shimizu M, Sato H, Narimatsu K, et al. Free cholesterol accumulation in hepatic stellate cells: Mechanism of liver fibrosis aggravation in nonalcoholic steatohepatitis in mice. *Hepatology.* (2014) 59 (1):154–69. doi: 10.1002/hep.26604

11. Ioannou GN, Subramanian S, Chait A, Haigh WG, Yeh MM, Farrell GC, et al. Cholesterol crystallization within hepatocyte lipid droplets and its role in murine NASH. *J Lipid Res* (2017) 58(6):1067–79. doi: 10.1194/jlr.M072454

12. Devisscher L, Verhelst X, Colle I, Van Vlierberghe H, Geerts A. The role of macrophages in obesity-driven chronic liver disease. *J Leukoc Biol* (2016) 99 (5):693–8. doi: 10.1189/jlb.5RU0116-016R

13. Park JW, Jeong G, Kim SJ, Kim MK, Park SM. Predictors reflecting the pathological severity of non-alcoholic fatty liver disease: Comprehensive study of clinical and immunohistochemical findings in younger Asian patients. *J Gastroenterol Hepatol* (2007) 22(4):491–7. doi: 10.1111/j.1440-1746.2006.04758.x

14. Han J, Zhang X, Lau JK, Fu K, Lau HC, Xu W, et al. Bone marrow-derived macrophage contributes to fibrosing steatohepatitis through activating hepatic stellate cells. *J Pathol* (2019) 248(4):488–500. doi: 10.1002/path.5275

15. Kazankov K, Jørgensen SMD, Thomsen KL, Møller HJ, Vilstrup H, George J, et al. The role of macrophages in nonalcoholic fatty liver disease and nonalcoholic steatohepatitis. *Nat Rev Gastroenterol Hepatol* (2019) 16(3):145–59. doi: 10.1038/s41575-018-0082-x

16. Huang W, Metlakunta A, Dedousis N, Zhang P, Sipula I, Dube JJ, et al. Depletion of liver kupffer cells prevents the development of diet-induced hepatic steatosis and insulin resistance. *Diabetes* (2010) 59(2):347–57. doi: 10.2337/db09-0016

17. Im YR, Hunter H, de Gracia Hahn D, Duret A, Cheah Q, Dong J, et al. A systematic review of animal models of NAFLD finds high-fat, high-fructose diets most closely resemble human NAFLD. *Hepatology* (2021) 74(4):1884–901. doi: 10.1002/hep.31897

18. Wang X, Zheng Z, Caviglia JM, Corey KE, Herfel TM, Cai B, et al. Hepatocyte TAZ/WWTR1 promotes inflammation and fibrosis in nonalcoholic steatohepatitis. *Cell Metab* (2016) 24(6):848–62. doi: 10.1016/j.cmet.2016.09.016

19. Akinrinmade OA, Chetty S, Daramola AK, Islam MU, Thepen T, Barth S. CD64: An attractive immunotherapeutic target for M1-type macrophage mediated chronic inflammatory diseases. *Biomedicines.* (2017) 5(3):56. doi: 10.3390/biomedicines5030056

20. Cai B, Dongiovanni P, Corey KE, Wang X, Shmarakov IO, Zheng Z, et al. Macrophage MerTK promotes liver fibrosis in nonalcoholic steatohepatitis. *Cell Metab* (2020) 31(2):406–21.e7. doi: 10.1016/j.cmet.2019.11.013

21. Wang C, Ma C, Gong L, Guo Y, Fu K, Zhang Y, et al. Macrophage polarization and its role in liver disease. *Front Immunol* (2021) 12:803037. doi: 10.3389/fimmu.2021.803037

22. Patro R, Duggal G, Love MI, Irizarry RA, Kingsford C. Salmon provides fast and bias-aware quantification of transcript expression. *Nat Methods* (2017) 14 (4):417–9. doi: 10.1038/nmeth.4197

23. Soneson C, Love MI, Robinson MD. Differential analyses for RNA-seq: transcript-level estimates improve gene-level inferences. *F1000Res.* (2015) 4:1521. doi: 10.12688/f1000research.7563.1

24. Love MI, Huber W, Anders S. Moderated estimation of fold change and dispersion for RNA-seq data with DESeq2. *Genome Biol* (2014) 15(12):550. doi: 10.1186/s13059-014-0550-8

25. Krämer A, Green J, Pollard J, Tugendreich S. Causal analysis approaches in ingenuity pathway analysis. *Bioinformatics.* (2014) 30(4):523–30. doi: 10.1093/bioinformatics/btt703

26. Subramanian A, Tamayo P, Mootha VK, Mukherjee S, Ebert BL, Gillette MA, et al. Gene set enrichment analysis: A knowledge-based approach for interpreting genome-wide expression profiles. *Proc Natl Acad Sci U S A.* (2005) 102(43):15545–50. doi: 10.1073/pnas.0506580102

27. Mi H, Muruganujan A, Ebert D, Huang X, Thomas PD. PANTHER version 14: more genomes, a new PANTHER GO-slim and improvements in enrichment analysis tools. *Nucleic Acids Res* (2019) 47(D1):D419–D26. doi: 10.1093/nar/gky1038

28. Edgar R, Domrachev M, Lash AE. Gene expression omnibus: NCBI gene expression and hybridization array data repository. *Nucleic Acids Res* (2002) 30 (1):207–10. doi: 10.1093/nar/30.1.207

29. Li H, Zhou Y, Wang H, Zhang M, Qiu P, Zhang R, et al. Crosstalk between liver macrophages and surrounding cells in nonalcoholic steatohepatitis. *Front Immunol* (2020) 11:1169. doi: 10.3389/fimmu.2020.01169

30. Hirsova P, Bamidele AO, Wang H, Povero D, Revelo XS. Emerging roles of T cells in the pathogenesis of nonalcoholic steatohepatitis and hepatocellular carcinoma. *Front Endocrinol (Lausanne)* (2021) 12:760860. doi: 10.3389/fendo.2021.760860

31. Michel T, Hentges F, Zimmer J. Consequences of the crosstalk between monocytes/macrophages and natural killer cells. *Front Immunol* (2012) 3:403. doi: 10.3389/fimmu.2012.00403

32. Chen Y, Tian Z. Roles of hepatic innate and innate-like lymphocytes in nonalcoholic steatohepatitis. *Front Immunol* (2020) 11:1500. doi: 10.3389/fimmu.2020.01500

33. Savard C, Tartaglione EV, Kuver R, Haigh WG, Farrell GC, Subramanian S, et al. Synergistic interaction of dietary cholesterol and dietary fat in inducing experimental steatohepatitis. *Hepatology* (2013) 57(1):81–92. doi: 10.1002/hep.25789

34. McGettigan B, McMahan R, Orlicky D, Burchill M, Danhorn T, Francis P, et al. Dietary lipids differentially shape nonalcoholic steatohepatitis progression and the transcriptome of kupffer cells and infiltrating macrophages. *Hepatology* (2019) 70(1):67–83. doi: 10.1002/hep.30401

35. Bieghs V, Hendrikx T, van Gorp PJ, Verheyen F, Guichot YD, Walenbergh SM, et al. The cholesterol derivative 27-hydroxycholesterol reduces steatohepatitis in mice. *Gastroenterology* (2013) 144(1):167–78.e1. doi: 10.1053/j.gastro.2012.09.062

36. Del Prete A, Martínez-Muñoz L, Mazzon C, Toffali L, Sozio F, Za L, et al. The atypical receptor CCRL2 is required for CXCR2-dependent neutrophil recruitment and tissue damage. *Blood* (2017) 130(10):1223–34. doi: 10.1182/blood-2017-04-777680

37. Henkel J, Gärtner D, Dorn C, Hellerbrand C, Schanze N, Elz SR, et al. Oncostatin m produced in kupffer cells in response to PGE2: Possible contributor to hepatic insulin resistance and steatosis. *Lab Invest* (2011) 91(7):1107–17. doi: 10.1038/labinvest.2011.47

38. Foglia B, Sutti S, Pedicini D, Cannito S, Bocca C, Maggiora M, et al. A profibrogenic mediator overexpressed in non-alcoholic fatty liver disease, stimulates migration of hepatic myofibroblasts. *Cells* (2019) 9(1):28. doi: 10.3390/cells9010028

39. Di Maira G, Foglia B, Napione L, Turato C, Maggiora M, Sutti S, et al. Oncostatin m is overexpressed in NASH-related hepatocellular carcinoma and promotes cancer cell invasiveness and angiogenesis. *J Pathol* (2022) 257(1):82–95. doi: 10.1002/path.5871

40. Xu L, Chen Y, Nagashimada M, Ni Y, Zhuge F, Chen G, et al. CC chemokine ligand 3 deficiency ameliorates diet-induced steatohepatitis by regulating liver macrophage recruitment and M1/M2 status in mice. *Metabolism* (2021) 125:154914. doi: 10.1016/j.metabol.2021.154914

41. Zhang X, Li J, Qin JJ, Cheng WL, Zhu X, Gong FH, et al. Oncostatin m receptor β deficiency attenuates atherogenesis by inhibiting JAK2/STAT3 signaling in macrophages. *J Lipid Res* (2017) 58(5):895–906. doi: 10.1194/jlr.M074112

42. Tan Z, Liu Q, Jiang R, Lv L, Shoto SS, Maillet I, et al. Interleukin-33 drives hepatic fibrosis through activation of hepatic stellate cells. *Cell Mol Immunol* (2018) 15(4):388–98. doi: 10.1038/cmi.2016.63

43. Gao Y, Liu Y, Yang M, Guo X, Zhang M, Li H, et al. IL-33 treatment attenuated diet-induced hepatic steatosis but aggravated hepatic fibrosis. *Oncotarget.* (2016) 7(23):33649–61. doi: 10.18632/oncotarget.9259

44. Kakino S, Ohki T, Nakayama H, Yuan X, Otabe S, Hashinaga T, et al. Pivotal role of TNF-α in the development and progression of nonalcoholic fatty liver disease in a murine model. *Horm Metab Res* (2018) 50(1):80–7. doi: 10.1055/s-0043-118666

45. Deveaux V, Cadoudal T, Ichigotani Y, Teixeira-Clerc F, Louvet A, Manin S, et al. Cannabinoid CB2 receptor potentiates obesity-associated inflammation, insulin resistance and hepatic steatosis. *PloS One* (2009) 4(6):e5844. doi: 10.1371/journal.pone.0005844

46. Fourman LT, Stanley TL, Billingsley JM, Sui SJH, Feldpausch MN, Boutin A, et al. Delineating tesamorelin response pathways in HIV-associated NAFLD using a targeted proteomic and transcriptomic approach. *Sci Rep* (2021) 11(1):10485. doi: 10.1038/s41598-021-89966-y

47. Moles A, Murphy L, Wilson CL, Chakraborty JB, Fox C, Park EJ, et al. A TLR2/S100A9/CXCL-2 signaling network is necessary for neutrophil recruitment in acute and chronic liver injury in the mouse. *J Hepatol* (2014) 60(4):782–91. doi: 10.1016/j.jhep.2013.12.005

48. Zhou SL, Zhou ZJ, Hu ZQ, Huang XW, Wang Z, Chen EB, et al. Tumor-associated neutrophils recruit macrophages and T-regulatory cells to promote progression of hepatocellular carcinoma and resistance to sorafenib. *Gastroenterology* (2016) 150(7):1646–58.e17. doi: 10.1053/j.gastro.2016.02.040

49. Gordon RA, Grigoriev G, Lee A, Kalliolias GD, Ivashkiv LB. The interferon signature and STAT1 expression in rheumatoid arthritis synovial fluid macrophages are induced by tumor necrosis factor α and counter-regulated by the synovial fluid microenvironment. *Arthritis Rheumatol* (2012) 64(10):3119–28. doi: 10.1002/art.34544

50. Møhlenberg M, Terczynska-Dyla E, Thomsen KL, George J, Eslam M, Grønbæk H, et al. The role of IFN in the development of NAFLD and NASH. *Cytokine.* (2019) 124:154519. doi: 10.1016/j.cyto.2018.08.013

51. Yamaguchi K, Itoh Y, Yokomizo C, Nishimura T, Niimi T, Fujii H, et al. Blockade of interleukin-6 signaling enhances hepatic steatosis but improves liver injury in methionine choline-deficient diet-fed mice. *Lab Invest* (2010) 90(8):1169–78. doi: 10.1038/labinvest.2010.75

52. Barreby E, Chen P, Aouadi M. Macrophage functional diversity in NAFLD - more than inflammation. *Nat Rev Endocrinol* (2022) 18:461–72. doi: 10.1038/s41574-022-00675-6

53. Tall AR, Yvan-Charvet L. Cholesterol, inflammation and innate immunity. *Nat Rev Immunol* (2015) 15(2):104–16. doi: 10.1038/nri3793

54. Ramachandran P, Pellicoro A, Vernon MA, Boulter L, Aucott RL, Ali A, et al. Differential ly-6C expression identifies the recruited macrophage phenotype, which orchestrates the regression of murine liver fibrosis. *Proc Natl Acad Sci USA* (2012) 109(46):E3186–95. doi: 10.1073/pnas.1119964109

55. Triantafyllou E, Pop OT, Possamai LA, Wilhelm A, Liaskou E, Singanayagam A, et al. MerTK expressing hepatic macrophages promote the resolution of inflammation in acute liver failure. *Gut* (2018) 67(2):333–47. doi: 10.1136/gutjnl-2016-313615

56. Choi JY, Seo JY, Yoon YS, Lee YJ, Kim HS, Kang JL. Mer signaling increases the abundance of the transcription factor LXR to promote the resolution of acute sterile inflammation. *Sci Signal* (2015) 8(365):ra21. doi: 10.1126/scisignal.2005864

57. Mak KM, Mei R. Basement membrane type IV collagen and laminin: An overview of their biology and value as fibrosis biomarkers of liver disease. *Anat Rec (Hoboken)* (2017) 300(8):1371–90. doi: 10.1002/ar.23567

58. Martinez-Hernandez A, Martinez J. The role of capillarization in hepatic failure: studies in carbon tetrachloride-induced cirrhosis. *Hepatology* (1991) 14 (5):864–74. doi: 10.1002/hep.1840140519

59. Huang H, Zhang G, Ge Z. lncRNA MALAT1 promotes renal fibrosis in diabetic nephropathy by targeting the miR-2355-3p/IL6ST axis. *Front Pharmacol* (2021) 12:647650. doi: 10.3389/fphar.2021.647650

60. Yu C, Wang F, Jin C, Huang X, Miller DL, Basilico C, et al. Role of fibroblast growth factor type 1 and 2 in carbon tetrachloride-induced hepatic injury and fibrogenesis. *Am J Pathol* (2003) 163(4):1653–62. doi: 10.1016/S0002-9440(10)63522-5

61. Wang C, Li Y, Li H, Zhang Y, Ying Z, Wang X, et al. Disruption of FGF signaling ameliorates inflammatory response in hepatic stellate cells. *Front Cell Dev Biol* (2020) 8:601. doi: 10.3389/fcell.2020.00601

62. Lee KS, Buck M, Houglum K, Chojkier M. Activation of hepatic stellate cells by TGF alpha and collagen type I is mediated by oxidative stress through c-myb expression. *J Clin Invest* (1995) 96(5):2461–8. doi: 10.1172/JCI118304

63. Borkham-Kamphorst E, Meurer SK, Van de Leur E, Haas U, Tihaa L, Weiskirchen R. PDGF-d signaling in portal myofibroblasts and hepatic stellate cells proves identical to PDGF-b *via* both PDGF receptor type α and β. *Cell Signal* (2015) 27(7):1305–14. doi: 10.1016/j.cellsig.2015.03.012

64. Fichtner-Feigl S, Strober W, Kawakami K, Puri RK, Kitani A. IL-13 signaling through the IL-13alpha2 receptor is involved in induction of TGF-beta1 production and fibrosis. *Nat Med* (2006) 12(1):99–106. doi: 10.1038/nm1332

65. Thayer TE, Lino Cardenas CL, Martyn T, Nicholson CJ, Traeger L, Wunderer F, et al. The role of bone morphogenetic protein signaling in non-alcoholic fatty liver disease. *Sci Rep* (2020) 10(1):9831. doi: 10.1038/s41598-020-66770-8

66. Arndt S, Wacker E, Dorn C, Koch A, Saugspier M, Thasler WE, et al. Enhanced expression of BMP6 inhibits hepatic fibrosis in non-alcoholic fatty liver disease. *Gut.* (2015) 64(6):973–81. doi: 10.1136/gutjnl-2014-306968

frontiers | Frontiers in Immunology

TYPE Original Research
PUBLISHED 26 January 2023
DOI 10.3389/fimmu.2023.1113883

OPEN ACCESS

EDITED BY
Daming Zuo,
Southern Medical University, China

REVIEWED BY
Jinglin Wang,
Nanjing Drum Tower Hospital, China
Ayaka Ito,
Nagoya University, Japan

*CORRESPONDENCE
Xiaofeng Yang
xfyang@temple.edu

†These authors share the first authorship

SPECIALTY SECTION
This article was submitted to Molecular Innate Immunity, a section of the journal Frontiers in Immunology

RECEIVED 01 December 2022
ACCEPTED 06 January 2023
PUBLISHED 26 January 2023

CITATION
Drummer C IV, Saaoud F, Jhala NC, Cueto R, Sun Y, Xu K, Shao Y, Lu Y, Shen H, Yang L, Zhou Y, Yu J, Wu S, Snyder NW, Hu W, Zhuo J'J, Zhong Y, Jiang X, Wang H and Yang X (2023) Caspase-11 promotes high-fat diet-induced NAFLD by increasing glycolysis, OXPHOS, and pyroptosis in macrophages.
Front. Immunol. 14:1113883.
doi: 10.3389/fimmu.2023.1113883

Caspase-11 promotes high-fat diet-induced NAFLD by increasing glycolysis, OXPHOS, and pyroptosis in macrophages

Charles Drummer IV[1†], Fatma Saaoud[1†], Nirag C. Jhala[2], Ramon Cueto[3], Yu Sun[1], Keman Xu[1], Ying Shao[1], Yifan Lu[1], Huimin Shen[3], Ling Yang[4], Yan Zhou[5], Jun Yu[3], Sheng Wu[3], Nathaniel W. Snyder[3], Wenhui Hu[3], Jia 'Joe' Zhuo[6], Yinghui Zhong[7], Xiaohua Jiang[3], Hong Wang[3] and Xiaofeng Yang[1,3*]

[1]Centers of Cardiovascular Research, Temple University Lewis Katz School of Medicine, Philadelphia, PA, United States, [2]Department of Pathology and Laboratory Medicine, Temple University Lewis Katz School of Medicine, Philadelphia, PA, United States, [3]Metabolic Disease Research and Thrombosis Research Center, Departments of Cardiovascular Sciences, Temple University Lewis Katz School of Medicine, Philadelphia, PA, United States, [4]Department of Medical Genetics and Molecular Biochemistry, Temple University Lewis Katz School of Medicine, Philadelphia, PA, United States, [5]Biostatistics and Bioinformatics Facility, Fox Chase Cancer Center, Temple Health, Philadelphia, PA, United States, [6]Tulane Hypertension & Renal Center of Excellence, Tulane University School of Medicine, New Orleans, LA, United States, [7]School of Biomedical Engineering, Science and Health Systems, Drexel University, Philadelphia, PA, United States

Introduction: Non-alcoholic fatty liver disease (NAFLD) has a global prevalence of 25% of the population and is a leading cause of cirrhosis and hepatocellular carcinoma. NAFLD ranges from simple steatosis (non-alcoholic fatty liver) to non-alcoholic steatohepatitis (NASH). Hepatic macrophages, specifically Kupffer cells (KCs) and monocyte-derived macrophages, act as key players in the progression of NAFLD. Caspases are a family of endoproteases that provide critical connections to cell regulatory networks that sense disease risk factors, control inflammation, and mediate inflammatory cell death (pyroptosis). Caspase-11 can cleave gasdermin D (GSDMD) to induce pyroptosis and specifically defends against bacterial pathogens that invade the cytosol. However, it's still unknown whether high fat diet (HFD)-facilitated gut microbiota-generated cytoplasmic lipopolysaccharides (LPS) activate caspase-11 and promote NAFLD.

Methods: To examine this hypothesis, we performed liver pathological analysis, RNA-seq, FACS, Western blots, Seahorse mitochondrial stress analyses of macrophages and bone marrow transplantation on HFD-induced NAFLD in WT and Casp11−/− mice.

Results and Discussion: Our results showed that 1) HFD increases body wight, liver wight, plasma cholesterol levels, liver fat deposition, and NAFLD activity score (NAS score) in wild-type (WT) mice; 2) HFD increases the expression of caspase-11, GSDMD, interleukin-1β, and guanylate-binding proteins in WT mice; 3) Caspase-11 deficiency decreases fat liver deposition and NAS score; 4) Caspase-11 deficiency decreases bone marrow monocyte-derived macrophage (MDM) pyroptosis

(inflammatory cell death) and inflammatory monocyte (IM) surface GSDMD expression; 5) Caspase-11 deficiency re-programs liver transcriptomes and reduces HFD-induced NAFLD; 6) Caspase-11 deficiency decreases extracellular acidification rates (glycolysis) and oxidative phosphorylation (OXPHOS) in inflammatory fatty acid palmitic acid-stimulated macrophages, indicating that caspase-11 significantly contributes to maintain dual fuel bioenergetics—glycolysis and OXPHOS for promoting pyroptosis in macrophages. These results provide novel insights on the roles of the caspase-11-GSDMD pathway in promoting hepatic macrophage inflammation and pyroptosis and novel targets for future therapeutic interventions involving the transition of NAFLD to NASH, hyperlipidemia, type II diabetes, metabolic syndrome, metabolically healthy obesity, atherosclerotic cardiovascular diseases, autoimmune diseases, liver transplantation, and hepatic cancers.

KEYWORDS

non-alcoholic fatty liver disease (NAFLD), non-alcoholic steatohepatitis (NASH), caspase-11, inflammation, pyroptosis

1 Introduction

Nonalcoholic fatty liver disease (NAFLD) is the most common form of chronic liver disease in the Western world. 10% to 40% of adults in the United States are estimated to have some form of NAFLD (1–3). NAFLD is an umbrella term referring to two underlying conditions: nonalcoholic fatty liver (NAFL; also known as hepatic steatosis) and nonalcoholic steatohepatitis (NASH) (4), the inflammatory phase of the disease. Inflammatory liver damage associated with NASH can lead to liver cirrhosis, liver failure, and hepatocellular carcinoma (1, 5–8). NAFLD is considered the hepatic manifestation of metabolic syndrome and metabolically healthy obesity (9–12). In addition, NAFLD is associated with adverse cardiovascular events and contributes to subclinical atherosclerosis (13, 14). Histologically, NAFLD is different from the alcoholic liver disease in at least 11 histologic features results from lipid metabolism imbalance leading to the accumulation of fatty acids in hepatocytes (15, 16). Changes in fatty acid uptake, fatty acid synthesis, lipolysis, β-oxidation and circulating lipoprotein result in hepatocytes exceeding their capacity to safely store lipids (16). These changes lead to the accumulation of toxic lipid species (ceramides, diacylglycerol, lipid peroxides, and oxidized phospholipids) and the subsequent proinflammatory, lipotoxicity-induced hepatocyte cell death (17).

The liver has the highest number of macrophages of any solid organ, which are classified as Kupffer cells (KCs) and monocyte derived macrophages (MDMs) (18–20). Macrophages play a critical role in the initiation and propagation of inflammation in both patients and animal models of NAFLD/NASH (21–25). This is illustrated by the fact that the depletion of KCs is sufficient in halting the NAFL to NASH transitions and preventing the recruitment of bone marrow generated MDMs significantly decreases inflammation associated with NASH (21, 26). Microenvironmental stimuli ultimately determine the function and phenotypic characteristics of the two macrophage subsets and both populations are involved in the development of NAFLD (27–30). Both KCs and MDMs can further differentiate into proinflammatory type 1 (M1) macrophages, which are the primary sources of proinflammatory cytokine secretion and generators of reactive oxygen species (ROS) (31–36) or anti-inflammatory and inflammation resolution type 2 (M2) macrophages (26). True differentiation/polarization of these populations requires single cell transcriptomic analysis of key mediators (22, 23). Therefore, this study will focus on both populations and referred to them collectively as "hepatic macrophages (HMΦs)". KCs are liver tissue-resident macrophages and reside within liver acinus zone 1 (22, 23). Activated KCs in NAFLD/NASH patients are F4/80^{+}, CD14^{+}, CD16^{+} and CD68^{+} (21, 27, 37–40) and in NAFLD mouse models are F4/80^{+}, CD11b^{low}, CD68^{+} and Clec4f^{+} (21, 27, 38). KCs have several homeostatic functions including clearance of damaged red blood cells, iron metabolism, bilirubin metabolism, and cholesterol metabolism (18, 19, 31, 41–43).

MDMs arise from Ly6C$^{+/high}$ bone marrow (BM)-derived monocytes recruited to the liver in response to liver inflammation (21–23). Upon maturation, MDMs transition to a Ly6C$^{-/low}$ status and reside in hepatic acinus zones 2 and zone 3 (22, 23, 44, 45). These MDMs repopulate the liver macrophage niche in hepatic acinus zone 1, with the microenvironment and secretomes from liver sinusoidal endothelial cells (LSECs) allowing for the development of a "KC-like" phenotype and functionality (27, 29, 30, 38). Recent studies have added more context to this binary system (46). Hepatic macrophages play a significant role in NAFLD (21, 47–50). MDMs are a population of HMΦs capable of repopulating the liver when KCs are depleted in chronic liver diseases. Furthermore, clinical trials have demonstrated that preventing MDM infiltration decreases inflammatory liver damages (21, 23, 27, 29, 30, 38, 50–54).

Inflammasomes and inflammatory caspases, such as caspase-1 and caspase-4 (humans)/caspase-11 (mice), have two coupled functions: 1) serve as sensors for danger associated molecular patterns (DAMPs) and viral and bacterial infections-related pathogen associated molecular patterns (PAMPs) and 2) initiate

inflammation signaling and promote inflammatory cell death (pyroptosis) (55–70), which specifically antagonize infection but can cause detrimental inflammation as well (71). Recent studies have shown promise in treating NAFLD with therapeutics targeting the nucleotide-binding domain (NOD)-, leucine-rich repeat (LRR)- and pyrin domain-containing protein 3 (NLRP3) inflammasome, suggesting that targeting pyroptosis is a viable option for treating the disease (72, 73). While current pyroptosis targeting therapeutics focus on the inflammasomes that activate caspase-1, the caspase-11-dependent pathway presents a novel therapeutic target. Our group and others have demonstrated that caspase-1 deficiency is protective against HFD-induced NAFLD to NASH progression (57, 74). However, the roles of caspase-11-dependent pathway have not been defined in HFD-induced NAFLD (75, 76).

As we recently published in our novel data mining analysis of 4249 genes in 27 mouse models of NAFLD, caspase-11 mediates liver pyroptosis in both patients and mouse models of NASH *via* lipid peroxidation and trained immunity (innate immune memory) pathways (77). Other studies have demonstrated that lipid peroxidation can generate endogenous ligand for caspase-11, which impacts animal models of sepsis (78–80).

Endotoxin levels and gut-derived Gram-negative bacteria are elevated in patients with NAFLD (81). A previous study involving two obese individuals showed that the nonvirulent endotoxin-producing strains of pathogenic species that were overgrowing in obese people's guts can cause NAFLD and related metabolic problems. The most upstream and crucial biological process that causes all phenotypes in NAFLD and other related metabolic disorders is the host's TLR4 receptor (82). Another study involved Nine hundred and twenty adults randomly selected from the government's census database and underwent proton-magnetic resonance spectroscopy to assess hepatic steatosis showed that NAFLD patients had slightly higher lipopolysaccharide-binding protein (LBP) endotoxin markers associated with insulin resistance and dyslipidemia and that people with modest alcohol consumption have lower serum endotoxin (83). Similarly, another study involving one hundred and fifty-five patients with NAFLD and twenty-three control individuals showed that endotoxin levels were significantly higher in NAFLD patients than in controls, with particularly noticeable increases in early-stage fibrosis (84). However, several important questions remain to be addressed: 1) Why NAFLD cannot be developed in germ-free mice; and why LPS-containing Gram-negative bacteria overgrowing in human gut microbiota are linked to NAFLD (82). 2) Why NAFLD can be a significant proinflammatory driver for second wave of atherosclerosis (11, 12). We previously reported a novel metabolically healthy obesity mouse model, in which atherosclerosis is decreased due to proinflammatory microRNA-155 (miR155) deficiency in apolipoprotein E deficient ($ApoE^{-/-}$) mice but NAFLD development is sustained (10). 3) Why HFD model becomes an essential component for all 27 models of NAFLD. Here we sought to determine whether caspase-11 plays a role in promoting HFD-induced NAFLD. We found that HFD feeding for 12 weeks drives NAFLD in WT mice, which are transcriptionally distinct from WT liver fed with normal chow diet (NCD). HFD increased gene expressions of caspase-11, gasdermin D (GSDMD), interleukin-1β (IL-1β), and guanylate-binding proteins (GBPs) in liver. However, caspase-11 deficiency significantly decreased liver IL-1β concentrations, reduced N-terminal GSDMD expression on plasma membrane, significantly re-programed liver transcriptomes, and attenuated hepatic monocyte/macrophage pyroptosis in HFD-induced NAFLD. BM-derived monocytes/macrophages play more significant roles than liver resident monocytes/macrophages in developing pyroptosis. To determine the underlying mechanisms, we performed a set of experiments and found that caspase-11 deficiency significantly decreased extracellular acidification rate (ECAR) from glycolysis and oxidative phosphorylation (OXPHOS), indicating that caspase-11 significantly contributes to maintain dual fuel bioenergetics — glycolysis and OXPHOS in proinflammatory fatty acid palmitic acid-stimulated macrophages, and potentially promotes transition of M2 macrophages into M1 macrophages. These results provide novel insights on the roles of caspase-11-GSDMD pathway in promoting hepatic macrophage inflammation and novel targets for future therapeutic interventions involving transition of NAFLD to NASH, hyperlipidemia, type-II diabetes, metabolic syndrome, atherosclerotic cardiovascular diseases, autoimmune diseases, liver transplantation, and hepatic cancers.

2 Materials and methods

2.1 Animal care

All animal experiments were performed in accordance with the Institutional Animal Care and Use Committee (IACUC) guidelines and were approved by the IACUC of Lewis Katz School of Medicine (LKSOM) at Temple University. Wild-type (WT) mice were of a C57BL/6J background, and caspase-11 knockout ($Casp11^{-/-}$) mice were purchased from Jackson Laboratories (Bar Harbor, ME). Mice were housed under controlled conditions in the LKSOM Animal Facility, where they had *ad libitum* access to standard chow diet control/HFD, water, and were subject to a 12-hour light-dark cycle. Mice were age-matched and gender-specific in all experiment groups. At eight to ten weeks old, male mice either remained on normal chow diet (10.7% fat, 23.9% protein, 5.1% fiber, 58.7% carbohydrate/other, 200ppm cholesterol; Labdiet 5001) or switched to HFD [20% (w/w) fat, 17.4% protein, 5% fiber, 49.9% carbohydrate/other, 2027 ppm cholesterol (0.15% (w/w) cholesterol); AIN-76A] (Research Diets, NJ).

2.2 Histological NAFLD activity score analysis

There are different parameters used to histologically grade NAFLD/NASH progression including: macrovesicular steatosis, microvesicular steatosis, lobular inflammation, Mallory Body occurrence, hepatocellular iron, KC activation, and hepatocyte ballooning (1, 85, 86). The most common NAFLD/NASH grading rubric is the "NAFLD Activity (NAS) Score" which combines (macrovesicular) steatosis, lobular inflammation, and hepatocyte ballooning on a scale from 0 (no NAFLD) to 8 (severe disease) (1, 85, 86). Mice were sacrificed *via* ketamine overdose and cervical dislocation. Body weight was measured then mice were affixed to a Styrofoam surface. Blood was collected *via* cardiac puncture and the

liver was perfused *via* the portal vein with 10 ml of phosphate buffered saline (PBS). Isolated liver was weight, washed with PBS. A liver sample was collected and preserved in 10% formalin for 8 – 10 hours at room temperature (RT), washed with PBS then stored in 75% ethanol. Hematoxylin and eosin staining was carried out by AML Laboratories (St. Augustine, FL). NAFLD Activity Score (NAS) was determined by Dr. Nirag Jhala, MD (Professor, Pathology and Laboratory Medicine) from Temple University Hospital (Philadelphia, PA).

2.3 Plasma cholesterol measurement

Blood was collected in 5% coated tubes *via* from the cardiac puncture of anesthetized animals. Plasma was collected by low-speed centrifugation for 20 minutes at 4°C. Plasma cholesterol levels in each sample were analyzed at the Mouse Metabolic Phenotyping Center at the University of Cincinnati (C1052-lipid Profiles) by colorimetric assays using Cholesterol Reagent Set. Reactions were run in microtiter plates and analyzed on a plate reader (https://med.uc.edu/institutes/mmpc/select-a-test/lipid-metabolism).

2.4 Bone marrow transplantation

Six to eight weeks old recipient (male, $CD45.2^+$) mice were irradiated with 750 to 950 cGy (RS-2000 Biological Irradiator, Buford, GA). Eight to ten weeks old donor (male, $CD45.1^+$) mice were sacrificed as described above. After euthanasia, femur and tibia were amputated and stored in PBS on ice. Marrow was flushed from the bone, passed through a 70-um filter. Red blood cells were eliminated using erythrocyte lysis buffer (8.29 g/L NH_4Cl, 1 g/L $KHCO_3$, 37.2 mg/L EDTA, double-distilled H_2O, pHed to pH 7.2). $1x10^6$ cells from donor mice were transplanted by retro-orbital injection into recipient mice.

2.5 Liver single cell suspension and immune cell fractionation

Mice were sacrificed, and liver was perfused *via* the portal vein with 10 ml of PBS. Isolated liver was weight, cut into 1-1.5 mm pieces and stored in 5 ml Liver Digestion Medium (ThermoFisher, 17703034) on ice until ready for digestion. Liver suspensions were incubated in a 37 °C water bath for 20-30 minutes on an orbital shaker. Digestion medium was collected in 5.0 ml Eppendorf tubes for cytokine analysis. Liver suspensions were filtered through a 70-um filter. Red blood cells were eliminated using erythrocyte lysis buffer. HMΦs were separated from hepatocytes using 33% Percoll solution (Sigma-Aldrich, P1644).

2.6 Western blot and ELISA analysis

Immune cell fraction was prepared from mouse liver as described above. Fractionated immune cells were lysed and protein isolated using an acid-guanidinium-phenol based reagent TRIzol (ThermoFisher, GE17-0891-01) according to manufacturer's instructions. Protein was concentrated using Protein Concentrator polyethersulfone (PES), 10K molecular weight cutoff (MWCO) (ThermoFisher, 88503). Protein was quantified using colorimetric Pierce BCA Protein Assay Kit (ThermoFisher 23225). Protein was run on 12.5% gel and transferred to polyvinylidene difluoride (PVDF) membrane. Membranes were blocked using 5% bovine serum albumin (BSA) for 1 hour. Primary antibodies were diluted in Tris-buffered saline (TBS) (0.2% Tween-20) buffer and incubated at 4°C overnight. Primary antibodies used: caspase-11 (ThermoFisher, 14-9935-82), GSDMD (Abcam, ab209845), and β-Actin (Sigma-Aldrich, ab6276). Secondary antibodies were diluted in TBS (0.2% Tween-20, 0.01% SDS) and incubated for 30 minutes to 1 hour at RT. Secondary antibody used: IRDye 680RD (LI-COR), IRDye 800CW (LI-COR). Membranes were scanned using LI-COR Odyssey Crx (Li-Cor Biosciences, Lincoln, NE). Image processing was performed using Image Studio Analysis (LI-COR). Liver IL-1β levels were assessed using the Mouse IL-1 beta/IL-1F2 Quantikine ELISA Kit (R&D Systems, MLB003) following the manufacturer's instruction.

2.7 Flow cytometric quantification of hepatic macrophages and noncanonical pyroptosis

Animals were sacrificed and livers were collected as described above. Fractionated immune cells were collected. Cells were incubated with CD16/CD32 FcR-blocking antibody (BD Bioscience, 553142) on ice for 20 minutes. Live/Dead staining was performed using Zombie Aqua (Biolegend, 423101) with a 30-minute incubation on ice. HMΦ surface staining was performed using the following panel: APC-Cy7_CD45 (BioLegend, 103116), FITC_I-A/I-E (MHCII) (BioLegend, 107605), PerCP-Cy5.5_CD11b (BioLegend, 101228), BV510_Ly6G (BioLegend, 127633), BUV395_F4/80 (BD Biosciences, 565614), BV421_CCR2 (BioLegend, 150605), APC_Ly6C (BioLegend, 128016), PE-Cy7_CD206 (ThermoFisher, 25-2061-82), BV785_CD86 (BioLegend, 105043). HMΦ pyroptosis was performed using the following panel: FAM-LEHD-FMK (caspase-11 activity assay), APC-Cy7_CD45 (BioLegend, 103116), BV510_Ly6G (BioLegend, 127633), PerCP-Cy5.5_CD11b (BioLegend, 101228), Ly-6C_AF700 (BioLegend, 128024), BUV395_F4/80 (BD Biosciences, 565614), GSDMDC1_AF674 (Santa Cruz Biotechnology, sc-393581 AF647). Flow cytometric data was acquired using LSR-II Flow Cytometer (BD Bioscience). Mean fluorescent intensity (MFI) and population percentages were analyzed using FlowJo (Ashland, OR).

2.8 RNA-sequencing

RNA-seq was performed using the immune cell fraction from male WT and $Casp11^{-/-}$ mice fed 12-week HFD. Animals were sacrificed and livers were collected. Fractionated immune cells were lysed and RNA isolated using TRIzol (ThermoFisher, GE17-0891-01) according to manufacturer's instructions. RNA was quantified using Nanodrop (ThermoFisher). Frozen RNA samples were sent to Genewiz (South Plainfield, NJ) for RNA-seq analysis. Total RNA

libraries were prepared by using Pico Input SMARTer Stranded Total RNA-seq Kit (Takara). In short, 10 ng total RNA from each sample was reverse transcribed *via* random priming and reverse transcriptase. Full-length cDNA was obtained with SMART (Switching Mechanism At 5′ end of RNA Template) technology. The template-switching reaction was used to keep the strand orientation of the RNA. The ribosomal cDNA was hybridized to mammalian-specific R-Probes and then cleaved by ZapR. Libraries containing Illumina adapter with TruSeq HT indexes were subsequently pooled and loaded to the Hiseq 2500. Single end reads at 75 bp with 30 million reads per sample were generated for bioinformatic analysis FASTQ files were mapped to the mouse mm10 genome using STAR Aligner and BAM alignment files were imported into Qlucore Omics Explorer and used to generate expression data (transcripts per million, TPM). All original RNA-seq data were deposited in the NCBI's Gene Expression Omnibus database (GSE221005).

2.9 Measurement of extracellular acidification rate and mitochondrial parameters in palmitic acid stimulated bone marrow-derived macrophages

Bone marrow-derived macrophages were isolated from tibias and femurs of WT and Casp11$^{-/-}$ as we previously reported (12). Briefly, femurs and tibias were sprayed with 75% alcohol in Petri dish containing Roswell Park Memorial Institute medium (RPMI) 1640 (Gibco, Grand Island, NY) with 2% FBS. The bones were cut off at both ends and elute morrow into 50-mL conical tubes with RPMI-1640 with 2% FBS and penicillin/streptomycin (p/s) (Gibco, Grand Island, NY) using 10-mL syringes and 25-G needles. The cell suspension was filtered through a 70-μm cell strainer (BD Biosciences, San Jose, CA) into a sterile conical tube and centrifuged (500 g for 5 minutes). The pellet was resuspended well in 5 to 10 mL ACK red blood cell lysis buffer (Sigma-Aldrich, St Louis, MO) for 1 minute followed by the addition of RPMI-1640 and centrifugation (600 g for 7 minutes) to terminate the lysis. The pellet was washed using RPMI-1640 with 10% FBS once more, resuspended in differentiation medium (RPMI-1640, 10% FBS, 20% L929 conditional medium, p/s), and cultured at 37℃ in a 5% CO2 incubator. At day 3, the supernatant was carefully removed, and the medium was replaced. At day 7, cells were harvested and transferred to 96-well plate for seahorse assay. Seahorse XF96 analyzer (Seahorse Bioscience, Agilent, Santa Clara, CA) was used to measure the extracellular acidification rate (glycolysis) and six mitochondrial parameters (Mito Stress Test) in bone marrow-derived macrophages, including basal respiration, maximal respiration, proton leak, ATP production, spare respiratory capacity, and non-mitochondrial respiration as we previously reported (87, 88). Briefly, 100,000 cell/well were seeded in a 96-well plate and cultured overnight in XF assay medium supplemented with 10 mM glucose, 1 mM pyruvate and 2 mM L-glutamine. Cells were stimulated with palmitic acid 500 μM for 8 hours (89). Culturing media was changed to modified DMEM media and placed into a 37°C non-CO2 incubator for 1 hour. After preparation of drugs and XF Cell Mito Stress Test Kit and glycolytic rate kit (Seahorse Bioscience) into cartridge ports, the cartridge and cell culture plates were loaded into XF96 analyzer (Seahorse Bioscience). Experiments were performed in triplicates.

2.10 Statistical analysis

All data was reported as mean ± standard deviation (SD). Statistical analysis comparing genotype-diet groups (WT-HFD versus (vs) WT-NCD, Casp11$^{-/-}$HFD vs Casp11$^{-/-}$NCD, Casp11$^{-/-}$ NCD vs WT-NCD) were calculated by 1-way or 2-way ANOVA using Prism (GraphPad) or Qlucore Omics Explorer (Qlucore). Statistical significance was set at $p \leq 0.05$.

3 Results

3.1 High-fat diet promotes nonalcoholic fatty liver disease, and lipid accumulation are temporally earlier than liver inflammation

HFD feeding is a commonly used rodent model of Western diet-induced obesity and NAFLD (90–92). The HFD not only increases intake of saturated fatty acid (SFA) but also induces metabolic endotoxemia, defined as an HFD-associated increase in circulating LPS (93). The 12- and 16-week HFD-feeding schemes have been shown to induce obesity and NAFLD in male C57BL/6 mice (94). Therefore, we compared WT mice fed either HFD or normal chow diet (NCD) (as controls) for 12 weeks (Figure 1A). We found that HFD significantly increased mouse body weight (Figure 1B), liver weigh (Figure 1C), and plasma cholesterol levels (Figure 1D). HFD for 12 weeks has been shown to discolor the liver and increase macrovesicular steatosis (1, 85, 86). Our results also showed that the liver color of the HFD group appeared light yellow compared to dark red in the NCD group (Figure 1E), consistent with the HFD promoted hepatic steatosis.

After 12 weeks of HFD, there was a NAFLD/NASH histological phenotype with deposits of fat determined by pathohistological staining (Figure 1F). The NAFLD activity score (NAS) is a pathological measure of grade and represent the sum of scores for steatosis (0-3), hepatocyte ballooning (0-3), and lobular inflammation (0-3). In grade 0, steatosis less than 5%, no hepatocyte ballooning, and no inflammation. Grade 1 showed mild steatosis (5-33%), mild hepatocyte ballooning, and minimal inflammation. Grade 2 has moderate steatosis (33-66%), moderate hepatocyte ballooning, and mild inflammation. Grade 3 has severe steatosis (> 66%), severe hepatocyte ballooning, and moderate inflammation. However, grade 4 has severe inflammation (4) (Figure 1G). In addition, HFD significantly increased NAS score (Figure 1H), steatosis score (Figure 1I), and slightly but not statistically significant increase in lobular inflammation (Figure 1K), and no change in hepatocyte ballooning (Figure 1J) compared to NCD controls.

Additionally, our new RNA-seq data indicated that the livers of HFD mice were transcriptionally distinct from that of NCD-fed mouse liver controls (Figure 1L). As shown in the Volcano plot analysis (Figure 1M), HFD modulated the expressions of 3895 genes, among them 2918 genes were significantly upregulated, and 977 gene downregulated (FC ≥ 1.5 and p value ≤ 0.01). Taken together, these results have demonstrated that HFD promotes NAFLD phenotypes, and induce gross pathological and transcriptomic changes in the liver characterized by deposits of fat that appear temporally earlier than liver inflammation.

10.3389/fimmu.2023.1113883

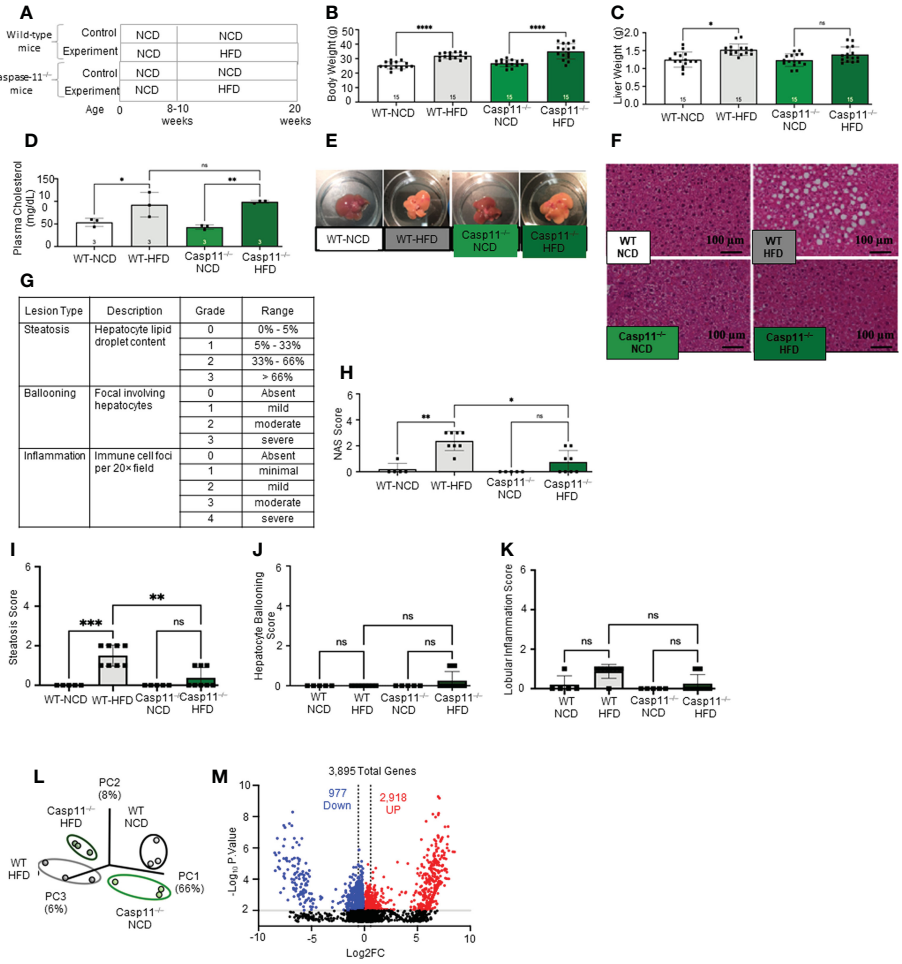

FIGURE 1
High-fat diet (HFD) promotes non-alcoholic fatty liver disease (NAFLD) and Caspase-11 deficiency decreases lipid droplet, steatosis score, and NAS score in HFD-induced NAFLD but does not change liver weight or gross anatomic fatty liver pathology. **(A)** Experimental diet timeline. 8-10 weeks old Wild-type (WT) male mice and Caspase-11 deficient (Casp11−/−) mice were fed HFD or normal chow diet (NCD) for 12 weeks. **(B)** Body weight (n = 15). **(C)** Liver weight (n = 15). **(D)** Plasma cholesterol levels (n = 3). **(E)** Representative images showed that HFD feeding changed liver color to light yellow color. **(F)** Representative 20X images of hematoxylin and eosin (H&E) staining showing hepatic steatosis in 12-week HFD-fed WT and Casp11−/− male mice compared to 12-week NCD. Scale bar 100 µm. **(G)**. Description and grades of NAS scare. NAFLD activity score analysis indicated that lipids accumulation as judged by liver steatosis and ballooning is precedent to liver inflammation. In grade 1, when steatosis reaches 5-33%, and ballooning reaches mild, inflammation is minimal. Steatosis was in the graded section as: are 0, steatotic; 0% to 1, 5% greater than 5% to 33% of hepatocytes are steatotic; 2, greater than 33% to as: 66%; 0, absent; and 3, 1, greater mild (focal; than 66%. involving Ballooning fewer than 3 hepatocytes); 2, moderate (focal and involving 3 or more hepatocytes or multifocal); and 3, severe (multifocal, with more than 2 foci of 3 or more hepatocytes). (0 or 1 Inflammation focus per 20× was field); graded 2, as: mild 0, (2 absent; foci); 3, moderate (3 foci); and 4, severe (4 or more foci per 20× field). **(H)** Total NAS score for WT-NCD (n = 5), WT-HFD (n = 8), Casp11−/−NCD (n = 5) and Casp11−/−HFD (n = 8). **(I)** Hepatic steatosis score. **(J)** Hepatocyte ballooning. **(K)** Lobular inflammation. **(L)** Principal component analysis (PCA) demonstrating that WT-NCD, WT-HFD, Casp11−/−NCD, and Casp11−/−HFD mice are transcriptionally distinct (n = 3). **(M)** Volcano plot analysis showed the 3895 differentially expressed genes (DEGs) in the WT liver of 12-week HFD compared to12-week NCD control. Among 3895 DEGs, 2918 genes were significantly upregulated (red), and 977 genes downregulated (blue). (FC) > 1.5 and $p < 0.05$. Statistical Analysis: Bulk RNA-Seq analysis was performed using Qlucore Omics Explorer. PCA plot generated using significantly differentially regulated genes). Volcano plot generated using GraphPad Prism with significantly differentially regulated genes. Statistical Analysis: One-Way ANOVA. *$p < 0.05$, **$p < 0.001$, ***$p < 0.0001$ ****$p < 0.0001$. ns, Non-significant.

3.2 HFD upregulates the expressions of proinflammatory, NASH-related hepatic macrophage markers, guanylate binding proteins, caspase-11, and increases N-terminal gasdermin D (GSDMD) cleavage

Hepatic acini form hexagonal structures with a central vein and portal triads at every other vertices. The hepatic acinus can be histologically divided into three zones (Figures 2A, B). Zone 1 represents the portal triad, which includes hepatic artery, portal vein, and bile duct. Zone 2 represents the parenchymal area, structurally consisting primarily of hepatocytes with a central vasculature composed of LSECs. Mature immune cells including B cells, T cells, innate-like lymphoid cells (ILCs), natural killer cells (NK cells), and KCs reside in hepatic acinus zone 1 and 2. Zone 3 represents the central vein, the innermost hepatocytes, and infiltrating immune cells. The portal vein contains nutrient-rich blood that is contaminated by microbial pathogen associated molecular patterns (PAMPs) such as LPS and bacteria, both arising from the intestines (95).

In the noncanonical pyroptosis pathway (Figure 2C), the guanylate binding proteins (GBPs) promote exposure of LPS from

10.3389/fimmu.2023.1113883

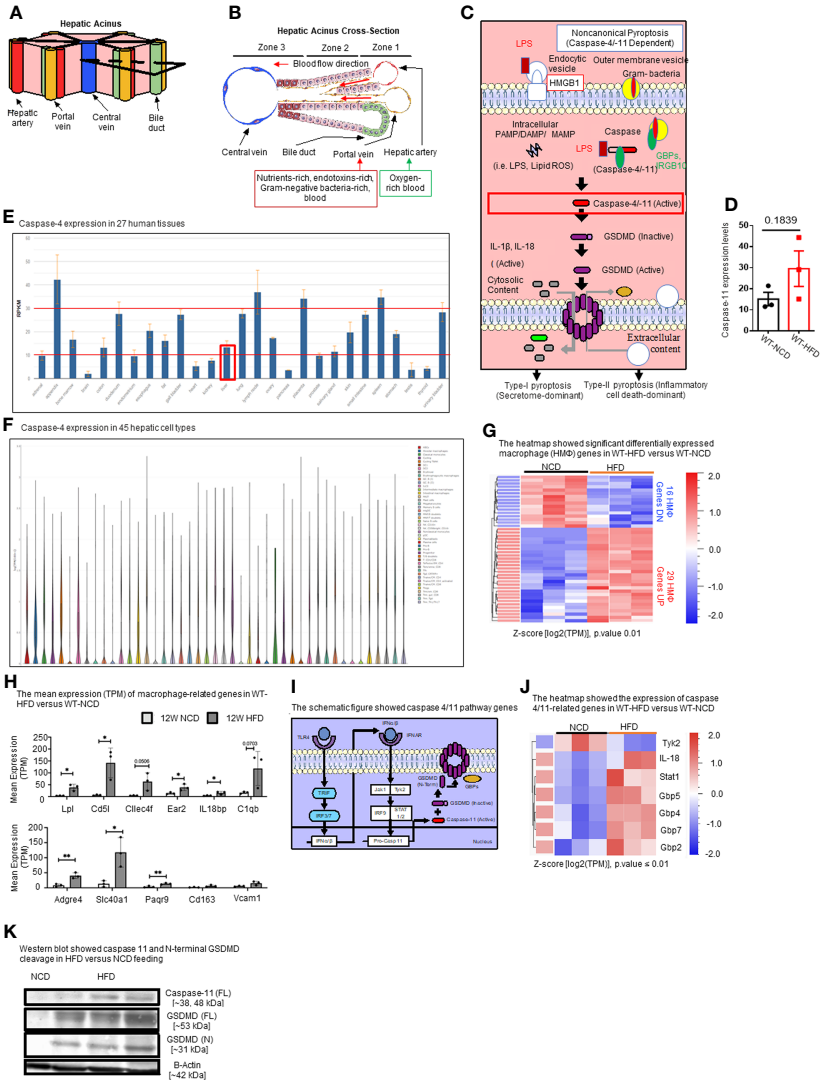

FIGURE 2
HFD upregulates the expressions of proinflammatory, NASH-related hepatic macrophage markers, GBPs, caspase-11, and increases N-terminal GSDMD cleavage. **(A, B)** The structure of hepatic acinus suggests that the liver is the first organ exposed to endotoxins-rich and Gram bacteria-rich blood in the body. Liver parenchymal and nonparenchymal cells are organized into structures called "acinus". Hepatic acini form hexagonal structures with a central vein and portal triad at the vertices. The hepatic acinus can be histologically divided into three zones. Zone 1 represents the portal triad which includes a hepatic artery, a portal vein, and a bile duct. Zone 2 represents the parenchymal area, structurally consisting primarily of hepatocytes with a central vasculature composed of liver sinusoidal endothelial cells (LSECs). Mature immune cells including B cells, T cells, innate-like lymphoid cells (ILCs), natural killer cells (NK cells), and tissue-resident macrophages (Kupffer cells) reside in hepatic acinus zone 1 and 2. Zone 3 represents the central vein, the innermost hepatocytes, and infiltrating immune cells. The portal vein contains nutrient-rich, endotoxins-rich, and gram bacteria-rich blood. **(C)** Noncanonical pyroptosis is caspase-4 (human), caspase-11 (mouse) dependent. Guanylate binding proteins (GBPs) promote the outer membrane vesicles from gram-bacteria to activate caspase-11. Intracellular sources of inflammation (including LPS and oxidized phospholipids) directly bind to caspase-4/-11. Caspase-4/-11 cleaves gasdermin-D to initiate noncanonical pyroptosis. **(D)** The expressions of caspase-11 in the liver were in an upregulation trend in high-fat diet-fed wild-type mice. The microarray data were achieved from the NIH-NCBI-Geo-Profiles database (GDS4811). **(E)** Caspase-4 expression in 27 human tissues. The expression of caspase-4 in the liver is at a medium level among all 27 human tissues. Caspase-4 RNA-Seq data were analyzed from the NIH-NCBI-Gene database (https://www.ncbi.nlm.nih.gov/gene/837). **(F)** Caspase-4 expression in 45 hepatic cell types. Caspase-4 is expressed in all 40 immune cell types, the single-cell RNA-Seq data were analyzed from the MIT Broad Institute Single Cell RNA-Seq (scRNA-Seq) Porter database (https://singlecell.broadinstitute.org/single_cell/study/SCP1845/cross-tissue-immune-cell-analysis-reveals-tissue-specific-features-in-humans?genes=casp4&tab=distribution#study-visualize). Among 45 immune cell types identified in scRNA-Seq, 19 immune cell types are significantly enriched in the human liver including dendritic cell 1 (DC1), DC2, classical monocytes, non-classical monocytes, erythrophagocytic macrophages, mononuclear phagocytes (MNP)/B doublets, age-associated B cells (ABCs), plasma cells, Plasmablasts, MNP/B doublets, T/B doublets, mucosal-associated invariant T (MAIT), T_CD4/CD8, T effector memory (Tem)/effector memory re-expressing CD45RA (emra)_CD8, T resident memory cell/effector memory cell (Trm/em)_CD8, gamma-delta T cell (Tgd)_CRTAM+, Cycling T cell & natural killer cell (NK), NK_CD16+, and NK-CD56bright_CD16-. **(G)** 12-week HFD promotes expression of HMΦ activation mediators in the WT liver. 8-10 weeks old male WT mice were fed with HFD for 12 weeks. Heatmap of significant, differentially regulated macrophage (HMΦ) genes. **(H)** Bulk RNA-seq expression (mean transcripts per kilobase million, TPM) of macrophage mediators. **(I)** Schematic representing caspase-4/11 pathway genes. **(J)** Bulk RNA-seq expression (mean TPM) of noncanonical pyroptosis-associated mediators. **(K)** Western blot analysis showed that HFD feeding increased caspase-11 and N-terminal GSDMD cleavage. Statistical Analysis: Bulk RNAseq analysis was performed using Qlucore Omics Explorer. Heatmap was generated using significantly differentially regulated genes (p.adj < 0.01). Differential gene expression presented as Z-score calculated from log2 transformed TPM. *P < 0.05, **p < 0.01.

Gram-negative bacteria to activate caspase-11 (96, 97). Cytosolic LPS then directly binds to and activates caspase-4/11, leading to GSDMD cleavage to generate the N-terminal active fragment (GSDMD-NT). GSDMD-NT-mediated plasma membrane perforation triggers membrane rupture associated with release of proinflammatory cytokines such as IL-1β (type-I pyroptosis or secretome-dominant) and cell death (type-II pyroptosis or inflammatory cell death-dominant) (97–100). Previous studies have shown the role of inflammasomes and caspase-1 in NAFLD (101, 102), and the role of caspase-11 in methionine-, choline-deficient diet (MCD)-induced NASH was reported (76). However, the roles of caspase-11 in HFD-induced NAFLD have not been extensively studied. Therefore, we examined the expression levels of caspase-11 in the liver of HFD-fed WT mice from microarray data from the NIH-NCBI-Geo-Profiles database (GDS4811). The results showed that caspase-11 expression was increased in the liver of HFD fed mice (Figure 2D). We further checked the expression of caspase-4 in the normal human tissues from RNA-seq data performed on tissue samples from 95 human individuals representing 27 different tissues, data were analyzed from the NIH-NCBI-Gene database (https://www.ncbi.nlm.nih.gov/gene/837) (103). Our data analysis showed that caspase-4 expression in the liver is at a medium level among all 27 human tissues (Figure 2E). Furthermore, we analyzed the expression of caspase-4 in 45 immune cell types from single-cell RNA-seq data collected from the MIT Broad Institute Single Cell RNA-seq (scRNA-seq) Porter database (https://singlecell.broadinstitute.org/single_cell/study/SCP1845/cross-tissue-immune-cell-analysis-reveals-tissue-specific-features-in-humans?genes=casp4&tab=distribution#study-visualize) (104). Our data analysis showed that caspase-4 was expressed in all 45 immune cell types (Figure 2F). Among 45 immune cell types identified in scRNA-seq, 19 immune cell types are significantly enriched in the human liver including dendritic cell 1 (DC1), DC2, classical monocytes, non-classical monocytes, erythrophagocytic macrophages, mononuclear phagocytes (MNP)/B doublets, age-associated B cells (ABCs), plasma cells, plasmablasts, MNP/B doublets, T/B doublets, mucosal-associated invariant T (MAIT), T_CD4/CD8, T effector memory (Tem)/effector memory re-expressing CD45RA (emra)_CD8, T resident memory cell/effector memory cell (Trm/em)_CD8, gamma-delta T cell (Tgd)_CRTAM+, Cycling T cell & natural killer cell (NK), NK_CD16+, and NK-CD56bright_CD16.

Liver has the highest number of macrophages of any solid organ (18–20), therefore, we focused on inflammatory features of liver macrophages to determine the inflammatory pathways underlying HFD-driven NAFLD transition to NASH. Our RNA-seq data analysis of liver immune cells showed that HFD increased the expression of fifteen NASH-associated inflammatory macrophage markers including fatty acid binding protein 7 (Fabp7), C-C motif chemokine ligand 24 (Ccl24), lipoprotein lipase (Lpl), matrix metallopeptidase 12 (Mmp12), complement C1q B chain (C1qb), interleukin 18 binding protein (Il18bp), C-type lectin domain family 4 member F (Clec4f), CD5 molecule like (Cd5l), phospholipid transfer protein (Pltp), nuclear receptor subfamily 2 group F member 6 (NR2F6, Ear2), insulin like growth factor 1 (Igf1), apolipoprotein C1 (Apoc1), WAP four-disulfide core domain 17 (Wfdc17), membrane spanning 4-domains A7 (Ms4a7), and matrix metallopeptidase 12 (Mmp12) (Figures 2G, H). Ten healthy, inactivate HMΦ markers were also increased in HFD including macrophage receptor with collagenous structure (Marco), C-X-C motif chemokine ligand 13 (Cxcl13), CD163 molecule (Cd163), adhesion G protein-coupled receptor E4, pseudogene (Adgre4), progestin and adipoQ receptor family member 9 (Paqr9), solute carrier family 40 member 1 (Slc40a1), ficolin 3 (Fcna), mannose receptor C-type 1 (Mrc1), syndecan 3 (Sdc3), and heme oxygenase 1 (Hmox1), likely signifying an expansion of KCs in preparation for HFD-induced activation (Figures 2G, H). In addition, the expressions of other genes in the caspase-11 pathway, shown in schematic Figure 2I including signal transducer and activator of transcription 1 (Stat1), guanylate binding protein 2 (Gbp2), Gbp4, Gbp5, Gbp7, and interleukin-18 (IL-18) were significantly increased in the livers of HFD fed mice (Figure 2J). Western blot analysis also showed that caspase-11 and GSDMD-NT protein expressions were increased by HFD (Figure 2K). Tyrosine kinase 2 (Tyk2) as a part of Janus kinase (JAK)-signal transducer and activator of transcription (STAT) (JAK/STAT) signaling downstream of interferon-α/β receptor (IFNAR) has been shown to increase caspase-11 expression in splenic myeloid cells in response to LPS stimulations (105). IL-18 is the other IL-1 family cytokine cleaved by proinflammatory caspases in pyroptosis (102). The N-terminal of cleaved GSDMD is required for GSDMD-pore formation on plasma membrane and demonstrates caspase-11 activity. Guanylate-binding protein (GBP) expression have been shown to bind to cytosolic Gram-negative bacteria and expose LPS for sensing by caspase-11 (106). Taken together, these results have demonstrated that HFD upregulates the expressions of proinflammatory, NASH-related hepatic macrophage markers, GBPs, caspase-11, GSDMD, and increases GSDMD-NT cleavage and membrane expression.

3.3 Caspase-11 deficiency decreases lipid droplet, steatosis score, and non-alcoholic steatosis score in HFD-induced NAFLD but does not change liver weight or gross anatomic fatty liver pathology

To determine the roles of caspase-11 in NAFLD, we compared pathological progression of NAFLD in Casp11$^{-/-}$mice with that of WT control mice (Figure 1A). We found that HFD significantly increased body weight for both Casp11$^{-/-}$ and WT mice (Figure 1B). While liver weight significantly increased in HFD fed WT mice, the liver weight of Casp11$^{-/-}$ mice did not increase significantly (Figure 1C). However, HFD promoted steatosis and significantly increased circulating cholesterol levels in both Casp11$^{-/-}$ and WT mice (Figures 1D). Along these lines, HFD increased lipid droplet formation (macrovesicular steatosis), NAS score and steatosis score (107) in WT mice. However, HFD in Casp11$^{-/-}$ mice dramatically reduced lipid droplet, NAS score, and steatosis score compared to WT mice on HFD (Figures 1E, I) and slightly but statistically non-significant decreased lobular inflammation (Figure 1K). Interestingly, caspase-11 deficiency led to slightly but statistically non-significant increases in hepatocyte ballooning (swollen hepatocytes with rarefied cytoplasm) (108), which was not seen in any of the other groups (Figure 1J). Decreased steatosis and increased hepatocyte ballooning suggest differential roles for caspase-11 in both

hepatocytes and HMΦs, respectively. Our principal component analysis (PCA) of liver RNA-seq data showed that liver transcriptomes of WT and Casp11$^{-/-}$ mice on HFD were transcriptionally distinct from the respective NCD controls (Figure 1L). In summary, our results have demonstrated that although slightly increasing hepatocyte ballooning, caspase-11 deficiency decreases NAFLD progression and lobular inflammation in HFD-induced NAFLD.

3.4 Caspase-11 deficiency reprograms liver transcriptomes and attenuates hepatic macrophage pyroptosis in HFD-induced NAFLD; caspase-11 cleaves N-terminal GSDMD in normal chow diet livers more than that in HFD-induced NAFLD; and bone marrow-derived macrophages play more significant roles than liver resident macrophages in facilitating pyroptosis

The results so far demonstrated that HFD promotes fatty liver in WT mice, however, caspase-11 deficiency decreases macrovesicular steatosis and lobular inflammation, which were well correlated with a report showing decreased macrophage recruitment into atherosclerotic lesion in Casp11$^{-/-}$/ApoE$^{-/-}$ atherogenic mice (109). Studies have shown that HMΦs drive inflammation and canonical pyroptosis in NAFLD, however, the role of noncanonical pyroptosis has not been well studied. Therefore, we next sought out to evaluate HMΦ pyroptosis. The transcripts of six NASH-associated activated macrophage markers including Cd5l, Clec4f, C1qb, Lpl, Folr2, and Il18bp were upregulated in both WT and Casp11$^{-/-}$ mice (Figure 3A). Furthermore, we used flow cytometry analysis to examine liver macrophages (Figure 3B) and found that HFD promoted F4/80^{+} expression in HMΦs in both Casp11$^{-/-}$ and WT mice (Figures 3C), indicating that HFD-induced NAFLD drives the increase of NASH-related F4/80^{+} HMΦs in WT mice, which are caspase-11 independent.

We examined caspase-11 and GSDMD expression in WT and Casp11$^{-/-}$ HMΦs. We found that HFD increased caspase-11 and GSDMD expression in the inflammatory monocyte (IM) of WT mice while there were no significant changes in Casp11$^{-/-}$ mice (Figure 4A). Liver expressions of IL-1β were significantly increased in WT mice upon HFD-feeding but the trending increase in IL-1β concentrations did not reach statistical significance in Casp11$^{-/-}$ mice fed with HFD compared to Casp11$^{-/-}$ mice fed with NCD (Figure 4B), suggesting that although caspase-1, other caspases (110), and neutrophil elastase (111) that are also capable of cleaving pro-IL1β are not deficient, HFD feeding induced IL-1β generation is mostly attributed by caspase-11 function. These results have demonstrated that HFD induced cytokine responses requires caspase-11.

Since 60% of mouse liver macrophages in disease conditions are derived from the bone marrow (25), to determine whether these changes were due to caspase-11 activity in bone marrow-derived macrophages, we performed bone marrow transplantation (BMT) (36). Bone marrow cells from WT donor mice (CD45.1) were transplanted into either WT recipient mice (CD45.2^{+}) or Casp11$^{-/-}$ mice after irradiation (Figure 4C). WT recipient mice (CD45.2^{+}) that received BM from WT mice (CD45.1^{+}) maintained significantly elevated GSDMD^{+} inflammatory monocytes (IMs) and noncanonical pyroptosis mature HMΦs (Figures 4D, E). Conversely, Casp11$^{-/-}$ recipient mice (CD45.2^{+}) that received bone

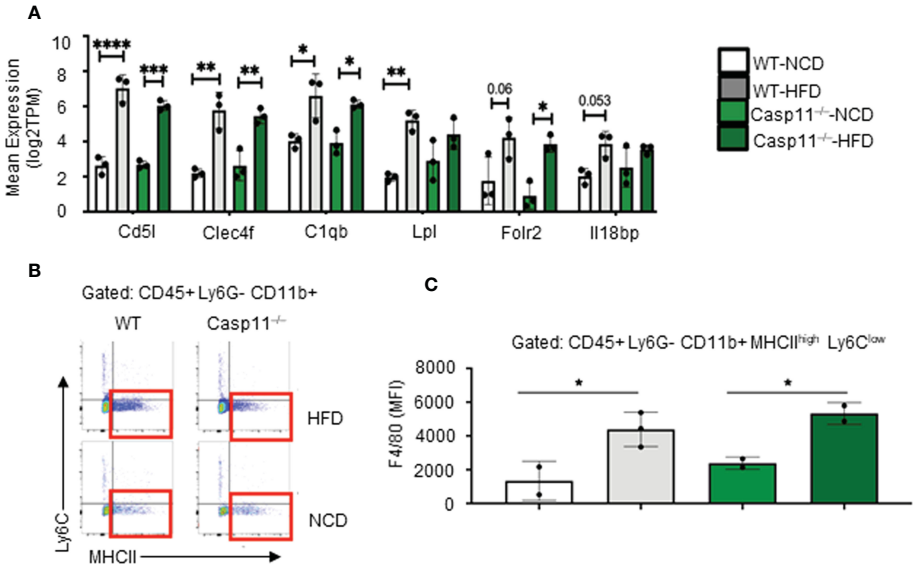

FIGURE 3
High-fat diet (HFD)-induced non-alcoholic fatty liver disease (NAFLD) drives the increase of NASH-related F4/80+ hepatic macrophages (HMΦs) in WT mice, which are caspase-11 activation-independent. 8-10 weeks old male WT and Casp11$^{-/-}$ mice were fed HFD for 12 weeks. **(A)** Bulk RNA-seq expression (TPM) of NASH-associated activated HMΦ genes. **(B)** Representative flow cytometry gating of HMΦ. Gated on CD45+ > CD11b+ Ly6G- > Ly6Clow MHCIIhigh. **(C)** F4/80+ mean fluorescence intensity (MFI) for HMΦ populations. Statistical Analysis: Bulk RNAseq analysis was performed using Qlucore Omics Explorer. PCA generated using significantly differentially regulated genes (p.adj < 0.01). Included genes were significant (p < 0.05) in multi-variant analysis (Two-Way ANOVA). Marked significance (*) determined by One-Way ANOVA. *p < 0.05, **p < 0.001, ***p < 0.0001 ****p < 0.0001. Flow cytometry data was analyzed with FlowJo, and statistical analysis was performed using Prism. One-Way ANOVA.

10.3389/fimmu.2023.1113883

marrow from WT mice (CD45.1^{+}) had significantly regained GSDMD^{+} IM's and noncanonical pyroptosis mature HMΦs (Figures 4D, E). These data indicate that WT mice had more monocyte migration and more hepatic pyroptosis, however, Casp11$^{-/-}$ mice had less monocyte migration and hepatic pyroptosis presumably resulting in an unchanged total number of hepatic macrophages (Figure 4F). Taken together, our results have demonstrated that 1) caspase-11 deficiency significantly reprograms liver transcriptomes in NCD and HFD livers; 2) caspase-11 deficiency attenuates hepatic macrophage pyroptosis in HFD-induced NAFLD; 3) caspase-11 cleaves GSDMD-NT in NCD livers more than that in HFD-induced NAFLD; and 4) BM-derived macrophages play more significant roles than liver resident macrophages in developing and facilitating pyroptosis.

3.5 Caspase-11 deficiency significantly reduced extracellular acidification rates from glycolysis and mitochondrial electron transport chain functions suggesting that caspase-11 contributes to maintain dual fuel bioenergetics — glycolysis and oxidative phosphorylation in macrophages potentially for cholesterol biosynthesis

Our recent paper reported that two pathways such as fatty acid β-oxidation (112) and stearate biosynthesis are upregulated and shared by human NASH, NAFLD mouse models with glycine N-methyltransferase deficiency (GNMT-KO), and high-fat-cholesterol diet (HFCD) models (77). Our Casp11$^{-/-}$ mice showed significant

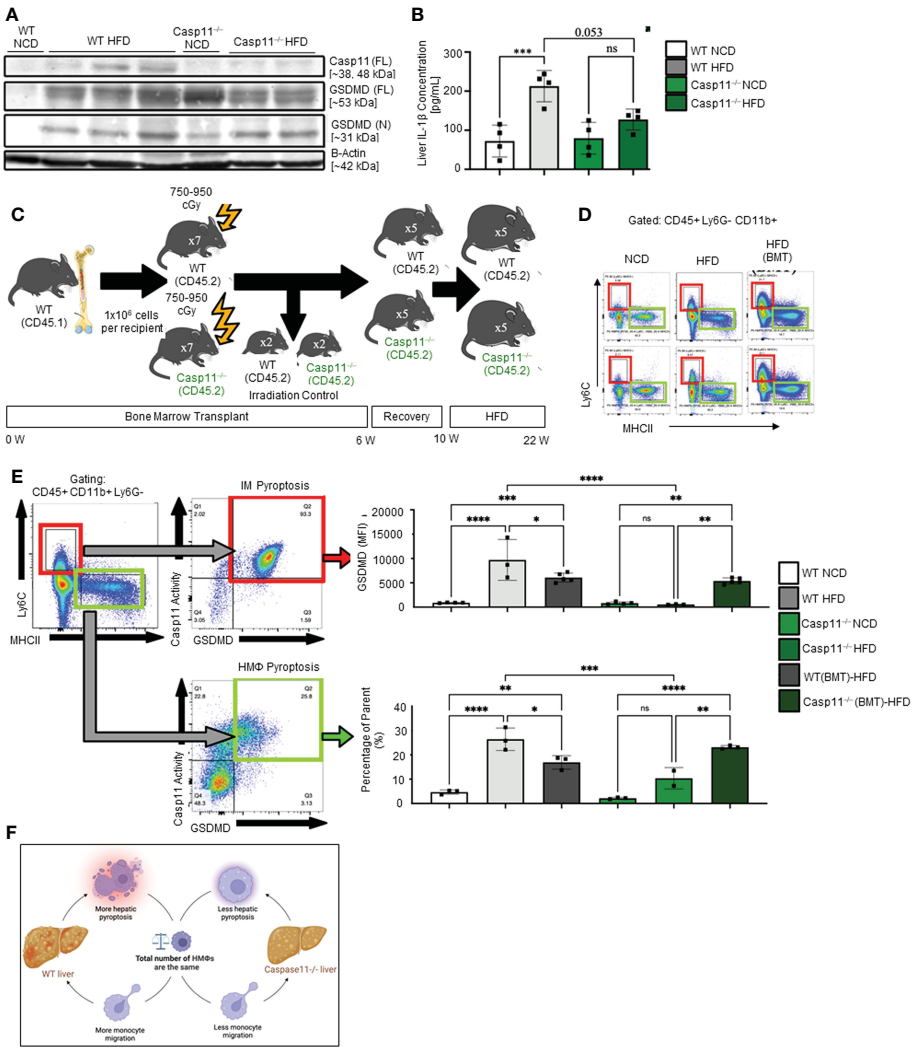

FIGURE 4
Hepatic inflammatory monocyte (IM) and monocyte-derived macrophage (MDM) caspase-11 deficiency protective against pyroptosis, WT bone marrow transplantation to Casp11$^{-/-}$ mice restored IM and MDM pyroptosis. 8-10 weeks old male WT and Casp11$^{-/-}$ mice were fed HFD for 12 weeks. **(A)** Western blot for noncanonical pyroptosis mediators. **(B)** Liver IL-1β concentrations. **(C)** Experimental design for bone marrow transplantation (BMT). **(D)** Representative flow cytometry gating of hepatic macrophages (HMΦ, Green, CD45+ > CD11b+ Ly6G- > Ly6Clow MHCIIhigh) inflammatory monocytes (IM, Red, CD45+ > CD11b+ Ly6G- > Ly6Chigh MHCIIlow). **(E)** Gating strategy for designing pyroptosis populations. HMΦs and IMs gated on GSDMD MFI vs. Casp11-Inhibitor MFI. RED: GSDMD MFI for IM (CD45+ > CD11b+ Ly6G- > Ly6Chigh MHCIIlow). GREEN: Percentage of the parent for HMΦ pyroptosis gating CD45+ > CD11b+ Ly6G- > Ly6Chigh MHCIIlow > Casp11 Activity vs GSDMD). **(F)** Schematic diagram showed that WT mice had more monocyte migration and more hepatic pyroptosis, however, Casp11−/− had less monocyte migration and hepatic pyroptosis resulting in an unchanged total number of hepatic macrophages. Statistical Analysis: Flow cytometry data was analyzed with FlowJo, and statistical analysis was performed using Prism. One-Way ANOVA. One-Way ANOVA. *p < 0.05, **p < 0.001, ***p < 0.0001 ****p < 0.0001. ns, Non-significant.

inhibition of NAFLD (Figure 1), implying that caspase-11 promotes cholesterol biosynthesis and fatty acid β-oxidation. We and others reported that increased acetyl-CoA promotes innate immune memory (trained immunity) (65, 88, 113–116); and fatty acid β-oxidation provides acetyl-CoA to fuel mitochondrial tricarboxylic acid (TCA) cycle and ATP production, which thus may not be limited to M2 macrophages (117). Previous reports showed that proinflammatory fatty acid palmitic acid induces hepatocellular lipotoxicity, endoplasmic reticulum (ER) stress, pyroptosis, and upregulate NLRP3 inflammasome, caspase-1 and IL-1β (118); and that caspase-11 deficiency leads to reduced activations of procaspase-1, IL-1β and caspase-7 and reduced production of glycolysis-promoted CXCL1 (119). In addition, caspase-11 may promote metabolic reprogramming and trained immunity (persistent hyperactivation of inflammation) (65, 113, 114, 120) as our transcriptomic data mining report suggested (77). One report supported this argument and showed that caspase-11 deficiency increases antimycin A-induced mitochondrial reactive oxygen species (mitoROS) (121–126) generation in macrophages (127), implying that caspase-11 inhibits mitochondrial electron transport chain (ETC) dysfunction and contributes the maintenance of mitochondrial ETC functions. We hypothesized that caspase-11 promote mitochondrial ETC functions in macrophages stimulated by palmitic acid. To examine the differences in the operation of mitochondrial energy pathways between WT and Casp11$^{-/-}$ macrophages stimulated by NAFLD, gut derived endotoxins LPS, related (93, 128) proinflammatory saturated fatty acid palmitic acid using the method reported (93), we performed extracellular metabolic flux analysis. The extracellular acidification rates (ECAR) or proton efflux rate (PER), considered a proxy for glycolysis (129), were decreased in Casp11$^{-/-}$ macrophages (Figure 5A). In addition, using the method we reported (87, 124–126), mitochondrial stress test results showed that six mitochondrial electron transport chain (ETC) functions including ATP production, maximal respiration, spare respiratory capacity (uncoupling of OXPHOS induced by carbonyl cyanide-p-trifluoromethoxyphenylhydrazone, FCCP), basal, proton leak and non-mitochondrial oxygen consumption were decreased in Casp11$^{-/-}$ macrophages in comparison to that of WT macrophages in response to palmitic acid stimulation, especially ATP production, basal respiration, maximal respiration, and spare respiratory capacity (Figure 5B). Caspase-11 functions in maintaining both glycolysis and OXPHOS in macrophages stimulated by proinflammatory fatty acid palmitic acid are the same as that unique metabolic activation identified in adipose tissue macrophages (ATM) (130). The significance of the dual fuel bioenergetics in macrophages stimulated by hyperlipidemia and in adipose tissues may be related to an intermediate polarization status, their buffering capacity, or the result of a mixed population of distinctly polarized ATMs (131) and unique functions of caspase-11 in promoting HFD-induced NAFLD potentially by switching/transdifferentiating fatty acid β-oxidation -fueled OXPHOS in M2 macrophages into proinflammatory glycolysis-dominance in M1 macrophages (46). Taken together, these results have demonstrated that caspase-11 contributes significantly to the maintenance of glycolysis and mitochondrial electron transport chain functions in macrophages, in which acetyl-coenzyme A (acetyl-CoA) production is shared between glycolysis (acetyl-CoA transport into mitochondria) and TCA cycle (transport from mitochondria into cytosol for cholesterol synthesis); and both acetyl-CoA generation and cholesterol biosynthesis (132) are the key metabolic pathways for establishing trained immunity (69, 77, 114, 120), which are well correlated with our report on downregulation of 45.6% of 101 trained immunity pathway enzymes (71 glycolysis enzymes, 23 acetyl-CoA generation enzymes and 7 mevalonate synthesis enzymes) in Casp11$^{-/-}$ transcriptome (GSE115094) (133) (77, 114).

4 Discussion

Nonalcoholic fatty liver disease (NAFLD) is the second leading cause of liver transplantation in the United States, and with obesity driven NAFLD on the rise worldwide, there is a great need for NAFLD research and therapeutic development (134, 135). Hepatic macrophage (HMΦ) activation and recruitment are important factors in driving the inflammatory phase of NAFLD and NASH (21, 47–50). While inhibition of macrophage activation and recruitment significantly decreases liver inflammation in NAFLD animal models, this may have unintended side effects due to the prevention of the physiological roles of HMΦs (18, 19, 31, 41–43). Therefore, a more targeted approach is required. Anti-inflammasome therapeutics have been shown to be a viable treatment option for inflammatory metabolic disease (72). While these therapies focus on the canonical pyroptotic pathway, the caspase11-dependent pyroptosis pathway provides a novel target and pathway for the treatment of NAFLD.

Based on our and other's previous publications (77, 114, 136), HFD is one of the major drivers of innate immune memory (trained immunity). Glycolysis, Acetyl CoA generation (cytosolic and OXPHOS generated), increased mevalonate pathway, increased glutaminolysis, TCA cycle metabolite accumulation such as fumarate, and the epigenetic modification have all been identified as critical pathways for establishing trained immunity in trained immune cells. Furthermore, the proinflammatory cytokines including tumor necrosis factor-α (TNF- α), IL-1β, and IL-16 are the major read outs for trained immunity. In addition, inflammasomes control the maturation and secretion of proinflammatory IL-1β and IL-18 through GSDMD pores on the cell membrane and induce an inflammatory cell death (pyroptosis) (137). Therefore, the metabolic reprograming such as glycolysis in trained immune cells enhanced the release of IL1β through N-terminal GSDMD pores and promotes pyroptosis".

The role of caspase-11 in driving pyroptosis in the pathogenesis of NAFLD in methionine- and choline-deficient diet (MCD)-induced NAFLD mouse model has been demonstrated (76). However, the role of caspase-11 in driving pyroptosis in HFD-induced NAFLD mice model have not been studied which we reported in this manuscript. Our team previously examined the expression changes of macrophage markers, macrophage proinflammatory cytokines, and macrophage metabolism genes in 10 macrophage subsets in liver inflammatory diseases, digestive inflammatory diseases, type-1 and type-2 diabetes, metabolic syndrome, and familial hypercholesterolemia and demonstrated that liver inflammatory diseases have predominant M1 macrophage status. In addition, M1 macrophage status have a significant upregulation of proinflammatory cytokine IL-1β, which secreted during pyroptosis mechanisms (138) and also reported in

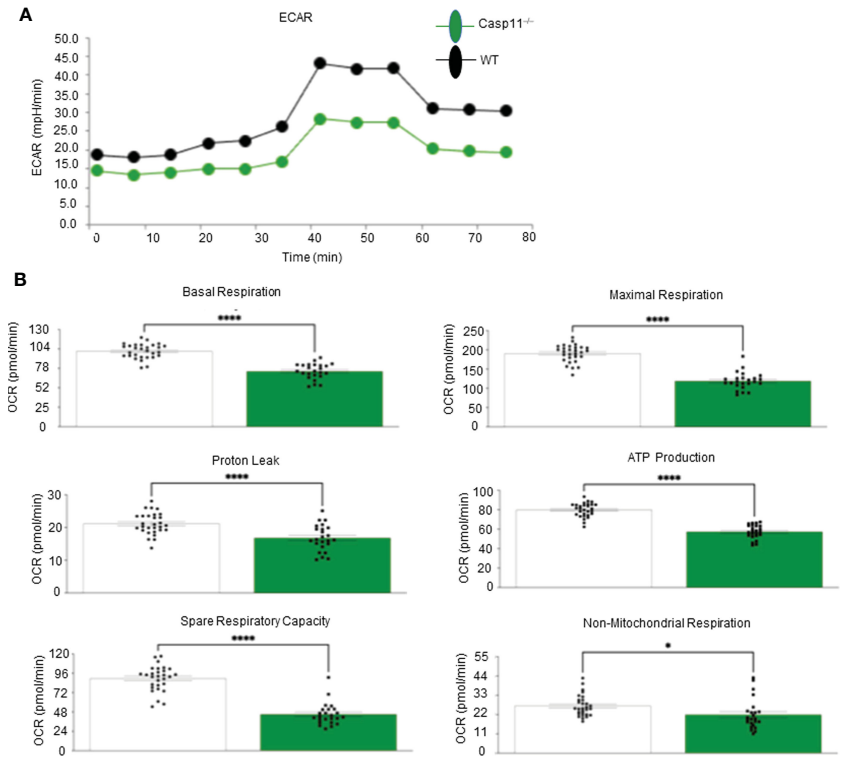

FIGURE 5
Caspase-11 significantly contributes to maintaining dual fuel bioenergetics- glycolysis and OXPHOS in macrophages potentially for cholesterol synthesis and trained immunity. Bone marrow macrophages were isolated from 3 WT and 3 Casp11$^{-/-}$ mice and treated with palmitic acid (500 μM) for 8 hours then pulled for seahorse analysis. **(A)** Seahorse XF96 Extracellular Flux Analyzer to measure extracellular acidification rate (glycolysis) of Casp11$^{-/-}$ vs WT BMDMs in palmitic acid supplemented medium. **(B)** Seahorse mitochondrial function assay of Casp11$^{-/-}$ vs WT BMDMs in palmitic acid supplemented medium.*P < 0.0, ****p < 0.0001.

our recent papers (77, 139). We also found that M1 macrophages related to metabolic diseases have a significant increase in glycolysis while M2 macrophages related to TCA cycle metabolites (46). Therefore, ECAR and OXPHOS are related to cholesterol biosynthesis *via* increasing M1 macrophage glycolysis and increased generation of acetyl CoA which is the initial and key molecule for cholesterol biosynthesis as well as M2 macrophages which increases TCA cycle metabolites. IL-1 β is a major driver and regulator for innate immune memory (trained immunity) which characterized by increased glycolysis, increased acetyl CoA generation, and increased cholesterol biosynthesis (88, 140, 141).

Given the central role of HMΦs in the progression of NAFLD (21, 47, 49, 50) and the significance of pyroptosis in both patients and animal models of NAFLD outlined in our recent publication (77), we hypothesize that caspase-11-dependent pyroptosis promotes NAFLD *via* glycolysis and OXPHOS dual fuel bioenergetics and bone marrow-derived macrophage pyroptosis. We performed histopathological analysis, RNA-seq and scRNA-seq data analysis, FACS, Western blots, Seahorse mitochondrial stress analyses of macrophages and bone marrow transplantation on HFD-induced NAFLD in WT and Casp11$^{-/-}$ mice, we made the following findings: 1) HFD feeding for 12 weeks drives increases NAFLD in WT mice, which are transcriptionally distinct from NCD control mouse livers; 2) Noncanonical pyroptosis mediators including caspase-11, GSDMD, IL-1β, and GBPs are increased in response to HFD; 3) HFD promotes type-I, secretome dominant, caspase-11-GSDMD pyroptosis other than type-II, inflammatory cell death-dominant, caspase-11-GSDMD pyroptosis; 4) Casp11$^{-/-}$ mice have decreased NAFLD (reduced NAS score, steatosis score and lobular inflammation) with no significant liver weight changes; 5) Caspase-11 deficiency significantly decreases liver IL-1β concentrations and GSDMD expression; 6) Caspase-11 deficiency significantly reprogram liver transcriptomes in NCD and HFD livers, attenuates hepatic macrophage pyroptosis in HFD-induced NAFLD; 7) caspase-11 cleaves GSDMD-NT in NCD livers more than that in HFD-induced NAFLD; 8) bone marrow-derived macrophages play more significant roles than liver resident monocytes/macrophages in facilitating pyroptosis; and 9) Caspase-11 significantly contributes to maintain dual fuel bioenergetics — glycolysis and OXPHOS in palmitic acid-stimulated macrophages potentially *via* promoting transition of M2 macrophages into M1 macrophages.

Based on our results, we propose a new working model; as shown in Figure 6, HFD increased hepatic lipid accumulation (steatosis). In addition, HFD promotes increase of gut microbiota Gram-negative bacteria-generated endotoxin LPS, leading to elevations in circulating LPS and metabolic endotoxemia (142), and increased LPS endocytosis (143) and cytosolic LPS. Furthermore, Gram-negative bacteria promoted by HFD enter the blood stream and enter cells, which are mediated by GBPs (144, 145) to increase intracellular bacteria and LPS to activate caspase-11. Caspase-11 activation is triggered by its

interaction with LPS from Gram-negative bacteria. Being an initiator caspase, activated caspase-11 functions primarily through its cleavage of key substrates. GSDMD is the primary substrate of caspase-11, and the N-terminal GSDMD cleavage fragment generated (GSDMD-NT) leads to the formation of pores (protein channels) in the plasma membrane and secretion of caspase-1 produced IL-1β and other caspase-1 dependent secretomes and caspase-11-dependent secretomes (139, 146) into the extracellular space to promote liver inflammation (NASH), and subsequently increased hepatic pyroptosis and promotes NAFLD. Thus, caspase-11 functions as an intracellular sensor for LPS and an innate immune effector. Palmitic acid produced by lipolysis in HFD-fed mice activates caspase-11 and GSDMD cleavage. Furthermore, LPS-induced caspase-11 activation and GSDMD cleavage also maintain dual fuel bioenergetics — glycolysis and OXPHOS. Casp11$^{-/-}$ decreases GSMDM cleavage and IL-1β secretion, reduces liver inflammation, and hepatic pyroptosis. These results provide novel insights on the roles of caspase-11-GSDMD pathway in promoting hepatic macrophage inflammation and pyroptosis and novel targets for future therapeutic interventions involving transition of NAFLD to NASH, hyperlipidemia, type-II

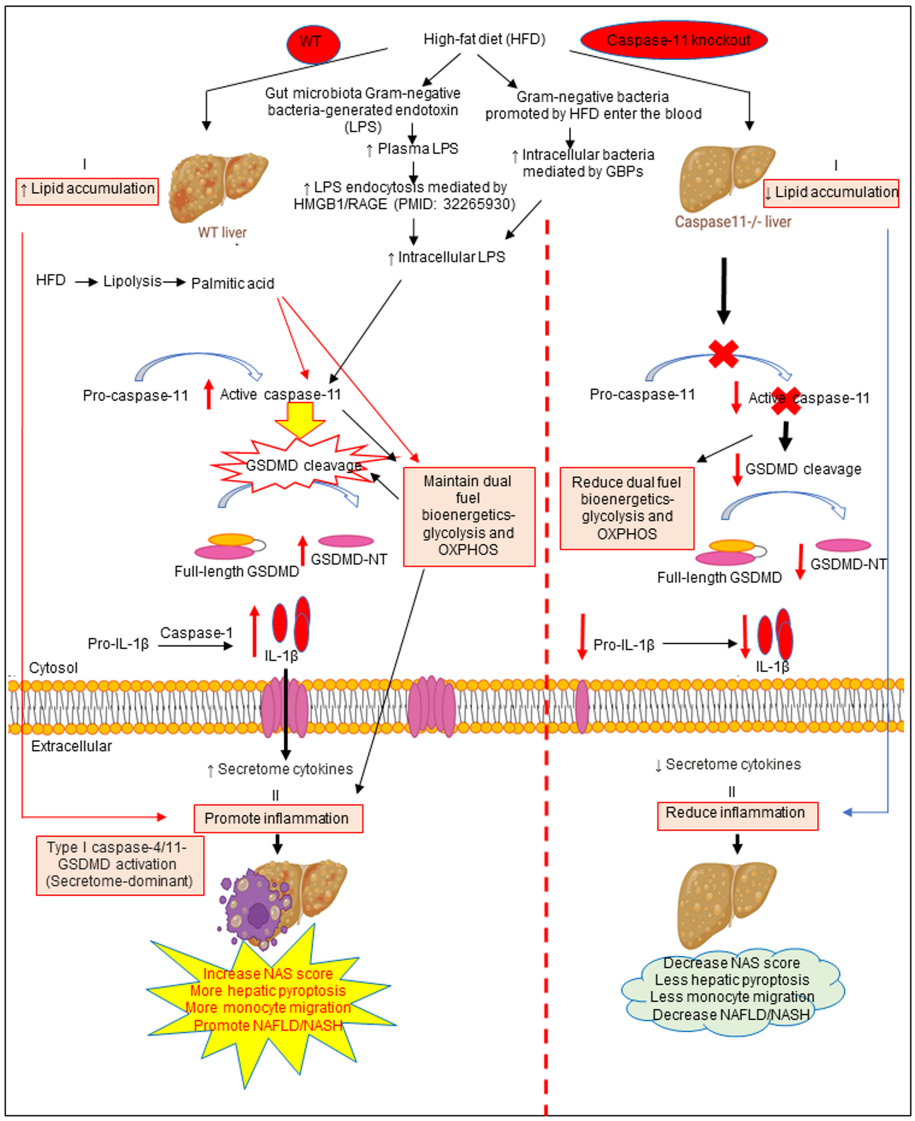

FIGURE 6
The working model showed that HFD increased hepatic lipid accumulation (steatosis). HFD promotes increased gut microbiota Gram-negative bacteria-generated endotoxin LPS leading to elevations in circulating LPS and metabolic endotoxemia and increased LPS endocytosis and intracellular LPS. Gram-negative bacteria promoted by HFD enter the bloodstream and enter cells which are mediated by GBPs to increase intracellular bacteria and LPS to activate caspase-11. Caspase-11 activation is triggered by its interaction with LPS from Gram-negative bacteria. Being an initiator caspase, activated caspase-11 functions primarily through its cleavage of key substrates. GSDMD is the primary substrate of caspase-11, and the GSDMD cleavage fragment generated (GSDMD-NT) leads to the formation of pores in the plasma membrane and secretion of caspase-1 produced IL-1B into the extracellular space to promote liver inflammation (NASH) and subsequently increased hepatic pyroptosis and promotes NAFLD. Thus, caspase-11 functions as an intracellular sensor for LPS and an immune effector. Palmitic acid produced by lipolysis in HFD-fed mice caspase-11 activation and GSDMD cleavage. Furthermore, LPS-induced caspase-11 activation and GSDMD cleavage also maintain dual fuel bioenergetics-glycolysis and OXPHOS and. Casp11$^{-/-}$ decreased GSMDM cleavage and IL-1β secretion, reduced liver inflammation, and hepatic pyroptosis.

diabetes, metabolic syndrome, atherosclerotic cardiovascular diseases, autoimmune diseases, liver transplantation, and hepatic cancers.

Data availability statement

Our RNA sequencing data presented in the study are deposited in the NCBI's Gene Expression Omnibus database repository, accession number GSE221005. Other RNA seq and single cell RNA seq data were obtained the NIH-NCBI-Gene database (https://www.ncbi.nlm.nih.gov/gene/837. Single Cell RNA-seq (scRNA-seq) Porter database from the MIT Broad Institute (https://singlecell.broadinstitute.org/single_cell/study/SCP1845/cross-tissue-immune-cell-analysis-reveals-tissue-specific-features-in-humans?genes=casp4&tab=distribution study-visualize were deposited in the ArrayExpress database at EMBL-EBI (www.ebi.ac.uk/arrayexpress) under accession number E-MTAB-11536).

Ethics statement

The animal study was reviewed and approved by Institutional Animal Care and Use Committee (IACUC) and approved by the IACUC of Lewis Katz School of Medicine (LKSOM) at Temple University.

Author contributions

CD and FS carried out the data gathering, data analysis and prepared the tables and figures. NJ, RC, YSu, KX, YSh, YL, HS, YZ, LY, JY, SW, NS, WH, JZ, YHZ, XJ, HW, aided with analysis of the data. XY supervised the experimental design, data analysis, and manuscript writing. All authors read and approved the final manuscript.

Funding

Our research activities are supported by grants from the National Institutes of Health (NIH)/National Heart, Lung, and Blood Institute (HL131460, HL132399, HL138749, HL147565, DK104116, and DK113775). The content in this article is solely the responsibility of the authors and does not necessarily represent the official views of the NIH. We are very grateful to Dr. Edward A. Miao in the Department of Immunology at Duke University School of Medicine for his most insightful advices and corrections.

Conflict of interest

The authors declare that the research was conducted in the absence of any commercial or financial relationships that could be construed as a potential conflict of interest.

Publisher's note

Supplementary material

The Supplementary Material for this article can be found online at: https://www.frontiersin.org/articles/10.3389/fimmu.2023.1113883/full#supplementary-material

References

1. Brunt EM, Wong VW, Nobili V, Day CP, Sookoian S, Maher JJ, et al. Nonalcoholic fatty liver disease. *Nat Rev Dis Primers* (2015) 1:15080. doi: 10.1038/nrdp.2015.80

2. Ryu JE, Jo W, Choi HJ, Jang S, Lee HJ, Woo DC, et al. Evaluation of nonalcoholic fatty liver disease in C57BL/6J mice by using MRI and histopathologic analyses. *Comp Med* (2015) 65(5):409–15.

3. Van Herck MA, Vonghia L, Francque SM. Animal models of nonalcoholic fatty liver disease-a starter's guide. *Nutrients* (2017) 9(10):1072. doi: 10.3390/nu9101072

4. Sheka AC, Adeyi O, Thompson J, Hameed B, Crawford PA, Ikramuddin S. Nonalcoholic steatohepatitis: A review. *Jama* (2020) 323(12):1175–83. doi: 10.1001/jama.2020.2298

5. Pais R, Barritt AS 4th, Calmus Y, Scatton O, Runge T, Lebray P, et al. NAFLD and liver transplantation: Current burden and expected challenges. *J Hepatol* (2016) 65(6):1245–57. doi: 10.1016/j.jhep.2016.07.033

6. Sayiner M, Koenig A, Henry L, Younossi ZM. Epidemiology of nonalcoholic fatty liver disease and nonalcoholic steatohepatitis in the united states and the rest of the world. *Clin Liver Dis* (2016) 20(2):205–14. doi: 10.1016/j.cld.2015.10.001

7. Younossi Z, Henry L. Contribution of alcoholic and nonalcoholic fatty liver disease to the burden of liver-related morbidity and mortality. *Gastroenterology* (2016) 150(8):1778–85. doi: 10.1053/j.gastro.2016.03.005

8. Younossi ZM, Koenig AB, Abdelatif D, Fazel Y, Henry L, Wymer M. Global epidemiology of nonalcoholic fatty liver disease-meta-analytic assessment of prevalence, incidence, and outcomes. *Hepatology* (2016) 64(1):73–84. doi: 10.1002/hep.28431

9. Kim CH, Younossi ZM. Nonalcoholic fatty liver disease: a manifestation of the metabolic syndrome. *Cleve Clin J Med* (2008) 75(10):721–8. doi: 10.3949/ccjm.75.10.721

10. Virtue A, Johnson C, Lopez-Pastraña J, Shao Y, Fu H, Li X, et al. MicroRNA-155 deficiency leads to decreased atherosclerosis, increased white adipose tissue obesity, and non-alcoholic fatty liver disease: A NOVEL MOUSE MODEL OF OBESITY PARADOX. *J Biol Chem* (2017) 292(4):1267–87. doi: 10.1074/jbc.M116.739839

11. Johnson C, Drummer C 4th, Virtue A, Gao T, Wu S, Hernandez M, et al. Increased expression of resistin in MicroRNA-155-Deficient white adipose tissues may be a possible driver of metabolically healthy obesity transition to classical obesity. *Front Physiol* (2018) 9:1297. doi: 10.3389/fphys.2018.01297

12. Johnson C, Drummer C Iv, Shan H, Shao Y, Sun Y, Lu Y, et al. A novel subset of CD95(+) pro-inflammatory macrophages overcome miR155 deficiency and may serve as a switch from metabolically healthy obesity to metabolically unhealthy obesity. *Front Immunol* (2020) 11:619951. doi: 10.3389/fimmu.2020.619951

13. Valencia-Rodriguez A, Vera-Barajas A, Barranco-Fragoso B, Kúsulas-Delint D, Qi X, et al. New insights into the association between non-alcoholic fatty liver disease and atherosclerosis. *Ann Transl Med* (2019) 7(Suppl 8):S300. doi: 10.21037/atm.2019.11.13

14. Zhou YY, Zhou XD, Wu SJ, Fan DH, Van Poucke S, Chen YP, et al. Nonalcoholic fatty liver disease contributes to subclinical atherosclerosis: A systematic review and meta-analysis. *Hepatol Commun* (2018) 2(4):376–92. doi: 10.1002/hep4.1155

15. Sakhuja P. Pathology of alcoholic liver disease, can it be differentiated from nonalcoholic steatohepatitis? *World J Gastroenterol* (2014) 20(44):16474–9. doi: 10.3748/wjg.v20.i44.16474

16. Gluchowski NL, et al. Lipid droplets and liver disease: from basic biology to clinical implications. *Nat Rev Gastroenterol Hepatol* (2017) 14(6):343–55. doi: 10.1038/nrgastro.2017.32

17. Hirsova P, Ibrabim SH, Gores GJ, Malhi H. Lipotoxic lethal and sublethal stress signaling in hepatocytes: relevance to NASH pathogenesis. *J Lipid Res* (2016) 57 (10):1758–70. doi: 10.1194/jlr.R066357

18. Lopez BG, Tsai MS, Baratta JL, Longmuir KJ, Robertson RT. Characterization of kupffer cells in livers of developing mice. *Comp Hepatol* (2011) 10(1):2. doi: 10.1186/1476-5926-10-2

19. Ju C, Tacke F. Hepatic macrophages in homeostasis and liver diseases: from pathogenesis to novel therapeutic strategies. *Cell Mol Immunol* (2016) 13(3):316–27. doi: 10.1038/cmi.2015.104

20. Guilliams M, Dutertre CA, Scott CL, McGovern N, Sichien D, Chakarov S, et al. Unsupervised high-dimensional analysis aligns dendritic cells across tissues and species. *Immunity* (2016) 45(3):669–84. doi: 10.1016/j.immuni.2016.08.015

21. Krenkel O, Tacke F. Liver macrophages in tissue homeostasis and disease. *Nat Rev Immunol* (2017) 17(5):306–21. doi: 10.1038/nri.2017.11

22. MacParland SA, Liu JC, Ma XZ, Innes BT, Bartczak AM, Gage BK, et al. Single cell RNA sequencing of human liver reveals distinct intrahepatic macrophage populations. *Nat Commun* (2018) 9(1):4383. doi: 10.1038/s41467-018-06318-7

23. Seidman JS, Troutman TD, Sakai M, Gola A, Spann NJ, Bennett H, et al. Niche-specific reprogramming of epigenetic landscapes drives myeloid cell diversity in nonalcoholic steatohepatitis. *Immunity* (2020) 52(6):1057–1074.e7. doi: 10.1016/j.immuni.2020.04.001

24. Sakai M, Troutman TD, Seidman JS, Ouyang Z, Spann NJ, Abe Y, et al. Liver-derived signals sequentially reprogram myeloid enhancers to initiate and maintain kupffer cell identity. *Immunity* (2019) 51(4):655–670.e8. doi: 10.1016/j.immuni.2019.09.002

25. Barreby E, Chen P, Aouadi M. Macrophage functional diversity in NAFLD - more than inflammation. *Nat Rev Endocrinol* (2022) 18(8):461–72. doi: 10.1038/s41574-022-00675-6

26. Kazankov K, Jørgensen SMD, Thomsen KL, Møller HJ, Vilstrup H, George J, et al. The role of macrophages in nonalcoholic fatty liver disease and nonalcoholic steatohepatitis. *Nat Rev Gastroenterol Hepatol* (2019) 16(3):145–59. doi: 10.1038/s41575-018-0082-x

27. Scott CL, Zheng F, De Baetselier P, Martens L, Saeys Y, De Prijck S, et al. Bone marrow-derived monocytes give rise to self-renewing and fully differentiated kupffer cells. *Nat Commun* (2016) 7:10321. doi: 10.1038/ncomms10321

28. Heymann F, Hammerich L, Storch D, Bartneck M, Huss S, Rüsseler V, et al. Hepatic macrophage migration and differentiation critical for liver fibrosis is mediated by the chemokine receptor c-c motif chemokine receptor 8 in mice. *Hepatology* (2012) 55 (3):898–909. doi: 10.1002/hep.24764

29. David BA, Rezende RM, Antunes MM, Santos MM, Freitas Lopes MA, Diniz AB, et al. Combination of mass cytometry and imaging analysis reveals origin, location, and functional repopulation of liver myeloid cells in mice. *Gastroenterology* (2016) 151 (6):1176–91. doi: 10.1053/j.gastro.2016.08.024

30. Beattie L, Sawtell A, Mann J, Frame TCM, Teal B, de Labastida Rivera F, et al. Bone marrow-derived and resident liver macrophages display unique transcriptomic signatures but similar biological functions. *J Hepatol* (2016) 65(4):758–68. doi: 10.1016/j.jhep.2016.05.037

31. Tacke F, Zimmermann HW. Macrophage heterogeneity in liver injury and fibrosis. *J Hepatol* (2014) 60(5):1090–6. doi: 10.1016/j.jhep.2013.12.025

32. Ramachandran P, Pellicoro A, Vernon MA, Boulter L, Aucott RL, Ali A, et al. Differential ly-6C expression identifies the recruited macrophage phenotype, which orchestrates the regression of murine liver fibrosis. *Proc Natl Acad Sci U.S.A.* (2012) 109(46):E3186–95. doi: 10.1073/pnas.1119964109

33. Pellicoro A, Ramachandran P, Iredale JP, Fallowfield JA. Liver fibrosis and repair: immune regulation of wound healing in a solid organ. *Nat Rev Immunol* (2014) 14 (3):181–94. doi: 10.1038/nri3623

34. Mehal WZ, Schuppan D. Antifibrotic therapies in the liver. *Semin Liver Dis* (2015) 35(2):184–98. doi: 10.1055/s-0035-1550055

35. Karlmark KR, Weiskirchen R, Zimmermann HW, Gassler N, Ginhoux F, Weber C, et al. Hepatic recruitment of the inflammatory Gr1+ monocyte subset upon liver injury promotes hepatic fibrosis. *Hepatology* (2009) 50(1):261–74. doi: 10.1002/hep.22950

36. Saaoud F, Wang J, Iwanowycz S, Wang Y, Altomare D, Shao Y, et al. Bone marrow deficiency of mRNA decaying protein tristetraprolin increases inflammation and mitochondrial ROS but reduces hepatic lipoprotein production in LDLR knockout mice. *Redox Biol* (2020) 37:101609. doi: 10.1016/j.redox.2020.101609

37. Liaskou E, et al. Monocyte subsets in human liver disease show distinct phenotypic and functional characteristics. *Hepatology* (2013) 57(1):385–98. doi: 10.1002/hep.26016

38. Lavin Y, Winter D, Blecher-Gonen R, David E, Keren-Shaul H, Merad M, et al. Tissue-resident macrophage enhancer landscapes are shaped by the local microenvironment. *Cell* (2014) 159(6):1312–26. doi: 10.1016/j.cell.2014.11.018

39. Ingersoll MA, Spanbroek R, Lottaz C, Gautier EL, Frankenberger M, Hoffmann R, et al. Comparison of gene expression profiles between human and mouse monocyte subsets. *Blood* (2010) 115(3):e10–9. doi: 10.1182/blood-2009-07-235028

40. Gao B, Jeong WI, Tian Z. Liver: An organ with predominant innate immunity. *Hepatology* (2008) 47(2):729–36. doi: 10.1002/hep.22034

41. Willekens FL, Werre JM, Kruijt JK, Roerdinkholder-Stoelwinder B, Groenen-Döpp YA, van den Bos AG, et al. Liver kupffer cells rapidly remove red blood cell-derived vesicles from the circulation by scavenger receptors. *Blood* (2005) 105(5):2141–5. doi: 10.1182/blood-2004-04-1578

42. Naito M, Hasegawa G, Ebe Y, Yamamoto T. Differentiation and function of kupffer cells. *Med Electron Microsc* (2004) 37(1):16–28. doi: 10.1007/s00795-003-0228-x

43. Gammella E, et al. Macrophages: central regulators of iron balance. *Metallomics* (2014) 6(8):1336–45. doi: 10.1039/C4MT00104D

44. Mossanen JC, Krenkel O, Ergen C, Govaere O, Liepelt A, Puengel T, et al. Chemokine (C-c motif) receptor 2-positive monocytes aggravate the early phase of acetaminophen-induced acute liver injury. *Hepatology* (2016) 64(5):1667–82. doi: 10.1002/hep.28682

45. Dal-Secco D, Wang J, Zeng Z, Kolaczkowska E, Wong CH, Petri B, et al. A dynamic spectrum of monocytes arising from the in situ reprogramming of CCR2+ monocytes at a site of sterile injury. *J Exp Med* (2015) 212(4):447–56. doi: 10.1084/jem.20141539

46. Lai B, Wang J, Fagenson A, Sun Y, Saredy J, Lu Y, et al. Twenty novel disease group-specific and 12 new shared macrophage pathways in eight groups of 34 diseases including 24 inflammatory organ diseases and 10 types of tumors. *Front Immunol* (2019) 10:2612. doi: 10.3389/fimmu.2019.02612

47. Wu S, Wu F, Ding Y, Hou J, Bi J, Zhang Z. Association of non-alcoholic fatty liver disease with major adverse cardiovascular events: A systematic review and meta-analysis. *Sci Rep* (2016) 6:33386. doi: 10.1038/srep33386

48. Wu R, Nakatsu G, Zhang X, Yu J. Pathophysiological mechanisms and therapeutic potentials of macrophages in non-alcoholic steatohepatitis. *Expert Opin Ther Targets* (2016) 20(5):615–26. doi: 10.1517/14728222.2016.1125883

49. Reid DT, Reyes JL, McDonald BA, Vo T, Reimer RA, Eksteen B. Kupffer cells undergo fundamental changes during the development of experimental NASH and are critical in initiating liver damage and inflammation. *PloS One* (2016) 11(7):e0159524. doi: 10.1371/journal.pone.0159524

50. Krenkel O, Tacke F. Macrophages in nonalcoholic fatty liver disease: A role model of pathogenic immunometabolism. *Semin Liver Dis* (2017) 37(3):189–97. doi: 10.1055/s-0037-1604480

51. Tacke F. Cenicriviroc for the treatment of non-alcoholic steatohepatitis and liver fibrosis. *Expert Opin Investig Drugs* (2018) 27(3):301–11. doi: 10.1080/13543784.2018.1442436

52. Lefebvre E, Moyle G, Reshef R, Richman LP, Thompson M, Hong F, et al. Antifibrotic effects of the dual CCR2/CCR5 antagonist cenicriviroc in animal models of liver and kidney fibrosis. *PloS One* (2016) 11(6):e0158156. doi: 10.1371/journal.pone.0158156

53. Friedman S, Sanyal A, Goodman Z, Lefebvre E, Gottwald M, Fischer L, et al. Efficacy and safety study of cenicriviroc for the treatment of non-alcoholic steatohepatitis in adult subjects with liver fibrosis: CENTAUR phase 2b study design. *Contemp Clin Trials* (2016) 47:356–65. doi: 10.1016/j.cct.2016.02.012

54. Krenkel O, Puengel T, Govaere O, Abdallah AT, Mossanen JC, Kohlhepp M, et al. Therapeutic inhibition of inflammatory monocyte recruitment reduces steatohepatitis and liver fibrosis. *Hepatology* (2018) 67(4):1270–83. doi: 10.1002/hep.29544

55. Yang XF, Yin Y, Wang H. Vascular inflammation and atherogenesis are activated via receptors for pamps and suppressed by regulatory T cells. *Drug Discovery Today Ther Strateg* (2008) 5(2):125–42. doi: 10.1016/j.ddstr.2008.11.003

56. Yin Y, Li X, Sha X, Xi H, Li YF, Shao Y, et al. Early hyperlipidemia promotes endothelial activation via a caspase-1-sirtuin 1 pathway. *Arterioscler Thromb Vasc Biol* (2015) 35(4):804–16. doi: 10.1161/ATVBAHA.115.305282

57. Yin Y, Pastrana JL, Li X, Huang X, Mallilankaraman K, Choi ET, et al. Inflammasomes: sensors of metabolic stresses for vascular inflammation. *Front Biosci* (2013) 18:638–49. doi: 10.2741/4127

58. Yin Y, Yan Y, Jiang X, Mai J, Chen NC, Wang H, et al. Inflammasomes are differentially expressed in cardiovascular and other tissues. *Int J Immunopathol Pharmacol* (2009) 22(2):311–22. doi: 10.1177/039463200902200208

59. Shen J, Yin Y, Mai J, Xiong X, Pansuria M, Liu J, et al. Caspase-1 recognizes extended cleavage sites in its natural substrates. *Atherosclerosis* (2010) 210(2):422–9. doi: 10.1016/j.atherosclerosis.2009.12.017

60. Lopez-Pastrana J, Ferrer LM, Li YF, Xiong X, Xi H, Cueto R, et al. Inhibition of caspase-1 activation in endothelial cells improves angiogenesis -a novel therapeutic potential for ischemia. *J Biol Chem* (2015) 290(28):17485–94. doi: 10.1074/jbc.M115.641191

61. Li YF, Huang X, Li X, Gong R, Yin Y, Nelson J, et al. Caspase-1 mediates hyperlipidemia-weakened progenitor cell vessel repair. *Front Biosci* (2016) 21:178–91. doi: 10.2741/4383

62. Wang L, Fu H, Nanayakkara G, Li Y, Shao Y, Johnson C, et al. Novel extracellular and nuclear caspase-1 and inflammasomes propagate inflammation and regulate gene expression: a comprehensive database mining study. *J Hematol Oncol* (2016) 9(1):122. doi: 10.1186/s13045-016-0351-5

63. Wang J, Lai B, Nanayakkara G, Yang Q, Sun Y, Lu Y, et al. Experimental data-mining analyses reveal new roles of low-intensity ultrasound in differentiating cell death regulatome in cancer and non-cancer cells via potential modulation of chromatin long-range interactions. *Front Oncol* (2019) 9:600. doi: 10.3389/fonc.2019.00600

64. Ferrer LM, Monroy AM, Lopez-Pastrana J, Nanayakkara G, Cueto R, Li YF, et al. Caspase-1 plays a critical role in accelerating chronic kidney disease-promoted neointimal hyperplasia in the carotid artery. *J Cardiovasc Transl Res* (2016) 9(2):135–44. doi: 10.1007/s12265-016-9683-3

65. Fagenson AM, Xu K, Saaoud F, Nanayakkara G, Jhala NC, Liu L, et al. Liver ischemia reperfusion injury, enhanced by trained immunity, is attenuated in caspase 1/Caspase 11 double gene knockout mice. *Pathogens* (2020) 9(11):879. doi: 10.3390/pathogens9110879

66. Yang J, Fang P, Yu D, Zhang L, Zhang D, Jiang X, et al. Chronic kidney disease induces inflammatory CD40+ monocyte differentiation via homocysteine elevation and

DNA hypomethylation. *Circ Res* (2016) 119(11):1226–41. doi: 10.1161/CIRCRESAHA.116.308750

67. Xi H, Zhang Y, Xu Y, Yang WY, Jiang X, Sha X, et al. Caspase-1 inflammasome activation mediates homocysteine-induced pyrop-apoptosis in endothelial cells. *Circ Res* (2016) 118(10):1525–39. doi: 10.1161/CIRCRESAHA.116.308501

68. Xu K, Khan M, Yu J, Snyder NW, Wu S, Vazquez-Padron RI, et al. Editorial: Insights in cardiovascular therapeutics: 2021 - cell death, cardiovascular injuries, and novel targets of cardiovascular therapeutics. *Front Cardiovasc Med* (2022) 9:981544. doi: 10.3389/fcvm.2022.981544

69. Shao Y, Saredy J, Yang WY, Sun Y, Lu Y, Saaoud F, et al. Vascular endothelial cells and innate immunity. *Arterioscler Thromb Vasc Biol* (2020) 40(6):e138–52. doi: 10.1161/ATVBAHA.120.314330

70. Lu Y, Nanayakkara G, Sun Y, Liu L, Xu K, Drummer CT, et al. Procaspase-1 patrolled to the nucleus of proatherogenic lipid LPC-activated human aortic endothelial cells induces ROS promoter CYP1B1 and strong inflammation. *Redox Biol* (2021) 47:102142. doi: 10.1016/j.redox.2021.102142

71. Wei X, Xie F, Zhou X, Wu Y, Yan H, Liu T, et al. Role of pyroptosis in inflammation and cancer. *Cell Mol Immunol* (2022) 19(9):971–92. doi: 10.1038/s41423-022-00905-x

72. Colak Y, Hasan B, Erkalma B, Tandon K, Zervos X, Menzo EL, et al. Pathogenetic mechanisms of nonalcoholic fatty liver disease and inhibition of the inflammasome as a new therapeutic target. *Clin Res Hepatol Gastroenterol* (2021) 45(4):101710. doi: 10.1016/j.clinre.2021.101710

73. de Carvalho Ribeiro M, Szabo G. Role of the inflammasome in liver disease. *Annu Rev Pathol* (2022) 17:345–65. doi: 10.1146/annurev-pathmechdis-032521-102529

74. Dixon LJ, Flask CA, Papouchado BG, Feldstein AE, Nagy LE. Caspase-1 as a central regulator of high fat diet-induced non-alcoholic steatohepatitis. *PloS One* (2013) 8 (2):e56100. doi: 10.1371/journal.pone.0056100

75. Yi YS. Regulatory roles of caspase-11 non-canonical inflammasome in inflammatory liver diseases. *Int J Mol Sci* (2022) 23(9):4986. doi: 10.3390/ijms23094986

76. Zhu Y, Zhao H, Lu J, Lin K, Ni J, Wu G, et al. Caspase-11-Mediated hepatocytic pyroptosis promotes the progression of nonalcoholic steatohepatitis. *Cell Mol Gastroenterol Hepatol* (2021) 12(2):653–64. doi: 10.1016/j.jcmgh.2021.04.009

77. Drummer CIV, Saaoud F, Sun Y, Atar D, Xu K, Lu Y, et al. Hyperlipidemia may synergize with hypomethylation in establishing trained immunity and promoting inflammation in NASH and NAFLD. *J Immunol Res 2021* (2021) p:3928323. doi: 10.1155/2021/3928323

78. Kang R, Zeng L, Zhu S, Xie Y, Liu J, Wen Q, et al. Lipid peroxidation drives gasdermin d-mediated pyroptosis in lethal polymicrobial sepsis. *Cell Host Microbe* (2018) 24(1):97–108.e4. doi: 10.1016/j.chom.2018.05.009

79. Chu LH, Indramohan M, Ratsimandresey RA, Gangopadhyay A, Morris EP, Monack DM, et al. The oxidized phospholipid oxPAPC protects from septic shock by targeting the non-canonical inflammasome in macrophages. *Nat Commun* (2018) 9 (1):996. doi: 10.1038/s41467-018-03409-3

80. Zanoni I, Tan Y, Di Gioia M, Broggi A, Ruan J, Shi J, et al. An endogenous caspase-11 ligand elicits interleukin-1 release from living dendritic cells. *Science* (2016) 352 (6290):1232–6. doi: 10.1126/science.aaf3036

81. Bruneau A, Hundertmark J, Guillot A, Tacke F. Molecular and cellular mediators of the gut-liver axis in the progression of liver diseases. *Front Med* (2021) 8:725390. doi: 10.3389/fmed.2021.725390

82. Fei N, Bruneau A, Zhang X, Wang R, Wang J, Rabot S, et al. Endotoxin producers overgrowing in human gut microbiota as the causative agents for nonalcoholic fatty liver disease. *mBio* (2020) 11(1):e03263–19. doi: 10.1128/mBio.03263-19

83. Wong VW, Wong GL, Chan HY, Yeung DK, Chan RS, Chim AM, et al. Bacterial endotoxin and non-alcoholic fatty liver disease in the general population: a prospective cohort study. *Aliment Pharmacol Ther* (2015) 42(6):731–40. doi: 10.1111/apt.13327

84. Harte AL, da Silva NF, Creely SJ, McGee KC, Billyard T, Youssef-Elabd EM, et al. Elevated endotoxin levels in non-alcoholic fatty liver disease. *J Inflammation* (2010) 7:15. doi: 10.1186/1476-9255-7-15

85. Brunt EM. Grading and staging the histopathological lesions of chronic hepatitis: the knodell histology activity index and beyond. *Hepatology* (2000) 31(1):241–6. doi: 10.1002/hep.510310136

86. Brunt EM, Janney CG, Di Bisceglie AM, Neuschwander-Tetri BA, Bacon BR. Nonalcoholic steatohepatitis: a proposal for grading and staging the histological lesions. *Am J Gastroenterol* (1999) 94(9):2467–74. doi: 10.1111/j.1572-0241.1999.01377.x

87. Li X, Fang P, Li Y, Kuo Y-M, Andrews AJ, Nanayakkara G, et al. Mitochondrial reactive oxygen species mediate lysophosphatidylcholine-induced endothelial cell ActivationHighlights. *Arteriosclerosis Thrombosis Vasc Biol* (2016) 36(6):1090–100. doi: 10.1161/ATVBAHA.115.306964

88. Saaoud F, Liu L, Xu K, Cueto R, Shao Y, Lu Y, et al. Aorta- and liver-generated TMAO enhances trained immunity for increased inflammation via ER stress-mitochondrial ROS/glycolysis pathways. *JCI Insight* (2022) 8(1):e158183. doi: 10.1172/jci.insight.158183

89. Chiappini F, Coilly A, Kadar H, Gual P, Tran A, Desterke C, et al. Metabolism dysregulation induces a specific lipid signature of nonalcoholic steatohepatitis in patients. *Sci Rep* (2017) 7:46658. doi: 10.1038/srep46658

90. Ratziu V, Giral P, Charlotte F, Bruckert E, Thibault V, Theodorou I, et al. Liver fibrosis in overweight patients. *Gastroenterology* (2000) 118(6):1117–23. doi: 10.1016/S0016-5085(00)70364-7

91. Marchesini G, Brizi M, Morselli-Labate AM, Bianchi G, Bugianesi E, McCullough AJ, et al. Association of nonalcoholic fatty liver disease with insulin resistance. *Am J Med* (1999) 107(5):450–5. doi: 10.1016/S0002-9343(99)00271-5

92. Lau JKC, Zhang X, Yu J. Animal models of non-alcoholic fatty liver diseases and its associated liver cancer. *Adv Exp Med Biol* (2018) 1061:139–47. doi: 10.1007/978-981-10-8684-7_11

93. Li Y, Lu Z, Ru JH, Lopes-Virella MF, Lyons TJ, Huang Y. Saturated fatty acid combined with lipopolysaccharide stimulates a strong inflammatory response in hepatocytes in vivo and in vitro. *Am J Physiol Endocrinol Metab* (2018) 315(5):E745–57. doi: 10.1152/ajpendo.00015.2018

94. Eccleston HB, Andringa KK, Betancourt AM, King AL, Mantena SK, Swain TM, et al. Chronic exposure to a high-fat diet induces hepatic steatosis, impairs nitric oxide bioavailability, and modifies the mitochondrial proteome in mice. *Antioxid Redox Signal* (2011) 15(2):447–59. doi: 10.1089/ars.2010.3395

95. Vernon H, Wehrle CJ, Kasi A. Anatomy, abdomen and pelvis, liver. In: *StatPearls*. Treasure Island (FL: StatPearls Publishing LLC (2022).

96. Finethy R, Luoma S, Orench-Rivera N, Feeley EM, Haldar AK, Yamamoto M, et al. Inflammasome activation by bacterial outer membrane vesicles requires guanylate binding proteins. *mBio* (2017) 8(5):e01188–17. doi: 10.1128/mBio.01188-17

97. Agnew A, Nulty C, Creagh EM. Regulation, activation and function of caspase-11 during health and disease. *Int J Mol Sci* (2021) 22(4):1506. doi: 10.3390/ijms22041506

98. Finethy R, Luoma S, Orench-Rivera N, Feeley EM, Haldar AK, Yamamoto M, et al. Dynamin-related irgm proteins modulate LPS-induced caspase-11 activation and septic shock. *EMBO Rep* (2020) 21(11):e50830. doi: 10.15252/embr.202050830

99. Ruhl S, Broz P. Regulation of lytic and non-lytic functions of gasdermin pores. *J Mol Biol* (2022) 434(4):167246. doi: 10.1016/j.jmb.2021.167246

100. Karmakar M, Minns M, Greenberg EN, Diaz-Aponte J, Pestonjamasp K, Johnson JL, et al. N-GSDMD trafficking to neutrophil organelles facilitates IL-1beta release independently of plasma membrane pores and pyroptosis. *Nat Commun* (2020) 11 (1):2212. doi: 10.1038/s41467-020-16043-9

101. Cai C, Zhu X, Li P, Li J, Gong J, Shen W, et al. NLRP3 deletion inhibits the non-alcoholic steatohepatitis development and inflammation in kupffer cells induced by palmitic acid. *Inflammation* (2017) 40(6):1875–83. doi: 10.1007/s10753-017-0628-z

102. Szabo G, Petrasek J. Inflammasome activation and function in liver disease. *Nat Rev Gastroenterol Hepatol* (2015) 12(7):387–400. doi: 10.1038/nrgastro.2015.94

103. Fagerberg L, Hallström BM, Oksvold P, Kampf C, Djureinovic D, Odeberg J, et al. Analysis of the human tissue-specific expression by genome-wide integration of transcriptomics and antibody-based proteomics. *Mol Cell Proteomics* (2014) 13(2):397–406. doi: 10.1074/mcp.M113.035600

104. Domínguez Conde C, Xu C, Jarvis LB, Rainbow DB, Wells SB, Gomes T, et al. Cross-tissue immune cell analysis reveals tissue-specific features in humans. *Science* (2022) 376(6594):eabl5197. doi: 10.1126/science.abl5197

105. Yen JH, Ganea D. Interferon beta induces mature dendritic cell apoptosis through caspase-11/caspase-3 activation. *Blood* (2009) 114(7):1344–54. doi: 10.1182/blood-2008-12-196592

106. Pilla-Moffett D, Barber MF, Taylor GA, Coers J. Interferon-inducible GTPases in host resistance, inflammation and disease. *J Mol Biol* (2016) 428(17):3495–513. doi: 10.1016/j.jmb.2016.04.032

107. Shao C, Ye J, Li X, Lin Y, Feng S, Liao B, et al. Discrepancies between nonalcoholic and metabolic-associated fatty liver disease by multiple steatosis assessment. *J Clin Transl Hepatol* (2022) 10(6):1013–26. doi: 10.14218/JCTH.2021.00371

108. Takahashi Y, Fukusato T. Histopathology of nonalcoholic fatty liver disease/nonalcoholic steatohepatitis. *World J Gastroenterol* (2014) 20(42):15539–48. doi: 10.3748/wjg.v20.i42.15539

109. Jiang M, Sun X, Liu S, Tang Y, Shi Y, Bai Y, et al. Caspase-11-Gasdermin d-mediated pyroptosis is involved in the pathogenesis of atherosclerosis. *Front Pharmacol* (2021) 12:657486. doi: 10.3389/fphar.2021.657486

110. Liu X, Xia S, Zhang Z, Wu H, Lieberman J.. Channelling inflammation: gasdermins in physiology and disease. *Nat Rev Drug Discovery* (2021) 20(5):384–405. doi: 10.1038/s41573-021-00154-z

111. Chen KW, Demarco B, Broz P. Beyond inflammasomes: emerging function of gasdermins during apoptosis and NETosis. *EMBO J* (2020) 39(2):e103397. doi: 10.15252/embj.2019103397

112. Nan J, Lee JS, Lee SA, Lee DS, Park KS, Chung SS. An essential role of the n-terminal region of ACSL1 in linking free fatty acids to mitochondrial beta-oxidation in C2C12 myotubes. *Mol Cells* (2021) 44(9):637–46. doi: 10.14348/molcells.2021.0077

113. Lu Y, Sun Y, Drummer CT, Nanayakkara GK, Shao Y, Saaoud F, et al. Increased acetylation of H3K14 in the genomic regions that encode trained immunity enzymes in lysophosphatidylcholine-activated human aortic endothelial cells - novel qualification markers for chronic disease risk factors and conditional DAMPs. *Redox Biol* (2019) 24:101221. doi: 10.1016/j.redox.2019.101221

114. Drummer CT, Saaoud F, Shao Y, Sun Y, Xu K, Lu Y, et al. Trained immunity and reactivity of macrophages and endothelial cells. *Arterioscler Thromb Vasc Biol* (2021) 41 (3):1032–46. doi: 10.1161/ATVBAHA.120.315452

115. Li X, Fang P, Sun Y, Shao Y, Yang WY, Jiang X, et al. Anti-inflammatory cytokines IL-35 and IL-10 block atherogenic lysophosphatidylcholine-induced, mitochondrial ROS-mediated innate immune activation, but spare innate immune memory signature in endothelial cells. *Redox Biol* (2020) 28:101373. doi: 10.1016/j.redox.2019.101373

116. Shao Y, Saredy J, Xu K, Sun Y, Saaoud F, Drummer CT, et al. Endothelial immunity trained by coronavirus infections, DAMP stimulations and regulated by anti-oxidant NRF2 may contribute to inflammations, myelopoiesis, COVID-19 cytokine storms and thromboembolism. *Front Immunol* (2021) 12:653110. doi: 10.3389/fimmu.2021.653110

117. Batista-Gonzalez A, Vidal R, Criollo A, Carreno LJ. New insights on the role of lipid metabolism in the metabolic reprogramming of macrophages. *Front Immunol* (2019) 10:2993. doi: 10.3389/fimmu.2019.02993

118. Zeng X, Zhu M, Liu X, Chen X, Yuan Y, Li L, et al. Oleic acid ameliorates palmitic acid induced hepatocellular lipotoxicity by inhibition of ER stress and pyroptosis. *Nutr Metab (Lond)* (2020) 17:11. doi: 10.1186/s12986-020-0434-8

119. Greuter T, Yaqoob U, Gan C, Jalan-Sakrikar N, Kostallari E, Lu J, et al. Mechanotransduction-induced glycolysis epigenetically regulates a CXCL1-dominant angiocrine signaling program in liver sinusoidal endothelial cells in vitro and in vivo. *J Hepatol* (2022) 77(3):723–34. doi: 10.1016/j.jhep.2022.03.029

120. Zhong C, Yang X, Feng Y, Yu J. Trained immunity: An underlying driver of inflammatory atherosclerosis. *Front Immunol* (2020) 11:284. doi: 10.3389/fimmu.2020.00284

121. Li X, Fang P, Li Y, Kuo YM, Andrews AJ, Nanayakkara G, et al. Mitochondrial reactive oxygen species mediate lysophosphatidylcholine-induced endothelial cell activation. *Arterioscler Thromb Vasc Biol* (2016) 36(6):1090–100. doi: 10.1161/ATVBAHA.115.306964

122. Li X, Fang P, Mai J, Choi ET, Wang H, Yang XF. Targeting mitochondrial reactive oxygen species as novel therapy for inflammatory diseases and cancers. *J Hematol Oncol* (2013) 6:19. doi: 10.1186/1756-8722-6-19

123. Li X, Fang P, Yang WY, Chan K, Lavallee M, Xu K, et al. Mitochondrial ROS, uncoupled from ATP synthesis, determine endothelial activation for both physiological recruitment of patrolling cells and pathological recruitment of inflammatory cells. *Can J Physiol Pharmacol* (2017) 95(3):247–52. doi: 10.1139/cjpp-2016-0515

124. Li X, Shao Y, Sha X, Fang P, Kuo YM, Andrews AJ, et al. IL-35 (Interleukin-35) suppresses endothelial cell activation by inhibiting mitochondrial reactive oxygen species-mediated site-specific acetylation of H3K14 (Histone 3 lysine 14). *Arterioscler Thromb Vasc Biol* (2018) 38(3):599–609. doi: 10.1161/ATVBAHA.117.310626

125. Cheng J, Nanayakkara G, Shao Y, Cueto R, Wang L, Yang WY, et al. Mitochondrial proton leak plays a critical role in pathogenesis of cardiovascular diseases. *Adv Exp Med Biol* (2017) 982:359–70. doi: 10.1007/978-3-319-55330-6_20

126. Nanayakkara GK, Wang H, Yang X. Proton leak regulates mitochondrial reactive oxygen species generation in endothelial cell activation and inflammation - a novel concept. *Arch Biochem Biophys* (2019) 662:68–74. doi: 10.1016/j.abb.2018.12.002

127. Krause K, Daily K, Estfanous S, Hamilton K, Badr A, Abu Khweek A, et al. Caspase-11 counteracts mitochondrial ROS-mediated clearance of staphylococcus aureus in macrophages. *EMBO Rep* (2019) 20(12):e48109. doi: 10.15252/embr.201948109

128. Ogawa Y, Imajo K, Honda Y, Kessoku T, Tomeno W, Kato S, et al. Palmitate-induced lipotoxicity is crucial for the pathogenesis of nonalcoholic fatty liver disease in cooperation with gut-derived endotoxin. *Sci Rep* (2018) 8(1):11365. doi: 10.1038/s41598-018-29735-6

129. Tanner LB, Goglia AG, Wei MH, Sehgal T, Parsons LR, Park JO, et al. Four key steps control glycolytic flux in mammalian cells. *Cell Syst* (2018) 7(1):49–62.e8. doi: 10.1016/j.cels.2018.06.003

130. Boutens L, Hooiveld GJ, Dhingra S, Cramer RA, Netea MG, Stienstra R. Unique metabolic activation of adipose tissue macrophages in obesity promotes inflammatory responses. *Diabetologia* (2018) 61(4):942–53. doi: 10.1007/s00125-017-4526-6

131. Caslin HL, Bhanot M, Bolus WR, Hasty AH. Adipose tissue macrophages: Unique polarization and bioenergetics in obesity. *Immunol Rev* (2020) 295(1):101–13. doi: 10.1111/imr.12853

132. Saeed S, Quintin J, Kerstens HH, Rao NA, Aghajanirefah A, Matarese F, et al. Epigenetic programming of monocyte-to-macrophage differentiation and trained innate immunity. *Science* (2014) 345(6204):1251086. doi: 10.1126/science.1251086

133. Mandal P, Feng Y, Lyons JD, Berger SB, Otani S, DeLaney A, et al. Caspase-8 collaborates with caspase-11 to drive tissue damage and execution of endotoxic shock. *Immunity* (2018) 49(1):42–55.e6. doi: 10.1016/j.immuni.2018.06.011

134. Neuschwander-Tetri BA. Lifestyle modification as the primary treatment of NASH. *Clin Liver Dis* (2009) 13(4):649–65. doi: 10.1016/j.cld.2009.07.006

135. Younossi ZM, Blissett D, Blissett R, Henry L, Stepanova M, Younossi Y, et al. The economic and clinical burden of nonalcoholic fatty liver disease in the united states and Europe. *Hepatology* (2016) 64(5):1577–86. doi: 10.1002/hep.28785

136. Christ A, Günther P, Lauterbach MAR, Duewell P, Biswas D, Pelka K, et al. Western Diet triggers NLRP3-dependent innate immune reprogramming. *Cell* (2018) 172(1-2):162–175.e14. doi: 10.1016/j.cell.2017.12.013

137. He WT, Wan H, Hu L, Chen P, Wang X, Huang Z, et al. Gasdermin d is an executor of pyroptosis and required for interleukin-1β secretion. *Cell Res* (2015) 25(12):1285–98. doi: 10.1038/cr.2015.139

138. Wei G, Luo S, Wu W, Hu J, Zhou R. Activation of interleukin-1β release and pyroptosis by transmissible gastroenteritis virus is dependent on the NOD-like receptor protein 3 inflammasome in porcine intestinal epithelial cell line. *Viral Immunol* (2021) 34(6):401–9. doi: 10.1089/vim.2020.0227

139. Lu Y, Sun Y, Xu K, Saaoud F, Shao Y, Drummer CT, et al. Aorta in pathologies may function as an immune organ by upregulating secretomes for immune and vascular cell activation, differentiation and trans-Differentiation-Early secretomes may serve as drivers for trained immunity. *Front Immunol* (2022) 13:858256. doi: 10.3389/fimmu.2022.858256

140. Mitroulis I, Ruppova K, Wang B, Chen LS, Grzybek M, Grinenko T, et al. Modulation of myelopoiesis progenitors is an integral component of trained immunity. *Cell* (2018) 172(1-2):147–161.e12. doi: 10.1016/j.cell.2017.11.034

141. Arts RJW, Moorlag S, Novakovic B, Li Y, Wang SY, Oosting M, et al. BCG Vaccination protects against experimental viral infection in humans through the induction of cytokines associated with trained immunity. *Cell Host Microbe* (2018) 23(1):89–100.e5. doi: 10.1016/j.chom.2017.12.010

142. Kim KA, Gu W, Lee IA, Joh EH, Kim DH. High fat diet-induced gut microbiota exacerbates inflammation and obesity in mice via the TLR4 signaling pathway. *PloS One* (2012) 7(10):e47713. doi: 10.1371/journal.pone.0047713

143. Yang H, Liu H, Zeng Q, Imperato GH, Addorisio ME, Li J, et al. Inhibition of HMGB1/RAGE-mediated endocytosis by HMGB1 antagonist box a, anti-HMGB1 antibodies, and cholinergic agonists suppresses inflammation. *Mol Med* (2019) 25(1):13. doi: 10.1186/s10020-019-0081-6

144. Wandel MP, Kim BH, Park ES, Boyle KB, Nayak K, Lagrange B, et al. Guanylate-binding proteins convert cytosolic bacteria into caspase-4 signaling platforms. *Nat Immunol* (2020) 21(8):880–91. doi: 10.1038/s41590-020-0697-2

145. Rathinam VAK, Zhao Y, Shao F. Innate immunity to intracellular LPS. *Nat Immunol* (2019) 20(5):527–33. doi: 10.1038/s41590-019-0368-3

146. Ni D, Tang T, Lu Y, Xu K, Shao Y, Saaoud F, et al. Canonical secretomes, innate immune caspase-1-, 4/11-gasdermin d non-canonical secretomes and exosomes may contribute to maintain treg-ness for treg immunosuppression, tissue repair and modulate anti-tumor immunity via ROS pathways. *Front Immunol* (2021) 12:678201. doi: 10.3389/fimmu.2021.678201

frontiers | Frontiers in Immunology

TYPE Original Research
PUBLISHED 09 February 2023
DOI 10.3389/fimmu.2023.1034356

OPEN ACCESS

EDITED BY
Yankai Wen,
University of Texas Health Science Center at Houston, United States

REVIEWED BY
Fudi Zhong,
Guangxi Medical University, China
Adil Bhat,
University of California, Los Angeles, United States
Yunlong Ma,
Zhejiang University, China

*CORRESPONDENCE
Yifang Gao
gaoyf26@mail.sysu.edu.cn
Yi Ma
mayi@mail.sysu.edu.cn

†These authors have contributed equally to this work

SPECIALTY SECTION
This article was submitted to Inflammation, a section of the journal Frontiers in Immunology

RECEIVED 01 September 2022
ACCEPTED 12 January 2023
PUBLISHED 09 February 2023

CITATION
Ren A, He W, Rao J, Ye D, Cheng P, Jian Q, Fu Z, Zhang X, Deng R, Gao Y and Ma Y (2023) Dysregulation of innate cell types in the hepatic immune microenvironment of alcoholic liver cirrhosis.
Front. Immunol. 14:1034356.
doi: 10.3389/fimmu.2023.1034356

Dysregulation of innate cell types in the hepatic immune microenvironment of alcoholic liver cirrhosis

Ao Ren[1,2,3†], Wenjing He[1,2,3†], Jiawei Rao[1,2,3†], Dongmei Ye[1,2,3], Pengrui Cheng[1,2,3], Qian Jian[1,2,3], Zongli Fu[1,2,3], Xuzhi Zhang[1,2,3], Ronghai Deng[1,2,3], Yifang Gao[1,2,3*] and Yi Ma[1,2,3*]

[1]Organ Transplant Center, The First Affiliated Hospital, Sun Yat-sen University, Guangzhou, China, [2]Guangdong Provincial Key Laboratory of Organ Donation and Transplant Immunology, The First Affiliated Hospital, Sun Yat-sen University, Guangzhou, China, [3]Guangdong Provincial International Cooperation Base of Science and Technology (Organ Transplantation), The First Affiliated Hospital, Sun Yat-sen University, Guangzhou, China

Introduction: The risk of alcoholic cirrhosis increases in a dose- and time-dependent manner with alcohol consumption and ethanol metabolism in the liver. Currently, no effective antifibrotic therapies are available. We aimed to obtain a better understanding of the cellular and molecular mechanisms involved in the pathogenesis of liver cirrhosis.

Methods: We performed single-cell RNA-sequencing to analyze immune cells from the liver tissue and peripheral blood form patients with alcoholic cirrhosis and healthy controls to profile the transcriptomes of more than 100,000 single human cells and yield molecular definitions for non-parenchymal cell types. In addition, we performed single-cell RNA-sequencing analysis to reveal the immune microenvironment related to alcoholic liver cirrhosis. Hematoxylin and eosin, Immunofluorescence staining and Flow cytometric analysis were employed to study the difference between tissues and cells with or without alcoholic cirrhosis.

Results: We identified a fibrosis-associated M1 subpopulation of macrophages that expands in liver fibrosis, differentiates from circulating monocytes, and is pro-fibrogenic. We also define mucosal-associated invariant T (MAIT) cells that expand in alcoholic cirrhosis and are topographically restricted to the fibrotic niche. Multilineage modeling of ligand and receptor interactions between the fibrosis-associated macrophages, MAIT, and NK cells revealed the intra-fibrotic activity of several pro-fibrogenic pathways, including responses to cytokines and antigen processing and presentation, natural killer cell-mediated cytotoxicity, cell adhesion molecules, Th1/Th2/Th17 cell differentiation, IL-17 signaling pathway, and Toll-like receptor signaling pathway.

Discussion: Our work dissects unanticipated aspects of the cellular and molecular basis of human organ alcoholic fibrosis at the single-cell level and provides a conceptual framework for the discovery of rational therapeutic targets in liver alcoholic cirrhosis.

KEYWORDS

scRNA-seq, MAIT cells, NKT cells, macrophages, fibrosis

Introduction

Liver cirrhosis is a morbid, multisystem disease associated with frequent hospitalizations and high mortality rates, accounting for 1.2 million annual deaths worldwide and ranking as the 14th and 10th leading cause of death in the world and most developed countries, respectively (1–3). The risk of alcoholic cirrhosis increases in a dose- and time-dependent manner with alcohol consumption, and is related to one's ethanol metabolism ability (4, 5). With continued alcohol consumption, the alcoholic liver disease progresses to a stage of severely damaged liver cells known as "alcoholic cirrhosis", which is characterized by progressive hepatic fibrosis and nodules (6). Hence, effective antifibrotic therapies are urgently needed for patients with alcoholic liver cirrhosis (7).

The liver hosts a complex range of immunocompetent cells under physiological and pathological conditions, which may interact with other non-parenchymal cell (NPC) lineages, such as endothelial and mesenchymal cells, to promote the progression of liver fibrosis (8, 9). Gao et al. reviewed inflammatory pathways in alcoholic steatohepatitis and showed that natural killer (NK) T cells may promote alcoholic liver injury *via* the activation of macrophages and that mucosa-associated invariant T cells (MAIT) cells are reduced in patients with alcohol-related liver disease (ALD) (10–12). These immune cells might be associated with the pathogenesis of alcoholic liver cirrhosis and may provide a target for future treatments. Therefore, understanding the functional heterogeneity and interactome of cell lineages that contribute to the fibrotic niche of alcoholic cirrhosis is necessary.

Single-cell RNA sequencing (scRNA-seq) allows us to explore disease mechanisms and individual cell populations at an unprecedented resolution. In this study, using scRNA-seq, we profiled mononuclear immune cells from the liver and blood of patients with alcoholic cirrhosis and healthy patients.

Methods

Three patients were pathologically diagnosed with alcoholic cirrhosis, and two donors of liver transplantation as healthy controls at The First Affiliated Hospital, Sun Yat sen University. The available clinicopathological features of these patients were summarized in Supplementary Tables 1. Admission criteria: onset of jaundice within prior 8weeks; ongoing consumption of>40(female) or 60(male)g alcohol/day for ≥6 months, with<60 days of abstinence before the onset of jaundice; AST>50, AST/ALT>1.5, and both values<400IU/L; serum total bilirubin>3.0 mg/dL; pathological findings confirmed cirrhosis. Exclusion criteria: hepatic failure;hepatitis virus, nonalcoholic fatty and autoimmune liver disease. Informed consent for the sample collection for single-cell RNA sequencing was obtained from the donor's family delegate. Organs were managed according to organ procurement guidelines. This study was approved by the Ethics Committee for Clinical Research and Animal Trials of the First Affiliated Hospital of Sun Yat-sen University (permit no. [2021]113) and was conducted in accordance with the Declaration of Helsinki principles.

Abbreviations: MAIT, mucosal-associated invariant T; NK, natural killer; NPC, non-parenchymal cell; ALD, alcohol-related liver disease; scRNA-seq, Single-cell RNA sequencing; PBMCs, peripheral blood mononuclear cells; A, Liver tissue of patients with alcoholic cirrhosis; AP, PBMC of patients with alcoholic cirrhosis (AP); H, Liver tissue of healthy patients(H); HP, PBMC of healthy patients(HP); QuSAGE, quantitative gene set enrichment.

Hematoxylin and eosin and immunofluorescence analyses

Small pieces of freshly dissected liver were fixed with 10% formalin, embedded in paraffin, cut into 3–5 μm thick sections, and stained with anti-CD80, anti-68, and anti-CD206 monoclonal antibodies (mAbs), according to the manufacturer's protocols. M1 macrophages were defined as CD68+CD80+, while M2 macrophages were defined as CD68+CD206+.

Flow cytometric analysis

Liver cells were stained with the indicated fluorescent mAbs and analyzed on a flow cytometer (BD LSRFortessa, USA). MAIT cells were defined as CD3+CD161+TCRVα7.2+. With respect to macrophages analysis, liver cells were stained with the indicated fluorescent conjugated mAbs and analyzed on a full spectrum flow cytometer (Cytek Aurora, USA). M1 macrophages were defined as CD45+CD68+CD86+CD80+, and M2 macrophages were defined as CD45+CD68+CD163+CD206+. Data were analyzed using the FlowJo software (v10.5.3).

Single-cell RNA statistical analysis

Single-cell RNA (scRNA-seq) data analysis was performed by NovelBio Co., Ltd. with NovelBrain Cloud Analysis Platform (www.novelbrain.com). We applied fastp (13) with default parameters, filtered the adapter sequence, and removed low-quality reads to achieve clean data. Then, the feature-barcode matrices were obtained by aligning reads to the human genome (GRCh38 Ensemble: version 100) using CellRanger v5.0.1. We performed the downsample analysis among samples sequenced according to the mapped barcoded reads per cell of each sample and finally achieved the aggregated matrix. Cells containing over 200 expressed genes and mitochondrial UMI rates below 20% passed the cell quality filtering, and mitochondrial genes were removed from the expression table.

The Seurat package (version: 3.1.4, https://satijalab.org/seurat/) was used for cell normalization and regression based on the expression table, UMI counts of each sample, and percentage of mitochondrial rate to obtain the scaled data. Principal component analysis (PCA) was constructed based on the scaled data with the top 2000 highly variable genes, and the top 10 principals were used for UMAP construction. Using the graph-based cluster method, we acquired the unsupervised cell cluster result based on the PCA top 10 principal, and we calculated the marker genes using the FindAllMarkers function with the Wilcoxon rank-sum test algorithm under the following criteria:1. lnFC > 0.25; 2. P< 0.05; 3. min.pct > 0.1. To identify the cell type in detail, clusters of the same cell type were selected for re-tSNE analysis, graph-based clustering, and marker analysis.

Pseudotime analysis

Single-cell trajectory analysis was performed using Monocle2 (http://cole-trapnell-lab.github.io/monocle-release) using DDR-Tree and default parameters. Before Monocle analysis, we selected marker genes based on the Seurat clustering results and raw expression counts of the filtered cells. Based on the pseudotime analysis, branch expression analysis modeling (BEAM analysis) was applied for branch fate-determined gene analysis.

Differential gene expression analysis

To identify differentially expressed genes (DEG) among samples, the function FindMarkers with the Wilcoxon rank-sum test algorithm was used under the following criteria:1. lnFC > 0.25; 2. P< 0.05; 3. min.pct>0.1.

Cell communication analysis

To enable a systematic analysis of cell-cell communication molecules, we applied cell communication analysis based on the Cell Phone DB toolset (14), a public repository of ligands, receptors, and their interactions. The membrane, secreted, and peripheral proteins of the cluster at different time points were annotated. Significant mean and cell communication significance (P < 0.05) were calculated based on the interaction and the normalized cell-matrix achieved by Seurat normalization.

Gene enrichment and co-regulated gene analyses

To characterize the relative activation of a given gene set, such as pathway activation, we performed QuSAGE (2.16.1) analysis (15). To characterize the relative activation of a given gene set, such as the KEGG PATHWAY gene set, we performed GSVA (1.32.0) to calculate it for each cell. To discover the gene co-regulation network, the "find gene modules" function of monocle3 was used with the default parameters (16).

Data-driven regression discontinuity plot

To display the expression levels of chemokine genes, cytokine genes, and anti-tags in cell species, we used the Seurat package (version: 3.1.4, https://satijalab.org/seurat/) to draw feature, bubble, and violin plots.

Statistical analyses

Statistical analyses of zonation figures were performed using GraphPad Prism v5.0. Data are expressed as mean ± standard deviation, and the statistical test used is listed in each figure caption. Statistical significance was evaluated using ANOVA with a Bonferroni post-test*** P < 0.001, ** P < 0.01, * P < 0.05.

Results

A single-cell atlas of human Liver NPCs

Non-parenchymal cells (NPCs) were isolated from the livers of patients with alcoholic cirrhosis and healthy controls. $CD45^+$ leukocytes and other $CD45^-$ NPCs were screened by flow cytometry before scRNA-seq analysis. To better understand the pathogenesis of alcoholic cirrhosis and discriminate between liver-resident and circulating leukocytes, we also collected $CD45^+$ peripheral blood mononuclear cells (PBMCs) to perform scRNA-seq analysis (Figure 1A). The combined liver NPC and PBMC datasets were partitioned into clusters and annotated using signatures of known lineage markers. The datasets were divided into 19 clusters.

Re-clustering of the 21638 liver-resident cells and PBMCs from five livers and peripheral blood (n = 2 healthy; n = 3 alcoholic cirrhosis) revealed 19 populations, across 12 cell lineages, including T, B, plasma, endothelial, dendritic, erythroid, plasmacytoid dendritic, and stellate cells, as well as macrophages and monocytes (Figures 1B, C). And patient demographics and clinical information were shown in Supplementary Table 1. Subpopulations and markers were identified across all clusters and lineages, and the top differentially expressed genes (DEGs) for the cellular subclusters are presented in the heatmap (Figure 1D). Notably, we identified several distinct types of immune cells: T cells characterized with high expression of the cell markers CD3D and CD3G; monocytes, macrophages, and dendritic cells specifically expressing the cell markers CD1C, C1QA, and S100A9; plasmacytoid dendritic cells highly expressing joining chain of multimeric IgA and IgM (JCHAIN) and major histocompatibility complex class II DR alpha (HLA-DRA); erythroid cells with high beta-globin (HBB) expression; cholangiocytes specifically expressing the markers EPCAM and KRT18; endothelial cells highly expressing fms related receptor tyrosine kinase 1 (FLT1) and platelet endothelial cell adhesion molecule-1 (PECAM1); B cells and plasma cells expressing CD79A and MS4; stellate and smooth muscle cells with high decorin (DCN), actin alpha 2 (ACTA2), and transgelin (TAGLN) expression; and hepatocytes highly expressing albumin (ALB) and haptoglobin (HP). The expression patterns of cluster-specific marker genes in cellular populations are shown in Figure 1E. T cells, monocytes, and macrophages accounted for approximately 57%, 18%, and 2%, respectively in the A and AP groups, and approximately 53%, 32%, and 1%, respectively in the H and HP groups (Figure 1F) (A: Liver tissue of patients with alcoholic cirrhosis; AP: PBMC of patients with alcoholic cirrhosis; H: Liver tissue of healthy patients; HP: PBMC of healthy patients). Therefore, T cells, macrophages, and monocytes accounted for the largest proportion of immune cells. Additionally, the proportion of T cells was higher in the liver tissues of healthy individuals than in PBMCs, while that in patients with alcoholic cirrhosis was higher in liver tissue. Macrophages were more abundant in the liver tissues than in the PBMCS in both healthy individuals and patients with alcoholic liver cirrhosis (Supplementary Table 2). There is no consensus regarding which immune cells are responsible for the progression of alcoholic cirrhosis; we hypothesized that it is caused by the interaction of multiple immune cells. Therefore, we analyzed the effects of related immune cells on the progression of alcoholic liver cirrhosis.

10.3389/fimmu.2023.1034356

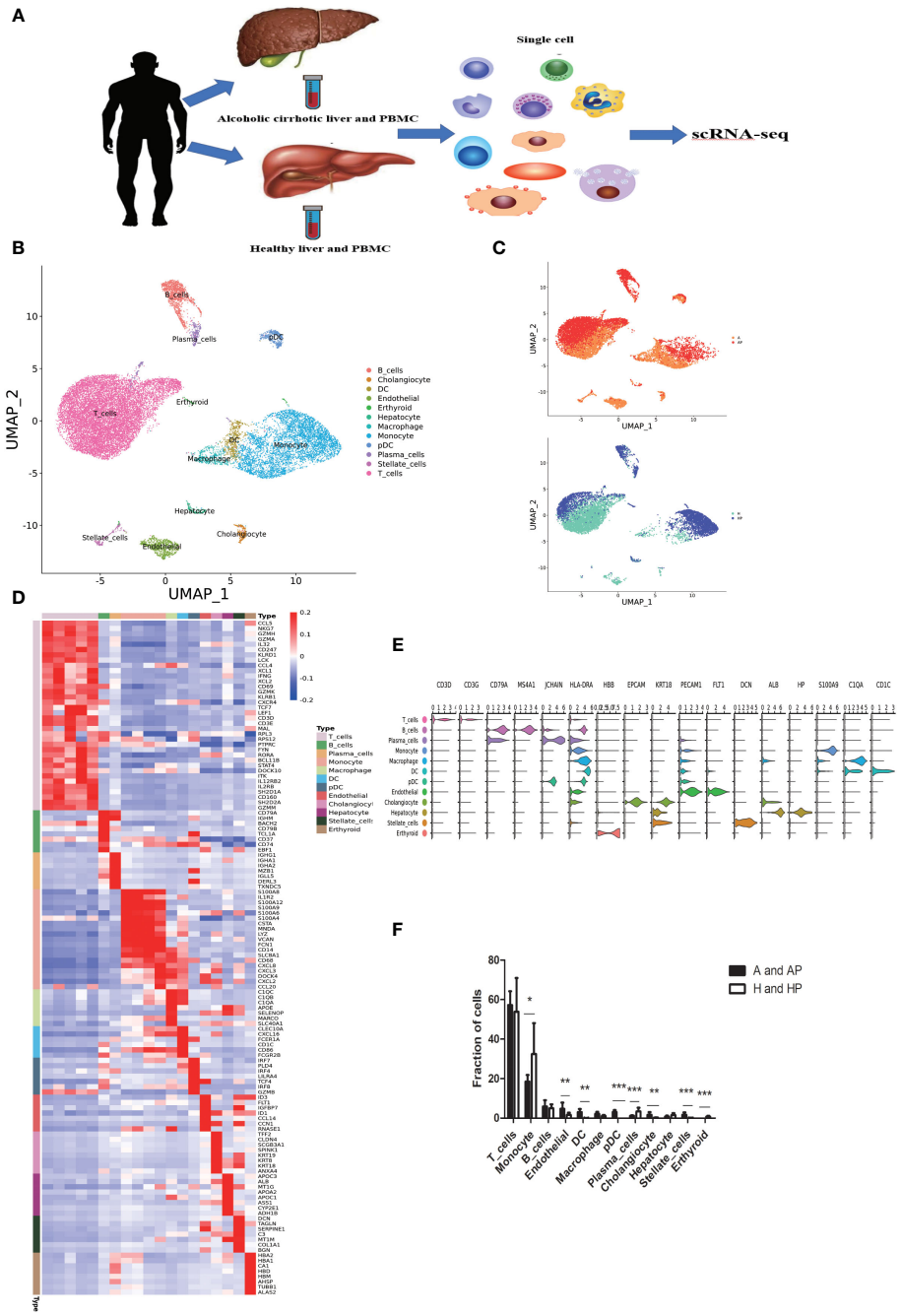

FIGURE 1
Single-cell atlas of human liver non-parenchymal cells (NPCs). **(A)** An overview of the isolation, FACS, and single-cell sequencing (scRNA-seq) analyses of NPC fractions from liver tissue and peripheral blood mononuclear cells (PBMCs). **(B)** Clustering of 21638 liver-resident cells and PBMCs from five liver tissue and peripheral blood samples (n = 2 healthy and n = 3 alcoholic cirrhosis) **(C)** Annotation of the conditions of the patients. **(D)** Heatmap of cluster marker genes. **(E)** Scaled gene expression of NPCs cells. **(F)** Fraction of cells from NPCs. (*P < 0.05, **P < 0.01, ***P < 0.001).

Role of monocytes and macrophages in alcoholic cirrhosis

Monocytes and macrophages have been shown to play an important role in liver cirrhosis (17). We identified a total of 5176 monocytes and macrophages from five liver and peripheral blood samples (n = 2 healthy and n = 3 alcoholic cirrhosis). Monocytes and macrophages clustered into 11 clusters: IRF1 mono, RNASE2 mono, IL1R2 mono, SERPINB2 mono, CCL20 mono, H1-4 mono, CD52 mono, FCGR3A mono, C1QC macro, SLC40A1 macro, and CD163 macro (Figures 2A, B). Subpopulations and markers were identified across all clusters and lineages. The top DEGs for the cellular subclusters are presented in a heatmap in Figure 2C, and the expression patterns of the cluster-specific marker genes in the cellular populations are shown in Figure 2D. Quantification of monocytes and macrophages revealed that clusters CD52 mono, IRF1 mono, SERPINB2 mono, C1QC macro, and SLC40A1 macro were expanded in liver tissues and PBMCs of patients with alcoholic cirrhotic livers (P < 0.05) (Figures 2B, E). In particular, clusters CD52 mono, C1QC macro, and SLC40A1 macro were more enriched in the

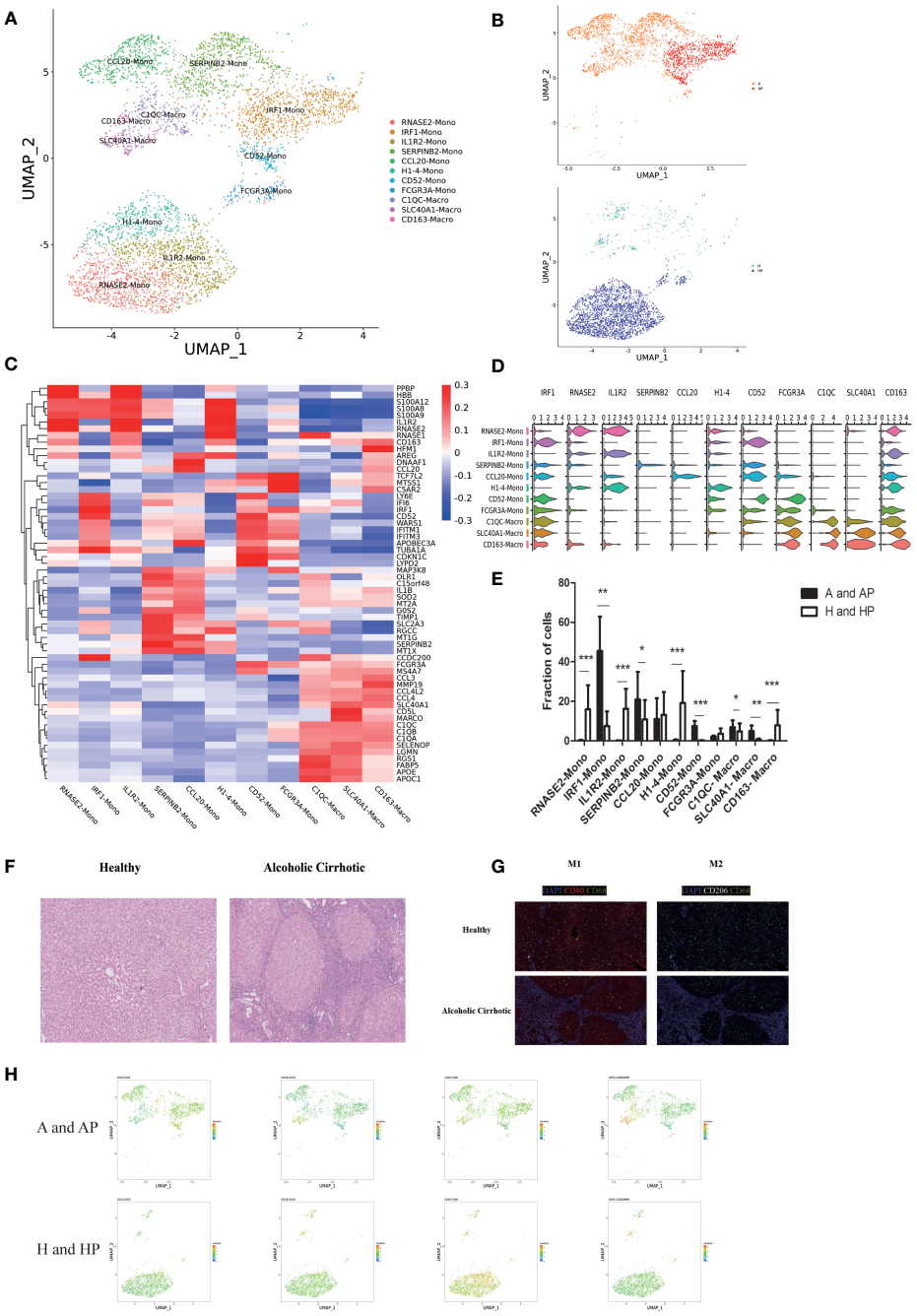

FIGURE 2
The monocyte and macrophage subpopulations. **(A)** Clustering of 5176 monocytes and macrophages from five liver tissue and peripheral blood samples (n = 2 healthy and n = 3 alcoholic cirrhosis) **(B)** Annotation of monocytes and macrophages by patient's condition. **(C)** Heatmap of MP cluster marker genes. **(D)** Scaled gene expression of monocytes and macrophages. **(E)** Fraction of monocyte and macrophage cells. **(F)** Pathological changes in the liver tissues of patients with alcoholic cirrhosis (10×). **(G)** Representative immunofluorescent images of CD80 (red), CD206 (white), CD68 (green), and DAPI (blue) in alcoholic cirrhotic livers (10×), and the distribution of M1 and M2 in healthy and alcoholic cirrhotic livers. **(H)** Proteomic analysis of CD80, CD52, CD163, and CD206. (*P < 0.05, **P < 0.01, ***P < 0.001).

PBMCs than in the liver tissues of patients with alcoholic liver cirrhosis. SERPINB2 mono was more enriched in the PBMCs than in the liver of patients with alcoholic liver cirrhosis. All the above mentioned clusters were more enriched in patients with alcoholic liver cirrhosis than in healthy individuals. IRF1 mono was more enriched in PBMCs than in the liver tissues of patients with alcoholic liver cirrhosis; however, it was generally more enriched in healthy individuals (Supplementary Table 3). Histological analysis confirmed the presence of characteristic pathological changes of cirrhosis, such as destruction of the liver lobule destroyed, fibrous tissue hyperplasia, and pseudolobuli formation, in the liver tissue samples of patients with alcoholic cirrhosis but not in those of healthy individuals (Figure 2F). Immunofluorescence analysis showed that M1 macrophages and M2 macrophages (CD206CD68 and CD80CD68, respectively) were more abundant in patients with alcoholic liver cirrhosis than in healthy individuals (Figure 2G). Flow cytometric

analysis showed that M1 macrophages and M2 macrophages accounted for 54.25 ± 3.35% (mean ± SEM) and 65 ± 6.76% (mean ± SEM) in CD68+macrophages, respectively. (Supplementary Figure 1) Furthermore, proteomic analysis revealed that CD80, CD52, CD163, and CD206 were more expressed in the A and AP groups (Figure 2H).

To determine the origin of macrophages, we performed an *in silico* pseudo-trajectory analysis on a combined dataset of peripheral blood monocytes and liver-resident macrophages (Figure 3A). The R package monocle was then used to sort single cells and construct a tree-like structure of the entire lineage differentiation trajectory. Along with trajectory progression, cells experienced three states: the starting point of branching (pre-branch) and the two other branches (Fate1 and Fate2). RNASE2 mono, IRF1 mono, IL1R2 mono, and H1-4 mono were mainly observed at the beginning of the trajectory. CD163 macro, C1QC macro, CCL20 mono, SERPINB2 mono, and SLC40A1 macro were mostly observed at the end of trajectory branch 1. Therefore, our findings suggest that RNASE2 mono, IRF1 mono, IL1R2 mono, and H1-4 mono could be the origin of macrophages and may transform into two distinct types of monocytes and macrophages during the progression of alcoholic cirrhosis. Moreover, the gene expression patterns in the cell state transition along with the progression trajectory were dissected, and 100 dynamic genes with significant expression changes were determined (Figure 3B). Our results showed that several crucial drivers, including regulators that are potentially associated with the progression of cirrhosis, such as SLC40A1, DAB2, FOLR2, GPAT3, and CDA, were upregulated during fibrosis. In contrast, transcriptional factors involved in immune cell differentiation and proliferation, such as CD52, CAMK1, HLA-DMB, and CD48, were remarkably downregulated in the trajectory transition process.

Role of MAIT cells in alcoholic cirrhosis

MAIT cells are present in peripheral blood and are highly abundant in mucosal tissues and the liver. Clustering of human MAIT cells identified seven subpopulations: FTH1-MAIT, STAT1-MAIT, IFNr-MAIT, CD69-MAIT, GZMB-MAIT, LTB-MAIT, and GNLY-MAIT (Figures 4A, B). Subpopulations and markers were identified across all clusters and lineages. The DEGs for the cellular subclusters were presented in a heatmap in Figure 4C, and the expression patterns of the cluster-specific marker genes in the cellular populations are presented in Figure 4D. Quantification of MAIT cells revealed that clusters of GZMB-MAIT cells and LTB-MAIT cells were expanded in the livers and PBMCs of patients with alcoholic cirrhosis ($P < 0.05$) (Figures 4B, E).

GZMB-MAIT cluster was more enriched in the liver than in the PBMCs of patients with alcoholic liver cirrhosis and were more enriched than that in healthy individuals. LTB-MAIT was more enriched in the PBMCs than in the liver of patients with alcoholic liver cirrhosis and less enriched than that in healthy individuals. (Supplementary Table 4). Additionally, flow cytometry analysis revealed that MAIT cells were more abundant in healthy individuals than in patients with alcoholic liver cirrhosis (Figure 4F).

Furthermore, we performed a quantitative gene set enrichment (QuSAGE) analysis to characterize the relative activation of a given gene set. The patients in the HP group had fewer MAIT cells; thus, they were not included in the analysis. QuSAGE analysis revealed that the most enriched terms in the alcoholic cirrhosis group included antigen processing and presentation, the intestinal immune network for IgA production, glycosaminoglycan biosynthesis, Th17 cell differentiation, ferroptosis, and glycolysis/gluconeogenesis (Figure 4G). Moreover, single-sample GSEA (ssGSEA) analysis, an extension of gene set enrichment analysis (GSEA), revealed that the Foxo signaling

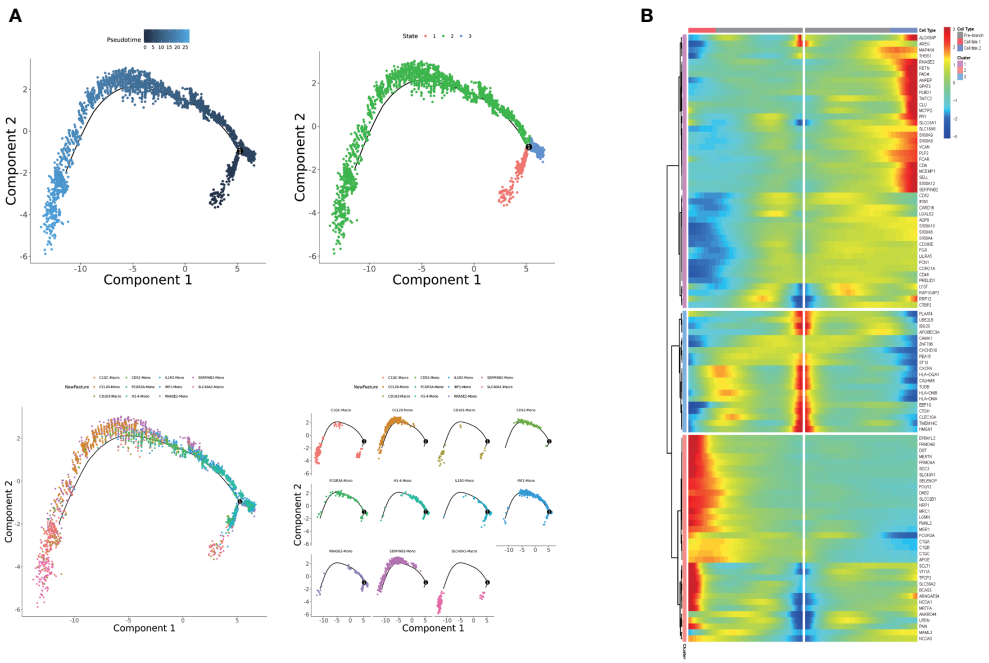

FIGURE 3
(A) Pseudotime analysis of monocyte and macrophage subpopulations. **(B)** Heatmap displaying the expressions of selected marker genes in monocytes and macrophages that are arranged along the pseudotime trajectory.

10.3389/fimmu.2023.1034356

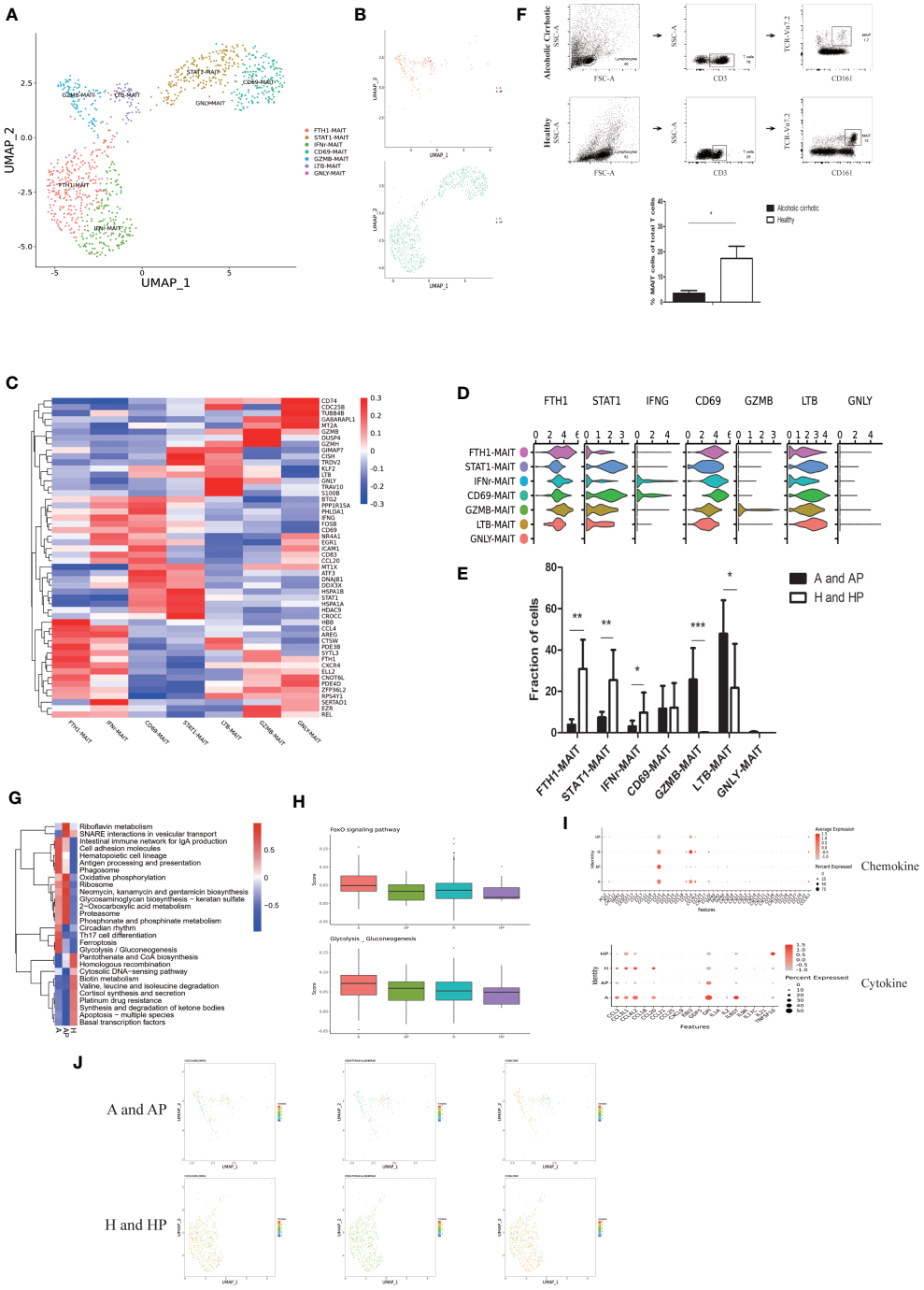

FIGURE 4
Identifying MAIT cell subpopulations. **(A)** Clustering of 969 mucosal-associated invariant T (MAIT) cells from five liver tissue and peripheral blood samples (n = 2 healthy and n = 3 alcoholic cirrhosis) **(B)** Annotation of MAIT cells by patient's condition. **(C)** Heatmap of MAIT cell cluster marker genes. **(D)** Scaled gene expression in MAIT cells. **(E)** Fraction of MAIT cells. **(F)** Flow analysis of MAIT cells in each group. **(G)** QuSAGE analysis of MAIT cells in the A, AP, and H groups. **(H)** Single-sample GSEA (ssGSEA) analysis of MAIT cells in the A, AP, H, and HP groups. **(I)** Cytokine and chemokine analyses of MAIT cells in the A, AP, H, and HP groups. **(J)** Proteomic analysis of KLRG1, CD69, and TCR. (*P < 0.05, **P < 0.01, ***P < 0.001).

pathway and glycolysis/gluconeogenesis were significantly upregulated in the A and AP groups (Figure 4H). The chemokine analysis, revealed that CCL5, XCL1, CXCL2, CCL2, and CXCL8 were significantly upregulated in the A and AP, groups whereas the cytokine analysis showed that EBI3, GDF5, GPI, IL21, TNFSF10, and IL1A, were significantly upregulated in the A and AP groups (Figure 4I). Moreover, the proteomic analysis revealed that CD69 and TCR Vα24-Jα18 were more expressed in the A and AP groups (Figure 4J).

Role of NK cells in alcoholic cirrhosis

NK cells are thought to be involved in controlling the development and progression of liver fibrosis. Clustering of 3578 NK cells from five livers and peripheral blood (n = 2 healthy and n = 3 alcoholic cirrhosis) was performed and five subpopulations were identified: GNLY NK, GZMK NK, SELL-NK, LAG3 NK, and XCL2 NK (Figures 5A, B). Subpopulations and markers were identified

across all clusters and lineages. The DEGs for the cellular subclusters are presented in a heatmap in Figure 5C, and the expression patterns of the cluster-specific marker genes in the cellular populations are presented in Figure 5D. Clusters of SELL-NK were expanded in the livers and PBMCS of patients with alcoholic liver cirrhosis (Figure 5E) ($P < 0.05$) and were more enriched in healthy individuals (Supplementary Table 5).

Furthermore, QuSAGE analysis revealed that the most enriched terms in the alcoholic cirrhosis group included antigen processing and presentation, natural killer cell-mediated cytotoxicity, cell adhesion molecules, Th1/Th2/Th17 cell differentiation, IL-17 signaling pathway, and toll-like receptor (TLR) signaling pathway (Figure 5F). The HP group was not included in the analysis because they presented a low number of NK cells. Additionally, ssGSEA showed that antigen processing and presentation, IL-17 signaling pathway, and Th1 and Th2 cell differentiation were significantly enhanced in the A and AP groups (Figure 5G). In the chemokine analysis, CCL13, CXCL12, CXCL8, CXCL3, and CXCL2 were significantly enhanced in the A and AP groups. The cytokine analysis revealed that BMP6, CCL3, CCL3L1, CNTF, CSF3, CXCL6, IL13, IL17RB, and TNFSF10, among others, were significantly activated in the A and AP groups (Figure 5H). The proteomic analysis revealed that CD62L and CD44 were more highly expressed in the A and AP groups (Figure 5I).

Multilineage interactome in the fibrotic niche

Having defined the populations of monocytes, macrophages, MAIT cells, and NK cells, we confirmed the close topographical association of these cells with alcoholic cirrhosis. To characterize the immune microenvironment of alcoholic cirrhosis, the Cell Phone toolset was used to detect intercellular communication among immune cells. In the output of the results of the ligand–receptor, the heatmap plot function was used to analyze the interactions among immune cells, which showed that macrophages and monocytes were significantly activated and interacted with MAIT and NK cells (Figures 6A, B).

Numerous statistically significant interactions were detected between ligands and cognate receptors expressed by macrophages, MAIT cells, and NK cells. In group A, macrophages, as ligands, interact with NK and MAIT cells. C1QC macro and SLC40A1 as ligands mainly interact with GNLY N, GZMB-MAIT, and LTB-MAIT. In the AP group, the C1QC macro, as a ligand, mainly interacts with GZMK-NK, SELL-NK, GNLY-NK, and LTB-MAIT (Figure 6B). In group A, C1QC macro expressed CCL3 and CCL4 signaling to cognate receptors CCR5 on LTB-MAIT and GZMB-MAIT cells, and SLC40A1 macro expressed CXCL8 signaling to cognate receptors CXCR2 on GNLY NK cells. In the AP group, C1QC macro expressed CXCL2 signaling to cognate receptors DPP4 on STAT1 MAIT, CD69 MAIT, and LTB-MAIT cells, and expressed CXCL16 signaling to cognate receptors CXCR6 on GZMK NK cells (Figure 6C). Therefore, our unbiased dissection of the key ligand-receptor interactions between fibrosis-associated NPCs highlights macrophages, MAIT, and NK cells as important regulators within the human liver alcoholic fibrotic niche.

Discussion

The pathogenesis of alcoholic liver cirrhosis remains unknown. Only a few heavy drinkers develop alcoholic cirrhosis, which indicates that there are other factors other than alcohol contributing to the progression of alcoholic cirrhosis (18). Alcoholic cirrhosis is a complex and multifactorial ALD that is affected by the interactions of environmental or host factors, which partly explains the large inter-individual variability in the likelihood of developing cirrhosis and affected by ethanol metabolism.

The deficiency of certain enzymes related to alcohol metabolism could result in alcohol intolerance (18). For instance, there is a clear dose relationship between the amount of alcohol, an environmental factor, and the development of alcoholic cirrhosis (19, 20), whereas coffee seems to protect against ALD (21). Other environmental factors, such as obesity, smoking, and viral hepatitis infections, are recognized as important promoters of ALD (22–25). Several studies have shown that the genetic background, a host factor, might affect the progression of ALD; women are at greater risk of alcohol-related cirrhosis, and race may affect the individual's alcohol sensitivity, since Hispanic men and women have a higher risk for developing alcoholic cirrhosis than black men and women in the United States (26–28). Additionally, some studies have found that certain variants are associated with the risk of developing ALD, such as PNPLA3, which was found to modulate the evolution of steatosis, necroinflammation, fibrosis, and HCC in alcoholics (29). The pathogenesis of ALD can also be conceptually divided into i) ethanol-mediated liver injury, ii) inflammatory immune response to injury, and iii) intestinal permeability and microbiome changes (30). The inflammatory immune response plays an important role in ALD. The interferon regulatory factor 3 is phosphorylated upon alcohol response, leading to the activation of an inflammatory response, which is required for the intrinsic (mitochondrial) apoptosis pathway in hepatocytes (31, 32). Bacteria-derived LPS interacts with TLR4 of the Kupffer cells, leading to the production of proinflammatory cytokines through the IRF-3 signaling pathway (30). Murine studies identified Interleukin-1 receptor-associated kinase 4 (IRAK4), the master kinase of Toll-like receptor (TLR)/IL-1R-mediated signalling activation, inhibiting IRAK4 kinase activity improves ethanol-induced liver injury in mice (10). Therefore, the immune and inflammatory responses play important roles in the progression of ALD and alcoholic cirrhosis. Here, we explored the relationship between immune cells and alcoholic liver cirrhosis using scRNA-seq.

Inflammatory processes are the primary contributors to the development and progression of ALD (10). A variety of cells in the liver and PBMCs are involved in inflammation, including macrophages, monocytes, NK cells, MAIT cells, which may be contribute to disease severity in patients with severe alcoholic hepatitis (10, 33).. In mild and chronic alcoholic steatohepatitis (ASH), the number of hepatic macrophages is increased, possibly due to infiltrating monocyte-derived macrophages, which also contributes to the pathogenesis of ASH (34). Kupffer cells become sensitized to TLR4-induced signaling after chronic ethanol exposure. These proinflammatory macrophages, together with infiltrating macrophages dictated by LPS, interferon-γ, and granulocyte-macrophage colony stimulatory factor (GM-CSF) signaling, are commonly classified as M1 macrophages as opposed to M2

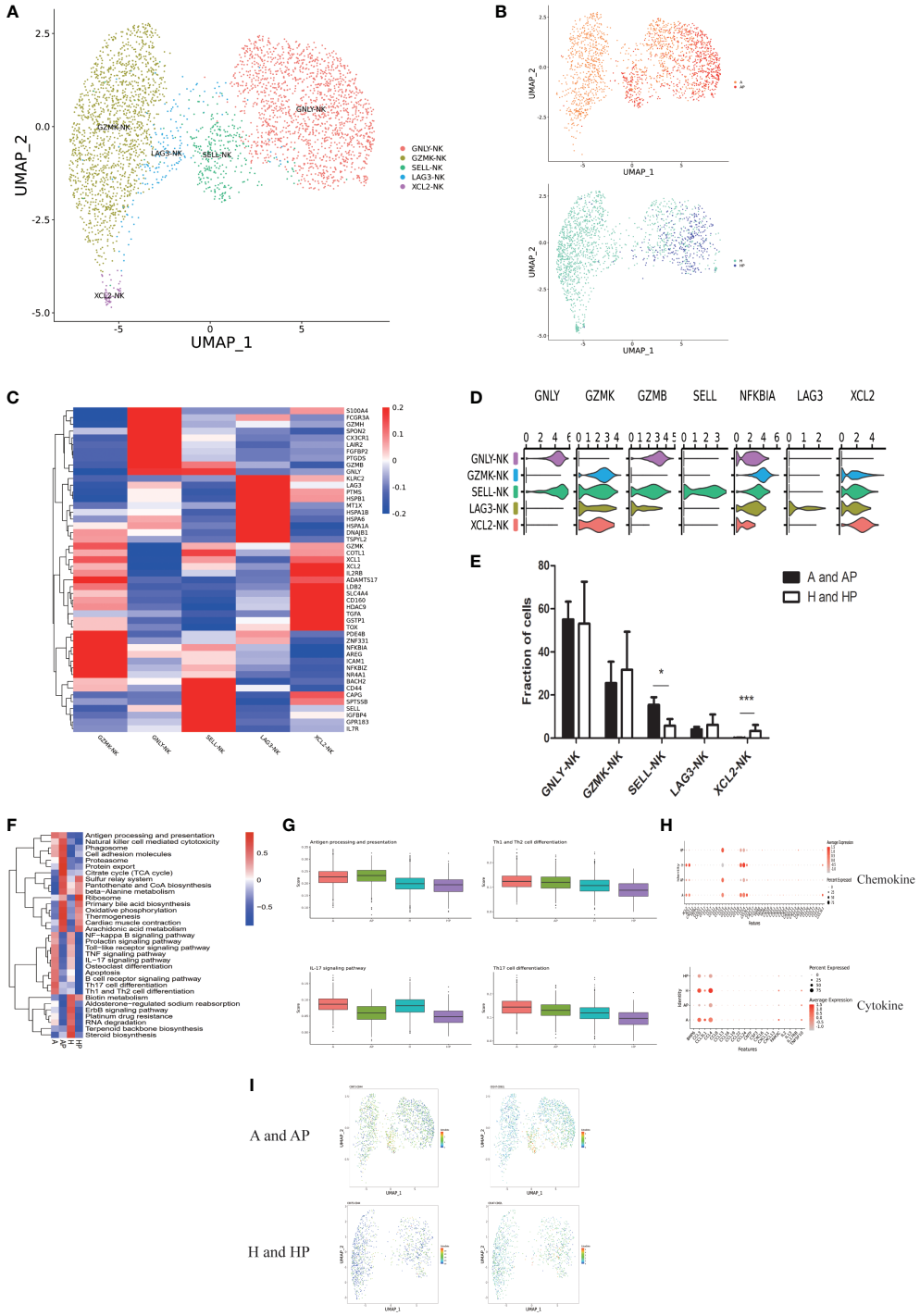

FIGURE 5
Identifying NK cell subpopulations. **(A)** Clustering of 3578 natural killer (NK) cells from five liver tissue and peripheral blood samples (n = 2 healthy and n = 3 alcoholic cirrhosis). **(B)** Annotation of NK cells by patient's condition. **(C)** Heatmap of NK cell cluster marker genes. **(D)** Scaled gene expression in NK cells. **(E)** Fraction of NK cells. **(F)** QuSAGE analysis of NK cells in the A, AP, H, and HP groups. **(G)** Single-sample GSEA (ssGSEA) analysis of NK cells in the A, AP, H, and HP groups. **(H)** Cytokine and chemokine analyses of NK cells in the A, AP, H, and HP groups. **(I)** Proteomic analysis of CD62L and CD44. (*P < 0.05, **P < 0.01, ***P < 0.001).

macrophages that usually arise in Th2 responses in allergy, granuloma formation, and wound healing (10). It is generally believed that activated M1 macrophages produce high amounts of cytokines, such as IL-1β, TNFα, IL-12, IL-18, and IL-23, which help to induce antigen-specific Th1 and Th17 cell inflammatory responses, thereby promoting inflammation. In contrast, activated M2 macrophages secrete large amounts of IL-10, IL-1R antagonist, and TGF-β and subsequently suppress inflammation and promote tissue repair (10). Infiltrating monocytes develop into M1-like hepatic macrophages *via* Notch-1 dependent mitochondrial reprogramming in ASH (35). However, the role of macrophages in the development of alcoholic cirrhosis and the specific underlying mechanisms of the disease remain to be studied.

Patients with ALD have significant infiltration and activation of CD4+ and CD8+ T cells in the liver (36). Studies have shown that NKT

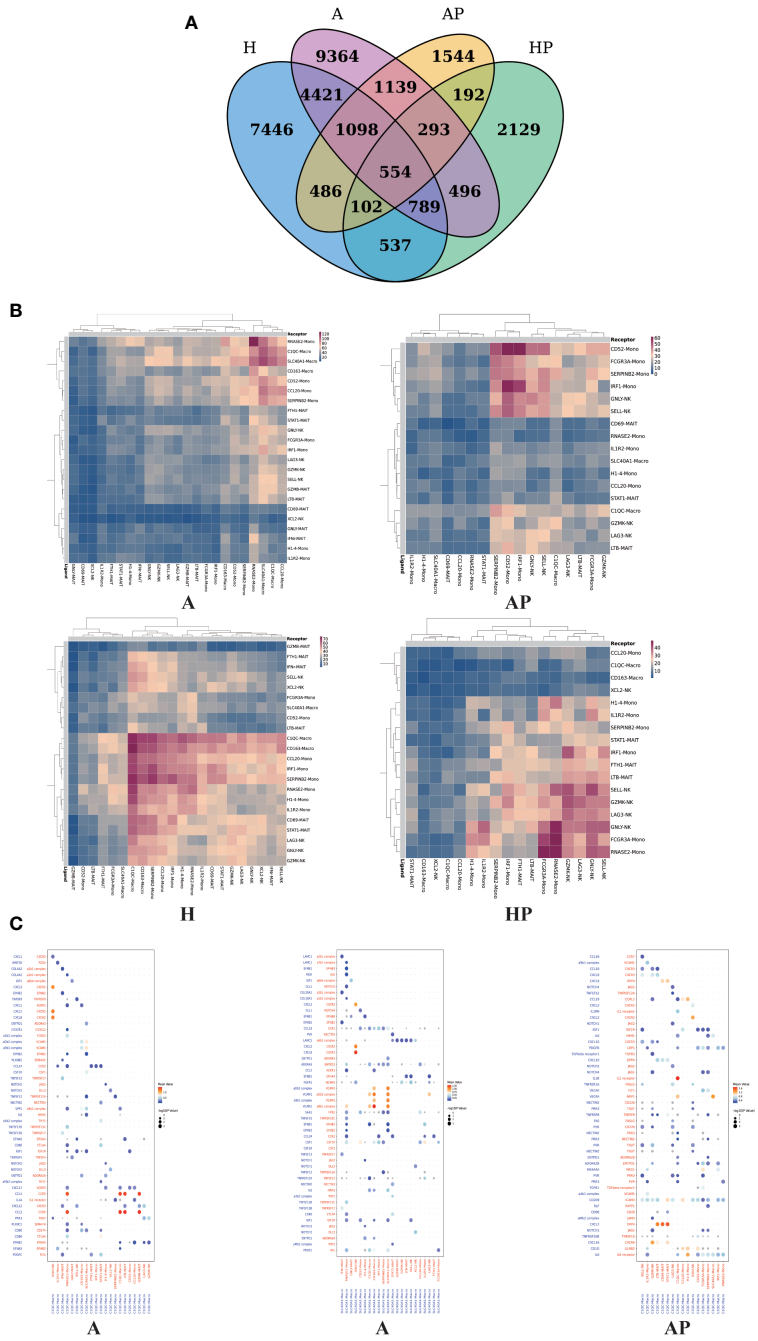

FIGURE 6
The interactions among NK cells, macrophages, and MAIT cells in the A, AP, H, and HP groups. **(A)** Venn diagram comparing different groups. **(B)** Heatmap showing the interactions among NK cells, macrophages, and MAIT cells in the A, AP, H, and HP groups. **(C)** Dot plot of ligand–receptor interactions among macrophages, MAIT, and NK cells in the A and AP groups.

cells promote ALD *via* activation of Kupffer cells and macrophages in mice (11). However, the number of NK T cells in humans is low; hence, NKT cells likely play a less important role in the pathogenesis of alcoholic cirrhosis. In contrast, the liver contains MAIT cells, representing 20%–50% of intrahepatic T cells, which play a key role in controlling bacterial infections (10). Patients with ALD exhibit a marked reduction in MAIT cells, possibly contributing to the increased risk of bacterial infections (37). In conclusion, macrophages, NK T cells, and MAIT cells may play a role in the development of ALD; however, their role in the progression of alcoholic cirrhosis remains unknown.

Here, using scRNA-seq, we dissected the fibrotic niche of human alcoholic cirrhosis, identifying pathogenic subpopulations of macrophages, NK cells, and MAIT cells producing fibroblasts. Several studies have shown that C1QC and SLC40A1 macrophages are associated with the tumor microenvironment, and patients with high C1QC TAM gene signatures have the best prognosis (38–40). Through Cell Phone analysis, we found that C1QC and SLC40A1 macrophages were also associated with liver fibrosis and cirrhosis, which might act by interacting with NK and MAIT cells. These macrophages might have originated from RNASE2 mono, IRF1

mono, IL1R2 mono, and H1-4 mono. Among CD8+ T lymphocytes, GZMB+ effector cells, which express high levels of cytotoxic molecules, and LTB has been reported to play an important role in fibrosis (41, 42). The SELL gene encodes a cell surface adhesion molecule, L-selectin, which belongs to the adhesion/homing receptor family and plays a role in promoting the migration of leukocytes to lymphoid organs, which plays an important role in the immune response (43, 44).

We dissected a complex, profibrotic interactome among multiple fibrosis-associated cell lineages and identified highly relevant intra-fibrosis pathways that can potentially be therapeutic targets for the treatment of alcoholic liver cirrhosis. In this era of precision medicine, this unbiased multilineage approach can help design highly targeted combination therapies that are necessary for an effective antifibrotic potency. The application of our novel fibrosis-associated cell markers could also potentially inform molecular pathology-based patient stratification, which is fundamental to the prosecution of successful antifibrotic clinical trials. Our study has several limitations: the limited number of samples might bias the results. Also, we confirmed that the interaction between MAIT, NK and macrophage lead to the progression of alcoholic cirrhosis, but its specific mechanism requires further study. Our work illustrates the power of single-cell transcriptomics to determine the cellular and molecular basis of human organ fibrosis, providing a conceptual framework for the discovery of relevant therapeutic targets to treat patients with a broad range of alcoholic fibrotic diseases.

Data availability statement

The datasets presented in this study can be found in online repositories. The names of the repository/repositories and accession number(s) can be found below: PRJNA928204 (SRA).

Ethics statement

The studies involving human participants were reviewed and approved by the Ethics Committee for Clinical Research and Animal Trials of the First Affiliated Hospital of Sun Yat-sen University. The patients/participants provided their written informed consent to participate in this study.

Author contributions

AR, YG and YM designed the study. AR, WH, YG and YM conducted experiments. AR, WH, DY and JR harvested the surgical specimen. AR and YG interpreted the histology. AR, WH, JR, DY, PC, QJ, ZF, RD, YG and YM analyzed and interpreted the data. AR, YG and YM prepared the manuscript with critical revision from all authors. All authors contributed to the article and approved the submitted version.

Funding

This research was supported by grants from Natural Science Foundation of Guangdong Province, China (2022A1515011052), National Natural Science Foundation of China, China (81873591), The Science and Technology Planning Project of Guangdong Province, China (2018A050506030). The Guangdong Provincial Key Laboratory Construction Projection on Organ Donation and Transplant Immunology (2020B1212060026 and 2017B030314018), Guangdong Provincial International Cooperation Base of Science and Technology (Organ Transplantation) (2015B050501002).

Acknowledgments

Thanks to NovelBio for the technical support of single cell sequencing.

Conflict of interest

The authors declare that the research was conducted in the absence of any commercial or financial relationships that could be construed as a potential conflict of interest.

Publisher's note

Supplementary material

The Supplementary Material for this article can be found online at: https://www.frontiersin.org/articles/10.3389/fimmu.2023.1034356/full#supplementary-material

References

1. Thomson MJ, Tapper EB, Lok ASF. Dos and don'ts in the management of cirrhosis: A view from the 21st century. *Am J Gastroenterol* (2018) 113(7):927–31. doi: 10.1038/s41395-018-0028-5

2. Wilde B, Katsounas A. Immune dysfunction and albumin-related immunity in liver cirrhosis. *Mediators Inflamm* (2019) 2019:7537649. doi: 10.1155/2019/7537649

3. Tsochatzis EA, Bosch J, Burroughs AK. Liver cirrhosis. *Lancet* (2014) 383 (9930):1749–61. doi: 10.1016/S0140-6736(14)60121-5

4. Mann RE, Smart RG, Govoni R. The epidemiology of alcoholic liver disease. *Alcohol Res Health* (2003) 27(3):209–19.

5. Lucey MR. Alcohol-associated cirrhosis. *Clin Liver Dis* (2019) 23(1):115–26. doi: 10.1016/j.cld.2018.09.013

6. Shirazi F, Singal AK, Wong RJ. Alcohol-associated cirrhosis and alcoholic hepatitis hospitalization trends in the united states. *J Clin Gastroenterol* (2021) 55(2):174–9. doi: 10.1097/MCG.0000000000001378

7. Testino G, Leone S, Fagoonee S, Pellicano R. Alcoholic liver fibrosis: Detection and treatment. *Minerva Med* (2018) 109(6):457–71. doi: 10.23736/S0026-4806.18.05844-5

8. Sica A, Invernizzi P, Mantovani A. Macrophage plasticity and polarization in liver homeostasis and pathology. *Hepatology* (2014) 59(5):2034–42. doi: 10.1002/hep.26754

9. Ramachandran P, Dobie R, Wilson-Kanamori JR, Dora EF, Henderson BEP, Luu NT, et al. Resolving the fibrotic niche of human liver cirrhosis at single-cell level. *Nature* (2019) 575(7783):512–8. doi: 10.1038/s41586-019-1631-3

10. Gao B, Ahmad MF, Nagy LE, Tsukamoto H. Inflammatory pathways in alcoholic steatohepatitis. *J Hepatol* (2019) 70(2):249–59. doi: 10.1016/j.jhep.2018.10.023

11. Cui K, Yan G, Xu C, Chen Y, Wang J, Zhou R, et al. Invariant NKT cells promote alcohol-induced steatohepatitis through interleukin-1beta in mice. *J Hepatol* (2015) 62:1311–8. doi: 10.1016/j.jhep.2014.12.027

12. Gao B, Ma J, Xiang X. MAIT cells: A novel therapeutic target for alcoholic liver disease? *Gut* (2018) 67:784–6. doi: 10.1136/gutjnl-2017-315284

13. Chen S, Zhou Y, Chen Y, Gu J. Fastp: An ultra-fast all-in-one FASTQ preprocessor. *Bioinformatics* (2018) 34(17):i884. doi: 10.1093/bioinformatics/bty560

14. Vento-Tormo R, Efremova M, Botting RA, Turco MY, Vento-Tormo M, Meyer KB, et al. Single-cell reconstruction of the early maternal–fetal interface in humans. *Nature* (2018) 563(7731):347. doi: 10.1038/s41586-018-0698-6

15. Gur Y, Bolen CR, Juilee T, Kleinstein SH. Quantitative set analysis for gene expression: A method to quantify gene set differential expression including gene-gene correlations. *Nucleic Acids Res* (2013) 41(18):e170. doi: 10.1093/nar/gkt660

16. Cao J, Spielmann M, Qiu X, Huang X, Ibrahim DM, Hill AJ, et al. The single-cell transcriptional landscape of mammalian organogenesis. *Nature* (2019) 566:496–502. doi: 10.1038/s41586-019-0969-x

17. Riva A, Mehta G. Regulation of monocyte-macrophage responses in cirrhosis-role of innate immune programming and checkpoint receptors. *Front Immunol* (2019) 10:167. doi: 10.3389/fimmu.2019.00167

18. Stickel F, Datz C, Hampe J, Bataller R. Pathophysiology and management of alcoholic liver disease: Update 2016. *Gut Liver* (2017) 11(2):173–88. doi: 10.5009/gnl16477

19. Sørensen TI, Orholm M, Bentsen KD, Høybye G, Eghøje K, Christ-offersen P. Prospective evaluation of alcohol abuse and alcoholic liver injury in men as predictors of development of cirrhosis. *Lancet* (1984) 2:241–4. doi: 10.1016/S0140-6736(84)90295-2

20. Kamper-Jørgensen M, Grønbaek M, Tolstrup J, Becker U. Alcohol and cirrhosis: Dose. response or threshold effect? *J Hepatol* (2004) 41:25–30. doi: 10.1016/j.jhep.2004.03.002

21. Kennedy OJ, Roderick P, Buchanan R, Fallowfield JA, Hayes PC, Parkes J. Systematic review with meta-analysis: Coffee consumption and the risk of cirrhosis. *Aliment Pharmacol Ther* (2016) 43:562–74. doi: 10.1111/apt.13523

22. Dam MK, Flensborg-Madsen T, Eliasen M, Becker U, Tolstrup JS. Smoking and risk of liver cirrhosis: A population-based cohort study. *Scand J Gastroenterol* (2013) 48:585–91. doi: 10.3109/00365521.2013.777469

23. Shoreibah M, Anand BS, Singal AK. Alcoholic hepatitis and concomitant hepatitis c virus infection. *World J Gastroenterol* (2014) 20:11929–34. doi: 10.3748/wjg.v20.i34.11929

24. Gitto S, Micco L, Conti F, Andreone P, Bernardi M. Alcohol and viral hepatitis: A mini-review. *Dig Liver Dis* (2009) 41:67–70. doi: 10.1016/j.dld.2008.05.009

25. Naveau S, Giraud V, Borotto E, Aubert A, Capron F, Chaput JC. Excess weight risk factor for alcoholic liver disease. *Hepatology* (1997) 25:108–11. doi: 10.1002/hep.510250120

26. Reed T, Page WF, Viken RJ, Christian JC. Genetic predisposition to organ-specific endpoints of alcoholism. *Alcohol Clin Exp Res* (1996) 20:1528–33. doi: 10.1111/j.1530-0277.1996.tb01695.x

27. Stinson FS, Grant BF, Dufour MC. The critical dimension of ethnicity in liver cirrhosis mortality statistics. *Alcohol Clin Exp Res* (2001) 25:1181–7. doi: 10.1111/j.1530-0277.2001.tb02333.x

28. Levy RE, Catana AM, Durbin-Johnson B, Halsted CH, Medici V. Ethnic differences in presentation and severity of alcoholic liver disease. *Alcohol Clin Exp Res* (2015) 39:566–74. doi: 10.1111/acer.12660

29. Stickel F, Moreno C, Hampe J, Morgan MY. The genetics of alcohol dependence and alcohol-related liver disease. *J Hepatol* (2017) 66:195–211. doi: 10.1016/j.jhep.2016.08.011

30. Dunn W, Shah VH. Pathogenesis of alcoholic liver disease. *Clin Liver Dis* (2016) 20(3):445–56. doi: 10.1016/j.cld.2016.02.004

31. Petrasek J, Iracheta-Vellve A, Csak T, Satishchandran A, Kodys K, Kurt-Jones EA, et al. STING-IRF3 pathway links endoplasmic reticulum stress with hepatocyte apoptosis in early alcoholic liver disease. *Proc Natl Acad Sci United States America* (2013) 110(41):16544–9. doi: 10.1073/pnas.1308331110

32. Petrasek J, Dolganiuc A, Csak T, Nath B, Hritz I, Kodys K, et al. Interferon regulatory factor 3 and type I interferons are protective in alcoholic liver injury in mice by way of crosstalk of parenchymal and myeloid cells. *Hepatology* (2011) 53(2):649–60. doi: 10.1002/hep.24059

33. Maras JS, Das S, Bhat A, Kumar Vyas A, Yadav G, Chaudhary S, et al. Dysregulated lipid transport proteins correlate with pathogenesis and outcome in severe alcoholic hepatitis. *Hepatol Commun* (2019) 3(12):1598–625. doi: 10.1002/hep4.1438

34. Wang M, You Q, Lor K, Chen F, Gao B, Ju C. Chronic alcohol ingestion modulates hepatic macrophage populations and functions in mice. *J Leukoc Biol* (2014) 96:657–65. doi: 10.1189/jlb.6A0114-004RR

35. Xu J, Chi F, Guo T, Punj V, Lee WN, French SW, et al. NOTCH reprograms mitochondrial metabolism for proinflammatory macrophage activation. *J Clin Invest* (2015) 125:1579–90. doi: 10.1172/JCI76468

36. Chedid A, Mendenhall CL, Moritz TE, French SW, Chen TS, Morgan TR, et al. Cell-mediated hepatic injury in alcoholic liver disease. veterans affairs cooperative study group 275. *Gastroenterology* (1993) 105:254–66. doi: 10.1016/0016-5085(93)90034-A

37. Ge X, Antoine DJ, Lu Y, Arriazu E, Leung TM, Klepper AL, et al. High mobility group box-1 (HMGB1) participates in the pathogenesis of alcoholic liver disease (ALD). *J Biol Chem* (2014) 289:22672–91. doi: 10.1074/jbc.M114.552141

38. Li X, Zhang Q, Chen G, Luo D. Multi-omics analysis showed the clinical value of gene signatures of C1QC+ and SPP1+ TAMs in cervical cancer. *Front Immunol* (2021) 12:694801. doi: 10.3389/fimmu.2021.694801

39. Chen LH, Liu JF, Lu Y, He XY, Zhang C, Zhou HH. Complement C1q (C1qA, C1qB, and C1qC) may be a potential prognostic factor and an index of tumor microenvironment remodeling in osteosarcoma. *Front Oncol* (2021) 11:642144. doi: 10.3389/fonc.2021.642144

40. Zhang Q, He Y, Luo N, Patel SJ, Han Y, Gao R, et al. Landscape and dynamics of single immune cells in hepatocellular carcinoma. *Cell* (2019) 179(4):829–845.e20. doi: 10.1016/j.cell.2019.10.003

41. Notarbartolo S, Ranzani V, Bandera A, Gruarin P, Bevilacqua V, Putignano AR, et al. Integrated longitudinal immunophenotypic, transcriptional and repertoire analyses delineate immune responses in COVID-19 patients. *Sci Immunol* (2021) 6(62):eabg5021. doi: 10.1126/sciimmunol.abg5021

42. Brozova J, Karlova I, Novak J. Analysis of the phenotype and function of the subpopulations of mucosal-associated invariant T cells. *Scand J Immunol* (2016) 84(4):245–51. doi: 10.1111/sji.12467

43. Xu H, Chen J, Wang Y, Wu Y, Liang Y. SELL and IFI44 as potential biomarkers of sjögren's syndrome and their correlation with immune cell infiltration. *Genes Genet Syst* (2021) 96(2):71–80. doi: 10.1266/ggs.20-00053

44. Wedepohl S, Beceren-Braun F, Riese S, Buscher K, Enders S, Bernhard G, et al. L-selectin–a dynamic regulator of leukocyte migration. *Eur J Cell Biol* (2012) 91(4):257–64. doi: 10.1016/j.ejcb.2011.02.007

frontiers | Frontiers in Immunology

TYPE Review
PUBLISHED 25 August 2023
DOI 10.3389/fimmu.2023.1238452

OPEN ACCESS

EDITED BY
Thiago Almeida Pereira,
Stanford University, United States

REVIEWED BY
Zhaojun Wang,
Shanghai Jiao Tong University, China
Janos G. Filep,
Montreal University, Canada

*CORRESPONDENCE
Jo A. Van Ginderachter
jo.van.ginderachter@vub.be

†These authors share senior authorship

RECEIVED 11 June 2023
ACCEPTED 11 August 2023
PUBLISHED 25 August 2023

CITATION
Musrati MA, De Baetselier P, Movahedi K and Van Ginderachter JA (2023) Ontogeny, functions and reprogramming of Kupffer cells upon infectious disease.
Front. Immunol. 14:1238452.
doi: 10.3389/fimmu.2023.1238452

Ontogeny, functions and reprogramming of Kupffer cells upon infectious disease

Mohamed Amer Musrati[1,2], Patrick De Baetselier[1,2], Kiavash Movahedi[1,2,3†] and Jo A. Van Ginderachter[1,2*†]

[1]Lab of Cellular and Molecular Immunology, Vrije Universiteit Brussel, Brussels, Belgium, [2]Myeloid Cell Immunology Lab, VIB Center for Inflammation Research, Brussels, Belgium, [3]Lab of Molecular and Cellular Therapy, Vrije Universiteit Brussel, Brussels, Belgium

The liver is a vital metabolic organ that also performs important immune-regulatory functions. In the context of infections, the liver represents a target site for various pathogens, while also having an outstanding capacity to filter the blood from pathogens and to contain infections. Pathogen scavenging by the liver is primarily performed by its large and heterogeneous macrophage population. The major liver-resident macrophage population is located within the hepatic microcirculation and is known as Kupffer cells (KCs). Although other minor macrophages reside in the liver as well, KCs remain the best characterized and are the best well-known hepatic macrophage population to be functionally involved in the clearance of infections. The response of KCs to pathogenic insults often governs the overall severity and outcome of infections on the host. Moreover, infections also impart long-lasting, and rarely studied changes to the KC pool. In this review, we discuss current knowledge on the biology and the various roles of liver macrophages during infections. In addition, we reflect on the potential of infection history to imprint long-lasting effects on macrophages, in particular liver macrophages.

KEYWORDS

liver, Kupffer cell, liver macrophages, infectious diseases, macrophage ontogeny

Liver macrophage heterogeneity and functions during homeostasis

Ontogeny of Kupffer cells

The liver harbors a large and heterogeneous population of resident macrophages (Figure 1). Work on mouse models has generated extensive information on the major resident macrophage population in the liver, known as KCs, which resides in the sinusoidal vessels and reaches into the perisinusoidal space of Disse towards hepatic stellate cells and hepatocytes (2). KCs are established embryonically and originate from yolk sac erythro-myeloid progenitors that seed the fetal liver by E10.5, later becoming heavily diluted by fetal

10.3389/fimmu.2023.1238452

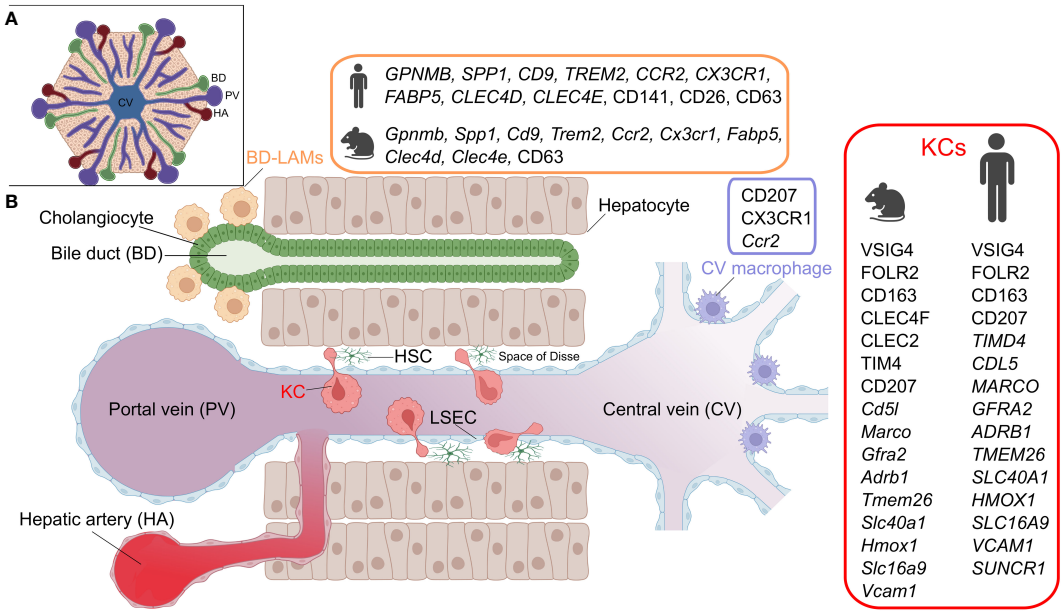

FIGURE 1
Hepatic macrophage subsets. A) The structure of the liver lobule. B) A cross section of liver sinusoids illustrating the different resident-macrophage populations. KC, Kupffer cell; LAM, lipid-associated macrophage; LSEC, liver sinusoidal endothelial cell; HSC, hepatic stellate cell. Marker details adapted from (1). Figure created with BioRender.com.

liver monocytes (3–6), while also receiving a minor contribution from blood monocytes during the post-natal period (7). Studies have highlighted the importance of the transcription factors *Id3* and *Nr1h3* (coding for LXRα) for normal KC development and maintenance of identity, respectively (8, 9).

During homeostatic conditions, KCs self-maintain and are only marginally replenished by adult bone marrow-derived monocytes (3, 5, 10). However, as will be discussed in later sections, bone marrow contribution to KCs increases dramatically in response to certain liver insults that trigger KC depletion. An important question is whether ontogeny is important for KC functionality. Work utilizing a murine model of diphtheria toxin-mediated specific KC depletion (*Clec4f*-DTR mice), demonstrated that circulating monocytes engraft in the liver upon KC depletion and give rise to monocyte-derived KCs (moKCs) that are highly reminiscent of their embryonic KC (emKCs) predecessors, at least at the transcriptome level (7). Monocyte engraftment as moKCs is orchestrated by the cellular niche of KCs, comprised of hepatocytes, liver sinusoidal endothelial cells (LSECs), and hepatic stellate cells and mediated via niche-derived signals such as DLL4, bone morphogenetic proteins (BMPs), TGFβ and desmosterol (2, 11). In particular, the ALK1-BMP9/10 axis, involving ALK1 (KCs) and BMP9/10 (stellate cells), is of critical importance for KC homeostasis, as ALK1 loss leads to defects in KC development and maintenance (12, 13).

Phenotypically, murine KCs can be readily identified by their unique surface expression of the endocytic C-type lectin receptor CLEC4F (7, 14). Additionally, KCs can be distinguished from other liver macrophages by TIM4, CLEC1B and VSIG4 expression, although these markers can also be expressed by other tissue-resident macrophages outside the liver (14, 15). One outstanding current challenge is to phenotypically distinguish between moKCs and emKCs. Given that TIM4 is acquired in the late stages of KC development, several studies relied on the lack of TIM4 expression to define moKCs in models of non-alcoholic steatohepatitis and irradiation-induced liver injury (7, 16–18). However, it is likely that the temporal regulation of TIM4 acquisition is model-dependent. Indeed, in the context of natural KC development during embryogenesis, *Timd4* expression occurs relatively early and precedes the upregulation of other KC marker genes such as *Clec4f* (2). Likewise, *Cd163* mRNA has been shown to be mainly enriched in emKCs (7, 17). However, *in situ* translatome analysis using a Cre-driven RiboTag reporter revealed that emKCs and moKCs express similar levels of CD163 (19). One marker that appears to be highly enriched in emKCs, and lowly expressed by moKCs across models is MARCO (17, 19). However, whether MARCO expression by itself enables a clear distinction between the two subsets has not been tested. Consequently, genetic fate-mapping, using transgenic mouse strains that report bone marrow ontogeny, remains the most reliable and non-invasive method for separating em- and moKCs.

Functions of Kupffer cells

KCs perform a wide array of homeostatic functions that support liver functionality and limit tissue injury. KCs play a key role in maintaining immunological **tolerance** in the liver under baseline conditions. For instance, human KCs secrete IL-10 in response to LPS stimulation *in vitro* (20). Murine KCs scavenge circulating

particles, promote the expansion of Foxp3$^+$IL-10$^+$ T regulatory cells (21) and suppress dendritic cell-induced T-cell activation by the action of prostaglandins (22). Moreover, the liver is a major site for **iron metabolism** (23) and murine KCs are implicated in regulating iron homeostasis as they express key genes involved in macrophage heme-iron metabolism, such as *Spi-c* and *Nfe2l2* (24). Murine KCs scavenge damaged and aged red blood cells and are strategically located to deliver iron to hepatocytes (2, 24, 25). Murine KCs are also thought to control body iron levels by regulating hepcidin expression (26), although this remains controversial (27). In addition to their erythro-phagocytic capacity, murine KCs are implicated in **maintaining hemostasis** by contributing to the clearance of aged platelets (28, 29). This is mediated by the Ashwell-Morell receptor and macrophage galactose lectin, as well as CLEC4F (28, 29). As such, KC depletion in mice via clodronate liposomes was associated with adverse platelet dysfunctions, as manifested by increased bleeding following wounding (29). Furthermore, murine KCs participate in the efferocytosis of apoptotic cells (30), and are also thought to regulate circulating neutrophil numbers by mediating the clearance of apoptotic neutrophils (31, 32). KCs are also implicated in **lipid metabolism** as they are enriched in the expression of liver X-family of receptors (LXRs) and peroxisome proliferator-activated family of receptors (PPARs), involved in various aspects of cholesterol transport and metabolism (reviewed in (33)). Murine KCs are abundantly equipped with low density lipoprotein (LDL) receptor, and appear to serve as gatekeepers for LDL cholesterol transport to hepatocytes (34). In line with this, in *Csf1r* knockout rats, which exhibit major deficiencies in many tissue-resident macrophages including KCs, the liver shows a vast dysregulation of genes related to lipid metabolism, liver growth and function, and endures extensive age-progressive steatosis (35). Additionally, murine KCs have recently been shown to be the major source of miR-690 within the liver, a microRNA that negatively regulates hepatocyte lipogenesis and hepatic stellate cell fibrogenic activation (36). Deletion of miR-690 shifts KCs towards a pro-inflammatory polarization, suggesting that this microRNA regulates some KC functions in the steady state liver (36). Consistent with this, treatment with miR-690 can reverse the impaired erythro-phagocytic capacity of KCs associated with non-alcoholic steatohepatitis (36).

Liver macrophage heterogeneity

A recent study has identified two distinct subpopulations of embryonically-derived KCs in mice: a major CD206^{low}ESAM$^-$ population (KC1) and a minor CD206^{high}ESAM$^+$ population (KC2) (37). Although they share the expression of core KC genes, KC1 mainly expresses genes associated with immune functions, while KC2 exhibits a higher expression of endothelial markers and genes associated with metabolic pathways such as lipid metabolism. Accordingly, the depletion of KC2 has been shown to prevent diet-induced obesity (37). Subsequent reports argued that the KC2 might represent endothelial cell-KC doublets, hence, these populations are still a current subject of debate (12, 38, 39).

Although KCs represent the major population of liver-resident macrophages, the steady state liver also hosts other macrophage populations that are spatially segregated (Figure 1) (12). These include bile duct-associated macrophages, which show transcriptional similarities to lipid-associated macrophages, expressing genes such as *Gpnmb*, *Spp1* and *Trem2* (12). Notably, a similar counterpart is also present in human livers (12). Moreover, another population of *Cd207*-expressing macrophages has been detected around the central veins of the murine liver (12). Apart from some data suggesting that murine bile duct macrophages exhibit a lower pro-inflammatory response to LPS stimulation than KCs, these newly identified macrophages generally lack functional characterization (12). Finally, the murine liver also harbors another population of macrophages residing in its capsule (40). These CX3CR1-expressing capsular macrophages are derived from monocytes, and accumulate after weaning in a microbiota-dependent manner and perform defensive functions against peritoneal pathogens (40).

Human Kupffer cells

A number of studies sought to characterize KCs in human livers (1) and we hereby review notable findings. Single cell RNA-sequencing (scRNA-seq) of *CD163+VSIG4+* cells from human livers has revealed subpopulations with distinct gene expression signatures, including *MARCO+LILRB5+* and *CD1C+FCER1A+* populations, enriched in metabolic/immunoregulatory and antigen presentation pathways, respectively (41). Another study also reported a *VSIG4+MARCO+* population based on scRNA-seq of human livers and has histologically shown that these cells are concentrated in periportal areas (42). Moreover, analysis of healthy and cirrhotic human livers identified two KC-like populations that were commonly enriched in *CD163*, *MARCO* and *CD5L,* while differing in *TIMD4* expression. Noteworthy, the *MARCO+TIMD4-* population was less present in the cirrhotic livers. Immunohistochemistry showed that while *TIMD4+* cells were equally present in both the healthy and cirrhotic livers, *MARCO+* cells were reduced during cirrhosis (43). A recent analysis of healthy human livers, using spatial proteo-genomics and single-cell sequencing approaches, identified a macrophage population that resembles murine KCs (12). The human KC-like population highly expressed core murine KC markers, including *CD5L, VSIG4, SLC1A3, CD163, FOLR2, TIMD4, MARCO, GFRA2, ADRB1, TMEM26, SLC4OA1, HMOX1, SLC16A9* and *VCAM1* (Figure 1), and appears to be localized in the mid zones of the liver lobules. Additionally, the same study detected a moKC-like hepatic macrophage subset in human livers, which expresses many of the core KC genes but lacks *TIMD4* expression (12). It is noteworthy that human KCs lack the expression of the specific murine KC marker CLEC4F, and in contrast to murine counterparts, express *SUCNR1* (12) (discrepancies in KC markers between species and studies were recently reviewed in (1)). Although delineating the ontogeny of KCs in humans is difficult to achieve, it is clear that humans generally endure a variety of pathological insults that affect the liver throughout life. Several insults that are known to alter KC

ontogeny in mice, such as infections, a high-fat diet and alcohol consumption, are highly relevant for humans. It is therefore likely that the ontogeny of human KCs varies across individuals, and may possibly be a mixture of bone marrow-derived as well as embryonic KCs. Variability likely also exists at the level of the activation status of human KCs since exposure to inflammatory episodes can imprint prolonged changes on macrophages, as elaborated later in this review.

Liver macrophages in the context of infections

Bacterial infections

The liver has an outstanding capacity to filter circulating bacteria (44, 45). This superior microbial scavenging property is underlined by the presence of KCs in the hepatic vasculature (44, 46). Due to their remarkable pattern of zonation around the periportal tracts of the liver blood vessels (47), KCs are among the first cells to encounter the incoming antigen-rich portal blood. KCs form an extensive scavenger network that actively monitors sinusoidal blood and captures circulating bacteria (48–50). KCs are equipped with a large repertoire of phagocytic receptors that facilitates the clearance of bacterial pathogens (49–51). A well characterized KC receptor that plays an essential role in bacterial clearance is VSIG4 (48–50). In addition to serving as a complement receptor for C3-opsonized bacteria (50), VSIG4 can directly bind the lipoteichoic acid component of the gram-positive bacterial cell wall, enabling their phagocytosis by KCs (48). Indeed, loss of *Vsig4* results in enhanced bacterial dissemination and increased mortality in mice infected with *Listeria monocytogenes* (50). Deletion of *Vsig4* in a mouse model of alcoholic liver disease hinders the phagocytosis of *Enterococcus faecalis* by KCs, and associates with increased systemic dissemination of gut-translocated bacteria as well as exacerbated pathology (52). Noteworthy, decreased *Vsig4* expression and a reduced percentage of $VSIG4^{+}$ macrophages is seen in the livers of patients with alcohol-related liver disease (52). Aside from the direct role in bacterial clearance via phagocytosis, KCs can indirectly instruct other innate immune cells to launch anti-microbial responses. For example, during *Borrelia burgdorferi* infection, murine KCs present antigen to invariant natural killer T cells (iNKT) in a CD1d-dependent manner, leading to iNKT cell activation and interferon-γ production (46). Activated iNKT cells in turn restrict the extra-hepatic dissemination of bacteria (46). Furthermore, the capture of certain bacterial pathogens such as *Bacillus cereus* and Methicillin-resistant *Staphylococcus aureus* (MRSA) by murine KCs has been shown to induce platelet aggregation on KCs (53). This process requires interactions between GPIb and GPIIb on platelets with von Willebrand factor (vWF) on KCs. Platelet aggregation appears to serve an important protective function in response to *B. cereus* infection in mice as GPIbα deficiency leads to increased mortality, impaired bacterial clearance, exacerbated liver damage and vascular injury (53). Interestingly, murine KCs possess dual-track mechanisms to remove bacteria that permit either the slow or fast clearance of bacterial pathogens (49). The former clearance route is regulated by time-dependent opsonization of bacteria by platelets via interaction with complement proteins. These bacteria-platelet complexes exhibit a relatively increased half-life in the circulation and are subsequently captured by VSIG4 on KCs. Conversely, the fast clearance route is mediated by scavenger receptors in a platelet-independent manner, hence allowing the rapid removal of bacteria (49). This dual-track clearance mechanism ensures the balance between rapid removal of bacteria while also maintaining antigen availability for the priming of adaptive immune responses (49). Interestingly, the anti-bacterial properties of murine KCs are strongly regulated by the gut microbiome (particularly the bacterial microbiome), and depletion of the gut microbiota associates with defective KC responses and results in higher vulnerability to infection (47, 54). Remarkably, the spatial distribution of KCs around the periportal tracts in the liver is in itself microbiota-dependent (47). Mechanistically, microbiome-derived signals regulate the composition of the extracellular matrix of LSECs in a MyD88-dependent manner, causing CXCL9 retention on periportal LSECs, hence allowing interaction with CXCR3 on KCs (47). Moreover, continuous crosstalk with gut commensals can directly shape the bacterial killing properties of KCs in a microbiome-derived, D-lactate-dependent manner (54). In addition, murine KCs exhibit a loss of their typical phenotype, gene signature and spatial zonation upon the deletion of *Alk1*, and this associates with impaired bacterial clearance and ultimately increased mortality in response to bacterial infection (13).

Intriguingly, encounter with some bacterial pathogens seems to compromise KC viability, resulting in the death and transient depletion of KCs. For instance, the facultative intracellular bacterial pathogens *L. monocytogenes*, as well as *Salmonella enterica* serovar Typhimurium, are known to infect murine liver macrophages leading to macrophage death (55). KCs respond to *L. monocytogenes* infection by undergoing necroptosis (55), a form of programmed lytic cell death via Receptor-Interacting Protein Kinase 3 (RIPK3) activation of Mixed Lineage Kinase Domain-like (MLKL) (56). Dying KCs become massively replaced by CCR2-dependent, monocyte-derived macrophages that proliferate intrahepatically, driven by signals including CSF1, hepatocyte-derived IL-33 and basophil-derived IL-4 (55). Interestingly, *L. monocytogenes*-induced KC necroptosis is thought to serve a beneficial host response by orchestrating a type 2 inflammation that limits excessive liver injury. Mechanistically, the necroptosis of KCs promotes hepatocyte production of IL-33, which presumably induces IL-4 production by basophils and thereby the alternative activation of liver macrophages (55). Paradoxically, another study reported that *L. monocytogenes* induces rapid cell death in murine liver macrophages in an IRF3-dependent manner, and showed that *Irf3* deletion rescues KC death and reduces hepatic bacterial burden (57), suggesting a pathogenic consequence associated with KC death in this context. Notably, no restoration of emKCs is observed following *L. monocytogenes* infection, and instead, recruited moKCs appear to dominate and engraft durably in the liver after the clearance of infection (55). Whether this change alters KC responses to subsequent bacterial infections is unknown. However, murine moKCs have been shown to exhibit a markedly

superior phagocytosis of a number of bacterial pathogens, including *L. monocytogenes* (17), suggesting that the modulation of KC ontogeny might lead to functional consequences. In contrast, *in vitro* examination has shown that moKCs generated in the *Clec4f*-DTR mouse model are equally phagocytic as emKCs (7). Nevertheless, the latter finding might reflect functional changes associated with the loss of the natural KC microenvironment, or even the artificial, non-physiological method of moKCs generation. Noteworthy, the phagocytic capacity of KCs can be altered by exposure to environmental factors. For instance, certain clinical drugs have been shown to negatively modulate the scavenging properties of murine KCs (58, 59). For example, tacrolimus, a commonly used drug to prevent graft rejection after solid organ transplantation and to treat graft-versus-host disease after bone marrow transplantation, has been shown to inhibit bacterial uptake and killing by KCs in mice (59). In humans, the risk of *Staphylococcus aureus* infection is associated with higher tacrolimus concentrations in liver transplant recipients (59). An overdose of acetaminophen has also been shown to imprint an immune-suppressive profile on murine KCs by upregulating PD1 at the cell surface, and to impair their phagocytic properties (58). Intriguingly, contrasting the negative effect of the aforementioned drugs on KCs, physical exercise has been shown to boost the phagocytic capacity of murine KCs, and to increase their expression of the phagocytic receptors MARCO and SR-A, which associates with enhanced endotoxin clearance from the blood circulation (60). Moreover, exercise training imprints a long-lasting anti-inflammatory profile on murine KCs, manifested in a lowered production of pro-inflammatory cytokines and an enhanced secretion of IL-10 and IL-1Ra in response to an LPS challenge (61). This exercise-induced anti-inflammatory reprogramming of KCs is regulated by itaconate metabolism, and can be recapitulated by KC treatment with itaconate, whereas the deletion of *Irg1* (which codes for cis-aconitate decarboxylase) abrogates this beneficial effect of exercise in mice (61). Importantly, the livers of exercised mice undergo less injury and necrosis following an LPS challenge (61), thus highlighting the effects of physical exercise in modulating the response to infectious inflammation in the liver. Aside from the various roles played by KCs during microbial infections, murine liver capsular macrophages are also implicated in the response to bacteria. They are thought to limit peritoneal pathogen dissemination to the liver by recruiting neutrophils, although the underlying mechanism remains vague (40).

In summary, in addition to their typical scavenging role, KCs regulate complex processes that facilitate the containment of bacterial infections and tissue injury. Moreover, the bactericidal properties of KCs are subject to regulation by environmental factors.

Viral infections

Hepato-tropic viruses, such as hepatitis B virus (HBV), can establish life-long persistent infections (62) and KCs seem to be implicated in the different aspects of HBV pathogenesis. Mouse experiments utilizing clodronate liposome-mediated KC depletion have suggested that KCs exhibit suppressive effects on $CD8^+$ T cells during HBV infection (63). As such, KC depletion lessens HBV persistence and associates with enhanced numbers and activation of $CD8^+$ T cells (63). Interestingly, KC-mediated suppression of $CD8^+$ T cells has been shown to be TLR2-dependent, as KCs from WT but not TLR2 KO mice abundantly produced the $CD8^+$ T cell-suppressive cytokine IL10 following *in vitro* stimulation with the hepatitis B core antigen (63). Murine KCs have also been reported to use an IL-10-dependent mechanism to promote systemic specific humoral tolerance to HBV (64). Recent work further explored the cellular and molecular mechanisms responsible for $CD8^+$ T cell dysfunction during HBV infection. To dissect the consequences of hepatocellular-mediated priming versus KC-mediated priming of $CD8^+$ T cells, a recent study performed cell-selective HBV targeting to either hepatocytes (natural target of HBV) or KCs (non-natural targets of HBV) in mice. This approach revealed that hepatocellular priming of virus-specific $CD8^+$ T cells generates dysfunctional $CD8^+$ T cells with impaired antiviral capacity (65). Conversely, KC-mediated priming leads to $CD8^+$ T-cell differentiation into effector cells endowed with potent antiviral functions (65). KC-primed $CD8^+$ T cells exhibit higher expression of activation markers such as *Gzma*, *Gzmb* and *Ifng* and show increased expression of *Il2*, the critical T-cell growth factor (65, 66). In line with these observations, treatment with recombinant IL-2 (IL-2-c) rescues and restores the antiviral functions of hepatocellularly-primed murine $CD8^+$ T cells (65). Follow-up work has shown that the ability of IL-2-c treatment to rejuvenate dysfunctional $CD8^+$ T cells during HBV infection is mediated by the KC2 subset, that is enriched in the expression of IL-2 signaling components (67). As such, the depletion of KC2 significantly impairs the efficacy of IL-2-c treatment (67).

Viral infections are also known to elicit dynamic compositional changes in the liver macrophage pool (68, 69). For instance, rapid IRF3-dependent KC death is seen in mice following infection with human adenovirus (57). Intriguingly, KC death during these settings appears functionally relevant. Indeed, although KC death was spared in IRF3 knockout mice, these mice exhibited higher hepatic viral loads. These data suggested either a pathogenic role for KCs during adenovirus infection, or an IRF3-mediated macrophage death pathway that serves a protective role during this infection (57). KC death also occurs after intravenous delivery of adenovirus vectors in mice (70). This was shown to be complement C3-dependent and to require VSIG4 expression, given that KC death is rescued in VSIG4- or C3-deficient mice (71). The process of KC death and replenishment by monocytes has also been explored in the context of vaccinia virus (VACV)-induced acute hepatitis in mice (69). During VACV infection, IFNAR triggering in myeloid cells, including KCs, contributes to the early control of the infection (69). In these settings, KCs are depleted and become replenished by infiltrating monocytes that differentiate into moKCs. Interestingly, bone marrow chimera experiments revealed that IFNAR signaling in monocytes delays their differentiation into moKCs (69). Hence, IFNAR-knockout monocytes engrafted more efficiently in the livers of VACV-infected mice than WT monocytes. This appeared to be a result of a direct IFNAR triggering of monocytes in the liver, as both WT and IFNAR knockout moKCs became equally engrafted in the KC population upon cessation of hepatic IFNAR triggering (69).

In conclusion, KCs clearly perform various and occasionally contrasting roles during viral infections.

Parasitic and fungal infections

KCs are implicated in the pathology of several parasitic infections, and their contribution ranges from beneficial to detrimental. For instance, during experimental trypanosome infections, KCs perform an essential role in parasite clearance, as KC depletion by clodronate liposomes results in uncontrolled parasitemia and rapid mortality (72). In fact, VSIG4 is critical for the anti-trypanosomal response of KCs as it contributes to parasite clearance in a complement C3-dependent manner (72). Furthermore, murine hepatic macrophages, including KCs, are thought to be a source of CXCL16 during *Trypanosoma brucei* infection, and are hence suspected to be implicated in the recruitment of pathogenic $CXCR6^{+}$ $CD4^{+}$ T cells that promote aggravated liver damage and increased mortality during infection (73). Noteworthy, VSIG4-complement interactions seem of crucial importance to universal KC defense responses, since KCs utilize a similar mechanism to contain fungal infections (74). This is highlighted by impaired blood clearance and heightened infection burden in clodronate liposome-treated, as well as VSIG4 knockout or C3 knockout mice following *Cryptococcus neoformans* infection (74).

Remarkably, some parasites manage to circumvent the clearance by KCs. In case of *Plasmodium* infection, sporozoites rapidly target the liver to establish hepatocyte infection (75). Strikingly, experimental work has shown that sporozoites traverse through KCs to cross the endothelial barrier and infect hepatocytes (76–78). It has been illustrated that sporozoite crossing of KCs induces extensive KC death, with only a small fraction of KCs appearing to survive the crossing event (78). Although sporozoites can also traverse through LSECs, this process appears less common than KC traversal (78). Consistent with this, *in vitro* work showed that LSECs are less permissive to sporozoite traversal relative to KCs (76), overall suggesting that sporozoites utilize and favor KC crossing to overcome the sinusoidal lining and establish hepatocyte infection. Furthermore, it appears that sporozoites modulate KC functionalities to favor their intracellular survival, as illustrated by *in vitro* work showing that sporozoites can suppress the respiratory burst in KCs by increasing intracellular cAMP (79). This mechanism is mediated by the parasite circumsporozoite protein, and is inhibited by the blockade of CD91 or the removal of surface proteoglycans on KCs (79). By altering intracellular levels of cAMP, sporozoites are also thought to inhibit inflammatory cytokine production by KCs, instead favoring IL-10 secretion (80). Additionally, the phagocytic capacity of murine KCs towards bacteria has been shown to be substantially impaired during *Plasmodium* infection (81), further highlighting the compromising effects of malarial infection on KCs. The notion that KCs might exhibit pathogenic features during malarial infection is further supported by the finding that osteopetrotic (op/op) mice, which show a severe deficiency of mononuclear phagocytes including KCs, exhibit reduced hepatic infection (82). Paradoxically, depletion of KCs by clodronate liposomes augments parasitemia and hepatic infection (78, 82). Notably, clodronate liposome-mediated depletion of KCs is thought to compromise the structural integrity of the hepatic sinusoids, particularly by inducing gaps in the sinusoidal wall (82). Although this has been speculated to be the reason for the contradiction between the infection outcome following the aforementioned methods of KC-depletion, the authors provide no data to indicate that the integrity of the sinusoidal lining is unaltered in op/op mice (82).

Moreover, in a murine model of self-resolving *Plasmodium* infection invoked by the injection of parasitized erythrocytes, KCs are partially lost and replaced by infiltrating monocytes that in turn gave rise to long-lasting moKCs (83). In this model, KC loss occurs prior to the peak of blood parasitemia and coincides with an increase in the infiltration of monocytic cells (83). Notably, *in vitro* work has also suggested a role for ferroptosis and the deposition of hemozoin (81), a crystallized by-product of hemoglobin catabolism that is released in the circulation during malarial infection (84), as a trigger of KC death during *Plasmodium* infection (81). It is worth mentioning that a common feature in the pathology of many parasitic infections, including those invoked by *Plasmodium* and *Trypanosoma*, is the occurrence of anemia. In such settings, erythrocytes exhibit surface alterations resulting in enhanced erythro-phagocytosis by phagocytic cells (85, 86). As they are implicated in the clearance of damaged erythrocytes (24, 25), the erythro-phagocytic functions of KCs might also contribute to their response to parasitic infections. In this regard, erythro-phagocytosis has been shown to imprint an anti-inflammatory signature on KCs that is manifested in a lower expression of *Ifng*, *Tnf*, *Il12b*, *Cxcl9* and *Cxcl10* and MHCII-related genes in a mouse model of hemolytic anemia (87). Whether reprogramming due to erythro-phagocytosis functionally contributes to the response to parasitic infections is unclear.

During schistosomiasis, the main pathology results from the host type 2 immune response to the parasite eggs deposited in the liver. The eggs become surrounded by a granulomatous reaction encompassing mononuclear cells, eosinophils, neutrophils and fibroblasts, ultimately resulting in fibrosis (88). Alternatively activated macrophages, including KCs and monocyte-derived macrophages, are implicated in mediating the type 2 immune response and pathology in this context. Murine *Schistosoma mansoni* infection leads to the accumulation of $Ly6C^{hi}$ monocytes in the liver, which proliferate and differentiate into $CD11b^{hi}$ macrophages that gradually become the predominant hepatic macrophage population during the infection (89). KCs are steadily ablated as the infection proceeds, and although they showed little, if any, proliferative activity, they remain mainly of embryonic origin up to 10 weeks post-infection. Nevertheless, at this time-point, a minor but significant bone marrow contribution to the KC pool was observed (89). $CD11b^{hi}$ macrophages are alternatively activated in the infected livers and exhibit an IL4Ra-dependent upregulation of Ym1 and Relm-α. Although granuloma size was increased upon the deletion of *Il4ra* in myeloid cells ($Lyz2^{Cre}$), this did not alter the survival kinetics (89). A recent scRNA-seq of *Schistosoma japonica*-infected murine livers also provided insights into macrophage heterogeneity during

schistosomiasis (90). This study reported the presence of two major macrophage populations in the infected liver, a KC population (*Timd4*, *Cd163*, *Marco*), and a *Ccr2*+ population that lacked the expression of KC markers, and might hence represent infiltrating monocyte-derived macrophages (90). Noteworthy, the two populations were enriched in *Chil3* expression, although KCs were notably more enriched in *Arg1* and *Retnla,* suggesting a general alternative activation of macrophages in this context (90). Moreover, hepatic macrophages from *S. mansoni*-infected mice produce IL-6, IL-10, IL-4 and IL-13 in response to stimulation with soluble worm antigens and are thought to present worm antigens to hepatic T cells, promoting their type 2 differentiation (91). KCs are also implicated in tapeworm infection, particularly in cystic echinococcosis, as they uptake, via CLEC4F, the mucins of the laminated layer that protect the larval stages (hydatids) of *Echinococcus granulosus* parasites (92).

Overall, while KCs mount protective responses in some types of parasitic infections, they seem to be overwhelmed and even hijacked in other cases of parasitic insults. Notably, most experimental work investigating the roles of KCs in parasitic infection models has been done using non-specific KC targeting and identification methods that complicates the interpretation of the results. Hence, the recent advances in KC targeting and identification techniques might help resolve ambiguous aspects of KC biology during parasitic infections.

Perspectives: infection history and reprogramming of Kupffer cell function

As detailed previously, KCs are highly implicated in the response to pathogens. Given the wide range of pathogens that directly or indirectly target the liver, KC-pathogen interactions are probably a recurrent phenomenon during infections. In this regard, an increasing number of studies have shown that exposure to infections can alter tissue macrophage properties in the long-term. This effect can be mediated by ontogenic shifts, transcriptional and epigenetic reprogramming as well as alteration of the macrophage microenvironment (93–95). It is therefore likely that KCs are similarly subject to such modulation and that their functional properties are continuously shaped by infection history. For instance, although monocytes replenish KCs during almost all types of infectious diseases, it is unknown whether moKCs generated under these inflammatory scenarios are functionally distinct from emKCs. Although several studies report that moKCs generated following artificial KC-depletion during steady-state adopt the emKC identity and share some functional properties (7, 11, 17), this might not necessarily apply to situations where moKCs are generated in an inflammatory context. In support of this notion, it has been shown that monocyte-derived alveolar macrophages (moAMs), generated during influenza infection, are transcriptionally and epigenetically distinct from their embryonic counterparts and exhibit superior antibacterial functions (94). However, these enhanced antibacterial properties fail to develop when moAMs are generated following clodronate liposome-induced depletion of alveolar macrophages (94), confirming the need of inflammation to confer distinctive properties on monocyte-derived macrophages. In line with this, studies have highlighted some functional differences between emKCs and the moKCs generated during inflammatory contexts (17, 96). For instance, irradiation-generated moKCs are clearly superior to emKCs in the phagocytosis of a number of bacterial pathogens *in vivo* (17). In contrast, moKCs generated under lipemic conditions appear inferior to emKCs in their capacity to load and process lipids (96). Likewise, emKCs are more efficient in scavenging acetylated low density lipoprotein than irradiation-generated moKCs (17), indicating differences in the context of lipid metabolism. Moreover, emKCs are relatively radio-resistant as they upregulate the expression of *Cdkna1* to resist and survive irradiation, whereas moKCs seem to lack this property (19). Importantly, although some of the distinctions between moKCs and emKCs might readily be made on the basis of the transcriptome, some may be represented in forms of "hidden" alterations at the level of the epigenome. In this context, despite several weeks of intrahepatic residency after irradiation, moKCs only recover less than half of the tissue-specific enhancer regions found in emKCs (14), further supporting the idea that ontogeny or the timing of moKC generation associates with differential functionality.

In addition to ontogeny-related effects, pathogens may directly alter macrophages, or their microenvironment. For instance, exposure to pathogens or their components is well documented to drive a persistent remodelling of the epigenomic landscapes of macrophages (95, 97). For instance, peripheral LPS administration can reprogram murine microglia and associates with altered responses to neurological disease (97). Likewise, exposure to inflammatory signals commonly encountered during infections, such as interferon-γ (paradigm of type 1 inflammation) or IL-4 (paradigm of type 2 inflammation), reshapes the macrophage epigenome and triggers the generation of latent enhancers associated with faster and more robust responses upon secondary stimulation (98, 99). Although this concept is rarely studied in KCs, a recent study has shown that *in vitro* treatment of KCs with β-glucan induces trained immunity, promoting an anti-inflammatory response to a secondary stimulation with LPS (61), confirming that KCs are amenable to reprogramming. Tissue macrophages, including KCs, rely on local signals provided by stromal cells in their tissue of residence in order to maintain their identity (2, 100–103). It is therefore logical that changes to the KC niche as a result of infections might subsequently reprogram KC identity and functions. This concept is exemplified in the lung, where changes in the microenvironment resulting from a previous exposure to experimental pneumonia can epigenetically reprogram embryonically-derived alveolar macrophages, leading to long-term impairment of their phagocytic function (95). In conclusion, despite the fact that KCs frequently and dynamically respond to infections, studies exploring whether a past exposure to infectious inflammation alters the KC phenotype are largely lacking. Major questions include whether infection history alters KC biology, and if so, for how long that lasts, and whether such effects are reversible. Importantly, what is the physiological consequence of such changes on the overall response to secondary inflammation? Given the

frequent exposure of humans to infections and the important roles played by liver macrophages during infections, this topic warrants further investigation.

Author contributions

The manuscript was written by MM and revised by PB, KM and JG. All authors contributed to the article and approved the submitted version.

Funding

MM, KM and JG are supported by FWO (MM: 1157718N). KM holds an ERC Consolidator Grant.

Conflict of interest

The authors declare that the research was conducted in the absence of any commercial or financial relationships that could be construed as a potential conflict of interest.

Publisher's note

References

1. Guilliams M, Scott CL. Liver macrophages in health and disease. *Immunity* (2022) 55(9):1515–29. doi: 10.1016/j.immuni.2022.08.002

2. Bonnardel J, T'Jonck W, Gaublomme D, Browaeys R, Scott CL, Martens L, et al. Stellate cells, hepatocytes, and endothelial cells imprint the kupffer cell identity on monocytes colonizing the liver macrophage niche. *Immunity* (2019) 51(4):638–54.e9. doi: 10.1016/j.immuni.2019.08.017

3. Schulz C, Perdiguero EG, Chorro L, Szabo-Rogers H, Cagnard N, Kierdorf K, et al. A lineage of myeloid cells independent of myb and hematopoietic stem cells. *Science* (2012) 336(6077):86. doi: 10.1126/science.1219179

4. Hoeffel G, Chen J, Lavin Y, Low D, Almeida Francisca F, See P, et al. C-myb+ Erythro-myeloid progenitor-derived fetal monocytes give rise to adult tissue-resident macrophages. *Immunity* (2015) 42(4):665–78. doi: 10.1016/j.immuni.2015.03.011

5. Gomez Perdiguero E, Klapproth K, Schulz C, Busch K, Azzoni E, Crozet L, et al. Tissue-resident macrophages originate from yolk-sac-derived erythro-myeloid progenitors. *Nature* (2015) 518(7540):547–51. doi: 10.1038/nature13989

6. Sheng J, Ruedl C, Karjalainen K. Most tissue-resident macrophages except microglia are derived from fetal hematopoietic stem cells. *Immunity* (2015) 43 (2):382–93. doi: 10.1016/j.immuni.2015.07.016

7. Scott CL, Zheng F, De Baetselier P, Martens L, Saeys Y, De Prijck S, et al. Bone marrow-derived monocytes give rise to self-renewing and fully differentiated kupffer cells. *Nat Commun* (2016) 7(1):10321. doi: 10.1038/ncomms10321

8. Mass E, Ballesteros I, Farlik M, Halbritter F, Günther P, Crozet L, et al. Specification of tissue-resident macrophages during organogenesis. *Science* (2016) 353(6304):aaf4238. doi: 10.1126/science.aaf4238

9. Scott CL, T'Jonck W, Martens L, Todorov H, Sichien D, Soen B, et al. The transcription factor zeb2 is required to maintain the tissue-specific identities of macrophages. *Immunity* (2018) 49(2):312–25.e5. doi: 10.1016/j.immuni.2018.07.004

10. Hagemeyer N, Kierdorf K, Frenzel K, Xue J, Ringelhan M, Abdullah Z, et al. Transcriptome-based profiling of yolk sac-derived macrophages reveals a role for irf8 in macrophage maturation. *EMBO J* (2016) 35(16):1730–44. doi: 10.15252/embj.201693801

11. Sakai M, Troutman TD, Seidman JS, Ouyang Z, Spann NJ, Abe Y, et al. Liver-derived signals sequentially reprogram myeloid enhancers to initiate and maintain kupffer cell identity. *Immunity* (2019) 51(4):655–70.e8. doi: 10.1016/j.immuni.2019.09.002

12. Guilliams M, Bonnardel J, Haest B, Vanderborght B, Wagner C, Remmerie A, et al. Spatial proteogenomics reveals distinct and evolutionarily conserved hepatic macrophage niches. *Cell* (2022) 185(2):379–96.e38. doi: 10.1016/j.cell.2021.12.018

13. Zhao D, Yang F, Wang Y, Li S, Li Y, Hou F, et al. Alk1 signaling is required for the homeostasis of kupffer cells and prevention of bacterial infection. *J Clin Invest* (2022) 132(3). doi: 10.1172/JCI150489

14. Lavin Y, Winter D, Blecher-Gonen R, David E, Keren-Shaul H, Merad M, et al. Tissue-resident macrophage enhancer landscapes are shaped by the local microenvironment. *Cell* (2014) 159(6):1312–26. doi: 10.1016/j.cell.2014.11.018

15. Gautier EL, Shay T, Miller J, Greter M, Jakubzick C, Ivanov S, et al. Gene-expression profiles and transcriptional regulatory pathways that underlie the identity and diversity of mouse tissue macrophages. *Nat Immunol* (2012) 13(11):1118–28. doi: 10.1038/ni.2419

16. Remmerie A, Martens L, Thoné T, Castoldi A, Seurinck R, Pavie B, et al. Osteopontin expression identifies a subset of recruited macrophages distinct from kupffer cells in the fatty liver. *Immunity* (2020) 53(3):641–57.e14. doi: 10.1016/j.immuni.2020.08.004

17. Beattie L, Sawtell A, Mann J, Frame TCM, Teal B, de Labastida Rivera F, et al. Bone marrow-derived and resident liver macrophages display unique transcriptomic signatures but similar biological functions. *J Hepatol* (2016) 65(4):758–68. doi: 10.1016/j.jhep.2016.05.037

18. Daemen S, Gainullina A, Kalugotla G, He L, Chan MM, Beals JW, et al. Dynamic shifts in the composition of resident and recruited macrophages influence tissue remodeling in nash. *Cell Rep* (2021) 34(2). doi: 10.1016/j.celrep.2020.108626

19. Soysa R, Lampert S, Yuen S, Douglass AN, Li W, Pfeffer K, et al. Fetal origin confers radioresistance on liver macrophages via P21cip1/waf1. *J Hepatol* (2019) 71 (3):553–62. doi: 10.1016/j.jhep.2019.04.015

20. Knoll P, Schlaak J, Uhrig A, Kempf P, zum Büschenfelde K-HM, Gerken G. Human kupffer cells secrete il-10 in response to lipopolysaccharide (Lps) challenge. *J Hepatol* (1995) 22(2):226–9. doi: 10.1016/0168-8278(95)80433-1

21. Heymann F, Peusquens J, Ludwig-Portugall I, Kohlhepp M, Ergen C, Niemietz P, et al. Liver inflammation abrogates immunological tolerance induced by kupffer cells. *Hepatol (Baltimore Md)* (2015) 62(1):279–91. doi: 10.1002/hep.27793

22. You Q, Cheng L, Kedl RM, Ju C. Mechanism of T cell tolerance induction by murine hepatic kupffer cells. *Hepatol (Baltimore Md)* (2008) 48(3):978–90. doi: 10.1002/hep.22395

23. Nairz M, Theurl I, Swirski FK, Weiss G. "Pumping iron"-how macrophages handle iron at the systemic, microenvironmental, and cellular levels. *Pflugers Arch* (2017) 469(3-4):397–418. doi: 10.1007/s00424-017-1944-8

24. Theurl I, Hilgendorf I, Nairz M, Tymoszuk P, Haschka D, Asshoff M, et al. On-demand erythrocyte disposal and iron recycling requires transient macrophages in the liver. *Nat Med* (2016) 22(8):945–51. doi: 10.1038/nm.4146

25. Terpstra V, van Berkel TJC. Scavenger receptors on liver kupffer cells mediate the in vivo uptake of oxidatively damaged red blood cells in mice. *Blood* (2000) 95 (6):2157–63. doi: 10.1182/blood.V95.6.2157

26. Theurl M, Theurl I, Hochegger K, Obrist P, Subramaniam N, van Rooijen N, et al. Kupffer cells modulate iron homeostasis in mice via regulation of hepcidin expression. *J Mol Med* (2008) 86(7):825. doi: 10.1007/s00109-008-0346-y

27. Lou D-Q, Lesbordes J-C, Nicolas G, Viatte L, Bennoun M, Van Rooijen N, et al. Iron- and inflammation-induced hepcidin gene expression in mice is not mediated by kupffer cells in vivo. *Hepatol (Baltimore Md)* (2005) 41(5):1056–64. doi: 10.1002/hep.20663

28. Li Y, Fu J, Ling Y, Yago T, McDaniel JM, Song J, et al. Sialylation on O-glycans protects platelets from clearance by liver kupffer cells. *Proc Natl Acad Sci* (2017) 114 (31):8360. doi: 10.1073/pnas.1707662114

29. Deppermann C, Kratofil RM, Peiseler M, David BA, Zindel J, Castanheira FVES, et al. Macrophage galactose lectin is critical for kupffer cells to clear aged platelets. *J Exp Med* (2020) 217(4). doi: 10.1084/jem.20190723

30. Roberts AW, Lee BL, Deguine J, John S, Shlomchik MJ, Barton GM. Tissue-resident macrophages are locally programmed for silent clearance of apoptotic cells. *Immunity* (2017) 47(5):913–27.e6. doi: 10.1016/j.immuni.2017.10.006

31. Shi J, Fujieda H, Kokubo Y, Wake K. Apoptosis of neutrophils and their elimination by kupffer cells in rat liver. *Hepatol (Baltimore Md)* (1996) 24(5):1256–63. doi: 10.1002/hep.510240545

32. Shi J, Gilbert GE, Kokubo Y, Ohashi T. Role of the liver in regulating numbers of circulating neutrophils. *Blood* (2001) 98(4):1226–30. doi: 10.1182/blood.V98.4.1226

33. Remmerie A, Scott CL. Macrophages and lipid metabolism. *Cell Immunol* (2018) 330:27–42. doi: 10.1016/j.cellimm.2018.01.020

34. Demetz E, Tymoszuk P, Hilbe R, Volani C, Haschka D, Heim C, et al. The haemochromatosis gene hfe and kupffer cells control ldl cholesterol homeostasis and impact on atherosclerosis development. *Eur Heart J* (2020) 41(40):3949–59. doi: 10.1093/eurheartj/ehaa140

35. Keshvari S, Caruso M, Teakle N, Batoon L, Sehgal A, Patkar OL, et al. Csf1r-dependent macrophages control postnatal somatic growth and organ maturation. *PloS Genet* (2021) 17(6):e1009605. doi: 10.1371/journal.pgen.1009605

36. Gao H, Jin Z, Bandyopadhyay G, Cunha e Rocha K, Liu X, Zhao H, et al. Mir-690 treatment causes decreased fibrosis and steatosis and restores specific kupffer cell functions in Nash. *Cell Metab* (2022) 34(7):978–90.e4. doi: 10.1016/j.cmet.2022.05.008

37. Blériot C, Barreby E, Dunsmore G, Ballaire R, Chakarov S, Ficht X, et al. A subset of kupffer cells regulates metabolism through the expression of cd36. *Immunity* (2021) 54(9):2101–16.e6. doi: 10.1016/j.immuni.2021.08.006

38. Hume DA, Offermanns S, Bonnavion R. Contamination of isolated mouse kupffer cells with liver sinusoidal endothelial cells. *Immunity* (2022) 55(7):1139–40. doi: 10.1016/j.immuni.2022.06.010

39. Iannacone M, Blériot C, Andreata F, Ficht X, Laura C, Garcia-Manteiga JM, et al. Response to contamination of isolated mouse kupffer cells with liver sinusoidal endothelial cells. *Immunity* (2022) 55(7):1141–2. doi: 10.1016/j.immuni.2022.06.012

40. Sierro F, Evrard M, Rizzetto S, Melino M, Mitchell AJ, Florido M, et al. A liver capsular network of monocyte-derived macrophages restricts hepatic dissemination of intraperitoneal bacteria by neutrophil recruitment. *Immunity* (2017) 47(2):374–88.e6. doi: 10.1016/j.immuni.2017.07.018

41. Aizarani N, Saviano A, Sagar, Mailly L, Durand S, Herman JS, et al. A human liver cell atlas reveals heterogeneity and epithelial progenitors. *Nature* (2019) 572 (7768):199–204. doi: 10.1038/s41586-019-1373-2

42. MacParland SA, Liu JC, Ma X-Z, Innes BT, Bartczak AM, Gage BK, et al. Single cell rna sequencing of human liver reveals distinct intrahepatic macrophage populations. *Nat Commun* (2018) 9(1):4383. doi: 10.1038/s41467-018-06318-7

43. Ramachandran P, Dobie R, Wilson-Kanamori JR, Dora EF, Henderson BEP, Luu NT, et al. Resolving the fibrotic niche of human liver cirrhosis at single-cell level. *Nature* (2019) 575(7783):512–8. doi: 10.1038/s41586-019-1631-3

44. Balmer ML, Slack E, de Gottardi A, Lawson MAE, Hapfelmeier S, Miele L, et al. The liver may act as a firewall mediating mutualism between the host and its gut commensal microbiota. *Sci Trans Med* (2014) 6(237):237ra66–ra66. doi: 10.1126/scitranslmed.3008618

45. David BA, Rezende RM, Antunes MM, Santos MM, Freitas Lopes MA, Diniz AB, et al. Combination of Mass Cytometry and Imaging Analysis Reveals origin, Location, and Functional Repopulation Of liver myeloid Cells in Mice. *Gastroenterology* (2016) 151(6):1176–91. doi: 10.1053/j.gastro.2016.08.024

46. Lee W-Y, Moriarty TJ, Wong CHY, Zhou H, Strieter RM, van Rooijen N, et al. An intravascular immune response to borrelia burgdorferi involves kupffer cells and inkt cells. *Nat Immunol* (2010) 11(4):295–302. doi: 10.1038/ni.1855

47. Gola A, Dorrington MG, Speranza E, Sala C, Shih RM, Radtke AJ, et al. Commensal-driven immune zonation of the liver promotes host defence. *Nature* (2021) 589(7840):131–6. doi: 10.1038/s41586-020-2977-2

48. Zeng Z, Surewaard BG, Wong CH, Geoghegan JA, Jenne CN, Kubes P. Crig functions as a macrophage pattern recognition receptor to directly bind and capture blood-borne gram-positive bacteria. *Cell Host Microbe* (2016) 20(1):99–106. doi: 10.1016/j.chom.2016.06.002

49. Broadley Steven P, Plaumann A, Coletti R, Lehmann C, Wanisch A, Seidlmeier A, et al. Dual-track clearance of circulating bacteria balances rapid restoration of blood sterility with induction of adaptive immunity. *Cell Host Microbe* (2016) 20(1):36–48. doi: 10.1016/j.chom.2016.05.023

50. Helmy KY, Katschke KJ, Gorgani NN, Kljavin NM, Elliott JM, Diehl L, et al. Crig: A macrophage complement receptor required for phagocytosis of circulating pathogens. *Cell* (2006) 124(5):915–27. doi: 10.1016/j.cell.2005.12.039

51. Min C, Park J, Kim G, Moon H, Lee S-A, Kim D, et al. Tim-4 functions as a scavenger receptor for phagocytosis of exogenous particles. *Cell Death Dis* (2020) 11 (7):561. doi: 10.1038/s41419-020-02773-7

52. Duan Y, Chu H, Brandl K, Jiang L, Zeng S, Meshgin N, et al. Crig on liver macrophages clears pathobionts and protects against alcoholic liver disease. *Nat Commun* (2021) 12(1):7172. doi: 10.1038/s41467-021-27385-3

53. Wong CHY, Jenne CN, Petri B, Chrobok NL, Kubes P. Nucleation of platelets with blood-borne pathogens on kupffer cells precedes other innate immunity and contributes to bacterial clearance. *Nat Immunol* (2013) 14(8):785–92. doi: 10.1038/ni.2631

54. McDonald B, Zucoloto AZ, Yu I-L, Burkhard R, Brown K, Geuking MB, et al. Programing of an intravascular immune firewall by the gut microbiota protects against pathogen dissemination during infection. *Cell Host Microbe* (2020) 28(5):660–8.e4. doi: 10.1016/j.chom.2020.07.014

55. Bleriot C, Dupuis T, Jouvion G, Eberl G, Disson O, Lecuit M. Liver-resident macrophage necroptosis orchestrates type 1 microbicidal inflammation and type-2-mediated tissue repair during bacterial infection. *Immunity* (2015) 42(1):145–58. doi: 10.1016/j.immuni.2014.12.020

56. Jorgensen I, Rayamajhi M, Miao EA. Programmed cell death as a defence against infection. *Nat Rev Immunol* (2017) 17(3):151. doi: 10.1038/nri.2016.147

57. Di Paolo Nelson C, Doronin K, Baldwin Lisa K, Papayannopoulou T, Shayakhmetov Dmitry M. The transcription factor irf3 triggers "Defensive suicide" necrosis in response to viral and bacterial pathogens. *Cell Rep* (2013) 3(6):1840–6. doi: 10.1016/j.celrep.2013.05.025

58. Triantafyllou E, Gudd CLC, Mawhin M-A, Husbyn HC, Trovato FM, Siggins MK, et al. Pd-1 blockade improves kupffer cell bacterial clearance in acute liver injury. *J Clin Invest* (2021) 131(4). doi: 10.1172/JCI140196

59. Deppermann C, Peiseler M, Zindel J, Zbytnuik L, Lee W-Y, Pasini E, et al. Tacrolimus impairs kupffer cell capacity to control bacteremia: why transplant recipients are susceptible to infection. *Hepatol (Baltimore Md)* (2021) 73(5):1967–84. doi: 10.1002/hep.31499

60. Komine S, Akiyama K, Warabi E, Oh S, Kuga K, Ishige K, et al. Exercise training enhances in vivo clearance of endotoxin and attenuates inflammatory responses by potentiating kupffer cell phagocytosis. *Sci Rep* (2017) 7(1):11977. doi: 10.1038/s41598-017-12358-8

61. Zhang H, Chen T, Ren J, Xia Y, Onuma A, Wang Y, et al. Pre-operative exercise therapy triggers anti-inflammatory trained immunity of kupffer cells through metabolic reprogramming. *Nat Metab* (2021) 3(6):843–58. doi: 10.1038/s42255-021-00402-x

62. Wong YC, Tay SS, McCaughan GW, Bowen DG, Bertolino P. Immune outcomes in the liver: is cd8 T cell fate determined by the environment? *J Hepatol* (2015) 63 (4):1005–14. doi: 10.1016/j.jhep.2015.05.033

63. Li M, Sun R, Xu L, Yin W, Chen Y, Zheng X, et al. Kupffer cells support hepatitis B virus–mediated cd8+ T cell exhaustion via hepatitis B core antigen–tlr2 interactions in mice. *J Immunol* (2015) 195(7):3100–9. doi: 10.4049/jimmunol.1500839

64. Xu L, Yin W, Sun R, Wei H, Tian Z. Kupffer cell-derived il-10 plays a key role in maintaining humoral immune tolerance in hepatitis B virus-persistent mice. *Hepatol (Baltimore Md)* (2014) 59(2):443–52. doi: 10.1002/hep.26668

65. Bénéchet AP, De Simone G, Di Lucia P, Cilenti F, Barbiera G, Le Bert N, et al. Dynamics and genomic landscape of cd8+ T cells undergoing hepatic priming. *Nature* (2019) 574(7777):200–5. doi: 10.1038/s41586-019-1620-6

66. Spolski R, Li P, Leonard WJ. Biology and regulation of il-2: from molecular mechanisms to human therapy. *Nat Rev Immunol* (2018) 18(10):648–59. doi: 10.1038/s41577-018-0046-y

67. De Simone G, Andreata F, Bleriot C, Fumagalli V, Laura C, Garcia-Manteiga JM, et al. Identification of a kupffer cell subset capable of reverting the T Cell dysfunction induced by hepatocellular priming. *Immunity* (2021) 54(9):2089–100.e8. doi: 10.1016/j.immuni.2021.05.005

68. Wu LL, Peng WH, Wu HL, Miaw SC, Yeh SH, Yang HC, et al. Lymphocyte antigen 6 complex, locus C+ Monocytes and kupffer cells orchestrate liver immune responses against hepatitis B virus in mice. *Hepatol (Baltimore Md)* (2019) 69(6):2364–80. doi: 10.1002/hep.30510

69. Borst K, Frenz T, Spanier J, Tegtmeyer P-K, Chhatbar C, Skerra J, et al. Type I interferon receptor signaling delays kupffer cell replenishment during acute fulminant viral hepatitis. *J Hepatol* (2018) 68(4):682–90. doi: 10.1016/j.jhep.2017.11.029

70. Manickan E, Smith JS, Tian J, Eggerman TL, Lozier JN, Muller J, et al. Rapid kupffer cell death after intravenous injection of adenovirus vectors. *Mol Ther* (2006) 13 (1):108–17. doi: 10.1016/j.ymthe.2005.08.007

71. He JQ, Katschke KJ Jr., Gribling P, Suto E, Lee WP, Diehl L, et al. Crig mediates early kupffer cell responses to adenovirus. *J leukocyte Biol* (2013) 93(2):301–6. doi: 10.1189/jlb.0612311

72. Liu G, Fu Y, Yosri M, Chen Y, Sun P, Xu J, et al. Crig plays an essential role in intravascular clearance of bloodborne parasites by interacting with complement. *Proc Natl Acad Sci* (2019) 116(48):24214–20. doi: 10.1073/pnas.1913443116

73. Liu G, Abas O, Strickland AB, Chen Y, Shi M. Cxcr6+Cd4+ T cells promote mortality during trypanosoma brucei infection. *PloS Pathog* (2021) 17(10):e1009968. doi: 10.1371/journal.ppat.1009968

74. Sun D, Sun P, Li H, Zhang M, Liu G, Strickland AB, et al. Fungal dissemination is limited by liver macrophage filtration of the blood. *Nat Commun* (2019) 10(1):4566. doi: 10.1038/s41467-019-12381-5

75. Schofield L, Grau GE. Immunological processes in malaria pathogenesis. *Nat Rev Immunol* (2005) 5(9):722–35. doi: 10.1038/nri1686

76. Pradel G, Frevert U. Malaria sporozoites actively enter and pass through rat kupffer cells prior to hepatocyte invasion. *Hepatol (Baltimore Md)* (2001) 33(5):1154–65. doi: 10.1053/jhep.2001.24237

77. Frevert U, Engelmann S, Zougbédé S, Stange J, Ng B, Matuschewski K, et al. Intravital observation of plasmodium berghei sporozoite infection of the liver. *PloS Biol* (2005) 3(6):e192. doi: 10.1371/journal.pbio.0030192

78. Tavares J, Formaglio P, Thiberge S, Mordelet E, Van Rooijen N, Medvinsky A, et al. Role of host cell traversal by the malaria sporozoite during liver infection. *J Exp Med* (2013) 210(5):905–15. doi: 10.1084/jem.20121130

79. Usynin I, Klotz C, Frevert U. Malaria circumsporozoite protein inhibits the respiratory burst in kupffer cells. *Cell Microbiol* (2007) 9(11):2610–28. doi: 10.1111/j.1462-5822.2007.00982.x

80. Klotz C, Frevert U. Plasmodium yoelii sporozoites modulate cytokine profile and induce apoptosis in murine kupffer cells. *Int J Parasitol* (2008) 38(14):1639–50. doi: 10.1016/j.ijpara.2008.05.018

81. Hirako IC, Antunes MM, Rezende RM, Hojo-Souza NS, Figueiredo MM, Dias T, et al. Uptake of plasmodium chabaudi hemozoin drives kupffer cell death and fuels superinfections. *Sci Rep* (2022) 12(1):19805. doi: 10.1038/s41598-022-23858-7

82. Baer K, Roosevelt M, Clarkson AB Jr., Van Rooijen N, Schnieder T, Frevert U. Kupffer cells are obligatory for plasmodium yoelii sporozoite infection of the liver. *Cell Microbiol* (2007) 9(2):397–412. doi: 10.1111/j.1462-5822.2006.00798.x

83. Lai SM, Sheng J, Gupta P, Renia L, Duan K, Zolezzi F, et al. Organ-specific fate, recruitment, and refilling dynamics of tissue-resident macrophages during blood-stage malaria. *Cell Rep* (2018) 25(11):3099–109. doi: 10.1016/j.celrep.2018.11.059

84. Olivier M, Van Den Ham K, Shio M, Kassa F, Fougeray S. Malarial pigment hemozoin and the innate inflammatory response. *Front Immunol* (2014) 5. doi: 10.3389/fimmu.2014.00025

85. Stijlemans B, Cnops J, Naniima P, Vaast A, Bockstal V, De Baetselier P, et al. Development of a phrodo-based assay for the assessment of in vitro and in vivo erythrophagocytosis during experimental trypanosomosis. *PloS Negl Trop Dis* (2015) 9 (3):e0003561. doi: 10.1371/journal.pntd.0003561

86. Waitumbi JN, Opollo MO, Muga RO, Misore AO, Stoute JA. Red cell surface changes and erythrophagocytosis in children with severe plasmodium falciparum anemia. *Blood* (2000) 95(4):1481–6. doi: 10.1182/blood.V95.4.1481.004k15_1481_1486

87. Pfefferlé M, Ingoglia G, Schaer CA, Yalamanoglu A, Buzzi R, Dubach IL, et al. Hemolysis transforms liver macrophages into antiinflammatory erythrophagocytes. *J Clin Invest* (2020) 130(10):5576–90. doi: 10.1172/JCI137282

88. Anthony BJ, Ramm GA, McManus DP. Role of resident liver cells in the pathogenesis of schistosomiasis. *Trends Parasitol* (2012) 28(12):572–9. doi: 10.1016/j.pt.2012.09.005

89. Rolot M, Dougall AM, Javaux J, Lallemand F, Machiels B, Martinive P, et al. Recruitment of hepatic macrophages from monocytes is independent of il-4rα but is associated with ablation of resident macrophages in schistosomiasis. *Eur J Immunol* (2019) 49(7):1067–81. doi: 10.1002/eji.201847796

90. Zhang Y, Li J, Li H, Jiang J, Guo C, Zhou C, et al. Single-cell rna sequencing to dissect the immunological network of liver fibrosis in schistosoma japonicum-infected mice. *Front Immunol* (2022) 13:980872. doi: 10.3389/fimmu.2022.980872

91. Hayashi N, Matsui K, Tsutsui H, Osada Y, Mohamed RT, Nakano H, et al. Kupffer cells from schistosoma mansoni-infected mice participate in the prompt type 2 differentiation of hepatic T cells in response to worm antigens1. *J Immunol* (1999) 163 (12):6702–11. doi: 10.4049/jimmunol.163.12.6702

92. Barrios AA, Mouhape C, Schreiber L, Zhang L, Nell J, Suárez-Martins M, et al. Mucins shed from the laminated layer in cystic echinococcosis are captured by kupffer cells via the lectin receptor clec4f. *Infection Immun* (2023) 91(6):e00031–23. doi: 10.1128/iai.00031-23

93. Rua R, Lee JY, Silva AB, Swafford IS, Maric D, Johnson KR, et al. Infection drives meningeal engraftment by inflammatory monocytes that impairs cns immunity. *Nat Immunol* (2019) 20(4):407–19. doi: 10.1038/s41590-019-0344-y

94. Aegerter H, Kulikauskaite J, Crotta S, Patel H, Kelly G, Hessel EM, et al. Influenza-induced monocyte-derived alveolar macrophages confer prolonged antibacterial protection. *Nat Immunol* (2020) 21(2):145–57. doi: 10.1038/s41590-019-0568-x

95. Roquilly A, Jacqueline C, Davieau M, Mollé A, Sadek A, Fourgeux C, et al. Alveolar macrophages are epigenetically altered after inflammation, leading to long-term lung immunoparalysis. *Nat Immunol* (2020) 21(6):636–48. doi: 10.1038/s41590-020-0673-x

96. Tran S, Baba I, Poupel L, Dussaud S, Moreau M, Gélineau A, et al. Impaired kupffer cell self-renewal alters the liver response to lipid overload during non-alcoholic steatohepatitis. *Immunity* (2020) 53(3):627–40.e5. doi: 10.1016/j.immuni.2020.06.003

97. Wendeln A-C, Degenhardt K, Kaurani L, Gertig M, Ulas T, Jain G, et al. Innate immune memory in the brain shapes neurological disease hallmarks. *Nature* (2018) 556 (7701):332–8. doi: 10.1038/s41586-018-0023-4

98. Ostuni R, Piccolo V, Barozzi I, Polletti S, Termanini A, Bonifacio S, et al. Latent enhancers activated by stimulation in differentiated cells. *Cell* (2013) 152(1):157–71. doi: 10.1016/j.cell.2012.12.018

99. Kang K, Park SH, Chen J, Qiao Y, Giannopoulou E, Berg K, et al. Interferon-Γ Represses M2 gene expression in human macrophages by disassembling enhancers bound by the transcription factor maf. *Immunity* (2017) 47(2):235–50.e4. doi: 10.1016/j.immuni.2017.07.017

100. Bellomo A, Mondor I, Spinelli L, Lagueyrie M, Stewart BJ, Brouilly N, et al. Reticular fibroblasts expressing the transcription factor wt1 define a stromal niche that maintains and replenishes splenic red pulp macrophages. *Immunity* (2020) 53(1):127–42.e7. doi: 10.1016/j.immuni.2020.06.008

101. Buechler MB, Kim K-W, Onufer EJ, Williams JW, Little CC, Dominguez CX, et al. A stromal niche defined by expression of the transcription factor wt1 mediates programming and homeostasis of cavity-resident macrophages. *Immunity* (2019) 51 (1):119–30.e5. doi: 10.1016/j.immuni.2019.05.010

102. Masuda T, Amann L, Monaco G, Sankowski R, Staszewski O, Krueger M, et al. Specification of cns macrophage subsets occurs postnatally in defined niches. *Nature* (2022) 604(7907):740–8. doi: 10.1038/s41586-022-04596-2

103. Mondor I, Baratin M, Lagueyrie M, Saro L, Henri S, Gentek R, et al. Lymphatic endothelial cells are essential components of the subcapsular sinus macrophage niche. *Immunity* (2019) 50(6):1453–66.e4. doi: 10.1016/j.immuni.2019.04.002

frontiers | Frontiers in Immunology

TYPE Review
PUBLISHED 25 October 2023
DOI 10.3389/fimmu.2023.1238972

OPEN ACCESS

EDITED BY
Perenlei Enkhbaatar,
University of Texas Medical Branch at Galveston, United States

REVIEWED BY
Bin Guo,
University of Houston, United States
Hamza Yazdani,
University of Pittsburgh, United States

*CORRESPONDENCE
Xihong Li
hilixihong@163.com

RECEIVED 23 July 2023
ACCEPTED 17 October 2023
PUBLISHED 25 October 2023

CITATION
Chen Y, Yang L and Li X (2023) Advances in Mesenchymal stem cells regulating macrophage polarization and treatment of sepsis-induced liver injury.
Front. Immunol. 14:1238972.
doi: 10.3389/fimmu.2023.1238972

Advances in Mesenchymal stem cells regulating macrophage polarization and treatment of sepsis-induced liver injury

Yuhao Chen[1,2], Lihong Yang[1,2] and Xihong Li[1,2]*

[1]Department of Emergency Medicine, West China Second Hospital of Sichuan University, Sichuan, China, [2]Key Laboratory of Birth Defects and Related Diseases of Women and Children, Sichuan University, Ministry of Education, Sichuan, China

Sepsis is a syndrome of dysregulated host response caused by infection, which leads to life-threatening organ dysfunction. It is a familiar reason of death in critically ill patients. Liver injury frequently occurs in septic patients, yet the development of targeted and effective treatment strategies remains a pressing challenge. Macrophages are essential parts of immunity system. M1 macrophages drive inflammation, whereas M2 macrophages possess anti-inflammatory properties and contribute to tissue repair processes. Mesenchymal stem cells (MSCs), known for their remarkable attributes including homing capabilities, immunomodulation, anti-inflammatory effects, and tissue regeneration potential, hold promise in enhancing the prognosis of sepsis-induced liver injury by harmonizing the delicate balance of M1/M2 macrophage polarization. This review discusses the mechanisms by which MSCs regulate macrophage polarization, alongside the signaling pathways involved, providing an idea for innovative directions in the treatment of sepsis-induced liver injury.

KEYWORDS

mesenchymal stem cells (MSCs), sepsis, liver injury, kupffer cells, macrophage polarization

1 Introduction

1.1 Sepsis-induced liver injury

In 2016, the Sepsis-3 Workgroup introduced revised definitions for sepsis and septic shock, aiming to enhance accuracy and clinical identification. Sepsis is now defined as a critical condition wherein organ dysfunction arises from a dysregulated host response to infection. Septic shock is identified by the clinical requirement of vasopressors to maintain a mean arterial pressure equal to or above 65 mmHg, accompanied by a serum lactate level exceeding 2 mmol/L, without evidence of hypovolemia (1). Liver injury is a familiar organ damaged in patients with sepsis. It can be viewed as a primary dysfunction that occurs

within the first hour after the initial injury, which is usually associated with liver hypoperfusion. This can result in diffuse intravascular coagulation and multiple organ failure (2). Concurrently, sepsis can induce dysfunction in the intestinal microcirculation, facilitating the infiltration of intestinal toxins and bacteria into the liver through the portal vein, thereby initiating a cascade of hepatic inflammation. Within the context of sepsis, the liver becomes a hub of intensified oxidative stress reactions, generating byproducts that activate neutrophils and exacerbate hepatic damage (3). There is evidence that liver injury and failure, particularly as a severe complication of sepsis, contribute directly to disease progression and patients' death (4).

Sepsis is most common in people with weakened immune systems, such as the elderly, infants and patients with certain underlying medical conditions. Sepsis will become more common as the number of elderly patients grows (5). The average annual increase percentage in sepsis incidence was 13%-13.3% (6). Currently, the main way to improve outcomes is to recognize sepsis early and treat it appropriately in the initial hours. However, targeted and effective treatment strategies are still lacking. As a result, it is urgent to investigate a treatment for sepsis-induced liver injury.

1.2 Macrophage

Kupffer cells, the specialized macrophages residing in the liver, distinguish themselves from monocyte-derived macrophages by their distinct localization and rapid accumulation within the damaged liver. As resident tissue macrophages, Kupffer cells exhibit a mature phenotype that demonstrates remarkable plasticity. Their functional activity dynamically evolves in response to the specific metabolic and local immune environment (7). Macrophages exhibit a classification into two distinct phenotypes: M1 and M2. M1 macrophages, also known as classically activated macrophages, possess the ability to release elevated levels of proinflammatory cytokines, including TNF-α, IL-6, IL-12, and inducible nitric oxide synthase (iNOS). In contrast, M2 macrophages, alternatively activated macrophages, display a different profile. They tend to release lower levels of proinflammatory cytokines and instead exhibit higher levels of anti-inflammatory mediators, such as IL-10 and transforming growth factor beta (TGF-β) (8). Therefore, inhibition of excess polarization of M1 macrophages and promotion of polarization of M2 macrophages in patients with sepsis may help improve the condition (9). Emerging data has revealed significant heterogeneity even within the traditional M1 and M2 macrophage classifications, underscoring the oversimplification of the M1/M2 categorization. In fact, the M2 phenotype has been further subdivided into distinct subtypes, namely M2a, M2b, M2c, and M2d, reflecting the diverse functional states and responses exhibited by these macrophages (Figure 1). The subtypes have unique cell surface marker proteins and distinct functions, and they are induced by various regulators (10). This refined categorization highlights the intricate and multifaceted nature of macrophage polarization, emphasizing the need for a more comprehensive understanding of the various subpopulations and their specific roles in immune regulation, inflammation, and tissue repair.

1.3 The role of macrophages in sepsis

1.3.1 Bacterial clearance

The liver is an essential component of the inflammatory response and is crucial for germ limitation and toxin elimination in sepsis (11). In animal models, more than 60% of the total number of bacteria can be eliminated from the blood and limited in the liver after 10 minutes, and more than 80% of them can be limited in the liver after 6 hours (12). In bacterial infections, lipopolysaccharide (LPS) serves as a crucial inflammatory trigger. Notably, the liver plays a pivotal role in eliminating LPS from the circulation (13). When the liver sustains damage, its capacity for efficient bacterial clearance becomes compromised. This impairment in bacterial clearance increases the risk of sepsis and systemic infection can spread unchecked. Thus, liver damage becomes a significant factor contributing to the heightened vulnerability to sepsis (14). The mediation of bacterial phagocytosis and clearance within the liver involves a diverse range of cells. These cells operate as the initial line of defense against the translocation of bacteria through the bloodstream. The active participation in this process is undertaken by Kupffer cells, liver sinusoidal endothelial cells (LSECs), and stellate cells (15). Kupffer cells, as resident macrophages inhabiting the hepatic sinusoids, are cells with an exceptional capacity for phagocytosis. These specialized cells play a crucial role in the liver's immune defense system by efficiently removing bacteria and soluble bacterial products from the bloodstream (2, 16).

Platelets and neutrophils work along with Kupffer cells to remove bacteria from the blood. Platelets release many antimicrobial molecules and play a direct role in infection defense. Platelets can also enhance the killing capacity of Kupffer cells (16). By secreting Kupffer cell chemokines, neutrophils move and gather in the hepatic sinusoids during sepsis. Then, neutrophils and platelets interact to jointly promote the release of neutrophil extracellular traps to trap and clear pathogens (17). The impaired bacterial clearance observed in the liver during sepsis is attributed to a combination of factors, including the direct impact of reduced platelet count on immune responses, the damage inflicted on the reticuloendothelial system responsible for bacteria phagocytosis and clearance, and the compromised function of neutrophils, leading to reduced phagocytosis and intracellular killing capacity (18).

1.3.2 Liver-mediated pro-inflammatory response

In sepsis patients, the liver serves as a prominent site of inflammatory responses triggered by bacterial endotoxins. Additionally, the liver itself can contribute to the production and release of inflammatory mediators. Meanwhile, other organs may have significant and deadly inflammatory reactions because of the damaged liver (19).

Kupffer cells are in charge of generating inflammatory cytokines and mediating liver injury in the early stages of sepsis. Upon

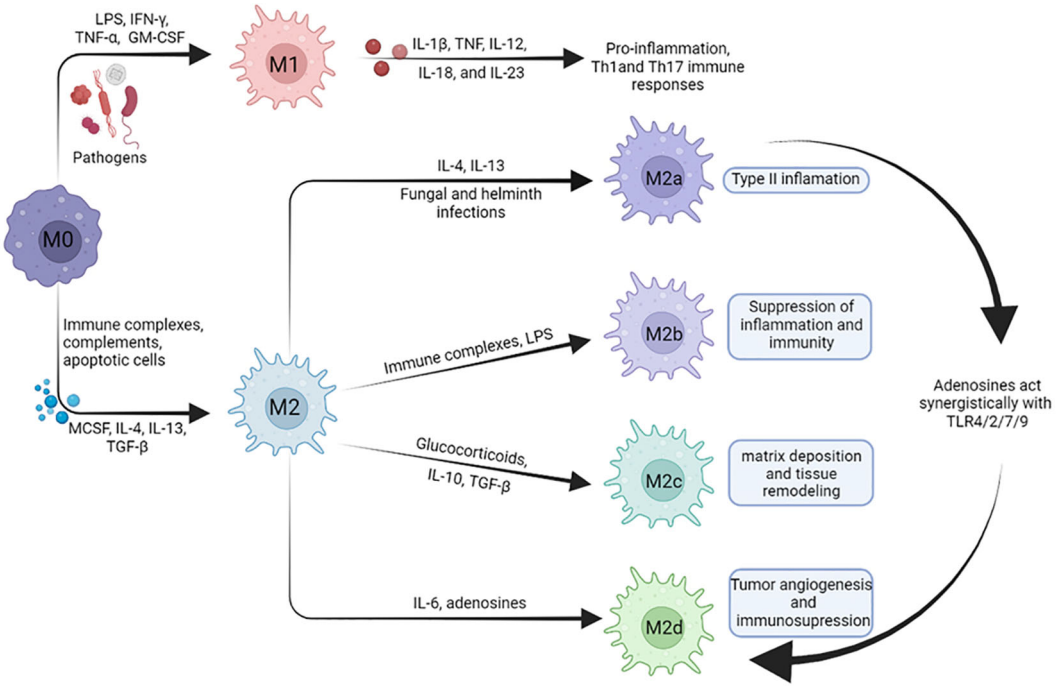

FIGURE 1
Macrophages exhibit remarkable plasticity and can undergo polarization into either M1 macrophages or M2 macrophages in response to specific microenvironmental cues. M1 macrophages are characterized by the secretion of various pro-inflammatory cytokines and inflammatory mediators, contributing to tissue damage and robust inflammatory responses. M2 macrophages has been subdivided into distinct subtypes, including M2a, M2b, M2c, and M2d. Under certain conditions, M2a can be transformed into M2d. Activated M2a macrophages can be involved in type II inflammation. M2b macrophages can be involved in the supression of inflammation and immunity response. M2c macrophages can be involved in matrix deposition and tissue remodeling. M2d macrophages can be involved in tumor angiogenesis and immunosupression.

encountering harmful bacteria or endotoxins, Kupffer cells respond by augmenting the release of several early proinflammatory mediators. These include IL-1, IL-6, IL-8, TNF-α, IFN-γ, and monocyte chemotactic protein 1 (11). Studies have shown that inducing Kupffer cell exhaustion through the administration of gadolinium chloride before cecal ligation and puncture (CLP) can have beneficial effects during the early stages of sepsis in rats. This exhaustion of Kupffer cells leads to a reduction in the secretion of pro-inflammatory cytokines. Additionally, it helps improve hepatic microcirculation disorders, reduce hepatic cell apoptosis, and prevent the development of liver injury. However, hepatic bacterial clearance impaired due to Kupffer cells loss, finally the survival of septic rats was remarkably decreased (20). The modulation of Kupffer cell differentiation represents a novel strategy with the potential to suppress inflammation and protect organs from injury.

Inflammation and chemokine production are also mediated by hepatocytes, hepatic stellate cells, and LSECs. Pathogen proteins are identified by hepatic stellate cells and LSECs through pattern recognition receptors such as the Toll-like receptor (TLR), enabling them to assume the role of liver antigen-presenting cells. In collaboration with Kupffer cells, these cells orchestrate a series of immunological events in sepsis. They activate hepatic natural killer T cells, classical T cells (CD4+ and CD8+ T lymphocytes), recruit neutrophils to the liver, and initiate both local and systemic inflammatory responses (2).

1.3.3 Liver-mediated immunosuppression

Liver has a special innate immune microenvironment and plays a crucial part in surveillance for immune homeostasis (21, 22). Due to its unique dual blood supply, the liver is subjected to a constant exposure to circulating antigens, pathogens, and pathogen-associated toxins. These agents gain access to the liver through multiple routes, including the gastrointestinal tract, portal vein, and systemic circulation via arterial blood (23). Thus, liver cells act as gatekeepers to initiate or suppress immune responses as needed. The liver harbors a significant population of intra-tissue macrophages, primarily represented by Kupffer cells located within the hepatic sinusoids. These Kupffer cells serve as the predominant phagocytic cells in the liver and constitute more than 80% of the macrophage population in a healthy human liver. Additionally, it contains lymphoid (such as natural killer cells, T cells, or B cells) and myeloid (such as neutrophils or macrophages) immune cells, which collectively compose both innate and acquired immune responses (22).

The complexity of sepsis ranges from the initial stage of inflammatory response to the later stages of immunosuppression (24). The initial phase manifests as systemic inflammatory response syndrome, which include systemic inflammation, cytokine storm and multi-organ damage (25). When the body's immune cells detect bacteria or endotoxins, a potent inflammatory response is triggered. If the process is not properly controlled, monocytes become unable to respond to further endotoxin attacks, and they begin to produce

anti-inflammatory cytokines (TGF-β, IL-10), the spesis will enter a state of immunosuppression. Endotoxin tolerance is one of the main mechanisms of immunosuppression in sepsis. It is the diminished reactivity to endotoxin challenge following the initial exposure (26, 27). Endotoxin tolerance can protect body from lethal endotoxin attack and prevents infection and ischemia-reperfusion injury. In the meantime, endotoxin tolerance has a significant impact on patients' vulnerability to reinfection, which in septic patients can be fatal (24). Uncontrolled inflammatory responses produce cytokine storms that lead to abroad tissue damage and pathological manifestations states such as sepsis (27).

1.4 Mesenchymal stem cells

Mesenchymal stem cells (MSCs) possess an immense capacity for self-renewal and multi-differentiation. These remarkable cells can be sourced from various tissues, such as bone marrow, adipose tissue, umbilical cord, and placental tissue (28, 29). MSCs exhibit a variety of advantageous characteristics in inflammatory diseases, including the ability of homing, reduce inflammatory response, regulate immune homeostasis, mitigate organ damage, and stimulate tissue regeneration (30). Based on the characteristics, MSCs have widespread application in the fields of cell therapies and bioengineering (28, 29). As a result, MSCs appear to be promising as one of the treatments for sepsis (31).

2 How MSCs regulate macrophage polarization

2.1 Paracrine effects of MSCs

MSCs can reduce inflammatory response, promote tissue repair and regeneration through paracrine soluble factors (32). MSCs possess the capability to modulate the polarization of macrophages and regulate the secretion of inflammatory factors. Through the paracrine signaling of prostaglandin E2 (PGE2). PGE2 exerts inhibitory effects on the nucleotide-binding and oligomerization domain-like receptor 3 (NLRP3) inflammasome, resulting in the reduction of inflammatory cytokine secretion, including IL-1β, IL-6, and IL-18. By attenuating the activation of the NLRP3 inflammasome, MSCs can effectively mitigate acute liver inflammation, thereby contributing to the amelioration of liver injury and the restoration of immune homeostasis (33). MSCs control the Hippo-YAP pathway of macrophages in a mouse model of inflammatory liver injury by secreting PGE2 to prevent the phosphorylation of mammalian Ste20-like kinase 1/2 and large tumor suppressor 1, to boost the translocation of YAP from cytoplasm to nucleus. By directly interacting with YAP and β-catenin to activate NLRP3, the Hippo pathway then regulates XBP1 to reduce NLRP3/caspase-1 activity and IL-1 production, which in turn facilitate hepatic macrophages to polarize toward M2 phenotype (34). MSCs produce PGE2, which not only inhibits inflammatory cytokine secretion but also facilitates the polarization of hepatic macrophages towards the M2 phenotype (35, 36). This process is mediated by the activation and phosphorylation of the transcription factor signal transducers and activators of transcription 6 (STAT6). PGE2, through its interaction with specific receptors on macrophages, triggers the activation and phosphorylation of STAT6, a classical mechanism involved in M2 macrophage polarization. This shift towards the M2 phenotype promotes an anti-inflammatory environment and supports tissue repair processes in the liver, further contributing to the resolution of inflammation and the promotion of liver recovery (33, 35) (Figure 2).

When the expression of MSCs-derived TSG-6 (TNF-α-stimulated gene 6) was inhibited, there was a notable impact on the macrophage population in the pancreatic and liver tissues of rats with severe acute pancreatitis. Specifically, the presence of iNOS+ M1 macrophages significantly increased, while the abundance of CD163+ M2 macrophages significantly decreased. Inhibition of TSG-6 expression disrupts this regulatory mechanism, leading to an imbalance in macrophage phenotypes and potentially exacerbating the inflammatory state associated with severe acute pancreatitis in the pancreatic and liver tissues of rats (37). Within the inflammatory state of the host, the generation and secretion of IL-4 by bone marrow-derived MSCs occur, triggering the activation of host liver macrophage reprogramming. Simultaneously, the upregulation of Wnt-3a expression is induced by MSCs. Facilitating the shift from the M1 pro-inflammatory phenotype to the M2 anti-inflammatory phenotype (38). Through the co-encapsulation of hepatocytes and human umbilical cord MSCs (HNF4α-UMSCs), a series of beneficial effects have been observed. This co-encapsulation approach has demonstrated the capacity to diminish liver damage induced by LPS/D-galactosamine, elevate the survival rate of mice with acute liver failure (ALF), and enhance the survival, proliferation, and metabolic function of hepatocytes. These positive outcomes are achieved by facilitating the polarization shift of macrophages from the M1 to the M2 phenotype, and leveraging paracrine mechanisms (39). Through the augmentation of HNF4α expression, an elevation in the transcriptional activity of IL-10 is achieved, consequently promoting the polarization of M2 macrophages via the activation of the IL-10/STAT3 pathway (40). Using paracrine soluble substances, especially through controlling macrophage activity, can help to reduce excessive inflammatory reactions (Figure 3).

2.2 Exosomes of MSCs

The International Society for Extracellular Vesicles (ISEV) endorses the term "extracellular vesicle" (EV) as the universal terminology for naturally released particles originating from cells. These vesicles are characterized by a lipid bilayer membrane, lack the ability to replicate and do not possess a functional nucleus within their structure (41). EVs are commonly categorized into three subtypes based on their size and biogenesis: exosomes (Exos), microvesicles, and apoptotic bodies. Exos are generated through the fusion of multivesicular bodies with the plasma membrane, resulting in their release into the extracellular space (42). EVs can

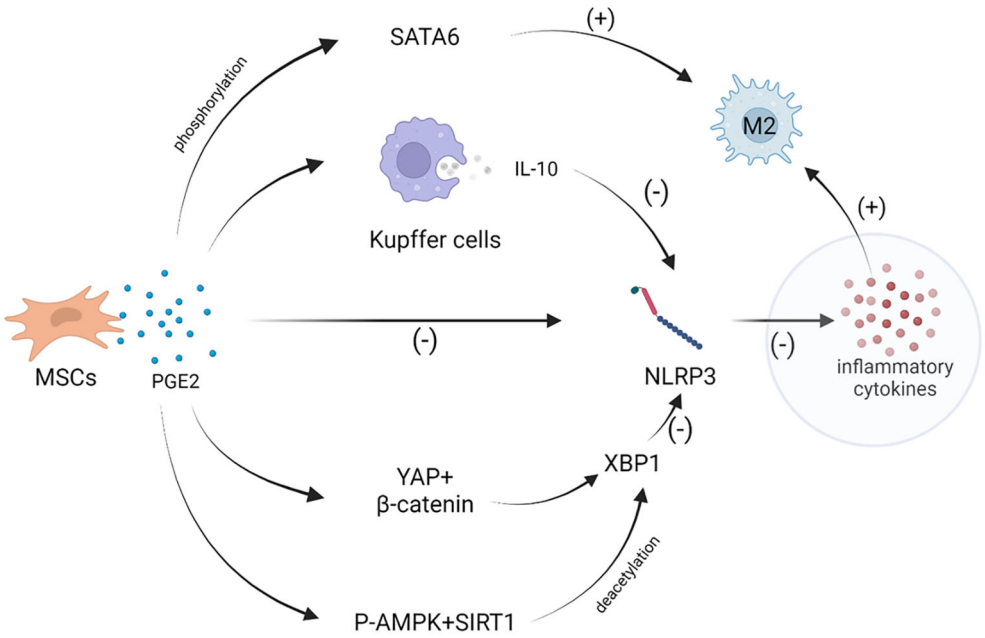

FIGURE 2
MSCs can paracrine PGE2 and affect the macrophages polarization through a variety of ways. PGE2 inhibits NLRP3 inflammasome to lessen the secretion of inflammatory cytokines. PGE2 control the Hippo-YAP pathway of macrophages and increase the expression of p-AMPK and SIRT1, then regulates XBP1 to reduce NLRP3 inflammasome activity, which promotes macrophages polarization toward M2 phenotype. In addition, PGE2 can stimulate the phosphorylation and activation of STAT6, induces macrophages to M2 polarization.

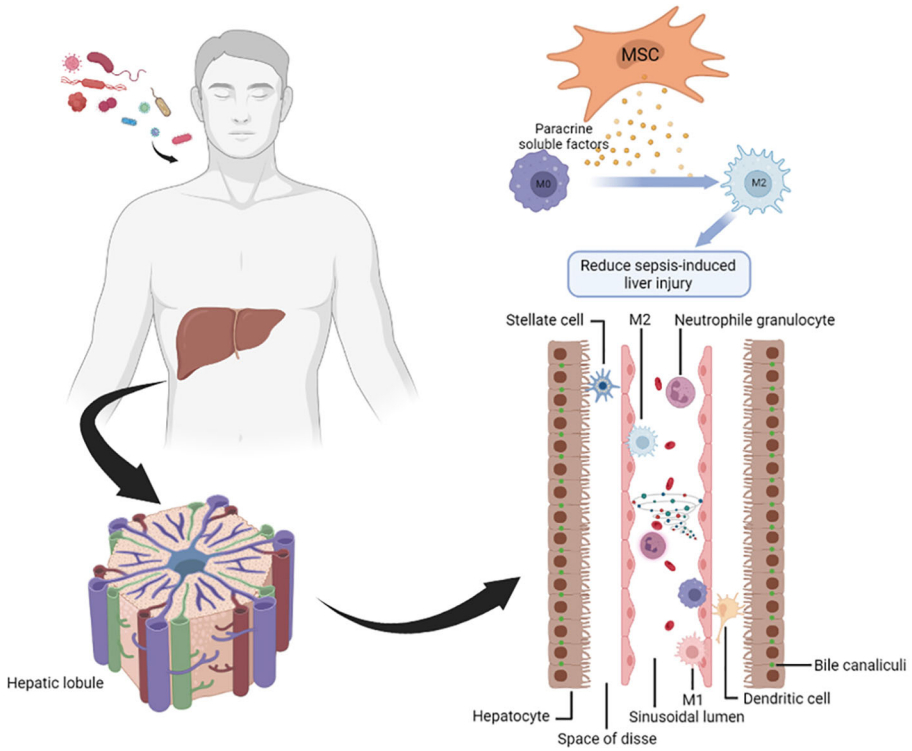

FIGURE 3
MSCs attenuate sepsis-induced liver injury through paracrine soluble factors. Immune cells, such as neutrophils and Kupffer cells, accumulates in the hepatic sinuses and produce a large number of cytokines, resulting in a cytokine storm. MSCs can play a pivotal role in attenuating sepsis-induced liver injury through the immunoregulation effects of paracrine soluble factor.

carry complex macromolecular substances such as proteins and nucleic acids, and introduced into recipient cells to take a variety of biological effects (8). Exos serve as both providers of biologically active molecules and essential carriers to protect the molecules and deliver them to the appropriate targets. Exos are preferentially endocytosed in the injured tissue because Exos uptake is reliant on the acidity of the intracellular and microenvironment and tissue injury is typically characterized by acidosis (43).

The immunomodulatory effects displayed by MSC-Exos, akin to those exerted by MSCs, have been demonstrated both *in vitro* and *in vivo* settings (44, 45). MSC-Exos were found to repair injured liver tissue in ALF model mice and reduce the expression of NLRP3 inflammasome and caspase-1, IL-1β and IL-6 in acute liver failure (46), thereby promoting macrophage polarization toward the M2 phenotype (34). MSC-Exos accumulated in the liver 6 hours after injection in the mouse model of partial hepatectomy and was primarily absorbed by liver macrophages, MSC-Exos exert their hepatoregenerative effects through the modulation of macrophage phenotypic transformations (45). Anti-inflammatory-related miRNA-299-3p had been found up-regulated in TNF-α pretreatment of umbilical cord MSC-derived Exos. Their high expression may contribute to the reduction of blood levels of alanine aminotransferase (ALT), aspartate aminotransferase (AST), pro-IL-1 and pro-IL-18, pro-inflammatory cytokines, attenuation of liver injury, and inhibition of NLRP3 inflammation-associated pathway proteins (47). The miRNA-17, abundant in MSC-Exo cargo, can also suppress NLRP3 inflammasome activation by targeting thioredoxin-interacting protein (TXNIP) in macrophages (48). The miRNA-182-5p was significantly enriched in MSC-Exos. By preventing the production of the forkhead box transcription factor 1 (FOXO1) in macrophages, the miRNA-182-5p of MSC-Exos reduced the expression of the TLR4 and triggered an anti-inflammatory response (45).

Experiments conducted *in vitro* have demonstrated that MSC-Exos decrease inflammatory responses and may control macrophage polarization by preventing hypoxia-inducible factor 1 (HIF-1) from mediating glycolysis, significantly inhibiting M1 polarization and promoting M2 polarization (49). It was discovered by Zhang Y et al. that Kupffer cell M2 polarization is dependent on the presence of IL-10 within MSC-EVs, as opposed to free IL-10. The EVs carrying IL-10 were collected by Kupffer cells, subsequently inducing the expression of PTPN22. This, in turn, facilitated macrophage polarization towards the M2 phenotype, leading to a reduction in liver inflammation and damage (50).

In the study conducted by Siyuan et al., it was demonstrated that miRNA-148a, which is enriched within the extracellular vesicles (Exos), exerts regulatory effects on Kruppel-like factor 6 (KLF6). Through this regulatory interaction, miRNA-148a exhibits the capability to suppress M1 macrophages while simultaneously promoting the polarization of M2 macrophages. This modulation is achieved by inhibiting the STAT3 pathway (51). However, Hui et al. found that MSC-Exos induced macrophage polarization toward M2 with arginase-1 high expression mainly through transporting the activated STAT3 (52). The mechanism of regulating STAT3 pathway affecting macrophage polarization needs to be further studied.

2.3 Homing

Stem cell homing refers to the process in which autologous or exogenous stem cells can migrate to target tissues and colonize under the action of various factors (53). In a mouse model of sepsis-induced liver injury, the use of iron oxide-based synthetic nanoparticles containing MSCs (SPION-MSCs) was found to facilitate the polarization of macrophages towards the M2 phenotype. The introduction of SPIONs did not compromise the fundamental characteristics of MSCs. Instead, it stimulated the expression of Haem oxygenase 1 within MSCs, allowing for the regulation of their activity within an inflammatory environment (9). Following infusion, SPION-MSCs exhibited a rapid homing to the lungs and subsequently became trapped in the liver for a period exceeding 10 days. In contrast, their residence in other organs was infrequently observed. Importantly, the promotion of M2 macrophage polarization was attributed to the phagocytosis of SPION-MSCs by these macrophages. This phenomenon suggests that the interaction between SPION-MSCs and M2 macrophages plays a significant role in facilitating the polarization of macrophages towards the M2 phenotype (54). Additionally, the expression of TNF receptor-associated factor 1 by SPION-MSCs was found to be crucial for the promotion of macrophage polarization and the subsequent reduction of sepsis in mice (9).

In conclusion, the regulation of macrophage polarization by MSCs can occur through various mechanisms, including the secretion of paracrine soluble factors, the release of Exos, and the process of homing (Table 1). Consequently, this regulatory capacity holds great promise as a therapeutic approach for addressing sepsis-induced liver injury.

3 MSCs-regulated signaling pathways of macrophage polarization

3.1 NF-κB signaling pathway

NF-κB is a universal transcription factor and a critical regulator of gene expression during severe infections, including sepsis (57). It is one of important transcription factor associated with the activation of M1 macrophages (58). Studies demonstrated that inhibition of NF-κB activation by MSCs can remarkably reduce sepsis-induced liver injury (59). Therefore, inhibition of NF-κB pathway by MSCs may be a significant molecular mechanism in the treatment of sepsis-induced liver injury. P50 NF-κB protein can inhibit NF-κB signaling pathway, and activate the M2 polarization (60). The miRNA-27b supplied by MSC-derived exos could decrease the inflammatory response and prevent sepsis by downregulating p65 NF-κB, which can activate the NF-κB signal pathway (61). Jie et al. found that small EVs from MSCs can limit the phosphorylation of the NF-κB pathway (62). Thus, EVs acting on the NF-κB pathway may be one of the effective ways to treat sepsis.

TABLE 1 The ways of MSCs regulate macrophage polarization.

Authors	Publication time	Sources of MSCs	Regulation of macrophage polarization	Results
Lee KC et al. (55)	2015	Mice bone marrow	Paracrine soluble factors: IL1Ra	MSCs reduced liver injury by increasing IL10 production through an IL1Ra dependent M2 polarization of macrophage.
Miao CM et al. (36)	2016	Mice bone marrow	Paracrine soluble factors: PGE2	MSCs secrete PGE2 to inhibit M1 Kupffer cells and promote M2 Kupffer cells, enhancing IL-10 release.
Liu Y et al. (48)	2018	Mice adipose	MSCs-derived exosomal miRNA -17	MSC-Exos protect against ALF by inhibiting NLRP3 inflammasome activation in macrophages via miR-17-mediated TXNIP inhibition.
Li C et al. (34)	2019	Mice bone marrow	Paracrine soluble factors: PGE2	Mesenchymal stem cells promoted the macrophage Hippo pathway, reduced NLRP3/caspase-1 activity, leading to reprogramming of macrophages to the M2 phenotype.
Jiang L et al. (46)	2019	Human umbilical cord	MSC-Exos	MSC-Exos repaired liver tissue, reducing NLRP3 inflammasome expression and levels of ALT and AST in a mouse ALF model.
Kong D et al. (39)	2020	Human umbilical cord	Paracrine soluble factors:HB-EGF	Co-encapsulation of HNF4α-MSCs and hepatocytes promoted M2 macrophage polarization and attenuated the inflammatory response.
Zhang S et al. (47)	2020	Human umbilical cord	MSCs-derived exosomal miRNA-299-3p	T-Exos effectively reduced serum levels of ALT, AST, and proinflammatory cytokines, suppressed the activation of NLRP3 inflammation-associated pathway proteins, and mitigated pathological liver damage in ALF.
Wang J et al. (33)	2021	Mice bone marrow	Paracrine soluble factors: PGE2	MSC-derived PGE2 induces M2 macrophage polarization in liver through STAT6 and mTOR signaling pathways.
Chang CY et al. (52)	2021	Human placenta choriodecidual membrane	MSCs-derived exosomal let-7i-5p miRNA	Exos therapy restores metabolic homeostasis, reduces oxidation and inflammation, and promotes the polarization of macrophages towards the M2 phenotype.
Zhang Y et al. (50)	2021	Mice bone marrow	MSCs-derived EVs containing IL-10	IL-10-containing EVs were captured by Kupffer cells, leading to the upregulation of protein tyrosine phosphatase non-receptor 22 (PTPN22). This resulted in the transformation of Kupffer cells into the M2 phenotype, effectively mitigating liver inflammation.
Xu Y et al. (9)	2021	Human umbilical cord	Homing of MSCs	The enhanced macrophages polarization towards the M2 phenotype observed in sepsis-induced liver injury in mice is attributed to the phagocytosis of SPION-MSCs.
Sun W et al. (44)	2022	Human umbilical cord	MSC-Exos	Exos derived from MSCs exhibit potent anti-inflammatory and immunosuppressive effects, thereby preventing critical organ injury by promoting the polarization of M2 macrophages and regulatory T cells.
Tian S et al. (51)	2022	Human umbilical cord	MSCs-derived exosomal miRNA-148a	MiR-148a, abundant in MSC-Exos, selectively targets Kruppel-like factor 6 (KLF6) to suppress M1 macrophages while promoting M2 macrophages through the inhibition of the STAT3 pathway.
Wang J et al. (38)	2022	Mice bone marrow	MSCs-derived exosomal IL-4	Transplanting allogeneic MSCs alleviated ALF by inducing a switch of macrophages towards the M2 phenotype, and this effect was dependent on IL-4.
Xu J et al. (45)	2022	Mice bone marrow	MSCs-derived exosomal miRNA-182- 5p	Hypoxic MSC-Exos promote macrophage polarization to the M2 phenotype during liver regeneration by modulating the FOXO1/TLR4 signaling pathway.
Yu Y et al. (40)	2022	Human umbilical cord	Paracrine soluble factors: IL-10	Overexpressing HNF4α in MSCs alleviated ALF and induced macrophage polarization to the M2 phenotype via the IL10/STAT3 pathway.
Watanabe Y et al. (56)	2022	Human gingival tissue	MSCs-derived exosomal CD73, CD5L	MSC-Exos, when stimulated with the combination of TNF-α and IFN-α, enhance macrophage polarization to the M2 phenotype through the upregulation of exosomal CD73 and CD5L.

3.2 JAK/STAT signaling pathway

The Janus family of kinases (JAK) encompasses four major members, namely JAK1, JAK2, JAK3, and Tyk2. These proteins, belonging to the tyrosine kinase family, exhibit high homology and share similar structural characteristics (63). Many cellular functions are reliant upon the pivotal role played by the STAT (Signal Transducer and Activator of Transcription) family, consisting of essential members such as STAT1, STAT2, STAT3, STAT4, STAT5A, STAT5B, and STAT6 (64). To regulate the expression of associated genes, the JAK enzymes are capable of phosphorylating STAT proteins, giving rise to what is commonly

referred to as the JAK-STAT signaling pathway. This intricate pathway exerts significant control over immunological responses, cell growth, proliferation, and differentiation processes (63).

An investigation found that the potential functions of the JAK/STAT pathway in regulating the systemic inflammatory response elicited by septic challenge were examined *in vivo*. The researchers observed that JAK2 exhibited rapid activation in septic rats, with maximal activation occurring in hepatic tissues after 6 hours. Notably, in septic rats induced by CLP, they demonstrated that the JAK/STAT pathway could potentially exert control over the development of organ damage in various organs. These findings shed light on the role of the JAK/STAT pathway in the pathogenesis of sepsis and suggest its involvement in orchestrating the inflammatory response and subsequent organ injury during septic conditions (65). A study found that inhibiting the JAK2/STAT3 signaling pathway might diminish the production of proinflammatory cytokines including TNF-α and IL-6, as well as mitigate multiple organ failure in severe sepsis (66). Lentsch et al. made an intriguing discovery regarding the dysregulated activation of the transcription factor NF-κB in STAT6-deficient mice. This dysregulation led to an augmented production of pro-inflammatory cytokines and chemokines in the liver, including MIP-1, MIP-2, IP-10, and MCP-1. Additionally, upon endotoxin stimulation, STAT6-deficient animals exhibited a higher accumulation of neutrophils and leukocytes within the liver. This enhanced accumulation of immune cells may potentially contribute to organ damage (67).

Mesenchymal stem cells stimulate the phosphorylation and activation of STAT6 by paracrine PGE2, which in turn induces macrophages to M2 polarization. Increasing M2 macrophages by MSC treatment can activate the IL-4/STAT6 signaling pathway to control the acute-phase response in the liver (35).

3.3 AMPK/SIRT1 signaling pathway

AMP-activated protein kinase (AMPK) is an important regulator of energy metabolism at the cellular level. Sirtuin (SIRT) is a NAD^+-dependent protein deacetylase, SIRT1 is one of the most concerned members, it plays a key role in the regulation of inflammation, immune response, metabolism and apoptosis/aging. In the aspect of maintaining energy homeostasis, AMPK and SIRT1 often show synergistic effect, and also interact to regulate each other's expression. The target of AMPK/SIRT1 is a classical upstream signaling pathway of oxidative stress and crucial for maintaining metabolic homeostasis (68). Jagged1 treatment significantly raised the amount of PGE2 that MSCs secreted. PGE2 then increased the expression of p-AMPK and SIRT1, which in turn caused XBP1s to be deacetylated and the NLRP3 inflammasome to be inhibited in macrophages (69), thereby promoting macrophage polarization toward the M2 phenotype (34).

3.4 Notch signaling pathway

Recent studies have highlighted the participation of the Notch pathway in critical processes such as liver regeneration and repair, liver fibrosis, and metabolism. These findings suggest that the Notch signaling pathway plays a significant role in maintaining liver homeostasis and responding to physiological and pathological changes within the liver (70). Notch signaling pathway is crucial in macrophage polarization (71). It can up-regulate miRNA-148a-3p expression in macrophages, when miRNA-148a-3p can accelerate M1 polarization of macrophages (72). Through activation of NF-κB, activated Notch1 and expression of the Notch target genes remarkably regulate the production of TNF-α, IL-6, and IL-10 (71). MSC transplantation remarkably reduced Notch1 receptor in liver failure rats, suppressing the M1 polarization of macrophage. The impact of MSCs on hepatocyte regeneration may be influenced by the down-regulation of Notch signaling (73). Further investigations into the intricate mechanisms underlying Notch pathway regulation hold promise for developing novel therapeutic strategies targeting liver-related disorders.

4 MSCs treatment sepsis-induced liver injury

As the liver serves as the primary defense against infections and also plays a crucial role in drug metabolism, it is susceptible to injuries induced by both infections and drugs. In a study conducted, mice were intravenously administered with MSCs one hour before being subjected to a CLP challenge. Following the CLP challenge, there was a significant increase in the levels of AST and ALT. However, the intervention involving the administration of MSCs effectively mitigated the elevated levels of AST and ALT, alleviated pathological injury of the liver and enhanced the survival rate of mice in the sepsis model (74).

When MSCs were administered into a mouse model with CLP-induced sepsis, there was a notable attenuation in the expression of TNF-α and IL-6, while concurrently witnessing an upsurge in the expression of IL-4 and IL-10. This not only mitigated the pronounced hepatic swelling and necrosis observed in the liver but also led to a decline in the elevated levels of AST and ALT. Additionally, there was a discernible reduction in the presence of Bax- and Caspase-3-positive apoptosis cells, coupled with an enhanced glycogen deposition within the liver, ultimately contributing to an improved survival rate (59, 75). It's noteworthy to mention that SPION-MSCs exhibited a more pronounced ameliorative effect on these pathological symptoms in both CLP and LPS sepsis mouse models in comparison to when MSCs were used in isolation (9).

5 Conclusion

In summary, the modulation of macrophage polarization by MSCs offers a promising therapeutic approach for sepsis-induced liver injury. The paracrine secretion of soluble factors, exosomes, and the ability of MSCs to home to the liver contribute to their beneficial effects in reducing liver injury and promoting tissue repair. Further understanding of the signaling pathways involved and optimization of MSC-based therapies will pave the way for their

clinical application in treating sepsis-induced liver injury, offering new hope for patients facing this challenging condition.

Author contributions

YC: Writing - Original draft. LY and XL: Writing -Review and Editing. All authors contributed to the article and approved the submitted version.

Funding

The author(s) declare financial support was received for the research, authorship, and/or publication of this article. This work was supported by the National Science Foundation of China (grant nos. 82071353).

Acknowledgments

The authors thanks Biorender (https://biorender.com) for their help in drawing pictures.

Conflict of interest

The authors declare that the research was conducted in the absence of any commercial or financial relationships that could be construed as a potential conflict of interest.

Publisher's note

References

1. Singer M, Deutschman CS, Seymour CW, Shankar-Hari M, Annane D, Bauer M, Shankar-Hari M, Annane D, Bauer M, et al. The third international consensus definitions for sepsis and septic shock (Sepsis-3). *JAMA* (2016) 315(8):801–10. doi: 10.1001/jama.2016.0287

2. Dhainaut JF, Marin N, Mignon A, Vinsonneau C. Hepatic response to sepsis: interaction between coagulation and inflammatory processes. *Crit Care Med* (2001) 29 (7 Suppl):S42–7. doi: 10.1097/00003246-200107001-00016

3. Sun J, Zhang J, Wang X, Ji F, Ronco C, Tian J, et al. Gut-liver crosstalk in sepsis-induced liver injury. *Crit Care* (2020) 24:614. doi: 10.1186/s13054-020-03327-1

4. Lelubre C, Vincent JL. Mechanisms and treatment of organ failure in sepsis. *Nat Rev Nephrol* (2018) 14(7):417–27. doi: 10.1038/s41581-018-0005-7

5. Iwashyna TJ, Cooke CR, Wunsch H, Kahn JM. Population burden of long-term survivorship after severe sepsis in older Americans. *J Am Geriatr Soc* (2012) 60 (6):1070–7. doi: 10.1111/j.1532-5415.2012.03989.x

6. Gaieski DF, Edwards JM, Kallan MJ, Carr BG. Benchmarking the incidence and mortality of severe sepsis in the United States. *Crit Care Med* (2013) 41(5):1167–74. doi: 10.1097/CCM.0b013e31827c09f8

7. Dixon LJ, Barnes M, Tang H, Pritchard MT, Nagy LE. Kupffer cells in the liver. *Compr Physiol* (2013) 3(2):785–97. doi: 10.1002/cphy.c120026

8. Arabpour M, Saghazadeh A, Rezaei N. Anti-inflammatory and M2 macrophage polarization-promoting effect of mesenchymal stem cell-derived exosomes. *Int Immunopharmacol* (2021) 97:107823. doi: 10.1016/j.intimp.2021.107823

9. Xu Y, Liu X, Li Y, Dou H, Liang H, Hou Y. SPION-MSCs enhance therapeutic efficacy in sepsis by regulating MSC-expressed TRAF1-dependent macrophage polarization. *Stem Cell Res Ther* (2021) 12(1):531. doi: 10.1186/s13287-021-02593-2

10. Anders CB, Lawton T, Smith HL, Garret J, Doucette MM, Ammons M. Use of integrated metabolomics, transcriptomics, and signal protein profile to characterize the effector function and associated metabotype of polarized macrophage phenotypes. *J Leukoc Biol* (2022) 111(3):667–93. doi: 10.1002/JLB.6A1120-744R

11. Yan J, Li S, Li S. The role of the liver in sepsis. *Int Rev Immunol* (2014) 33 (6):498–510. doi: 10.3109/08830185.2014.889129

12. Gonnert FA, Kunisch E, Gajda M, Lambeck S, Weber M, Claus RA, Lambeck S, Weber M, Claus RA, et al. Hepatic fibrosis in a long-term murine model of sepsis. *Shock* (2012) 37(4):399–407. doi: 10.1097/SHK.0b013e31824a670b

13. Deng M, Scott MJ, Loughran P, Gibson G, Sodhi C, Watkins S, Gibson G, Sodhi C, Watkins S, et al. Lipopolysaccharide clearance, bacterial clearance, and systemic inflammatory responses are regulated by cell type-specific functions of TLR4 during sepsis. *J Immunol* (2013) 190(10):5152–60. doi: 10.4049/jimmunol.1300496

14. Foreman MG, Mannino DM, Moss M. Cirrhosis as a risk factor for sepsis and death: analysis of the National Hospital Discharge Survey. *Chest* (2003) 124(3):1016–20. doi: 10.1378/chest.124.3.1016

15. Protzer U, Maini MK, Knolle PA. Living in the liver: hepatic infections. *Nat Rev Immunol* (2012) 12(3):201–13. doi: 10.1038/nri3169

16. Wong CH, Jenne CN, Petri B, Chrobok NL, Kubes P. Nucleation of platelets with blood-borne pathogens on Kupffer cells precedes other innate immunity and contributes to bacterial clearance. *Nat Immunol* (2013) 14(8):785–92. doi: 10.1038/ni.2631

17. McDonald B, Urrutia R, Yipp BG, Jenne CN, Kubes P. Intravascular neutrophil extracellular traps capture bacteria from the bloodstream during sepsis. *Cell Host Microbe* (2012) 12(3):324–33. doi: 10.1016/j.chom.2012.06.011

18. Wasmuth HE, Kunz D, Yagmur E, Timmer-Stranghöner A, Vidacek D, Siewert E, Timmer-Stranghöner A, Vidacek D, Siewert E, et al. Patients with acute on chronic liver failure display "sepsis-like" immune paralysis. *J Hepatol* (2005) 42(2):195–201. doi: 10.1016/j.jhep.2004.10.019

19. Gustot T, Durand F, Lebrec D, Vincent JL, Moreau R. Severe sepsis in cirrhosis. *Hepatology* (2009) 50(6):2022–33. doi: 10.1002/hep.23264

20. Koo DJ, Chaudry IH, Wang P. Kupffer cells are responsible for producing inflammatory cytokines and hepatocellular dysfunction during early sepsis. *J Surg Res* (1999) 83(2):151–7. doi: 10.1006/jsre.1999.5584

21. Krenkel O, Tacke F. Liver macrophages in tissue homeostasis and disease. *Nat Rev Immunol* (2017) 17(5):306–21. doi: 10.1038/nri.2017.11

22. Heymann F, Tacke F. Immunology in the liver–from homeostasis to disease. *Nat Rev Gastroenterol Hepatol* (2016) 13(2):88–110. doi: 10.1038/nrgastro.2015.200

23. Strnad P, Tacke F, Koch A, Trautwein C. Liver - guardian, modifier and target of sepsis. *Nat Rev Gastroenterol Hepatol* (2017) 14(1):55–66. doi: 10.1038/nrgastro.2016.168

24. Monneret G, Venet F, Pachot A, Lepape A. Monitoring immune dysfunctions in the septic patient: a new skin for the old ceremony. *Mol Med* (2008) 14(1-2):64–78. doi: 10.2119/2007-00102.Monneret

25. Adib-Conquy M, Cavaillon JM. Compensatory anti-inflammatory response syndrome. *Thromb Haemost* (2009) 101(1):36–47.

26. Ackerman MH, Ahrens T, Kelly J, Pontillo A. Sepsis. *Crit Care Nurs Clin North Am* (2021) 33(4):407–18. doi: 10.1016/j.cnc.2021.08.003

27. Biswas SK, Lopez-Collazo E. Endotoxin tolerance: new mechanisms, molecules and clinical significance. *Trends Immunol* (2009) 30(10):475–87. doi: 10.1016/j.it.2009.07.009

28. Maqsood M, Kang M, Wu X, Chen J, Teng L, Qiu L. Adult mesenchymal stem cells and their exosomes: Sources, characteristics, and application in regenerative medicine. *Life Sci* (2020) 256:118002. doi: 10.1016/j.lfs.2020.118002

29. Brown C, McKee C, Bakshi S, Walker K, Hakman E, Halassy S, Walker K, Hakman E, Halassy S, et al. Mesenchymal stem cells: Cell therapy and regeneration potential. *J Tissue Eng Regener Med* (2019) 13(9):1738–55. doi: 10.1002/term.2914

30. Liang H, Ding X, Yu Y, Zhang H, Wang L, Kan Q, et al. Adipose-derived mesenchymal stem cells ameliorate acute liver injury in rat model of CLP induced-sepsis via sTNFR1. *Exp Cell Res* (2019) 383(1):111465. doi: 10.1016/j.yexcr.2019.06.010

31. Daniel M, Bedoui Y, Vagner D, Raffray L, Ah-Pine F, Doray B, et al. Pathophysiology of sepsis and genesis of septic shock: the critical role of mesenchymal stem cells (MSCs). *Int J Mol Sci* (2022) 23(16).

32. Alvites R, Branquinho M, Sousa AC, Lopes B, Sousa P, Maurício AC. Mesenchymal stem/stromal cells and their paracrine activity-immunomodulation mechanisms and how to influence the therapeutic potential. *Pharmaceutics* (2022) 14 (2).

33. Wang J, Liu Y, Ding H, Shi X, Ren H. Mesenchymal stem cell-secreted prostaglandin E(2) ameliorates acute liver failure via attenuation of cell death and regulation of macrophage polarization. *Stem Cell Res Ther* (2021) 12(1):15.

34. Li C, Jin Y, Wei S, Sun Y, Jiang L, Zhu Q, et al. Hippo signaling controls NLR family pyrin domain containing 3 activation and governs immunoregulation of mesenchymal stem cells in mouse liver injury. *Hepatology* (2019) 70(5):1714–31.

35. Li Y, Sheng Q, Zhang C, Han C, Bai H, Lai P, et al. STAT6 up-regulation amplifies M2 macrophage anti-inflammatory capacity through mesenchymal stem cells. *Int Immunopharmacol* (2021) 91:107266.

36. Miao CM, Jiang XW, He K, Li P-Z, Liu Z-J, Cao D, et al. Bone marrow stromal cells attenuate LPS-induced mouse acute liver injury via the prostaglandin E 2-dependent repression of the NLRP3 inflammasome in Kupffer cells. *Immunol Lett* (2016) 179:102–13.

37. Huang Q, Cheng X, Luo C, Yang S, Li S, Wang B, et al. Placental chorionic plate-derived mesenchymal stem cells ameliorate severe acute pancreatitis by regulating macrophage polarization via secreting TSG-6. *Stem Cell Res Ther* (2021) 12(1):337.

38. Wang J, Ding H, Zhou J, Xia S, Shi X, Ren H. Transplantation of mesenchymal stem cells attenuates acute liver failure in mice via an interleukin-4-dependent switch to the M2 macrophage anti-inflammatory phenotype. *J Clin Transl Hepatol* (2022) 10 (4):669–79.

39. Kong D, Xu H, Chen M, Yu Y, Qian Y, Qin T, et al. Co-encapsulation of HNF4α overexpressing UMSCs and human primary hepatocytes ameliorates mouse acute liver failure. *Stem Cell Res Ther* (2020) 11(1):449.

40. Yu Y, Zhang Q, Wu N, Xia L, Cao J, Xia Q, et al. HNF4α overexpression enhances the therapeutic potential of umbilical cord mesenchymal stem/stromal cells in mice with acute liver failure. *FEBS Lett* (2022).

41. Théry C, Witwer KW, Aikawa E, Alcaraz MJ, Anderson JD, Andriantsitohaina R, et al. Minimal information for studies of extracellular vesicles 2018 (MISEV2018): a position statement of the International Society for Extracellular Vesicles and update of the MISEV2014 guidelines. *J Extracell Vesicles* (2018) 7(1):1535750.

42. Wang J, Xia J, Huang R, Hu Y, Fan J, Shu Q, et al. Mesenchymal stem cell-derived extracellular vesicles alter disease outcomes via endorsement of macrophage polarization. *Stem Cell Res Ther* (2020) 11(1):424. doi: 10.1186/s13287-020-01937-8

43. Lai RC, Yeo RW, Lim SK. Mesenchymal stem cell exosomes. *Semin Cell Dev Biol* (2015) 40:82–8. doi: 10.1016/j.semcdb.2015.03.001

44. Sun W, Yan S, Yang C, Yang J, Wang H, Li C, et al. Mesenchymal stem cells-derived exosomes ameliorate lupus by inducing M2 macrophage polarization and regulatory T cell expansion in MRL/lpr mice. *Immunol Invest* (2022) 51(6):1785–803. doi: 10.1080/08820139.2022.2055478

45. Xu J, Chen P, Yu C, Shi Q, Wei S, Li Y, et al. Hypoxic bone marrow mesenchymal stromal cells-derived exosomal miR-182-5p promotes liver regeneration via FOXO1-mediated macrophage polarization. *FASEB J* (2022) 36(10):e22553. doi: 10.1096/fj.202101868RRR

46. Jiang L, Zhang S, Hu H, Yang J, Wang X, Ma Y, et al. Exosomes derived from human umbilical cord mesenchymal stem cells alleviate acute liver failure by reducing the activity of the NLRP3 inflammasome in macrophages. *Biochem Biophys Res Commun* (2019) 508(3):735–41. doi: 10.1016/j.bbrc.2018.11.189

47. Zhang S, Jiang L, Hu H, Wang H, Wang X, Jiang J, et al. Pretreatment of exosomes derived from hUCMSCs with TNF-α ameliorates acute liver failure by inhibiting the activation of NLRP3 in macrophage. *Life Sci* (2020) 246:117401. doi: 10.1016/j.lfs.2020.117401

48. Liu Y, Lou G, Li A, Zhang T, Qi J, Ye D, et al. AMSC-derived exosomes alleviate lipopolysaccharide/d-galactosamine-induced acute liver failure by miR-17-mediated reduction of TXNIP/NLRP3 inflammasome activation in macrophages. *EBioMedicine* (2018) 36:140–50. doi: 10.1016/j.ebiom.2018.08.054

49. Deng H, Wu L, Liu M, Zhu L, Chen Y, Zhou H, et al. Bone marrow mesenchymal stem cell-derived exosomes attenuate LPS-induced ARDS by modulating macrophage polarization through inhibiting glycolysis in macrophages. *Shock* (2020) 54(6):828–43. doi: 10.1097/SHK.0000000000001549

50. Zhang Y, Zhang X, Zhang H, Song P, Pan W, Xu P, et al. Mesenchymal stem cells derived extracellular vesicles alleviate traumatic hemorrhagic shock induced hepatic injury via IL-10/PTPN22-mediated M2 kupffer cell polarization. *Front Immunol* (2021) 12:811164. doi: 10.3389/fimmu.2021.811164

51. Tian S, Zhou X, Zhang M, Cui L, Li B, Liu Y, et al. Mesenchymal stem cell-derived exosomes protect against liver fibrosis via delivering miR-148a to target KLF6/STAT3 pathway in macrophages. *Stem Cell Res Ther* (2022) 13(1):330. doi: 10.1186/s13287-022-03010-y

52. Zhao H, Shang Q, Pan Z, Bai Y, Li Z, Zhang H, et al. Exosomes from adipose-derived stem cells attenuate adipose inflammation and obesity through polarizing M2 macrophages and beiging in white adipose tissue. *Diabetes* (2018) 67(2):235–47. doi: 10.2337/db17-0356

53. Karp JM, Leng Teo GS. Mesenchymal stem cell homing: the devil is in the details. *Cell Stem Cell* (2009) 4(3):206–16. doi: 10.1016/j.stem.2009.02.001

54. Pan Y, Li J, Wang J, Jiang Q, Yang J, Dou H, et al. Ferroptotic MSCs protect mice against sepsis via promoting macrophage efferocytosis. *Cell Death Dis* (2022) 13(9):825. doi: 10.1038/s41419-022-05264-z

55. Lee KC, Lin HC, Huang YH, Hung SC. Allo-transplantation of mesenchymal stem cells attenuates hepatic injury through IL1Ra dependent macrophage switch in a mouse model of liver disease. *J Hepatol* (2015) 63(6):1405–12. doi: 10.1016/j.jhep.2015.07.035

56. Watanabe Y, Fukuda T, Hayashi C, Nakao Y, Toyoda M, Kawakami K, et al. Extracellular vesicles derived from GMSCs stimulated with TNF-α and IFN-α promote M2 macrophage polarization via enhanced CD73 and CD5L expression. *Sci Rep* (2022) 12(1):13344. doi: 10.1038/s41598-022-17692-0

57. Jin LY, Li CF, Zhu GF, Wu CT, Wang J, Yan SF. Effect of siRNA against NF-κB on sepsis–induced acute lung injury in a mouse model. *Mol Med Rep* (2014) 10(2):631–7. doi: 10.3892/mmr.2014.2299

58. Sica A, Mantovani A. Macrophage plasticity and polarization: in *vivo* veritas. *J Clin Invest* (2012) 122(3):787–95. doi: 10.1172/JCI59643

59. Liang X, Li T, Zhou Q, Pi S, Li Y, Chen X, et al. Mesenchymal stem cells attenuate sepsis-induced liver injury via inhibiting M1 polarization of Kupffer cells. *Mol Cell Biochem* (2019) 452(1-2):187–97. doi: 10.1007/s11010-018-3424-7

60. Porta C, Rimoldi M, Raes G, Brys L, Ghezzi P, Di Liberto D, et al. Tolerance and M2 (alternative) macrophage polarization are related processes orchestrated by p50 nuclear factor kappaB. *Proc Natl Acad Sci USA* (2009) 106(35):14978–83. doi: 10.1073/pnas.0809784106

61. Sun J, Sun X, Chen J, Liao X, He Y, Wang J, et al. microRNA-27b shuttled by mesenchymal stem cell-derived exosomes prevents sepsis by targeting JMJD3 and downregulating NF-κB signaling pathway. *Stem Cell Res Ther* (2021) 12(1):14.

62. Chen J, Li C, Liang Z, Li C, Li Y, Zhao Z, et al. Human mesenchymal stromal cells small extracellular vesicles attenuate sepsis-induced acute lung injury in a mouse model: the role of oxidative stress and the mitogen-activated protein kinase/nuclear factor kappa B pathway. *Cytotherapy* (2021) 23(10):918–30. doi: 10.1016/j.jcyt.2021.05.009

63. Xu P, Shen P, Yu B, Xu X, Ge R, Cheng X, et al. Janus kinases (JAKs): The efficient therapeutic targets for autoimmune diseases and myeloproliferative disorders. *Eur J Med Chem* (2020) 192:112155. doi: 10.1016/j.ejmech.2020.112155

64. Cai B, Cai JP, Luo YL, Chen C, Zhang S. The specific roles of JAK/STAT signaling pathway in sepsis. *Inflammation* (2015) 38(4):1599–608. doi: 10.1007/s10753-015-0135-z

65. Hui L, Yao Y, Wang S, Yu Y, Dong N, Li H, et al. Inhibition of Janus kinase 2 and signal transduction and activator of transcription 3 protect against cecal ligation and puncture-induced multiple organ damage and mortality. *J Trauma* (2009) 66(3):859–65. doi: 10.1097/TA.0b013e318164d05f

66. Zhang W, Sun Q, Gao X, Jiang Y, Li R, Ye J. Anti-inflammation of spirocyclopiperazinium salt compound LXM-10 targeting α7 nAChR and M4 mAChR and inhibiting JAK2/STAT3 pathway in rats. *PloS One* (2013) 8(6):e66895. doi: 10.1371/journal.pone.0066895

67. Lentsch AB, Kato A, Davis B, Wang W, Chao C, Edwards MJ. STAT4 and STAT6 regulate systemic inflammation and protect against lethal endotoxemia. *J Clin Invest* (2001) 108(10):1475–82. doi: 10.1172/JCI200113763

68. Cheng AW, Tan X, Sun JY, Gu CM, Liu C, Guo X. Catechin attenuates TNF-α induced inflammatory response via AMPK-SIRT1 pathway in 3T3-L1 adipocytes. *PloS One* (2019) 14(5):e0217090. doi: 10.1371/journal.pone.0217090

69. Yu M, Zhou M, Li J, Zong R, Yan Y, Kong L, et al. Notch-activated mesenchymal stromal/stem cells enhance the protective effect against acetaminophen-induced acute liver injury by activating AMPK/SIRT1 pathway. *Stem Cell Res Ther* (2022) 13(1):318. doi: 10.1186/s13287-022-02999-6

70. Adams JM, Jafar-Nejad H. The roles of notch signaling in liver development and disease. *Biomolecules* (2019) 9(10). doi: 10.3390/biom9100608

71. Wei W, Li ZP, Bian ZX, Han QB. Astragalus polysaccharide RAP induces macrophage phenotype polarization to M1 via the notch signaling pathway. *Molecules* (2019) 24(10). doi: 10.3390/molecules24102016

72. Huang F, Zhao JL, Wang L, Gao C-C, Liang S-Q, An D-J, et al. miR-148a-3p mediates notch signaling to promote the differentiation and M1 activation of macrophages. *Front Immunol* (2017) 8:1327. doi: 10.3389/fimmu.2017.01327

73. He Y, Guo X, Lan T, Xia J, Wang J, Li B, et al. Human umbilical cord-derived mesenchymal stem cells improve the function of liver in rats with acute-on-chronic liver failure via downregulating Notch and Stat1/Stat3 signaling. *Stem Cell Res Ther* (2021) 12(1):396. doi: 10.1186/s13287-021-02468-6

74. Cai J, Tang D, Hao X, Liu E, Li W, Shi J. Mesenchymal stem cell-derived exosome alleviates sepsis- associated acute liver injury by suppressing MALAT1 through microRNA-26a-5p: an innovative immunopharmacological intervention and therapeutic approach for sepsis. *Front Immunol* (2023) 14:1157793. doi: 10.3389/fimmu.2023.1157793

75. Cóndor JM, Rodrigues CE, Rd SM, Canale D, Volpini RA, Shimizu MH, et al. Treatment with human wharton's jelly-derived mesenchymal stem cells attenuates sepsis-induced kidney injury, liver injury, and endothelial dysfunction. *Stem Cells Transl Med* (2016) 5:1048–57. doi: 10.5966/sctm.2015-0138

frontiers | Frontiers in Immunology

TYPE Review
PUBLISHED 26 October 2023
DOI 10.3389/fimmu.2023.1279264

OPEN ACCESS

EDITED BY
Balachandran Ravindran,
Institute of Life Sciences (ILS), India

REVIEWED BY
Santosh Panda,
Washington University in St. Louis, United States
Edward N. Harris,
University of Nebraska System, United States

*CORRESPONDENCE
Shi Ouyang
ouyangshi@gzhmu.edu.cn

RECEIVED 17 August 2023
ACCEPTED 16 October 2023
PUBLISHED 26 October 2023

CITATION
Xie D and Ouyang S (2023) The role and mechanisms of macrophage polarization and hepatocyte pyroptosis in acute liver failure. *Front. Immunol.* 14:1279264. doi: 10.3389/fimmu.2023.1279264

The role and mechanisms of macrophage polarization and hepatocyte pyroptosis in acute liver failure

Dan Xie and Shi Ouyang*

Key Laboratory of Biological Targeting Diagnosis, Therapy and Rehabilitation of Guangdong Higher Education Institutes, Department of Infectious Diseases, The Fifth Affiliated Hospital of Guangzhou Medical University, Guangzhou, China

Acute liver failure (ALF) is a severe liver disease caused by disruptions in the body's immune microenvironment. In the early stages of ALF, Kupffer cells (KCs) become depleted and recruit monocytes derived from the bone marrow or abdomen to replace the depleted macrophages entering the liver. These monocytes differentiate into mature macrophages, which are activated in the immune microenvironment of the liver and polarized to perform various functions. Macrophage polarization can occur in two directions: pro-inflammatory M1 macrophages and anti-inflammatory M2 macrophages. Controlling the ratio and direction of M1 and M2 in ALF can help reduce liver injury. However, the liver damage caused by pyroptosis should not be underestimated, as it is a caspase-dependent form of cell death. Inhibiting pyroptosis has been shown to effectively reduce liver damage induced by ALF. Furthermore, macrophage polarization and pyroptosis share common binding sites, signaling pathways, and outcomes. In the review, we describe the role of macrophage polarization and pyroptosis in the pathogenesis of ALF. Additionally, we preliminarily explore the relationship between macrophage polarization and pyroptosis, as well as their effects on ALF.

KEYWORDS

acute liver failure (ALF), macrophage, polarization, pyroptosis, immune

1 Introduction

The liver plays a crucial role in the immune system by serving as a vital organ responsible for removing toxins, producing immune proteins, and maintaining metabolic homeostasis (1). The first point to note is that the liver contains a high concentration of both innate and adaptive immune cells. These cells have the ability to trigger inflammation and liver damage in response to disease, but also have the capability of maintaining a state of tolerance during homeostasis. The liver is home to a variety of T cell subsets, including regulatory T cells and cytotoxic T lymphocytes, which play an essential role in maintaining liver tolerance (2–4). Not only that, innate immune cells, particularly liver-resident

macrophages known as Kupffer cells (KCs), work together with acquired immune cells to eliminate common pathogen-associated molecular patterns (PAMPs) and damage-associated molecular patterns (DAMPs) in the body. Besides, KCs also have a crucial role in maintaining liver homeostasis by engaging in phagocytosis, eliminating dead and senescent cells, and promoting tissue repair (5–7). In addition, the liver has the highest concentration of macrophages, which are dispersed throughout a network of circulatory channels that can quickly detect pathogens in the hepatic portal system (8).

The liver has a unique anatomy because it receives blood from both the hepatic artery and portal vein. This dual blood supply nourishes to the diverse structures and cells within the liver (8). The hepatic arterial and portal circulation terminate in the liver sinusoidal endothelial cells (LSECs), which consist of a thin, porous network of special capillaries and complement KCs in the hepatic sinusoids to form a solid surveillance system (9, 10) (Figure 1). The blood flows in sinusoidal waves at a slow pace, which allows for prolonged exposure to antigens within the sinusoids. This facilitates the recognition and handling of antigens by both immune and non-immune cells. The portal vein supplies the liver with the majority of its blood supply (9). In addition to being rich in nutrients, the portal vein is also rich in pathogenic molecules such as lipopolysaccharide (LPS) (11). When intestinal epithelial damage or failure, it can lead to the entry of infections into the bloodstream. Then, these infections can travel from the portal vein to the liver, bypassing conventional immune organs such as the spleen and lymph nodes (8, 11, 12).

Meanwhile, the liver conducts circulating immune surveillance by mobilizing immune cells (e.g., KCs) within the liver to eliminate pathogens or toxins and maintain immune homeostasis in the liver and throughout the body. A study found that KCs crawling within the hepatic vascular system were able to effectively capture blood-borne disseminating *Borrelia burgdorferi*, thus creating an efficient surveillance and filtering system. Additionally, KCs can induce the formation of chemokine receptor (CXCR)3-dependent clusters of activated invariant natural killer T cells (*i*NKT cells) after ingesting *Borrelia burgdorferi*. This clustering prevents the spread of pathogens to organs, such as the joints (13). Therefore, KCs in the liver are considered the body's first line of defense against any pathogens that are transmitted (8). The effect was similarly demonstrated in animal experiments by depleting KCs following intravenous administration of liposome-entrapped clodronate or using CRISPR/Cas9-mediated genome editing to prepare lacking liver immune receptor models. It has been discovered that in a mouse model, the depletion of KCs or immune receptors in the liver leads to 100% mortality from a sub-lethal dose of *Listeria* monocytogenes. However, removing the spleen did not have any impact on host immunity or survival (8, 14, 15). In short, this suggests that the liver plays a crucial role in detecting pathogens and defending the host. When the function or structure of the liver is compromised, especially for KCs, it becomes vulnerable to systemic diseases and can cause damage to multiple organs, resulting in disruptions to the immune microenvironment.

The main pathophysiological features of acute liver failure (ALF) are massive hepatocyte death and immune-inflammatory response (16). Among these, immune-mediated liver injury starts early in ALF and is primarily caused by innate immunity followed by an adaptive immune response that leads to further injury. The early activation of the innate immune system is specific to the

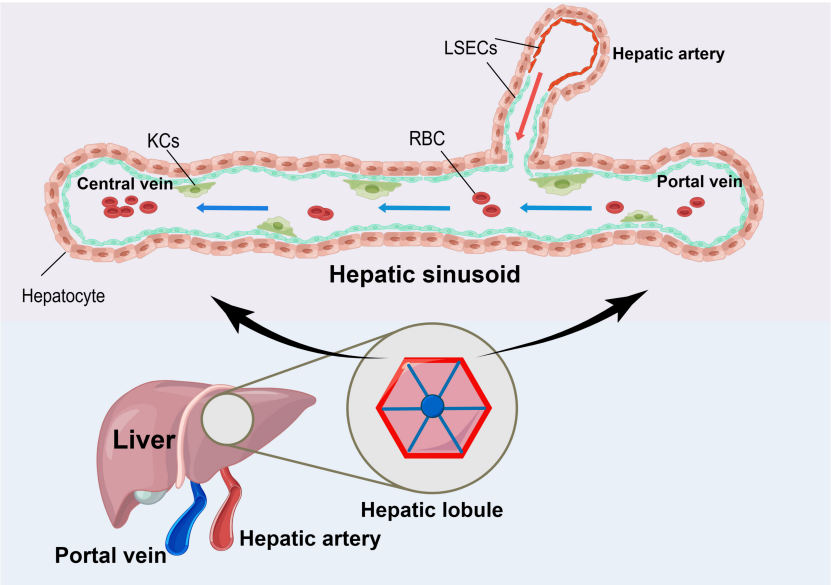

FIGURE 1
The Unique Anatomy of the Liver. The liver has a unique anatomy in that it receives blood from both the hepatic artery and the portal vein. Both sets of blood supplies end in liver sinusoidal endothelial cells (LSEC) with a large number of Kupffer cells (KCs) attached to their surface. When the blood flows through this area, it moves slowly in sinusoidal waves at a slow pace. This allows for the effective absorption of nutrients and nourishment of the liver tissues. Additionally, it enables the attached KCs to remove disease-causing substances, thereby maintaining the body's homeostasis.

activating substances, such as PAMPs and DAMPs. PAMPs play a more significant role in ALF induced by liver pathogens, while DAMPs are released from damaged cells and are crucial in ALF caused by hepatotoxic substances (17, 18). Monocytes and macrophages are essential components of the innate and adaptive immune response because they possess receptors on their cell surface that recognize PAMPs and DAMPs. Upon activation, they can modulate the immune response by producing reactive oxygen radicals and either anti-inflammatory or pro-inflammatory cytokines (17–19). Based on the anatomy of the liver, KCs are located in the hepatic blood sinusoids as an important defense device within the liver. They have a scavenging and filtering effect on the incoming and outgoing blood, effectively identifying toxic substances or pathogens in the blood (20, 21). In the diseased state, mononuclear macrophages recruited from outside the liver differentiate into various subsets of macrophage, leading to different functions. This process, known as polarization, determines changes in the local hepatic immune microenvironment and even the systemic immune state, especially in cases of ALF (11, 22).

Another major cause of damage in ALF is the destruction of hepatocytes by toxic substances and their death. In addition to necrosis and apoptosis, which are the accepted modes of cell death, several new modes of cell death have been identified and confirmed over the past decade. These include pyroptosis, necroptosis, and ferroptosis, which are available for study (16, 23–25). Pyroptosis is a newly discovered form of programmed cell death that specifically targets the innate immune defenses of intracellular bacteria. It plays a crucial role in defending against pathogens and danger signals (26, 27). However, excessive pyroptosis can lead to the development of ALF, as demonstrated in LPS/D-galactosamine(D-GalN)-induced ALF mice models (28). Therefore, inhibiting cellular pyroptosis has also been used as a research hotspot for ALF treatment in recent years.

At the same time, there has been interest in the relationship between cell death and the immune-inflammatory response. In ALF, dying hepatocytes release DAMPs that bind to evolutionarily conserved pattern recognition receptors of the innate immune system. These receptors are found in both liver-resident cells (e.g., KCs, LSECs) and cells that are recruited in response to injury (e.g., monocytes, macrophages, NK cells). This binding triggers the release of inflammatory mediators, including cytokines and chemokines. In turn, inflammatory mediators lead to further cell death, establishing a highly hepatotoxic feedforward cycle of inflammation and cell death (29). As important intrinsic immune cells, macrophages and their polarization play a crucial role in this process. However, there is a lack of clear description and discussion regarding the novel cell death modality known as pyroptosis. Therefore, this paper will discuss the roles and molecular mechanisms of macrophage polarization and hepatocyte pyroptosis in ALF. It will further explore how these processes alter the immune microenvironment of the liver, leading to immune dysfunction in the liver or even the entire circulatory system. Additionally, this paper will delve into the crosstalk between macrophage polarization and hepatocyte pyroptosis to provide a new theoretical basis for the pathogenesis and immunotherapy of ALF in the future.

2 Macrophages

2.1 Macrophages in normal liver

As mentioned before, the liver is supplied by two blood supply systems: the hepatic artery and the portal vein. It has immune regulation and circulatory immune monitoring functions. The portal vein is rich in both nutrients and molecules that can cause diseases, such as LPS (11). The circulating blood flows through the portal system and directly into the liver, where it undergoes a detoxifying and removal process (30). The process is primarily carried out by immune cells in the liver, with hepatic macrophages playing a crucial role (21).

The source of macrophages in a healthy liver mainly consists of self-renewing tissue-resident macrophages, such as KCs. These cells are located in the hepatic sinusoids and account for 80% of systemic macrophages (22). They also make up 20-25% of non-parenchymal cells in the liver and are the largest population of innate immune cells in the liver. KCs maintain hepatic homeostasis by removing pathogens through the portal vein (31). This regulatory immune and clearance function plays a vital role in maintaining liver function and immune system balance. Firstly, the immunomodulatory function of macrophages is to regulate both innate and acquired immune responses by releasing pro- and anti-inflammatory mediators. This helps to maintain immune balance in the body. Secondly, macrophages are also able to function as antigen-presenting cells and regulate the adaptive immune response (32). Thirdly, macrophages also function to clear harmful substances from the blood and prevent infection. This includes the clearance of translocated gut microbiota (20). Particularly, KCs are capable of specifically phagocytosing particulate material larger than 200 nm (20, 33).

But, under normal circumstances, the intestinal flora also releases some LPS into the bloodstream. So, how does the liver maintain immune tolerance without causing local inflammation? This issue is closely intertwined with the LSECs to which KCs are attached. LSECs mainly form highly permeable capillaries without basement membranes in the hepatic sinusoids. They share similar functions with KCs as antigen-presenting cells and are involved in the process of phagocytosis. LSECs and KCs collaborate to phagocytose blood-borne pathogens and substances present in the hepatic arteries and portal veins, preventing their further systemic circulation and averting widespread inflammatory reactions. However, it is important to note that LSECs have a higher responsiveness to LPS compared to KCs. This is predominantly due to the presence of Toll-like receptor 4(TLR4) and cluster of differentiation 14 (CD14) on the surface of LSECs, which enables them to directly interact with LPS, a byproduct of bacterial degradation. This interaction triggers a decrease in the expression of CD54 molecules on the surface of LSECs, which in turn reduces the adherence of leukocytes to LSECs (34). Ultimately, this leads to a decrease in localized inflammatory responses and promotes immune tolerance. In addition, LSECs bind LPS and produce prostaglandins, including prostaglandin E_2, which can inhibit downstream gene expression induced by TLR4 ligands through nuclear receptors (35). This mechanism promotes immunological

tolerance to LPS in normal conditions by inhibiting leukocyte adhesion and local activation, thereby maintaining the integrity of the liver endothelial cell layer.

The regulation of LPS tolerance by LSECs is very delicate. Because LSECs can initially tolerate LPS at a certain concentration, but as the LPS concentration gradually increases, LSECs can overcome their initial tolerance and simultaneously activate KCs. This not only ensures immune tolerance within the physiological range, but also enables an accurate response to bacterial infection during this period (36). Mechanistically, when the concentration of LPS is too high, LSECs instead increase the expression level of CD54 on the surface. This leads to an increase in leukocyte adhesion and aggregation, facilitating the local clearance of toxic substances against pathogens. Meanwhile, it has been found that LSECs can directly respond to LPS stimulation in an inflammatory environment by altering the expression pattern of their chemokine genes, such as C-C motif chemokine ligand 2(CCL2), CCL3, CCL4, and CCL7 (37, 38). Specifically, CCL2 plays a role in recruiting inflammatory monocytes into the liver (37). Therefore, LSECs and KCs play a crucial role in maintaining local immune tolerance in the liver. They have a significant regulatory function in accurately detecting high levels of LPS and facilitating the recruitment of monocytes to enhance the initial signaling, thereby initiating the downstream inflammatory cascade response.

2.2 Macrophages in ALF

When a liver injury occurs, the macrophage population in the liver undergoes changes. This process is primarily caused by the release of pro-inflammatory mediators or chemokines from activated KCs into the bloodstream. This triggers the accumulation of peritoneal macrophages and monocyte-derived macrophages (MoMFs) in the liver and is implicated in the development of various liver diseases (21, 22, 39).

In the pathogenesis of ALF, hepatocytes are exposed to foreign toxic substances such as acetaminophen (APAP), pathogens, and LPS produced by bacteria, which can lead to a significant number of hepatocyte deaths in the liver (40, 41). The disease progression leads to the regeneration and repair of hepatocytes, but they may not be able to fully compensate for the damage caused by cell death. After that, the dead cells release DAMPs (39), which can bind to pattern-recognition receptors (PRRs) such as Toll-like receptors (TLRs), cytoplasmic Nod-like receptors (NLRs), Retinoic acid-inducible gene (RIG)-I-like receptors (RLRs), and C-type lectin receptors (CLRs) (42). PRRs are expressed on the surface of immune cells and upon binding cause the immune cells to transform their phenotype and become activated (43), which initiates an inflammatory response. This ultimately leads to changes in the immune microenvironment in the liver (44).

As the predominant intrinsic immune cells in the liver, activated KCs release inflammatory mediators and chemokines into the bloodstream, which recruit bone marrow-derived monocytes to develop into mature MoMFs. However, in the early stages of ALF, the liver-resident KCs are gradually depleted (22, 45–48). Recent research has found that the acute injury model induced by carbon tetrachloride (CCl4) in mice has three distinct phases: necroinflammation, early repair, and late repair. At the gene and protein level, the immune microenvironment of the liver was characterized by MoMFs-induced immune damage, with lower levels of KCs observed during the necroinflammation. This finding indicates a potential role for MoMFs in the phagocytosis of necrotic hepatocytes. However, the opposite cellular distribution was observed during the repair (48). Therefore, the majority of macrophages in ALF are replaced by MoMFs, which can perform either pro-inflammatory or anti-inflammatory functions.

The pro-inflammatory and anti-inflammatory effects described here are illustrated in two main ways. To begin with, the pro-inflammatory effect of MoMFs is due to their high expression of the C-C motif chemokine receptor 2(CCR2) and surface marker Ly-6C ($CCR2^{+}$Ly-$6C^{high}$ MoMFs). Their main function is to clear toxic substances from the liver by releasing vasoactive and inflammatory mediators such as Term1 and S100 calcium binding protein A8 and A9 (S100A8/9) into the peripheral blood during the early phase of acute liver injury (11, 49). S100A8/9 is a novel molecule of DAMPs that can bind to TLR4 receptors, promoting inflammation propagation and activating other relevant immune cells (50, 51). During the disease's repair phase, MoMFs and yolk sac-derived KCs undergo a transformation into anti-inflammatory MoMFs after being stimulated by macrophage-colony stimulating factor 1 (CSF1) (52, 53). The phenotypic transition from pro-inflammatory $CCR2^{+}$Ly-$6C^{high}$ MoMFs to anti-inflammatory $CCR2^{-}$Ly-$6C^{low}$ MoMFs, which secrete anti-inflammatory factors, facilitate hepatic repair, suppresses inflammation, and maintain the stability of the hepatic immune microenvironment (11, 22, 49, 54). In addition, the release of anti-inflammatory factors from $CCR2^{-}$Ly-$6C^{low}$ MoMFs into the bloodstream contributes to the deactivation of functional monocytes and increases the risk of sepsis (22, 54). Briefly, it was observed that MoMFs had the ability to undergo differentiation towards either M1 macrophages, representing a classic proinflammatory phenotype, or M2 macrophages, representing an alternative anti-inflammatory phenotype in different phases of the disease (55, 56).

However, monocytes and other immune cells are recruited to the liver from the systemic circulation, resulting in a relative decrease in the number of immune cells and immunity in the systemic circulation. This can lead to an increased risk of systemic opportunistic infections (45, 57). In particular, the occurrence of bacterial translocation in the gut releases PAMPs, which can easily initiate systemic infections (43, 58) and enhances hepatocyte death by binding to TLRs (59). In conjunction with macrophage-derived mediators, they can also cause vascular endothelial dysfunction and microcirculatory disturbances. These disturbances can result in extrahepatic organ dysfunction (22), which is part of a larger process known as systemic inflammatory response syndrome (SIRS). If left untreated, SIRS can progress to sepsis, septicemia, or even multi-organ failure, ultimately leading to a poor prognosis for patients with ALF (60–62).

Therefore, there is a conflict regarding the role of macrophages in ALF. Some studies suggest that recruited monocytes develop into mature macrophages with an improved ability to clear hepatotoxic substances and alleviate liver damage. At the same time, some scholars believe that the pro-inflammatory capacity of macrophages

in ALF will further exacerbate liver damage and induce SIRS. Moreover, simply eliminating or impairing the function of various immune cells will unavoidably cause a delay in the healing process of damaged tissue. This underscores the crucial role of the immune system in tissue repair. In general, liver macrophages cannot be restricted to a single role. Their phenotypes can change according to the altered immune microenvironment in the liver, and they perform different functions both in the liver and systemically to maintain the balance of the immune microenvironment. Such conflicting and mutually limiting roles also pose one of the main challenges in the development of ALF immunotherapies. This is because potential molecular targets may have varying local and systemic effects (22, 32, 54).

3 Macrophage polarization

In addition to regulating the immune system and performing phagocytosis, macrophages are also highly diverse and adaptable. They can exhibit various functions depending on the stimuli or proteins present in the immune microenvironment and can differentiate into different subtypes through a process known as polarization (63–67). Macrophages can be classified into two phenotypes: pro-inflammatory (M1) and anti-inflammatory (M2). These phenotypes are determined by various factors, including microorganisms, tissue microenvironment, and cytokine signals (64, 68, 69). M1 macrophages are induced by various stimuli, including LPS, interferon-γ (IFN-γ), and tumor necrosis factor-α (TNF-α), which are Th1 cytokines. Additionally, inducible nitric oxide synthase (iNOS) and granulocyte-macrophage colony-stimulating factor (GM-CSF) can also induce M1 macrophages (31, 70). Primitive macrophages differentiate into M1 macrophages, which produce a large number of pro-inflammatory factors, such as interleukin (IL)-1β, reactive oxygen species (ROS), and TNF-α. These factors mediate antimicrobial defense, tissue destruction, and antitumor resistance (31, 70, 71). In contrast, M2 macrophages are induced by anti-inflammatory factors such as IL-4, IL-13 (which are Th2 cytokines), IL-10, and transforming growth factor-β (TGF-β). These macrophages produce anti-inflammatory factors. M2 macrophages are primarily involved in wound repair, angiogenesis, resistance to parasites, and promotion of tumor growth (67, 70–72). The underlying mechanisms are even more complex, involving multiple signaling pathways and associated regulatory factors (Figure 2).

3.1 M1 macrophage

M1 macrophages, also known as classically activated macrophages (CAMs), are characterized by the release of large amounts of inflammatory cytokines, Th1 chemokines, and ROS/RNS products. They also act as positive feedback to unpolarized macrophages (70, 73, 74). The regulation of M1 polarization is primarily controlled by the TLR/nuclear factor-kB (NF-kB)

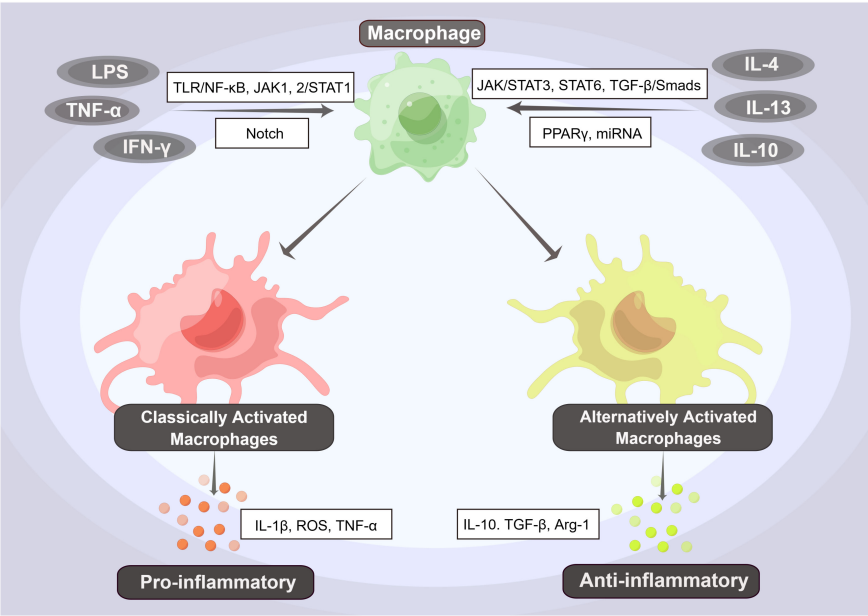

FIGURE 2
The Phenotypes and Pathways of Macrophage Polarization. Primary macrophages can differentiate into pro-inflammatory (M1) and anti-inflammatory (M2) macrophages by activating various factors and pathways. Among them, factors such as LPS, interferon-γ (IFN-γ), and tumor necrosis factor-α (TNF-α) can induce the differentiation of primitive macrophages into M1-type macrophages, i.e., classically activated macrophages (CAMs), through activation of the TLR/NF-κB, JAK1,2/STAT1, and Notch signaling pathways. These M1-type macrophages produce a large number of pro-inflammatory factors, such as interleukin (IL)-1β, reactive oxygen species (ROS), and TNF-α, further inducing a proinflammatory response. In contrast, when anti-inflammatory factors such as IL-4, IL-13, and IL-10 activate the JAK/STAT3, STAT6, and TGF-β/Smads signaling pathways, they induce the differentiation of M2-type macrophages, also known as alternatively activated macrophages (AAMs). These macrophages produce anti-inflammatory factors such as IL-10, TGF-β, and Arg-1, which initiate an anti-inflammatory response.

signaling pathway, the Janus kinase 1, 2 (JAK1, 2)/signal transducer and activator of transcription 1 (STAT1), and the Notch signaling pathway. LPS is the main factor for the activation of the TLR/NF-κB signaling pathway (75). It promotes the polarization of CAMs by binding to TLR4 receptors on the surface of initial macrophages and activating NF-κB via the MyD88-dependent pathway or interferon regulatory factor 3 (IRF3). This activation leads to the production of IL-6 and iNOS (76, 77), while the level of IL-10 decreases. Ultimately, this process mediates the formation of the pro-inflammatory phenotype of CAMs (71, 78, 79). Activation of NF-κB p65 is a marker of CAM activation (79). However, the binding of IFN-γ to its receptor (IFN-γR) activates JAK1 and JAK2, which are members of the tyrosine kinase family. This activation leads to the phosphorylation of STAT1, which then translocates into the nucleus to bind the conserved Gamma interferon activation site (GAS) DNA element. This binding activates the transcription of interferon-stimulated genes (ISGs), resulting in the formation of CAMs and the promotion of chemokine and antigen-presenting molecule production (80, 81) (Figure 3). Moreover, the JAK1,2/STAT1 signaling pathway and TLR/NF-κB signaling pathway have synergistic effects (67, 81, 82).

Recently, the Notch signaling pathway has also received widespread attention in the polarization of CAMs. Macrophages stably express Notch ligands and Notch 1, 2, and 4 receptors on their surface, which can bind to ligands or receptors in adjacent cells. On the ligand cells, endocytosis of the ligand-receptor complexes leads to a change in the mechanical conformation of the endocytosed receptor. This change exposes the complexes to the hydrolysis site 2 (S2) in the extracellular near-membrane region. The complexes are cleaved by tumor necrosis factor-α-converting enzyme (TACE) and hydrolyzed by the γ-secretase complex (located at the S3 site in the transmembrane region). This process forms a soluble Notch intracellular domain (NICD) that enters the cytoplasm and translocates to the nucleus. NICD binds to the nuclear CSL transcription factor complex and activates the hairy enhancer of split (Hes) and Hes with YRPW motif (Hey) family members, which are classical Notch target genes. These genes induce CAMs and mediate the release of inflammatory factors (Figure 3). On the other hand, blocking Notch signaling could promote the polarization of M2 cells (66, 83–85). Not only that, but the Notch pathway regulates a variety of biological properties of macrophages that still need further exploration.

3.2 M2 macrophage

M2 macrophages are also known as alternatively activated macrophages (AAMs). AAMs are characterized by the production

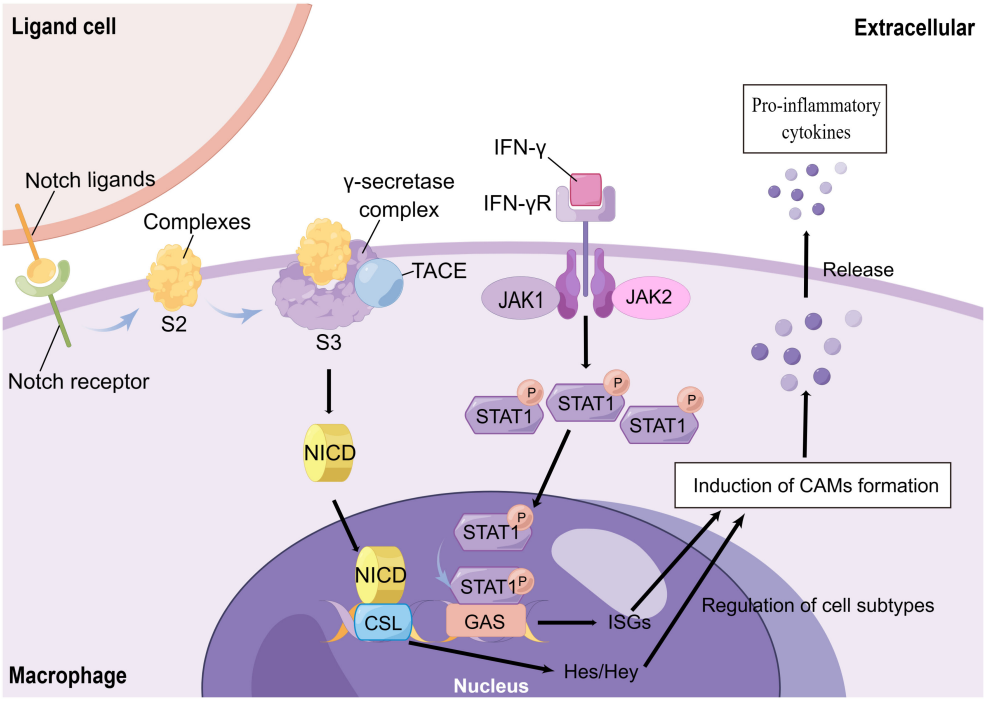

FIGURE 3
The Mechanisms of CAMs Formation. Notch receptors, which are expressed on the surface of macrophages, bind to neighboring cellular ligands. The ligand-receptor complex is formed and then exposed to hydrolysis site 2 (S2) in the extracellular proximal membrane region after endocytosis. After cleavage by tumor necrosis factor-α-converting enzyme (TACE) and hydrolysis of the γ-secretase complex (located at site S3 in the transmembrane region), a soluble Notch intracellular domain (NICD) is formed. This NICD then enters the cytoplasm and translocates to the nucleus, where it binds to the nuclear CSL transcription factor complex. This binding further activates Hes and Hey, induces the formation of CAMs, and mediates the release of inflammatory factors. On the other hand, the interferon-γ (IFN-γ) receptor (IFN-γR) on the surface of macrophages activates JAK1/JAK2 upon IFN-γ stimulation, which leads to the phosphorylation of intracellular STAT1. Phosphorylated STAT1 then enters the nucleus and binds to the Gamma interferon activation site (GAS) DNA element. This binding induces the transcription of interferon-stimulated genes (ISGs) and triggers the formation of CAMs.

of large amounts of anti-inflammatory cytokines, Th2 chemokines, C-type lectins, clearance receptors, and polyamines (66, 78). It is mainly regulated by signaling pathways such as JAK/STAT3, STAT6, TGF-β/Smads, peroxisome proliferator-activated receptor γ (PPARγ), and certain miRNAs. Th2 cytokines IL-4 and IL-13 inhibit M1 polarization and promote AAM formation mainly through the corresponding receptors (IL-4Rα), which ultimately activate STAT6. Furthermore, STAT3 is equally important for the formation of AAMs, in addition to IL-4 and IL-13, other cytokines such as IL-10 are also activated (67, 78, 86, 87). Similarly, TGF-β induces phosphorylation of type I receptors by binding to type II receptors on the macrophage surface. This leads to the activation of Smad2 and Smad3 (88), which promotes the formation of AAMs and suppresses CAMs (67, 89). PPARγ is an essential transcription factor for cell differentiation (67, 90). It coordinates M1/M2 cell homeostasis with NF-κB and promotes the polarization of M2 cells (91). Activation of NF-κB p50 is critically important for the polarization of AAMs *in vitro* and *in vivo* (79). In recent years, the development of stem cell transplantation technology has raised significant interest in the immunomodulatory role of stem cells in various diseases, especially in the regulation of immune cells. Stem cells primarily exert their effects through the release of exosomes. It contains a large number of functional microRNAs (miRNAs) that regulate M1 and M2 macrophage polarization by targeting various transcription factors (74, 92, 93). Besides the classical signaling pathways mentioned above, the Wnt/β-catenin pathway and the PI3K/Akt/mTOR pathway have been demonstrated to have a significant impact on the regulation of macrophage polarization (94, 95). Nevertheless, M2 macrophage typing can be refined and further subdivided into M2a, M2b, M2c, and M2d subtypes, depending on their specific function and the genes they express (96).

3.3 Macrophage polarization in ALF

The pathogenesis of ALF is complex and involves interactions between pathogenic agents and the host immune system. This interaction leads to the disorganization of the hepatic immune microenvironment and the simultaneous apoptosis of hepatocytes. Therefore, polarization is a dynamic process in ALF, as the polarized CAMs and AAMs still retain their plasticity and can interconvert again depending on the changing environment (22, 46). In the early stage of ALF, liver damage predominates due to immune injury. When the liver is invaded by foreign toxins or bacteria, or exposed to hepatotoxic substances, it can result in the death of hepatocytes. This, in turn, triggers the release of PAMPs by pathogens and DAMPs by dying hepatocytes. These PAMPs and DAMPs activate macrophages by binding to PR receptors (e.g., TLRs, NLRs) on the surface of macrophages. This activation prompts macrophages to shift towards the M1 pro-inflammatory phenotype and release inflammatory mediators into the bloodstream. Consequently, this process recruits and activates numerous inflammatory cells in the liver in order to eliminate pathogenic bacteria from the liver (97). However, simultaneously, it leads to a substantial infiltration of inflammatory cells and the formation of an excessive release of cytokines in the liver, initiating a "cascade activation" that results in a detrimental cycle (22). This phenomenon has also been observed during the early stages of injury in the model of ALF induced by APAP (31). Such an excessive inflammatory response not only exacerbates liver necrosis and injury but also increases the risk of extrahepatic and systemic infections. Hence, during the middle and late stages of ALF, the immune system of the body is functionally suppressed as a consequence of macrophages being excessively activated. This in turn leads to the suppression of both the functions of presenting antigens and pro-inflammatory functions. Consequently, a state of functional depletion arises. Both intrahepatic and extrahepatic immune components exhibit signs of immune paralysis (98). Furthermore, the remaining macrophages undergo a shift in function from the inflammatory M1 phenotype to the anti-inflammatory M2 phenotype, which facilitates tissue repair (99, 100). This is an antagonistic effect of the body aimed at protecting against an early, excessive inflammatory response (101). However, as a result of premature over-activation and depletion, the immune cells and their function become compromised, elevating the vulnerability to opportunistic infections. Consequently, the immune function of the body is further weakened. It is important to note that the direction of macrophage polarization during ALF is not absolute and relies on the influence of various cytokines and mediators in the immune microenvironment on primitive macrophages (99). Therefore, macrophage M1/M2 regulation can significantly modulate the systemic immune microenvironment and initiate a cascade of immune responses.

The imbalance of M1/M2 macrophage polarization is a key factor in the pathogenesis of ALF and plays a central role in the imbalance of the immune microenvironment in ALF (102). In the thioacetamide (TAA)-induced acute liver injury (TAA-ALI) mice model, the expression of senescence-associated secretory phenotype (SASP) was significantly increased, inducing M1 macrophage polarization. This exacerbates liver injury in ALI through repression of autophagy-related gene 5 (ATG5) (103). Similarly, the CC-5013, a TNF-α inhibitor, was able to significantly ameliorate liver damage in ALF by reducing the proportion of CAMs through the inhibition of the TNF-α/HMGB1 signaling pathway (104). Overall, CAMs have a positive effect on liver injury, making them a potential strategy for ALF treatment. Upregulating STAT6 by mesenchymal stem cells (MSCs) can increase the proportion of AAMs and significantly alleviate liver injury in a study, which demonstrates a positive therapeutic effect in ALF (105). Similarly, the overexpression of hepatocyte nuclear factor 4α (HNF4α) increased the transcription of IL-10 and promoted the polarization of AAMs through the IL-10/STAT3 pathway. This novel therapy for ALF resulted in the alleviation of ALF (106). In the D-GalN/LPS-induced ALF mice model, treatment with JWH-13, a cannabinoid receptor 2 (CB2) agonist, attenuated alanine aminotransferase (ALT) levels and reduced the production of pro-inflammatory cytokines, thereby protecting against ALF-associated death. Not only that, pretreatment of macrophages *in vitro* with JWH-133 significantly increased the secretion of the anti-inflammatory cytokine IL-10 in CAMs. It also enhanced the expression of AAMs markers, such as Arg and IL-10. These

findings suggest that JWH-133 promotes the transformation of M1 to M2 macrophage phenotype, thereby improving ALF (107). At the same time, exosomes derived from human umbilical cord MSCs inhibited macrophage activation and the production of inflammatory cytokines *in vitro* and *in vivo* when exposed to LPS. This was achieved by releasing miR-455-3p, which resulted in reduced levels of serum inflammatory factors and improved IL-6-induced acute liver injury in ALF (108). In addition, stem cells can also regulate the direction of macrophage polarization by releasing cytokines (74). A study reported that treatment with MSCs in a D-GalN-induced ALF model induces the MSCs to secrete IL-4 in a paracrine manner. This secretion promotes the phenotypic conversion of inflammatory CAMs to anti-inflammatory AAMs, leading to improved ALF (109). Therefore, adjusting the proportion of M1/M2 macrophages has become a hot topic in ALF therapy. However, it also presents a new challenge for clinical application, as CAMs are essential cells for the clearance of toxic substances in the liver. The timing of their application still requires further experimental validation. This validation should consider the benefits and adverse consequences of reducing initial immune activation and its harmful downstream effects.

4 Pyroptosis

4.1 The mechanisms of pyroptosis

Pyroptosis, as a novel mode of cell death, has received much attention in recent years, and its specific mechanisms have been well explained (26). There are two activation pathways for pyroptosis: the canonical pathway, which depends on Caspase-1, and the non-canonical pathway, which depends on Caspase-4/5/11 activations (26, 27). When damage mediators enter the tissue, they induce the release of pro-inflammatory factors and the activation of immune cells, further stimulating the formation of the intracellular inflammasome, which can be found in various cells, such as macrophages, neutrophils, and hepatocytes (110). Inflammasomes, intracellular multiprotein complexes, consist of three parts: a cytosolic sensor, a bridging adaptor, and an effector (27, 111). The cytosolic sensor of the inflammasome is formed by nucleotide-binding oligomerization domain NLRs, with NLRP3 predominantly mediating pyroptosis. Apoptosis-associated speck-like proteins containing caspase recruitment domains (ASCs) act as bridging junctions for the inflammasome, with pro-caspase-1 serving as the effector. Therefore, NLPR3 and pro-caspase-1 form an inflammasome by binding to ASCs (27, 112, 113). The canonical pathway is initiated by the recognition of different endogenous and exogenous damage factors, such as DAMPs and PAMPs, by the inflammasome. This recognition triggers the activation pro-caspase-1, leading to its maturation into caspase-1, the effector molecule. It is released into the cytoplasm act on the NF-κB signaling pathway and promotes the cleavage of pro-IL-1β and pro-IL-18 into mature cytokines (27, 113). Activated Caspase-1 cleaves the gasdermin D (GSDMD) protein into N- and C-terminal fragments (114, 115). The GSDMD-N-terminal protein folds on the cell surface, forming a membrane pore. This pore allows for the release of cell contents, including IL-1β and IL-18 pro-inflammatory cytokines, outside the cell. As a result, the cell becomes swollen and highly permeable to the plasma membrane due to an imbalance of intra- and extracellular fluids. Eventually, the cell rapidly lyses, a process known as pyroptosis (27, 114–116).

In the non-canonical pathway, LPS, which is the primary stimulus in the non-classical pathway, enters the cell directly. Its Lipid A portion then binds to the CARD structural domain on the pro-Caspase-4/5/11, promoting the activation of mature Caspase-4/5/11 (117, 118). Caspase-4/5/11 not only cleaves GSDMD to form pore membranes like the canonical pathway that leads to pyroptosis, but it can also activate pannexin-1, the membrane channel for ATP, which induces the extracellular release of ATP (27). In the extracellular space, ATP binds to the P2X7 receptor through an autocrine or paracrine mechanism, causing the opening of the P2X7 pore and resulting in pyroptosis (119, 120). At the same time, Caspase-4/5/11 induces the formation of the NLRP3 inflammasome by promoting K-ion efflux and activating the classical scorch pathway (27, 119). Therefore, there is a distinction and link between the non-canonical and canonical pathways (Figure 4). The nature of pyroptosis is an effective immune defense against bacteria-infected cells in the internal environment. And IL-1β and IL-18, released from the cleaved cell by pyroptosis, are potent pro-inflammatory cytokines that can recruit innate immune cells to the site of infection and regulate acquired immune cells, aiding in the capture and clearance of pathogens (121, 122). This immune response towards pathogens facilitates the elimination of foreign microorganisms. However, if not well regulated, this excessive pro-inflammatory cascade response and host cell pyroptosis can be harmful to healthy tissue (27, 120, 123). Moreover, mature IL-18 can promote the production of IFN-γ and enhance the cytolytic activity of NK cells and T cells. (121, 122).

4.2 Pyroptosis in ALF

Inflammasome formation is also present in hepatocytes. Hepatocyte pyroptosis, induced by the activation of the specific NLRP3 inflammasome in hepatocytes, is considered to be a significant contributor to liver injury and liver fibrosis (27, 124). The production of NLRP3 inflammasome, cleavage of Caspase-1, and elevated levels of IL-1β factor have been observed in the concanavalin (ConA) and LPS/D-GalN induced liver failure models (27, 125, 126). In addition, the levels of proteins associated with pyroptosis, including caspase 1/4, GSDMD-N, IL-1β, IL-18, TNFα, and IFN-γ, were also detected in liver tissue from patients with ALF (127). Therefore, numerous studies have been conducted to alleviate liver damage in ALF by inhibiting key proteins or genes involved in pyroptosis. This is considered a potential therapeutic mechanism for treating ALF.

GSDMD, as a pyroptosis executioner (128), has been the primary focus of several studies. Using necrosulfonamide (NSA), an inhibitor of GSDMD, on the LPS/D-GalN-induced ALF mouse model resulted in a significant improvement in the pathophysiology and serology of liver damage. Additionally, it significantly decreased

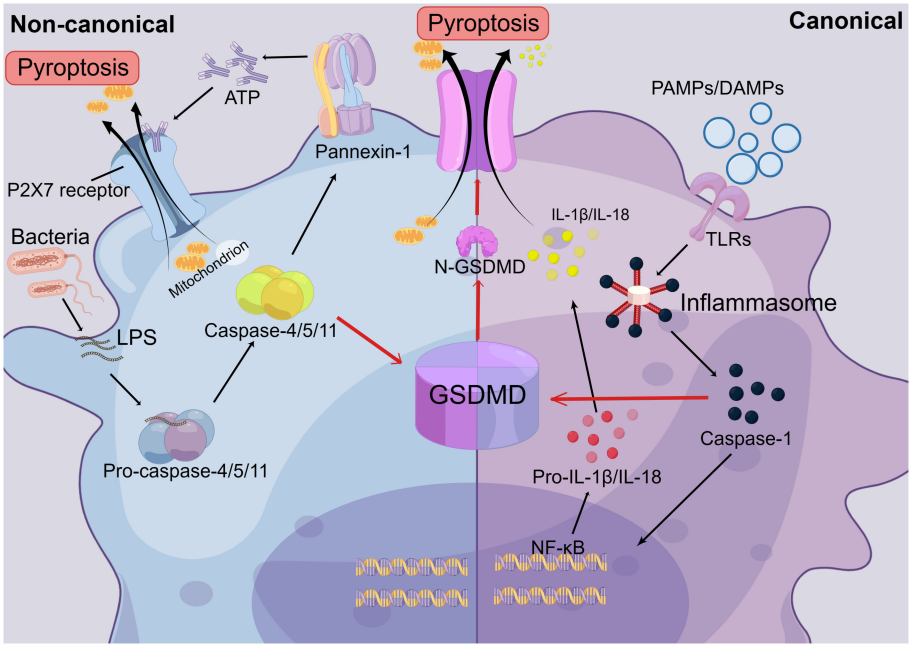

FIGURE 4
The Mechanisms of Pyroptosis. In the canonical pathway of pyroptosis, Toll-like receptors (TLRs) recognize extracellular pathogen-associated molecular patterns (PAMPs) and damage-associated molecular patterns (DAMPs), leading to the formation of inflammasomes. This, in turn, activates pro-caspase-1, causing it to mature into caspase-1. Caspase-1 is then released into the cytoplasm and acts on the NF-κB signaling pathway, promoting the maturation of IL-1β and IL-18. Secondly, activated caspase-1 cleaves the gasdermin D (GSDMD) protein into N-terminal and C-terminal fragments. The N-GSDMD fragments form pore membranes on the cell surface, allowing the release of IL-1β and IL-18 from the cell, thereby triggering inflammatory responses. Cell contents can also flow out through the pore membrane, resulting in an imbalance of intracellular and extracellular fluids and rapid cell lysis. In the non-canonical pathway, extracellular LPS can directly enter the cell and bind to the CARD domain on the intracellular Caspase-4/5/11 precursor, promoting the activation of mature Caspase-4/5/11. This activation leads to the formation of the N-GSDMD pore membrane, which triggers cellular pyroptosis. Additionally, it activates the ATP membrane channel, pannexin-1, which leads to the release of ATP from the cell. ATP binds to the P2X7 receptor through autocrine or paracrine mechanisms, resulting in the opening of the P2X7 pore. This leads to the release of cellular contents and ultimately triggers pyroptosis.

the levels of GSDMD, NLRP3, Caspase-1, and IL-1β (28). This study not only highlights the significance of pyroptosis in the progression of ALF but also demonstrates that inhibiting pyroptosis *in vivo* can effectively mitigate liver damage associated with ALF and yield therapeutic benefits. Similarly, limonin was able to inhibit LPS-induced pyroptosis by preventing cell membrane rupture and GSDMD activation. Additionally, limonin could prevent LPS-induced liver injury by primarily reducing the expression of NLRP3 and Caspase-1-related proteins, thereby inhibiting IL-1β (129). The 3,4-dihydroxyphenylethyl alcohol glycoside (DAG) isolated from Sargentodoxa cuneata has been shown to possess antioxidant, anti-apoptotic, and anti-inflammatory effects. Further studies have revealed that DAG reduces the levels of pyroptosis-related factors IL-1β, IL-18, and ROS. It also inhibits the expression of Caspase-1 and GSDMD in a dose-dependent manner, thereby inhibiting pyroptosis to treat APAP-induced ALF (130). The tyrosine-alanine (YA) peptide, which is a significant constituent of oyster (Crassostrea gigas) hydrolysate (OH), has demonstrated a hepatoprotective effect. It reduces the upregulation of GSDMD, the activation of caspase-1, and the cleavage of the C-terminus of GSDMD in mice injected with LPS/D-GalN (131).

Besides that, it has also been reported that PAMPs and DAMPs can directly or indirectly cause hepatocyte pyroptosis through cell-to-cell crosstalk (27). And it is not only hepatocyte pyroptosis, but macrophage pyroptosis also contributes to the development of liver disease (132, 133). In summary, pyroptosis is a promising therapeutic target for inflammatory diseases. This can be achieved by blocking related molecules such as NLRP3, Caspase-1, and GSDMD, which ultimately affects the progression of ALF. However, pyroptosis is an important defense mechanism against pathogenic invasion by its nature. Under physiological circumstances, moderate pyroptosis plays an important role in host defense against pathogenic microorganisms (134). Many pathogens have developed antimicrobial activity against macrophages, which are intrinsic immune cells. These pathogens can invade and replicate within macrophages, effectively isolating themselves from extracellular immune defenses and allowing them to escape the immune system. However, these pathogens cannot resist extracellular immunity (135). Bacteria, on the other hand, can activate the formation of various pyroptosis-associated inflammasomes, such as Listeriolysin released by *Listeria* monocytogenes, *B. anthracis* protease lethal factor (LF), Pneumolysin (PLY), and α-hemolysin released by *Staphylococcus aureus*. All of these are known to be activators of NLRP3 (136). LF was the first activator of pyroptosis to be identified and discovered. Mechanistically, LF is cleaved intracellularly and further degraded by the proteasome (137). The degradation product can then participate in the formation of CARD at the C-terminus of Caspase-1 (138, 139).

This activation leads to the formation of inflammasomes and triggers the canonical pathway, inducing pyroptosis. As a result, infected cells rupture, releasing pathogens into the extracellular environment and initiating an immune response to eliminate the pathogens. In addition, the gene sequence of LPS released by Gram-negative bacteria, LipidA, is a highly conserved. LipidA binds to Caspase-11/4/5 and triggers the oligomerization and activation of caspases, leading to the induction of the non-canonical cellular pyroptosis (140, 141). Overall, this mechanism serves as a clearance mechanism for the organism to defend against invading pathogens and plays a crucial role in protecting the organism from such pathogens. Therefore, therapeutic interventions aimed at inhibiting pyroptosis may have inherent flaws. It can worsen the existing pathogenic invasion and increase the risk of opportunistic infections. Furthermore, when regulating the local signaling pathways or key proteins in the organism, it is necessary to consider the systemic response that it triggers. The pros and cons of this issue are unavoidable and will require extensive research before it can be translated into clinical treatment. It is indisputable that conducting comprehensive studies on pyroptosis is essential for understanding the pathogenesis of ALF and for the development of drugs targeting this process.

5 The crosstalk of pyroptosis and macrophage polarization in ALF

Macrophage polarization and pyroptosis are important for the development of ALF and share certain signaling pathways or regulatory mediators. Therefore, it is reasonable to speculate that there is an interaction between macrophage polarization and pyroptosis. However, there are fewer studies on the mutual regulation and crosstalk between macrophage polarization and pyroptosis. Cluster of Differentiation 38 (CD38) is a type II transmembrane protein that is widely expressed in immune cells. It controls the innate immune response and inflammatory pathways triggered by infection (122, 142). It was found that liver-injured mice with CD38 knockdown exhibited more severe pyroptosis and liver damage. By comparing protein expression in WT and CD38-deficient mice, researchers found elevated expression of M1 macrophage marker proteins such as TLR4, MyD88, and phosphorylated NF-κB p65 in CD38-deficient mice. Furthermore, the increased expression of pyroptosis-associated markers caused by CD38 knockdown could be reversed by TLR4 mutation. This suggests that the more severe liver damage and pyroptosis caused by CD38 deficiency are related to the TLR4 signaling pathway. However, further research is needed to elucidate the role of CD38 in M1 macrophages and pyroptosis through the TLR4 signaling pathway is not available (122). TLR receptor activation has been found to induce the production of the NLRP3 inflammasome and the development of pyroptosis (143). Therefore, we can speculate that CD38 inhibits pyroptosis by regulating the TLR4 signaling pathway. But it remains to be considered whether CD38 further regulates pyroptosis through the polarization of M1 macrophages.

High mobility group box protein 1 (HMGB1) is a nuclear DNA-binding protein that activates Caspase-1-dependent pyroptosis in hepatocytes, thereby exacerbating the inflammatory response and damage. This process can be ameliorated by HMGB1 inhibitors (144). In addition, HMGB1 also acts as a DAMP that easily translocates to the outside of cells in response to endogenous tissue damage or exogenous microbial invasion. It activates immune cells and releases pro-inflammatory factors, which cause an inflammatory response (145). When the DAMPs activate macrophages by binding to PRR on the surface of the macrophage, the activated macrophage will secrete the pro-inflammatory HMGB1 (22, 144). Once HMGB1 translocates to the outside of the cell membrane or is transported to target cells via extracellular vesicles, it binds to its receptor RAGE or TLR4 and initiates as a DAMP molecule. This leads to the activation of the NLRP3 inflammasome, inducing pyroptosis in recipient cells and provoking an inflammatory response (144, 146–148). Moreover, the HMGB1 outside the cell could activate the MyD88-dependent TLR4 signaling pathway and enhance NF-κB expression through TLR4 binding (122, 144). Therefore, macrophages following LPS induction will release HMGB1 to initiate hepatocyte pyroptosis. This process can also induce the formation of the NLRP3-inflammasome through activation of the TLR4/MyD88/NF-κB signaling pathway (144). As discussed in a previous paragraph, this pathway is also considered a classical pathway for M1 macrophage polarization. Although the role of macrophage polarization is not highlighted in this article, HMGB1 plays an important role in liver damage of ALF as a common mediator of both macrophage polarization and pyroptosis, and the therapeutic effect of HMGB1 inhibition on ALF has been demonstrated in several studies. Besides, in the LPS/D-GalN-induced ALF mouse model, it was discovered that lenalidomide (CC-5013) treatment significantly reduced the activation of the TNF-α/HMGB1 signaling pathway. This reduction resulted in a decrease in the number of M1 macrophages in both liver and kidney tissues, ultimately leading to a decrease in intra-tissue pyroptosis levels (104).

M2 macrophages play a crucial role in protecting the liver in ALF. They exhibit hepatoprotective effects by releasing the anti-inflammatory cytokine IL-10 and pro-fibrosis (149). Additionally, M2 macrophages exert hepatoprotective effects by expressing the Galectin-3 (GAL3) gene, which inhibits the expression of pyroptosis signaling proteins in ALF mice (150). Surely, the one-way regulatory mechanism is incomplete. Some studies have suggested that hepatocyte pyroptosis mediated by GSDMD can recruit macrophages to release inflammatory mediators through the upregulation of the monocyte chemotactic protein 1/CC chemokine receptor-2 (MCRP1/CCR2) signaling pathway, leading to the spread of the inflammatory response. Furthermore, immunohistochemistry of the liver showed a significant decrease in the expression of the macrophage-specific protein F4/80 in the D-GalN/LPS ALF mouse model with GSDMD knockout, compared to the wild type(WT) D-GalN/LPS ALF model (127). This phenomenon suggests that inhibiting GSDMD-induced pyroptosis can significantly decrease macrophage infiltration in ALF liver tissue. In a wore, all of this evidence suggests a positive feedback loop between macrophage polarization and hepatocyte pyroptosis, which can induce an inflammatory cascade response in ALF. Given these observations, further research is needed to understand the cellular crosstalk between macrophage polarization and hepatocyte pyroptosis and its contribution to the progression of ALF. Additionally, the complex signaling pathways

between these two processes should be explored and confirmed through additional experiments (Figure 5).

6 Conclusion and future directions

The study of the hepatocyte pyroptosis pathway in ALF is still in its preliminary stage. All factors that induce liver injury led to pyroptosis, and the late stage of hepatocyte pyroptosis, accompanied by the release of inflammatory factors such as IL-1β and IL-18, is central to the exacerbation of ALF (132, 151). The inflammatory factors released from hepatocyte pyroptosis enhance the activation of the NF-κB signaling pathway in hepatocytes and macrophages, thereby further promoting the inflammatory response. At the same time, the release of pro-inflammatory factors can recruit mononuclear macrophages in the body, leading to a more severe inflammatory response and ultimately causing massive hepatocyte death (22, 152). The suggestion of improving liver damage and inflammatory response by inhibiting pyroptosis in ALF has also been the focus of several studies. However, inhibiting pyroptosis is equivalent to compromising the system's ability to clear microorganisms, which can potentially lead to opportunistic infections and even the development of adverse outcomes like bacteremia and sepsis. Therefore, further exploration is needed in the therapeutic strategy of treating ALF by inhibiting pyroptosis. This is important to consider due to the local intrahepatic damage and the systemic state. The aim is to find more precise methods of targeting intrahepatic pyroptosis.

The role of hepatic macrophages in ALF has been controversial. It is mentioned in our paper that macrophage activation is influenced by various factors in the immune microenvironment and can polarize in either a pro-inflammatory or an anti-inflammatory direction. However, polarized macrophages can still switch their polarization depending on the cytokines and mediators present in the immune microenvironment. Depending on the stage of ALF disease, macrophages can either perpetuate inflammation or promote its remission. These contradictions and inconsistencies are attributed to the diversity of macrophage subtypes. For this reason, regulating the direction of macrophage polarization has become a therapeutic approach in the study of ALF. However, therapies targeted at macrophages for the treatment of ALF carry certain risks and challenges. Firstly. However, promoting the anti-inflammatory effects of macrophages, they can improve liver damage and disease progression in ALF, but at the same time, they can also facilitate the spread of pathogens in the system and increase susceptibility to infection. Secondly, by promoting the pro-inflammatory effects of macrophages, it can effectively inhibit opportunistic infections and remove foreign pathogens. However, it can also easily induce a severe inflammatory response, resulting in the release of inflammatory mediators that are dispersed throughout the system via the bloodstream. This can lead to multi-organ damage and even failure. The contradictions of the approaches described for macrophage-targeted therapy highlight the challenges of immunotherapeutic strategies in ALF. The local hepatic immune microenvironment and the systemic immune microenvironment mutually regulate and influence each other. Anti-inflammatory therapy in the local hepatic

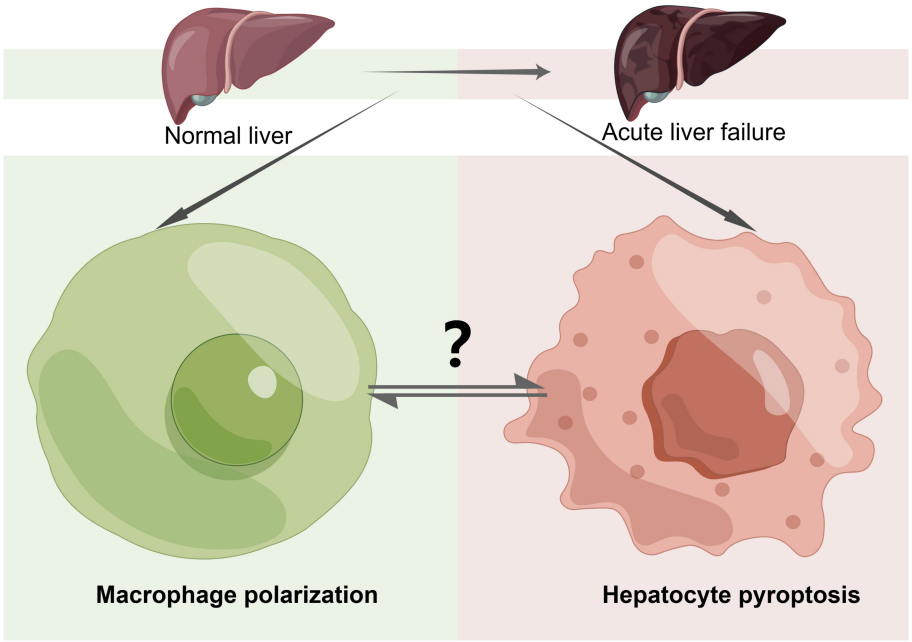

FIGURE 5
The Crosstalk of Pyroptosis and Macrophage Polarization in ALF. Macrophage polarization and hepatocyte pyroptosis play important roles in acute liver failure (ALF). The mutual crosstalk and regulation between these two processes can impact the progression of the disease. However, the specific mechanisms involved require further study and exploration. "?": there are many unknown relationships between macrophage polarization and hepatocyte pyroptosis in ALF that need to be further explored and investigated in the future, including the impact of their mutual regulation and constraints on disease progression in ALF as well as the specific pathways of action.

immune microenvironment is effective in alleviating liver damage and repairing tissue. However, it has the opposite effect in controlling systemic pathogen dissemination. The timing of targeting application to induce different macrophage polarization directions needs to be precisely controlled, especially in order to clarify the function and composition of macrophages at different stages of ALF in humans.

Combining the signaling pathways and mechanisms of macrophage polarization and pyroptosis mentioned above, it is clear that several signaling pathways are shared between the two. For example, the TLR/NF-κB pathway not only plays an important role in M1 polarization but also induces cell pyroptosis (27, 67). In addition, several studies have also implicitly suggested that there is a reciprocal regulation between macrophage polarization and pyroptosis. For example, the knockdown of CD38 promotes the expression of molecules related to M1 polarization and also triggers more severe cell pyroptosis. CD38 serves as a common regulatory mediator of both processes (122). The interaction between macrophage polarization and pyroptosis still requires further investigation and exploration. In particular, the roles of both factors are crucial to the development of the disease. However, it is unclear whether they are mutually independent, whether they regulate each other, or if they even trigger a more severe inflammatory response through positive feedback. This assessment cannot be made without further experiments and studies to confirm.

In summary, this paper describes the mechanisms and regulatory pathways of macrophage polarization and pyroptosis in ALF. It also explores the interplay between macrophage polarization and pyroptosis. Fundamentally, macrophage polarization and pyroptosis in ALF are significant factors that have been extensively studied in recent years. However, there are still numerous unanswered questions that require further exploration. It is hoped that future research will address these questions, leading to new insights into the pathogenesis and therapeutic strategies for ALF.

Author contributions

DX: Conceptualization, Writing – original draft. SO: Conceptualization, Writing – review & editing.

Funding

The author(s) declare financial support was received for the research, authorship, and/or publication of this article. This work was supported by the National Natural Science Foundation of China (81803884), Plan on enhancing scientific research in GMU (02-410-2302092XM), 2022 Guangzhou Medical University discipline construction projects (02-410-2206013), the 2022 Student Innovation Capacity Enhancement Program Project of Guangzhou Medical University (02-408-2304-19064XM), 2023 City school (college) enterprise joint funding projects (2023A03J0421), the Undergraduate Capacity Enhancement Innovation Project of Guangzhou Medical University (2022JXA003), the 2023 Artificial Liver Special Fund (iGandanF-1082023-RGG023), the Key Medical Discipline of Guangzhou [2021-2023] and the Key Laboratory of Guangdong Higher Education Institutes (2021KSYS009).

Acknowledgments

All figures created by Figdraw.

Conflict of interest

The authors declare that the research was conducted in the absence of any commercial or financial relationships that could be construed as a potential conflict of interest.

Publisher's note

References

1. Cheng ML, Nakib D, Perciani CT, MacParland SA. The immune niche of the liver. *Clin Sci (Lond)* (2021) 135(20):2445–66. doi: 10.1042/CS20190654

2. Nakano T, Lai CY, Goto S, Hsu LW, Kawamoto S, Ono K, et al. Immunological and regenerative aspects of hepatic mast cells in liver allograft rejection and tolerance. *PloS One* (2012) 7(5):e37202. doi: 10.1371/journal.pone.0037202

3. Herkel J. Regulatory T cells in hepatic immune tolerance and autoimmune liver diseases. *Dig Dis* (2015) 33 Suppl 2:70–4. doi: 10.1159/000440750

4. Drescher HK, Bartsch LM, Weiskirchen S, Weiskirchen R. Intrahepatic T(H)17/T (Reg) cells in homeostasis and disease-it's all about the balance. *Front Pharmacol* (2020) 11:588436. doi: 10.3389/fphar.2020.588436

5. Robinson MW, Harmon C, O'Farrelly C. Liver immunology and its role in inflammation and homeostasis. *Cell Mol Immunol* (2016) 13(3):267–76. doi: 10.1038/cmi.2016.3

6. Shetty S, Lalor PF, Adams DH. Liver sinusoidal endothelial cells - gatekeepers of hepatic immunity. *Nat Rev Gastroenterol Hepatol* (2018) 15(9):555–67. doi: 10.1038/s41575-018-0020-y

7. Sakai M, Troutman TD, Seidman JS, Ouyang Z, Spann NJ, Abe Y, et al. Liver-derived signals sequentially reprogram myeloid enhancers to initiate and maintain kupffer cell identity. *Immunity* (2019) 51(4):655–670.e658. doi: 10.1016/j.immuni.2019.09.002

8. Jenne CN, Kubes P. Immune surveillance by the liver. *Nat Immunol* (2013) 14 (10):996–1006. doi: 10.1038/ni.2691

9. McDonald B, Kubes P. Innate immune cell trafficking and function during sterile inflammation of the liver. *Gastroenterology* (2016) 151(6):1087–95. doi: 10.1053/j.gastro.2016.09.048

10. Trefts E, Gannon M, Wasserman DH. The liver. *Curr Biol* (2017) 27(21):R1147–51. doi: 10.1016/j.cub.2017.09.019

11. Kubes P, Jenne C. Immune responses in the liver. *Annu Rev Immunol* (2018) 36:247–77. doi: 10.1146/annurev-immunol-051116-052415

12. Son G, Kremer M, Hines IN. Contribution of gut bacteria to liver pathobiology. *Gastroenterol Res Pract* (2010) 2010:1–13. doi: 10.1155/2010/453563

13. Lee WY, Moriarty TJ, Wong CH, Zhou H, Strieter RM, van Rooijen N, et al. An intravascular immune response to Borrelia burgdorferi involves Kupffer cells and iNKT cells. *Nat Immunol* (2010) 11(4):295–302. doi: 10.1038/ni.1855

14. Ebe Y, Hasegawa G, Takatsuka H, Umezu H, Mitsuyama M, Arakawa M, et al. The role of Kupffer cells and regulation of neutrophil migration into the liver by macrophage inflammatory protein-2 in primary listeriosis in mice. *Pathol Int* (1999) 49 (6):519–32. doi: 10.1046/j.1440-1827.1999.00910.x

15. Zhao D, Yang F, Wang Y, Li S, Li Y, Hou F, et al. ALK1 signaling is required for the homeostasis of Kupffer cells and prevention of bacterial infection. *J Clin Invest* (2022) 132(3):e150489. doi: 10.1172/JCI150489

16. Schwabe RF, Luedde T. Apoptosis and necroptosis in the liver: a matter of life and death. *Nat Rev Gastroenterol Hepatol* (2018) 15(12):738–52. doi: 10.1038/s41575-018-0065-y

17. Chung RT, Stravitz RT, Fontana RJ, Schiodt FV, Mehal WZ, Reddy KR, et al. Pathogenesis of liver injury in acute liver failure. *Gastroenterology* (2012) 143(3):e1–7. doi: 10.1053/j.gastro.2012.07.011

18. Dong V, Nanchal R, Karvellas CJ. Pathophysiology of acute liver failure. *Nutr Clin Pract* (2020) 35(1):24–9. doi: 10.1002/ncp.10459

19. Kumagai K, Mawatari S, Ido A. [Pathophysiology of acute liver failure from onset to liver regeneration]. *Nihon Shokakibyo Gakkai Zasshi* (2020) 117(9):750–5. doi: 10.11405/nisshoshi.117.750

20. Abdullah Z, Knolle PA. Liver macrophages in healthy and diseased liver. *Pflugers Arch* (2017) 469(3-4):553–60. doi: 10.1007/s00424-017-1954-6

21. Krenkel O, Tacke F. Liver macrophages in tissue homeostasis and disease. *Nat Rev Immunol* (2017) 17(5):306–21. doi: 10.1038/nri.2017.11

22. Triantafyllou E, Woollard KJ, McPhail MJW, Antoniades CG, Possamai LA. The role of monocytes and macrophages in acute and acute-on-chronic liver failure. *Front Immunol* (2018) 9:2948. doi: 10.3389/fimmu.2018.02948

23. Linkermann A, Green DR. Necroptosis. *N Engl J Med* (2014) 370(5):455–65. doi: 10.1056/NEJMra1310050

24. Vande Walle L, Lamkanfi M. Pyroptosis. *Curr Biol* (2016) 26(13):R568–72. doi: 10.1016/j.cub.2016.02.019

25. Stockwell BR, Friedmann Angeli JP, Bayir H, Bush AI, Conrad M, Dixon SJ, et al. Ferroptosis: A regulated cell death nexus linking metabolism, redox biology, and disease. *Cell* (2017) 171(2):273–85. doi: 10.1016/j.cell.2017.09.021

26. Shi J, Gao W, Shao F. Pyroptosis: gasdermin-mediated programmed necrotic cell death. *Trends Biochem Sci* (2017) 42(4):245–54. doi: 10.1016/j.tibs.2016.10.004

27. Wu J, Lin S, Wan B, Velani B, Zhu Y. Pyroptosis in liver disease: new insights into disease mechanisms. *Aging Dis* (2019) 10(5):1094–108. doi: 10.14336/AD.2019.0116

28. Wu YL, Ou WJ, Zhong M, Lin S, Zhu YY. Gasdermin D inhibitor necrosulfonamide alleviates lipopolysaccharide/D-galactosamine-induced acute liver failure in mice. *J Clin Transl Hepatol* (2022) 10(6):1148–54. doi: 10.14218/JCTH.2021.00560

29. Brenner C, Galluzzi L, Kepp O, Kroemer G. Decoding cell death signals in liver inflammation. *J Hepatol* (2013) 59(3):583–94. doi: 10.1016/j.jhep.2013.03.033

30. Strnad P, Tacke F, Koch A, Trautwein C. Liver - guardian, modifier and target of sepsis. *Nat Rev Gastroenterol Hepatol* (2017) 14(1):55–66. doi: 10.1038/nrgastro.2016.168

31. Dou L, Shi X, He X, Gao Y. Macrophage phenotype and function in liver disorder. *Front Immunol* (2019) 10:3112. doi: 10.3389/fimmu.2019.03112

32. Shan Z, Ju C. Hepatic macrophages in liver injury. *Front Immunol* (2020) 11:322. doi: 10.3389/fimmu.2020.00322

33. Kempka G, Kolb-Bachofen V. Binding, uptake, and transcytosis of ligands for mannose-specific receptors in rat liver: an electron microscopic study. *Exp Cell Res* (1988) 176(1):38–48. doi: 10.1016/0014-4827(88)90118-8

34. Uhrig A, Banafsche R, Kremer M, Hegenbarth S, Hamann A, Neurath M, et al. Development and functional consequences of LPS tolerance in sinusoidal endothelial cells of the liver. *J Leukoc Biol* (2005) 77(5):626–33. doi: 10.1189/jlb.0604332

35. Rieder H, Ramadori G, Allmann KH, Meyer zum Buschenfelde KH. Prostanoid release of cultured liver sinusoidal endothelial cells in response to endotoxin and tumor necrosis factor. Comparison with umbilical vein endothelial cells. *J Hepatol* (1990) 11 (3):359–66. doi: 10.1016/0168-8278(90)90222-d

36. Kastenbauer S, Ziegler-Heitbrock HW. NF-kappaB1 (p50) is upregulated in lipopolysaccharide tolerance and can block tumor necrosis factor gene expression. *Infect Immun* (1999) 67(4):1553–9. doi: 10.1128/IAI.67.4.1553-1559.1999

37. Gschwandtner M, Derler R, Midwood KS. More than just attractive: how CCL2 influences myeloid cell behavior beyond chemotaxis. *Front Immunol* (2019) 10:2759. doi: 10.3389/fimmu.2019.02759

38. Papaioannou S, See JX, Jeong M, de la Torre C, Ast V, Reiners-Koch PS, et al. Liver sinusoidal endothelial cells orchestrate NK cell recruitment and activation in acute inflammatory liver injury. *Cell Rep* (2023) 42(8):112836. doi: 10.1016/j.celrep.2023.112836

39. Woolbright BL, Jaeschke H. The impact of sterile inflammation in acute liver injury. *J Clin Transl Res* (2017) 3(Suppl 1):170–88. doi: 10.18053/jctres.03.2017S1.003

40. Ramachandran A, Jaeschke H. Acetaminophen hepatotoxicity. *Semin Liver Dis* (2019) 39(2):221–34. doi: 10.1055/s-0039-1679919

41. Stravitz RT, Lee WM. Acute liver failure. *Lancet* (2019) 394(10201):869–81. doi: 10.1016/S0140-6736(19)31894-X

42. Takeuchi O, Akira S. Pattern recognition receptors and inflammation. *Cell* (2010) 140(6):805–20. doi: 10.1016/j.cell.2010.01.022

43. Zindel J, Kubes P. DAMPs, PAMPs, and LAMPs in immunity and sterile inflammation. *Annu Rev Pathol* (2020) 15:493–518. doi: 10.1146/annurev-pathmechdis-012419-032847

44. Mihm S. Danger-associated molecular patterns (DAMPs): molecular triggers for sterile inflammation in the liver. *Int J Mol Sci* (2018) 19(10):3104. doi: 10.3390/ijms19103104

45. Gale RP, Sparkes RS, Golde DW. Bone marrow origin of hepatic macrophages (Kupffer cells) in humans. *Science* (1978) 201(4359):937–8. doi: 10.1126/science.356266

46. Beattie L, Sawtell A, Mann J, Frame TCM, Teal B, de Labastida Rivera F, et al. Bone marrow-derived and resident liver macrophages display unique transcriptomic signatures but similar biological functions. *J Hepatol* (2016) 65(4):758–68. doi: 10.1016/j.jhep.2016.05.037

47. Triantafyllou E, Pop OT, Possamai LA, Wilhelm A, Liaskou E, Singanayagam A, et al. MerTK expressing hepatic macrophages promote the resolution of inflammation in acute liver failure. *Gut* (2018) 67(2):333–47. doi: 10.1136/gutjnl-2016-313615

48. Flores Molina M, Abdelnabi MN, Mazouz S, Villafranca-Baughman D, Trinh VQ, Muhammad S, et al. Distinct spatial distribution and roles of Kupffer cells and monocyte-derived macrophages in mouse acute liver injury. *Front Immunol* (2022) 13:994480. doi: 10.3389/fimmu.2022.994480

49. Mossanen JC, Krenkel O, Ergen C, Govaere O, Liepelt A, Puengel T, et al. Chemokine (C-C motif) receptor 2-positive monocytes aggravate the early phase of acetaminophen-induced acute liver injury. *Hepatology* (2016) 64(5):1667–82. doi: 10.1002/hep.28682

50. Wu R, Zhang Y, Xiang Y, Tang Y, Cui F, Cao J, et al. Association between serum S100A9 levels and liver necroinflammation in chronic hepatitis B. *J Transl Med* (2018) 16(1):83. doi: 10.1186/s12967-018-1462-2

51. Bai L, Kong M, Duan Z, Liu S, Zheng S, Chen Y. M2-like macrophages exert hepatoprotection in acute-on-chronic liver failure through inhibiting necroptosis-S100A9-necroinflammation axis. *Cell Death Dis* (2021) 12(1):93. doi: 10.1038/s41419-020-03378-w

52. Stutchfield BM, Antoine DJ, Mackinnon AC, Gow DJ, Bain CC, Hawley CA, et al. CSF1 restores innate immunity after liver injury in mice and serum levels indicate outcomes of patients with acute liver failure. *Gastroenterology* (2015) 149(7):1896–1909.e1814. doi: 10.1053/j.gastro.2015.08.053

53. Tacke F. Targeting hepatic macrophages to treat liver diseases. *J Hepatol* (2017) 66(6):1300–12. doi: 10.1016/j.jhep.2017.02.026

54. Yang T, Wang H, Wang X, Li J, Jiang L. The dual role of innate immune response in acetaminophen-induced liver injury. *Biol (Basel)* (2022) 11(7):1057. doi: 10.3390/biology11071057

55. Zhou D, Yang K, Chen L, Wang Y, Zhang W, Xu Z, et al. Macrophage polarization and function: new prospects for fibrotic disease. *Immunol Cell Biol* (2017) 95(10):864–9. doi: 10.1038/icb.2017.64

56. Li H, Zhou Y, Wang H, Zhang M, Qiu P, Zhang M, et al. Crosstalk between liver macrophages and surrounding cells in nonalcoholic steatohepatitis. *Front Immunol* (2020) 11:1169. doi: 10.3389/fimmu.2020.01169

57. Wang J, Kubes P. A reservoir of mature cavity macrophages that can rapidly invade visceral organs to affect tissue repair. *Cell* (2016) 165(3):668–78. doi: 10.1016/j.cell.2016.03.009

58. Tujios S, Stravitz RT, Lee WM. Management of acute liver failure: update 2022. *Semin Liver Dis* (2022) 42(3):362–78. doi: 10.1055/s-0042-1755274

59. Filliol A, Piquet-Pellorce C, Raguenes-Nicol C, Dion S, Farooq M, Lucas-Clerc C, et al. RIPK1 protects hepatocytes from Kupffer cells-mediated TNF-induced apoptosis in mouse models of PAMP-induced hepatitis. *J Hepatol* (2017) 66(6):1205–13. doi: 10.1016/j.jhep.2017.01.005

60. Rolando N, Wade J, Davalos M, Wendon J, Philpott-Howard J, Williams R. The systemic inflammatory response syndrome in acute liver failure. *Hepatology* (2000) 32 (4 Pt 1):734–9. doi: 10.1053/jhep.2000.17687

61. Choudhury A, Kumar M, Sharma BC, Maiwall R, Pamecha V, Moreau R, et al. Systemic inflammatory response syndrome in acute-on-chronic liver failure: Relevance of 'golden window': A prospective study. *J Gastroenterol Hepatol* (2017) 32(12):1989–97. doi: 10.1111/jgh.13799

62. Yang R, Zou X, Tenhunen J, Tonnessen TI. HMGB1 and extracellular histones significantly contribute to systemic inflammation and multiple organ failure in acute liver failure. *Mediators Inflamm* (2017) 2017:5928078. doi: 10.1155/2017/5928078

63. Funes SC, Rios M, Escobar-Vera J, Kalergis AM. Implications of macrophage polarization in autoimmunity. *Immunology* (2018) 154(2):186–95. doi: 10.1111/imm.12910

64. Thapa B, Lee K. Metabolic influence on macrophage polarization and pathogenesis. *BMB Rep* (2019) 52(6):360–72. doi: 10.5483/BMBRep.2019.52.6.140

65. Locati M, Curtale G, Mantovani A. Diversity, mechanisms, and significance of macrophage plasticity. *Annu Rev Pathol* (2020) 15:123–47. doi: 10.1146/annurev-pathmechdis-012418-012718

66. Chen W, Liu Y, Chen J, Ma Y, Song Y, Cen Y, et al. The Notch signaling pathway regulates macrophage polarization in liver diseases. *Int Immunopharmacol* (2021) 99:107938. doi: 10.1016/j.intimp.2021.107938

67. Wang C, Ma C, Gong L, Guo Y, Fu K, Zhang Y, et al. Macrophage polarization and its role in liver disease. *Front Immunol* (2021) 12:803037. doi: 10.3389/fimmu.2021.803037

68. Kadomoto S, Izumi K, Mizokami A. Macrophage polarity and disease control. *Int J Mol Sci* (2021) 23(1):144. doi: 10.3390/ijms23010144

69. Lampiasi N. Macrophage polarization: learning to manage it. *Int J Mol Sci* (2022) 23(13):7208. doi: 10.3390/ijms23137208

70. Yao Y, Xu XH, Jin L. Macrophage polarization in physiological and pathological pregnancy. *Front Immunol* (2019) 10:792. doi: 10.3389/fimmu.2019.00792

71. Bosco MC. Macrophage polarization: Reaching across the aisle? *J Allergy Clin Immunol* (2019) 143(4):1348–50. doi: 10.1016/j.jaci.2018.12.995

72. Martinez FO, Gordon S. The M1 and M2 paradigm of macrophage activation: time for reassessment. *F1000Prime Rep* (2014) 6:13. doi: 10.12703/P6-13

73. Parisi L, Gini E, Baci D, Tremolati M, Fanuli M, Bassani B, et al. Macrophage polarization in chronic inflammatory diseases: killers or builders? *J Immunol Res* (2018) 2018:8917804. doi: 10.1155/2018/8917804

74. Arabpour M, Saghazadeh A, Rezaei N. Anti-inflammatory and M2 macrophage polarization-promoting effect of mesenchymal stem cell-derived exosomes. *Int Immunopharmacol* (2021) 97:107823. doi: 10.1016/j.intimp.2021.107823

75. Ciesielska A, Matyjek M, Kwiatkowska K. TLR4 and CD14 trafficking and its influence on LPS-induced pro-inflammatory signaling. *Cell Mol Life Sci* (2021) 78 (4):1233–61. doi: 10.1007/s00018-020-03656-y

76. Chen XX, Tang L, Fu YM, Wang Y, Han ZH, Meng JG. Paralemmin-3 contributes to lipopolysaccharide-induced inflammatory response and is involved in lipopolysaccharide-Toll-like receptor-4 signaling in alveolar macrophages. *Int J Mol Med* (2017) 40(6):1921–31. doi: 10.3892/ijmm.2017.3161

77. Gong J, Li J, Dong H, Chen G, Qin X, Hu M, et al. Inhibitory effects of berberine on proinflammatory M1 macrophage polarization through interfering with the interaction between TLR4 and MyD88. *BMC Complement Altern Med* (2019) 19 (1):314. doi: 10.1186/s12906-019-2710-6

78. Shapouri-Moghaddam A, Mohammadian S, Vazini H, Taghadosi M, Esmaeili SA, Mardani F, et al. Macrophage plasticity, polarization, and function in health and disease. *J Cell Physiol* (2018) 233(9):6425–40. doi: 10.1002/jcp.26429

79. Wang LX, Zhang SX, Wu HJ, Rong XL, Guo J. M2b macrophage polarization and its roles in diseases. *J Leukoc Biol* (2019) 106(2):345–58. doi: 10.1002/JLB.3RU1018-378RR

80. Villarino AV, Kanno Y, O'Shea JJ. Mechanisms and consequences of Jak-STAT signaling in the immune system. *Nat Immunol* (2017) 18(4):374–84. doi: 10.1038/ni.3691

81. Ivashkiv LB. IFNgamma: signalling, epigenetics and roles in immunity, metabolism, disease and cancer immunotherapy. *Nat Rev Immunol* (2018) 18 (9):545–58. doi: 10.1038/s41577-018-0029-z

82. Wang F, Zhang S, Jeon R, Vuckovic I, Jiang X, Lerman A, et al. Interferon gamma induces reversible metabolic reprogramming of M1 macrophages to sustain cell viability and pro-inflammatory activity. *EBioMedicine* (2018) 30:303–16. doi: 10.1016/j.ebiom.2018.02.009

83. Suresh S, Irvine AE. The NOTCH signaling pathway in normal and Malignant blood cell production. *J Cell Commun Signal* (2015) 9(1):5–13. doi: 10.1007/s12079-015-0271-0

84. Wu G, Wilson G, George J, Qiao L. Modulation of Notch signaling as a therapeutic approach for liver cancer. *Curr Gene Ther* (2015) 15(2):171–81. doi: 10.2174/1566523214666141224100319

85. Aval SF, Lotfi H, Sheervalilou R, Zarghami N. Tuning of major signaling networks (TGF-beta, Wnt, Notch and Hedgehog) by miRNAs in human stem cells commitment to different lineages: Possible clinical application. *BioMed Pharmacother* (2017) 91:849–60. doi: 10.1016/j.biopha.2017.05.020

86. Wang N, Liang H, Zen K. Molecular mechanisms that influence the macrophage m1-m2 polarization balance. *Front Immunol* (2014) 5:614. doi: 10.3389/fimmu.2014.00614

87. Porta C, Riboldi E, Ippolito A, Sica A. Molecular and epigenetic basis of macrophage polarized activation. *Semin Immunol* (2015) 27(4):237–48. doi: 10.1016/j.smim.2015.10.003

88. Travis MA, Sheppard D. TGF-beta activation and function in immunity. *Annu Rev Immunol* (2014) 32:51–82. doi: 10.1146/annurev-immunol-032713-120257

89. Wang L, Li Y, Wang X, Wang P, Essandoh K, Cui S, et al. GDF3 protects mice against sepsis-induced cardiac dysfunction and mortality by suppression of macrophage pro-inflammatory phenotype. *Cells* (2020) 9(1):120. doi: 10.3390/cells9010120

90. Marion-Letellier R, Savoye G, Ghosh S. Fatty acids, eicosanoids and PPAR gamma. *Eur J Pharmacol* (2016) 785:44–9. doi: 10.1016/j.ejphar.2015.11.004

91. Luo W, Xu Q, Wang Q, Wu H, Hua J. Effect of modulation of PPAR-gamma activity on Kupffer cells M1/M2 polarization in the development of non-alcoholic fatty liver disease. *Sci Rep* (2017) 7:44612. doi: 10.1038/srep44612

92. Essandoh K, Li Y, Huo J, Fan GC. MiRNA-mediated macrophage polarization and its potential role in the regulation of inflammatory response. *Shock* (2016) 46 (2):122–31. doi: 10.1097/SHK.0000000000000604

93. Lo Sicco C, Reverberi D, Balbi C, Ulivi V, Principi E, Pascucci L, et al. Mesenchymal stem cell-derived extracellular vesicles as mediators of anti-inflammatory effects: endorsement of macrophage polarization. *Stem Cells Transl Med* (2017) 6(3):1018–28. doi: 10.1002/sctm.16-0363

94. Vergadi E, Ieronymaki E, Lyroni K, Vaporidi K, Tsatsanis C. Akt signaling pathway in macrophage activation and M1/M2 polarization. *J Immunol* (2017) 198 (3):1006–14. doi: 10.4049/jimmunol.1601515

95. Feng Y, Ren J, Gui Y, Wei W, Shu B, Lu Q, et al. Wnt/beta-catenin-promoted macrophage alternative activation contributes to kidney fibrosis. *J Am Soc Nephrol* (2018) 29(1):182–93. doi: 10.1681/ASN.2017040391

96. Huang X, Li Y, Fu M, Xin HB. Polarizing macrophages *in vitro*. *Methods Mol Biol* (2018) 1784:119–26. doi: 10.1007/978-1-4939-7837-3_12

97. Jaeschke H, Ramachandran A. Mechanisms and pathophysiological significance of sterile inflammation during acetaminophen hepatotoxicity. *Food Chem Toxicol* (2020) 138:111240. doi: 10.1016/j.fct.2020.111240

98. Wasmuth HE, Kunz D, Yagmur E, Timmer-Stranghoner A, Vidacek D, Siewert E, et al. Patients with acute on chronic liver failure display "sepsis-like" immune paralysis. *J Hepatol* (2005) 42(2):195–201. doi: 10.1016/j.jhep.2004.10.019

99. Sica A, Mantovani A. Macrophage plasticity and polarization: *in vivo* veritas. *J Clin Invest* (2012) 122(3):787–95. doi: 10.1172/JCI59643

100. Chan MWY, Viswanathan S. Recent progress on developing exogenous monocyte/macrophage-based therapies for inflammatory and degenerative diseases. *Cytotherapy* (2019) 21(4):393–415. doi: 10.1016/j.jcyt.2019.02.002

101. Dambach DM, Watson LM, Gray KR, Durham SK, Laskin DL. Role of CCR2 in macrophage migration into the liver during acetaminophen-induced hepatotoxicity in the mouse. *Hepatology* (2002) 35(5):1093–103. doi: 10.1053/jhep.2002.33162

102. Possamai LA, Thursz MR, Wendon JA, Antoniades CG. Modulation of monocyte/macrophage function: a therapeutic strategy in the treatment of acute liver failure. *J Hepatol* (2014) 61(2):439–45. doi: 10.1016/j.jhep.2014.03.031

103. Liu R, Cui J, Sun Y, Xu W, Wang Z, Wu M, et al. Autophagy deficiency promotes M1 macrophage polarization to exacerbate acute liver injury via ATG5 repression during aging. *Cell Death Discov* (2021) 7(1):397. doi: 10.1038/s41420-021-00797-2

104. Wang Y, Zhang H, Chen Q, Jiao F, Shi C, Pei M, et al. TNF-alpha/HMGB1 inflammation signalling pathway regulates pyroptosis during liver failure and acute kidney injury. *Cell Prolif* (2020) 53(6):e12829. doi: 10.1111/cpr.12829

105. Li Y, Sheng Q, Zhang C, Han C, Bai H, Lai P, et al. STAT6 up-regulation amplifies M2 macrophage anti-inflammatory capacity through mesenchymal stem cells. *Int Immunopharmacol* (2021) 91:107266. doi: 10.1016/j.intimp.2020.107266

106. Yu Y, Zhang Q, Wu N, Xia L, Cao J, Xia Q, et al. HNF4alpha overexpression enhances the therapeutic potential of umbilical cord mesenchymal stem/stromal cells in mice with acute liver failure. *FEBS Lett* (2022) 596(24):3176–90. doi: 10.1002/1873-3468.14453

107. Tomar S, Zumbrun EE, Nagarkatti M, Nagarkatti PS. Protective role of cannabinoid receptor 2 activation in galactosamine/lipopolysaccharide-induced acute liver failure through regulation of macrophage polarization and microRNAs. *J Pharmacol Exp Ther* (2015) 353(2):369–79. doi: 10.1124/jpet.114.220368

108. Shao M, Xu Q, Wu Z, Chen Y, Shu Y, Cao X, et al. Exosomes derived from human umbilical cord mesenchymal stem cells ameliorate IL-6-induced acute liver injury through miR-455-3p. *Stem Cell Res Ther* (2020) 11(1):37. doi: 10.1186/s13287-020-1550-0

109. Li YW, Zhang C, Sheng QJ, Bai H, Ding Y, Dou XG. Mesenchymal stem cells rescue acute hepatic failure by polarizing M2 macrophages. *World J Gastroenterol* (2017) 23(45):7978–88. doi: 10.3748/wjg.v23.i45.7978

110. Gan C, Cai Q, Tang C, Gao J. Inflammasomes and pyroptosis of liver cells in liver fibrosis. *Front Immunol* (2022) 13:896473. doi: 10.3389/fimmu.2022.896473

111. Szabo G, Petrasek J. Inflammasome activation and function in liver disease. *Nat Rev Gastroenterol Hepatol* (2015) 12(7):387–400. doi: 10.1038/nrgastro.2015.94

112. Broz P, Dixit VM. Inflammasomes: mechanism of assembly, regulation and signalling. *Nat Rev Immunol* (2016) 16(7):407–20. doi: 10.1038/nri.2016.58

113. Rathinam VA, Fitzgerald KA. Inflammasome complexes: emerging mechanisms and effector functions. *Cell* (2016) 165(4):792–800. doi: 10.1016/j.cell.2016.03.046

114. Kovacs SB, Miao EA. Gasdermins: effectors of pyroptosis. *Trends Cell Biol* (2017) 27(9):673–84. doi: 10.1016/j.tcb.2017.05.005

115. Liu X, Lieberman J. A mechanistic understanding of pyroptosis: the fiery death triggered by invasive infection. *Adv Immunol* (2017) 135:81–117. doi: 10.1016/bs.ai.2017.02.002

116. Liu X, Zhang Z, Ruan J, Pan Y, Magupalli VG, Wu H, et al. Inflammasome-activated gasdermin D causes pyroptosis by forming membrane pores. *Nature* (2016) 535(7610):153–8. doi: 10.1038/nature18629

117. Shi J, Zhao Y, Wang Y, Gao W, Ding J, Li P, et al. Inflammatory caspases are innate immune receptors for intracellular LPS. *Nature* (2014) 514(7521):187–92. doi: 10.1038/nature13683

118. Downs KP, Nguyen H, Dorfleutner A, Stehlik C. An overview of the non-canonical inflammasome. *Mol Aspects Med* (2020) 76:100924. doi: 10.1016/j.mam.2020.100924

119. Yang D, He Y, Munoz-Planillo R, Liu Q, Nunez G. Caspase-11 requires the pannexin-1 channel and the purinergic P2X7 pore to mediate pyroptosis and endotoxic shock. *Immunity* (2015) 43(5):923–32. doi: 10.1016/j.immuni.2015.10.009

120. You R, He X, Zeng Z, Zhan Y, Xiao Y, Xiao R. Pyroptosis and its role in autoimmune disease: A potential therapeutic target. *Front Immunol* (2022) 13:841732. doi: 10.3389/fimmu.2022.841732

121. He Y, Hara H, Nunez G. Mechanism and regulation of NLRP3 inflammasome activation. *Trends Biochem Sci* (2016) 41(12):1012–21. doi: 10.1016/j.tibs.2016.09.002

122. Zhang H, Du Y, Guo Y, Wang Z, Li H, Lv Z, et al. TLR4-NLRP3-GSDMD-mediated pyroptosis plays an important role in aggravated liver injury of CD38(-/-) sepsis mice. *J Immunol Res* (2021) 2021:6687555. doi: 10.1155/2021/6687555

123. Mira JC, Gentile LF, Mathias BJ, Efron PA, Brakenridge SC, Mohr AM, et al. Sepsis pathophysiology, chronic critical illness, and persistent inflammation-immunosuppression and catabolism syndrome. *Crit Care Med* (2017) 45(2):253–62. doi: 10.1097/CCM.0000000000002074

124. Gaul S, Leszczynska A, Alegre F, Kaufmann B, Johnson CD, Adams LA, et al. Hepatocyte pyroptosis and release of inflammasome particles induce stellate cell activation and liver fibrosis. *J Hepatol* (2021) 74(1):156–67. doi: 10.1016/j.jhep.2020.07.041

125. Luan J, Zhang X, Wang S, Li Y, Fan J, Chen W, et al. NOD-like receptor protein 3 inflammasome-dependent IL-1beta accelerated conA-induced hepatitis. *Front Immunol* (2018) 9:758. doi: 10.3389/fimmu.2018.00758

126. Wang Y, Chen Q, Jiao F, Shi C, Pei M, Wang L, et al. Histone deacetylase 2 regulates ULK1 mediated pyroptosis during acute liver failure by the K68 acetylation site. *Cell Death Dis* (2021) 12(1):55. doi: 10.1038/s41419-020-03317-9

127. Li H, Zhao XK, Cheng YJ, Zhang Q, Wu J, Lu S, et al. Gasdermin D-mediated hepatocyte pyroptosis expands inflammatory responses that aggravate acute liver failure by upregulating monocyte chemotactic protein 1/CC chemokine receptor-2 to recruit macrophages. *World J Gastroenterol* (2019) 25(44):6527–40. doi: 10.3748/wjg.v25.i44.6527

128. Liu M, He J, Zheng S, Zhang K, Ouyang Y, Zhang Y, et al. Human umbilical cord mesenchymal stem cells ameliorate acute liver failure by inhibiting apoptosis, inflammation and pyroptosis. *Ann Transl Med* (2021) 9(21):1615. doi: 10.21037/atm-21-2885

129. Yang R, Yu H, Chen J, Zhu J, Song C, Zhou L, et al. Limonin attenuates LPS-induced hepatotoxicity by inhibiting pyroptosis via NLRP3/gasdermin D signaling pathway. *J Agric Food Chem* (2021) 69(3):982–91. doi: 10.1021/acs.jafc.0c06775

130. Liu T, Yang L, Gao H, Zhuo Y, Tu Z, Wang Y, et al. 3,4-dihydroxyphenylethyl alcohol glycoside reduces acetaminophen-induced acute liver failure in mice by inhibiting hepatocyte ferroptosis and pyroptosis. *PeerJ* (2022) 10:e13082. doi: 10.7717/peerj.13082

131. Siregar AS, Nyiramana MM, Kim EJ, Cho SB, Woo MS, Lee DK, et al. Oyster-derived tyr-ala (YA) peptide prevents lipopolysaccharide/D-galactosamine-induced acute liver failure by suppressing inflammatory, apoptotic, ferroptotic, and pyroptotic signals. *Mar Drugs* (2021) 19(11):614. doi: 10.3390/md19110614

132. Shu B, Zhou YX, Li H, Zhang RZ, He C, Yang X. The METTL3/MALAT1/PTBP1/USP8/TAK1 axis promotes pyroptosis and M1 polarization of macrophages and contributes to liver fibrosis. *Cell Death Discov* (2021) 7(1):368. doi: 10.1038/s41420-021-00756-x

133. Yang W, Tao K, Zhang P, Chen X, Sun X, Li R. Maresin 1 protects against lipopolysaccharide/d-galactosamine-induced acute liver injury by inhibiting macrophage pyroptosis and inflammatory response. *Biochem Pharmacol* (2022) 195:114863. doi: 10.1016/j.bcp.2021.114863

134. Rao Z, Zhu Y, Yang P, Chen Z, Xia Y, Qiao C, et al. Pyroptosis in inflammatory diseases and cancer. *Theranostics* (2022) 12(9):4310–29. doi: 10.7150/thno.71086

135. Aachoui Y, Sagulenko V, Miao EA, Stacey KJ. Inflammasome-mediated pyroptotic and apoptotic cell death, and defense against infection. *Curr Opin Microbiol* (2013) 16(3):319–26. doi: 10.1016/j.mib.2013.04.004

136. Greaney AJ, Leppla SH, Moayeri M. Bacterial exotoxins and the inflammasome. *Front Immunol* (2015) 6:570. doi: 10.3389/fimmu.2015.00570

137. Friedlander AM. Macrophages are sensitive to anthrax lethal toxin through an acid-dependent process. *J Biol Chem* (1986) 261(16):7123–6. doi: 10.1016/S0021-9258(17)38364-3

138. Chui AJ, Okondo MC, Rao SD, Gai K, Griswold AR, Johnson DC, et al. N-terminal degradation activates the NLRP1B inflammasome. *Science* (2019) 364(6435):82–5. doi: 10.1126/science.aau1208

139. Sandstrom A, Mitchell PS, Goers L, Mu EW, Lesser CF, Vance RE. Functional degradation: A mechanism of NLRP1 inflammasome activation by diverse pathogen enzymes. *Science* (2019) 364(6435):eaau1330. doi: 10.1126/science.aau1330

140. Kayagaki N, Warming S, Lamkanfi M, Vande Walle L, Louie S, Dong J, et al. Non-canonical inflammasome activation targets caspase-11. *Nature* (2011) 479(7371):117–21. doi: 10.1038/nature10558

141. Kayagaki N, Wong MT, Stowe IB, Ramani SR, Gonzalez LC, Akashi-Takamura S, et al. Noncanonical inflammasome activation by intracellular LPS independent of TLR4. *Science* (2013) 341(6151):1246–9. doi: 10.1126/science.1240248

142. Glaria E, Valledor AF. Roles of CD38 in the immune response to infection. *Cells* (2020) 9(1):228. doi: 10.3390/cells9010228

143. Kinra M, Nampoothiri M, Arora D, Mudgal J. Reviewing the importance of TLR-NLRP3-pyroptosis pathway and mechanism of experimental NLRP3 inflammasome inhibitors. *Scand J Immunol* (2022) 95(2):e13124. doi: 10.1111/sji.13124

144. Hou W, Wei X, Liang J, Fang P, Ma C, Zhang Q, et al. HMGB1-induced hepatocyte pyroptosis expanding inflammatory responses contributes to the pathogenesis of acute-on-chronic liver failure (ACLF). *J Inflamm Res* (2021) 14:7295–313. doi: 10.2147/JIR.S336626

145. Murao A, Aziz M, Wang H, Brenner M, Wang P. Release mechanisms of major DAMPs. *Apoptosis* (2021) 26(3-4):152–62. doi: 10.1007/s10495-021-01663-3

146. Dong W, Zhu Q, Yang B, Qin Q, Wang Y, Xia X, et al. Polychlorinated biphenyl quinone induces caspase 1-mediated pyroptosis through induction of pro-inflammatory HMGB1-TLR4-NLRP3-GSDMD signal axis. *Chem Res Toxicol* (2019) 32(6):1051–7. doi: 10.1021/acs.chemrestox.8b00376

147. Jia C, Zhang J, Chen H, Zhuge Y, Chen H, Qian F, et al. Endothelial cell pyroptosis plays an important role in Kawasaki disease via HMGB1/RAGE/cathespin B signaling pathway and NLRP3 inflammasome activation. *Cell Death Dis* (2019) 10(10):778. doi: 10.1038/s41419-019-2021-3

148. Sun Z, Nyanzu M, Yang S, Zhu X, Wang K, Ru J, et al. VX765 attenuates pyroptosis and HMGB1/TLR4/NF-kappaB pathways to improve functional outcomes in TBI mice. *Oxid Med Cell Longev* (2020) 2020:7879629. doi: 10.1155/2020/7879629

149. Wang J, Ren H, Yuan X, Ma H, Shi X, Ding Y. Interleukin-10 secreted by mesenchymal stem cells attenuates acute liver failure through inhibiting pyroptosis. *Hepatol Res* (2018) 48(3):E194–202. doi: 10.1111/hepr.12969

150. Bai L, Lu W, Tang S, Tang H, Xu M, Liang C, et al. Galectin-3 critically mediates the hepatoprotection conferred by M2-like macrophages in ACLF by inhibiting pyroptosis but not necroptosis signalling. *Cell Death Dis* (2022) 13(9):775. doi: 10.1038/s41419-022-05181-1

151. de Carvalho Ribeiro M, Szabo G. Role of the inflammasome in liver disease. *Annu Rev Pathol* (2022) 17:345–65. doi: 10.1146/annurev-pathmechdis-032521-102529

152. Bertheloot D, Latz E, Franklin BS. Necroptosis, pyroptosis and apoptosis: an intricate game of cell death. *Cell Mol Immunol* (2021) 18(5):1106–21. doi: 10.1038/s41423-020-00630-3

frontiers | Frontiers in Immunology

TYPE Original Research
PUBLISHED 29 November 2023
DOI 10.3389/fimmu.2023.1303921

OPEN ACCESS

EDITED BY
Heiko Mühl,
Goethe University Frankfurt, Germany

REVIEWED BY
Yankai Wen,
University of Texas Health Science Center at Houston, United States
Yeonhee Cho,
Amgen, United States

*CORRESPONDENCE
Bryan L. Copple
copple@msu.edu

RECEIVED 28 September 2023
ACCEPTED 13 November 2023
PUBLISHED 29 November 2023

CITATION
Roth K, Strickland J, Pant A, Freeborn R, Kennedy R, Rockwell CE, Luyendyk JP and Copple BL (2023) Interleukin-10 disrupts liver repair in acetaminophen-induced acute liver failure.
Front. Immunol. 14:1303921.
doi: 10.3389/fimmu.2023.1303921

Interleukin-10 disrupts liver repair in acetaminophen-induced acute liver failure

Katherine Roth[1,2,3,4], Jenna Strickland[1,2,3,4], Asmita Pant[5], Robert Freeborn[1,2], Rebekah Kennedy[1,2], Cheryl E. Rockwell[1,2,3,4], James P. Luyendyk[2,5] and Bryan L. Copple[1,2,3,4]*

[1]Department of Pharmacology and Toxicology, Michigan State University, East Lansing, MI, United States, [2]Institute for Integrative Toxicology, Michigan State University, East Lansing, MI, United States, [3]Cell and Molecular Biology Program, Michigan State University, East Lansing, MI, United States, [4]College of Human Medicine, Michigan State University, East Lansing, MI, United States, [5]Pathobiology and Diagnostic Investigation, Michigan State University, East Lansing, MI, United States

Introduction: Systemic levels of the anti-inflammatory cytokine interleukin 10 (IL-10) are highest in acetaminophen (APAP)-induced acute liver failure (ALF) patients with the poorest prognosis. The mechanistic basis for this counterintuitive finding is not known, as induction of IL-10 is hypothesized to temper the pathological effects of immune cell activation. Aberrant production of IL-10 after severe liver injury could conceivably interfere with the beneficial, pro-reparative actions of immune cells, such as monocytes.

Methods: To test this possibility, we determined whether IL-10 levels are dysregulated in mice with APAP-induced ALF and further evaluated whether aberrant production of IL-10 prevents monocyte recruitment and/or the resolution of necrotic lesions by these cells.

Results: Our studies demonstrate that in mice challenged with 300 mg/kg acetaminophen (APAP), a hepatotoxic dose of APAP that fails to produce ALF (i.e., APAP-induced acute liver injury; AALI), Ly6C^{hi} monocytes were recruited to the liver and infiltrated the necrotic lesions by 48 hours coincident with the clearance of dead cell debris. At 72 hours, IL-10 was upregulated, culminating in the resolution of hepatic inflammation. By contrast, in mice treated with 600 mg/kg APAP, a dose that produces clinical features of ALF (i.e., APAP-induced ALF; AALF), IL-10 levels were markedly elevated by 24 hours. Early induction of IL-10 was associated with a reduction in the hepatic numbers of Ly6C^{hi} monocytes resulting in the persistence of dead cell debris. Inhibition of IL-10 in AALF mice, beginning at 24 hours after APAP treatment, increased the hepatic numbers of monocytes which coincided with a reduction in the necrotic area. Moreover, pharmacologic elevation of systemic IL-10 levels in AALI mice reduced hepatic myeloid cell numbers and increased the area of necrosis.

Discussion: Collectively, these results indicate that during ALF, aberrant production of IL-10 disrupts the hepatic recruitment of monocytes, which prevents the clearance of dead cell debris. These are the first studies to document a mechanistic basis for the link between high IL-10 levels and poor outcome in patients with ALF.

KEYWORDS

acetaminophen, acute liver failure, interleukin-10, inflammation, monocytes

Introduction

In severe cases of acetaminophen (APAP) overdose, acute liver injury rapidly progresses to acute liver failure (ALF), producing life threatening cardiac instability, hepatic encephalopathy, and multiorgan dysfunction syndrome (MODS) (1, 2). First line therapy for APAP overdose is N-acetyl cysteine (NAC), which is most efficacious when administered within 8 hours of APAP ingestion (3, 4). If NAC fails to limit the progression to ALF, supportive medical care and liver transplantation are the only remaining modes of therapy. Unfortunately, despite significant improvements to critical care medicine and emergency liver transplantation, mortality associated with ALF remains high (i.e., approximately 30%), underscoring the importance of identifying new therapeutic targets (2).

Components of innate immunity exacerbate early liver injury after APAP overdose in mice. Consequently, deficiency of the neutrophil chemokine, Cxcl1, or antibody-mediated depletion of neutrophils reduces blood biomarkers of hepatocyte injury in APAP-treated mice (5, 6). Moreover, deficiency in the anti-inflammatory cytokine, interleukin-10 (IL-10), enhances liver injury and inflammation in APAP-treated mice, whereas administration of recombinant IL-10 early after APAP overdose reduces liver injury (7–9). These findings have set current dogma that innate immunity is predominately detrimental to outcome after APAP overdose. As a result, it has been proposed that therapeutic intervention with exogenous IL-10 could improve outcomes in APAP overdose patients that have become refractory to standard care (9). Although this could be viewed as a game changer for critically ill patients, the prevailing belief that the innate immune system is solely harmful contrasts with findings from clinical studies where severe immune suppression is frequently observed in this patient population (10–12).

APAP-induced ALF patients with the poorest prognosis develop compensatory anti-inflammatory response syndrome (CARS), a condition characterized by severe systemic immune suppression (10, 13). Blood monocytes collected from ALF patients demonstrate a reduced capacity to phagocytose bacteria, produce lower levels of proinflammatory cytokines, and display features of myeloid-derived suppressor cells (MDSCs), including high level expression of the immune-suppressive, ligand-receptor pair, programmed death ligand 1 (PD-L1) and PD-1 (11, 14, 15). Moreover, high blood levels of the CARS-associated cytokine, IL-10, are an independent predictor of a poor outcome in these patients (10, 12). While the mechanistic basis for this seemingly paradoxical association is not known, these findings indicate that therapeutic intervention with IL-10 could be harmful to ALF patients. One mechanism by which high levels of IL-10 could negatively impact outcome in APAP overdose patients is by interfering with the beneficial, pro-reparative activities of innate immune cells.

Liver injury after APAP overdose stimulates the hepatic release of Ccl2, a chemokine that facilitates the recruitment of Ly6C^{hi} monocytes to the damaged liver in a Ccr2-dependent manner (16, 17). Once in the liver, these cells traffic to the necrotic foci where they become stimulated to phagocytose dead cell debris (17, 18). This process, along with proliferation of hepatocytes and nonparenchymal cells, facilitates repair of the damaged liver resulting in the restoration of hepatic function. Interventions that prevent the hepatic recruitment of monocytes, such as blockade of Ccr2, inhibit the clearance of dead cell debris, a key component of liver repair (16, 17). Because IL-10 is a potent anti-inflammatory cytokine, it is conceivable that high levels of IL-10 could interfere with certain pro-repair activities of immune cells, including resolution of necrotic lesions by monocytes. Interestingly, Bhushan and colleagues recently reported that necrotic cells persist in the livers of mice treated with a dose of APAP that produces clinically relevant ALF, including evidence of a coagulopathy, hepatic encephalopathy, and renal injury, a frequent component of MODS (19–22). Whether this is the result of amplified IL-10 levels, similar to APAP-induced ALF patients, however, was not investigated. Accordingly, in the present studies we tested the hypothesis that high levels of IL-10 in mice with APAP-induced ALF prevent the clearance of dead cell debris by monocytes.

Abbreviations: IL-10, interleukin-10, APAP, acetaminophen, AALF, acetaminophen-induced acute liver failure, AALI, acetaminophen-induced acute liver injury, MDM, monocyte-derived macrophage, PCNA, proliferating cell nuclear antigen, PE, phycoerythrin, SEM, standard error of the mean, ANOVA, analysis of variance, MDSC, myeloid-derived suppressor cell, H&E, hematoxylin and eosin, MODS, multiorgan dysfunction syndrome, NAC, N-acetylcysteine, CARS, compensatory anti-inflammatory response syndrome.

Materials and methods

Animals and treatments

12-16-week-old male C57BL/6J or IL-10 reporter mice (B6.129S6-Il10$^{tm1/flv}$/J; Jackson Laboratories) were used for all

studies. Mice were housed in a 12-hour light/dark cycle under controlled temperature (18-21°C) and humidity. Food (Rodent diet; Harlan-Teklad) and water were allowed *ad libitum*.

Mice were fasted for 16 hours prior to the administration of 300 mg/kg APAP (Sigma-Aldrich), 600 mg/kg APAP, or sterile saline vehicle by intraperitoneal injection, as described previously (20). Fasting was initiated at approximately 5:00 PM and APAP was injected at approximately 9:00 AM the following day. In all studies, rodent diet was returned immediately after APAP challenge.

For IL-10 neutralization studies, mice were injected with 0.5 mg *InVivo*MAb anti-mouse IL-10 antibody (Bio X Cell, clone JES5-2A5) or 0.5 mg isotype control antibody (Innovative Research, Rat IgG) both by intraperitoneal injection at 24 hours after APAP treatment. For recombinant IL-10 studies, mice were injected with 5 µg recombinant mouse IL-10 (Biolegend, San Diego, CA) or sterile saline both by intraperitoneal injection at 24 hours after APAP challenge. All studies were approved by the Michigan State University Institutional Animal Care and Use Committee.

Sample collection

Mice were anesthetized using Fatal-Plus Solution (Vortech Pharmaceuticals) or isoflurane. Blood was collected from the inferior vena cava and the livers were removed. A portion of each liver was fixed in 10% neutral-buffered formalin. The livers were embedded in paraffin, sectioned, and stained with hematoxylin and eosin. The area of necrosis was quantified as described by us previously (23). Briefly, 10 randomly chosen images were collected per liver section (2 sections per mouse taken from separate liver lobes) using a 20X objective. The areas of necrosis were outlined, and Image J was used to calculate the percent area of necrosis. Additional portions of the liver were homogenized in TRIzol Reagent (Thermo-Fisher Scientific) for RNA isolation or were snap-frozen in liquid nitrogen for sectioning and immunofluorescence staining.

Immunofluorescence

Immunofluorescence was used to detect CD68 as described by us previously (23). Briefly, 8 µm sections were cut from frozen livers and fixed for 10 minutes in 4% formalin. The sections were then incubated in blocking buffer (10% goat serum in phosphate-buffered saline (PBS)) followed by incubation with rat anti-CD68 antibody (Bio-Rad) diluted 1:500. After washing, the sections were incubated with goat anti-rat secondary antibody conjugated to Alexa Fluor 594 (diluted 1:500, Thermo Fisher Scientific). To quantify the area of CD68 fluorescent staining, 10 randomly chosen images were collected per liver section using a 20X objective. The area of positive CD68 staining was then quantified using Image J. Proliferating cell nuclear antigen (PCNA) was detected by immunohistochemistry and used as a biomarker of hepatocyte proliferation. Hepatocytes were identified based upon their larger size relative to that of nonparenchymal cells and quantified as described by us previously (23).

Luminex immunoassay

IL-10 protein levels were measured in blood serum samples by using the Bio-Plex Pro assay kit (Bio-Rad) according to manufacturer's instructions. Bead fluorescent readings were obtained using a Luminex 200 system.

Isolation of F4/80$^+$ and LY6C$^+$ cells from mouse livers

To isolate F4/80$^+$ and Ly6C$^+$ cells, livers from C57BL/6 mice were perfused and digested with collagenase (Collagenase H; Sigma-Aldrich), as described previously (24). After removal of hepatocytes by centrifugation, the nonparenchymal cells were centrifuged at 300 × *g* for 10 minutes. A total of 1 × 10^8 nonparenchymal cells was resuspended in 60 µL of MACS Buffer (2.5 g bovine serum albumin, 0.416 g EDTA, and 500 mL phosphate-buffered saline) containing 12 µL biotinylated anti-F4/80 antibody or biotinylated anti-Ly6C antibody (Miltenyi Biotec, Bergisch Gladbach, Germany). The cell suspension was incubated for 10 minutes at 4°C and then washed by adding 10 mL of MACS buffer and centrifugation (300 × *g* for 10 minutes). Streptavidin microbeads (Miltenyi Biotec), diluted 1:10 in 60 µL of MACs buffer, were added to the nonparenchymal pellet. Cells were resuspended and incubated at 4°C for 10 minutes and then washed by adding 10 mL of MACS buffer and centrifugation (300 × *g* for 10 minutes). The pellet was resuspended with 500 µL MACS buffer and applied to MACS LS columns (Miltenyi Biotec). The column was rinsed three times with 3 mL MACS buffer. F4/80$^+$ or Ly6C$^+$ cells were collected by removing the column from the midiMACS Separator (Miltenyi Biotec) and rinsing the column with 5 mL of MACS buffer. Cell purity was confirmed by flow cytometry and was routinely greater than 94% as reported by us previously (25). RNA was immediately isolated from the cells by using the E.Z.N.A. Total RNA Kit I (Omega, Bio-tek, Norcross, GA) and real-time PCR was performed as detailed below.

Flow cytometry

To isolate non-parenchymal cells, mouse livers were perfused and digested with collagenase (Collagenase H, Sigma Chemical Company) as described by us previously (26). Hepatocytes were removed by centrifugation (50 g for 2 minutes), and non-parenchymal cells were collected from the remaining solution by centrifugation at 300 g for 10 minutes. The non-parenchymal cells were washed and resuspended in FACs buffer (phosphate-buffered saline, 1% fetal bovine serum). The cells were then incubated with Fc blocking buffer (BD Biosciences; diluted 1:20) for 10 minutes at 4 °C,

rinsed, and then pelleted by centrifugation at 300 g for 5 minutes. The cells were incubated with anti-F4/80 conjugated to Pacific Blue, anti-Ly6C conjugated to APC/Cy7, and anti-Ly6G conjugated to Percp/Cy5.5 for 30 minutes at 4°C. All antibodies were purchased from Biolegend. For studies with IL-10 GFP reporter mice, the following antibodies were used for flow cytometry: anti-Axl (APC), anti-CD45.1 (Alexa 488), anti-F4/80 (pacific blue), anti-Cx3cr1 (Alexa 700), anti-Ly6C (APC/Cy7), anti-Cd11b (PE), anti-Marco (APC), anti-Ccr2 (BV650), anti-PD-L1 (PerCp/Cy5.5), anti-CD3 (BV510), anti-CD4 (AF700), anti-NK1.1 (BV711), anti-CD8a (PerCP), and CD11c (BV711). All antibodies were purchased from Biolegend, except anti-Marco and anti-Axl, which were purchased from Invitrogen. The fixable dye, Zombie Aqua (Biolegend), was used to determine cell viability. Following incubation, cells were washed twice and fixed in formalin (Sigma) for 15 minutes at 4°C. The fixed cells were washed twice and resuspended in FACs buffer. Flow cytometry was conducted on an Attune NxT flow cytometer (Life Technologies). Attune NxT software (Life Technologies) was used to analyze the data.

Real-time PCR

Total RNA was isolated from liver samples using TRIzol Reagent (Thermo-Fisher) and reverse transcribed into cDNA as described previously(24). Real-time PCR was performed on a QuantStudio 7 Flex Real-Time PCR System (Thermo-Fisher) using the iTaq Universal SYBR green Supermix (Bio-Rad). The following primer sequences were used: TNF-α: Forward-5'-AGGGTCTGGGCC ATAGAACT-3', Reverse-5'-CCACCACGCTCTTCTGTCTAC-3'; Cxcl1: Forward-5'-TGGCTGGGATTCACCTCAAG-3', Reverse-5'-GTGGCTATGACTTCGGTTTGG-3'; Ccl2: Forward- 5'-CCTGC TGTTCACAGTTGCC-3', Reverse- 5'-ATTGGGATCAT CTTGCTGGT-3'; Il-10: Forward- 5'-TGTCAAATTCATTCATG GCCT-3', Reverse- 5'-ATCGATTTCTCCCCTGTGAA-3': Rpl13a: Forward- 5'-GACCTCCTCCTTTCCCAGGC-3', Reverse- 5'-AAGTACCTGCTTGGCCACAA-3'; urokinase plasminogen activator (uPA): Forward-5'-GGGCTTGTTTTTCTCTGCAC-3', Reverse-5'-GCCCCACTACTATGGCTCTG-3'.

Microarray analysis

For reanalysis of microarray data from ALF patients, the.cel files were obtained from GEO database (accession number: GSE8075) and differential gene expression was determined using Transcriptome Analysis Console Software (ThermoFisher Scientific). Detailed patient information was reported previously (27). Upstream analysis was conducted using Ingenuity Pathway Analysis (Qiagen).

Statistical analysis

Results are presented as the mean + SEM. Data were analyzed by a one-way or two-way Analysis of Variance (ANOVA) where appropriate. Data expressed as a percentage were transformed by arcsine square root prior to analysis. Comparisons among group means were made using the Student-Newman-Keuls test. The criterion for significance was $p < 0.05$ for all studies.

Results

Persistence of necrotic cell debris in the livers of mice with APAP-induced ALF

Bhushan and colleagues previously reported that dead cells persist in the livers of mice with APAP-induced ALF (AALF) (20). Because monocytes are critical for the clearance of dead cells from the liver (28), these findings suggested a defect in monocyte recruitment and/or function in ALF. To examine this further, we treated groups of mice with 300 mg/kg APAP, a hepatotoxic dose of APAP that fails to produce ALF (i.e., APAP-induced acute liver injury; AALI), or with 600 mg/kg APAP, a dose that produces clinical features of AALF, including coagulopathy (22), renal injury (21), and hepatic encephalopathy (19).

As reported previously (20), liver necrosis peaked at approximately 24 hours in mice with AALI (Figures 1A, B). By 48 hours, extensive inflammatory infiltrates were evident within the necrotic foci (inset in Figure 1A, 24-hour AALI). The inflammatory cells, along with the necrotic cell debris, were largely cleared from the liver by 72 hours (Figures 1A, B). In mice with AALF, APAP produced a comparable initial hepatotoxic response (i.e., peak area of necrosis at 24 hours; Figures 1A, B), however, at this larger dose of APAP, the necrotic lesions were largely devoid of inflammatory cells (inset in Figure 1A, 24-hour AALF). Unlike AALI mice, the necrotic cells persisted in the liver at 72 hours, suggesting that the mechanisms driving dead cell clearance were impaired (Figure 1B) (17). While no deaths were noted in mice with AALI, in mice with AALF, 9 mice either died or were euthanized for humane reasons beyond 24 hours resulting in an overall mortality of 30% (n=30 mice with 9 deaths occurring at various times) by 72 hours. This mortality rate is similar to what was reported previously (20).

Reduced numbers of myeloid cells in the livers of mice with AALF

Because myeloid cells clear dead cell debris from the APAP-injured liver (28), we determined whether the numbers of these cells were impacted in the livers of AALF mice. To accomplish this, immunofluorescent staining was used to detect CD68 in sections of liver. CD68 is expressed at high levels by $Ly6C^{hi}$ monocytes and Kupffer cells (29). Moreover, prior studies revealed that $CD68^{+}$ myeloid cells accumulate in the livers of patients with APAP-induced ALF (18, 30, 31). By 24 hours in mice with AALI, $CD68^{+}$ myeloid cells were present in the liver and more concentrated near centrilobular regions where liver injury occurred (Figure 2A, CD68 staining appears red; arrows indicate the location of central veins in centrilobular regions which were visible under conditions of overexposure). By 48 hours, CD68 staining was markedly increased

in centrilobular regions which persisted at 72 hours (Figure 2A). In mice with AALF, fewer CD68$^+$ myeloid cells were present in the livers at all time points examined (Figures 2A, B). Moreover, these cells were evenly distributed throughout the liver lobule and not concentrated within centrilobular regions (Figures 2A, B).

Next, flow cytometry was used to better define the myeloid cell type(s) that were reduced in numbers in AALF mice. Gating for flow cytometry is shown in Figure 3A. As shown in Figures 3B, C the absolute number of Ly6G$^+$ cells (i.e., neutrophils) in the liver was not different between mice with AALI and AALF, however these cells did comprise a larger percentage of the CD45 population in AALF mice (Figure 3D). The number of Ly6C$^+$ cells (i.e., recruited monocytes; (32)) was markedly reduced in mice with AALF, whereas the number of F4/80$^+$ cells (i.e., Kupffer cells and monocytes that had differentiated into macrophages, monocyte-derived macrophages (MDMs)) was modestly higher (Figures 3B–D). Collectively, these findings demonstrate that recruited monocytes, which clear dead cell debris from the APAP-injured liver, were decreased in numbers in mice with AALF.

Increased levels of IL-10 in mice with AALF

High levels of IL-10 are associated with a worse outcome in ALF patients (10). Similar to these clinical findings, in mice with AALF, hepatic mRNA levels of IL-10 were increased by 24 hours and remained elevated at 72 hours (Figure 4A). Importantly, elevated mRNA levels were matched by increased IL-10 protein in the serum (Figure 4B). By contrast, in mice with AALI, IL-10 mRNA levels were not elevated until 72 hours after APAP treatment (Figures 4A, B). To determine whether myeloid cells were a source of IL-10, we purified F4/80$^+$ myeloid cells (i.e., Kupffer cells and MDMs) and Ly6C$^+$ myeloid cells (i.e., recruited monocytes) from the livers of AALF mice at 24 hours after APAP treatment and IL-10 mRNA

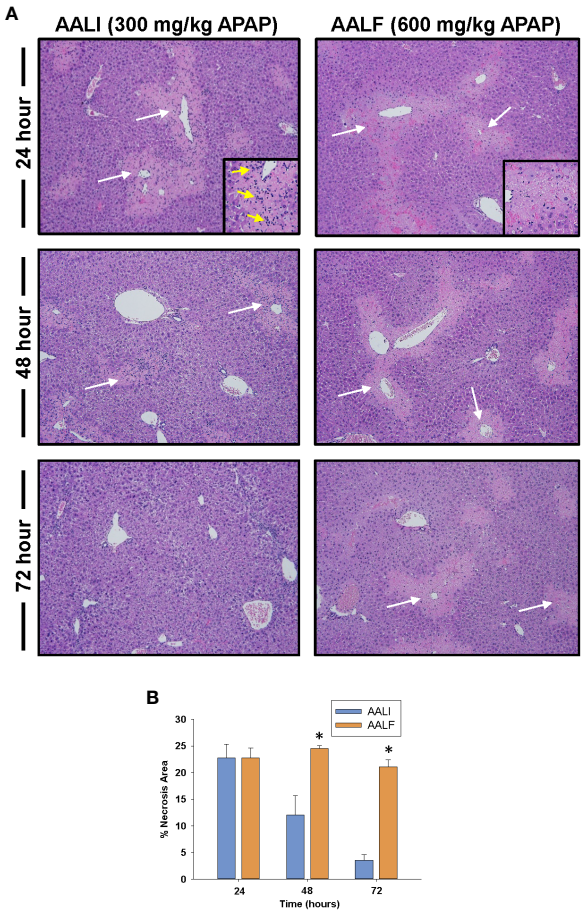

FIGURE 1
Liver injury and inflammation in APAP-treated mice. Mice were treated with either 300 mg/kg APAP (AALI) or 600 mg/kg APAP (AALF) for the indicated time. **(A)** Photomicrographs of H&E-stained liver sections. White arrows indicate areas of necrosis occurring in centrilobular regions. Higher power image of necrotic region in inset in 24 hour images. Arrows indicate evidence of inflammatory infiltrates. **(B)** Area of necrosis was quantified in sections of liver. *Significantly different from mice treated with 300 mg/kg APAP. All data are expressed as mean ± SEM; n = 5-10 mice per group.

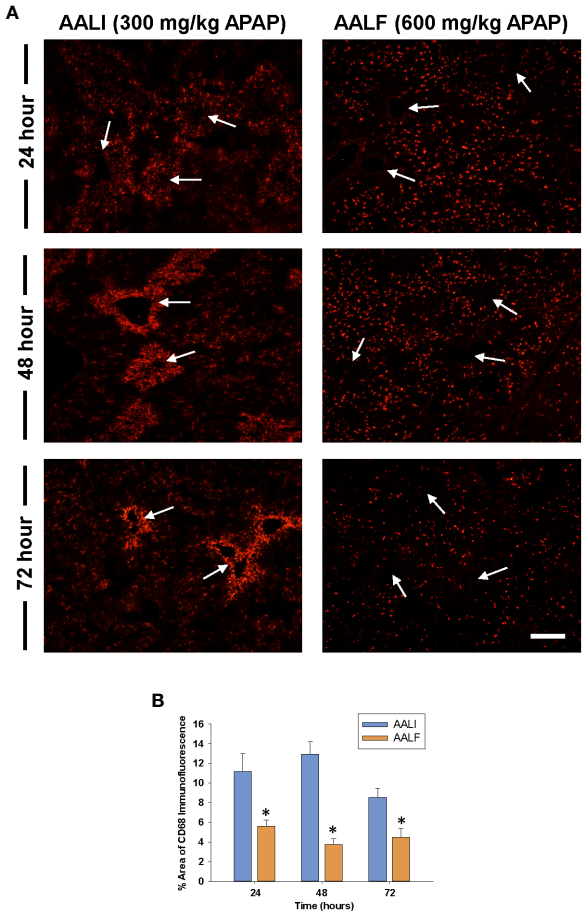

FIGURE 2
Accumulation of myeloid cells in the livers of mice treated with APAP. Mice were treated with either 300 mg/kg APAP (AALI) or 600 mg/kg APAP (AALF)for the indicated time. **(A)** Photomicrographs of CD68 immunofluorescent staining in liver sections. Positive staining appears red. Arrows indicate centrilobular regions. **(B)** The area of CD68 immunofluorescent staining was quantified in sections of liver. *Significantly different from mice treated with 300 mg/kg APAP. Data are expressed as mean ± SEM; n = 5 mice per group.

10.3389/fimmu.2023.1303921

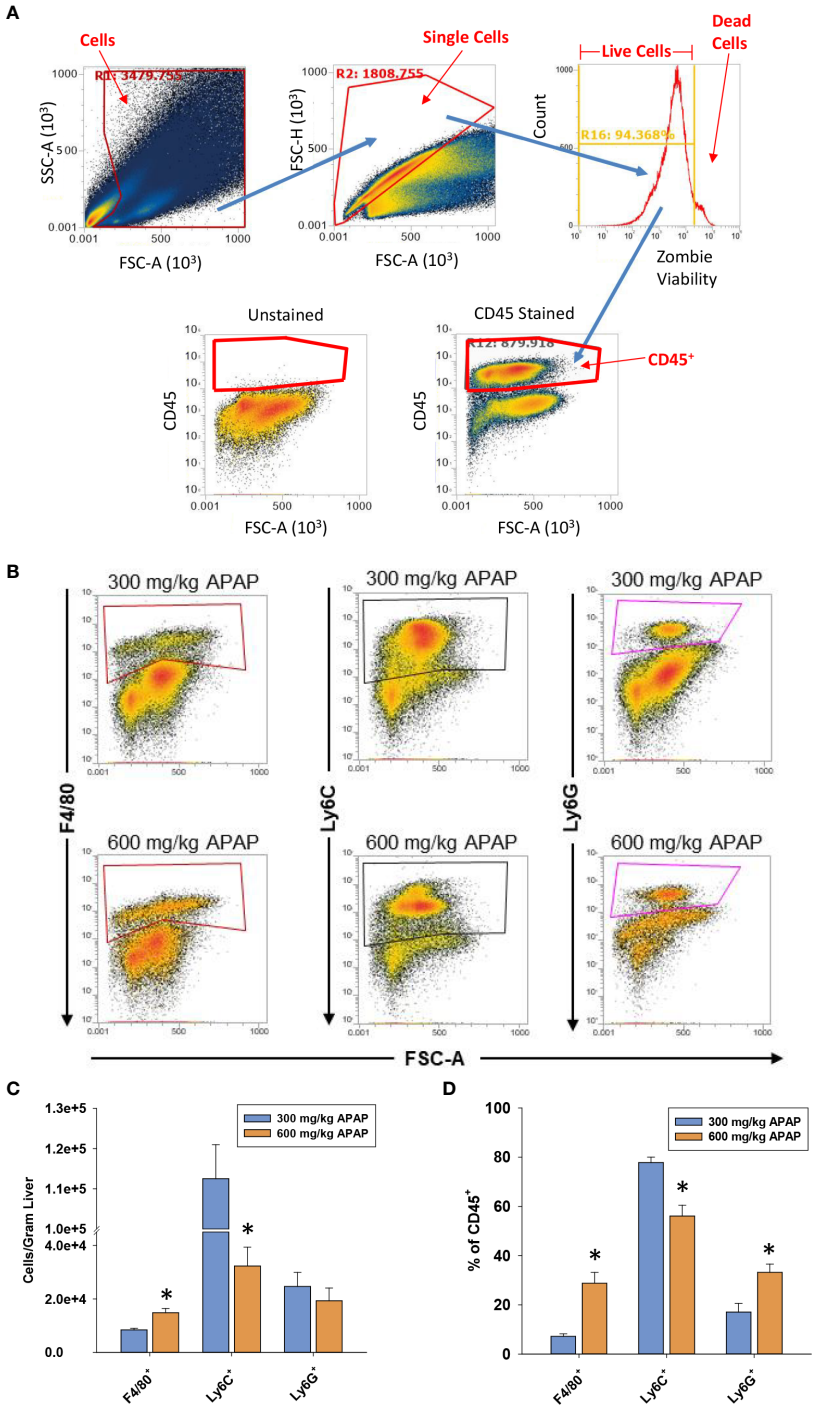

FIGURE 3
Hepatic myeloid cell accumulation in APAP-treated mice. Mice were treated with either 300 mg/kg APAP (AALI) or 600 mg/kg APAP (AALF)for the indicated time. **(A)** Gating for flow cytometry. **(B)** At 24 hours after APAP treatment, flow cytometry was used to detect F4/80$^+$, Ly6C$^+$, and Ly6G$^+$ cells in the liver. Boxes indicate the positive gate. **(C)** Absolute cell counts and the percentage of each myeloid cell population within the larger CD45$^+$ population by flow cytometry. *Significantly different from mice treated with 300 mg/kg APAP. All data are expressed as mean ± SEM; n = 5-10 mice per group.

levels were quantified. As shown in Figure 4C, IL-10 mRNA levels were greater in F4/80$^+$ cells isolated from AALF mice but were not different between Ly6C$^+$ cells isolated AALI and AALF mice (Figure 4C). We next confirmed these findings by using IL-10 reporter mice that express green fluorescent protein (GFP) under control of the IL-10 promoter. As shown in Figures 4D, E, greater numbers of GFP-expressing F4/80$^+$ cells were detected in the livers of IL-10 reporter mice with AALF.

Next, we determined whether other immune cell types express IL-10 in the livers of mice with AALF. As shown in Figure 5, IL-10

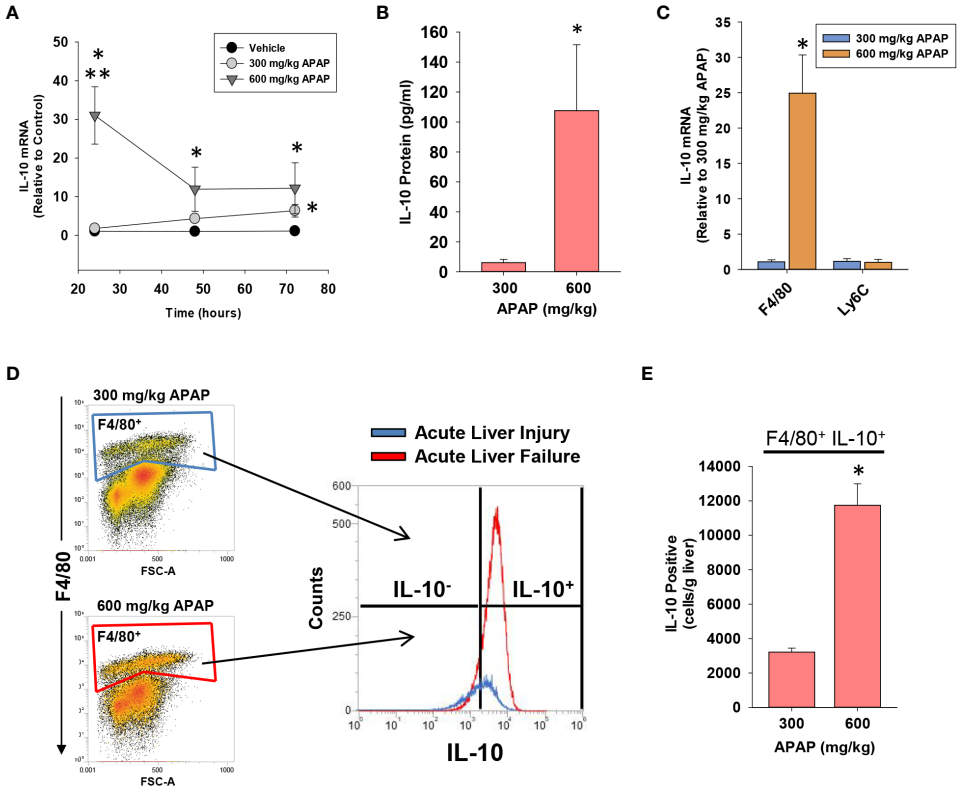

FIGURE 4
Hepatic and systemic levels of IL-10 in APAP-treated mice. Mice were treated with either 300 mg/kg APAP (AALI) or 600 mg/kg APAP (AALF). **(A)** At the indicated time, IL-10 mRNA levels were measured in the liver. **(B)** IL-10 protein was measured in serum at 72 hours after APAP treatment. **(C)** F4/80$^+$ and Ly6C$^+$ myeloid cells were isolated from the liver at 24 hours after treatment of mice with either 300 mg/kg APAP (AALI) or 600 mg/kg APAP (AALF), and IL-10 mRNA levels were measured. **(D)** Nonparenchymal cells were isolated from the livers of IL-10 reporter mice treated 24 hours earlier with 300 mg/kg APAP (AALI) or 600 mg/kg APAP (AALF). Flow cytometry was used to identify IL-10 expressing F4/80$^+$ cells. Gate for F4/80$^+$ cells indicated in the density plots. Representative histogram of IL-10 expression (i.e., GFP$^+$) in F4/80$^+$ cells. **(E)** Quantification of the number of F4/80$^+$ cells expressing IL-10 in the liver from flow cytometry. *Significantly different from mice treated with 300 mg/kg APAP. Data are expressed as mean ± SEM; n = 4-5 mice per group.

(GFP) was detected in all immune cell types evaluated. Compared to other immune cell populations, however, a larger fraction of NKT cells, NK cells, and F4/80$^+$ cells were positive for IL-10 in AALF mice (Figure 5C).

Immunophenotyping of IL-10$^+$ F4/80$^+$ cells in mice with AALF

Clinical studies have demonstrated that circulating monocytes express markers of MDSCs in ALF patients with the worst outcomes (11, 33). Therefore, we determined whether the hepatic, IL-10-expressing F4/80$^+$ cells (i.e., GFP$^+$) similarly expressed markers of MDSCs in AALF mice. Immunophenotyping by flow cytometry revealed that these cells expressed CD11b, PD-L1, Cx3Cr1, and Axl consistent with an MDSC-like phenotype (Figures 6A, B). Levels of additional markers commonly associated with MDSCs, however, including MARCO, Ly6C, Ccr2, and Ly6G, were only detected in a small percentage of IL-10-expressing F4/80$^+$ cells (Figures 6A, B).

Moore and colleagues previously performed gene array analysis on purified peripheral blood monocytes from patients with APAP-induced ALF (27). The analysis included 6 patients with AALF that spontaneously survived and 6 patients with AALF that either died or received a liver transplant (27). We reanalyzed this publicly available data set to determine whether IL-10 mRNA levels and levels of other MDSC-associated genes were differentially expressed between these two ALF patient populations.

As shown in Supplemental Table 1, 154 mRNAs were increased, while 37 mRNAs were decreased in blood monocytes from ALF patients that died when compared to those that survived. Many of these mRNAs, including IL-10 (indicated with a green arrow), have been associated with MDSCs (Figure 6C) (34, 35). Next, Ingenuity Pathway Analysis was used to identify potential upstream regulators that predict the observed mRNA changes. IPA identified several regulators as potential drivers of the observed transcriptional changes occurring in ALF patients that died (Figure 6D). Interestingly, many of these regulators have been linked to the differentiation, expansion, and/or activation of MDSCs (Figure 6D; MDSC drivers highlighted in red) (34, 35).

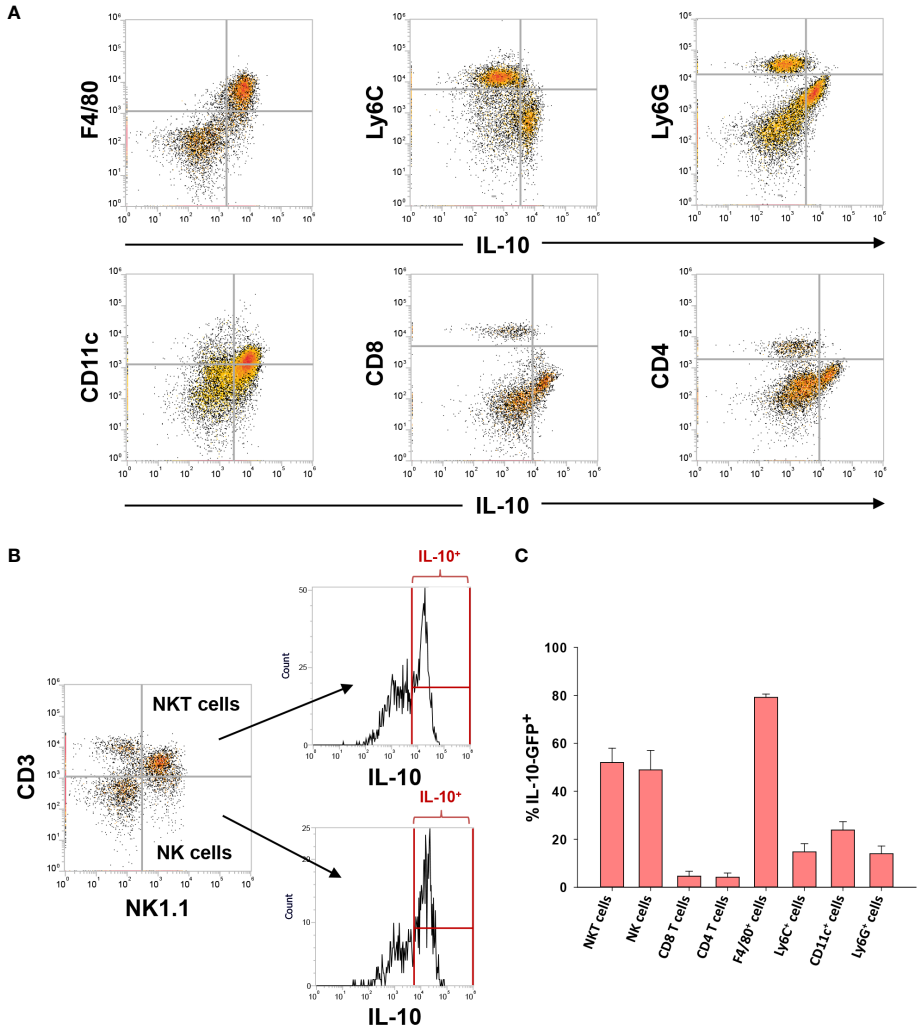

FIGURE 5
IL-10 expressing (GFP$^+$) cells in the livers of mice with AALF. **(A, B)** Representative dot plots of the indicated cell types expressing IL-10. **(C)** Percentage of each immune cell type expressing IL-10 in AALF.

Modulation of IL-10 levels impact myeloid cell accumulation and necrotic lesion size in mice treated with APAP

Our findings indicate that myeloid cell accumulation in the liver is disrupted in mice with AALF (Figures 1-3). Because of the potent immune inhibitory properties of IL-10, we tested the hypothesis that IL-10 contributes to this defect. To examine this, we utilized a loss of function approach (i.e., IL-10 neutralization in AALF mice) and a gain of function approach (i.e., injection of recombinant IL-10 into AALI mice). Prior studies demonstrated that IL-10 knockout mice develop markedly greater liver injury after APAP overdose (7). Accordingly, to avoid impacts on APAP-induced liver injury, we treated mice with IL-10 neutralizing antibody or recombinant IL-10 protein beginning at 24 hours after APAP treatment, a time where hepatocyte injury is complete (i.e., no additional increase in necrosis; Figure 1) and levels of hepatic glutathione, which detoxify the toxic APAP metabolite, N-acetyl-*p*-benzoquinone imine (NAPQI), have been restored (36).

Treatment of AALF mice with IL-10 neutralizing antibody increased mRNA levels of the pro-inflammatory cytokines, Ccl2, TNF-α, and Cxcl1 when compared to AALF mice treated with isotype control, demonstrating the efficacy of the IL-10 neutralizing antibody (Figures 7A–C). We also evaluated the impact of IL-10 neutralization on the levels of urokinase plasminogen activator (uPA) which converts the zymogen plasminogen into the fibrinolytic enzyme, plasmin. The rationale for this is that we demonstrated previously that inhibition of plasmin activity reduced monocyte-dependent clearance of dead cells from the livers of AALI mice and it is conceivable that diminished levels of uPA may contribute to the defective clearance of dead cell debris (18). As shown in Figure 7D, neutralization of IL-10 increased uPA mRNA levels in the livers of AALF mice. IL-10 neutralizing antibody, however, did not affect ALT activity in the serum (Figure 7E) or the number of PCNA positive cells in the liver (Figures 7F–H). In AALF mice treated with isotype control antibody, CD68$^+$ myeloid cells were distributed throughout the liver lobule similar to our earlier findings (Figure 8A). Treatment of

10.3389/fimmu.2023.1303921

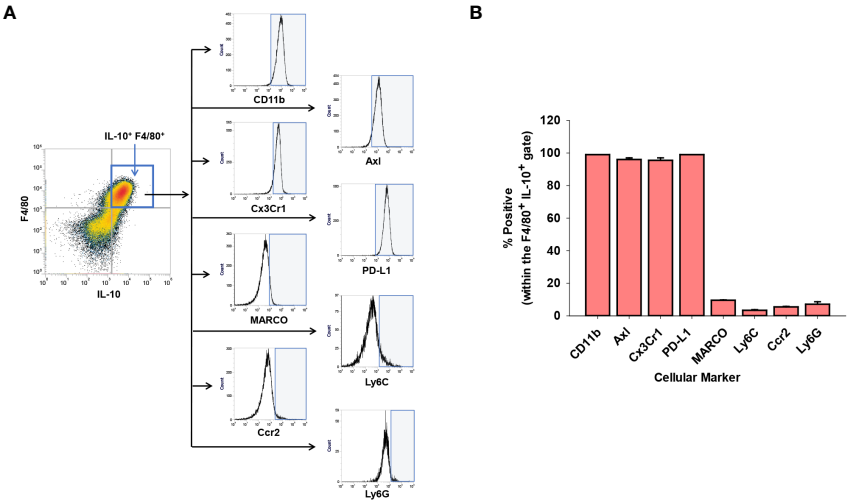

C

Gene	Fold Change	P value
MMP8	5.74	0.0077
IL1R2	5.31	0.0036
ADGRG3	4.08	0.0002
LRG1	2.46	0.0026
IL10	2.43	0.0373
BACH1	2.39	0.0416
ARG1	2.36	0.0295
CXCR1	2.3	0.0269
PPARG	2.29	0.0098
ID1	2.21	0.0009
PIM1	2.21	0.0047
FAM20C	2.13	0.0199
ORM1	2.1	0.0132
SLAMF1	2.09	0.0207
HIST1H2AK	2.08	0.0179
PAG1	2.07	0.0215
MSRA	2.06	0.0126
CEACAM1	2.05	0.0106
PCNA	2.02	0.0274
LRRC8C	2.01	0.0131

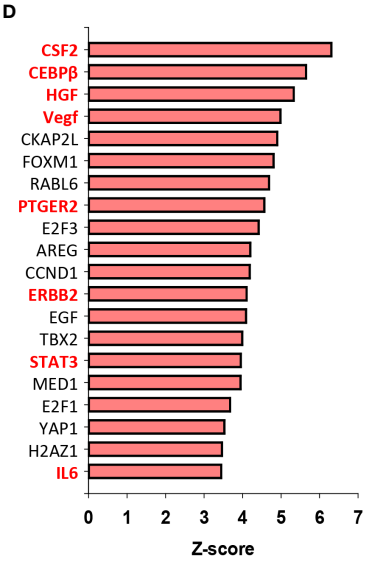

FIGURE 6
Immune suppressive phenotype of myeloid cells in APAP induced ALF. **(A)** Mice were treated with 600 mg/kg APAP. After 24 hours, flow cytometry was used to detect IL-10 expressing F4/80$^+$ cells, indicated by the blue box. Representative histograms of IL-10$^+$ F4/80$^+$ cells expressing the indicated marker (x-axis). Positive staining indicated by the blue shaded box. **(B)** Quantification of the flow cytometry in **(A)** Data are expressed as mean ± SEM; n = 4 mice per group. **(C)** Analysis of GEO dataset accession number GSE8075, containing gene array analysis of monocytes isolated from patients with APAP-induced ALF that survived and patients with APAP induced ALF that died. Fold change represents ALF patients that died relative to those that survived (e.g., IL-10 mRNA levels 2.43-fold higher in patients that died; indicated with a green arrow and highlighted green). **(D)** Ingenuity pathway analysis was used to identify upstream regulators in the GSE8075 GEO dataset. Regulators associated with MDSCs are highlighted in red. (n=6 patient samples per group).

these mice with IL-10 neutralizing antibody, however, increased the numbers of CD68$^+$ myeloid cells with a greater concentration in centrilobular regions (Figures 8A, C). Notably, the pattern of CD68$^+$ immunostaining observed in these mice resembled that in AALI (Figures 2A, 8B). Treatment of AALI mice with recombinant IL-10, on the other hand, reduced the numbers of CD68$^+$ cells particularly in centrilobular regions (Figures 8B, D) producing a pattern of CD68 immunostaining similar to that observed in AALF mice (Figures 2A, 8A).

Next, because recruited monocytes clear dead cell debris from the APAP-injured liver, we determined whether increasing or decreasing IL-10 levels impacted lesion size. As in Figure 8, the indicated treatments (i.e., antibody or recombinant protein) were initiated at 24 hours, a time when peak injury had occurred (Figure 1B). Therefore, differences in the area of necrosis beyond 24 hours would result from changes to the mechanisms that clear dead cell debris. In AALF mice, neutralization of IL-10 increased histological evidence of inflammatory cells within the necrotic foci (Figures 9A, B) consistent with the CD68 immunostaining (Figure 8A). Further, IL-10 neutralizing antibody reduced the area of necrosis compared to isotype control treated mice (Figure 9C), suggesting that an increase in number of myeloid cells (Figure 8) resulted in an increase in the clearance of dead cell debris. Similar to these findings, pharmacological elevation of IL-10 in AALI mice decreased evidence of inflammatory cells within the necrotic lesions while increasing the area of necrosis (Figures 9D–F).

10.3389/fimmu.2023.1303921

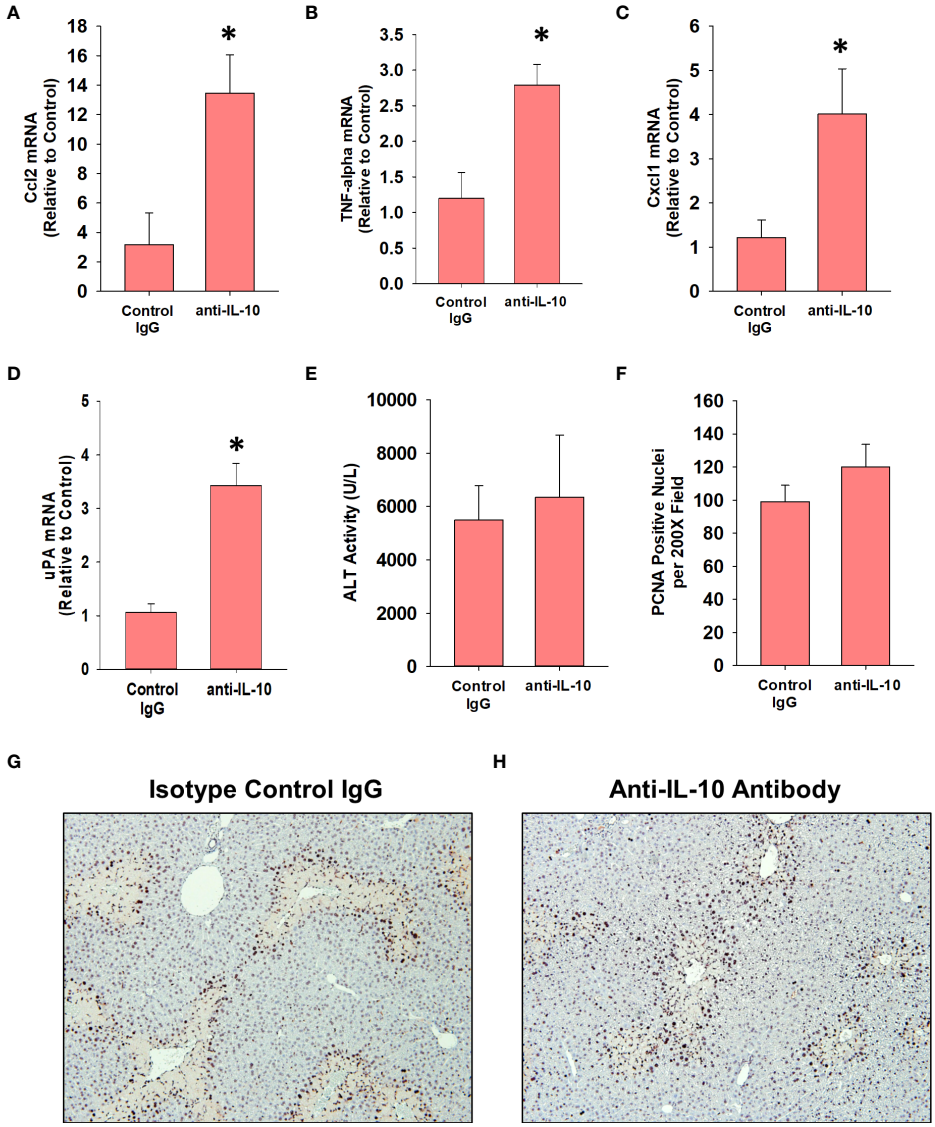

FIGURE 7
Impact of IL-10 neutralization in mice with APAP-induced ALF. Mice were treated with 600 mg/kg APAP (AALF) followed by treatment with control IgG or anti-IL-10 antibody 24 hours later. Livers were collected 72 hours after APAP treatment. **(A-D)** mRNA levels of the indicated protein were quantified in the liver by real-time PCR. **(E)** Serum activity of ALT. **(F)** The number of PCNA positive cells was quantified in sections of liver. Representative photomicrographs of immunohistochemistry staining for PCNA in liver sections from AALF mice treated with **(G)** isotype control IgG or **(H)** anti-IL-10 antibody. Positive staining appears dark brown. *Significantly different from mice treated with 600 mg/kg APAP and control IgG. All data are expressed as mean ± SEM; n = 5 mice per group.

Discussion

Toxicant-induced liver injury stimulates the synthesis and release of chemokines that recruit immune cells, including monocytes, to the liver. As the injury resolves, IL-10 is released to terminate the inflammatory response thereby preventing immune-mediated exacerbation of the injury. Evidence in support of this has demonstrated that deficiency of IL-10 (i.e., IL-10 knockout mice) exacerbates proinflammatory cytokine production and liver injury in APAP treated mice (7). More recently, it was reported that treatment of AALI mice with exogenous IL-10, beginning at 2 hours after APAP treatment, reduces liver injury (9). While these findings have driven current dogma that IL-10 is protective in experimental liver injury, they contrast with clinical findings where high levels of IL-10 are an independent predictor of a poor outcome in ALF patients (10). The mechanistic basis for this paradoxical association is not fully known, however, it has been proposed that high levels of IL-10 may prevent the clearance of nosocomial infections leading to sepsis (10). Investigations into this possibility, however, have been unable to demonstrate an association between high levels of IL-10 and increased risk of sepsis, suggesting that IL-10 impacts additional processes critical for recovery from ALF (10). Our current study provides an alternative explanation for these findings and reveals that high levels of IL-10 interfere with hepatic monocyte recruitment.

In mice with AALI, $CD68^+$ myeloid cells began to concentrate within centrilobular regions of the liver where APAP produces

10.3389/fimmu.2023.1303921

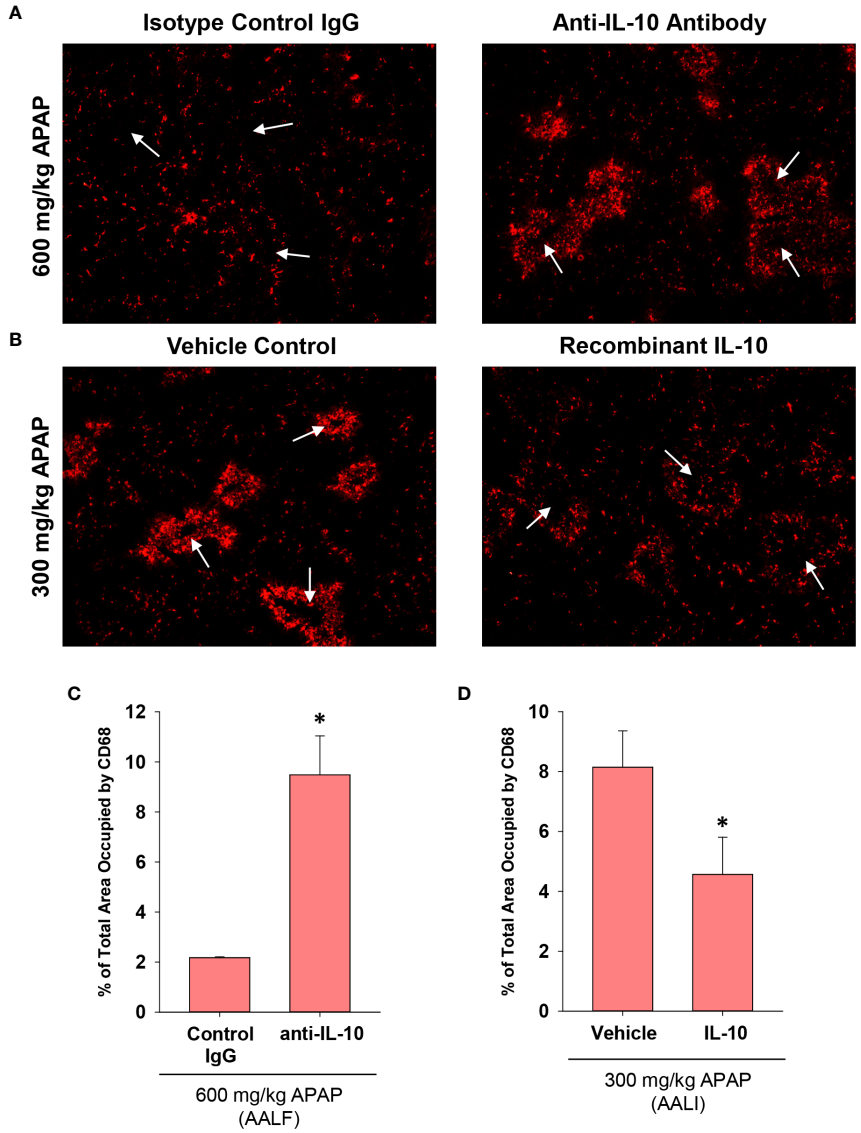

FIGURE 8
Impact of IL-10 on inflammation in mice treated with APAP. **(A)** Mice were treated with 600 mg/kg APAP (AALF) followed by treatment with control IgG or anti-IL-10 antibody 24 hours later. Livers were collected 72 hours after APAP treatment. CD68 was detected by immunofluorescence (red staining) in sections of liver. Arrows indicate centrilobular regions. **(B)** Mice were treated with 300 mg/kg APAP (AALI) followed by treatment with either vehicle or 5 mg recombinant IL-10 24 hours later. Livers were collected 48 hours after APAP treatment. CD68 was detected by immunofluorescence (red staining) in sections of liver. Arrows indicate centrilobular regions. **(A, B)** Representative photomicrographs from an n = 5 mice per group. **(C, D)** The area of CD68 staining was quantified in whole liver sections. n = 5 mice per group. *Significantly different at $p<0.05$.

injury (Figures 1, 2). Coincident with the accumulation of these cells, dead cell debris was cleared from the liver (Figures 1, 2) (17). By contrast, in mice with AALF, the numbers of $CD68^+$ myeloid cells were markedly lower at all time-points examined, and these cells were largely restricted to uninjured regions (Figure 2). Immunophenotyping of the hepatic myeloid cell populations demonstrated a reduction in the numbers of $Ly6C^+$ monocytes in the livers of AALF mice, indicating a defect in the recruitment of these cells from the systemic circulation (Figure 3). It was previously reported that manipulations which prevent the hepatic recruitment of monocytes (i.e., Ccr2 knockout mice) inhibit the clearance of necrotic cell debris from the APAP-injured liver (16, 17, 32). Consistent with these findings, our studies demonstrated that a paucity of $Ly6C^+$ monocytes in the livers of AALF mice coincided with a persistence of dead cell debris (Figures 1, 2). Collectively, these findings suggest that a failure of monocyte recruitment to the liver during AALF may prevent the clearance of necrotic cells. While it could be argued that the persistence of necrosis resulted from ongoing hepatocyte death that was compensated for by hepatocyte proliferation, this is unlikely in light of findings by Bhushan and colleagues demonstrating that hepatocyte proliferation is also markedly reduced in mice with AALF (20). Therefore, the persistence of the necrotic foci most likely resulted from a failure in the mechanisms controlling the clearance of dead cells. It would be difficult to assess whether there is a similar reduction in the hepatic accumulation of monocytes in the livers

10.3389/fimmu.2023.1303921

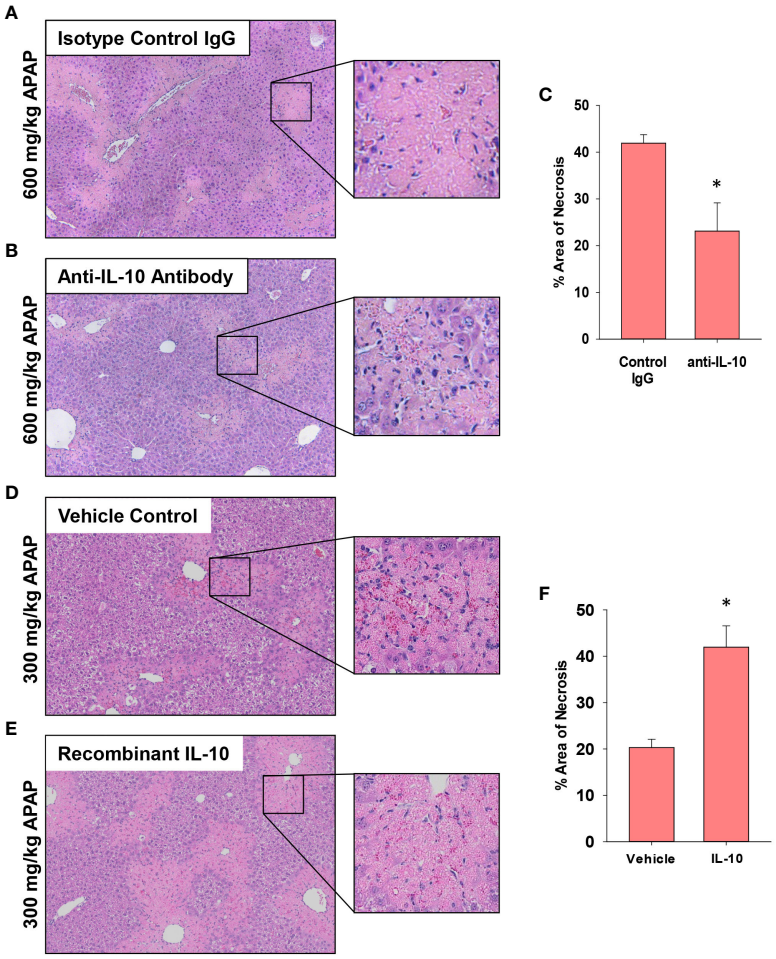

FIGURE 9
Impact of IL-10 on liver histology in mice treated with APAP. **(A–C)** Mice were treated with 600 mg/kg APAP (AALF) followed by treatment with control IgG or anti-IL-10 antibody 24 hours later. Livers were collected 72 hours after APAP treatment. **(D–F)** Mice were treated with 300 mg/kg APAP (AALI) followed by treatment with vehicle or 5 mg recombinant IL-10 24 hours later. Livers were collected 48 hours after APAP treatment. Representative photomicrographs of hematoxylin and eosin-stained liver sections from mice treated with **(A)** 600 mg/kg APAP (AALF) and control IgG, **(B)** 600 mg/kg APAP (AALF) and anti-IL-10 antibody, **(D)** 300 mg/kg APAP (AALI) and vehicle or **(E)** 300 mg/kg APAP (AALI) and recombinant IL-10. **(C, F)** The area of necrosis was quantified in the indicated liver sections. n = 5 mice per group. *Significantly different at $p<0.05$.

of patients with ALF. Although, it has been reported that ALF patients with the worst outcomes have reduced numbers of circulating monocytes when compared to ALF patients that recover (27).

Mechanistically, our studies indicate that early induction of IL-10 (Figure 4A) contributes to the defect in hepatic monocyte recruitment in AALF mice. In support of this, treatment of AALF mice with IL-10 neutralizing antibody increased monocyte numbers in the liver (Figure 8A), which coincided with a decrease in the area of necrosis, suggesting that the recovery of monocyte recruitment restored, in part, dead cell clearance (Figures 9A, B). The reduction in necrotic area in AALF mice treated with IL-10 neutralizing antibody cannot be attributed to a decrease in the severity of liver injury, as the antibody treatments were not initiated until 24 hours after APAP overdose, a time where hepatocyte injury is complete (i.e., no additional increase in necrosis; Figure 1) and levels of hepatic glutathione, which detoxify APAP, have been fully restored (36). Moreover, as mentioned above, a complete loss of IL-10 (i.e., IL-10 knockout mice) enhances rather than reduces liver injury (7). In further confirmation of the impact of IL-10 on liver repair, we demonstrated that pharmacological elevation of IL-10 in AALI mice, beginning at 24 hours after APAP treatment, reduced hepatic monocyte recruitment while increasing the area of necrosis (Figures 8, 9). These findings indicate that high levels of IL-10 prevent the recruitment of monocytes to the liver which inhibits the clearance of dead cells. As discussed earlier, it was recently reported that treatment of AALI mice with exogenous IL-10, early after APAP overdose (i.e., 2 hours), attenuated liver injury. While this approach might similarly reduce liver injury in APAP overdose patients, it would require administration soon after the overdose which is a time where NAC is well established to be safe and highly efficacious. Moreover, our studies indicate that initiation of IL-10 therapy, after liver injury has occurred, could disrupt liver repair potentially resulting in a worse outcome.

Despite the reduction in necrotic area, AALF mice treated with either IL-10 neutralizing antibody or isotype control antibody were

similarly moribund by 72 hours and were euthanized, indicating that the restoration of monocyte recruitment alone was insufficient to fully reverse the ALF pathology. One possible reason for this may be that neutralization of IL-10 failed to restore hepatocyte proliferation in AALF mice (Figure 7E). As discussed, Bhushan and colleagues reported previously that hepatocyte proliferation is markedly reduced in mice with AALF, and that this is reversed by pharmacological blockade of GSK-3β (37). Restoration of hepatocyte proliferation through GSK-3β inhibition, however, did not recover dead cell clearance and similar to our studies, was unable to improve survival (37). Therefore, it is possible that restoration of hepatocyte proliferation along with dead cell clearance mechanisms may be needed to promote a full recovery of liver function in ALF.

The mechanism by which neutralization of IL-10 enhanced monocyte recruitment to the liver was not fully uncovered from our studies, however, it may involve changes to the levels of the monocyte chemokine, Ccl2 or the fibrinolytic enzyme, uPA. Ccl2 is released after liver injury and binds to the Ccr2 receptor on circulating monocytes which triggers their recruitment towards sites of injury (16, 17). In our studies, neutralization of IL-10 increased hepatic Ccl2 levels (Figure 6A) which may have contributed to the enhanced recruitment of myeloid cells to the liver. A second mechanism by which IL-10 may prevent dead cell clearance from the liver is through inhibition of fibrinolysis. We previously showed that the fibrinolytic enzyme, plasmin, is critical for the clearance of dead cells from the livers of mice with AALI (18). The protease uPA cleaves the zymogen plasminogen to generate plasmin. Interestingly, prior studies demonstrated that IL-10 reduces uPA levels in cultured monocytes (38). Consistent with this *in vitro* finding, our studies show that neutralization of IL-10 in mice with AALF increased uPA levels suggesting that IL-10 may impact dead cell clearance by interfering with fibrinolysis. Additional studies are needed, however, to fully investigate these possibilities.

Increased numbers of circulating MDSCs have been reported in patients with ALF. Our studies complement these findings and indicate further that these cells are a potential source of IL-10 (Figure 5C). Notably, levels of IL-10 were greatest in circulating monocytes from patients with ALF that died or were referred for a liver transplant. Moreover, several mRNAs were increased in these cells that are associated with MDSCs, and ingenuity pathway analysis identified a number of upstream regulators that could contribute to the generation of these cells. Because of these findings, we determined whether the IL-10-expressing, F4/80$^+$ macrophages in the livers of mice with AALF also expressed markers of MDSCs. Interestingly, these cells expressed several proteins frequently associated MDSCs, including PD-L1, CD11b, Axl, and Cx3Cr1 (Figure 5) (35). They did not, however, express Ly6C, a key marker associated with monocytic MDSCs (35). Therefore, the IL-10 producing cells are either Kupffer cells or may have arisen from circulating MDSCs. Studies have shown that MDSCs recruited to the tumor microenvironment mature into tumor-associated macrophages that lose expression of Ly6C, gain expression of F4/80 and Cx3Cr1, and maintain expression of IL-10 and PD-L1. Although additional studies are needed to investigate this, it is possible that in AALF, circulating MDSCs accumulate in the liver and mature into F4/80$^+$ macrophages with an immune suppressive phenotype, similar to what occurs in solid tumors. Consistent with this possibility, our studies demonstrated that there were nearly twice as many F4/80$^+$ myeloid cells in the livers of mice with AALF when compared to AALI mice (Figure 3C). Additional studies are needed, however, to better define the source of these immune suppressive cells. Similarly, additional follow up is needed to evaluate the importance of NKT and NK cells as a source of IL-10 in AALF, as our studies show that a high percentage of these cells produce IL-10 in the liver during AALF (Figure 5).

Collectively, our findings demonstrate that IL-10 dysregulation is effectively recapitulated in mice treated with a high dose APAP that produces ALF. As such, this experimental setting provides a novel platform to interrogate mechanisms of immune dysregulation in ALF and to identify new therapeutic interventions. Further, by using this approach, our studies identified IL-10 as a central player in monocyte dysregulation in ALF, challenging the long-held belief that IL-10 is only hepatoprotective in APAP-induced ALF and providing a mechanism to explain the paradoxical association between high levels of IL-10 and poor outcome in ALF patients.

Data availability statement

The datasets presented in this study can be found in online repositories. The names of the repository/repositories and accession number(s) can be found in the article/Supplementary Material.

Ethics statement

Ethical approval was not required for the study involving humans in accordance with the local legislation and institutional requirements. Written informed consent to participate in this study was not required from the participants or the participants' legal guardians/next of kin in accordance with the national legislation and the institutional requirements. The animal study was approved by Institutional Animal Care and Use Committee, Michigan State University. The study was conducted in accordance with the local legislation and institutional requirements.

Author contributions

KR: Conceptualization, Data curation, Formal analysis, Investigation, Writing – review & editing. JS: Conceptualization, Data curation, Formal analysis, Investigation, Writing – review & editing. AP: Conceptualization, Data curation, Formal analysis, Investigation, Writing – review & editing. RF: Data curation, Formal analysis, Investigation, Writing – review & editing. RK: Data curation, Formal analysis, Investigation, Writing – review & editing. CR: Data curation, Formal analysis, Investigation, Supervision, Writing – review & editing. JL: Conceptualization, Data curation, Formal analysis, Funding acquisition, Investigation,

Supervision, Writing – review & editing. BC: Conceptualization, Data curation, Formal analysis, Funding acquisition, Investigation, Supervision, Writing – original draft.

Funding

The author(s) declare financial support was received for the research, authorship, and/or publication of this article. Supported by NIH Grants DK103895 to BC, DK105099 and DK120289 to JL and DK135649 to BC and JL. KR and JS were supported by NIEHS training grant, ES024966. JL was also supported by the USDA National Institute of Food and Agriculture.

Conflict of interest

The authors declare that the research was conducted in the absence of any commercial or financial relationships that could be construed as a potential conflict of interest.

The author(s) declared that they were an editorial board member of Frontiers, at the time of submission. This had no impact on the peer review process and the final decision.

Publisher's note

Supplementary material

The Supplementary Material for this article can be found online at: https://www.frontiersin.org/articles/10.3389/fimmu.2023.1303921/full#supplementary-material

References

1. Lee WM, Squires RH, Nyberg SL, Doo E, Hoofnagle JH. Acute liver failure: summary of A workshop. *Hepatology* (2008) 47:1401–15. doi: 10.1002/hep.22177

2. Bernal W, Wendon J. Acute liver failure. *N Engl J Med* (2013) 369:2525–34. doi: 10.1056/NEJMra1208937

3. Smilkstein MJ, Knapp GL, Kulig KW, Rumack BH. Efficacy of oral N-acetylcysteine in the treatment of acetaminophen overdose. Analysis of the national multicenter study, (1976 to 1985). *N Engl J Med* (1988) 319:1557–62. doi: 10.1056/NEJM198812153192401

4. Saito C, Zwingmann C, Jaeschke H. Novel mechanisms of protection against acetaminophen hepatotoxicity in mice by glutathione and N-acetylcysteine. *Hepatology* (2010) 51:246–54. doi: 10.1002/hep.23267

5. Huebener P, Pradere JP, Hernandez C, Gwak GY, Caviglia JM, Mu X, et al. The hmgb1/rage axis triggers neutrophil-mediated injury amplification following necrosis. *J Clin Invest* (2015) 125:539–50. doi: 10.1172/JCI76887

6. Nguyen NT, Umbaugh DS, Smith S, Adelusi OB, Sanchez-Guerrero G, Ramachandran A, et al. Dose-dependent pleiotropic role of neutrophils during acetaminophen-induced liver injury in male and female mice. *Arch Toxicol* (2023) 97:1397–412. doi: 10.1007/s00204-023-03478-4

7. Bourdi M, Masubuchi Y, Reilly TP, Amouzadeh HR, Martin JL, George JW, et al. Protection against acetaminophen-induced liver injury and lethality by interleukin 10: role of inducible nitric oxide synthase. *Hepatology* (2002) 35:289–98. doi: 10.1053/jhep.2002.30956

8. Bourdi M, Eiras DP, Holt MP, Webster MR, Reilly TP, Welch KD, et al. Role of il-6 in an il-10 and il-4 double knockout mouse model uniquely susceptible to acetaminophen-induced liver injury. *Chem Res Toxicol* (2007) 20:208–16. doi: 10.1021/tx060228l

9. Guo C, Liu W, Liu Z, Cai J, Yu X, Wang H, et al. Scavenger receptor A is A major homeostatic regulator that restrains drug-induced liver injury. *Hepatology* (2023) 78:45–57. doi: 10.1097/HEP.0000000000000044

10. Berry PA, Antoniades CG, Hussain MJ, Mcphail MJ, Bernal W, Vergani D, et al. Admission levels and early changes in serum interleukin-10 are predictive of poor outcome in acute liver failure and decompensated cirrhosis. *Liver Int* (2010) 30:733–40. doi: 10.1111/j.1478-3231.2010.02219.x

11. Triantafyllou E, Gudd CL, Mawhin MA, Husbyn HC, Trovato FM, Siggins MK, et al. Pd-1 blockade improves kupffer cell bacterial clearance in acute liver injury. *J Clin Invest* (2021) 131(4):e140196. doi: 10.1172/JCI140196

12. Woolbright BL, Nguyen NT, Mcgill MR, Sharpe MR, Curry SC, Jaeschke H. Generation of pro-and anti-inflammatory mediators after acetaminophen overdose in surviving and non-surviving patients. *Toxicol Lett* (2022) 367:59–66. doi: 10.1016/j.toxlet.2022.07.813

13. Antoniades CG, Berry PA, Wendon JA, Vergani D. The importance of immune dysfunction in determining outcome in acute liver failure. *J Hepatol* (2008) 49:845–61. doi: 10.1016/j.jhep.2008.08.009

14. Antoniades CG, Khamri W, Abeles RD, Taams LS, Triantafyllou E, Possamai LA, et al. Secretory leukocyte protease inhibitor: A pivotal mediator of anti-inflammatory responses in acetaminophen-induced acute liver failure. *Hepatology* (2014) 59:1564–76. doi: 10.1002/hep.26933

15. Triantafyllou E, Pop OT, Possamai LA, Wilhelm A, Liaskou E, Singanayagam A, et al. Mertk expressing hepatic macrophages promote the resolution of inflammation in acute liver failure. *Gut* (2018) 67:333–47. doi: 10.1136/gutjnl-2016-313615

16. Dambach DM, Watson LM, Gray KR, Durham SK, Laskin DL. Role of ccr2 in macrophage migration into the liver during acetaminophen-induced hepatotoxicity in the mouse. *Hepatology* (2002) 35:1093–103. doi: 10.1053/jhep.2002.33162

17. Holt MP, Cheng L, Ju C. Identification and characterization of infiltrating macrophages in acetaminophen-induced liver injury. *J Leukoc Biol* (2008) 84:1410–21. doi: 10.1189/jlb.0308173

18. Roth K, Strickland J, Joshi N, Deng M, Kennedy RC, Rockwell CE, et al. Dichotomous role of plasmin in regulation of macrophage function after acetaminophen overdose. *Am J Pathol* (2019) 189:1986–2001. doi: 10.1016/j.ajpath.2019.07.003

19. Shah N, Montes De Oca M, Jover-Cobos M, Tanamoto K, Muroi M, Sugiyama K, et al. Role of toll-like receptor 4 in mediating multiorgan dysfunction in mice with acetaminophen induced acute liver failure. *Liver Transpl* (2013) 19:751–61. doi: 10.1002/lt.23655

20. Bhushan B, Walesky C, Manley M, Gallagher T, Borude P, Edwards G, et al. Pro-regenerative signaling after acetaminophen-induced acute liver injury in mice identified using A novel incremental dose model. *Am J Pathol* (2014) 184:3013–25. doi: 10.1016/j.ajpath.2014.07.019

21. Akakpo JY, Ramachandran A, Orhan H, Curry SC, Rumack BH, Jaeschke H. 4-methylpyrazole protects against acetaminophen-induced acute kidney injury. *Toxicol Appl Pharmacol* (2020) 409:115317. doi: 10.1016/j.taap.2020.115317

22. Groeneveld DJ, Poole LG, Bouck EG, Schulte A, Wei Z, Williams KJ, et al. Robust coagulation activation and coagulopathy in mice with experimental acetaminophen-induced liver failure. *J Thromb Haemost* (2023) 21(9):2430–40. doi: 10.1016/j.jtha.2023.03.040

23. Mochizuki A, Pace A, Rockwell CE, Roth KJ, Chow A, O'brien KM, et al. Hepatic stellate cells orchestrate clearance of necrotic cells in A hypoxia-inducible factor-1α-dependent manner by modulating macrophage phenotype in mice. *J Immunol* (2014) 192:3847–57. doi: 10.4049/jimmunol.1303195

24. Kim ND, Moon JO, Slitt AL, Copple BL. Early growth response factor-1 is critical for cholestatic liver injury. *Toxicol Sci* (2006) 90:586–95. doi: 10.1093/toxsci/kfj111

25. Roth K, Rockwell CE, Copple BL. Differential sensitivity of kupffer cells and hepatic monocyte-derived macrophages to bacterial lipopolysaccharide. *Clin Exp Gastroenterol Hepatol* (2019) 1. doi: 10.31531/edwiser.jcegh.1000106

26. Allen K, Jaeschke H, Copple BL. Bile acids induce inflammatory genes in hepatocytes: A novel mechanism of inflammation during obstructive cholestasis. *Am J Pathol* (2011) 178:175–86. doi: 10.1016/j.ajpath.2010.11.026

27. Moore JK, Mackinnon AC, Man TY, Manning JR, Forbes SJ, Simpson KJ. Patients with the worst outcomes after paracetamol (Acetaminophen)-induced liver failure have an early monocytopenia. *Aliment Pharmacol Ther* (2017) 45:443–54. doi: 10.1111/apt.13878

28. You Q, Holt M, Yin H, Li G, Hu CJ, Ju C. Role of hepatic resident and infiltrating macrophages in liver repair after acute injury. *Biochem Pharmacol* (2013) 86:836–43. doi: 10.1016/j.bcp.2013.07.006

29. Iqbal AJ, Mcneill E, Kapellos TS, Regan-Komito D, Norman S, Burd S, et al. Human cd68 promoter gfp transgenic mice allow analysis of monocyte to macrophage differentiation *in vivo*. *Blood* (2014) 124:E33–44. doi: 10.1182/blood-2014-04-568691

30. Antoniades CG, Quaglia A, Taams LS, Mitry RR, Hussain M, Abeles R, et al. Source and characterization of hepatic macrophages in acetaminophen-induced acute liver failure in humans. *Hepatology* (2012) 56:735–46. doi: 10.1002/hep.25657

31. Mossanen JC, Krenkel O, Ergen C, Govaere O, Liepelt A, Puengel T, et al. Chemokine (C-C motif) receptor 2-positive monocytes aggravate the early phase of acetaminophen-induced acute liver injury. *Hepatology* (2016) 64:1667–82. doi: 10.1002/hep.28682

32. Zigmond E, Samia-Grinberg S, Pasmanik-Chor M, Brazowski E, Shibolet O, Halpern Z, et al. Infiltrating monocyte-derived macrophages and resident kupffer cells display different ontogeny and functions in acute liver injury. *J Immunol* (2014) 193:344–53. doi: 10.4049/jimmunol.1400574

33. Bernsmeier C, Triantafyllou E, Brenig R, Lebosse FJ, Singanayagam A, Patel VC, et al. Cd14. *Gut* (2018) 67:1155–67. doi: 10.1136/gutjnl-2017-314184

34. Veglia F, Perego M, Gabrilovich D. Myeloid-derived suppressor cells coming of age. *Nat Immunol* (2018) 19:108–19. doi: 10.1038/s41590-017-0022-x

35. Veglia F, Sanseviero E, Gabrilovich DI. Myeloid-derived suppressor cells in the era of increasing myeloid cell diversity. *Nat Rev Immunol* (2021) 21:485–98. doi: 10.1038/s41577-020-00490-y

36. Mirochnitchenko O, Weisbrot-Lefkowitz M, Reuhl K, Chen L, Yang C, Inouye M. Acetaminophen toxicity. Opposite effects of two forms of glutathione peroxidase. *J Biol Chem* (1999) 274:10349–55. doi: 10.1074/jbc.274.15.10349

37. Bhushan B, Poudel S, Manley MW, Roy N, Apte U. Inhibition of glycogen synthase kinase 3 accelerated liver regeneration after acetaminophen-induced hepatotoxicity in mice. *Am J Pathol* (2017) 187:543–52. doi: 10.1016/j.ajpath.2016.11.014

38. Paysant J, Vasse M, Soria J, Lenormand B, Pourtau J, Vannier JP, et al. Regulation of the upar/upa system expressed on monocytes by the deactivating cytokines, il-4, il-10 and il-13: consequences on cell adhesion to vitronectin and fibrinogen. *Br J Haematol* (1998) 100:45–51. doi: 10.1046/j.1365-2141.1998.00528.x

frontiers | Frontiers in Immunology

TYPE Original Research
PUBLISHED 07 December 2023
DOI 10.3389/fimmu.2023.1287136

OPEN ACCESS

EDITED BY
Xuchu Que,
University of California, San Diego,
United States

REVIEWED BY
Adil Bhat,
University of California, Los Angeles,
United States
Wang Qi,
First Affiliated Hospital of Anhui Medical
University, China

*CORRESPONDENCE
Cheng Lu
lv_cheng0816@163.com

RECEIVED 01 September 2023
ACCEPTED 23 November 2023
PUBLISHED 07 December 2023

CITATION
Cao Z, Lu P, Li L, Geng Q, Lin L, Yan L, Zhang L, Shi C, Li L, Zhao N, He X, Tan Y and Lu C (2023) Bioinformatics-led discovery of liver-specific genes and macrophage infiltration in acute liver injury. *Front. Immunol.* 14:1287136. doi: 10.3389/fimmu.2023.1287136

Bioinformatics-led discovery of liver-specific genes and macrophage infiltration in acute liver injury

Zhiwen Cao, Peipei Lu, Li Li, Qi Geng, Lin Lin, Lan Yan, Lulu Zhang, Changqi Shi, Li Li, Ning Zhao, Xiaojuan He, Yong Tan and Cheng Lu*

Institute of Basic Research in Clinical Medicine, China Academy of Chinese Medical Sciences, Beijing, China

Background: Acute liver injury (ALI) is an important global health concern, primarily caused by widespread hepatocyte cell death, coupled with a complex immune response and a lack of effective remedies. This study explores the underlying mechanisms, immune infiltration patterns, and potential targets for intervention and treatment ALI.

Methods: The datasets of acetaminophen (APAP), carbon tetrachloride (CCl4), and lipopolysaccharide (LPS)-induced ALI were obtained from the GEO database. Differentially expressed genes (DEGs) were individually identified using the limma packages. Functional enrichment analysis was performed using KEGG, GO, and GSEA methods. The overlapping genes were extracted from the three datasets, and hub genes were identified using MCODE and CytoHubba algorithms. Additionally, PPI networks were constructed based on the String database. Immune cell infiltration analysis was conducted using ImmuCellAI, and the correlation between hub genes and immune cells was determined using the Spearman method. The relationship between hub genes, immune cells, and biochemical indicators of liver function (ALT, AST) was validated using APAP and triptolide (TP) -induced ALI mouse models.

Results: Functional enrichment analysis indicated that all three ALI models were enriched in pathways linked to fatty acid metabolism, drug metabolism, inflammatory response, and immune regulation. Immune analysis revealed a significant rise in macrophage infiltration. A total of 79 overlapping genes were obtained, and 10 hub genes were identified that were consistent with the results of the biological information analysis after screening and validation. Among them, Clec4n, Ms4a6d, and Lilrb4 exhibited strong associations with macrophage infiltration and ALI.

KEYWORDS

acute liver injury, immunoinfiltration, bioinformatics, acetaminophen, triptolide

1 Introduction

The liver, a vital metabolic organ in the human body, is primarily responsible for various physiological functions, including metabolism, detoxification, and protein synthesis. Unfortunately, liver damage often occurs due to factors such as drug abuse and alcohol consumption. Acute liver injury (ALI) is a condition characterized by dysfunction in innate immunity and damage to liver cell, and its high mortality rate has attracted clinical attention (1, 2). The mechanisms involved in ALI are intricate, encompassing multiple signaling pathways, including oxidative stress, inflammatory responses, and immune reactions, among others (3, 4). Although there is a deep understanding of the pathological features of ALI, the molecular characteristics that induce ALI is still not thorough enough (5). ALI progresses rapidly, and currently, there are no drugs available to reverse this deteriorative process (5, 6). Therefore, exploring the general mechanisms and targets associated with ALI is of great significance in formulating effective treatment strategies.

The diverse factors responsible for local sterile inflammation within innate immunity are the primary culprits of liver injury and failure (7). In various ALI models, immune cell infiltration in the liver, including neutrophils, NK/NKT cells, T cells, and macrophages, represents a critical pathological feature, each playing distinct roles (8–12). For example, the activation of macrophages during ALI can lead to the release of reactive oxygen species, IL-6, and TNF-α, thereby inducing apoptosis of liver cells (13, 14). In the case of APAP-induced ALI, eosinophils can be recruited to the liver, exerting hepatoprotective effects (15). Therefore, understanding the immune response in ALI and identifying its potential regulatory targets is paramount.

Bioinformatics provides an efficient method to predict potential regulatory targets and associated mechanisms for diseases. It may be a new attempt to obtain the general regulatory characteristics of ALI by combining the open database to obtain the data sets of different liver injury models as predictive models, which may be a new attempt to explore potential strategies for addressing ALI.

In light of this, the present study employed a dataset encompassing acetaminophen (APAP), carbon tetrachloride (CCl4), and lipopolysaccharide (LPS)-induced ALI to investigate potential pathways, immune response mechanisms, and regulatory targets of ALI. The APAP and triptolide (TP)-induced ALI models were selected for validation of the predictive results. The ALI models induced by APAP, CCl4, and LPS have been widely used for exploring the mechanisms of ALI and validating drug efficacy. Previous studies have indicated that these models cover mechanisms of inflammation response, mitochondrial function, oxidative stress, immune regulation, apoptosis, necrosis, and more (1, 5, 16, 17). In clinical practice, the overdose or long-term abuse of APAP can deplete glutathione and lead to the accumulation of its metabolite, N-acetyl-p-benzoquinone imine (NAPQI), resulting in ALI. TP, the primary active component of Tripterygium wilfordii Hook.f, exhibits multi-organ toxicity, particularly hepatotoxicity, which limits its clinical application. The mechanisms underlying TP-induced ALI are associated with oxidative stress and immune imbalance (18–20). Through these three predictive datasets and two validated animal models, this study aims to explore the general gene regulatory profiles and immune infiltration characteristics in the progression of ALI (Figure 1). Such investigations will contribute to a deeper understanding of the pathogenesis of ALI and may pave the way for developing novel therapeutic strategies.

Abbreviations: AL, acute liver injury; APAP, acetaminophen; CCl4, carbon tetrachloride; LPS, lipopolysaccharide; DEGs, differentially expressed genes; TP, triptolide; NAPQI, N-acetyl-p benzoquinone imine; GO, Gene Ontology; KEGG, Kyoto Encyclopedia of Genes and Genomes; PPI, protein–protein interactions; BP, Biological Process; CC, Cellular Component; MF, Molecular Function.

2 Methods

2.1 Microarray data source

The datasets GSE167032, GSE167033, and GSE166488 were obtained from the GEO database (https://www.ncbi.nlm.nih.gov/geo/) (21). GSE167032 ([Mouse430_2] Affymetrix Mouse Genome 430 2.0 Array) is a mouse ALI model induced by a single injection of 300 mg/kg APAP, lasting 24 hours. This dataset comprises 5 control samples and 5 APAP-treated samples. The gene expression data of GSE167033 ([Mouse430_2] Affymetrix Mouse Genome 430 2.0 Array) consists of 10 samples obtained from mice treated with a single injection of 1.6 g/kg CCl4. These samples were collected at the 24-hour time point, including 5 samples from the control group and 5 samples from the model group. GSE166488 ([Mouse430_2] Affymetrix Mouse Genome 430 2.0 Array) is a mouse ALI model induced by a single injection of 750 μg/kg LPS for 24 hours. The dataset includes 5 samples from the model group and 3 samples from the control group.

2.2 Acquisition of microarray data and identifcation of DEGs

The three datasets were retrieved from the GEO database and processed using the limma package in R (22). Differential gene expression analysis was conducted on each dataset, applying a filtering criterion of $|logFC| > 0.75$ and a P. value < 0.05 to identify significant genes. The results of the differential gene analysis were visualized using volcano plots and heatmaps, created with the ggplot2 and pheatmap packages, respectively (23).

2.3 Functional enrichment analysis

Gene Ontology (GO) and Kyoto Encyclopedia of Genes and Genomes (KEGG) pathway enrichment analyses ware conducted using the R package clusterProfiler (24), with the DEGs criteria set as $|logFC|>0.75$ and P.Value<0.05. The resulting analysis outcomes ware then visualized using the gglot2 package (23). Additionally, GSEA analysis is performed using the clusterProfiler package with a pvalueCutoff of 0.05, and the obtained results ware further visualized using gglot2 for enhanced visualization and interpretation (23, 24).

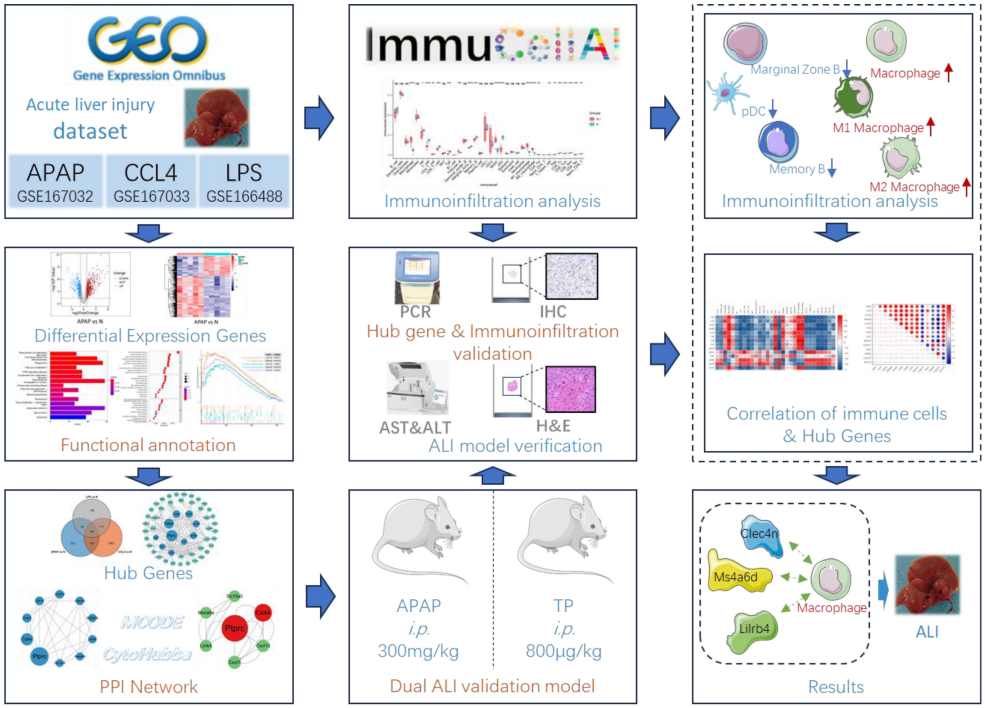

FIGURE 1
Flow chart of bioinformatics analysis and animal experiments. The figure was partly generated using Servier Medical Art, provided by Servier, licensed under a Creative Commons Attribution 3.0 unported license.

2.4 Analysis of protein–protein interactions and identifcation of Hub genes

Perform protein–protein interactions (PPI) analysis on the overlapping DEGs from three datasets using the String database (https://cn.string-db.org/) and visualize the results using Cytoscape 3.9.1 (25). Utilize the MCODE and CytoHubba plugins to respectively filter hub genes, and integrate the obtained DEGs to form a hub gene set (26, 27). Using the MCODE plugin in Cytoscape, the advanced options ware set as follows: in Network Scoring, the Degree Cutoff was set to 2 (26). In Cluster Finding, the Node Score Cutoff was set to 0.2, the K-Core was set to 2, and the Max Depth was set to 100. Plugin CytoHubba selected the MCC algorithm (27).

2.5 Immune infltration analysis

Immunoinfiltration analysis was conducted using ImmuCellAI-mouse (http://bioinfo.life.hust.edu.cn/ImmuCellAI-mouse/#!/) (28, 29). Due to the lower gene count in dataset GSE167032 compared to the other two datasets, immunoinfiltration analysis was focused on GSE167033 and GSE166488 datasets. The GSE167033 and GSE166488 datasets, as well as their combined normalized dataset, were individually assessed for the degree of infiltration of 36 immune cell types using ImmuCellAI-mouse. The resulting datasets underwent inter-group differential analysis using Wilcox.test and were then visualized using ggplot2 (23). The correlation analysis and visualization of hub genes and immune cells were conducted using OriginPro.

2.6 Establishment of animal model of ALI

According to previous reports, TP and APAP ALI models were constructed to verify the expression of Hub genes and immune infiltration. Female Balb/c mice (6-8 weeks old) obtained from Beijing Vital River Laboratory Animal Technology Co., Ltd (SCXK (jing) 2021–0006). Animal experiments strictly adhered to the Guide for the Care and Use of Laboratory Animals, and the experimental protocol was approved by the Research Ethics Committee of the Institute of Basic Theory of Chinese Medicine, China Academy of Chinese Medical Sciences (IBTCMCACMS21-2110-04). After one week of acclimatization, the mice were randomly divided into control, TP, and APAP groups. The control group received an equivalent volume of physiological saline, the TP group received 800ug/kg of TP, and the APAP group received 300mg/kg of APAP. All administrations were done via intraperitoneal injection. After 24 hours of drug administration, all mice were euthanized and liver tissue and serum samples were collected for subsequent analysis.

2.7 Detection of ALT/AST level

The blood samples were collected in centrifuge tubes without anticoagulants, and serum was obtained by centrifugation. The

levels of ALT and AST were detected using an automated biochemical analyzer.

2.8 RNA extraction and qRT–PCR

Liver tissue was homogenized, and RNA extraction was performed using the RNAsimple Total RNA Kit (Tiangen Biotech). RNA concentration was determined using NanoDrop2000, and reverse transcription was carried out using the First-Strand Synthesis Master Mix (Lablead Biotech). The qRT-PCR step was conducted using the SYBR Green PCR Fast mixture (Lablead Biotech), and the expression levels of the target genes were normalized to GAPDH. The primer sequences for all genes are provided in Table S1.

2.9 Immunohistochemistry

Paraffin-embedded sections were dewaxed to water, followed by antigen retrieval. A 3% hydrogen peroxide solution was added to block endogenous peroxidase activity, and 3% BSA was applied within the tissue area to block non-specific binding. The primary antibody was added and incubated overnight at 4°C. After washing, the sections were incubated with the secondary antibody. Subsequently, DAB staining was performed, followed by counterstaining the cell nuclei with hematoxylin. Finally, the slides were dehydrated, mounted, and observed under a microscope for image acquisition. The F4/80 positive area was counted using Image J software.

2.10 Prediction of a hub Gene-miRNAs network

The Hub genes selected after *in vivo* experiments were further input into the miRWalk database to predict potential miRNA regulatory networks. The results obtained were visualized using Cytoscape 3.9.1.

2.11 Statistical analysis

All data analysis was performed using GraphPad Prism 7 and the corresponding R packages. Experimental data are presented as mean ± standard deviation. An unpaired Student's t-test was used to compare continuous variables between groups. A p-value less than 0.05 was considered statistically significant.

3 Results

3.1 DEGs in ALI and functional enrichment analysis

Differential expression analysis results showed 799 DEGs in GSE167032, with 537 upregulated and 262 downregulated. In GSE167033, there were 1872 DEGs, including 1110 upregulated and 762 downregulated. Additionally, GSE166488 had 340 DEGs, with 235 upregulated and 105 downregulated. The differential analysis results were visualized as volcano plots and heatmaps (Figure 2).

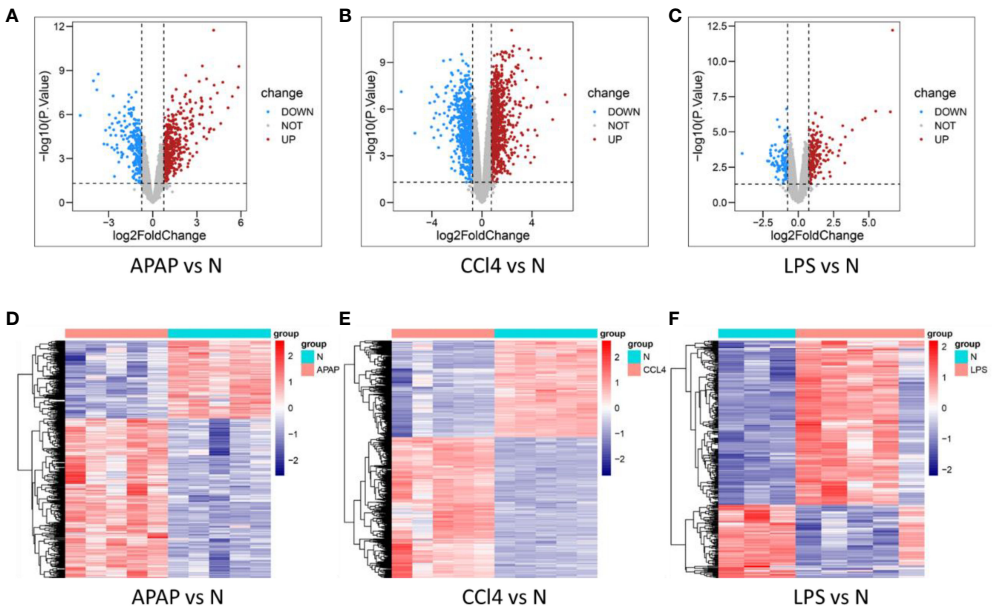

FIGURE 2
Determination of DEGs in three models. **(A–C)** volcano plot of DEGs in APAP, CCl4, and LPS. **(D–F)** Heat maps of DEGs in APAP, CCl4, and LPS.

KEGG enrichment analysis reveals that ALI induced by APAP, CCl4, and LPS primarily involves fatty acid metabolism, drug metabolism, PPAR signaling pathway, and IL-17 signaling pathway (Figures 3A–C).

The GO analysis results reveal that ALI is significantly associated with the GO terms in biological process (BP), cellular component (CC), and molecular function (MF). The enriched GO terms include fatty acid metabolism, inflammatory response, immune response, oxidation-reduction, and membrane microdomain, etc (Figures 3D–F).

GSEA analysis suggests that ALI induced by APAP, CCl4, or LPS is not only associated with biological processes such as apoptosis, fatty acid metabolism, and drug metabolism but is also closely related to inflammatory and immune-related pathways including the TNF signaling pathway, NF-kappa B signaling pathway, IL-17 signaling pathway, B cell receptor signaling pathway, and T cell receptor signaling pathway (Figures 3G–L).

3.2 PPI network analysis and hub DEGs identification

Integrating the DEGs from the three datasets yielded 79 overlapping genes, with 51 being upregulated and 21 being downregulated (Figure 4A). The 79 overlapping genes were subjected to network analysis using the String database, and the results were visualized using Cytoscape (Figure 4B). As indicated in the red nodes in Figure 4C, the top 10 ranked hub genes obtained using the MCC algorithm from the CytoHubba plugin were Ptprc, Cd14, Clec4n,

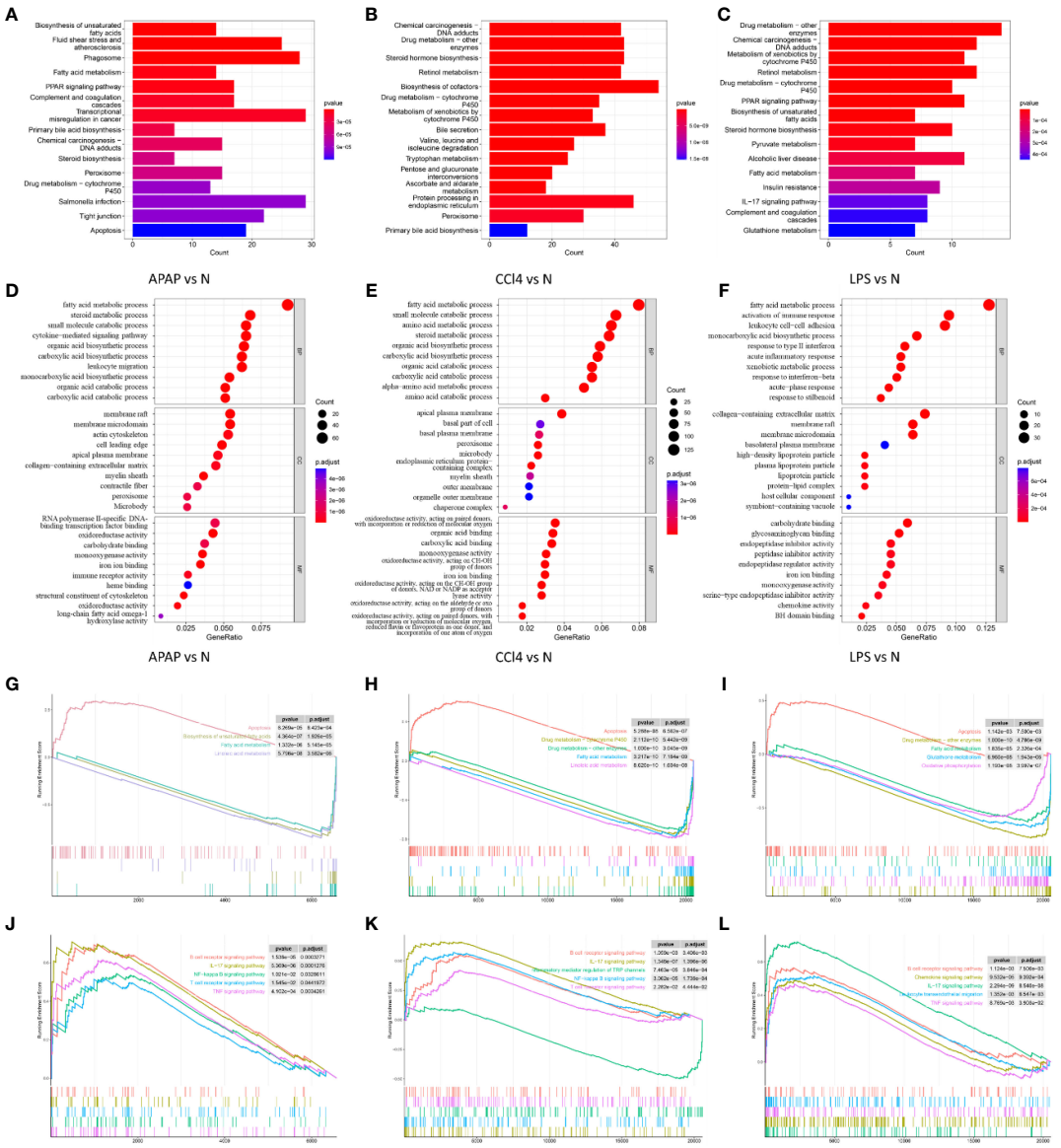

FIGURE 3
Functional enrichment analysis. **(A–C)** KEGG analysis of DEGs in APAP, CCl4, and LPS. **(D–F)** The top 10 functional enrichment in BP, CC, and MF analysis of APAP, CCl4, and LPS. **(G–I)** GSEA of apoptosis, fatty acid metabolism, and drug metabolism-related pathways in APAP, CCl4, and LPS. **(J–L)** GSEA sets of inflammatory response and immune response-related pathways in APAP, CCl4, and LPS.

10.3389/fimmu.2023.1287136

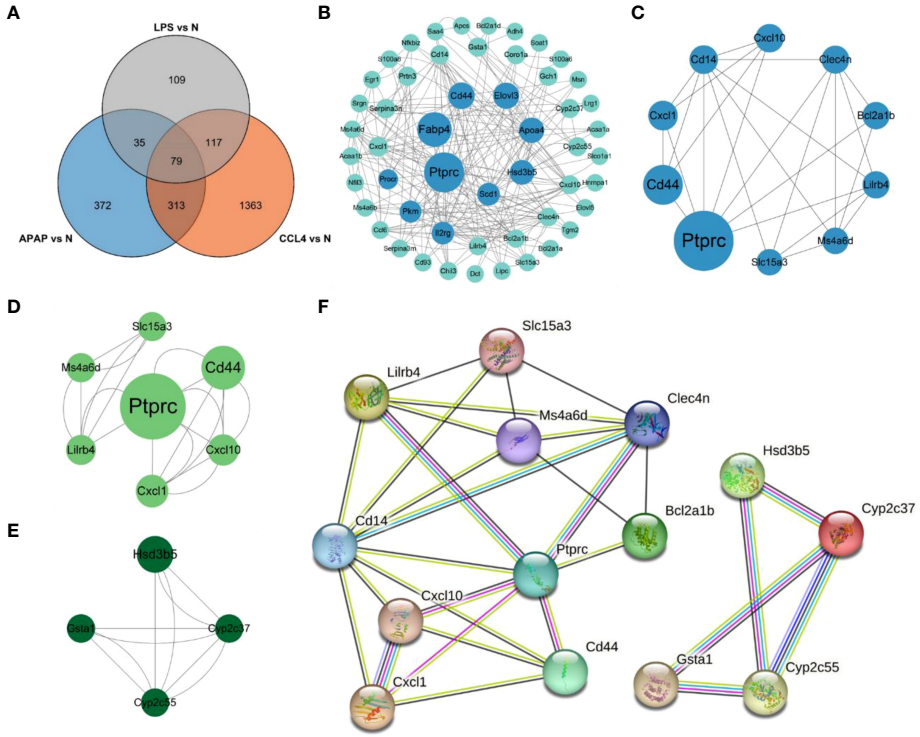

FIGURE 4
PPI network analysis and Hub gene identification. **(A)** Venn diagram shows the overlap of DEGs in APAP, CCl4 and LPS. **(B)** PPI network maps about 79 overlapping genes. The light green color represents the top 10 genes arranged according to betweenness. **(C)** Network diagram about the top10 DEGs of CytoHubba predictions. **(D, E)** Two clusters predicted by MCODE. **(F)** String analysis network diagram of 14 hub genes obtained by combining CytoHubba and MCODE algorithms.

Ms4a6d, Cxcl10, Cd44, Lilrb4, Cxcl1, Slc15a3 and Bcl2a1b. According to the MCODE plugin analysis, two significant gene clusters were identified in Figures 4D, E. They were referred to as Cluster1, which includes the genes Cyp2c37, Gsta1, Hsd3b5, and Cyp2c55, and Cluster2, which consists of the genes Lilrb4, Ptprc, Slc15a3, Cd44, Ms4a6d, Cxcl10, and Cxcl1. Combining the results of the two analysis methods, 14 potential hub genes associated with ALI were determined. These genes include Ptprc, Cd14, Clec4n, Ms4a6d, Cxcl10, Cd44, Lilrb4, Cxcl1, Bcl2a1b, Cyp2c37, Gsta1, Hsd3b5, Cyp2c55, and Slc15a3. Subsequently, the 14 identified hub genes were input into the String database to obtain the PPI network graph shown in Figure 4F.

3.3 Immune cell infiltration in ALI

After conducting immunoinfiltration analysis using the ImmuCell AI algorithm on the integrated results of GSE167033, GSE166488, and their respective datasets, significant differences in immune cell infiltration were observed between the ALI model and the control group. As displayed in Figures 5A, B and Figure S1, there is a significant increase in the infiltration of Macrophage, M1 Macrophage, and M2 Macrophage in the ALI model compared to the control group ($p < 0.05$). Conversely, Marginal Zone B, Memory B, and pDC infiltration decreased ($p < 0.05$). Further estimations were conducted on the correlation between immune cells, and the results showed a significant positive correlation between Macrophage, M1 Macrophage, and M2 Macrophage, as well as CD4 T cell, CD4 Tm, T helper cell, and Treg (Figure 5C). T cells negatively correlated with macrophage cells, M1 Macrophage, and M2 Macrophage.

3.5 Relationship between hub DEGs and immune cells

The potential correlation between immune cells and hub genes was analyzed. The results, as displayed in Figure 6A, indicate that hub genes exhibit contrasting correlations between macrophages and DC cells, T cells. Immunoinfiltration analysis determined a close association between macrophages and the ALI model. Focusing on macrophage analysis, there is a strong correlation between Clec4n (0.84), Ms4a6d (0.87), Lilrb4 (0.88), and macrophages, indicating their research significance in the context of macrophage infiltration-related ALI models. Through correlation analysis of hub genes, it was found that Clec4n exhibits strong correlations with Ptprc (0.87), Cd44 (0.90), Lilrb4 (0.88), Cxcl1 (0.82), Slc15a3 (0.90); Ms4a6d was associated with Cxcl10 (0.81), Bcl2a1b (0.87), Cyp2c55 (-0.88), Slc15a3 (0.81); and Lilrb4 was strongly correlated with Ptprc (0.84), Cd14 (0.81), Clec4n (0.88), Cxcl10 (0.81), Cd44 (0.87), Cxcl1 (0.82), Slc15a3 (0.84) (Figure 6B).

10.3389/fimmu.2023.1287136

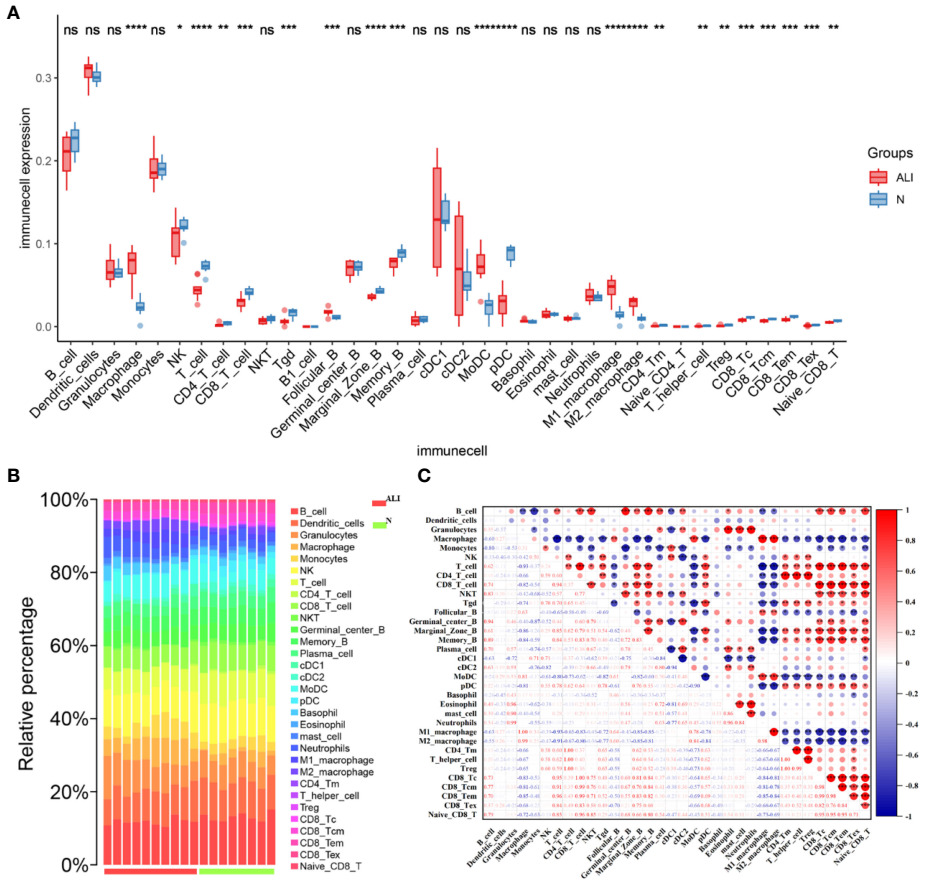

FIGURE 5
Characteristics of immune cell infiltration in ALI model. **(A)** Immune cell infiltration in ALI group and control group. **(B)** Stacked bar chart of immune cell infiltration in ALI group and control group. **(C)** The result of immune cell correlation analysis. *p<0.1, **p<0.05, ***p<0.01, ****p<0.001, ns, not significant.

3.6 Assessment of ALI and macrophage infiltration in validated models

Based on the above results, the APAP and TP-induced ALI models were selected to validate the relationship between hub genes, macrophage infiltration, and ALI. In the validated model of ALI, a significant increase in serum AST and ALT levels was observed after treatment with TP and APAP (Figures 7A, B). HE staining revealed a pronounced occurrence of hepatocyte steatosis in the mouse liver tissue following TP intervention, accompanied by hepatocyte swelling, hepatocyte necrosis, and localized infiltration of lymphocytes. In the APAP-induced ALI model, a substantial extent of hepatocyte necrosis was observed, accompanied by increased fibroblast proliferation, hepatocyte steatosis, and infiltration of lymphocytes and granulocytes (Figure 7C). Based on the analysis of immune infiltration, macrophage infiltration

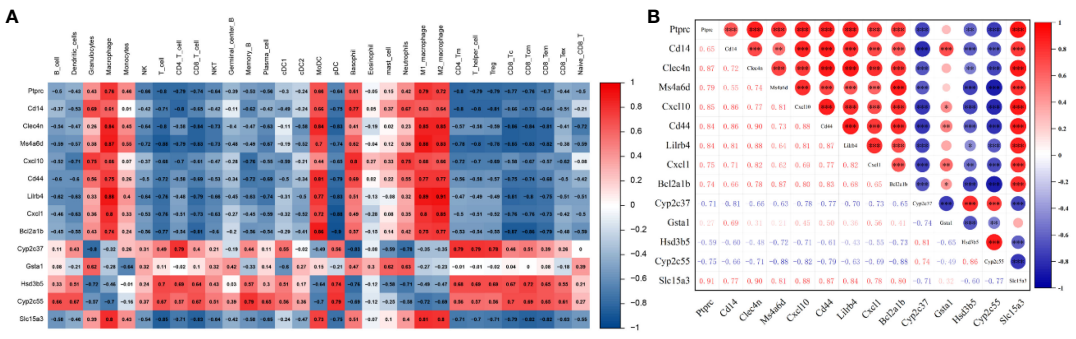

FIGURE 6
Relationship between hub genes and immune cells. **(A)** Correlation between hub genes and immune cells. **(B)** Correlation analysis of hub genes expression. *p<0.05, **p<0.01, ***p<0.001.

10.3389/fimmu.2023.1287136

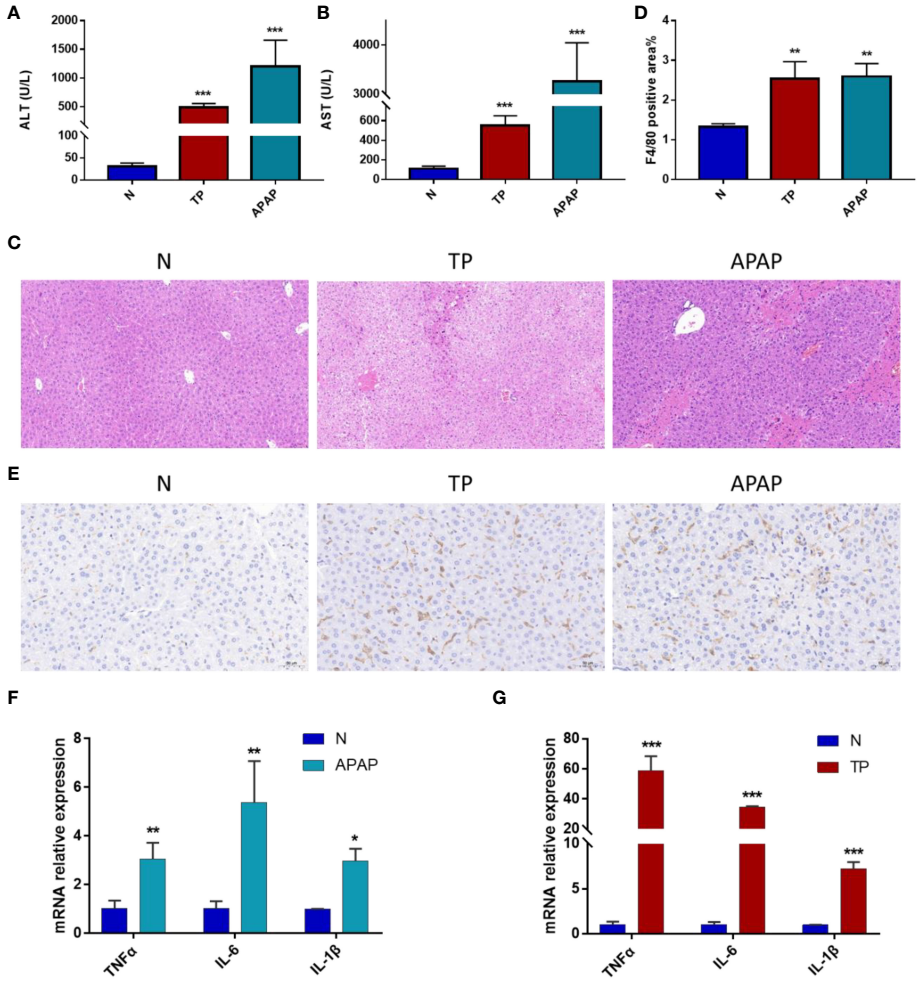

FIGURE 7
Validation of ALI model induced by APAP and TP. **(A)** ALT levels in serum. **(B)** AST levels in serum. **(C)** HE staining results of liver tissue. Scale bars: 50 μm. **(D)** Quantification of macrophage infiltration. **(E)** Immunohistochemical results. Scale bars: 50 μm. **(F)** mRNA expression of TNF-α, IL-6 and IL-1β in liver tissue of APAP model. **(G)** mRNA expression of TNF-α, IL-6 and IL-1β in liver tissue of TP model. *p<0.05, **p<0.01, ***p<0.001 APAP/TP vs N.

exhibited an increasing trend in all three models of ALI. Consequently, F4/80 staining was utilized to observe the distribution of macrophages in the TP and APAP-induced ALI models (8). It was found that compared to the control group, macrophage infiltration significantly increased in the TP and APAP groups, consistent with the previous analysis of immune infiltration (Figures 7D, E). Furthermore, the expression of macrophage-related inflammatory factors TNFα, IL-6, and IL-1β in liver tissue was evaluated. The results were as expected, with a significant upregulation of TNFα, IL-6, and IL-1β expression observed in the TP and APAP-induced ALI model (Figures 7F, G).

3.7 Experimental validations of hub DEGs expression in ALI mouse

Liver tissue RNA was extracted from mice with APAP- and TP-induced ALI to evaluate the expression levels of 14 hub genes using RT-qPCR. The results, as depicted in Figures 8A, B, demonstrate significant differences in the expression levels of Ptprc, Cd14, Clec4n, Ms4a6d, Cxcl10, Cd44, Lilrb4, Cxcl1, Bcl2a1b, and Slc15a3 in both validation models of ALI, exhibiting the expected trend. Moreover, the correlation between Clec4n, Ms4a6d, Lilrb4, and ALT, AST was analyzed (Figure 8C). The results revealed a strong correlation ($p<0.01$) between the PCR cycle numbers of Clec4n in both the APAP and TP models and ALT (-0.84, -0.88) and AST (-0.9, -0.94). Similarly, the PCR cycle numbers of Ms4a6d in the APAP and TP models showed a high correlation ($p<0.01$) with ALT (-0.9, -0.9) and AST (-0.96, -0.95). Furthermore, Lilrb4 displayed a significant correlation ($p<0.01$) with ALT (-0.9, -0.9) and AST (-0.96, -0.95) in both the APAP and TP models.

3.9 Prediction of hub gene and miRNA networks

The miRNA regulatory networks of the hub genes Clec4n, Ms4a6d, and Lilrb4 were predicted using the miRWalk database. The results only included the miRNA regulatory network associated

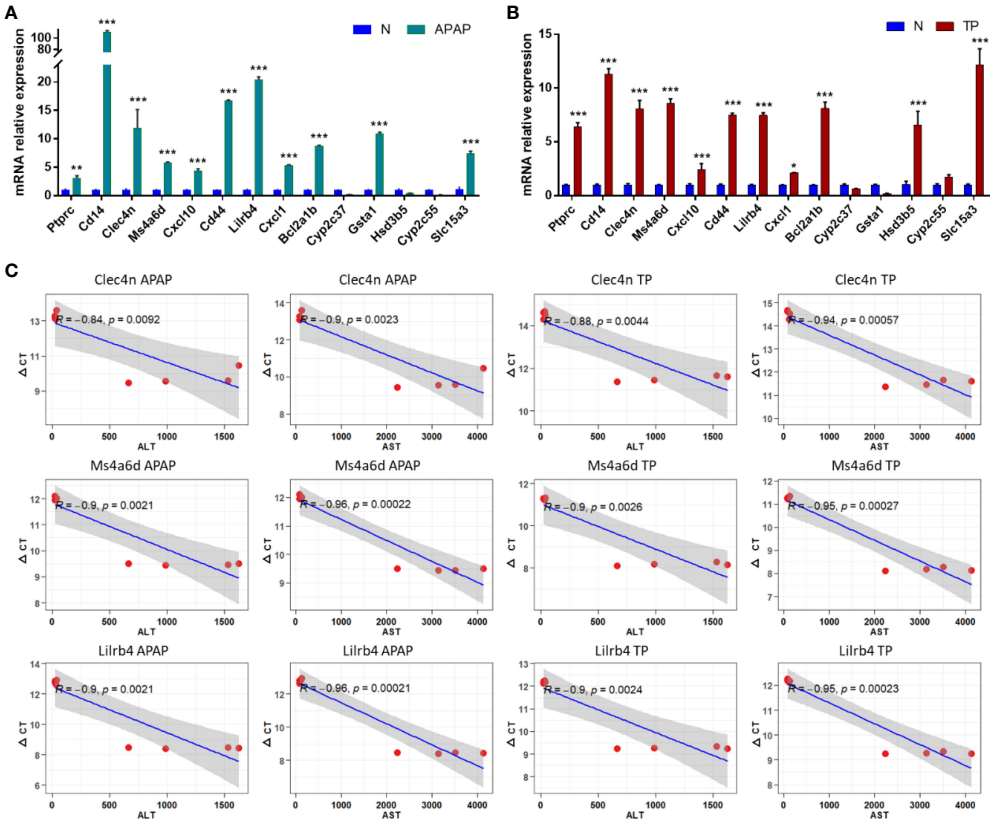

FIGURE 8
Hub DEGs expression in ALI mouse. **(A, B)** Validation of hub gene expression in APAP and TP models. **(C)** The correlation between Clec4n, Ms4a6d, Lilrb and liver function indicators ALT and AST. *p<0.05, **p<0.01, ***p<0.001 APAP/TP vs N.

with Clec4n and Ms4a6d, which comprised 223 nodes and 562 edges (Figure 9). Notably, miR-5126, miR-3109-5p, miR-7216-5p, miR-5128, miR-12201-5p, miR331-3p, miR-6939-5p, miR-5627-5p, miR-6988-5p, and miR-412-3p, were found to interact with the hub genes Clec4n and Ms4a6d. These results highlight the potential research value of these miRNAs in the context of ALI. However, it is important to note that further validation is required to establish their roles fully.

4 Discussion

The liver is an essential organ in the human body, performing a wide range of vital physiological functions. It plays a crucial role in metabolizing nutrients, detoxifying harmful substances, producing bile for digestion, storing vitamins and minerals, and synthesizing proteins and clotting factors. However, the liver is susceptible to various forms of injury, including ALI. ALI refers to the sudden and severe damage to liver cells, which can be caused by various factors such as viral infections, drug toxicity, alcohol abuse, or autoimmune reactions. When the liver experiences acute injury, its normal physiological functions can be significantly impaired. Understanding general mechanisms and regulatory targets is crucial for comprehending the ALI process and identifying potential therapeutic drugs. In this study, APAP, CCl4, and LPS were selected as the research subjects for ALI. These agents are commonly used in animal experiments to induce ALI and involve multiple mechanisms, including inflammation response, oxidative stress, immune response, apoptosis, and necrosis (1, 2, 5, 16). By employing various bioinformatics methods, this study screened and identified a set of common DEGs from three models. Through the predictions of MCODE and CytoHubba, a potential set of hub genes was identified. Functional enrichment analysis revealed that the three ALI datasets were primarily associated with pathways related to fatty acid metabolism, drug metabolism, inflammatory response, and immune response. Additionally, the infiltration characteristics of immune cells in different models were predicted, and the correlation between hub genes and immune cells was also examined. Finally, the immune infiltration and target gene expression results were validated by combining the APAP and TP-induced ALI models *in vivo*. By incorporating multiple models of ALI, this study may provide insights into the general regulatory mechanisms of ALI and offer references for exploring general solutions to ALI.

This study is the first attempt to combine three commonly used models of ALI to explore the general mechanisms underlying the occurrence of ALI. PPI network analysis identified 14 DEGs potentially connected to ALI. Through validation using a mouse model of ALI, a final selection of 10 genes (Ptprc, Cd14, Clec4n, Ms4a6d, Cxcl10, Cd44, Lilrb4, Cxcl1, Bcl2a1b, and Slc15a3) was confirmed to be significantly associated with ALI. These 10 hub genes have been reported to play regulatory roles in immune

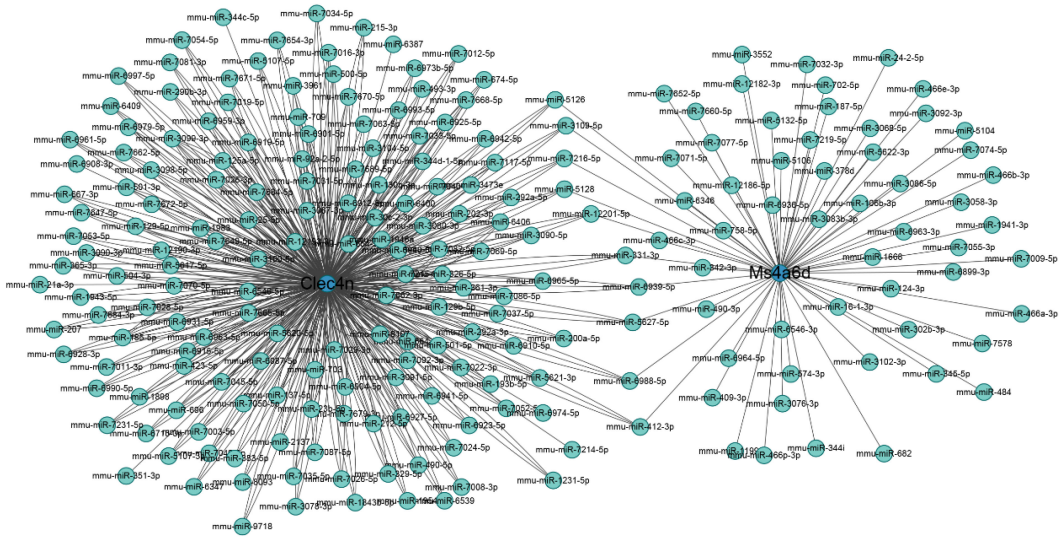

FIGURE 9
Regulatory networks on miRNA and macrophage-related genes. Blue circles represent genes, and cyan dots represent miRNA.

regulation and inflammatory response. For example, Ptprc, as a transmembrane glycoprotein, is an essential regulator of T cell and B cell antigen receptor-mediated activation. It is essential in immune deficiency, autoimmune diseases or malignant tumors (30). Due to its regulatory role in the immune response signaling pathway, Ptprc is also used as a target for treating certain immune diseases, such as organ transplant rejection and tumor metastasis, by selectively inhibiting Ptprc (31, 32). Bcl2a1b is associated with neutrophil proliferation and can serve as a potential marker for identifying proliferating neutrophils, aiding in the study and clinical identification and characterization of neutrophils in ALI. The accumulation of neutrophils contributes to the production of CCL6, thereby recruiting more macrophages (33, 34). Slc15a3 is highly expressed in macrophages and plays a vital role in inflammatory diseases. Studies have shown that knocking down Slc15a3 can reduce the production of TLR4-dependent TNF-α and IL-6. Furthermore, the expression of Slc15a3 positively correlates with the inflammatory process, indicating that Slc15a3 has value for the treatment and evaluation of inflammatory diseases (35, 36). Cxcl10 plays a crucial role in recruiting immune cells during the liver infiltration process in liver diseases. It has been confirmed that Cxcl10 is necessary for promoting inflammatory responses and can participate in hepatocyte apoptosis and inflammatory reactions through toll-like receptor 4 (37, 38). Cxcl1 has been reported to be associated with the recruitment of neutrophils and the severity of liver disease during liver injury. The detection of Cxcl1 levels may have clinical significance in assessing the progression of ALI (39, 40).

ALI is closely linked to dysfunction in innate immunity. GSEA analysis has revealed that all three ALI models are associated with signaling pathways related to inflammation, immune response, and apoptosis (2, 41). In this study, by comparing different immune cell infiltration in the ALI model and the control group, it was found that macrophage infiltration was significantly increased in the ALI model. Immunohistochemical staining showed that the distribution of macrophages in the TP and APAP-induced ALI models was significantly up-regulated. Macrophages are the most abundant immune cells in the liver and play a pivotal role in maintaining liver homeostasis and the potential mechanisms underlying liver diseases (42). In ALI, activated macrophages can increase the release of inflammatory cytokines (IL-6, TNF-α), nitrogen species, reactive oxygen species, and other factors, activating apoptotic pathways in liver cells. Furthermore, macrophage derived chemokines (IL-18, MCP-1) further recruit other immune cells to intervene in the process of liver injury (2, 13–15). Macrophage infiltration in the liver is a hallmark and contributor to liver inflammation and injury (43). Animal experiments have demonstrated that depleting of macrophages can effectively improve APAP-induced liver injury (44). Promoting the transition of macrophage functional characteristics from pro-inflammatory to anti-inflammatory can facilitate the resolution of tissue damage responses (45). Inhibiting macrophage migration to suppress pro-inflammatory immune activation can protect against ischemic liver injury (46). The transition of macrophage phenotypes from pro-inflammatory to anti-inflammatory can be regulated through various biological mechanisms, such as JAK/STATs, TLR4/NF-kB, PI3K/Akt/mTOR, PPARγ, TGF-β/Smads pathways, among others. Targeting these pathways involved in macrophage phenotype transition is a feasible strategy to alleviate ALI (47). For example, studies have found that reducing the expression of HIF-1α and activating the PI3K/Akt/mTOR signaling pathway can decrease oxidative stress and regulate macrophage polarization in the liver, thereby alleviating injury (48).

Integrating the results of hub gene and immune infiltration showed that Clec4n, Ms4a6d and Lilrb4 were strongly correlated with macrophages and serum ALT and AST levels. These results suggest that Clec4n, Ms4a6d, and Lilrb4 are associated with macrophage infiltration in ALI. Clec4n is a C-type lectin receptor expressed on dendritic cells and macrophages (49). Studies have shown that knocking down Clec4n in macrophages significantly affects the secretion of TNF-α, IL-6, or MIP-2 (50). Recent research has demonstrated that in acute inflammation, Ms4a6d in macrophages

promotes the transcription of pro-inflammatory genes and increases mitochondrial reactive oxygen species secretion through crosslinking with MHC Class II antigen (51). Lilrb4 is expressed on the surface of antigen-presenting cells such as macrophages and dendritic cells (52). Studies have found that Lilrb4 is involved in the pathological processes of various inflammatory diseases, and downregulation of Lilrb4 exacerbates local inflammatory responses (53). Knockout Lilrb4 in mice results in increased secretion of pro-inflammatory cytokines TNF-α and IL-6, and silencing Lilrb4 *in vitro* also leads to increased production of pro-inflammatory cytokines IL-6 and IL-1β (54, 55). These findings suggest that downregulation of Lilrb4 exacerbates the inflammatory process, and targeting Lilrb4 or its associated pathways may be an effective strategy for mitigating inflammation-induced injury in ALI.

However, there are some limitations in this study. For instance, the three ALI models used may not represent all types of ALI. The sample size was not sufficiently large, and the potential regulatory targets obtained were not validated in a more significant number of ALI models. Nevertheless, it is hoped that this study can lay the foundation for exploring the general regulatory targets and mechanisms of ALI, providing insights for clinical strategies to address ALI.

5 Conclusion

In summary, this study employed three datasets of ALI induced by APAP, CCl4, and LPS as generic models for liver injury research. A total of 79 overlapping genes were identified, identifying 14 potential hub genes associated with ALI. Functional enrichment analysis indicated that the ALI process may be linked to pathways related to fatty acid metabolism, drug metabolism, inflammatory response, and immune response. Immunoinfiltration studies revealed a significant increase in macrophage infiltration in ALI models. By constructing APAP and TP-induced ALI models, we validated the regulation of the 10 hub genes at the *in vivo* level, confirming consistency with the bioinformatics analysis results. Correlation analysis identified Clec4n, Ms4a6d, and Lilrb4 as significantly correlated with macrophage infiltration and liver function biochemical markers ALT and AST, suggesting their potential for further investigation in the prevention and treatment of ALI. Furthermore, using the miRWalk database, 10 miRNAs with potential research value in ALI were predicted.

Data availability statement

The original contributions presented in the study are included in the article/Supplementary Material. Further inquiries can be directed to the corresponding author.

Ethics statement

The experimental protocol was approved by the Research Ethics Committee of the Institute of Basic Theory of Chinese Medicine, China Academy of Chinese Medical Sciences (IBTCMCACMS21-2110-04). The study was conducted in accordance with the local legislation and institutional requirements.

Author contributions

ZC: Writing – original draft, Writing – review & editing. PL: Data curation, Formal analysis, Writing – review & editing. LL (3rd author): Conceptualization, Data curation, Writing – original draft. QG: Methodology, Visualization, Writing – original draft. LLin: Methodology, Writing – original draft. LY: Validation, Visualization, Writing – original draft. LZ: Validation, Writing – original draft. CS: Validation, Writing – original draft. LL (9th author): Writing – review & editing. NZ: Writing – review & editing. XH: Writing – review & editing. YT: Writing – review & editing. CL: Writing – review & editing.

Funding

The author(s) declare financial support was received for the research, authorship, and/or publication of this article. Youth Qihuang Scholar of National Administration of Traditional Chinese Medicine (2020), The National Natural Science Foundation of China (82074269), Innovation Team and Talents Cultivation Program of National Administration of Traditional Chinese Medicine (ZYYCXTD-D-202005).

Conflict of interest

The authors declare that the research was conducted in the absence of any commercial or financial relationships that could be construed as a potential conflict of interest.

Publisher's note

Supplementary material

The Supplementary Material for this article can be found online at: https://www.frontiersin.org/articles/10.3389/fimmu.2023.1287136/full#supplementary-material

References

1. Alkandahri MY, Pamungkas BT, Oktoba Z, Shafirany MZ, Sulastri L, Arfania M, et al. Hepatoprotective effect of kaempferol: A review of the dietary sources, bioavailability, mechanisms of action, and safety. *Adv Pharmacol Pharm Sci* (2023) 2023:1–16. doi: 10.1155/2023/1387665

2. Yang Y, Ni M, Zong R, Yu M, Sun Y, Li J, et al. Targeting notch1-yap circuit reprograms macrophage polarization and alleviates acute liver injury in mice. *Cell Mol Gastroenterol Hepatol* (2023) 15(5):1085–104. doi: 10.1016/j.jcmgh.2023.01.002

3. Qin C-C, Liu Y-N, Hu Y, Yang Y, Chen Z. Macrophage inflammatory protein-2 as mediator of inflammation in acute liver injury. *World J Gastroenterol* (2017) 23 (17):3043–52. doi: 10.3748/wjg.v23.i17.3043

4. Roth K, Strickland J, Copple BL. Regulation of macrophage activation in the liver after acute injury: role of the fibrinolytic system. *World J Gastroenterol* (2020) 26 (16):1879–87. doi: 10.3748/wjg.v26.i16.1879

5. Frank D, Savir S, Gruenbaum B, Melamed I, Grinshpun J, Kuts R, et al. Inducing acute liver injury in rats via carbon tetrachloride (Ccl4) exposure through an orogastric tube. *J visualized experiments JoVE* (2020) 158:e60695. doi: 10.3791/60695

6. Yu C, Chen P, Miao L, Di G. The role of the nlrp3 inflammasome and programmed cell death in acute liver injury. *Int J Mol Sci* (2023) 24(4):3067. doi: 10.3390/ijms24043067

7. Hirao H, Nakamura K, Kupiec-Weglinski J. Liver ischaemia-reperfusion injury: A new understanding of the role of innate immunity. *Nat Rev Gastroenterol Hepatol* (2022) 19(4):239–56. doi: 10.1038/s41575-021-00549-8

8. Xie Y, Zhong K-B, Hu Y, Xi Y-L, Guan S-X, Xu M, et al. Liver infiltration of multiple immune cells during the process of acute liver injury and repair. *World J Gastroenterol* (2022) 28(46):6537–50. doi: 10.3748/wjg.v28.i46.6537

9. Khoury T, Rmeileh A, Yosha L, Benson A, Daher S, Mizrahi M. Drug induced liver injury: review with a focus on genetic factors, tissue diagnosis, and treatment options. *J Clin Trans Hepatol* (2015) 3(2):99–108. doi: 10.14218/jcth.2015.00007

10. Bernal W, Auzinger G, Dhawan A, Wendon J. Acute liver failure. *Lancet (London England)* (2010) 376(9736):190–201. doi: 10.1016/s0140-6736(10)60274-7

11. Karlmark K, Wasmuth H, Trautwein C, Tacke F. Chemokine-directed immune cell infiltration in acute and chronic liver disease. *Expert Rev Gastroenterol Hepatol* (2008) 2(2):233–42. doi: 10.1586/17474124.2.2.233

12. Ayata C, Ganal S, Hockenjos B, Willim K, Vieira R, Grimm M, et al. Purinergic $P2y_2$ Receptors promote neutrophil infiltration and hepatocyte death in mice with acute liver injury. *Gastroenterology* (2012) 143(6):1620–9.e4. doi: 10.1053/j.gastro.2012.08.049

13. Brenner C, Galluzzi L, Kepp O, Kroemer G. Decoding cell death signals in liver inflammation. *J Hepatol* (2013) 59(3):583–94. doi: 10.1016/j.jhep.2013.03.033

14. Ilyas G, Zhao E, Liu K, Lin Y, Tesfa L, Tanaka K, et al. Macrophage autophagy limits acute toxic liver injury in mice through down regulation of interleukin-1β. *J Hepatol* (2016) 64(1):118–27. doi: 10.1016/j.jhep.2015.08.019

15. Xu L, Yang Y, Wen Y, Jeong J-M, Emontzpohl C, Atkins CL, et al. Hepatic recruitment of eosinophils and their protective function during acute liver injury. *J Hepatol* (2022) 77(2):344–52. doi: 10.1016/j.jhep.2022.02.024

16. Mohanraj R, Yao L, Chen W, Song K, Han C, Gandhi CR, et al. 15-hydroxyprostaglandin dehydrogenase (15-pgdh) prevents lipopolysaccharide (Lps)-induced acute liver injury. *PloS One* (2017) 12(4):e0176106. doi: 10.1371/journal.pone.0176106

17. Yan M, Huo Y, Yin S, Hu H. Mechanisms of acetaminophen-induced liver injury and its implications for therapeutic interventions. *Redox Biol* (2018) 17:274–83. doi: 10.1016/j.redox.2018.04.019

18. Zhang H, Yuan Z, Zhu Y, Yuan Z, Wang J, Nong C, et al. Th17/treg imbalance mediates hepatic intolerance to exogenous lipopolysaccharide and exacerbates liver injury in triptolide induced excessive immune response. *J Ethnopharmacology* (2022) 295:115422. doi: 10.1016/j.jep.2022.115422

19. Wang X, Sun L, Zhang L, Jiang Z. Effect of adoptive transfer or depletion of regulatory T cells on triptolide-induced liver injury. *Front Pharmacol* (2016) 7:99. doi: 10.3389/fphar.2016.00099

20. Feng Z, Zhou C, Dong S, Liu Z, Liu T, Zhou L, et al. Catalpol and panax notoginseng saponins synergistically alleviate triptolide-induced hepatotoxicity through nrf2/are pathway. *Toxicol In Vitro* (2019) 56:141–9. doi: 10.1016/j.tiv.2019.01.016

21. Holland CH, Ramirez Flores RO, Myllys M, Hassan R, Edlund K, Hofmann U, et al. Transcriptomic cross-species analysis of chronic liver disease reveals consistent regulation between humans and mice. *Hepatol Commun* (2021) 6(1):161–77. doi: 10.1002/hep4.1797

22. Ritchie ME, Phipson B, Wu D, Hu Y, Law CW, Shi W, et al. Limma powers differential expression analyses for rna-sequencing and microarray studies. *Nucleic Acids Res* (2015) 43(7):e47–e. doi: 10.1093/nar/gkv007

23. Gustavsson E, Zhang D, Reynolds R, Garcia-Ruiz S, Ryten M. Ggtranscript: an R package for the visualization and interpretation of transcript isoforms using ggplot2. *Bioinf (Oxford England)* (2022) 38(15):3844–6. doi: 10.1093/bioinformatics/btac409

24. Wu T, Hu E, Xu S, Chen M, Guo P, Dai Z, et al. Clusterprofiler 4.0: A universal enrichment tool for interpreting omics data. *Innovation* (2021) 2(3):100141. doi: 10.1016/j.xinn.2021.100141

25. Shannon P, Markiel A, Ozier O, Baliga NS, Wang JT, Ramage D, et al. Cytoscape: A software environment for integrated models of biomolecular interaction networks. *Genome Res* (2003) 13(11):2498–504. doi: 10.1101/gr.1239303

26. Bader G, Hogue C. An automated method for finding molecular complexes in large protein interaction networks. *BMC Bioinf* (2003) 4:2. doi: 10.1186/1471-2105-4-2

27. Chin C-H, Chen S-H, Wu H-H, Ho C-W, Ko M-T, Lin C-Y. Cytohubba: identifying hub objects and sub-networks from complex interactome. *BMC Syst Biol* (2014) 8(S4):S11. doi: 10.1186/1752-0509-8-s4-s11

28. Miao Y-R, Xia M, Luo M, Luo T, Yang M, Guo A-Y, et al. Immucellai-mouse: A tool for comprehensive prediction of mouse immune cell abundance and immune microenvironment depiction. *Bioinformatics* (2022) 38(3):785–91. doi: 10.1093/bioinformatics/btab711

29. Miao YR, Zhang Q, Lei Q, Luo M, Xie GY, Wang H, et al. Immucellai: A unique method for comprehensive T-cell subsets abundance prediction and its application in cancer immunotherapy. *Advanced Sci* (2020) 7(7):1902880. doi: 10.1002/advs.201902880

30. Al Barashdi MA, Ali A, McMullin MF, Mills K. Protein tyrosine phosphatase receptor type C (Ptprc or cd45). *J Clin Pathol* (2021) 74(9):548–52. doi: 10.1136/jclinpath-2020-206927

31. Urbanek R, Suchard S, Steelman G, Knappenberger K, Sygowski L, Veale C, et al. Potent reversible inhibitors of the protein tyrosine phosphatase cd45. *J medicinal Chem* (2001) 44(11):1777–93. doi: 10.1021/jm000447i

32. Perron M, Saragovi H. Inhibition of cd45 phosphatase activity induces cell cycle arrest and apoptosis of cd45 lymphoid tumors ex vivo and in vivo. *Mol Pharmacol* (2018) 93(6):575–80. doi: 10.1124/mol.117.110908

33. Liu Y, Zhang M, Liao Y, Chen H, Su D, Tao Y, et al. Human umbilical cord mesenchymal stem cell-derived exosomes promote murine skin wound healing by neutrophil and macrophage modulations revealed by single-cell rna sequencing. *Front Immunol* (2023) 14:1142088. doi: 10.3389/fimmu.2023.1142088

34. Cowburn A, Summers C, Dunmore B, Farahi N, Hayhoe R, Print C, et al. Granulocyte/macrophage colony-stimulating factor causes a paradoxical increase in the bh3-only pro-apoptotic protein bim in human neutrophils. *Am J Respir Cell Mol Biol* (2011) 44(6):879–87. doi: 10.1165/rcmb.2010-0101OC

35. Song F, Yi Y, Li C, Hu Y, Wang J, Smith DE, et al. Regulation and biological role of the peptide/histidine transporter slc15a3 in toll-like receptor-mediated inflammatory responses in macrophage. *Cell Death Dis* (2018) 9(7):770. doi: 10.1038/s41419-018-0809-1

36. Wang Y, Hu Y, Li P, Weng Y, Kamada N, Jiang H, et al. Expression and regulation of proton-coupled oligopeptide transporters in colonic tissue and immune cells of mice. *Biochem Pharmacol* (2018) 148:163–73. doi: 10.1016/j.bcp.2017.12.025

37. Liu H, Ling CC, Yeung WHO, Pang L, Liu J, Zhou J, et al. Monocytic mdsc mobilization promotes tumor recurrence after liver transplantation via cxcl10/tlr4/mmp14 signaling. *Cell Death Dis* (2021) 12(5):489. doi: 10.1038/s41419-021-03788-4

38. Hintermann E, Bayer M, Pfeilschifter J, Luster A, Christen U. Cxcl10 promotes liver fibrosis by prevention of nk cell mediated hepatic stellate cell inactivation. *J Autoimmun* (2010) 35(4):424–35. doi: 10.1016/j.jaut.2010.09.003

39. Chang B, Xu MJ, Zhou Z, Cai Y, Li M, Wang W, et al. Short- or long-term high-fat diet feeding plus acute ethanol binge synergistically induce acute liver injury in mice: an important role for cxcl1. *Hepatology* (2015) 62(4):1070–85. doi: 10.1002/hep.27921

40. Dominguez M, Miquel R, Colmenero J, Moreno M, García-Pagán J, Bosch J, et al. Hepatic expression of cxc chemokines predicts portal hypertension and survival in patients with alcoholic hepatitis. *Gastroenterology* (2009) 136(5):1639–50. doi: 10.1053/j.gastro.2009.01.056

41. Bernal W, Lee W, Wendon J, Larsen F, Williams R. Acute liver failure: A curable disease by 2024? *J Hepatol* (2015) 62:S112–20. doi: 10.1016/j.jhep.2014.12.016

42. Krenkel O, Tacke F. Liver macrophages in tissue homeostasis and disease. *Nat Rev Immunol* (2017) 17(5):306–21. doi: 10.1038/nri.2017.11

43. Liu Z, Wang M, Wang X, Bu Q, Wang Q, Su W, et al. Xbp1 deficiency promotes hepatocyte pyroptosis by impairing mitophagy to activate mtdna-cgas-sting signaling in macrophages during acute liver injury. *Redox Biol* (2022) 52:102305. doi: 10.1016/j.redox.2022.102305

44. Tang C, Cen L, Zeng H, Zhang X, Liu P, Chen Y, et al. Inhibiting hepatocyte uric acid synthesis and reabsorption ameliorates acetaminophen-induced acute liver injury in mice. *Cell Mol Gastroenterol Hepatol* (2023). doi: 10.1016/j.jcmgh.2023.10.005

45. Arnold L, Henry A, Poron F, Baba-Amer Y, van Rooijen N, Plonquet A, et al. Inflammatory Monocytes Recruited after Skeletal Muscle Injury Switch into Antiinflammatory Macrophages to Support Myogenesis. *J Exp Med* (2007) 204 (5):1057–69. doi: 10.1084/jem.20070075

46. Zhou H, Zhou S, Shi Y, Wang Q, Wei S, Wang P, et al. Tgr5/cathepsin E signaling regulates macrophage innate immune activation in liver ischemia and reperfusion injury. *Am J Transplant Off J Am Soc Transplant Am Soc Transplant Surgeons* (2021) 21(4):1453–64. doi: 10.1111/ajt.16327

47. Wang C, Ma C, Gong L, Guo Y, Fu K, Zhang Y, et al. Macrophage polarization and its role in liver disease. *Front Immunol* (2021) 12:803037. doi: 10.3389/fimmu.2021.803037

48. Song B, Zhang C, Hu W, Guo C, Xia Z, Hu W, et al. Nano-Designed Carbon Monoxide Donor Sma/Corm2 Exhibits Protective Effect against Acetaminophen Induced Liver Injury through Macrophage Reprograming and Promoting Liver Regeneration. *J Controlled release Off J Controlled Release Soc* (2021) 331:350–63. doi: 10.1016/j.jconrel.2021.01.025

49. Sun H, Xu X, Shao H, Su X, Wu X, Wang Q, et al. Dectin-2 is predominately macrophage restricted and exhibits conspicuous expression during aspergillus fumigatus invasion in human lung. *Cell Immunol* (2013) 284:60–7. doi: 10.1016/j.cellimm.2013.06.013

50. Viriyakosol S, MdP J, Saijo S, Fierer J, Deepe GS. Neither dectin-2 nor the mannose receptor is required for resistance to coccidioides immitis in mice. *Infection Immun* (2014) 82(3):1147–56. doi: 10.1128/iai.01355-13

51. Chen Y, Li S, Huang X, Wang C, Pan Y, Xiang Q, et al. Tetraspan ms4a6d is a coreceptor of mhc class ii antigen (Mhc-ii) that promotes macrophages-derived inflammation. *Mol Immunol* (2023) 160:121–32. doi: 10.1016/j.molimm.2023.07.003

52. Cella M, Döhring C, Samaridis J, Dessing M, Brockhaus M, Lanzavecchia A, et al. A novel inhibitory receptor (Ilt3) expressed on monocytes, macrophages, and dendritic cells involved in antigen processing. *J Exp Med* (1997) 185(10):1743–51. doi: 10.1084/jem.185.10.1743

53. Katz H. Inhibition of pathologic inflammation by leukocyte ig-like receptor B4 and related inhibitory receptors. *Immunol Rev* (2007) 217:222–30. doi: 10.1111/j.1600-065X.2007.00522.x

54. Jiang Z, Qin J-J, Zhang Y, Cheng W-L, Ji Y-X, Gong F-H, et al. Lilrb4 deficiency aggravates the development of atherosclerosis and plaque instability by increasing the macrophage inflammatory response via nf-Kb signaling. *Clin Sci* (2017) 131(17):2275–88. doi: 10.1042/cs20170198

55. Chang C, Liu Z, Vlad G, Qin H, Qiao X, Mancini D, et al. Ig-like transcript 3 regulates expression of proinflammatory cytokines and migration of activated T cells. *J Immunol (Baltimore Md 1950)* (2009) 182(9):5208–16. doi: 10.4049/jimmunol.0804048

frontiers | Frontiers in Immunology

TYPE Original Research
PUBLISHED 11 January 2024
DOI 10.3389/fimmu.2023.1302006

OPEN ACCESS

EDITED BY
Shouxiong Huang,
University of Cincinnati, United States

REVIEWED BY
Chi Ma,
National Institutes of Health (NIH), United States
Jianyun Liu,
Indiana University Bloomington, United States

*CORRESPONDENCE
Arion Kennedy
akmidget@ncsu.edu

RECEIVED 25 September 2023
ACCEPTED 28 November 2023
PUBLISHED 11 January 2024

CITATION
Adams VR, Collins LB, Williams TI, Holmes J, Hess P, Atkins HM, Scheidemantle G, Liu X, Lodge M, Johnson AJ and Kennedy A (2024) Myeloid cell MHC I expression drives CD8$^+$ T cell activation in nonalcoholic steatohepatitis. *Front. Immunol.* 14:1302006. doi: 10.3389/fimmu.2023.1302006

Myeloid cell MHC I expression drives CD8$^+$ T cell activation in nonalcoholic steatohepatitis

Victoria R. Adams[1], Leonard B. Collins[2], Taufika Islam Williams[2,3], Jennifer Holmes[4], Paul Hess[4], Hannah M. Atkins[5,6], Grace Scheidemantle[1], Xiaojing Liu[1], Mareca Lodge[1], Aaron J. Johnson[7] and Arion Kennedy[1]*

[1]Department of Molecular and Structural Biochemistry, NC State University, Raleigh, NC, United States, [2]Molecular Education, Technology and Research Innovation Center (METRIC), NC State University, Raleigh, NC, United States, [3]Department of Chemistry, NC State University, Raleigh, NC, United States, [4]College of Veterinary Medicine, NC State University, Raleigh, NC, United States, [5]Center for Human Health and Environment, NC State University, Raleigh, NC, United States, [6]Division of Comparative Medicine, UNC Chapel Hill, Chapel Hill, NC, United States, [7]Department of Immunology, Mayo Clinic, Rochester, MN, United States

Background & aims: Activated CD8$^+$ T cells are elevated in Nonalcoholic steatohepatitis (NASH) and are important for driving fibrosis and inflammation. Despite this, mechanisms of CD8$^+$ T cell activation in NASH are largely limited. Specific CD8$^+$ T cell subsets may become activated through metabolic signals or cytokines. However, studies in NASH have not evaluated the impact of antigen presentation or the involvement of specific antigens. Therefore, we determined if activated CD8$^+$ T cells are dependent on MHC class I expression in NASH to regulate fibrosis and inflammation.

Methods: We used H2Kb and H2Db deficient (MHC I KO), Kb transgenic mice, and myeloid cell Kb deficient mice (LysM Kb KO) to investigate how MHC class I impacts CD8$^+$ T cell function and NASH. Flow cytometry, gene expression, and histology were used to examine hepatic inflammation and fibrosis. The hepatic class I immunopeptidome was evaluated by mass spectrometry.

Results: In NASH, MHC class I isoform H2Kb was upregulated in myeloid cells. MHC I KO demonstrated protective effects against NASH-induced inflammation and fibrosis. Kb mice exhibited increased fibrosis in the absence of H2Db while LysM Kb KO mice showed protection against fibrosis but not inflammation. H2Kb restricted peptides identified a unique NASH peptide Ncf2 capable of CD8$^+$ T cell activation *in vitro*. The Ncf2 peptide was not detected during fibrosis resolution.

Conclusion: These results suggest that activated hepatic CD8$^+$ T cells are dependent on myeloid cell MHC class I expression in diet induced NASH to promote inflammation and fibrosis. Additionally, our studies suggest a role of NADPH oxidase in the production of Ncf2 peptide generation.

KEYWORDS

liver, NASH, fibrosis, H2Kb, CD8$^+$ T cells, immunopeptidome

1 Introduction

Nonalcoholic fatty liver disease (NAFLD) represents a spectrum of liver pathologies, beginning with hepatic steatosis progressing to nonalcoholic steatohepatitis (NASH) and even hepatocellular carcinoma (HCC) (1). NASH is characterized by immune cell infiltration, inflammation, oxidative stress, and fibrosis in the liver (2). Recent studies have demonstrated in obese models of NASH, a pathogenic subset of hepatic $CD8^+$ T cells that are elevated and regulate hepatic inflammation and fibrosis (3–8). Although liver fibrosis was thought to be irreversible, recent studies have shown NASH associated fibrosis can be resolved and is dependent on a protective subset of $CD8^+$ T cells during resolution in mice (9). Although studies have highlighted various subsets of $CD8^+$ T cells involved in both NASH development and resolution, further investigation is required to better understand mechanisms that regulate immune cell activation.

In both humans and mouse, NASH-induced B and T cell infiltration positively correlate with the presence of antibodies targeting antigens derived from oxidative stress (10). Oxidative stress in the liver is especially detrimental as it can play a role in cellular dysfunction, injury, and even cell death (11–13). With the advancement of single cell RNA sequence, current studies have identified multiple subsets of $CD8^+$ T cells in human and mouse models of NAFLD (9, 14). Resident pathogenic $CD8^+$ T cells in NASH are classified as auto-aggressive toward hepatocytes. This subset is characterized by expressing high levels of CXCR6, cytotoxicity (granzyme), and exhaustion marker PD-1. However, the hepatic $CD8^+$ T cells were discovered to act in an antigen-independent manner relying on IL-15 driven transcriptional reprogramming and metabolic signals acetate and ATP for activation (14). Additionally, a subset of $CD8^+$ T cells during NASH resolution operate in a CCR5-dependent chemoattractant manner also relying on IL-15 (9).

Major histocompatibility complex (MHC) class I molecules are expressed on all nucleated cells and are responsible for presenting short antigen peptides (8-11 amino acids in length) to $CD8^+$ T cells. In mice, this region is referred to as the histocompatibility 2 (H2) complex and expresses three class I loci (K, D, and L) equivalent to human class I loci HLA-A, HLA-B, and HLA-C. In humans, limited studies have addressed the impact of MHC Class I in regulating NAFLD associated pathologies. Human HLA class I alleles such as HLA*B27 are associated with advanced steatosis, while alleles HLA*C4, HLA*A31 and HLA*C6 correlate with NASH and advanced fibrosis (15, 16). These genes are highly polymorphic, having numerous alleles for each locus (k, d, b, k, q), and are involved in regulating the peptide binding activities of MHC I (17). Peptides are obtained through proteasomal degradation of ubiquitinated proteins where they are loaded onto MHC I molecules in the ER and brought to the cell surface. They are typically presented on classical antigen presenting cells (APCs) such as macrophages, monocytes, or dendritic cells. At the cell surface $CD8^+$ T cells are primarily activated by MHC class I bound peptides. Each T cell receptor has the capability for rearrangement which allows these cells to recognize many different peptides in order to become activated (8). However, it remains to determined how the MHC I immunopeptidome is altered during NASH and if this plays a role in $CD8^+$ T cell activation. Thus, understanding the role of peptide presentation by MHC class I is important for elucidating mechanisms of $CD8^+$ T cell activation in NASH.

Our findings indicate that $CD8^+$ T cell activation in NASH is dependent on H2Kb expression. Knockout of H2Kb and H2Db leads to significant reductions in $CD8^+$ T cell activation and hepatic fibrosis during NASH development. Lack of H2Kb in myeloid cells protected against liver fibrosis and $CD8^+$ T cell activation but not inflammation. Mice with NASH expressed a unique hepatic H2Kb immunopeptidome compared to steatosis and normal mouse. We identified the NASH peptide Ncf2 and demonstrated this peptide activates NASH $CD8^+$ T cells *in vitro*. Activated Ncf2 specific $CD8^+$ T cells were also detected in NASH mice *in vivo* This is further supported by the absence of the Ncf2 peptide during fibrosis resolution. Thus, the Ncf2 peptide may be a driving factor in antigen dependent $CD8^+$ T cell activation in NASH.

2 Materials and methods

2.1 Animal models

Male 5-wk-old C57BL/6J and low-density lipoprotein receptor knockout (LDLRKO) mice were originally purchased from Jackson Laboratories (Bar Harbor, ME) and further propagated in our colony. C57BL/6J mice were used to generate MHC I-deficient mice that lack endogenous H2Db and H2Kb (MHC I KO). Transgenic Kb mice were generated by introducing the H2Kb transgene (Kb LoxP) into MHC I KO mice developed by the Mayo Clinic Transgenic Mouse Core (Rochester, MN). Kb mice were then crossed with MHC I deficient mice expressing Cre recombinase under the LysM promoter (LysM Kb KO, myeloid cell specific). This cross generated a conditional knockout of Kb in myeloid cells. All Mouse genotypes were confirmed through flow cytometry. MHC I KO, Kb, and LysM Kb KO mice were donated from Dr. Aaron Johnson and further propagated in our colony (18).

WT Amylin NASH Model. Male 6-wk-old C57BL/6J (WT) mice were fed chow or amylin diet (AMLN, 40 kcal% fat, 20 kcal% fructose and 2% cholesterol, Diet # D09100310i, Research Diets) for 28 weeks. *LDLRKO NASH model*. Male 6-wk-old *LDLRKO* mice were fed chow or western diet (WD, 42 Kcal% fat with 0.2% added cholesterol, TD.22137; Harlan Laboratories) for 12 weeks. *WT Sucrose WD NASH model*. Male 6-wk-old C57BL/6J wild type (WT) mice were fed chow or western diet (WD, 42 Kcal% fat with 0.2% added cholesterol, TD.22137; Harlan Laboratories) with 30% glucose/fructose water for 25 weeks. *Taconic Amylin NASH Model*. C57BL/6NTac (Tac) male mice were purchased from Taconic Biosciences on chow or amylin diet (AMLN, 40 kcal% fat, 20 kcal% fructose and 2% cholesterol, Diet # D09100310i, Research Diets) remaining on diet for a total of 28 weeks. *Taconic Amylin Resolution Model*. Taconic mice were purchased from Taconic Biosciences on chow or amylin diet as described previously. For the resolution model (RES), NASH mice after 28 weeks on amylin diet were switched to a chow diet for 5 weeks.

MHC I KO, Kb, and LysM Kb KO Studies. 6-wk-old male mice from WT, MHC I KO, Kb, LysM Kb KO were fed chow or amylin diet (AMLN, 40 kcal% fat, 20 kcal% fructose and 2% cholesterol, Diet # D09100310i, Research Diets) for 28 weeks.

All Mice were housed with ad libitum access to food and water on a 12-hour light/dark cycle. Mice were sacrificed between the ages of 15-34 weeks. Tissues were snap-frozen and stored in -80°C freezer. All animal procedures were approved by the Institutional Animal Care and Use Committee (IACUC) at North Carolina State University under protocol 21-502-B.

2.2 Immune cell isolation from liver

Mice were anesthetized and perfused through the heart with 1X PBS. Mouse livers were collected and minced in RPMI, 1 mg/ml Collagenase IV, 2 mg/ml Collagenase II, 1 mg/ml Protease, and 0.01 mg/ml DNase and incubated at 37°C for 25 min shaking. The cell suspension was filtered through a 100-µm filter with wash buffer and centrifuged at 443 xg for 6 min at 4°C. Supernatant was discarded and the pellet washed and centrifuged at 443 xg for 6 min at 4°C. The pellet was resuspended in 33% Percoll and centrifuged at 850 xg for 15 min at 4°C with minimum break and accelerator. The pellet was resuspended in wash buffer and centrifuged at 300 xg for 5 min at 4°C and the supernatant discarded. The pellet was resuspended in ACK lysing buffer and incubated at room temperature for 5 min. After incubating, wash buffer was added and centrifuged at 300 xg for 5 min at 4°C. The supernatant was discarded and the pellet resuspended in FACS buffer filtered through a cell strainer cap tube and prepared for cell culture or flow cytometry.

2.3 $CD8^+$ T cell isolation from spleen

Mouse spleens were isolated and strained through a 100-µm filter with FACS buffer and centrifuged at 500 xg for 5 min at 4°C. Pellets were washed with FACS and centrifuged at 500 xg for 5 min at 4°C. Pellets were resuspended in ACK Lysing Buffer and incubated on ice for 5 mins. After incubation FACS buffer was added and centrifuged at 500 xg for 5 min at 4°C. Supernatants were discarded and pellets resuspended in 1ml FACS buffer and filtered through a cell strainer cap tube. Cells were centrifuged at 500 xg for 5 min at 4°C and resuspended in FACS buffer and prepared for T cell assays.

2.4 Flow cytometry

Isolated cells from the liver were incubated with Fc block followed by incubation with fluorophore conjugated antibodies on ice in FACS buffer for the following panels: T cell panel: CD8a (PE-Cy7, 1:200, BD Biosciences), TCRβ (APC-Cy7, 1:200, BD Biosciences), CD44 (A700, 1:200, BD Biosciences), and CD62L (APC, 1:200, BD Biosciences). T cell subsets panel: CD8a (PE-Cy7, 1:200, BD Biosciences), TCRβ (APC-Cy7, 1:200, BD Biosciences), CD44 (A700, 1:200, BD Biosciences), CD62L (APC, 1:200, BD Biosciences), CXCR6 (FITC, 1:100, Biolegend), CCR7 (PerCP-Cy5.5, 1:100, Biolegend), and Ncf2 Tetramer (PE, 1:100, NIH Tetramer Core Facility). NK T cell panel: NK1.1 (PE, 1:100, BD Biosciences), TCRβ (APC-Cy7, 1:200, BD Biosciences), CD8a (PE-Cy7, 1:200, BD Biosciences), and CD4 (AF488, 1:200, BD Biosciences). Macrophage Panel: F4/80 (A700, 1:200, Biolegend), CD64 (PE, 1:200, BD Biosciences), CD11b (FITC, 1:200, BD Biosciences), Ly6c (PerCP-Cy5.5, 1:200, BD Biosciences), H2Kb (APC-eFluor780, 1:200, ThermoFisher), and H2Db (PE-Cy7, 1:200, BD Biosciences). After incubation samples were washed twice with FACS buffer. Flow data was acquired on a Becton Dickinson LSRII machine in the NCSU flow Cytometry Core. All data was analyzed using FlowJo software v10.8. Flow gating strategies are provided (Supplementary Figures 1A, B).

2.5 Liver tissue histology staining

Paraffin-embedded sections from mouse livers were used for Hematoxylin and eosin (H&E) and Sirius red staining (7). Whole slide images were captured on BioTek Cytation 5 at 10X magnification.

2.6 RNA isolation and real time RT-PCR

For RNA isolation, 25 mg of frozen liver tissue was homogenized in Tri-Reagent (Fisher) and extracted using Direct-zol RNA MiniPrep kit (Genesee) according to manufacturer's instructions. cDNA was synthesized on a BioRad iQ5 thermocycler using qScript cDNA supermix (QuantaBio) according to manufacturer's instructions. Real-time RT-PCR analysis was performed using PerfeCTa qPCR FastMix II (QuantaBio) and TaqMan assay (ThermoFisher) on a 7500 fast Dx thermocycler. Relative gene expression was normalized to 18s expression and determined using the delta-delta CT method. All sample reactions performed in duplicate. All TaqMan assays used can be found in STAR methods.

2.7 Western analysis

A 50 mg piece of frozen liver was homogenized in 0.5 ml of RIPA buffer (150 mM Sodium Chloride, 1% Triton X-100, 0.5% Sodium Deoxycholate, 0.1% SDS, 50 mM Tris, and 1 mM EDTA) containing 1X protease and phosphatase inhibitor cocktail (Halt). Samples were centrifuged for 15 min at 12,000 rpm at 4°C. Supernatants were aspirated and protein quantified using Pierce BCA protein assay according to manufacturer's instructions. Proteins were separated by SDS-PAGE and transferred to activated PVDF membranes. Membranes were blocked with OneBlock blocking buffer (Prometheus, Genessee Scientific) for 1 hr at room temperature shaking. Membranes were then probed with antibodies specific for Ncf2 (ThermoFisher), H2Kb (BioXCell), or H2Db (Santa Cruz) at 4°C shaking overnight. All blots were

probed for β-actin (Cell Signaling Technology) 1 hr at room temperature. After blocking membranes were washed three times for 5 min in 1X PBS with 0.1% Tween-20 at room temperature. After washing membranes were incubated with Licor secondary antibodies goat anti-rabbit IRDye 800CW and goat anti-mouse IRDye 680RD at 1:10,000 dilutions with 0.1% Tween-20 for 1 hr at room temperature protected from light. Blots were washed again as described previously and imaged on Odyssey Infrared Imaging System. Band intensity quantification was obtained using Image Studio Lite version 5.2 software.

2.8 Isolation of H2Kb peptides from liver

Liver lysates were prepared following Kowalewski's methods with some modifications (19). Livers were isolated and pooled together 5 Control or 5 NASH age matched mice or isolated individually and immediately minced in one volume of 2x solubilization buffer (1X PBS, 12% CHAPS, protease inhibitor mini tablet (Pierce), and PhosSTOP inhibitor tablet (Roche). Lysates were then manually homogenized and rinsed in 1X solubilization buffer and stirred for 1 hr at 4°C. Lysates were sonicated with 120w of ultrasonic power and 30% pulse length for 3 min on ice and then stirred for 1 hr at 4°C. Lysates were then centrifuged at 2,000 x g for 20 min. Supernatants were collected and subjected to ultracentrifugation at 150,000 x g for 70 min at 4°C. Supernatants were collected and filtered through a 0.22 μm pore syringe filter.

Column preparation was modified from methods by Chen and colleagues (20). 1 ml HiTrap NHS-activated HP immunoaffinity columns (Cytiva) were prepared based on the following steps. Briefly, a drop of ice-cold 1 mM HCl was added to the top of the column and 6 ml of ice-cold 1 mM HCl was added to the column at a flow rate not exceeding 1 ml/min. For antibody coupling 10 ml of 1 mg/ml anti-H2Kb mAb (Clone:Y3, BioXCell) antibody in antibody coupling buffer (0.2 M of NaHCO3, 0.25 M NaCl, pH 8.3) was circulated at a flow rate of 1 ml/min for 4 hr at 4°C with a peristalsis pump. To deactivate any excess active groups, the column was injected with 3 x 2 ml buffer A (0.5 M ethanolamine, 0.25 M NaCl, pH 8.3) and 3 x 2 ml buffer B (0.1 M sodium acetate, 0.25 M NaCl, pH 4) alternatively with a syringe not exceeding 1 ml/min. After the column was left to rest at room temperature for 30 min, alternate washes of 3 x 2 ml buffer B and 3 x 2 ml buffer A were injected into the column. The prepared liver lysate was then continually circulated over the column overnight at a flow rate of 1 ml/min at 4°C. Columns were then washed with the following buffers: 15 ml of wash buffer 1 (50 mM Tris-HCl, pH 8, 75 mM NaCl, and 1% CHAPS), 15 ml of wash buffer 2 (50 mM Tris-HCl, pH 8, 75 mM NaCl in deionized H2O), 25 ml of wash buffer 3 (50 mM Tris-HCl, pH 8, 225 mM NaCl in deionized H2O), and 35 ml of wash buffer 4 (50 mM Tris-HCl, pH 8 in deionized H2O). H2Kb peptides were eluted in 6 ml of 10% acetic acid and filtered using a 3kDa ultrafiltration filter (Millipore) and frozen in -80°C. Frozen peptide elutes were lyophilized overnight and resuspended in 300 μL of 0.1% TFA. Peptide solutions were desalted using peptide desalting columns (Pierce) according to manufacturer's instructions.

2.9 Analysis of H2Kb peptides by LC-MS/MS

Immunoaffinity H2Kb captured peptide solutions were analyzed by a discovery proteomics workflow using a hybrid quadrupole-orbitrap mass spectrometer (Thermo Scientific™ Orbitrap Exploris™ 480, Bremen Germany) incorporating an Easy-Spray™ nanoelectrospray source (Thermo Scientific™, San Jose) coupled to an Easy-nLC™ 1200 nano-liquid-chromatography system (Thermo Scientific™, San Jose). Mass spectrometry data were acquired using non-targeted data-dependent acquisition (DDA) at top scan speed with a full experiment time of 3 seconds. Samples were injected in a random order. Commercially obtained, standardized bovine serum albumin (BSA) digest and HeLa digest were evaluated throughout the injection sequence to ensure proper nanoLC–MS/MS reproducibility. Proteins were identified by processing raw nanoLC/MS data with Proteome Discoverer 2.5 software (Thermo Scientific™, San Jose, CA) using a Mus musculus protein database obtained from Swiss-Prot (Taxon 10090 including sub-taxonomies; 17,090 sequences).

2.10 Analysis of lipid species by LC-MS/MS

Liver lipids were measured using methods previously described (21).

2.11 Peptide synthesis

Unique NASH H2Kb restricted peptides were synthesized at a crude purity from Peptide 2.0 Inc (Chantilly, VA). Synthetic peptides were used for functional assays and LC-MS/MS validation.

2.12 H2Kb peptide binding assay

RMA-S cells were seeded into a 96 well plate at $1x10^5$ per well in 100 μL of media (RPMI with 10% FBS) and incubated at 27°C for 18 hrs. Following incubation cells were treated with 100 μM of vehicle control, Ova, Ncf2 peptide, or Gpnmb peptide (FVYVFHTL) and incubated at 37°C for 5 hrs. Cells were harvested for flow cytometry and incubated with Fc block for 5 min followed by a 30 min incubation with fluorophore conjugated antibodies on ice in FACS buffer for H2Kb (APC-eFluor780, 1:200, ThermoFisher) and Propidium Iodide (PI, 1:10,000, ThermoFisher). Data for this assay was acquired on a BD Accuri C6 machine. All data was analyzed using FlowJo software v10.8.

2.13 $CD8^+$ T cell activation assay

96 well plates were initially coated with IgG (clone RTK2758, BioLegend) and incubated at room temperature for 3 hr. Plates were washed twice with PBS and coated with 1 μg/ml anti-CD3 (clone

145-2C11, Bio-Rad) and 1 μg/ml anti-CD28 (clone E18, Bio-Rad) overnight at 4°C. Plates were washed twice with PBS prior to plating cells. Unstimulated samples were not cultured with CD3 or CD28 and supplemented only with IL-2. Immune cells were isolated from livers or spleens of NASH mice as described previously and $CD8^+$ T cells were magnetically sorted using a $CD8^+$ T cell isolation kit (Miltenyi Biotec). $CD8^+$ T cells were stained with cell trace violet (Life Technologies) according to manufacturer's instructions. RMA-S cells were treated with vehicle control, Ova, Ncf2 peptide, or Gpnmb peptide as described previously. $CD8^+$ T cells were plated at $5x10^4$ per well and co-cultured with $1x10^4$ of treated RMA-S cells per well in a total of 200 μL of RPMI medium (Corning) supplemented with 10% FBS, L-glutamine (400 mM), penicillin (100 U/ml), streptomycin (100 μg/ml), 2-mercaptoethanol (50 μM), and IL-2 (100 ng). Cells were cultured at 37°C and harvested after 3 and 5 days and prepared for flow cytometry using the $CD8^+$ T cell panel. T cell activation assay for genotype comparisons of WT, MHC I KO, and Kb $CD8^+$ T cells were plated in 6 well plates with $1.5x10^5$ cells/well in 2 ml of media under stimulated or unstimulated conditions for 3 days and harvested for flow cytometry. Data for this assay was acquired on a Beckman Coulter CytoFLEX machine in the NCSU flow Cytometry Core. All data was analyzed using FlowJo software v10.8.

2.14 Cytokine analysis

Media from T cell activation assays were collected and analyzed using a 9-plex mouse luminex discovery assay targeting RANTES, Granzyme B, IFN-gamma, Il-2, IL-4, IL-6, IL-10, IL-13 and TNF alpha on the Bio-Rad Bio-Plex 200 multiplex suspension array system in the Advanced Analytical Core at UNC Chapel Hill. Media was diluted to 1:5 using assay buffer.

2.15 Statistical analysis

GraphPad Prism 10.0.2 software was used for all statistical analyses. Two-tailed unpaired Student's t-tests were performed for two group comparisons. Two-way ANOVA was performed for genotype versus diet studies followed by multiple T test comparisons. All data is presented as the mean ± SEM. Data was considered statistically significant for $P<0.05$ (*), $P<0.01$ (**), $P<0.001$(***), and $P<0.0001$(****).

3 Results

3.1 H2Kb and H2Db is upregulated in myeloid cells NASH

Our previous work has shown increased activated $CD8^+$ T cells in the LDLRKO obese/hyperlipidemia mouse model of NASH. We have shown that $CD8^+$ T cells play a key role in regulating inflammation and fibrosis through CD8 antibody depletion and adoptive transfer studies (7). However, limited studies have focused on how these cells are activated and how antigen presentation plays a role in their activation (14).

We demonstrate that activated $CD8^+$ T cells are significantly increased in obese mouse models of NASH using low density lipoprotein receptor knockout mice (LDLRKO) on western diet (WD) (Supplementary Figures 2A, B) and Taconic mice on amylin diet (Tac NASH) (Supplementary Figures 2C, D). Because $CD8^+$ T cells are class I restricted, we evaluated the expression of MHC I isoforms, H2Kb and H2Db, under NASH conditions. Total liver protein analysis revealed H2KB protein expression was significantly upregulated during NASH with increasing trends for H2DB expression (Figures 1A, B, Supplementary Figures 2E, F). We used flow cytometry analysis to determine if NASH impacts myeloid specific expression of H2Kb and H2Db in WT mice fed amylin diet for 28 weeks. Macrophages and recruited monocytes are elevated in NASH and crucial to inflammation, fibrosis, and immune cell activation in chronic liver diseases (22). In $CD11b^+$ myeloid cells, overall H2Kb expression was significantly increased compared to H2Db expression. Additionally, H2Kb expression was significantly increased in NASH compared to chow suggesting H2Kb may play a larger role in antigen presentation in NASH (Figure 1C). Our studies confirmed increased monocytes ($Ly6c^+$ $CD11b^+$), monocyte derived macrophages ($Ly6c^+CD11b^+F480^+CD64^+$), and macrophage populations ($Ly6c^-CD11b^+F480^+CD64^+$) in NASH (Figures 1D, G, J). Additionally, H2Kb and H2Db were significantly increased in the myeloid cell populations in NASH compared to chow controls (Figures 1E, F, H, I, K, L). These findings were consistent across Tac NASH and LDLRKO NASH models (Supplementary Figures 3A–O). In summary, H2Kb and H2Db are increased in myeloid cells in NASH livers. However, it remains unknown how changes in the expression of H2Kb or H2Db impact NASH progression.

3.2 Myeloid cell H2Kb controls NASH associated hepatic $CD8^+$ T cell activation

Given that H2Kb had higher overall expression in myeloid cells compared to H2Db, we then investigated the impacts of H2Kb on the activation of $CD8^+$ T cells in NASH. To probe the function of H2Kb in NASH, we used three genetically modified mouse models: mice lacking H2Kb and H2Db (MHC I KO), expressing only H2Kb and no H2Db (Kb), and conditional Kb knockout in myeloid cells (LysM Kb KO). By flow analysis, H2Kb and H2Db were not detected in the livers of MHC I KO mice. H2Kb was only detected with no H2Db expression in the Kb mouse model, and the LysM Kb KO mouse model was deficient in H2Kb on $CD11b^+$ cells (Supplementary Figures 4A–C).

After 28 weeks, amylin diet significantly increased epididymal fat in WT, MHC I KO, Kb, and LysM Kb KO mice. MHC I KO mice on amylin diet behaved most similar to WT with increased body weight and liver weights. Interestingly, Kb and LysM amylin fed mice had reduced liver weights compared to WT amylin fed mice and no changes in body weight in the Kb amylin fed mice (Figures 2A, B). To further understand how MHC I impacts NASH pathology, liver tissue sections were stained with H&E. WT amylin mice demonstrated diffuse lipid accumulation and

10.3389/fimmu.2023.1302006

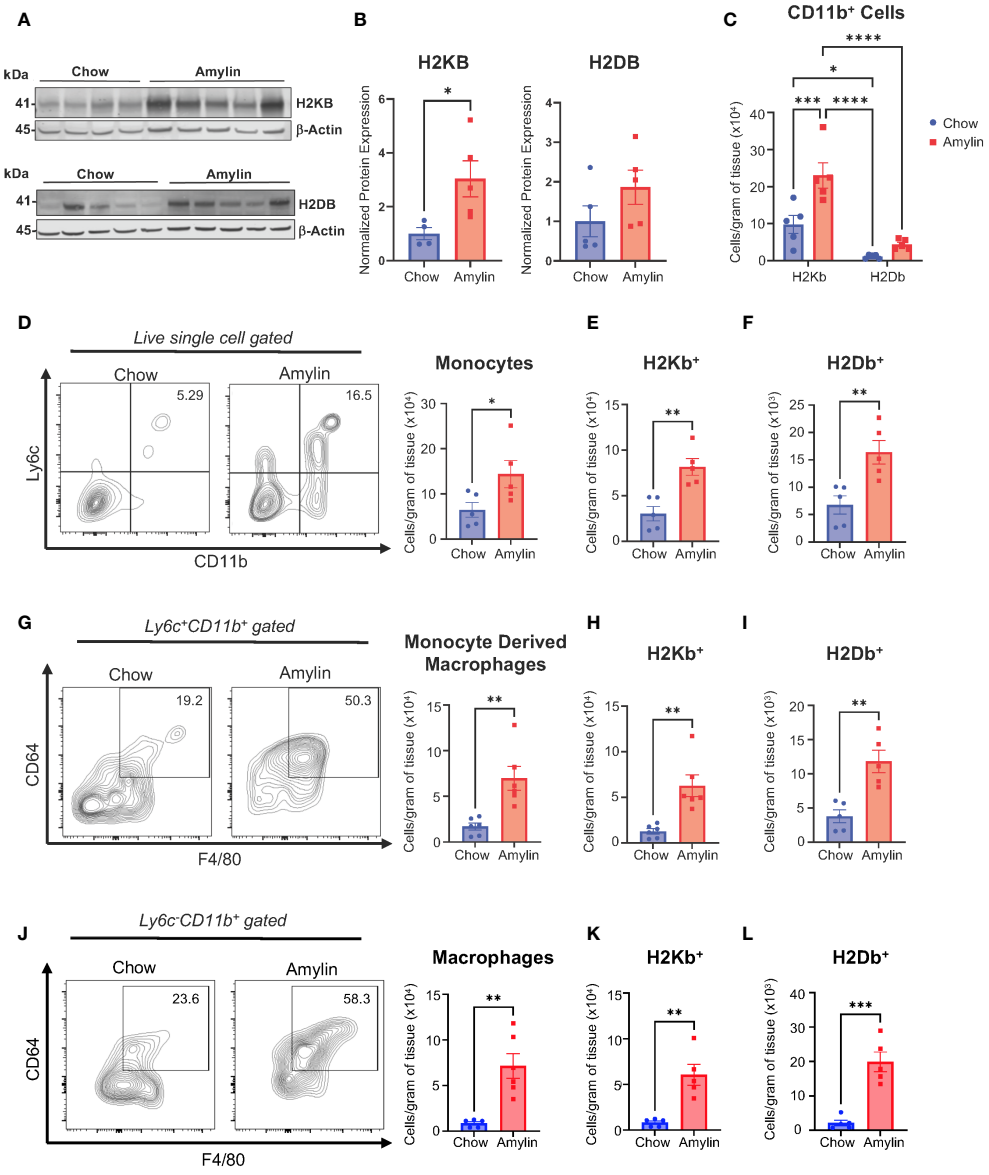

FIGURE 1
H2Kb is upregulated in myeloid cells in NASH. WT mice were fed chow or amylin diet for 28 wks (n=5 per group) in two replicate cohorts. **(A)** Total liver protein of H2KB and H2DB. **(B)** Quantification of protein expression normalized to β-actin. **(C)** Total CD11b$^+$ cells gated for H2Kb and H2Db. **(D)** Flow analysis of monocytes (*Ly6c$^+$CD11b$^+$*) and monocyte H2Kb **(E)** and H2Db **(F)** expression. **(G)** Flow analysis of monocyte derived macrophages (*Ly6c$^+$CD11b$^+$CD64$^+$F4/80$^+$*) monocyte derived macrophage H2Kb **(H)** and H2Db **(I)** expression. **(J)** Flow analysis of macrophages (*Ly6c$^-$CD11b$^+$CD64$^+$F4/80$^+$, CLEC4F$^+$*) and macrophage H2Kb **(K)** and H2Db **(L)** expression. Flow plots show percentage of parent gate. Data shown as the mean ± SEM. Two-tailed unpaired Student's t-tests and determined significant by P<0.05 (*), P<0.01 (**), P<0.001 (***), and P<0.0001(****).

minimal lymphatic inflammation compared to chow controls. However, no significant changes were detected between WT, MHC I KO, and LysM Kb KO mice on amylin diet. In contrast, Kb amylin fed mice displayed hepatocyte necrosis and oval cell hyperplasia (Figure 2C, Supplementary Table 1). Notably, MHC I KO and LysM Kb KO mice were protected against NASH induced increases in hepatic gene expression of immune cell markers *Cd8* and *Cd11b*. Whereas Kb mice responded similar to WT mice on amylin diet with increased expression of both markers (Figure 2D). Next, we determined how the loss of MHC I, H2Kb expression only, and H2Kb expression in myeloid cells impacts hepatic CD8$^+$ T cell activation during NASH development. Flow cytometry analysis demonstrated that MHC I KO and LysM Kb KO mice were protected from hepatic CD8$^+$ T cell activation compared to WT and Kb amylin mice (Figures 2E, F).

Because MHC I disruption can reduce CD8$^+$ T cell generation and impact natural killer (NK) T cell functions, we evaluated changes in CD8$^+$ T cells and NK cells in WT, MHC I KO, Kb, and LysM Kb KO chow mice. Interestingly, no significant changes were identified in the number of liver CD8$^+$ T cells between the WT and MHC I KO, Kb, or LysM Kb KO mice. However, MHC I KO mice demonstrated significant reductions in both spleen and blood CD8$^+$ T cell numbers (Supplementary Figure 4D) (23). We next evaluated if MHC I deletion impacts CD8$^+$ T cell function in

10.3389/fimmu.2023.1302006

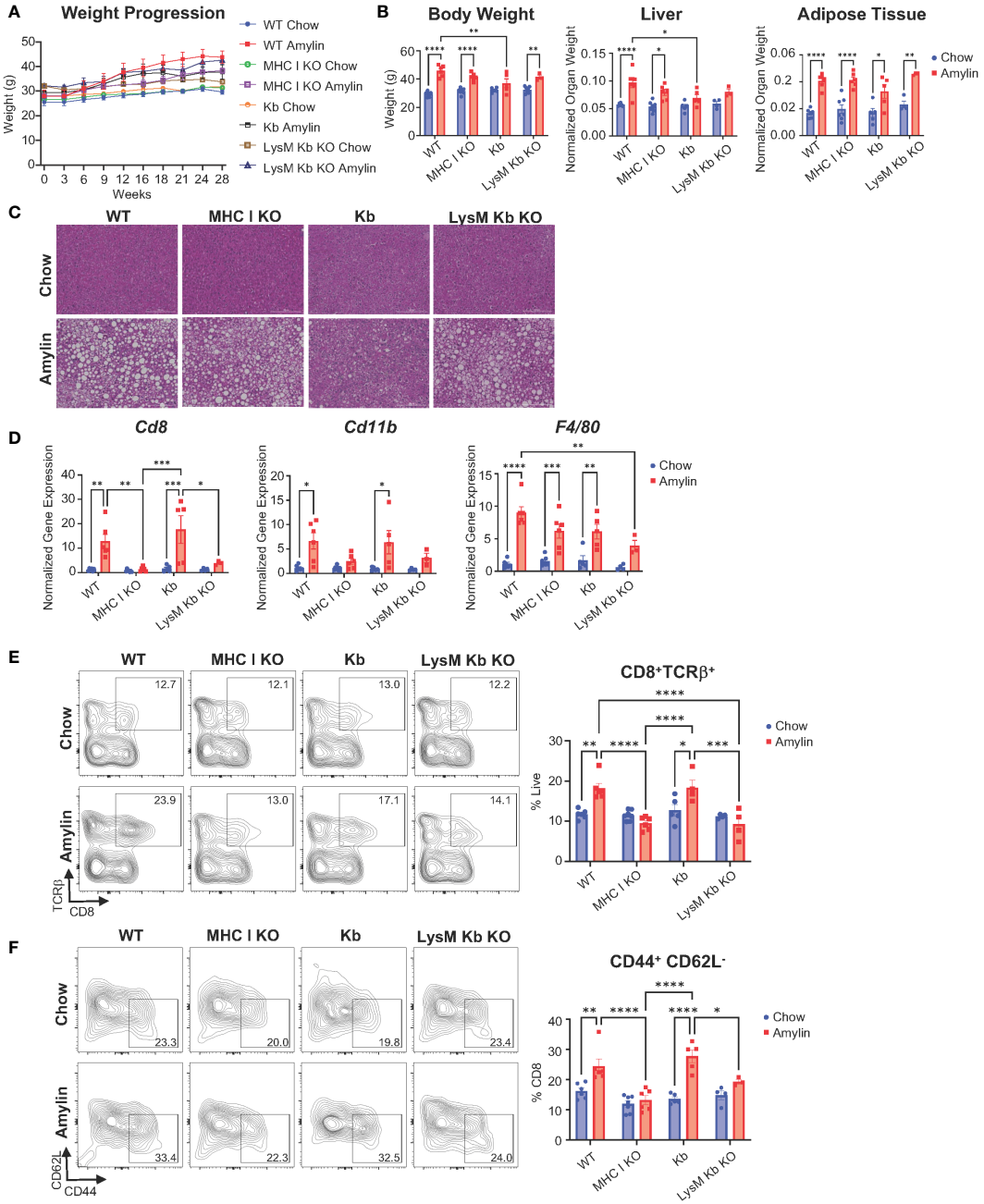

FIGURE 2
MHC I KO and LysM Kb KO prevent CD8$^+$ T cell activation in NASH. WT, MHC I KO, Kb or LysM Kb KO mice were on diet for 28 wks (n=3-7 per group) in two replicate cohorts. **(A)** Weight progression over time. **(B)** Body weight, liver weight, and adipose tissue weight after 28 wks on diet. **(C)** Representative images of H&E staining of mouse liver sections. **(D)** Hepatic gene expression. Flow analysis of *Tcrβ$^+$CD8$^+$* T cells **(E)** and activation (*CD44$^+$CD62L$^-$*). **(F)** Flow plots show percentage of parent gate. Data shown as the mean ± SEM. Two-way ANOVA were performed and determined significant by P<0.05 (*), P<0.01 (**), P<0.001 (***), and P<0.0001 (****).

both the spleen and liver. Isolated splenic or liver CD8$^+$ T cells were cultured under unstimulated or stimulated conditions with CD3/CD28 to confirm functionality in the MHC I KO genotype. Using flow cytometry, we identified less splenic CD8$^+$ T cells in the MHC I KO model and no differences between WT and Kb CD8$^+$ T cells. Both MHC I KO and Kb CD8$^+$ T cells responded to stimulation with increased activation (*CD44$^+$*, *CD62L$^-$*) and proliferation comparable to WT CD8$^+$ T cells (Supplementary Figures 4E–G). Previous studies have evaluated the impact of Kb deletion in myeloid cells on CD8$^+$ T cell development. These studies reported no significant changes in the proportion of CD8$^+$ T cells or changes in the TCR repertoire diversity (18). Liver CD8$^+$ T cells in the MHC I KO mice did not to respond to CD3/CD28 stimulus to the same extent as WT mice with less total CD8$^+$ TCRβ$^+$ cells present under stimulated conditions. However, MHC I KO CD8$^+$ T cells were still able to response to stimulus with increased activation and proliferation (Supplementary Figures 4H–J).

10.3389/fimmu.2023.1302006

To determine if altered MHC I expression impacts NK1.1+ and NK T cells, immune cells from livers of chow WT, MHC I KO, Kb, and LysM Kb KO mice were evaluated. Flow cytometry analysis revealed no significant differences in $NK1.1^{+}TCR\beta^{-}$ and $NK1.1^{+}TCR\beta^{+}$ cells between WT and MHC I KO, Kb, and LysM Kb KO mice (Supplementary Figures 5A,B). Additionally, no significant changes were detected in $NK1.1^{+}TCR\beta^{+}$ subsets for $CD4^{+}$ and $CD4^{-}CD8^{-}$ subsets (Supplementary Figures 5D, E). Previous studies support the lack of NK response to the missing MHC I as studies in β2m KO mice are not autoreactive and are tolerant to the MHC I deficiency (24–26).

Taken together, our results show that the absence of H2Kb and H2Db, and myeloid specific deletion of H2Kb protects against NASH associated $CD8^{+}$ T cell activation whereas H2Kb expression, in the absence of H2Db, increases $CD8^{+}$ T cell activation.

3.3 MHC I KO protects against NASH associated inflammation and fibrosis while LysM Kb KO only protects against fibrosis

We next evaluated the impact of MHC I function on hepatic inflammation and fibrosis. In the absence of H2Kb and H2Db, mice were protected from diet induced increases of inflammatory genes *Tnf*, *Il1b and Il10* and compared to WT amylin mice. However, Kb and LysM Kb KO mice demonstrated significant increases in *Tnf* with amylin diet. MHC I KO and Kb mice had significant reductions in Il10 expression while LysM Kb KO mice increased with amylin diet (Figure 3A). Interestingly, MHC I KO and LysM Kb KO mice were protected from diet induced fibrosis with significant reductions in hepatic gene expression of fibrotic markers *Col1a1* and *Tgfβ* in contrast to the significant increases in WT and Kb mice on amylin (Figure 3B). In correlation with gene expression, MHC I KO and LysM Kb KO mice showed significant reductions in Sirius red staining compared to WT and Kb amylin mice. Interestingly, Kb amylin mice demonstrated significantly increased collagen deposition compared to WT amylin mice. (Figure 3C). To examine hepatic steatosis, we performed mass spectrometry analysis of lipid species in the liver. We found total liver triglycerides and diglycerides were significantly upregulated with amylin diet and not impacted by genotype (Figure 3D).

Our findings suggest that H2Kb and H2Db are necessary for NASH induced $CD8^{+}$ T cell activation, inflammation, and fibrosis but do not regulate hepatic lipid accumulation. Additionally, H2Kb expression in the absence of H2Db leads to advanced NASH fibrosis. Meanwhile, H2Kb specific knockout in myeloid cells reduced fibrosis but not NASH associated inflammation.

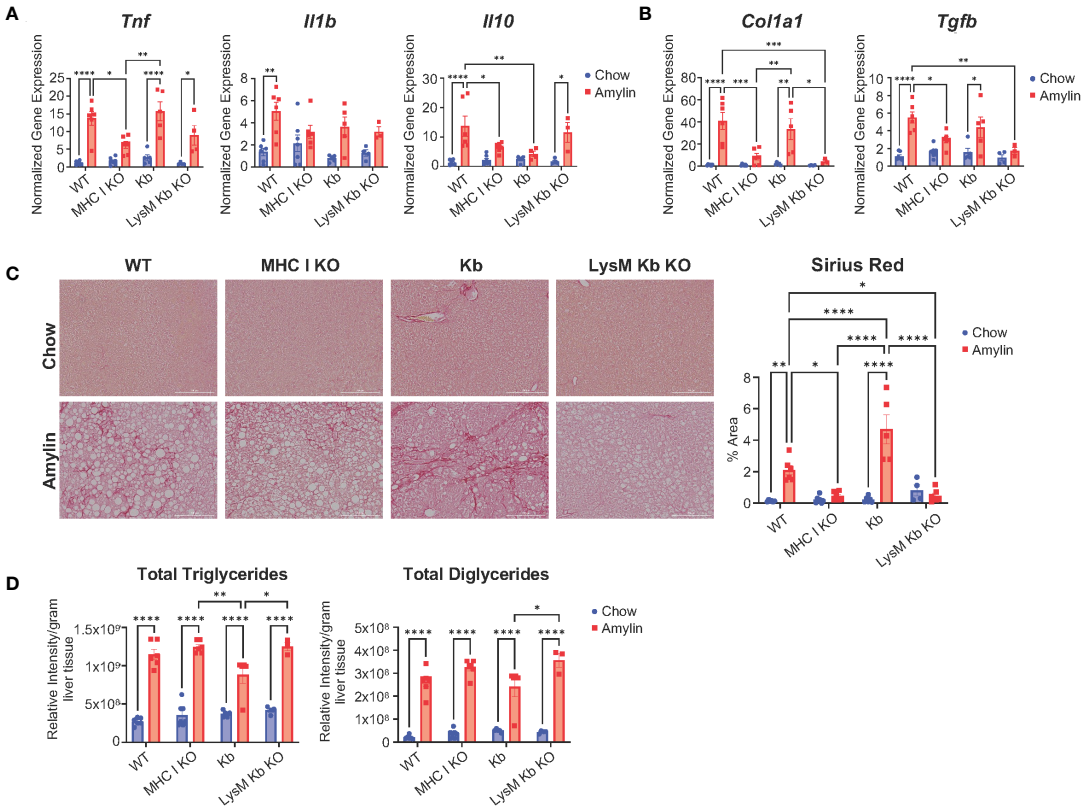

FIGURE 3
MHC I KO and LysM Kb KO are protective against NASH. WT, MHC I KO, Kb, or LysM Kb KO mice were on diet for 28 wks (n=3-7 per group, in two replicate cohorts). **(A, B)** Hepatic gene expression. **(C)** Representative figures of Sirius red staining of mouse liver sections and quantification. **(D)** Quantification of liver triglyceride and diglyceride lipid species detected by LC-MS/MS analysis. Data shown as the mean ± SEM. Two-way ANOVA were performed and determined significant by P<0.05 (*), P<0.01 (**), P<0.001 (***), and P<0.0001 (****).

3.4 Ncf2 is a unique H2Kb restricted peptide in NASH

Given H2Kb expression is important for CD8$^+$ T cell activation, we aimed to identify H2Kb restricted peptides in NASH. Peptides were isolated from livers of NASH mice using immunoaffinity chromatography in three different mouse models of NASH (LDLRKO, Tac, and WT) compared to chow controls. Using BioVenn filtering analysis, we identified unique NASH peptides in NASH mouse models by removing chow associated peptides (Figure 4A). NASH peptides demonstrated a preference for 8 amino acids in length (Figure 4B, Supplementary Figures 6A, B). BioVenn filtering identified 59 NASH peptides found in all three mouse models of NASH (Figure 4C). Pathway analysis of peptide related proteins revealed enrichment in pathways such as cellular response to stress, adaptive immune system, response to endoplasmic reticulum stress, and protein catabolic processes (Figure 4D). Using NetMHCPan-4.1, all peptides were predicted to be strong H2Kb binders (Supplementary Table 2).

Interestingly, the peptide VHYKYTVV (Ncf2 peptide) was found in all NASH models and predicted to strongly bind to H2Kb with high specificity and not predicted to bind to any other MHC I isoforms (Figure 4E, Supplementary Figure 6C). The Ncf2 peptide is associated with the p67phox protein, a critical subunit for NADPH oxidase activity (27–29). Protein and gene expression of Ncf2 was significantly upregulated in the LDLRKO NASH model (Supplementary Figures 6D, E). Interestingly, MHC I KO and LysM Kb KO mice showed reduced Ncf2 protein and gene expression compared to WT amylin mice. Additionally, Kb amylin behaved similar to WT amylin mice with increased Ncf2 expression (Figures 4F, G).

3.5 Ncf2 peptide activates hepatic NASH CD8$^+$ T cells *in vitro*

We determined the ability of the Ncf2 peptide to activate NASH CD8$^+$ T cells *in vitro*. To confirm Ncf2 predicted H2Kb binding, a peptide binding assay was performed using RMA-S cells. Cells were pulsed with a vehicle control containing no peptide (NP), a known H2Kb binding peptide ovalbumin (Ova), or the Ncf2 peptide. Flow cytometry analysis confirmed the peptides Ncf2 and Ova bind to H2Kb compared to NP control (Figure 5A). Next, we investigated whether Ncf2 could activate hepatic CD8$^+$ T cells isolated from NASH mice. Using the LDLRKO NASH model, hepatic CD8$^+$ T cells were isolated and co-cultured with RMA-S cells pulsed with NP, Ova, or Ncf2 and harvested for flow analysis at days 3 and 5. By day 3 samples treated with the Ncf2 peptide showed increased CD8$^+$ T cell activation (*CD44*$^+$ *CD62L*$^-$) and proliferation compared to both NP and Ova treated cells (Figures 5B, C). Additionally, the peptide binding assay confirmed peptide binding of another candidate peptide Gpnmb found in the LDLRKO NASH model (Figure 5D). To test whether Gpnmb activates CD8$^+$ T cells, RMA-S cells were treated with NP, Ncf2, or Gpnmb peptides and co-cultured with hepatic CD8$^+$ T cells. Interestingly, by day 5 only Ncf2 showed significant increases in both CD8$^+$ T cell activation and proliferation compared to both NP control and Gpnmb treated cells (Figures 5E, F). To test for cytotoxicity, cytokines from the media were evaluated and showed significant increases in IL-13, IFNγ, RANTES, and GRANZYME B by day 5 in Ncf2 treated cells compared to NP and Gpnmb (Figure 5G).

Comparable to the LDLRKO NASH model, hepatic CD8$^+$ T cells from the Tac NASH model also demonstrated significant increases in CD8$^+$ T cell activation and proliferation when exposed to the Ncf2 peptide compared to NP control by day 3 (Supplementary Figures 7A, B). Splenic CD8$^+$ T cells also demonstrated significant increases in T cell activation and proliferation in response to the Ncf2 peptide under both stimulated (Supplementary Figures 7C, D) and unstimulated conditions supplemented with IL-2 (Supplementary Figures 6E, F) in the Tac NASH model by day 5. Additionally, WT NASH and LDLRKO NASH models demonstrated CD8$^+$ T cell activation and proliferation by day 5 (Supplementary Figures 7C–H). Splenic CD8$^+$ T cells activated by the Ncf2 peptide shared a similar cytokine profile to hepatic CD8$^+$ T cells with significant increases in IFNγ, RANTES, and GRANZYME B (Supplementary Figure 7K).

To confirm CD8$^+$ T cell reactivity to the Ncf2 peptide, an H2Kb-Ncf2 tetramer was used to detect the presence of Ncf2 specific CD8$^+$ T cells *in vivo*. Immune cells were isolated from livers of Taconic chow or Amylin mice and stained for flow cytometry. Flow analysis confirmed increased CD8$^+$ T cells and activation in NASH. Additionally, CD8$^+$ T cell subsets were evaluated and identified significant increases in T cell effector memory (TEM, *CD62L*$^-$, *CD44*$^+$, *CCR7*$^-$, *CXCR6*$^-$) and T cell resident memory subsets (TRM, *CD62L*$^-$, *CD44*$^+$, *CCR7*$^-$, *CXCR6*$^+$) with no changes in T cell central memory cells (TCM, *CD6L2+*, *CD44*$^+$, *CCR7*$^+$) (Figures 6A, B). TEM and TRM CD8$^+$ T cell subsets showed a significant increase in Ncf2 Tetramer signal compared to chow controls with no significant changes detected in TCMs (Figures 6C–E). These results demonstrate that H2Kb restricted peptide Ncf2 can activate both hepatic and splenic CD8$^+$ T cells from NASH mice *in vitro* and with increased activation, proliferation, and cytotoxicity. Additionally, NASH mice have increased Ncf2 reactive hepatic TEM and TRM CD8$^+$ T cells detected *in vivo*.

3.6 Ncf2 peptide is not present during fibrosis resolution

A recent study has shown that tissue-resident memory (TRM) CD8$^+$ T cells play a key role in resolving fibrosis during resolution (RES). NASH RES can be established within 5 weeks of switching from a high fat high cholesterol diet to a chow diet. At 5 weeks of resolution CD8$^+$ T cells remain elevated, but mice show reductions in inflammation and fibrosis (9). Utilizing this model concept, we investigated if the expression of peptide Ncf2 is altered during RES at 5 weeks when CD8$^+$ T cells are still elevated (Figure 7A). As seen in previous studies, RES mice had significantly reduced body weight, liver weight, and adipose tissue compared to NASH mice after 5 weeks of resolution (Figures 7B–D) (9). Hepatic gene expression in RES mice showed significant reductions in

10.3389/fimmu.2023.1302006

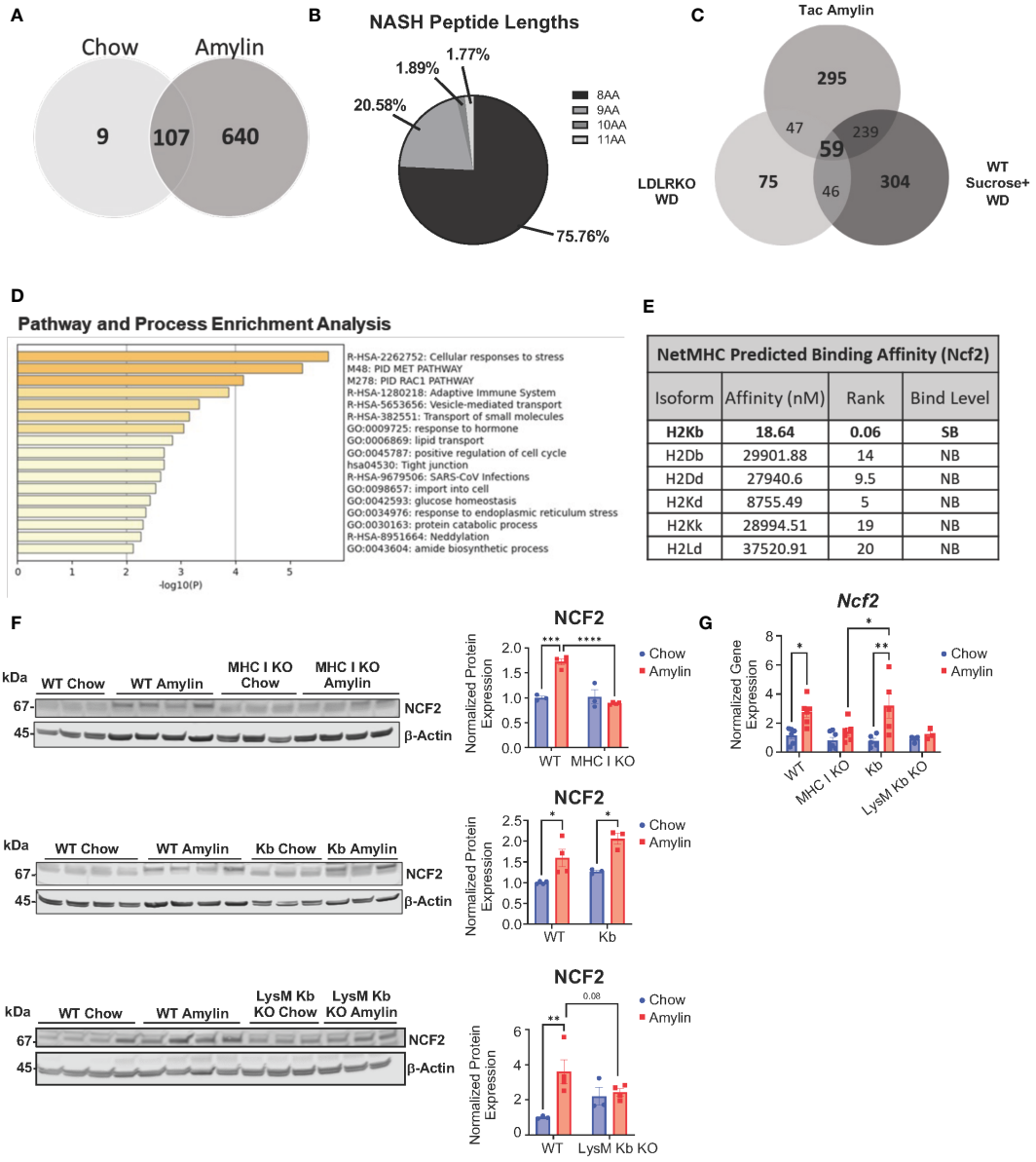

FIGURE 4
Unique H2Kb restricted peptides in NASH. Taconic mice on chow or amylin diet for 28 wks (n=5 mice per group, 2 replicate cohorts). LDLRKO mice on chow or WD for 12 wks (n=3-4 mice per group, 2 replicate cohorts). WT mice on chow or WD and sucrose water for 25 wks (n=5 mice per group, 1 cohort). WT, MHC I KO, Kb, or LysM Kb KO mice on chow or amylin diet (n= 3-7 mice per group, 2 replicate cohorts). **(A)** Venn diagram of the Taconic NASH model chow vs NASH peptides. **(B)** Pie chart of percentage of peptides with different amino acid lengths from Tac NASH model. **(C)** BioVenn filtered unique NASH peptides. **(D)** Bar graph of enriched terms across input gene lists, colored by p-values using Metascape. **(E)** NetMHC predicted binding affinities for Ncf2 peptide to MHC I isoforms for strong binders (SB) and non-binders (NB). Total liver Ncf2 protein **(F)** and gene expression **(G)** in WT, MHC I KO, Kb, and LysM Kb KO mice. Data shown as the mean ± SEM. Two-tailed unpaired Student's t-tests were performed for two group comparisons. Two-way ANOVA was performed for multiple genotypes versus diet studies. Data was considered statistically significant for P<0.05 (*), P<0.01 (**), P<0.001 (***), and P<0.0001 (****).

inflammation (*Tnf* and *Il10)* and fibrosis (*Col1a1)* compared to NASH mice (Figure 7E). Additionally, gene expression for immune cell markers *Cd8* and *Cd11b* remained elevated during resolution whereas *F4/80* expression was significantly reduced compared to NASH mice (Figure 7F). Next, we used mass spectrometry to evaluate if the Ncf2 peptide is present during resolution. Interestingly, the Ncf2 peptide was only present under NASH conditions (Figure 7G). Ncf2 hepatic protein and gene expression was also reduced during resolution compared to NASH mice (Figures 7H, I). These results indicate that the Ncf2 peptide may be necessary for *in vivo* pathogenic $CD8^+$ T cell activation in NASH and the presence of the peptide is dependent on dietary signals.

4 Discussion

In the present study, we demonstrate that hepatic $CD8^+$ T cell activation in NASH is dependent on H2Kb driving liver fibrosis

10.3389/fimmu.2023.1302006

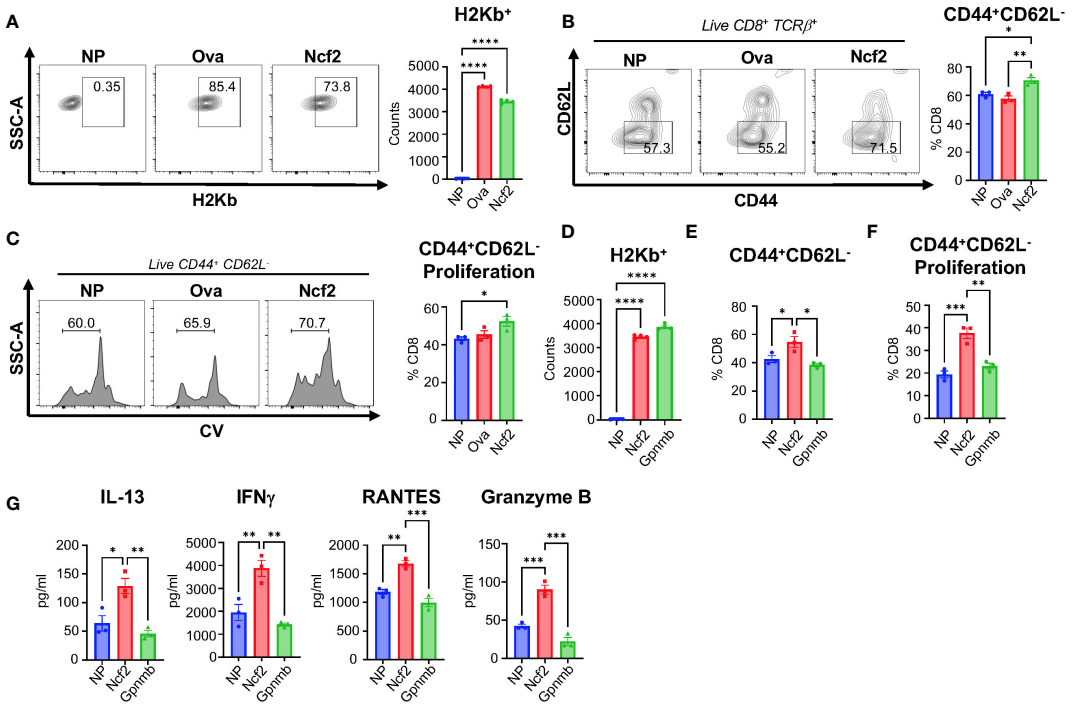

FIGURE 5
Ncf2 peptide activates hepatic NASH CD8$^+$ T cells *in vitro*. Hepatic CD8$^+$ T cells were isolated from LDLRKO NASH mice (2 combined NASH livers per cohort, 4 replicate cohorts, n=3 technical replicates per study). **(A)** Flow cytometry analysis of H2Kb expression to determine binding with NP, Ova, or Ncf2 peptide pulsed RMA-S cells (n=4 technical replicates, 3 replicate studies). T cell activation assay of hepatic CD8$^+$ T cells co-cultured with NP, Ova, or Ncf2 peptide pulsed RMA-S cells. Cells were harvested on day 3 for flow cytometry analysis of CD8$^+$ T cells (*CD8$^+$TCRβ$^+$*) and gated for **(B)** activation (*CD44$^+$ CD62L$^-$*) and **(C)** proliferation. **(D)** Representative flow cytometry analysis of peptide binding assay for NP, Ncf2, and Gpnmb peptides (n=4, 3 replicate studies). **(E, F)** Day 5 harvested cells for flow cytometry analysis of CD8$^+$ T cell activation **(E)** and proliferation **(F)**. **(G)** Cytokine analysis of media from day 5 of the T cell activation assay with hepatic LDLRKO NASH CD8$^+$ T cells. Flow plots show percentage of parent gate. Data shown as the mean ± SEM. Two-tailed unpaired Student's t-tests was performed for data sets with 2 groups and Two-way ANOVA was performed for groups more than 2 and was considered statistically significant for P<0.05 (*), P<0.01 (**), P<0.001 (***), and P<0.0001 (****).

with no impact on hepatic steatosis. H2Kb only expressing mice displayed worsened fibrosis in the absence of H2Db suggesting that H2Kb is the dominant isoform driving disease progression and H2Db may be protective in NASH. Additionally, myeloid cell expression of H2Kb is important for regulating CD8$^+$ T cell activation and fibrosis in NASH. NASH mice also demonstrate a unique H2Kb immunopeptidome and functional characterization of the Ncf2 peptide demonstrated the peptide induced activation, proliferation, and cytokine secretion of NASH CD8$^+$ T cells. Under fibrosis resolution the Ncf2 peptide is not detected, suggesting an antigen unique to the NASH environment. We determined that both gene and protein expression of Ncf2 were elevated during NASH and dependent on MHC class I expression. *Ncf2* gene expression is also upregulated in other liver fibrosis rodent models (30–32). This is surprising as peptides are normally generated during proteasomal degradation leading to reduced protein levels. This may be due to other cell types regulating p67phox expression versus a specific APC cell undergoing degradation or presenting the Ncf2 peptide. It remains to be determined the origin of this Ncf2 peptide and how MHC class I molecules regulate specific subsets of CD8$^+$ T cells during NASH development and progression.

Our data demonstrates that MHC I deficiency and H2Kb deficiency in myeloid cells can protect against liver fibrosis and CD8$^+$ T cell activation in NASH. In contrast, a recent study argues that CD8$^+$ T cells are activated through B cell stimulation through the IgA-FcR signaling in a choline deficient high fat (CD-HFD) model (33). This study showed that *in vitro* blocking of MHC I with an MHC I antibody is ineffective at preventing NASH CD8$^+$ T cell activation by intestinal B cells (33). However, previous work has shown that in a methionine and choline deficient high fat diet (MCD) model of NASH, CD8$^+$ T cells did not regulate hepatic inflammation, fibrosis, or stellate cell activation (7). Alternatively, β2m KO studies have shown that when using the CD-HFD model mice were protected from CD8$^+$ T cell activation, inflammation, and fibrosis. However, this model does not account for just MHC I antigen presentation as β2m is also present on CD1, Qa-1, and neonatal Fc receptor (FcRn) receptors impacting more than just CD8$^+$ T cells (5). Differences in choline content of the NASH diets may contribute to the factors that regulate CD8$^+$ T cell activation and function. CD8$^+$ T cells function may be altered under choline deficient conditions as activation of the T cell receptor (TCR) through antigen presentation upregulates components of their cholinergic system (34). Likewise, Tap1 deficient mice are protected from fructose induced NASH in mice (35). Therefore, targeting MHC I with an antibody may be ineffective as these molecules are typically bound with peptides when presented at the cell surface which could prevent the binding of blocking antibodies.

10.3389/fimmu.2023.1302006

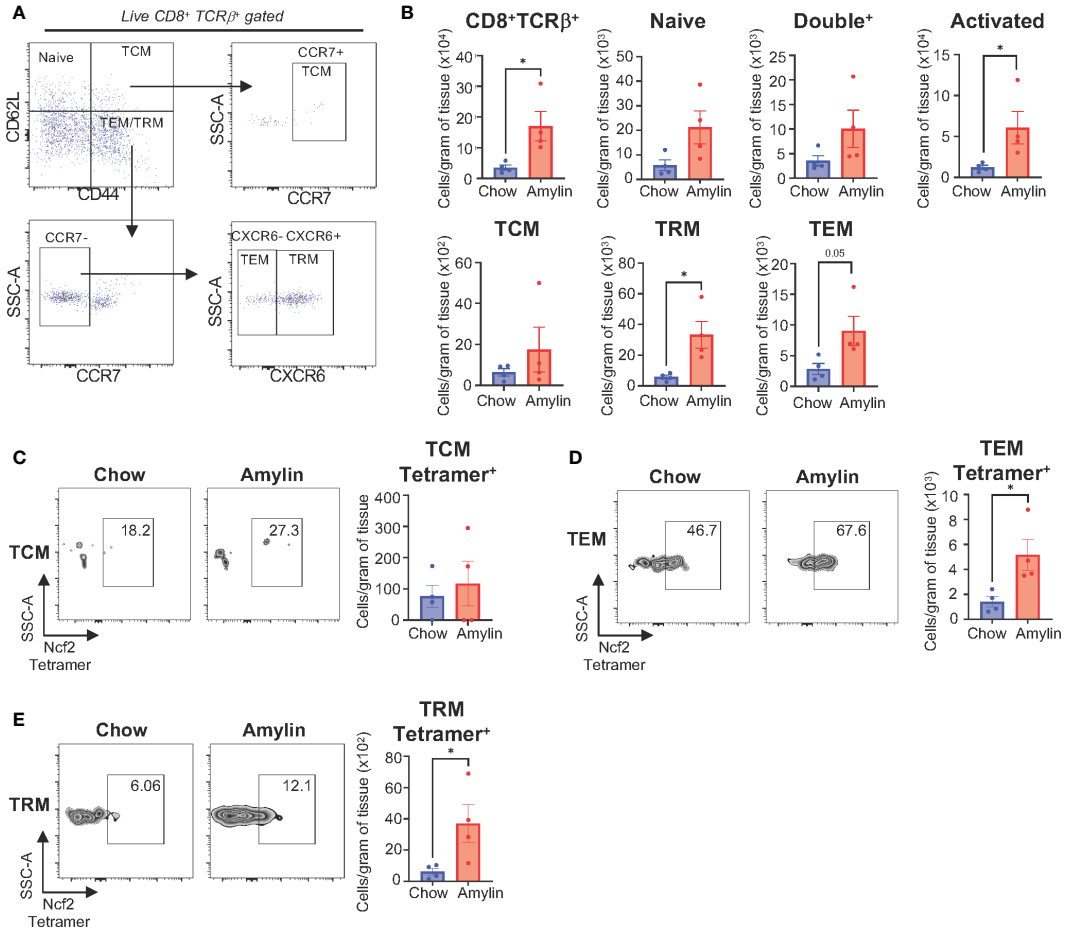

FIGURE 6
Ncf2 reactive CD8$^+$ T cells are detected *in vivo*. Tac NASH mice were fed chow or amylin diet for 28 wks (n=4 per group). **(A)** Flow cytometry CD8$^+$ T cell subsets gating strategy from CD8$^+$Tcrβ^+ liver lymphocytes. **(B)** Quantification of flow cytometry data. Representative Ncf2 Tetramer positive flow cytometry plots and quantification from liver CD8$^+$ T cell subsets: **(C)** TCM, **(D)** TEM, and **(E)** TRM cells. Quantification of flow cytometry data. Flow plots show percentage of parent gate. Data shown as the mean ± SEM. Two-tailed unpaired Student's t-tests was performed and considered statistically significant for P<0.05 (*).

Further studies are necessary to clarify the mechanisms of CD8$^+$ T cell activation across various dietary models of NASH. Alternative methods are also needed to better target MHC I molecules bound to specific NASH peptides.

Comparable to our findings, in a mouse model of cerebral malaria deficiency of H2Kb and H2Db led to reductions in CD8$^+$ T cell activation resulting in improved survival (36). Using the Kb and LysM Kb KO mouse models our data demonstrates that H2Kb on myeloid cells is required for regulating CD8$^+$ T cell activation and fibrosis in NASH. Interestingly, studies are beginning to highlight the distinct roles of H2Kb and H2Db in priming CD8$^+$ T cells and disease progression (37). In the context of Theiler's murine encephalomyelitis virus (TMEV) infection, H2Db, but not H2Kb, controls the development of brain atrophy (38, 39). In addition, CD8$^+$ T cell activation through an H2Db restricted TMEV-derived peptide contributes to brain atrophy (39). In lymphocytic choriomeningitis virus (LCMV) mouse models, deficiency of H2Db led to more severe liver pathology, increased hepatocyte apoptosis, and increased H2Kb restricted cytotoxic CD8$^+$ T cell numbers compared to WT and H2Kb KO mice (40). These studies in conjunction with our data, suggest that antigen presentation by different MHC I isoforms is important in regulating the type of CD8$^+$ T cell responses and are important factors in infection and chronic disease progression.

Hepatic inflammation has been linked to bone marrow derived monocyte infiltration into the liver driving NAFLD progression. Studies have shown that myeloid cells in the liver are also key players involved in fibrosis development (41–44). A recent transcriptomic study characterized macrophage subsets in NASH identifying increased pro-fibrotic and M2 macrophage subsets significantly correlated with degree of fibrosis in human patients (45). Our studies identified that myeloid cells have increased H2Kb expression demonstrating a potential mechanism by which antigens are presented to CD8$^+$ T cells in NASH driving fibrosis. This is further supported by H2Kb deletion on myeloid cells protecting mice against NASH induced CD8$^+$ T cell activation and fibrosis. CD8$^+$ T cells are also known to interact with hepatocytes (14), hepatic stellate cells, in addition to infiltrating myeloid cells (7) via antigen presentation. In particular, the p67phox protein associated with the Ncf2 peptide we identified is expressed by monocytes,

10.3389/fimmu.2023.1302006

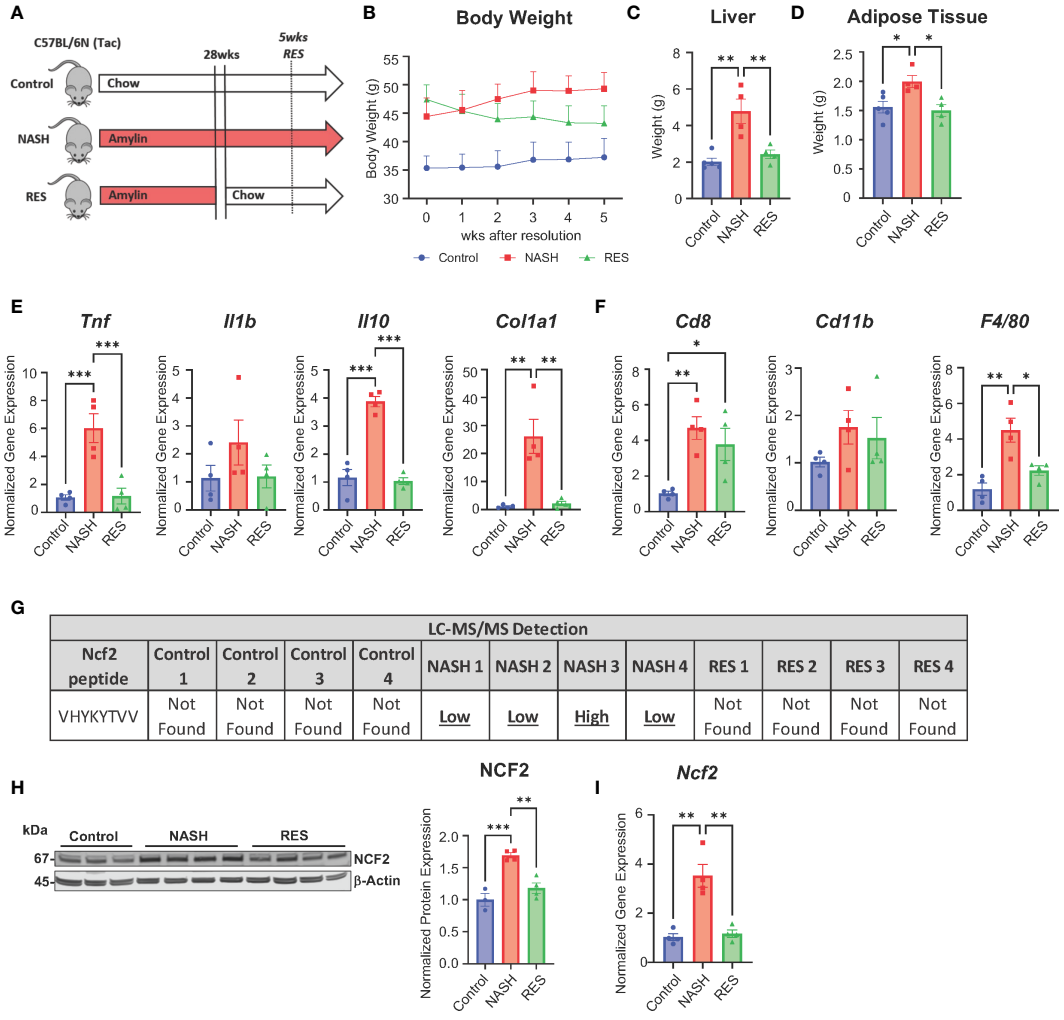

FIGURE 7
Ncf2 peptide is not found during NASH resolution. Tac NASH mice were fed chow or amylin diet for 33 wks. Tac RES mice were fed amylin diet for 28 wks and then switched to chow diet for 5 wks (n=4, 2 replicate cohorts). **(A)** Resolution study schematic. **(B)** Body weight progression. **(C)** Total liver weight. **(D)** Epididymal adipose tissue weight. **(E, F)** Hepatic gene expression. **(G)** LC-MS/MS detection of Ncf2 peptide from total livers of individual mice from control (chow), NASH, or RES (n=4). Total liver Ncf2 protein **(H)** and gene **(I)** expression. Data shown as the mean ± SEM. Two-way ANOVA was performed and considered statistically significant for P<0.05 (*), P<0.01 (**), and P<0.001 (***).

macrophages, hepatocytes, and dendritic cells under NASH conditions. Cross presentation by dendritic cells may also provide a mechanism for antigen presentation. Upon examination of dendritic subsets, classical dendritic cells (cDC1) were found to be elevated and drive liver injury and $CD8^+$ T cell activation (46). Similarly, adipose tissue dendritic cells are linked to metabolic dysfunction, were depletion of conventional dendritic cells prevents HFD model induced inflammation (47). Additionally, B cells have been highlighted to contribute to the progression of NASH through the production of pro-inflammatory mediators and antigen presentation. Studies have shown that B cell deficiency protects mice against liver fibrosis and inflammation in diet induced NASH models (48, 49). Studies also suggest that the gut microbiome can promote NASH progression through activation of intrahepatic B cells through microbial factors (49). However, MHC II is often upregulated in patients with NASH preceding $CD8^+$ T cell infiltration into the liver (48). It is known that B cells can activate $CD8^+$ T cells though IgA-FcR signaling, however it remains to be determined how B cell MHC I expression changes during NASH and how this impacts $CD8^+$ T cell activation (33). These findings highlight the ability of alternative APCs for antigen presentation that have not been evaluated in NASH.

During NASH progression and fibrosis resolution, analysis of the TCR repertoires of hepatic memory $CD8^+$ T cells demonstrated less diversity indicating possible antigen regulation (9). In high fat fed mice, we discovered previously that hepatic $CD8^+$ T cells share distinct clonotypes in their TCR repertoires with $CD8^+$ T cells from adipose tissue (50). In the current study we examined the hepatic immunopeptidome, which consists of all antigens bound to H2Kb in normal and NASH mouse livers. We identified 59 unique H2Kb dependent antigens in NASH livers with peptides associated to pathways such as tight junctions and cellular stress. Of these NASH peptides, we identified a $CD8^+$ T cell reactive Ncf2 peptide. This peptide is associated with the p67phox cytosolic subunit that makes

up part of the NOX2 NADPH oxidase protein complex (29, 51). Previous studies have shown that NOX2 is increased in NASH and NOX2 deficient mice are protected from diet induced steatosis and insulin resistance (52). Interestingly, in a lupus mouse model, knockdown of just the p67phox subunit reduces splenic $CD8^+$ T cells suggesting the Ncf2 peptide could be important for also activating $CD8^+$ T cells in other inflammatory diseases (53). Targeting the Ncf2 peptide or protein could provide new alternative therapies for targeting $CD8^+$ T cell activation in NASH and other inflammatory diseases.

The importance of myeloid specific H2Kb antigen presentation for $CD8^+$ T cell activation in NASH was highlighted in these studies. However, it remains to be determined the role of other candidate APC types and the origin of the Ncf2 peptide. The role of antigen presentation by other APCs such as hepatocytes, dendritic cells, and B cells can be evaluated using the Kb LoxP mouse model. Additionally, an effort to determine the source of the Ncf2 peptide needs to be addressed. It is unknown if the Ncf2 peptide is unique to the liver or generated in other metabolic tissues such as the intestine or adipose tissue. Gut microbes and oxidative stress related antigens may be generated in the intestine and travel to the liver driving $CD8^+$ T cells. It also remains to be determined if the Ncf2 peptide and Ncf2 reactive $CD8^+$ T cells are present in NASH in humans. Future studies targeting the Ncf2 protein or peptide may serve as a promising therapeutic target for regulating fibrosis in NASH.

Data availability statement

The data presented in the study can be found in the MassIVE Repository, accession number PXD047295.

Ethics statement

The animal study was approved by Institutional Animal Care and Use Committee (IACUC) at North Carolina State University. The study was conducted in accordance with the local legislation and institutional requirements.

Author contributions

VA: Data curation, Formal analysis, Methodology, Visualization, Writing – original draft, Writing – review & editing. LC: Data curation, Formal analysis, Methodology, Writing – review & editing. TW: Methodology, Writing – review & editing. JH: Resources, Writing – review & editing. PH: Resources, Writing – review & editing. HA: Formal analysis, Writing – review & editing. GS: Data curation, Writing – review & editing. XL: Data curation, Methodology, Writing – review & editing. ML: Data curation, Writing – review & editing. AJ: Methodology, Resources, Writing – review & editing. AK: Conceptualization, Data curation, Formal analysis, Funding acquisition, Investigation, Methodology, Project administration, Resources, Supervision, Validation, Writing – original draft, Writing – review & editing.

Funding

The author(s) declare financial support was received for the research, authorship, and/or publication of this article. This work was funded by the University of North Carolina at Chapel Hill Center for Gastrointestinal Biology and Disease (P30 DK034987 to AK) and Taconic Biosciences (Academic Grant Award to AK).

Conflict of interest

The authors declare that the research was conducted in the absence of any commercial or financial relationships that could be construed as a potential conflict of interest.

Publisher's note

Supplementary material

The Supplementary Material for this article can be found online at: https://www.frontiersin.org/articles/10.3389/fimmu.2023.1302006/full#supplementary-material

References

1. MaChado AP. Metabolic syndrome, atherosclerosis and thrombogenic risk. *Rev Port Cardiol* (2006) 25(2):173–8.

2. MaChado M, Cortez-Pinto H. Non-alcoholic steatohepatitis and metabolic syndrome. *Curr Opin Clin Nutr Metab Care* (2006) 9(5):637–42. doi: 10.1097/01.mco.0000241677.40170.17

3. Casini A, Ricci OE, Paoletti F, Surrenti C. Immune mechanisms for hepatic fibrogenesis. T-lymphocyte-mediated stimulation of fibroblast collagen production in chronic active hepatitis. *Liver* (1985) 5(3):134–41. doi: 10.1111/j.1600-0676.1985.tb00228.x

4. Safadi R, Ohta M, Alvarez CE, Fiel MI, Bansal M, Mehal WZ, et al. Immune stimulation of hepatic fibrogenesis by cd8 cells and attenuation by transgenic interleukin-10 from hepatocytes. *Gastroenterology* (2004) 127(3):870–82. doi: 10.1053/j.gastro.2004.04.062

5. Wolf MJ, Adili A, Piotrowitz K, Abdullah Z, Boege Y, Stemmer K, et al. Metabolic activation of intrahepatic cd8+ T cells and nkt cells causes nonalcoholic steatohepatitis and liver cancer via cross-talk with hepatocytes. *Cancer Cell* (2014) 26(4):549–64. doi: 10.1016/j.ccell.2014.09.003

6. Bhattacharjee J, Kirby M, Softic S, Miles L, Salazar-Gonzalez RM, Shivakumar P, et al. Hepatic natural killer T-cell and cd8+ T-cell signatures in mice with nonalcoholic steatohepatitis. *Hepatol Commun* (2017) 1(4):299–310. doi: 10.1002/hep4.1041

7. Breuer DA, Pacheco MC, Washington MK, Montgomery SA, Hasty AH, Kennedy AJ. Cd8. *Am J Physiol Gastrointest Liver Physiol* (2020) 318(2):G211–24. doi: 10.1152/ajpgi.00040.2019

8. Hirsova P, Bamidele AO, Wang H, Povero D, Revelo XS. Emerging roles of T cells in the pathogenesis of nonalcoholic steatohepatitis and hepatocellular carcinoma. *Front Endocrinol (Lausanne)* (2021) 12:760860. doi: 10.3389/fendo.2021.760860

9. Koda Y, Teratani T, Chu PS, Hagihara Y, Mikami Y, Harada Y, et al. Cd8. *Nat Commun* (2021) 12(1):4474. doi: 10.1038/s41467-021-24734-0

10. Ortiz-López N, Fuenzalida C, Dufeu MS, Pinto-León A, Escobar A, Poniachik J, et al. The immune response as a therapeutic target in non-alcoholic fatty liver disease. *Front Immunol* (2022) 13:954869. doi: 10.3389/fimmu.2022.954869

11. Del Ben M, Polimeni L, Carnevale R, Bartimoccia S, Nocella C, Baratta F, et al. Nox2-generated oxidative stress is associated with severity of ultrasound liver steatosis in patients with non-alcoholic fatty liver disease. *BMC Gastroenterol* (2014) 14:81. doi: 10.1186/1471-230X-14-81

12. Ashraf NU, Sheikh TA. Endoplasmic reticulum stress and oxidative stress in the pathogenesis of non-alcoholic fatty liver disease. *Free Radic Res* (2015) 49:1405-18. doi: 10.3109/10715762.2015.1078461

13. Arroyave-Ospina JC, Wu Z, Geng Y, Moshage H. Role of oxidative stress in the pathogenesis of non-alcoholic fatty liver disease: implications for prevention and therapy. *Antioxid (Basel)* (2021) 10(2):174. doi: 10.3390/antiox10020174

14. Dudek M, Pfister D, Donakonda S, Filpe P, Schneider A, Laschinger M, et al. Author correction: auto-aggressive cxcr6. *Nature* (2021) 593:no. doi: 10.1038/s41586-021-03568-2

15. Karrar A, Hariharan S, Fazel Y, Moosvi A, Houry M, Younoszai Z, et al. Analysis of human leukocyte antigen allele polymorphism in patients with non alcoholic fatty liver disease. *Med (Baltimore)* (2019) 98(32):e16704. doi: 10.1097/MD.0000000000016704

16. Govaere O, Cockell S, Tiniakos D, Queen R, Younes R, Vacca M, et al. Transcriptomic profiling across the nonalcoholic fatty liver disease spectrum reveals gene signatures for steatohepatitis and fibrosis. *Sci Transl Med* (2020) 12(572): eaba4448. doi: 10.1126/scitranslmed.aba4448

17. Klein J. The major histocompatibility complex of the mouse. *Science* (1979) 203 (4380):516–21. doi: 10.1126/science.104386

18. Malo CS, Huggins MA, Goddery EN, Tolcher HMA, Renner DN, Jin F, et al. Non-equivalent antigen presenting capabilities of dendritic cells and macrophages in generating brain-infiltrating Cd8. *Nat Commun* (2018) 9(1):633. doi: 10.1038/s41467-018-03037-x

19. Kowalewski DJ, Stevanović S. Biochemical large-scale identification of mhc class I ligands. *Methods Mol Biol* (2013) 960:145–57. doi: 10.1007/978-1-62703-218-6_12

20. Chen X, Wang S, Huang Y, Zhao X, Jia X, Meng G, et al. Obesity reshapes visceral fat-derived mhc I associated-immunopeptidomes and generates antigenic peptides to drive Cd8. *iScience* (2020) 23(4):100977. doi: 10.1016/j.isci.2020.100977

21. Duan L, Scheidemantle G, Lodge M, Cummings MJ, Pham E, Wang X, et al. Prioritize biologically relevant ions for data-independent acquisition (Bri-dia) in Lc-Ms/Ms-based lipidomics analysis. *Metabolomics* (2022) 18(8):55. doi: 10.1007/s11306-022-01913-8

22. Krenkel O, Tacke F. Liver macrophages in tissue homeostasis and disease. *Nat Rev Immunol* (2017) 17(5):306-321. doi: 10.1038/nri.2017.11

23. Vugmeyster Y, Glas R, Pérarnau B, Lemonnier FA, Eisen H, Ploegh H. Major histocompatibility complex (Mhc) class I kbdb -/- deficient mice possess functional cd8 + T cells and natural killer cells. *Proc Natl Acad Sci U.S.A.* (1998) 95(21):12492–7. doi: 10.1073/pnas.95.21.12492

24. Höglund P, Ohlén C, Carbone E, Franksson L, Ljunggren HG, Latour A, et al. Recognition of beta 2-microglobulin-negative (Beta 2m-) T-cell blasts by natural killer cells from normal but not from beta 2m- mice: nonresponsiveness controlled by beta 2m- bone marrow in chimeric mice. *Proc Natl Acad Sci U.S.A.* (1991) 88(22):10332–6. doi: 10.1073/pnas.88.22.10332

25. Liao NS, Bix M, Zijlstra M, Jaenisch R, Raulet D. Mhc class I deficiency: susceptibility to natural killer (Nk) cells and impaired Nk activity. *Science* (1991) 253 (5016):199–202. doi: 10.1126/science.1853205

26. Bern MD, Parikh BA, Yang L, Beckman DL, Poursine-Laurent J, Yokoyama WM. Inducible down-regulation of mhc class I results in natural killer cell tolerance. *J Exp Med* (2019) 216(1):99–116. doi: 10.1084/jem.20181076

27. Ming W, Li S, Billadeau DD, Quilliam LA, Dinauer MC. The Rac effector P67phox regulates phagocyte nadph oxidase by stimulating vav1 guanine nucleotide exchange activity. *Mol Cell Biol* (2007) 27(1):312–23. doi: 10.1128/MCB.00985-06

28. Feng D, Yang C, Geurts AM, Kurth T, Liang M, Lazar J, et al. Increased expression of nad(P)H oxidase subunit P67(Phox) in the renal medulla contributes to excess oxidative stress and salt-sensitive hypertension. *Cell Metab* (2012) 15(2):201–8. doi: 10.1016/j.cmet.2012.01.003

29. Jiang JX, Török NJ. Nadph oxidases in chronic liver diseases. *Adv Hepatol* (2014) 2014:742931. doi: 10.1155/2014/742931

30. Gan D, Zhang W, Huang C, Chen J, He W, Wang A, et al. Ursolic acid ameliorates ccl4-induced liver fibrosis through the noxs/ros pathway. *J Cell Physiol* (2018) 233(10):6799–813. doi: 10.1002/jcp.26541

31. Shiba K, Tsuchiya K, Komiya C, Miyachi Y, Mori K, Shimazu N, et al. Canagliflozin, an sglt2 inhibitor, attenuates the development of hepatocellular carcinoma in a mouse model of human nash. *Sci Rep* (2018) 8(1):2362. doi: 10.1038/s41598-018-19658-7

32. García-Jaramillo M, Lytle KA, Spooner MH, Jump DB. A lipidomic analysis of docosahexaenoic acid (22:6, Ω3) mediated attenuation of western diet induced nonalcoholic steatohepatitis in male. *Metabolites* (2019) 9(11):252. doi: 10.3390/metabo9110252

33. Kotsiliti E, Leone V, Schuehle S, Govaere O, Li H, Wolf MJ, et al. Intestinal B cells license metabolic T-cell activation in nash microbiota/antigen-independently and contribute to fibrosis by Iga-Fcr signalling. *J Hepatol* (2023) 79(2):296–313. doi: 10.1016/j.jhep.2023.04.037

34. Fujii T, Mashimo M, Moriwaki Y, Misawa H, Ono S, Horiguchi K, et al. Expression and function of the cholinergic system in immune cells. *Front Immunol* (2017) 8:1085. doi: 10.3389/fimmu.2017.01085

35. Arindkar S, Bhattacharjee J, Kumar JM, Das B, Upadhyay P, Asif S, et al. Antigen peptide transporter 1 is involved in the development of fructose-induced hepatic steatosis in mice. *J Gastroenterol Hepatol* (2013) 28(8):1403–9. doi: 10.1111/jgh.12186

36. Fain CE. H-2kb and H-2db class I molecules on cerebral endothelium differentially modulate Cd8 T cells dynamics and pathological outcomes in experimental cerebral malaria. *J Immunol* (2022) 208. doi: 10.4049/jimmunol.208.Supp.102.24

37. Tritz ZP, Orozco RC, Malo CS, Ayasoufi K, Fain CE, Khadka RH, et al. Conditional silencing of H-2d. *J Immunol* (2020) 205(5):1228–38. doi: 10.4049/jimmunol.2000340

38. Altintas A, Cai Z, Pease LR, Rodriguez M. Differential expression of H-2k and H-2d in the central nervous system of mice infected with theiler's virus. *J Immunol* (1993) 151(5):2803–12. doi: 10.4049/jimmunol.151.5.2803

39. Huseby Kelcher AM, Atanga PA, Gamez JD, Cumba Garcia LM, Teclaw SJ, Pavelko KD, et al. Brain atrophy in picornavirus-infected fvb mice is dependent on the H-2d. *FASEB J* (2017) 31(6):2267–75. doi: 10.1096/fj.201601055R

40. Xu HC, Huang J, Pandyra AA, Pandey P, Wang R, Zhang Z, et al. Single mhc-I expression promotes virus-induced liver immunopathology. *Hepatol Commun* (2022) 6 (7):1620–33. doi: 10.1002/hep4.1913

41. Duffield JS, Forbes SJ, Constandinou CM, Clay S, Partolina M, Vuthoori S, et al. Selective depletion of macrophages reveals distinct, opposing roles during liver injury and repair. *J Clin Invest* (2005) 115(1):56–65. doi: 10.1172/JCI22675

42. Pradere JP, Kluwe J, De Minicis S, Jiao JJ, Gwak GY, Dapito DH, et al. Hepatic macrophages but not dendritic cells contribute to liver fibrosis by promoting the survival of activated hepatic stellate cells in mice. *Hepatology* (2013) 58(4):1461–73. doi: 10.1002/hep.26429

43. Wynn TA, Chawla A, Pollard JW. Macrophage biology in development, homeostasis and disease. *Nature* (2013) 496(7446):445–55. doi: 10.1038/nature12034

44. Cai B, Dongiovanni P, Corey KE, Wang X, Shmarakov IO, Zheng Z, et al. Macrophage mertk promotes liver fibrosis in nonalcoholic steatohepatitis. *Cell Metab* (2020) 31(2):406–421.e7. doi: 10.1016/j.cmet.2019.11.013

45. He W, Huang Y, Shi X, Wang Q, Wu M, Li H, et al. Identifying a distinct fibrosis subset of nafld via molecular profiling and the involvement of profibrotic macrophages. *J Transl Med* (2023) 21(1):448. doi: 10.1186/s12967-023-04300-6

46. Deczkowska A, David E, Ramadori P, Pfister D, Safran M, Li B, et al. Xcr1. *Nat Med* (2021) 27(6):1043–54. doi: 10.1038/s41591-021-01344-3

47. Sundara Rajan S, Longhi MP. Dendritic cells and adipose tissue. *Immunology* (2016) 149:no. doi: 10.1111/imm.12653

48. Bruzzì S, Sutti S, Giudici G, Burlone ME, Ramavath NN, Toscani A, et al. B2-lymphocyte responses to oxidative stress-derived antigens contribute to the evolution of nonalcoholic fatty liver disease (Nafld). *Free Radic Biol Med* (2018) 124:249–59. doi: 10.1016/j.freeradbiomed.2018.06.015

49. Barrow F, Khan S, Fredrickson G, Wang H, Dietsche K, Robert S, et al. Microbiota-driven activation of intrahepatic B cells aggravates nash through innate and adaptive signaling. *Hepatology* (2021) 74(2):704–22. doi: 10.1002/hep.31755

50. McDonnell WJ, Koethe JR, Mallal SA, Pilkinton MA, Kirabo A, Ameka MK, et al. High Cd8 T-cell receptor clonality and altered Cdr3 properties are associated with elevated isolevuglandins in adipose tissue during diet-induced obesity. *Diabetes* (2018) 67(11):2361–76. doi: 10.2337/db18-0040

51. Gabbia D, Cannella L, De Martin S. The role of oxidative stress in nafld-nash-hcc transition-focus on nadph oxidases. *Biomedicines* (2021) 9(6):687. doi: 10.3390/biomedicines9060687

52. Kim SY, Jeong JM, Kim SJ, Seo W, Kim MH, Choi WM, et al. Pro-inflammatory hepatic macrophages generate ros through nadph oxidase 2 via endocytosis of monomeric Tlr4-Md2 complex. *Nat Commun* (2017) 8(1):2247. doi: 10.1038/s41467-017-02325-2

53. Jacob CO, Yu N, Yoo DG, Perez-Zapata LJ, Barbu EA, Kaplan MJ, et al. Haploinsufficiency of nadph oxidase subunit neutrophil cytosolic factor 2 is sufficient to accelerate full-blown lupus in nzm 2328 mice. *Arthritis Rheumatol* (2017) 69 (8):1647–60. doi: 10.1002/art.40141

frontiers | Frontiers in Immunology

TYPE Original Research
PUBLISHED 06 February 2024
DOI 10.3389/fimmu.2024.1346520

OPEN ACCESS

EDITED BY
Evangelos Triantafyllou,
Imperial College London, United Kingdom

REVIEWED BY
Chris John Weston,
University of Birmingham, United Kingdom
Wenhao Li,
Queen Mary University of London,
United Kingdom

*CORRESPONDENCE
Lukas Van Melkebeke
lukas.vanmelkebeke@kuleuven.be
Schalk van der Merwe
schalk.vandermerwe@uzleuven.be

†These authors share first authorship

‡These authors share senior authorship

RECEIVED 29 November 2023
ACCEPTED 22 January 2024
PUBLISHED 06 February 2024

CITATION
Van Melkebeke L, Verbeek J, Bihary D, Boesch M, Boeckx B, Feio-Azevedo R, Smets L, Wallays M, Claus E, Bonne L, Maleux G, Govaere O, Korf H, Lambrechts D and van der Merwe S (2024) Comparison of the single-cell and single-nucleus hepatic myeloid landscape within decompensated cirrhosis patients.
Front. Immunol. 15:1346520.
doi: 10.3389/fimmu.2024.1346520

Comparison of the single-cell and single-nucleus hepatic myeloid landscape within decompensated cirrhosis patients

Lukas Van Melkebeke[1,2*†], Jef Verbeek[1,2†], Dora Bihary[3,4], Markus Boesch[1], Bram Boeckx[3,4], Rita Feio-Azevedo[1], Lena Smets[1], Marie Wallays[1], Eveline Claus[5], Lawrence Bonne[5], Geert Maleux[5], Olivier Govaere[6], Hannelie Korf[1‡], Diether Lambrechts[3,4‡] and Schalk van der Merwe[1,2*‡]

[1]Laboratory of Hepatology, Department of Chronic Diseases and Metabolism, KU Leuven, Leuven, Belgium, [2]Department of Gastroenterology and Hepatology, University Hospitals Leuven, Leuven, Belgium, [3]Laboratory for Translational Genetics, Department of Human Genetics, KU Leuven, Leuven, Belgium, [4]VIB Center for Cancer Biology, Leuven, Belgium, [5]Department of Interventional Radiology, University Hospitals Leuven, Leuven, Belgium, [6]Department of Imaging and Pathology, Translational Cell and Tissue Research, KU Leuven and University Hospitals Leuven, Leuven, Belgium

Background and aims: A complete understanding of disease pathophysiology in advanced liver disease is hampered by the challenges posed by clinical specimen collection. Notably, in these patients, a transjugular liver biopsy (TJB) is the only safe way to obtain liver tissue. However, it remains unclear whether successful sequencing of this extremely small and fragile tissue can be achieved for downstream characterization of the hepatic landscape.

Methods: Here we leveraged in-house available single-cell RNA-sequencing (scRNA-seq) and single-nucleus (snRNA-seq) technologies and accompanying tissue processing protocols and performed an in-patient comparison on TJB's from decompensated cirrhosis patients (n = 3).

Results: We confirmed a high concordance between nuclear and whole cell transcriptomes and captured 31,410 single nuclei and 6,152 single cells, respectively. The two platforms revealed similar diversity since all 8 major cell types could be identified, albeit with different cellular proportions thereof. Most importantly, hepatocytes were most abundant in snRNA-seq, while lymphocyte frequencies were elevated in scRNA-seq. We next focused our attention on hepatic myeloid cells due to their key role in injury and repair during chronic liver disease. Comparison of their transcriptional signatures indicated that these were largely overlapping between the two platforms. However, the scRNA-seq platform failed to recover sufficient Kupffer cell numbers, and other monocytes/macrophages featured elevated expression of stress-related parameters.

10.3389/fimmu.2024.1346520

Conclusion: Our results indicate that single-nucleus transcriptome sequencing provides an effective means to overcome complications associated with clinical specimen collection and could sufficiently profile all major hepatic cell types including all myeloid cell subsets.

KEYWORDS

single cell sequence (scRNA-seq), single nucleus RNA sequencing, cirrhosis, transjugular biopsy, decompensated

Introduction

Cirrhosis represents a major cause of death worldwide and is characterized as the end stage of progressive liver fibrosis, in which the hepatic architecture is distorted, resulting in portal hypertension and loss of hepatic function (1). During the development of the advanced disease stage, cirrhosis is characterized by severe immune dysfunction and sustained systemic inflammation that may precipitate extrahepatic organ failure (2). Hepatic macrophages play a key role in this regard, as they contribute to both the progression and resolution of tissue inflammation (3). The recent application of single-cell RNA sequencing (scRNA-seq) and the development of a comprehensive human liver atlas have underscored the presence of a dense and diverse network of immune cells in the liver (3–5). In light of these findings, we can now recognize that the hepatic myeloid population is not exclusively composed of resident Kupffer cells but encompasses multiple populations of macrophages, even in a healthy state (4). Furthermore, during the development of cirrhosis, disease associated macrophage populations emerge that contribute to the maintenance of inflammation and the propagation of fibrosis (6–9). Moreover, spatial data enabled the identification and interaction of immune cells with other cells in their local environment, revealing signals that could direct niche-specific macrophage functions (9, 10).

Despite these advances, gaining a comprehensive understanding of human liver immune cells during advanced cirrhosis is significantly impeded by the challenges associated with clinical specimen collection and processing. For instance, fresh tissue necessitates immediate processing and enzymatic digestion, potentially resulting in the loss of sensitive or incompletely dissociated cells, along with alterations in gene expression. Moreover, the size of many structural hepatic cells may preclude their passage through microfluidic channels, leading to the non-recovery of their RNA cargo through this approach (11). Single-nucleus RNA-seq (snRNA-seq), on the other hand, could serve as an alternative strategy, involving the isolation of nuclei from frozen tissues, thereby circumventing the necessity for immediate sample processing. The drawback of this approach is that smaller subsets of cells, such as crucial macrophage subtypes, may be overshadowed by abundant structural cells. Nevertheless, snRNA-seq could still be the method of choice when dealing with specimens of extremely small size and fragility (12, 13).

In the context of investigating the hepatic landscape in decompensated cirrhosis, liver tissue can be safely obtained only through the transjugular route. However transjugular liver biopsies (TJBs) have an extremely small size (± 14.7mm^3 compared to 80.4mm^3 for 14G tru-cut needle biopsies), and successful sequencing of these specimens is yet to be demonstrated (14). In this study, we utilized in-house scRNA-seq and snRNA-seq technologies along with corresponding tissue processing protocols. We conducted a comparison of the data obtained from sequencing transjugular liver biopsies (TJBs) in patients with advanced cirrhosis. Importantly, we performed a within-patient comparison of both techniques to eliminate potential differences in cell subset frequencies arising from distinct disease states or stages among patients. Beyond assessing the global liver cell landscape, data quality, and cell recovery, we specifically examined how the transcriptomic profile of liver myeloid cells could be compared between the two techniques.

Our findings indicate that both scRNA-seq and snRNA-seq successfully identify myeloid cells from TJBs, with the gene signature of specific clusters and myeloid subpopulations being preserved between both techniques. However, the scRNA-seq platform failed to recover sufficient Kupffer cell numbers, and other monocytes/macrophages featured elevated expression of stress-related parameters. Moreover, our data offers valuable insights to consider when conducting sequencing experiments in the context of advanced cirrhosis.

Patients and methods

Patient population and sample collection

Liver biopsies were collected with ethics approval from the University Hospitals Leuven (ethical committee S64744) after written informed consent was given by the patient. From 3 patients with decompensated liver cirrhosis, a total of 5 TJBs per patient were taken with a standard 19G needle (Cook, Limerick, Ireland). The clinical characteristics are shown in Supplementary Table 1. All samples were immediately rinsed with an isotonic fluid.

For each patient, half of the samples were snap frozen in liquid nitrogen (-196°C) for snRNA-seq at a later timepoint while the other half was placed in phosphate-buffered saline (PBS) for immediate transfer for cell isolation and scRNA-seq.

Data availability statement

Raw sequence data has been deposited at the European Genome-phenome Archive (EGA), under accession number EGAS50000000073. This study did not generate any new code.

Single-cell RNA-sequencing

Upon arrival, samples were rapidly processed for scRNA-seq. Samples were transferred to 2mL digestion medium containing collagenase P (2mg mL^{-1}, ThermoFisher Scientific) and DNAse I (10U μL^{-1}, Sigma) in DMEM (ThermoFisher Scientific). Samples were incubated for 15min at 37°C and pipetted up and down for 1min using a P1000 pipette. Next, 3mL ice-cold PBS was added, and samples were filtered using a 40µm nylon mesh (ThermoFisher Scientific). Following centrifugation at 300×*g* at 4°C for 5min, the supernatant was aspirated and discarded, and the cell pellet was resuspended in 1ml red blood cell lysis buffer (Roche). Following a 5min incubation at room temperature, samples were centrifuged (300×*g*, 4°C, 5min) and resuspended in 1mL PBS containing 0.04% Bovine Serum Albumin (BSA) and filtered over Flowmi 40µm cell strainers (VWR) using wide-bore 1mL low-retention filter tips (Mettler-Toledo). Next, 10µL of this cell suspension was counted using a LUNA-FL dual fluorescence cell (Logos Biosystems) counter to determine the concentration of live cells. Libraries for scRNA-seq were generated using the Chromium Single Cell 3' library from 10x Genomics according to the manufacturers protocol. We aimed to profile 10,000 cells per library (if sufficient cells were retained during dissociation). The entire procedure, from the moment of biopsy until loading in the 10x Genomics device, was completed in <90 minutes. Afterwards, individual cells were emulsified and amplified with 3′ adaptors while attaching sample indices. Sequencing was performed using Novaseq 6000 (Illumina).

Single-nucleus RNA-sequencing

Upon collection, samples were immediately snap frozen in liquid nitrogen. At processing the samples were placed in 1 mL of TST-buffer (Supplementary Methods) on a petri dish and chopped into small pieces using a scalpel followed by tissue homogenization with a Dounce homogenizer (i.e., during 2.5 min with the loose pestle and 2.5 min with the tight pestle). The homogenized solution was then filtered through a 40 µm cell strainer (Falcon) and placed in a 50 mL Falcon tube. Afterwards the filter was washed once with 0.5 mL of ST-buffer (Supplementary Methods). This process was repeated on a 20 µm, a 10 µm and a 5 µm cell strainer (Falcon). Afterwards, the sample was transferred to a 15mL Falcon tube before being centrifuged at 4°C for 5min at 500g. The pellet was resuspended in 300µL of PBS containing 1.0% of BSA. Next, 10µL of this cell suspension was counted using a LUNA-FL dual fluorescence cell counter (Logos Biosystems) to determine the concentration of the nuclei. Libraries for snRNA-seq were generated using the Chromium Single Cell 3' library from 10x Genomics according to the manufacturers protocol. We aimed to profile 20,000 nuclei per library. The entire procedure was completed in <60 min. Afterwards, individual nuclei were emulsified and amplified with 3′ adaptors while attaching sample indices. Sequencing was performed using Novaseq 6000 (Illumina).

Data analysis

General statistics

Normally distributed data are reported as mean ± standard deviation, while non-normally distributed data are reported as median with interquartile range. Normality was tested using the Shapiro-Wilk test. The proportion and absolute numbers of cells and nuclei, the number of genes per cell/nuclei and the number of counts per cell/nuclei were compared using a paired sample t-test or Wilcoxon matched-pairs signed ranked test according to the type of data. Significance was defined as a two-sided $p<0.05$. Statistical analysis and graphs were produced using GraphPad Prism v9.0 (GraphPad Software) or the respective R v4.1.2 packages.

Preprocessing of scRNA-seq and snRNA-seq data

Raw sequencing reads were aligned to the human reference genome (GRCh38/hg38) and gene-expression matrices were generated with CellRanger (v3.0.2). Gene-cell matrix was used as input in Seurat (v4.1.1) for analysis (15). Genes expressed in less than three cells were excluded. The estimated ambient contamination fraction was calculated using SoupX (v1.6.2). The count matrix was filtered for cells exhibiting 800-8,000 genes as well as <30% mitochondrial genes of the total UMI counts (a comparable percentage as in other papers in the field of hepatology (8, 11)). Doublets were identified using DoubletFinder (v2.0.3) (16). Samples were log-normalized with a scale factor of 10,000 and anchor integrated. The variation between cells in UMI counts and mitochondrial gene content was regressed out. The number of reads and saturation per sample is stated in Supplementary Table 2.

Dimensionality, clustering and differential gene expression

Unsupervised clustering and differential gene expression analysis were performed in Seurat. Clustering on the transjugular liver biopsy samples was done using shared nearest neighbors with 30 principal components based on integrated dataset variability shown in principal component analysis (PCA). Louvain clustering with a resolution of 2 was used to determine the number of clusters. Next, clusters were combined and labeled based on published marker genes (8, 11, 17). Doublet clusters were identified using the DoubletScore and removed. Low quality clusters were identified

based on differentially expressed genes and removed. Several cell types were sub-clustered for further analysis. Each new Louvain clustering and uniform manifold approximation and projection (UMAP) reduction utilized dimensions between 10 and 20 for regression. Markers for each sub-cluster were identified with the FindAllMarkers functions, and cell types were manually annotated. Seurat was used together with ggplot2 (v3.3.6) and pheatmap (v1.0.12) packages to generate heatmaps, violin plots, barplots, dotplots and UMAP visualizations. Differential gene analysis in Seurat was performed with Wilcoxon Rank Sum with genes only present in at least 25% of cells. A correlation prediction score was calculated in the snRNA-seq and scRNA-seq dataset using the FindTransferAnchors and TransferData functions of the Seurat R Package using the scRNA-seq or sn-RNAseq as reference dataset respectively.

Comparison of scRNA-seq and snRNA-seq

We performed differential abundance analysis on the clusters and subclusters derived from different techniques, utilizing the miloR package (v1.2.0) to build a kNN graph (k=30, d=15-30) and define cell neighbourhoods (prop=0.2) (18). Neighbourhoods were quantified using countCells after calculating their distance with calcNhoodDistance (d=15-30). The differential abundance was evaluated with testNhoods across the conditions and visualized in a barplot. Significance was defined as an adjusted, two-sided p-value of <0.05. Spearman correlation was computed for the log2-transformed gene expression profiles of the cell and nucleus data (RNA-assay), specifically for the protein-coding genes. The set of protein coding human genes was downloaded from the Ensembl database (GRCh38.p14) using the BiomaRt R package. Gene set scores were calculated using the Addmodulescore function in Seurat and compared using a Wilcoxon-rank sum test. Single sample gene set enrichment analysis (ssGSEA) was performed using the R package GSVA (v1.46.0), and exporting the HallMark, KEGG, Reactome and Gene ontology (GO) gene sets from the MsigDB (v7.4) database using the R package GSEABase (v1.60.0). Limma (v3.54.2) was utilized to identify significantly (adjusted p-value <0.05, t-score >4) enriched gene sets across the calculated gene set scores. Plots were generated with ggplot2.

Results

SnRNA-seq and scRNA-seq of TJBs differentially recover all major hepatic cell types

SnRNA-seq and scRNA-seq was performed on transjugular liver biopsy material from the same patient (n = 3) (patients characteristics included in Supplementary Table 1). Hereby half of the material was snap-frozen and subjected to snRNA-seq, while the other half was immediately processed for scRNA-seq (Figure 1A). Both single-cell and single-nucleus libraries were prepared using the 10X Genomics platform. Following data integration, quality filtering and clustering analysis, we identified 31,410 single nuclei (10,470 ± 3,615 per sample) and 6,152 single cells (2,051 ± 1,204 per sample) for the two techniques, respectively (Figure 1B). Cells and nuclei were well integrated across the different patients (Supplementary Figures S1A, B).

Based on previously canonical described marker genes, all major hepatic cell types were identified in the integrated dataset of single cells and nuclei and in both datasets separately (Figures 1B–D; Supplementary Figures S1C, D) (8, 11, 17). (0.4%) These main clusters along with their signature genes include cholangiocytes (*KRT7, KRT19, SOX9*) (41.4%), hepatocytes (*CYP2A7, CYP2C9, BCHE*) (19.1%), endothelial cells (*CCL21, CCL14, FCN2)* (17.0%), mesenchymal cells (*ACTA2, COL1A1, PDE1A*) (15.6%), NK/T-lymphocytes (*CD2, GNLY, KLRB1*) (4.6%), myeloid cells (*MERTK, MARCO, VSIG4*) (2.3%) and B-lymphocytes (*IGHG1, IGKC, IGLC2*) (0.4%) (Figures 1B, E, Supplementary List 1). All major cell types were present in both techniques for every individual patient and formed separate clusters when integrated for each individual technique (Figures 1C, D; Supplementary Figure S1C, D). However only a limited amount of hepatocytes was present in scRNA-seq (n=58; 0.9%) compared to snRNA-seq (n=7,132; 22.7%).

To interrogate the frequencies of the cell types retrieved by both techniques, we implemented the MiloR package (Figures 1F, G) (18). This package was specifically designed for differential abundance testing in single-cell datasets and was tested on data from human liver biopsies to outperform alternative methods (18). In the snRNA-seq dataset, we detected a more abundant number of cholangiocytes (mean logFC=3.37, p_{adj}<0.01), hepatocytes (mean logFC=6.57, p_{adj}<0.01), mesenchymal cells (mean logFC=2.91, p_{adj}<0.01) and myeloid cells (mean logFC=1.71, p_{adj}<0.01) (Figure 1G). On the other hand, elevated frequencies of endothelial cells (mean logFC=1.04, p_{adj}<0.01), NK/T-lymphocytes (mean logFC=2.81, p_{adj}<0.01) and B-lymphocytes (mean logFC=0.41, p_{adj}<0.05) were present in the scRNA-seq dataset (Figure 1G).

Comparison of the hepatic myeloid landscape detected by snRNA-seq or scRNA-seq

We next performed a deeper analysis of the myeloid cell clusters and their frequencies within the integrated scRNA-seq and snRNA-seq datasets. We observed the presence of three transcriptionally distinct liver myeloid cell subpopulations (Figures 2A, B, Supplementary List 1). The first subset was characterized by the expression of markers associated with liver resident macrophages (Kupffer cells (5.9%)) (*MARCO, NDST3, TIMD4*) (Figures 2A, B) (3). The second cluster we could identify, expressed genes such as *CD9, SPP1, TREM2*, reminiscent of lipid-associated macrophages (LAM, 76.5%) (Figures 2A, B) (3). We further detected a population of monocytes typically expressing markers such as *FCN1, S100A8,*

10.3389/fimmu.2024.1346520

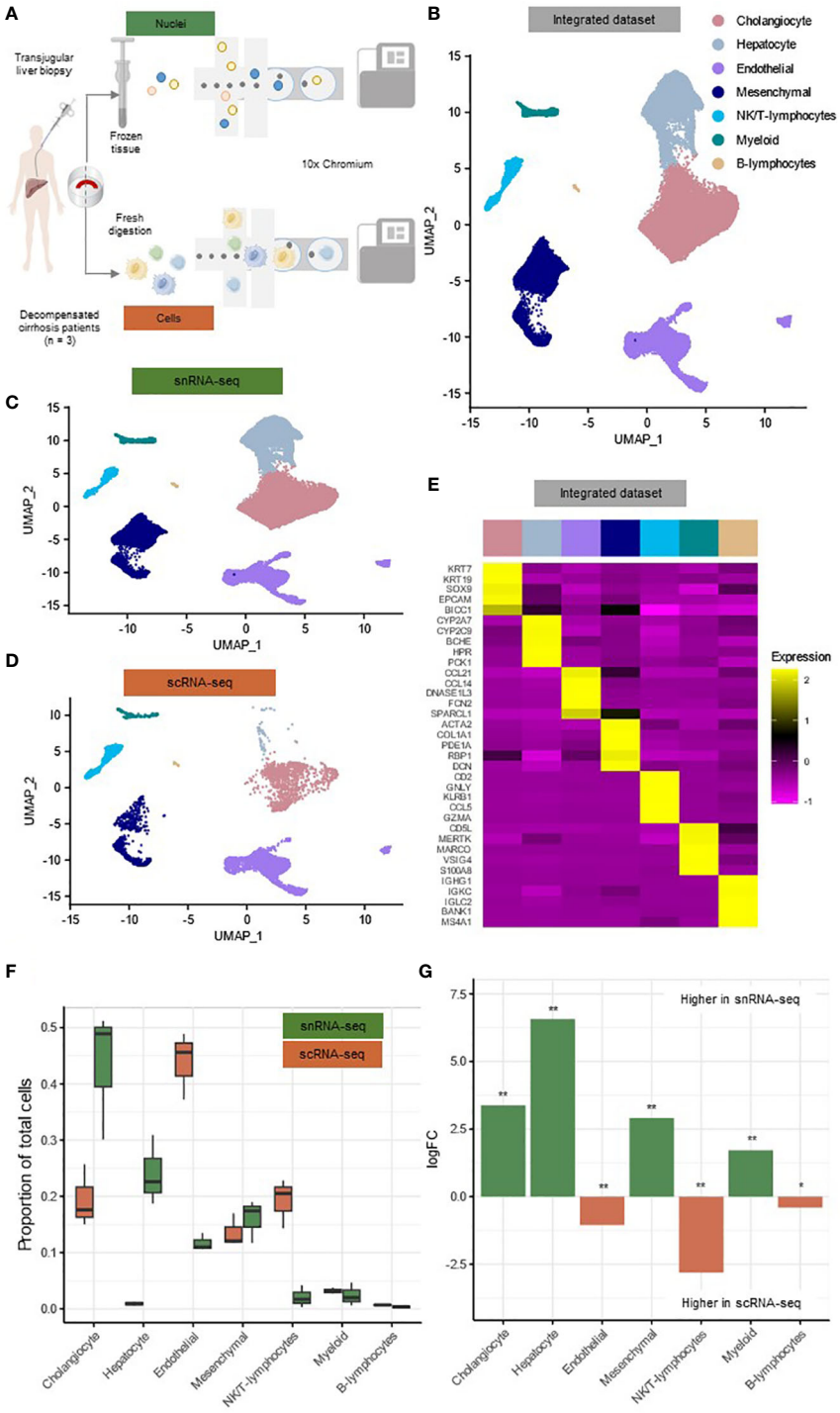

FIGURE 1
SnRNA-seq and scRNA-seq of TJBs differentially recover major hepatic cell types. **(A)** Depiction of the experimental design workflow. **(B)** Annotated UMAP plot of 31,410 single nuclei and 6,152 single cells, showing the different cell types. **(C)** Annotated UMAP plot of 31,410 single nuclei, showing the different cell types. **(D)** Annotated UMAP plot of 6,152 single cells, showing the different cell types. **(E)** Heatmap showing marker gene expression for the cell types of the full dataset. **(F)** Boxplot showing the percentage of every cluster in each sample. **(G)** Barplot showing mean logFC per cell type as calculated using MiloR. P-value adjusted for multiple testing being the minimum SpatialFDR. * p_{adj}<0.05, ** p_{adj}<0.01. *scRNA-seq, single-cell RNA-sequencing; snRNA-seq, single-nucleus RNA-sequencing; UMAP, uniform manifold approximation and projection*.

VCAN (17.6%) (Figures 2A, B) (3). The low percentage of Kupffer cells and high percentage of LAMs in patients with advanced liver disease is in line with the observations of previous reports (3, 9).

The cellular retrieval of the myeloid subpopulations in both techniques differed notably (Figures 2C-F). In snRNA-seq, only 10.06 ± 3.40% of all nuclei were monocytes, compared to 43.45 ± 11.01% of all scRNA-seq cells

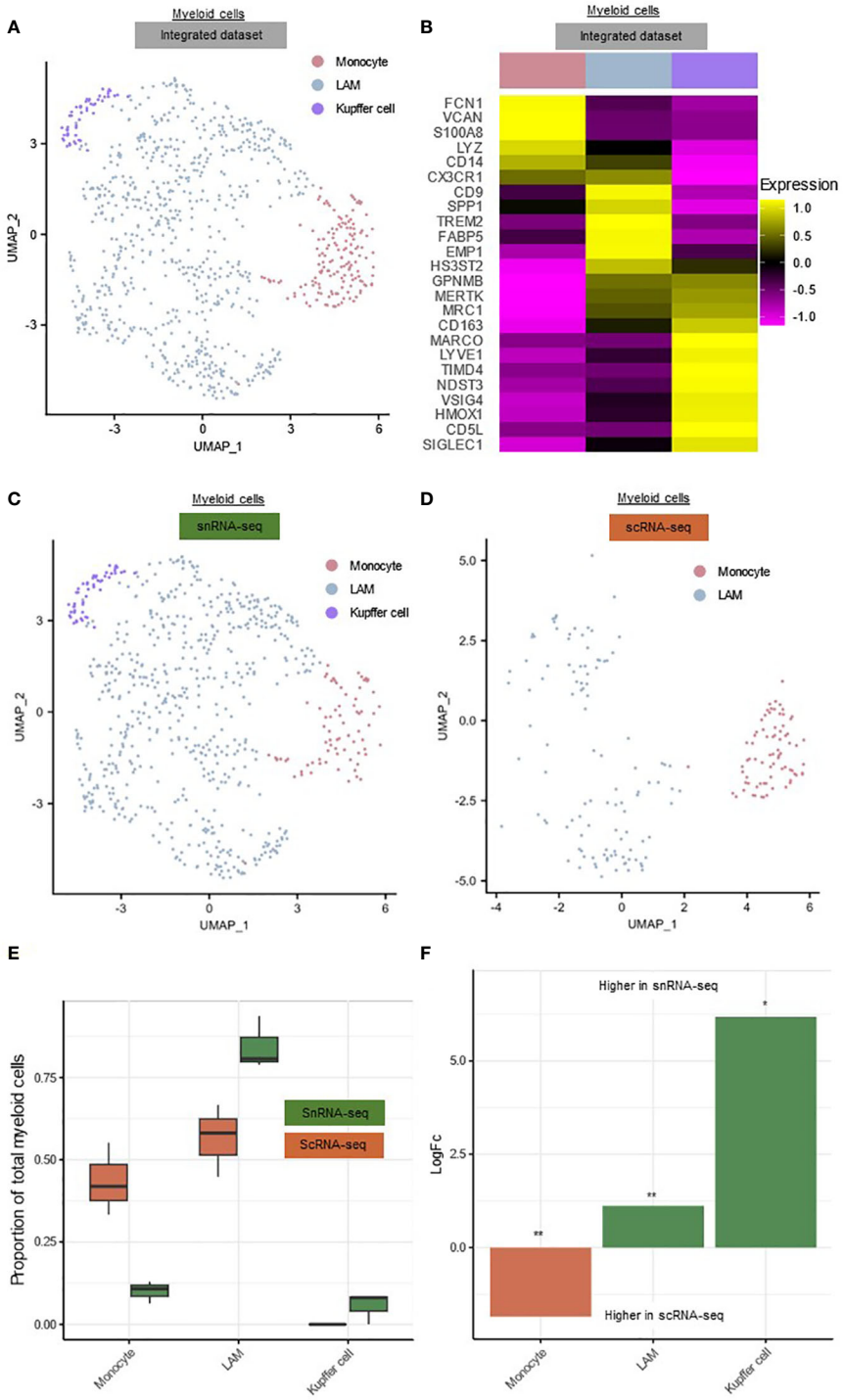

FIGURE 2
Comparison of the hepatic myeloid landscape detected by snRNA-seq or scRNA-seq. **(A)** Annotated UMAP plot of 689 single nuclei and 187 single cells of the myeloid cells, showing the different subpopulations. **(B)** Heatmap showing marker gene expression for the subclusters of the myeloid cells. **(C)** Annotated UMAP plot of 689 single nuclei of the myeloid cells, showing the different subpopulations **(D)** Annotated UMAP plot of 187 single cells of the myeloid cells, showing the different subpopulations **(E)** Boxplot showing the percentage of every myeloid subpopulation in each sample. **(F)** Barplot showing mean LogFC per subpopulation of the myeloid cells, as calculated using MiloR. P-value adjusted for multiple testing being the minimum SpatialFDR. * p_{adj}<0.05, ** p_{adj}<0.01, *scRNA-seq, single-cell RNA-sequencing; snRNA-seq, single-nucleus RNA-sequencing; UMAP, uniform manifold approximation and projection*.

(p=0.052) (Figure 2E). On the other hand, scRNA-seq failed to recover any Kupffer cells (Figure 2E). MiloR analysis showed that LAMs (mean logFC=1.12, p_{adj}<0.01) and Kupffer cells (mean logFC=6.18, p_{adj}<0.05) were significantly more abundant in snRNA-seq, while monocytes (mean logFC=1.85, p_{adj}<0.01) were significantly more present in scRNA-seq (Figure 2F). Because scRNA-seq was not able to detect Kupffer cells and retrieved less macrophages, this

technique seems less suitable for studying the hepatic myeloid cell landscape in TJB from decompensated cirrhosis patients.

Comparison of non-myeloid subclusters detected by snRNA-seq or scRNA-seq

The NK/T-lymphocytes could be subclustered into $CD4^+$ T-cells (*CD3D, CD3E, CD4*) (49.5%), $CD8^+$ T-cells (*CD3D, CD3E, CD8A, CD8B*) (24.1%), cytotoxic NK-cells (*GNLY, GZMB, KLRF1*) (10.0%) and tissue-resident NK-cells (*EOMES, NCAM1, XCL1*) (16.4%) (Figures 3A–C, Supplementary List 1) (19). Due to the limited total number of NK/T-lymphocytes, these subclusters were not subdivided further. The B-lymphocyte cluster could be subclustered into B-cells (*CD79A, CD79B, MS4A1*) (52.4%) and plasma cells (*IGHG1, IGHA1, JCHAIN*) (47.6%) (Figures 3C–E, Supplementary List 1).

Within the NK/T-lymphocytes, tissue-resident NK-cells (mean logFC=0.78, $p_{adj}<0.01$) were significantly more abundant in snRNA-seq, while $CD4^+$ T-cells (mean logFC=0.52, $p_{adj}<0.0001$), $CD8^+$ T-cells (mean logFC=0.72, $p_{adj}<0.01$) and cytotoxic NK-cells (mean logFC=0.87, $p_{adj}<0.01$) were significantly more abundant in scRNA-seq (Figure 3F). In the B-lymphocytes there were no significant differences in abundance, this could however be caused by the low number of cells and nuclei (Figure 3F).

The mesenchymal cells could be subdivided into fibroblasts (FB) (*COL4A4, NAV3, PTGDS*) (68.7%), hepatic stellate cells (HSC) (*ADAMTSL1, LRAT, RELN*) (6.2%) and vascular smooth muscle cells (VSMC) (*MYL9, ACTA2, MYH11*) (25.0%) (Figures 4A–C, Supplementary List 1) (8, 9, 11). As expected, HSCs and FBs clustered together because they have similar phenotypes, while the VSMCs clustered separately (Figure 4A) (8, 9, 11). We observed a high number of FBs compared to HSCs, which is in line with other data reported from cirrhotic human livers (8, 11). The endothelial cells could be subdivided into scar-associated endothelial cells (scarEC; *COL15A1, PLVAP, VWA1*) (72.2%), liver sinusoidal endothelial cells (LSEC; *CLEC4M, LYVE1, STAB2*) (5.9%), hepatic artery endothelial cells (*AIF1L, KLF2, SOX17*) (10.4%), venous endothelial cells (*CPE, LHX6, OPCML*) (2.8%) and lymphatic endothelial cells (*CCL21, PROX1, TSPAN5*) (8.7%) (Figures 4C–E, Supplementary List 1) (8, 9, 17). The number of scarECs was elevated compared to the number of LSECs, as was reported previously in human cirrhotic livers (Figure 4E) (8, 11).

Within the mesenchymal cells, scarECs (mean logFC=3.90, $p_{adj}<0.001$) and LSECs (mean logFC=1.83, $p_{adj}<0.05$) were significantly more abundant in snRNA-seq, while VSMCs (mean logFC=1.15, $p_{adj}<0.001$) were significantly more abundant in scRNA-seq (Figure 4F). There were no significant differences between both techniques for the endothelial cell subclusters (Figure 4F).

Comparison of gene signatures in snRNA-seq and scRNA-seq

After comparing both techniques for cluster and subcluster recovery, we next evaluated both techniques in terms of cell/nuclei recovery and gene signatures. The mean number of genes detected per nuclei/cell (2,851 ± 188 vs. 2,260 ± 16, $p<0.05$) was significantly elevated in the snRNA-seq dataset (Figure 5A). The number of counts per nuclei/cell was comparable between both techniques (6,274 ± 1082 vs. 6,669 ± 201, p NS) (Figure 5A).

To investigate if the core marker genes from the different subsets were comparable between both techniques, we used the gene signature of the single cells to predict the clustering of the single nuclei, and vice versa, using Seurat. Based on the gene signature of scRNA-seq and snRNA-seq, we could correctly identify the major cell types of 98.8% of the nuclei and 99.8% of the cells respectively (Supplementary Figures S2A, B). Specifically for the myeloid cluster, 99.4% of the nuclei and 99.5% of the cells were correctly predicted. This with a high mean correlation prediction score, as a measure for the certainty of the prediction, of 99.2 and 99.4 respectively, showing that the gene signature of myeloid cells was preserved in both techniques (Figures S2A, B).

In the myeloid subpopulations, we focused on the monocytes and LAMs since there were no Kupffer cells retrieved in scRNA-seq. For the monocytes, 100% of all nuclei and 77.6% of all cells were predicted correctly, with reasonable to good mean correlation prediction scores of 95.2 and 71.3 respectively (Supplementary Figures S2A, B). For the LAMs, 91.9% of all nuclei and 98.2% of all cells were predicted correctly, with good mean correlation prediction scores of 87.0 and 90.3 respectively (Supplementary Figures S2A, B). In addition, cell type intrinsic (pseudobulk) profiles of protein-coding genes were overall similar between snRNA-seq and scRNA-seq (Spearman correlation $\rho = 0.75$ in LAM and 0.73 in monocytes) (20). We calculated this in the myeloid subclusters (and not myeloid cluster), to minimize the effect of the differential abundance of specific subclusters in both techniques on the gene expression. This shows that also for the specific myeloid subpopulations, the gene signature was largely preserved in both techniques.

Nevertheless, also some important differences could be detected. In this regard, the transcriptomic data set from cells featured an elevated dissociation-induced stress signature (e.g. *FOS, HSPA8, JUNB*) (Figures 5B, C) as well as the expression of ribosomal (e.g. *RPL10, RPS8, RPS27*) and mitochondrial (e.g. *MT-CO1, MT-ND3, MT-ND4*) genes, similar to previous reports (20). In turn, nuclei exhibited elevated levels of long non-coding RNA (e.g. *AP000331.1, AP001011.1, AP003086.1*) (Figure 5C) (20–22). Furthermore, in a pathway analysis, immune-cell activation, apoptosis-related, phagocytosis, complement and stress-related pathways were increased in scRNA-seq compared to snRNA-seq, both in LAMs and monocytes (Figures 5D, E). Importantly, we also observed an elevated dissociation-induced stress signature in all other major clusters (Supplementary Figure S2C). This is compatible with an increased dissociation-induced stress in scRNA-seq.

Discussion

The capacity to examine advanced liver disease at the single-cell level could significantly enhance our comprehension of the pathophysiology in disorders such as acute-on-chronic liver failure (ACLF), severe alcoholic hepatitis, and decompensated

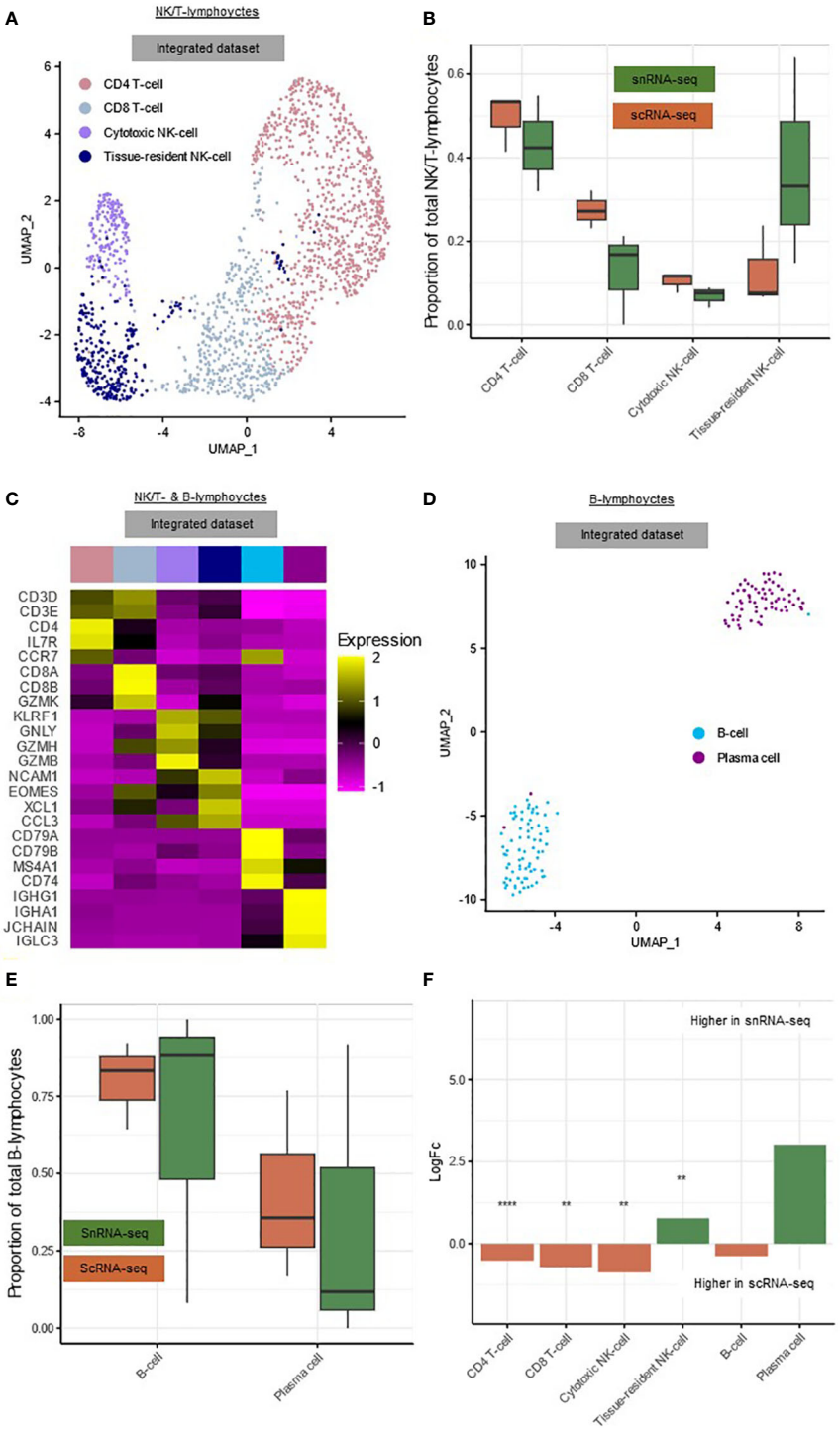

FIGURE 3
snRNA-seq and scRNA-seq differentially detect subclusters of hepatic lymphocytes. **(A)** Annotated UMAP plot of 573 single nuclei and 1,143 single cells of the NK/T-lymphocytes, showing the different subclusters. **(B)** Boxplot showing the percentage of every NK/T-lymphocyte subpopulation in each sample. **(C)** Heatmap showing marker gene expression for the subclusters of the NK/T- and B-lymphocytes. **(D)** Annotated UMAP plot of 99 single nuclei and 46 single cells of the B-lymphocytes, showing the different subclusters and techniques. **(E)** Boxplot showing the percentage of every B-lymphocyte subpopulation in each sample. **(F)** Barplot showing mean LogFC per subcluster of the immune cells, as calculated using MiloR. P-value adjusted for multiple testing being the minimum SpatialFDR. ** p_{adj}<0.01, **** p_{adj}<0.0001. *scRNA-seq, single-cell RNA-sequencing; snRNA-seq, single-nucleus RNA-sequencing; UMAP, uniform manifold approximation and projection.*

cirrhosis. It is crucial to acknowledge that in these advanced disease states, obtaining liver tissue safely is only possible through the transjugular route, resulting in extremely small and fragile liver biopsy specimens (14, 23). Currently, it remains uncertain whether successful sequencing of TJBs can be achieved for downstream characterization of the hepatic landscape. Therefore, we conducted an in-patient comparison of snRNA-seq and scRNA-seq protocols on TJBs obtained from 3 decompensated cirrhosis patients.

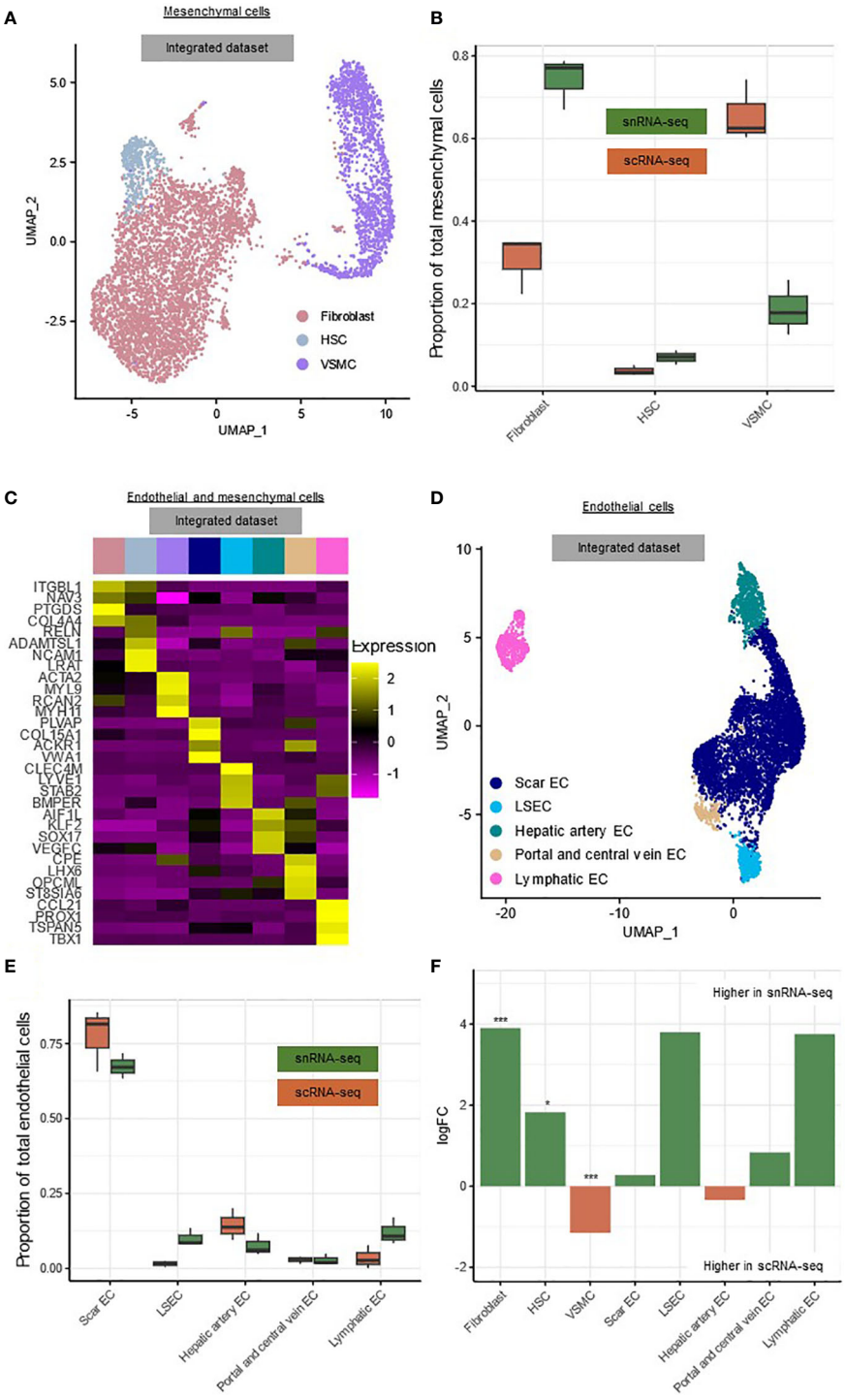

FIGURE 4
snRNA-seq and scRNA-seq differentially detect subclusters of mesenchymal cells. **(A)** Annotated UMAP plot of 5,023 single nuclei and 814 single cells of the mesenchymal cells, showing the different subclusters. **(B)** Boxplot showing the percentage of every mesenchymal subpopulation in each sample. **(C)** Heatmap showing marker gene expression for the subclusters of the mesenchymal- and endothelial cells. **(D)** Annotated UMAP plot of 3,666 single nuclei and 2,707 single cells of the endothelial cells, showing the different subclusters. **(E)** Boxplot showing the percentage of every endothelial subpopulation in each sample. **(F)** Barplot showing mean logFC per subcluster of the mesenchymal and endothelial cells, as calculated using MiloR. P-value adjusted for multiple testing being the minimum SpatialFDR. * p_{adj}<0.05, *** p_{adj}<0.001. *scRNA-seq, single-cell RNA-sequencing; snRNA-seq, single-nucleus RNA-sequencing; UMAP, uniform manifold approximation and projection.*

By following the appropriate protocol, we were able to consistently obtain approximately 10,000 single nuclei and 2,000 high-quality single cells per patient. Although the number of nuclei fell within the expected range, the count of cells tended to be lower than reported in the literature, likely attributable to the small size of the transjugular liver biopsy (11, 24). The data unveiled several differences that align with findings from comparable studies on the healthy human liver using whole liver lobes (11, 17). In particular,

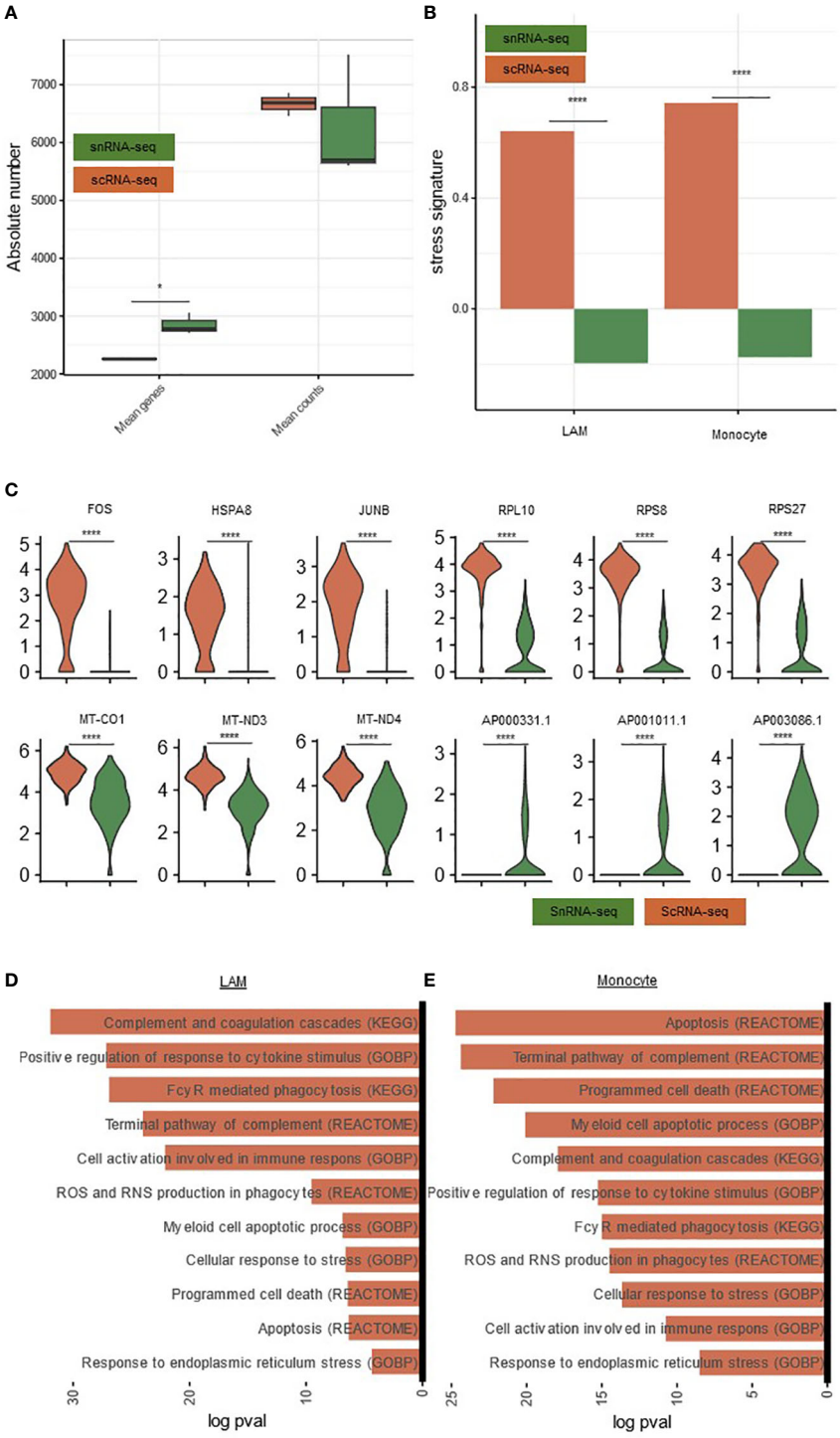

FIGURE 5
Comparison of gene expression and gene signatures in snRNA-seq and scRNA-seq. **(A)** Boxplots comparing scRNA-seq and snRNA-seq for mean genes and counts per sample. P-value calculated with a paired t-test. **(B)** Barplot comparing the stress signature between both techniques in monocytes and LAMs. Significance calculated using a Wilcoxon rank-sum test **(C)** Violin plot showing the expression of stress-related, ribosomal, mitochondrial and long non-coding RNA, comparing the snRNA-seq data with the scRNA-seq data. **(D)** Pathways significantly upregulated in scRNAseq compared to snRNA-seq in LAMs. **(E)** Pathways significantly upregulated in scRNA-seq compared to snRNA-seq in Monocytes.
* p_{adj}<0.05, **** p_{adj}<0.0001 *scRNA-seq, single-cell RNA-sequencing; snRNA-seq, single-nucleus RNA-sequencing.*

the snRNA-seq data showed a higher percentage of parenchymal and mesenchymal cells, but a lower percentage of endothelial cells and lymphocytes, in comparison to scRNA-seq (11). Similar to other studies on human liver biopsies, scRNA-seq revealed impaired recovery of hepatocytes, in contrast to snRNA-seq (8, 9). The reduced number of hepatocytes may be attributed to their vulnerability, rendering them susceptible to cell death during enzymatic dissociation. Alternatively their size could hinder their

passage through the microfluidic channels. Furthermore, we observed significant differences in the retrieval of subclusters, such as a higher frequency of hepatic stellate cells (HSCs) and fibroblasts in snRNA-seq compared to a higher frequency of vascular smooth muscle cells (VSMCs) in scRNA-seq. We propose that dissimilarities in cellular retrieval between the two techniques stem from variations in the dissociation protocols employed. In the case of snRNA-seq, where the goal is to exclusively recover nuclei, a robust mechanical dissociation protocol can be employed. Conversely, for scRNA-seq, the requirement for live cells during library preparation necessitates the use of a gentler enzymatic dissociation protocol. This method tends to selectively favour resilient and/or more easily dissociable cell types, such as lymphocytes.

Overall, we found that snRNA-seq performed well in terms of sensitivity and classification of all hepatic cell (sub)-types and exhibited less cell type bias, as has been observed in other types of human tissues (24, 25). On the other hand, scRNA-seq emerges as the preferred platform for investigating lymphocytes, benefitting from its distinct positive selection of these cells. This preference is further underscored by the low level of B- and T-cell receptor transcripts in sn-RNAseq data, a finding that is consistent with that of Andrews et al. (Supplementary Figure S2D) (11). Nevertheless, the snRNA-seq platform offered an additional advantage, as it decouples sample procurement from processing and allows multiplexing of samples collected over time, including biobanked material (24).

Concerning the hepatic myeloid compartment, it remains uncertain whether nuclei can serve as a viable alternative for cellular transcriptomes in the context of advanced liver disease and small sample sizes. This is significant, given that hepatic myeloid cells play a crucial role in both the progression and resolution of tissue inflammation and injury processes (3, 9).

Data analysis of the single nuclei sequenced myeloid cells consistently identify the primary monocyte/macrophage identities found in cirrhotic livers, including Kupffer cells, LAM, and monocytes (3). However, it is important to note that the scRNA-seq platform failed to capture sufficient numbers of Kupffer cells, the most prominent resident macrophage population in the healthy liver. This observation may be elucidated by the reduced presence of Kupffer cells in cirrhotic livers in combination with the limited absolute count of myeloid cells in our study. Additionally, scRNA-seq tends to favor cells that undergo easy dissociation, potentially contributing to the limited representation of myeloid cells in the dataset (3). Generally, snRNA-seq captured a higher percentage of macrophages compared to scRNA-seq, but a lower percentage of monocytes. The data further indicated that the gene signature of the myeloid subclusters was largely preserved in both snRNA-seq and scRNA-seq, with high mean prediction scores and good Pearson correlation coefficients when comparing both techniques. In scRNA-seq, we observed an increase in the expression of ribosomal and mitochondrial RNA, while in snRNA-seq, the expression of long non-coding RNA was notable. However, the most significant difference between both techniques was the heightened dissociation-induced stress signature in scRNA-seq, evident both at the gene level and in pathway analysis. This phenomenon may be attributed to the distinct methodologies employed in snRNA-seq and scRNA-seq. In snRNA-seq, cells undergo rapid freezing and mechanical dissociation, resulting in their swift demise. In contrast, scRNA-seq involves keeping the cells alive during enzymatic dissociation until loading, affording them an opportunity to develop a stress-response. This difference in treatment timelines could contribute to the observed variations in cellular outcomes between the two technique. Our findings strongly indicate that scRNA-seq is less suitable for studying the hepatic myeloid cell landscape in transjugular liver biopsies (TJB) from decompensated cirrhosis patients (3).

In summary, our data strongly suggests that snRNA-seq is superior in recapitulating the hepatic landscape without extensive population bias. The snRNA-seq platform also overcomes challenges related to streamlining clinical specimen collection and downstream experimental procedures, as the procedure can be performed on frozen tissue. Additionally, our results indicate that single-nucleus transcriptome sequencing is the platform of choice for studying myeloid cell populations, as scRNA-seq failed to recover Kupffer cells, and the remaining monocytes/macrophages exhibited increased expression of dissociation-induced stress parameters. Taken together, our data provide essential insights to be considered when undertaking similar sequencing experiments in advanced human cirrhosis.

Data availability statement

Raw sequence data has been deposited at the European Genome-phenome Archive (EGA), under accession number EGAS50000000073. This study did not generate any new code.

Ethics statement

The studies involving humans were approved by University Hospitals Leuven ethical committee. The studies were conducted in accordance with the local legislation and institutional requirements. The participants provided their written informed consent to participate in this study. Written informed consent was obtained from the individual(s) for the publication of any potentially identifiable images or data included in this article.

Author contributions

LM: Conceptualization, Data curation, Formal Analysis, Funding acquisition, Investigation, Methodology, Project administration, Resources, Software, Validation, Visualization, Writing – original draft, Writing – review & editing. JV: Conceptualization, Funding acquisition, Investigation, Methodology, Resources, Supervision, Visualization, Writing – original draft, Writing – review & editing. DB: Conceptualization, Data curation, Formal Analysis, Methodology, Software, Visualization, Writing – original draft. MB: Data curation, Formal Analysis, Methodology, Software, Visualization, Writing – review & editing. BB: Data curation, Methodology, Software, Writing – review & editing. RF-A: Investigation, Visualization, Writing – review & editing. LS:

Investigation, Writing – review & editing. MW: Investigation, Project administration, Writing – review & editing. EC: Investigation, Methodology, Writing – review & editing. LB: Investigation, Methodology, Writing – review & editing. GM: Investigation, Methodology, Resources, Supervision, Writing – review & editing. OG: Conceptualization, Investigation, Methodology, Supervision, Visualization, Writing – review & editing. HK: Conceptualization, Formal Analysis, Funding acquisition, Investigation, Methodology, Project administration, Supervision, Visualization, Writing – original draft, Writing – review & editing. DL: Conceptualization, Data curation, Funding acquisition, Investigation, Methodology, Project administration, Resources, Supervision, Writing – original draft, Writing – review & editing. SM: Conceptualization, Formal Analysis, Funding acquisition, Investigation, Methodology, Project administration, Resources, Supervision, Visualization, Writing – original draft, Writing – review & editing.

Funding

The author(s) declare financial support was received for the research, authorship, and/or publication of this article. This study was supported by a research grant from The Research Foundation – Flanders (FWO; Fonds voor Wetenschappelijk Onderzoek – Vlaanderen) (G082018N), LM (1110121N) received a junior research mandate and SM a senior research mandate from FWO. Additionally, our research was supported by internal funding from KU Leuven (C14/18/087, C14/23/135 & AKUL/19/039). Financial support was also received from the Belgian Association for the Study of the Liver and a research grant from the Belgian Week of Gastroenterology (BWGE) to LM and UZ Leuven (KOOR) to JV. The authors declare that this study also received funding from Gilead Sciences. The funder was not involved in the study design, collection, analysis, interpretation of data, the writing of this article, or the decision to submit it for publication.

Acknowledgments

We like to thank Rogier Schepers and Thomas Van Brussel for the practical support during the experiments. We would like to thank Gino Philips for his bio-informatic support. We would like to thank the hospital staff of the service of Hepatology and Intensive care in caring for our patients. Lastly, we would like to thank the patients for their willingness to participate in this study.

Conflict of interest

The authors declare that the research was conducted in the absence of any commercial or financial relationships that could be construed as a potential conflict of interest.

The author(s) declared that they were an editorial board member of Frontiers, at the time of submission. This had no impact on the peer review process and the final decision.

Publisher's note

Supplementary material

The Supplementary Material for this article can be found online at: https://www.frontiersin.org/articles/10.3389/fimmu.2024.1346520/full#supplementary-material

SUPPLEMENTARY FIGURE 1
Integration of both techniques and patients. **(A)** Annotated UMAP plot of 31,410 single nuclei, split per patient. **(B)** Annotated UMAP plot of 6,152 single cells, split per patient. **(C)** Annotated UMAP plot of 31,410 single nuclei, showing the different clusters. **(D)** Annotated UMAP plot of 6,152 single cells, showing the different clusters.

SUPPLEMENTARY FIGURE 2
Comparison of gene signatures in major clusters. **(A)** Barplot showing the mean prediction identity score per (sub)cluster of nuclei, predicted using the gene signature of the scRNA-seq data. Score ranging from 0 to 1. Calculated using Seurat-package (FindTransferAnchors, TransferData). **(B)** Barplot showing the mean prediction identity score per (sub)cluster of cells, predicted using the gene signature of the snRNA-seq data. Score ranging from 0 to 1. Calculated using Seurat-package (FindTransferAnchors, TransferData). **(C)** Barplot comparing the stress signature between both techniques in the major celltypes. Significance calculated using a Wilcoxon rank-sum test. **(D)** Dotplot showing the expression of T-cell and B-cell receptor genes in different techniques. The size of the dot shows the percentage of cells expressing the gene and the color the strength of expression.

SUPPLEMENTARY TABLE 1
Clinical characteristics of patients.

SUPPLEMENTARY TABLE 2
Number of reads and saturation per sample.

References

1. Marcellin P, Kutala BK. Liver diseases: A major, neglected global public health problem requiring urgent actions and large-scale screening. *Liver Int* (2018) 38 Suppl 1:2–6. doi: 10.1111/liv.13682

2. Albillos A, Martin-Mateos R, van der Merwe S, Wiest R, Jalan R, Álvarez-Mon M, et al. Cirrhosis-associated immune dysfunction. *Nat Rev Gastroenterol Hepatol* (2021) 19(2):112–34. doi: 10.1038/s41575-021-00520-7

3. Guilliams M, Scott CL. Liver macrophages in health and disease. *Immunity* (2022) 55:1515–29. doi: 10.1016/j.immuni.2022.08.002

4. Aizarani N, Saviano A, Sagar Mailly L, Durand S, Herman JS. A human liver cell atlas reveals heterogeneity and epithelial progenitors. *Nature* (2019) 572:199–204. doi: 10.1038/s41586-019-1373-2

5. Bernsmeier C, van der Merwe S, Périanin A. Innate immune cells in cirrhosis. *J Hepatol* (2020) 73:186–201. doi: 10.1016/j.jhep.2020.03.027

6. Sharma A, Wen Seow JJ, Dutertre C, Pai R, Blériot C, Mishra A, et al. Onco-fetal reprogramming of endothelial cells drives immunosuppressive macrophages in hepatocellular carcinoma. *Cell* (2020) 183:377–394.e21. doi: 10.1016/j.cell.2020.08.040

7. Krenkel O, Hundertmark J, Abdallah AT, Kohlhepp M, Puengel T, Roth T, et al. Myeloid cells in liver and bone marrow acquire a functionally distinct inflammatory phenotype during obesity-related steatohepatitis. *Gut* (2020) 69:551–63. doi: 10.1136/gutjnl-2019-318382

8. Ramachandran P, Dobie R, Wilson-Kanamori JR, Dora EF, Henderson BEP, Tuu NT, et al. Resolving the fibrotic niche of human liver cirrhosis at single-cell level. *Nature* (2019) 575:512–8. doi: 10.1038/s41586-019-1631-3

9. Guilliams M, Bonnardel J, Haest B, Vanderborght B, Wagner C, Remmerie A, et al. Spatial proteogenomics reveals distinct and evolutionarily conserved hepatic macrophage niches. *Cell* (2022) 185:379–396.e38. doi: 10.1016/j.cell.2021.12.018

10. Bonnardel J, T'Jonck W, Gaublomme D, Browaeys R, Scott CL, Martens L, et al. Stellate cells, hepatocytes, and endothelial cells imprint the kupffer cell identity on monocytes colonizing the liver macrophage niche. *Immunity* (2019) 51:638–654.e9. doi: 10.1016/j.immuni.2019.08.017

11. Andrews TS, Atif J, Liu JC, Perciani CT, Ma X, Thoeni C, et al. Single-cell, single-nucleus, and spatial RNA sequencing of the human liver identifies cholangiocyte and mesenchymal heterogeneity. *Hepatol Commun* (2021) 6(4):821–40. doi: 10.1002/HEP4.1854

12. Habib N, Avraham-Davidi I, Basu A, Burks T, Shekhar K, Hofree M, et al. Massively parallel single-nucleus RNA-seq with DroNc-seq. *Nat Methods* (2017) 14:955–8. doi: 10.1038/nmeth.4407

13. Habib N, Li Y, Heidenreich M, Swiech L, Avraham-Davidi I, Trombetta JJ, et al. Div-Seq: Single-nucleus RNA-Seq reveals dynamics of rare adult newborn neurons. *Science* (2016) 353:925–8. doi: 10.1126/science.aad7038

14. Reiberger T, Schwabl P, Trauner M, Peck-Radosavljevic M, Mandorfer M. Measurement of the hepatic venous pressure gradient and transjugular liver biopsy. *J Vis Exp* (2020) 2020:1–16. doi: 10.3791/58819

15. Hao Y, Hao S, Andersen-Nissen E, Mauck WM, Zheng S, Butler A, et al. Integrated analysis of multimodal single-cell data. *Cell* (2021) 184:3573–3587.e29. doi: 10.1016/j.cell.2021.04.048

16. McGinnis CS, Murrow LM, Gartner ZJ. DoubletFinder: doublet detection in single-cell RNA sequencing data using artificial nearest neighbors. *Cell Syst* (2019) 8:329–337.e4. doi: 10.1016/j.cels.2019.03.003

17. MacParland SA, Liu JC, Ma X, Innes BT, Bartczak AM, Gage BK, et al. Single cell RNA sequencing of human liver reveals distinct intrahepatic macrophage populations. *Nat Commun* (2018) 9:4383. doi: 10.1038/s41467-018-06318-7

18. Dann E, Henderson NC, Teichmann SA, Morgan MD, Marioni JC. Differential abundance testing on single-cell data using k-nearest neighbor graphs. *Nat Biotechnol* (2022) 40:245–53. doi: 10.1038/s41587-021-01033-z

19. Zhao J, Zhang S, Liu Y, He X, Qu M, Xu G, et al. Single-cell RNA sequencing reveals the heterogeneity of liver-resident immune cells in human. *Cell Discovery* (2020) 6:1–19. doi: 10.1038/s41421-020-0157-z

20. Eraslan G, Drokhlyansky E, Anand S, Fiskin E, Subramanian S, Slyper M, et al. Single-nucleus cross-tissue molecular reference maps toward understanding disease gene function. *Sci (1979)* (2022) 376. doi: 10.1126/science.abl4290

21. Van Den Brink SC, Sage F, Vértesy Á, Spanjaard B, Peterson-Maduro J, Baron CS, et al. Single-cell sequencing reveals dissociation-induced gene expression in tissue subpopulations. *Nat Methods* (2017) 14:935–6. doi: 10.1038/nmeth.4437

22. Wu H, Kirita Y, Donnelly EL, Humphreys BD. Advantages of single-nucleus over single-cell RNA sequencing of adult kidney: Rare cell types and novel cell states revealed in fibrosis. *J Am Soc Nephrol* (2019) 30:23–32. doi: 10.1681/ASN.2018090912

23. Sue MJ, Lee EW, Saab S, McWilliams J, Francisco D, El-Kabany M, et al. Transjugular liver biopsy: safe even in patients with severe coagulopathies and multiple biopsies. *Clin Transl Gastroenterol* (2019) 10. doi: 10.14309/ctg.0000000000000063

24. Slyper M, Porter CBM, Ashenberg O, Waldman J, Drokhlyansky E, Wakiro I, et al. A single-cell and single-nucleus RNA-Seq toolbox for fresh and frozen human tumors. *Nat Med* (2020) 26:792–802. doi: 10.1038/s41591-020-0844-1

25. Deleersnijder D, Callemeyn J, Arijs I, Naesens M, Van Craenenbroeck AH, Lambrechts D, et al. Current methodological challenges of single-cell and single-nucleus RNA-sequencing in glomerular diseases. *J Am Soc Nephrol* (2021) 32:1838–52. doi: 10.1681/ASN.2021020157

frontiers | Frontiers in Immunology

TYPE Original Research
PUBLISHED 13 March 2024
DOI 10.3389/fimmu.2024.1330536

OPEN ACCESS

EDITED BY
Jack Leslie,
Newcastle University, United Kingdom

REVIEWED BY
Scott A. Read,
Western Sydney University, Australia
Leo Marc Carlin,
University of Glasgow, United Kingdom

*CORRESPONDENCE
Patricia F. Lalor
p.f.lalor@bham.ac.uk

RECEIVED 31 October 2023
ACCEPTED 23 February 2024
PUBLISHED 13 March 2024

CITATION
Khan R, Salman S, Harford L, Sheriff L, Hazeldine J, Rajoriya N, Newsome PN and Lalor PF (2024) Circulating myeloid populations have prognostic utility in alcohol-related liver disease. *Front. Immunol.* 15:1330536. doi: 10.3389/fimmu.2024.1330536

Circulating myeloid populations have prognostic utility in alcohol-related liver disease

Reenam Khan[1], Shees Salman[2], Laura Harford[1], Lozan Sheriff[1], Jon Hazeldine[3], Neil Rajoriya[2], Philip N. Newsome[1,3] and Patricia F. Lalor[1]*

[1]Centre for Liver and Gastrointestinal Research, Institute of Immunology and Immunotherapy, Birmingham, United Kingdom, [2]The Liver Unit, Queen Elizabeth Hospital Birmingham, Birmingham, United Kingdom, [3]Institute of Inflammation and Ageing, University of Birmingham, and Birmingham National Institute for Health Research (NIHR), Biomedical Research Centre, Birmingham, United Kingdom

Introduction: Alcohol-related liver disease (ARLD) accounts for over one third of all deaths from liver conditions, and mortality from alcohol-related liver disease has increased nearly five-fold over the last 30 years. Severe alcohol-related hepatitis almost always occurs in patients with a background of chronic liver disease with extensive fibrosis or cirrhosis, can precipitate 'acute on chronic' liver failure and has a high short-term mortality. Patients with alcohol-related liver disease have impaired immune responses, and increased susceptibility to infections, thus prompt diagnosis of infection and careful patient management is required. The identification of early and non-invasive diagnostic and prognostic biomarkers in ARLD remains an unresolved challenge. Easily calculated predictors of infection and mortality are required for use in patients who often exhibit variable symptoms and disease severity and may not always present in a specialized gastroenterology unit.

Methods: We have used a simple haematological analyser to rapidly measure circulating myeloid cell parameters across the ARLD spectrum.

Results and Discussion: We demonstrate for the first time that immature granulocyte (IG) counts correlate with markers of disease severity, and our data suggests that elevated counts are associated with increased short-term mortality and risk of infection. Other myeloid populations such as eosinophils and basophils also show promise. Thus IG count has the potential to serve alongside established markers such as neutrophil: lymphocyte ratio as a simply calculated predictor of mortality and risk of infectious complications in patients with alcohol-related hepatitis. This would allow identification of patients who may require more intensive management.

KEYWORDS

cirrhosis, neutrophil, monocyte, alcohol, hepatitis, human

1 Introduction

It has been estimated that on a global scale, approximately half of the population currently drinks alcohol (1) with excess consumption a significant driver of disability and mortality. Alcohol-related liver disease (ARLD) accounts for over one third of all deaths from liver conditions (2), and mortality from alcohol-related liver disease has increased by 450% over the last 30 years (3). ARLD encompasses a spectrum that includes steatosis, steatohepatitis, fibrosis, cirrhosis, and subsequently hepatocellular carcinoma. Most individuals consuming >60g a day of alcohol will develop some degree of hepatic steatosis. A minority of these patients may develop the significant acute inflammatory condition called alcohol-related hepatitis (AH), and approximately 10-20% progress to liver cirrhosis (4). The presence of cirrhosis increases mortality risk by up to 10 fold (3), and much of the disease burden impacts people of working age (5). Thus, the economic cost of managing patients with ARLD is significant and growing.

Severe AH almost always occurs in patients with a background of chronic liver disease, with extensive fibrosis or cirrhosis. Severe AH can precipitate 'acute on chronic' liver failure (ACLF), associated with a multi-organ failure and a high short-term mortality (6). In patients hospitalized for alcohol-related cirrhosis, ACLF was associated with a three-month mortality of 60% vs 20% in patients in chronic decompensated cirrhosis (7). The most common causes of death in patients with AH include infections, GI bleeding, hepatic encephalopathy and hepatorenal syndrome. Sepsis is the most significant challenge in patients with AH with estimates suggesting that up to 25% of patients with AH have an infection on admission to hospital (8). Patients with AH have impaired immune responses, which increases their susceptibility to infections and often exhibit features of the systemic inflammatory response syndrome even in the absence of infection. This presents a challenge in the prompt diagnosis of infection and patient management. Patients with cirrhosis too exhibit immune dysfunction (9, 10) and this contributes to their overall poor outcome (11). The identification of early and non-invasive diagnostic and prognostic biomarkers in ARLD remains an unresolved challenge. In the absence of validated specific disease biomarkers, a definitive diagnosis of AH requires a biopsy (12) which carries risk in patients with compromised hepatic function. Scoring systems such as MELD and CLIF-C (13) can be used to identify at risk cirrhotic patients who need more intensive monitoring. However robust and easily calculated predictors of infection and mortality are required for use in patients who often exhibit variable presentation and disease severity and may not always present in a specialized gastroenterology unit.

Myeloid cells differentiate from bone marrow precursors to become mature circulating granulocytes (neutrophils, eosinophils, and basophils) and monocytes. These cells often function as a first line of defense against infection but can also precipitate end organ injury or drive resolution depending on the specific disease context (14). Such myeloid cells have been associated with the pathophysiology of ARLD. For example a high systemic neutrophil: lymphocyte ratio has been shown to be predictive of mortality (15), and acute kidney injury and infection (16) in the context of alcohol-related hepatitis. Similarly, recruitment of monocytes into the damaged liver contributes to inflammation and fibrosis in alcohol-related liver disease (17). Systemic inflammation or infection causes bone marrow stimulation and alterations in systemic myeloid cell counts and maturity (18). Studies suggest that elevated immature granulocyte (IG) counts may be useful as early markers of sepsis or inflammation (6, 7), although this has not been investigated in ARLD. Therefore, in this study, we use the Sysmex XN-1000 haematology analyser to investigate whether assessment of circulating myeloid cell populations also has potential prognostic utility in alcohol-related liver disease.

2 Materials and methods

2.1 Patient bloods and data collection

We collected peripheral blood from patients with alcohol-related hepatitis, (defined by ongoing alcohol use prior to admission, bilirubin >80mmol/L). We excluded patients if they had untreated sepsis, serum creatinine >500umol/L, malignancy, hepatitis B or C, or HCC or biliary obstruction. We also recruited patients with established chronic liver disease from hepatology outpatient clinics, including patients that were actively drinking and those that were abstinent >6 months. All samples were collected with informed patient consent and local LREC approval (Wales LREC reference 18-WA-0214). Healthy volunteers were also used as a control cohort. Patients were characterized into the following groups: Abstinent patients with chronic alcohol related liver disease (ARLD-Abstinent), and patients attending high dependency clinics who had alcohol-related cirrhosis and were still drinking (ARLD drinker). Demographic and clinical information was collated from digital healthcare records. Mortality outcomes were recorded up to 12 months after initial hospital admission for AH, and the presence of infection/use of antibiotics was reviewed up to 6 months post initial admittance. We supply the demographic information for our cohorts in Tables 1, 2. Whole blood was analyzed on a Sysmex XN-1000 analyzer according to manufacturer's protocols.

2.2 Functional analysis

In order to determine differences between immature PMN populations in patients with ARLD, whole blood was incubated for 30 mins with 2% dextran to allow erythrocyte sedimentation. The buffy coat was removed and layered on a density gradient of 56% and 80% Percoll. After centrifugation (220 x G for 20 minutes without brake), cells from either the upper (PBMC) or the lower (granulocyte) interface were removed and washed with RPMI-1640 + 1% PSG. Samples were then resuspended in 1ml HbSS and run on the Sysmex-XN 1000 analyser to determine differential cell counts. Neutrophil phagocytosis in heparin anticoagulated whole blood was assessed cytometrically using a PHAGOTEST kit (BD Biosciences, Oxford, UK) according to manufacturer's

TABLE 1 Combined clinical characteristics of our cohorts.

Parameter (and reference ranges)	Healthy controls (n=39)	ARLD (Abstinent) (n=39)	ARLD (Drinking) (n=11)	Alcohol-related Hepatitis (n=57)
Age	34 (27-41)	58 (36-77)	61 (42-72)	58 (20-65)
Female (%)	62	46	36	38
Alcohol units consumed per week		0	37.8 (15-75.6)	160 (21-420) [data available for 55 cases]
ALT (U/L) **Reference 0 - 55**		22 (10-61)****	27 (17-44)*	54 (15-204) [data available for 53 cases]
AST (U/L) **5 - 34**		27 (15-58)****	42 (24-91)***	130.9 (38-307) [data available for 46 cases]
ALP (U/L) **30 - 130**		106 (46-307)****	135 (64-227)	190.1 (92-562)
Urea (mmol/L) **2.5 – 7.8**		6.1 (2.1-20.8)*	5.6 (1.1-37)	5.2 (1.1-37)
Bilirubin (µmol/L) **< 21**		32 (5-205)****	18 (9-38)****	248 (51-732)
Creatinine (µmol/L) **64 - 104**		73 (41-156)***	73 (43-103)	69 (31-427)
Albumin (g/L) **35 - 50**		38 (21-45)****	38 (30-52)****	23 (12-45)
INR **0.8 – 1.2**		1.06 (1.0-1.9)****	1.1 (1-1.5)****	1.76 (1-3.2)
CRP (mg/L) **0 - 5**		4 (1-37)****	7 (1-18)**	43.29 (1-136)
FIB-4 points		2.4 (0.7-10.45)**** [data available for 33 cases]	3.4 (1.5-11.5)** [data available for 10 cases]	8.3 (2.4-49.7) [data available for 35 cases]
Encephalopathy (%)		7/39 (18)	1/11 (9)	12/57 (21%)
MELD score		8 (6-26)**** 18% MELD>15	9 (6-13)**** 0% MELD>15	24 (12-69) 95% MELD>15
UKELD score		50 (43-62)****	50(46-55)****	61 (51-72)
Child Pugh Score (points)		6 (5-11)****	6 (5-7)****	11 (6-14)
GAHS score		n/a	n/a	8 (5-11)
Maddrey score		n/a	n/a	54 (5.3-137) [data available for 40 cases]
1-month mortality (%)		0/39 (0)	0/11 (0)	10/56 (18%) [1 patient excluded as data not known]
6- month mortality (%)		2/36 (6) [3 patients excluded as data unknown]	0/11 (0)	12/43 (28%) [3 patients excluded as data not known]
12-month mortality (%)		2/23 (9) [16 patients excluded as data unknown]	0/7 (0) [4 patients excluded as data unknown]	16/35 (46%) [8 patients excluded as data not known]

Table summarizing the clinical data for all patients (used in functional assays and/or sysmex analyses). Peripheral blood samples were obtained from healthy controls (HC), and patients in indicated groups. Where appropriate, reference ranges are indicated in bold in the first column. Abstinent patients had ARLD and were on our transplant assessment list whilst those who were still drinking were being seen as outpatients in our high dependency clinic. Biochemistry data, patient symptoms and medication history were obtained from University Hospitals Birmingham electronic patient records. Age is rounded to the nearest year and mortality outcomes were assessed up to 12 months after hospital admission or sampling. Data is listed as mean (min, max values). Data were reviewed for normality (using the Shapiro Wilkes Test), and depending on the result, they were analysed using a one way ANOVA or Kruskal-Wallace test with Dunns multiple comparisons *p0.05, **p<0.001, *** p<0.005, ****p<0.0001 vs Alcoholic hepatitis cohort. ALT, alanine aminotransferase; AST aspartate aminotransferase; ALP, alkaline phosphatase; INR, international normalised ratio; MELD, Model for End-Stage Liver Disease; UKELD, United Kingdom Model for End-Stage Liver Disease; GAHS, Glasgow Alcoholic Hepatitis Score; Maddrey Score, Maddrey discriminant function).

TABLE 2 Infectious consequences in patients with ALD cirrhosis (abstinent and drinkers) and AH.

Parameter	ARLD-A (n=39)	ARLD-D (n=11)	AH (n=37)
Positive blood culture	0/39	0/11	1/36 (3) [1 patient excluded as data not known]
Microbial growth in urine (%)	0/39	0/11	1/37 [enterococcus faecalis]
Presence of CXR changes to support a diagnosis of pneumonia	0/39	0/11	12/37 [n=7 consolidation, n=5 atelectasis +/- pleural effusion
Bacterial peritonitis on ascitic tap	0/39	0/11	4/37 [n=1 had growth of Clostridium Tertium, n=1 had growth of Enterococcus Cloacae, n=2 had a polymorph count >250 but no bacterial growth]
Infection on skin swabs	0/39	0/11	2/37 [n=1 patient had fournier's gangrene, with multiple organisms on swab, one patient had growth of Staph Aureus]
Infection on nasal/ throat swabs	0/39	0/11	2/37 [n=2 tested positive for COVID19]
Infection on stool culture	0/39	0/11	1/37 [n=1 patient had C diff +ve stools]
Antibiotics (during hospital admission)	0/39	0/11	26/37 [16/26 were on antibiotics at the time of blood sampling]

Electronic patient records at University Hospitals Birmingham were reviewed to obtain data on the presence of infections (up to 6 months after initial blood sampling). Electronic drug charts were reviewed for evidence of antibiotic use. CXR, chest X-ray.

instructions. For NETosis assays, neutrophils were isolated using density gradient centrifugation and 200,000 cells per well were incubated with either 25nM PMA or vehicle control (DMSO). After incubation for 3 hours at 37°C, supernatant containing extruded nucleic acids was centrifuged at high speed (2,200G, 4°C, 10mins) transferred black, flat-bottomed, polystyrene, 96 well plates and labelled with 1μM SYTOX green dye (Invitrogen, S7020). Fluorescence was quantified using excitation 485nm and emission 530nm (BioTek-Synergy 2 plate reader). Values were compared with a standard curve of purified lambda DNA (Thermo Fisher Scientific, SD0011) to quantify the degree of NET production as described by Hazeldine et al. (19).

2.3 Statistical analysis

Graphical data are illustrated with individual symbols representing each patient with mean values for the cohort indicated. Tabulated data includes median and interquartile range for the cohort. Data were reviewed for normality (using the Shapiro Wilkes Test), and depending on the result, they were analysed using a one-way ANOVA or Kruskal-Wallace test with multiple comparisons. Correlations were calculated using the Spearman's rank correlation co-efficient.

3 Results

In this study we wished to understand the changes in peripheral blood myeloid populations which accompany alcohol-related liver disease with a view to identification of simply measured prognostic markers. Healthy volunteers were also used as a control cohort and although we aimed to match for donor age, our cohort was on average significantly younger than our patient groups (Table 1). Patients were composed of those recently admitted for AH, and abstinent patients with ARLD. In addition, a small number of our ARLD patients attending high dependency clinics were not abstinent (ARLD-Drinker). The AH patient group exhibited heterogeneity across multiple parameters on a par with the varied extent of drinking and underlying liver disease. For those patients whom we had the appropriate clinical parameters we calculated a FIB-4 score (20) as a simple noninvasive guide to likely fibrosis stage. This confirmed that the AH cohort had significantly higher FIB-4 scores than the ARLD patients (abstinent and drinkers). 89% of the AH patients had scores suggestive of an ISHAK fibrosis stage greater than 4, whilst 30% of drinking and 13% of abstinent patients fell into this category. The drinking patients with ARLD reported an average weekly alcohol unit consumption around 25% of that reported in the AH group but were a useful group to allow us to assess potential impact of alcohol superimposed on established disease given their consumption was over twice the recommended UK maximum weekly units. The AH patients exhibited significantly elevated MELD and Child Pugh scores compared to both ARLD groups ($p<0.0001$ for both), but MELD scores were similar across the ARLD groups. Decompensated liver function (evidenced by a MELD score >15) was observed in 95% of the AH patients whilst all the patients who were still drinking exhibited compensated liver function at time of assessment. In contrast nearly 20% of the abstinent ARLD patients had decompensated. The mortality risk was significantly elevated in the AH group as indicated by their elevated UKELD scores, and these patients had Maddrey's scores above 50 on average. Table 1 shows that these patients had an approximately 20% mortality risk at one month and this increased to around 30% at six months and to >40% at one year post initial presentation.

Patients with alcohol-related liver disease had elevated peripheral blood white cell count compared to healthy controls and this was particularly marked in those patients with alcohol-related hepatitis (Figure 1A). Here levels in AH significantly exceeded total white cell counts in abstinent ARLD and patients who were still drinking. Importantly neutrophils accounted for greater than 60% of the white cells in all individuals, with the largest proportion again in those individuals with AH (Figures 1B, C). Whilst the neutrophil percentage was consistently elevated in patients with AH, the neutrophil count showed significant

10.3389/fimmu.2024.1330536

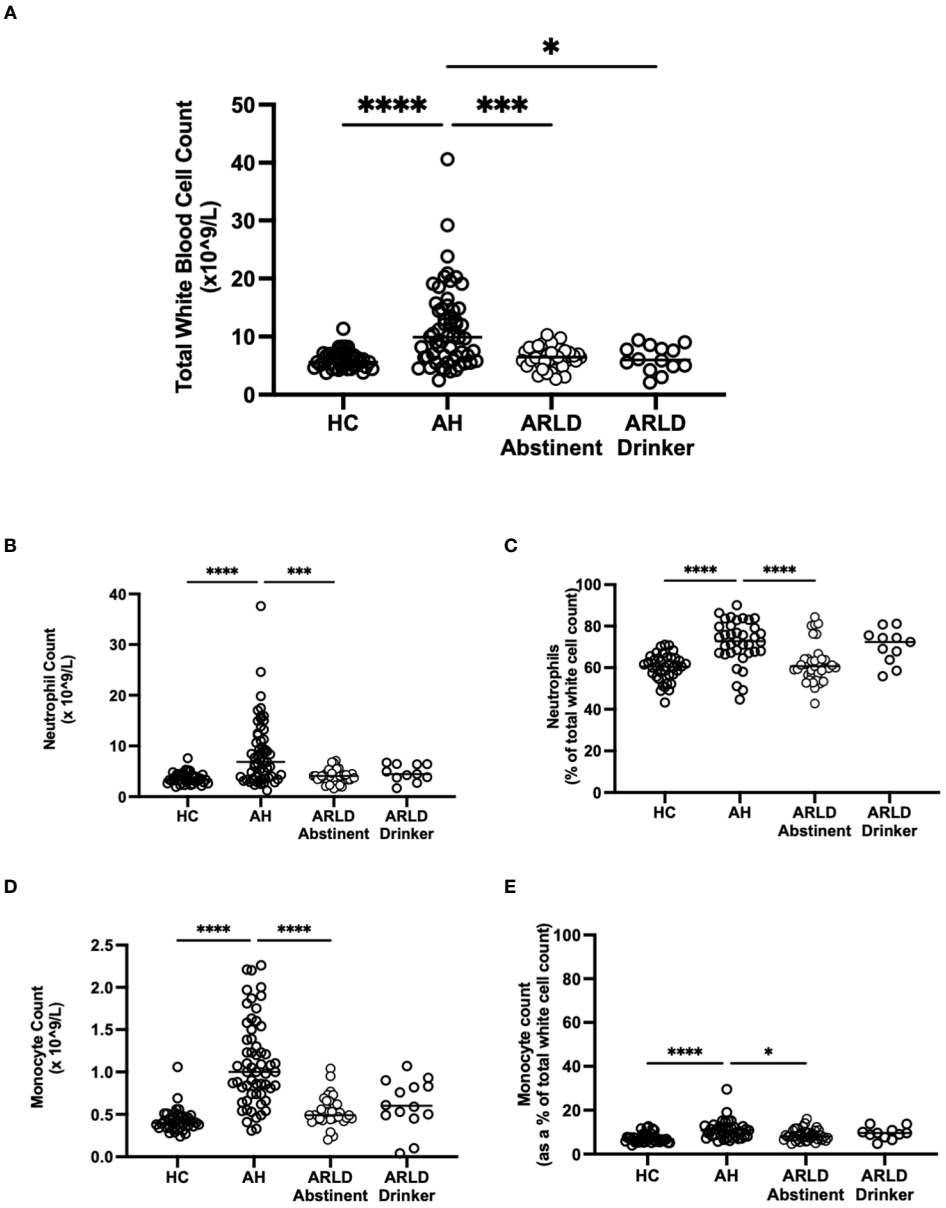

FIGURE 1
(A) Total white blood cell counts in whole blood samples obtained from patients with alcoholic hepatitis (AH), patients with alcohol related liver disease who were abstinent of alcohol, patients with alcohol related liver disease and ongoing drinking (Drinker), and healthy controls (HC), as measured by the Sysmex XN1000 analyser. **(B–E)** Neutrophil and Monocyte counts shown as total cell count or as a percentage of total WBC count as indicated. Individual data points represent a single patient, and the line is mean for the cohort. Multivariate ANOVA (Kruskal Wallis with Dunns correction) indicated significant differences between cohorts as indicated (p<0.05*, 0.01**, 0.001*** and 0.0001****).

interindividual variation ranging from (1.2 to 37.6 x10^9/L, Figure 1B). This correlated to a certain extent with disease severity since those patients with the highest Glasgow Alcoholic Hepatitis Score (GAHS) score/Maddrey function also tended to have the most increased peripheral neutrophil count (Supplementary Figure 2). The same was true for circulating monocytes with both % monocytes and total count significantly elevated in AH compared to healthy controls (Figures 1D, E) and increased compared to abstinent and drinking individuals with alcohol-related cirrhosis. These observations are in keeping with reported changes in neutrophil: lymphocyte ratio (NLR) (16) and monocyte ratio (21) in AH. In agreement, we confirmed that NLR was significantly elevated in both AH and ARLD (Figure 2A) and lymphocyte: monocyte ratio (LMR, Figure 2B) was significantly reduced in all our patient groups. This was associated with patient outcome parameters, with NLR in AH correlated with both GAHS (Figure 2C), MELD score (Figure 2D) and renal function (Creatine, Supplementary Figure 1). Similarly, when we compared survival in our AH cohort, both 28 day and 1 year survival were significantly reduced in patients with elevated NLR (Figures 2E, F).

10.3389/fimmu.2024.1330536

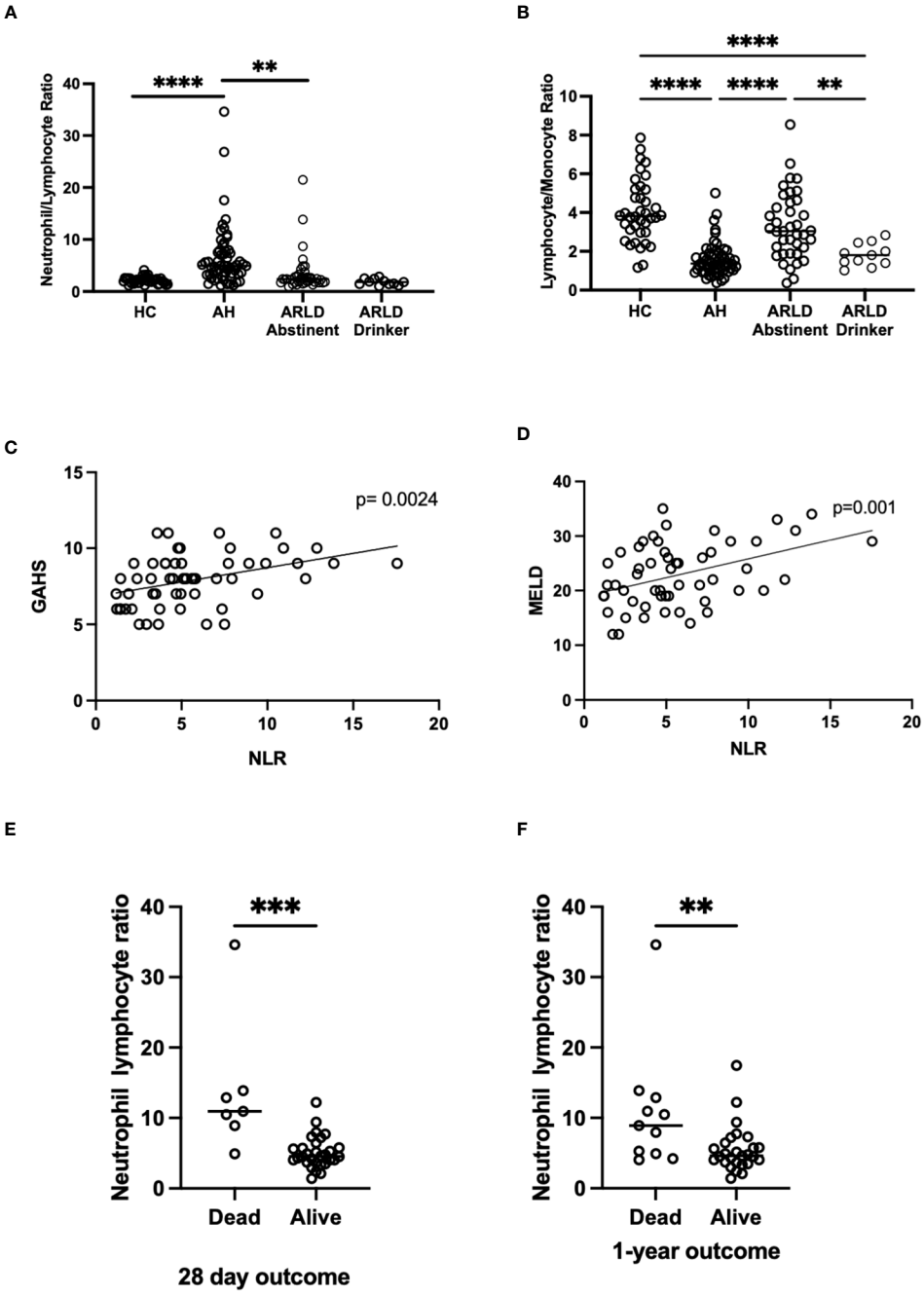

FIGURE 2
(A, B) Neutrophil: Lymphocyte, and Lymphocyte: Monocyte ratios in peripheral blood of patients with alcohol-related hepatitis (AH), patients with alcohol related liver disease who were abstinent of alcohol (ARLD-A) or still drinking (ARLD-D) and healthy controls (HC). **(C–E)** Mortality and infection data along with MELD, GAHS and biochemical characteristics were collected from electronic patient records of individuals with alcohol-related hepatitis. **(C, D)** Pearson r correlation analysis between NLR and GAHS or MELD score. Individual data points represent a single patient, and the line is best fit for the cohort. **(E, F)** NLR and survival data, multivariate ANOVA (Kruskal Wallis with Dunns correction) indicated significant differences between cohorts as indicated (p<0.05*, 0.01**, 0.001***, 0.0001****).

The Sysmex analyser permits assessment of key features of myeloid cell morphology such as cytoplasmic granularity and membrane fluorescence which can indicate functional status and maturity (22). Figure 3 shows the data for cytoplasmic granularity (NEUT-GI) and reactivity intensity (NEUT-RI) for peripheral blood neutrophils in patients with AH compared to healthy controls and patients with chronic disease. Patients with AH had more reactive neutrophils than both healthy controls and abstinent ARLD patients (Figure 3B). The number of patients in our drinking ARLD group was relatively small in comparison but these patients again tended to have higher numbers of more granular neutrophils compared to the abstinent group. However, when immature neutrophils were compared, it was clear that these were significantly elevated only in the context of alcohol-related

hepatitis and not in patients with chronic ARLD (even those still drinking, Figures 3C, D). This was an important distinction since the percentage of immature granulocytes in the peripheral blood population was associated with mortality outcomes. Figure 3E shows that there was a significant increase in the number of immature granulocytes in patients who died within 28 days of initial presentation, and that the impact persisted up to a year (panel F). Of note if we considered that patients with the top three highest NEUT-GI counts, this group all died by day 28, had a mean NEUT-GI of 154.8 and a mean NEUT-RI of 52.6. They also had an average GAHS score of 10.6 and were thus severely ill patients. Immature granulocytes have been reported previously to have altered immunosuppressive, phagocytic and metabolic functions (23, 24) and are found in elevated numbers in the blood of patients with conditions such as sepsis (23). These cells exhibit altered nuclear morphology and granule contents meaning they can be selected using differential centrifugation techniques. We were able to isolate and count cells from a small number of patients and we did indeed see elevated numbers of LD PMN separating into the lymphocyte band in AH compared to healthy controls (4.95 ± 0.6% of LD cells in AH vs 1.3 ± 0.4% in healthy controls). We also noted that isolated neutrophils from patients with AH had a reduced ability to

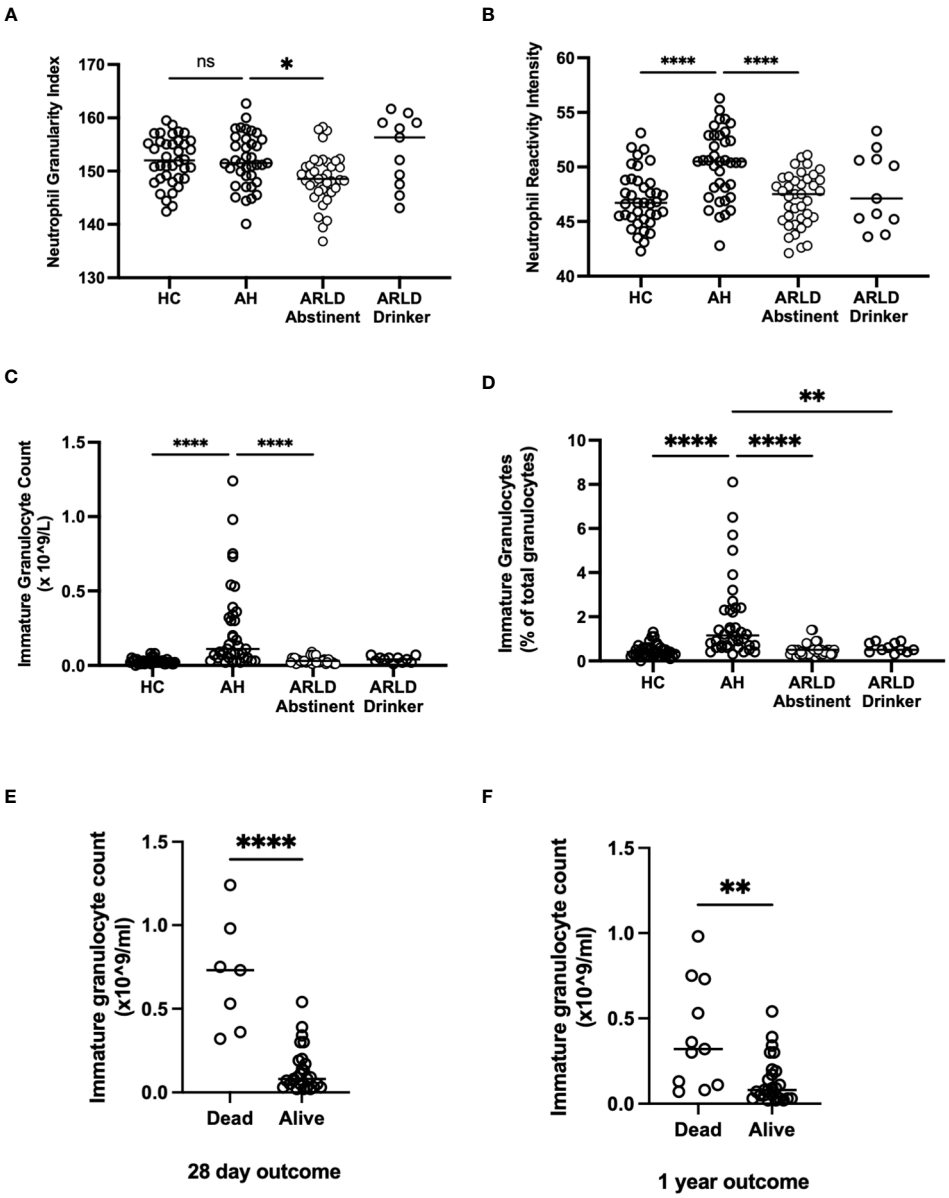

FIGURE 3
(A, B) Neutrophil granularity and reactivity intensity, **(C, D)** Immature granulocyte parameters and **(E, F)** Outcome data as assessed by Sysmex XN1000 analyser and extraction of data from electronic patient records. Values in peripheral blood from patients with alcohol-related hepatitis (AH), patients with alcohol related liver disease who were abstinent of alcohol (ARLD-A) or still drinking (ARLD-D) and healthy controls (HC). Mortality data was collected from electronic patient records of individuals with alcoholic hepatitis. Individual data points represent a single patient, and the line is mean for the cohort. Multivariate ANOVA (Kruskal Wallis with Dunns correction) indicated significant differences between cohorts as indicated ($p<0.05$*, 0.01**, 0.0001****) non-significant pairings are not annotated.

exteriorize NETS in response to PMA compared to both healthy controls and patients with ARLD (Supplementary Figure 3A). In AH neutrophil phagocytic response was also blunted compared to healthy controls (Supplementary Figure 3B), although this response was not significant in the small number of samples available. This is in keeping with reports of neutrophil dysfunction in other acute inflammatory settings (25, 26).

Although the proportion of AH patients in whom we could document evidence of infection (Table 2) was relatively low in our cohort we did observe respiratory infections and spontaneous bacterial peritonitis in the alcoholic hepatitis cohort with a total of 40/58 patients being administered antibiotics (Table 2). Those patients with the highest immature neutrophil counts had increased risk of developing infection (Figure 4A). Interestingly this held true when we considered some of the rarer granulocyte populations (eosinophils and basophils) too. Eosinophil number was variable in the cohorts (Healthy control: 0.15 ±0.015 $x10^9$/L, AH: 0.154 ±0.02 $x10^9$/L, ALD abstinent: 0.2 ±0.041 $x10^9$/L, ALD Drinker: 0.12 ±0.025 $x10^9$/L) but when the cell count was considered as a percentage of total WBC count, there was a significant increase in eosinophil % in those individuals who were alive at 28 days (Figure 4C). Again, there was a tendency for higher eosinophil counts in those patients who did not show signs of infection, but this was not significant (Figure 4B). A similar pattern was apparent for basophils where again individual counts varied across the groups but were reduced in all patients vs healthy controls (Healthy control: 0.36 ±0.16 $x10^9$/L, AH: 0.07 ±0.006 $x10^9$/L, ALD abstinent: 0.15 ±0.010 $x10^9$/L, ALD Drinker: 0.048 ±0.006 $x10^9$/L). Here, increased basophils as a percentage of WBC were observed in those patients who were alive at 28 days (Figure 4D).

4 Discussion

In the present study we utilized peripheral blood from cohorts of patients across the spectrum of ARLD to document changes in peripheral myeloid cells populations. We include data from patients with ARLD that are abstinent (ARLD-A) and patients with ARLD with ongoing alcohol use (ARLD-D). This permits consideration of whether differential findings observed in the AH patients simply due to the presence of chronic disease or alcohol alone. We confirmed that total white cell number is increased in acute alcohol-related hepatitis but not drinking or abstinent ARLD, and that elevation of myeloid cells in particular (both neutrophils and monocytes) may underlie this observation. These findings are in keeping with previously published work (16, 21), which reassures that our inclusion criteria and disease severity for the AH group are similar to those used in other settings (27). However, the variation

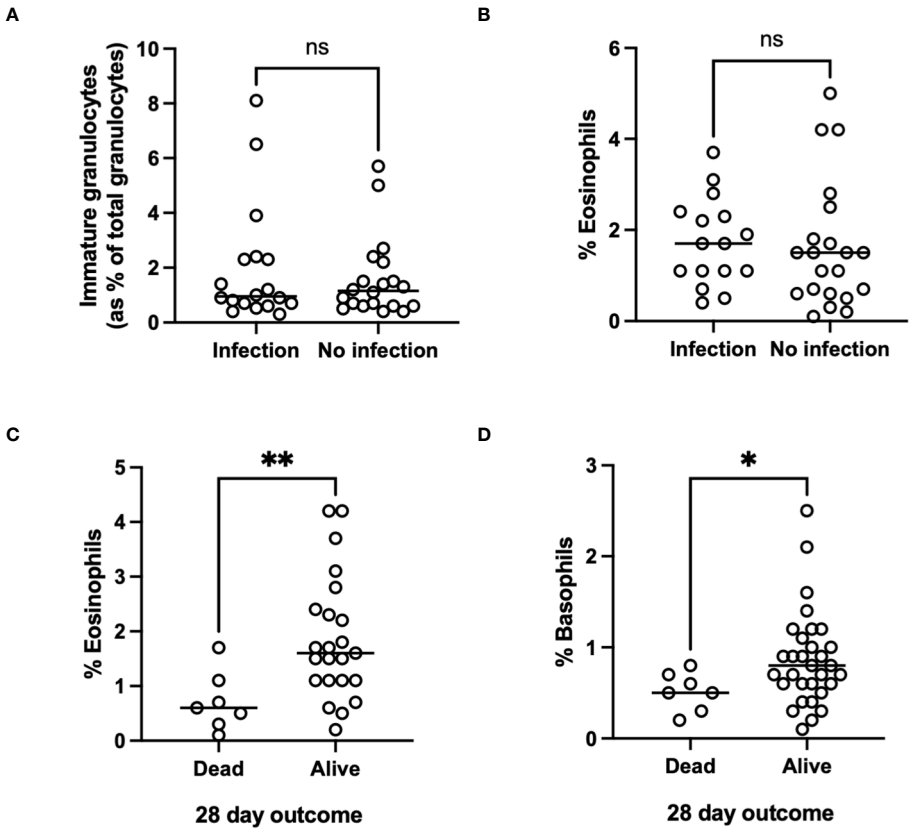

FIGURE 4
(A, B) Infectious outcome, or **(C, D)** Mortality at 28 days and 1 year in patients with alcohol-related hepatitis. Data was collected fusing Sysmex XN1000 analyser or from electronic patient records and individual data points represent a single patient, with the line indicating mean for the cohort. ANOVA indicated differences between cohorts as indicated (p<0.05*). p<0.01 **, ns, indicates no significant difference between indicated cohorts.

within our acute alcohol group (29/38 patients having a Maddrey DF>32, and 9/38 a Maddrey DF≤32) likely explains the spread of data for white cell parameters in this cohort, even though 95% of patients had a MELD> 15. It has been suggested that inflammation causes reciprocal production of granulocytes and lymphocytes in the bone marrow (28). Both cell types develop within the same niche, and therefore compete for resources. Inflammation associated reductions in growth and retention factors, such as stem cell factor and CXCL12, which act preferentially to inhibit lymphocyte development may explain the relative reductions in peripheral lymphocyte number (28). There is published data showing that neutrophil: lymphocyte ratios are elevated in patients with AH, and when incorporated within the GAHS score, can enhance the accuracy of the GAHS score in predicting mortality in AH (16). Similarly, data in cirrhotic patients listed for liver transplantation suggest that elevated NLR predicts poor outcome (29). Thus, it is interesting to observe that our drinking ARLD patients who were not listed for transplant and had higher average MELD score than the abstinent group, also had a higher NLR. We also report that those patients with the lowest NLR in AH had the best mortality outcomes at both 28 days and 1 year. Certainly, our data correlating NLR with both GAHS and renal function in the AH cohort are in keeping with these findings (16).

Circulating monocyte counts were also elevated particularly in the AH group compared to healthy controls and abstinent patients. Others using similar analytical approaches have suggested that monocyte distribution width (MDW, an indicator of cell activation) increases in response to infection and is an indicator of suspected sepsis (30). We were unable to show an association with infection in our relatively small cohort (although peripheral monocyte count was highest in those without sign of infection) and thus it would be interesting to explore MDW in future larger studies.

Perhaps the most significant and novel observation in our study was the presence of significant numbers of immature granulocytes in the peripheral blood of patients with alcohol-related hepatitis. The Sysmex analyser identifies these cells (NEUT-IG) based on both their cytoplasmic granular complexity and abundance of nucleic acids detected by fluorescent staining (31). The identified cells are typically myelocytes and there is a reported good correlation between the number of these cells as detected by the Sysmex instrument and traditional histopathological assessment of blood films (32). These correlate with disease severity (GAHS) and are associated with increased short-term mortality and likelihood of infection. The utility of the NEUT-IG parameter has been investigated for its diagnostic value in sepsis (26, 33–36) with the suggestion that emergency granulopoiesis and high frequencies of immature circulating cells are linked to poor outcome (37). Numbers of immature granulocytes are variable in the circulation of both healthy individuals and patients with inflammatory conditions, but there is a tendency for an increased numbers in disease (38). However an important caveat is that it has also been noted that in patients with some leukaemias or situations with elevated numbers of band neutrophils, the instrument may falsely elevate the IG count (39). One solution is to consider low density neutrophil (LDN) populations which have been suggested to represent immature neutrophil populations (23). We were able to use density gradient centrifugation to isolate low density neutrophils (LDN), and these were increased in AH. LDN have reduced ability to undergo phagocytosis, generate an oxidative burst and produce cytokines from whole blood. It is reported that these cells can include populations of more immature granulocytes, and that the extent of stimulated degranulation of neutrophils correlates with the number of low-density neutrophils present (23). However there is also evidence that some populations of LDN that separate within the lymphocytic cell fraction are actually a mature, primed cell population with enhanced ROS generation and phagocytic capacities (40). We were unable to purify sufficient LDN for detailed functional analysis, but we did note a tendency for reduced phagocytic capacity and stimulant liberated netosis of whole PMN populations from AH patient blood. Both would reduce the antimicrobial capacities of patient cells and have been linked to infection risk in other inflammatory contexts (25, 26). Our functional data would suggest that we are indeed considering immature cells as opposed to primed or 'suppressor' type cells (41), but further cytometric phenotyping of isolated cells would be necessary to absolutely confirm this (42).

It is currently unclear in the literature whether the absolute number of immature granulocytes versus the percentage of immature granulocytes provides more useful information. We found that absolute counts of immature granulocytes were more closely associated with disease severity and mortality than percentages. Whilst it is possible that the raised immature granulocyte count in AH is simply a marker of bone marrow stimulation, it is also feasible that the increased counts of immature granulocytes, which are less functional, contribute to the observed neutrophil dysfunction and risk of sepsis in AH (43, 44). Our total immature cell count was a relatively small proportion of total neutrophils but combined with reductions in both eosinophils and basophils could contribute to impaired pathogen clearance and thus explain our survival data. Our data also suggests a trend for worse infectious outcomes in patients with the lowest eosinophil and basophil number. Eosinophil number, and in particular eosinophil lymphocyte ratio has been considered as a marker of alcohol use in patients with bipolar disorder (45) may relate to increased IL-5 and TNF levels, and production and release of eosinophils from bone marrow (46). Recruitment of eosinophils to the liver is a protective feature in the context of acute hepatitis (47), so it is interesting to speculate whether patients with increased eosinophil release to the periphery may also show increased hepatic recruitment.

Of note along with an increase in immature neutrophils, we also demonstrated increased numbers of more granular and 'reactive' neutrophils (48) in alcoholic hepatitis and in the case of granularity this was also observed in our ARLD drinking cohort. Here the sysmex analyser measures relative membrane fluorescence (Neut-RI) along with cytoplasmic complexity and granule composition via 90° light scatted (NEUT-GI) to give an indication of proportions of more metabolically activated cells. These tend to be considered as more 'activated' and so our findings are in keeping with reports that patients with AH had increased neutrophil activation in comparison to healthy volunteers, as demonstrated by loss of CD62L expression and increased basal oxidant production (49).

Similar populations have been described in patients with autoimmune hepatitis (48), but we believe we are the first to use the Sysmex system to describe these more reactive cells in drinking patients with chronic ARLD and AH. Further consideration of the more unusual granulocyte populations (basophils and eosinophils) is also warranted based on our preliminary findings. Pro-inflammatory 'low density' neutrophils have been described in cirrhosis (50) and contribute to organ damage upon recruitment into tissue. These 'primed' cells are suggested by some to have impaired ROS production and compromised bacterial killing ability, although findings vary depending on the nature and severity of cirrhosis (50). Combined with reported deficiencies in neutrophil chemotaxis (51) and altered NET formation (52) in cirrhosis it is easy to appreciate how predisposition to bacterial infections may occur. However, we should note that our Unit has a cautious approach to initiation of antimicrobial therapy and thus overall, our reported incidence of, and mortality from infection was low. Similarly, infections which presented after discharge or patients who subsequently presented to other Centers would not feature in our data set. Thus, we may be underestimating the true incidence of infections in our study. Despite this and the relatively small size of our cohorts we believe there is potential to measure immature granulocyte counts as a simply calculated predictor of mortality and risk of infectious complications in alcohol related disease. This would allow identification of patients who may require more intensive management. Our study is novel in that we have tried to consider the full spectrum of alcohol related disease in humans from alcohol-related hepatitis to cirrhosis and have utilized a simple approach that translates to most clinical settings. A major advantage of using an automated hematology analyzer to obtain information on myeloid parameters is that no additional processing steps are required between obtaining the sample and running it on the analyser, which minimises the risk of inadvertent neutrophil activation during isolation/processing steps. Thus, in conclusion we suggest that measurement of myeloid parameters such as immature granulocyte count has potential prognostic ability in alcohol-related liver disease.

Data availability statement

Anonymised raw data supporting the conclusions of this article may be made available on personal request to the authors.

Ethics statement

The studies involving humans were approved by Wales Research Ethics Comittee (REC ref 18/WA/0214). The studies were conducted in accordance with the local legislation and institutional requirements. The participants provided their written informed consent to participate in this study.

Author contributions

RK: Data curation, Formal analysis, Investigation, Methodology, Writing – original draft. SS: Data curation, Formal analysis, Investigation, Writing – review & editing. LH: Data curation, Investigation, Writing – review & editing. LS: Data curation, Formal analysis, Methodology, Writing – review & editing. JH: Methodology, Writing – review & editing. NR: Writing – review & editing. PN: Funding acquisition, Supervision, Writing – review & editing. PL: Conceptualization, Data curation, Formal analysis, Funding acquisition, Supervision, Writing – original draft, Writing – review & editing.

Funding

The author(s) declare that financial support was received for the research, authorship, and/or publication of this article. This study represents independent research part funded by the MRC (MIMAH Stratified Medicine Initiative, and a fellowship for RK MR/S001581/1) and the Wellcome trust (MIDAS PhD studentship to LH) and carried out at the National Institute for Health and Care Research (NIHR) Birmingham Biomedical Research Centre (BRC). The views expressed are those of the author(s) and not necessarily those of the Wellcome Trust or MRC, the NIHR or the Department of Health and Social Care.

Conflict of interest

The authors declare that the research was conducted in the absence of any commercial or financial relationships that could be construed as a potential conflict of interest.

The author(s) declared that they were an editorial board member of Frontiers, at the time of submission. This had no impact on the peer review process and the final decision.

Publisher's note

Supplementary material

The Supplementary Material for this article can be found online at: https://www.frontiersin.org/articles/10.3389/fimmu.2024.1330536/full#supplementary-material

References

1. Devarbhavi H, Asrani SK, Arab JP, Nartey YA, Pose E, Kamath PS. Global burden of liver disease: 2023 update. *J Hepatol*. (2023) 79:516–37. doi: 10.1016/j.jhep.2023.03.017

2. N.E.o.L.C.I. Network. *Deaths from Liver Disease: Implications for End of Life Care in England*. (2012). Available at: https://www.ias.org.uk/uploads/pdf/News%20stories/nhs-endoflife-liverdisease-report.pdf.

3. A.o.M. Sciences. *Calling time – The nation's drinking as a major health issue*. London: A.o.M. Sciences. (2004).

4. Teli MR, Day CP, Burt AD, Bennett MK, James OF. Determinants of progression to cirrhosis or fibrosis in pure alcoholic fatty liver. *Lancet*. (1995) 346:987–90. doi: 10.1016/S0140-6736(95)91685-7

5. Singal AK, Arsalan A, Dunn W, Arab JP, Wong RJ, Kuo YF, et al. Alcohol-associated liver disease in the United States is associated with severe forms of disease among young, females and Hispanics. *Aliment Pharmacol Ther*. (2021) 54:451–61. doi: 10.1111/apt.16461

6. Gustot T, Jalan R. Acute-on-chronic liver failure in patients with alcohol-related liver disease. *J Hepatol*. (2019) 70:319–27. doi: 10.1016/j.jhep.2018.12.008

7. Katoonizadeh A, Laleman W, Verslype C, Wilmer A, Maleux G, Roskams T, et al. Early features of acute-on-chronic alcoholic liver failure: a prospective cohort study. *Gut*. (2010) 59:1561–9. doi: 10.1136/gut.2009.189639

8. Louvet A, Wartel F, Castel H, Dharancy S, Hollebecque A, Canva-Delcambre V, et al. Infection in patients with severe alcoholic hepatitis treated with steroids: early response to therapy is the key factor. *Gastroenterology*. (2009) 137:541–8. doi: 10.1053/j.gastro.2009.04.062

9. Ballester MP, Sittner R, Jalan R. Alcohol and acute-on-chronic liver failure. *J Clin Exp Hepatol*. (2022) 12:1360–70. doi: 10.1016/j.jceh.2021.12.010

10. Albillos A, Lario M, Alvarez-Mon M. Cirrhosis-associated immune dysfunction: distinctive features and clinical relevance. *J Hepatol*. (2014) 61:1385–96. doi: 10.1016/j.jhep.2014.08.010

11. Kasper P, Lang S, Steffen HM, Demir M. Management of alcoholic hepatitis: A clinical perspective. *Liver Int*. (2023) 43:2078–95. doi: 10.1111/liv.15701

12. Crabb DW, Bataller R, Chalasani NP, Kamath PS, Lucey M, Mathurin P, et al. Standard definitions and common data elements for clinical trials in patients with alcoholic hepatitis: recommendation from the NIAAA alcoholic hepatitis consortia. *Gastroenterology*. (2016) 150:785–90. doi: 10.1053/j.gastro.2016.02.042

13. Jalan R, Pavesi M, Saliba F, Amoros A, Fernandez J, Holland-Fischer P, et al. The CLIF Consortium Acute Decompensation score (CLIF-C ADs) for prognosis of hospitalised cirrhotic patients without acute-on-chronic liver failure. *J Hepatol*. (2015) 62:831–40. doi: 10.1016/j.jhep.2014.11.012

14. Xu W, Wu M, Chen B, Wang H. Myeloid cells in alcoholic liver diseases: Mechanism and prospect. *Front Immunol*. (2022) 13:971346. doi: 10.3389/fimmu.2022.971346

15. Vaz K, Little R, Majeed A, Kemp W, Roberts SK. Determinants of short- and long-term outcomes of an Australian cohort of patients admitted with alcoholic hepatitis. *Dig Dis Sci*. (2022) 67:3356–65. doi: 10.1007/s10620-021-07140-w

16. Forrest EH, Storey N, Sinha R, Atkinson SR, Vergis N, Richardson P, et al. Baseline neutrophil-to-lymphocyte ratio predicts response to corticosteroids and is associated with infection and renal dysfunction in alcoholic hepatitis. *Aliment Pharmacol Ther*. (2019) 50:442–53. doi: 10.1111/apt.15335

17. Ambade A, Lowe P, Kodys K, Catalano D, Gyongyosi B, Cho Y, et al. Pharmacological inhibition of CCR2/5 signaling prevents and reverses alcohol-induced liver damage, steatosis, and inflammation in mice. *Hepatology*. (2019) 69:1105–21. doi: 10.1002/hep.30249

18. Mare TA, Treacher DF, Shankar-Hari M, Beale R, Lewis SM, Chambers DJ, et al. The diagnostic and prognostic significance of monitoring blood levels of immature neutrophils in patients with systemic inflammation. *Crit Care*. (2015) 19:57. doi: 10.1186/s13054-015-0778-z

19. Hazeldine J, Harris P, Chapple IL, Grant M, Greenwood H, Livesey A, et al. Impaired neutrophil extracellular trap formation: a novel defect in the innate immune system of aged individuals. *Aging Cell*. (2014) 13:690–8. doi: 10.1111/acel.12222

20. Sterling RK, Lissen E, Clumeck N, Sola R, Correa MC, Montaner J, et al. Development of a simple noninvasive index to predict significant fibrosis in patients with HIV/HCV coinfection. *Hepatology*. (2006) 43:1317–25. doi: 10.1002/(ISSN)1527-3350

21. Voss JK, Li Z, Weinman SA. Elevated blood monocyte counts in alcohol-associated hepatitis. *JGH Open*. (2022) 6:148–51. doi: 10.1002/jgh3.12707

22. Farias MG, Garcia MP, Cagliari CR. Evaluation of the immature myeloid information (IMI) by Sysmex XE 2100(R) hematology analyzer in the identification of blasts of myeloid lineage. *Clin Chem Lab Med*. (2012) 50:1861–4. doi: 10.1515/cclm-2012-0147

23. Sun R, Huang J, Yang Y, Liu L, Shao Y, Li L, et al. Dysfunction of low-density neutrophils in peripheral circulation in patients with sepsis. *Sci Rep*. (2022) 12:685. doi: 10.1038/s41598-021-04682-x

24. Hsu BE, Tabaries S, Johnson RM, Andrzejewski S, Senecal J, Lehuede C, et al. Immature low-density neutrophils exhibit metabolic flexibility that facilitates breast cancer liver metastasis. *Cell Rep*. (2019) 27:3902–3915 e6. doi: 10.1016/j.celrep.2019.05.091

25. Taneja R, Sharma AP, Hallett MB, Findlay GP, Morris MR. Immature circulating neutrophils in sepsis have impaired phagocytosis and calcium signaling. *Shock*. (2008) 30:618–22. doi: 10.1097/SHK.0b013e318173ef9c

26. Hampson P, Dinsdale RJ, Wearn CM, Bamford AL, Bishop JRB, Hazeldine J, et al. Immature granulocytes, and cell-free DNA are early biomarkers of sepsis in burn-injured patients: A prospective observational cohort study. *Ann Surg*. (2017) 265:1241–9. doi: 10.1097/SLA.0000000000001807

27. Thursz MR, Richardson P, Allison M, Austin A, Bowers M, Day CP, et al. Prednisolone or pentoxifylline for alcoholic hepatitis. *N Engl J Med*. (2015) 372:1619–28. doi: 10.1056/NEJMoa1412278

28. Ueda Y, Kondo M, Kelsoe G. Inflammation and the reciprocal production of granulocytes and lymphocytes in bone marrow. *J Exp Med*. (2005) 201:1771–80. doi: 10.1084/jem.20041419

29. Leithead JA, Rajoriya N, Gunson BK, Ferguson JW. Neutrophil-to-lymphocyte ratio predicts mortality in patients listed for liver transplantation. *Liver Int*. (2015) 35:502–9. doi: 10.1111/liv.12688

30. Wu J, Li L, Luo J. Diagnostic and prognostic value of monocyte distribution width in sepsis. *J Inflammation Res*. (2022) 15:4107–17. doi: 10.2147/JIR.S372666

31. Kwiecien I, Rutkowska E, Kulik K, Klos K, Plewka K, Raniszewska A, et al. Reactivity and granularity research parameters to characterize and differentiate convalescent patients from active SARS-coV-2 infection. *Cells*. (2021) 10(9):2332. doi: 10.3390/cells10092332

32. Fujimoto H, Sakata T, Hamaguchi Y, Shiga S, Tohyama K, Ichiyama S, et al. Flow cytometric method for enumeration and classification of reactive immature granulocyte populations. *Cytometry*. (2000) 42:371–8. doi: 10.1002/(ISSN)1097-0320

33. Porizka M, Volny L, Kopecky P, Kunstyr J, Waldauf P, Balik M. Immature granulocytes as a sepsis predictor in patients undergoing cardiac surgery. *Interact Cardiovasc Thorac Surg*. (2019) 28:845–51. doi: 10.1093/icvts/ivy360

34. Karon BS, Tolan NV, Wockenfus AM, Block DR, Baumann NA, Bryant SC, et al. Evaluation of lactate, white blood cell count, neutrophil count, procalcitonin and immature granulocyte count as biomarkers for sepsis in emergency department patients. *Clin Biochem*. (2017) 50:956–8. doi: 10.1016/j.clinbiochem.2017.05.014

35. Ayres LS, Sgnaolin V, Munhoz TP. Immature granulocytes index as early marker of sepsis. *Int J Lab Hematol*. (2019) 41:392–6. doi: 10.1111/ijlh.12990

36. Ansari-Lari MA, Kickler TS, Borowitz MJ. Immature granulocyte measurement using the Sysmex XE-2100. *Relationship to infection sepsis. Am J Clin Pathol*. (2003) 120:795–9. doi: 10.1309/LT30BV9UJJV9CFHQ

37. Kwok AJ, Allcock A, Ferreira RC, Cano-Gamez E, Smee M, Burnham KL, et al. Neutrophils and emergency granulopoiesis drive immune suppression and an extreme response endotype during sepsis. *Nat Immunol*. (2023) 24:767–79. doi: 10.1038/s41590-023-01490-5

38. Morisaki T, Goya T, Ishimitsu T, Torisu M. The increase of low density subpopulations and CD10 (CALLA) negative neutrophils in severely infected patients. *Surg Today*. (1992) 22:322–7. doi: 10.1007/BF00308740

39. Lu Q, Li Y, Li T, Hou T, Zhao Y, Feng S, et al. Evaluation of immature granulocyte parameters in myeloid neoplasms assayed by Sysmex XN hematology analyzer. *J Hematop*. (2022) 15:1–6. doi: 10.1007/s12308-022-00484-w

40. Blanco-Camarillo C, Aleman OR, Rosales C. Low-density neutrophils in healthy individuals display a mature primed phenotype. *Front Immunol*. (2021) 12:672520. doi: 10.3389/fimmu.2021.672520

41. Singel KL, Emmons TR, Khan ANH, Mayor PC, Shen S, Wong JT, et al. Mature neutrophils suppress T cell immunity in ovarian cancer microenvironment. *JCI Insight*. (2019) 4(5):e122311. doi: 10.1172/jci.insight.122311

42. Hegde S, Leader AM, Merad M. MDSC: Markers, development, states, and unaddressed complexity. *Immunity*. (2021) 54:875–84. doi: 10.1016/j.immuni.2021.04.004

43. Tritto G, Bechlis Z, Stadlbauer V, Davies N, Frances R, Shah N, et al. Evidence of neutrophil functional defect despite inflammation in stable cirrhosis. *J Hepatol*. (2011) 55:574–81. doi: 10.1016/j.jhep.2010.11.034

44. Mookerjee RP, Stadlbauer V, Lidder S, Wright GA, Hodges SJ, Davies NA, et al. Neutrophil dysfunction in alcoholic hepatitis superimposed on cirrhosis is reversible and predicts the outcome. *Hepatology*. (2007) 46:831–40. doi: 10.1002/(ISSN)1527-3350

45. Dirani E, Bou Khalil R, Raad G, Richa S. Eosinophils to lymphocytes ratio (ELR) as a potential inflammatory biomarker in patients with dual diagnosis of bipolar and alcohol use disorders: A retrospective cohort study. *J Dual Diagn*. (2022) 18:144–52. doi: 10.1080/15504263.2022.2090650

46. Lampinen M, Carlson M, Hakansson LD, Venge P. Cytokine-regulated accumulation of eosinophils in inflammatory disease. *Allergy*. (2004) 59:793–805. doi: 10.1111/j.1398-9995.2004.00469.x

47. Xu L, Yang Y, Wen Y, Jeong JM, Emontzpohl C, Atkins CL, et al. Hepatic recruitment of eosinophils and their protective function during acute liver injury. *J Hepatol*. (2022) 77:344–52. doi: 10.1016/j.jhep.2022.02.024

48. Domerecka W, Kowalska-Kepczynska A, Homa-Mlak I, Michalak A, Mlak R, Mazurek M, et al. The usefulness of extended inflammation parameters and systemic

inflammatory response markers in the diagnostics of autoimmune hepatitis. *Cells*. (2022) 11(16):2554. doi: 10.3390/cells11162554

49. Taieb J, Mathurin P, Elbim C, Cluzel P, Arce-Vicioso M, Bernard B, et al. Blood neutrophil functions and cytokine release in severe alcoholic hepatitis: effect of corticosteroids. *J Hepatol*. (2000) 32:579–86. doi: 10.1016/S0168-8278(00)80219-6

50. Balazs I, Stadlbauer V. Circulating neutrophil anti-pathogen dysfunction in cirrhosis. *JHEP Rep*. (2023) 5:100871. doi: 10.1016/j.jhepr.2023.100871

51. Fiuza C, Salcedo M, Clemente G, Tellado JM. *In vivo* neutrophil dysfunction in cirrhotic patients with advanced liver disease. *J Infect Dis*. (2000) 182:526–33. doi: 10.1086/315742

52. Agraz-Cibrian JM, Delgado-Rizo V, Segura-Ortega JE, Maldonado-Gomez HA, Zambrano-Zaragoza JF, Duran-Avelar MJ, et al. Impaired neutrophil extracellular traps and inflammatory responses in the peritoneal fluid of patients with liver cirrhosis. *Scand J Immunol*. (2018) 88:e12714. doi: 10.1111/sji.12714

Frontiers in Immunology

Explores novel approaches and diagnoses to treat immune disorders.

The official journal of the International Union of Immunological Societies (IUIS) and the most cited in its field, leading the way for research across basic, translational and clinical immunology.

Discover the latest Research Topics

See more →

Frontiers

Avenue du Tribunal-Fédéral 34
1005 Lausanne, Switzerland
frontiersin.org

Contact us

+41 (0)21 510 17 00
frontiersin.org/about/contact